

**Online ISSN : 2395-602X**

**Print ISSN : 2395-6011**

[www.ijrst.com](http://www.ijrst.com)



**Conference  
Proceedings**

**Two Days National Conference on  
Material Science and Chemistry**

**4th and 5th Oct 2024**

**Organized By**

Department of Chemistry and  
Internal Quality Assurance Cell  
Yogeshwari Mahavidyalaya, Ambajogai.  
Dist. Beed, Maharashtra, India

**VOLUME 11, ISSUE 21, SEPTEMBER-OCTOBER-2024**

**INTERNATIONAL JOURNAL OF SCIENTIFIC  
RESEARCH IN SCIENCE AND TECHNOLOGY**

**PEER REVIEWED AND REFEREED INTERNATIONAL SCIENTIFIC RESEARCH JOURNAL**

Scientific Journal Impact Factor : 8.627

Email : [editor@ijrst.com](mailto:editor@ijrst.com) Website : <http://ijrst.com>



# **Two Days National Conference on Material Science and Chemistry**

4<sup>th</sup> and 5<sup>th</sup> Oct 2024

**Organized by**

Department of Chemistry and Internal Quality Assurance Cell  
Yogeshwari Mahavidyalaya, Ambajogai. Dist. Beed, Maharashtra, India

**Published By**

International Journal of Scientific Research in Science and Technology  
Print ISSN: 2395-6011 Online ISSN: 2395-602X

**Volume 11, Issue 21, September-October-2024**

International Peer Reviewed, Open Access Journal

**Published By**

**Technoscience Academy**

website: [www.technoscienceacademy.com](http://www.technoscienceacademy.com)

## CHIEF PATRONS

Mr. C.L. Bardapurkar  
President  
Y.E.S. Ambajogai

Mr. G. B. Vyas  
Vice-President  
Y.E.S. Ambajogai

Adv. Jagdish Chausalkar  
Executive Vice-President  
Y.E.S. Ambajogai

Mr. K. S. Chausalkar  
Secretary  
Y.E.S. Ambajogai

Dr. S. P. Vaidya  
Treasurer  
Y.E.S. Ambajogai

Mr. B. V. Shete  
Joint-Secretary  
Y.E.S. Ambajogai

## ORGANIZERS

Prof. Dr. M.V. Kanetkar  
I/C Principal, Yogeshwari Mahavidyalaya Ambajogai  
**Chief Organizing Secretary**

Dr. R. V. Kulkarni  
**Vice-Principal**  
Yogeshwari Mahavidyalaya Ambajogai

Dr. S. C. Jadhavar  
HOD Chemistry  
**Organizing Secretary**

Dr. Y. S. Handibag  
**IQAC Co-ordinator**  
Yogeshwari Mahavidyalaya Ambajogai

Dr. V. G. Kalalawe

**Convener**

Mr. J. M. Kondre

**Treasurer**

## **ADVISORY COMMITTEE**

Prof. Vijay Fulari (Hon. Vice-Chancellor, Dr. BAMU, Ch. Sambhajinagar)

Prof. Walmik Sarwade (Pro-Vice Chacellor, Dr. BAMU, Ch. Sambhajinagar)

Dr. S. T. Gaikwad (Sr. Professor, Dr. BAMU, Ch. Sambhajinagar)

Dr. Sunil Shankarwar (HOD, Chemistry, Dr. BAMU, Ch. Sambhajinagar)

Dr. Mrs. A.S. Rajbhoj (Sr. Professor, Dr. BAMU, Ch. Sambhajinagar)

Dr. Anil Shankarwar (Principal, S.B. College, Ch. Sanbhajinagar)

Dr. M. K. Lande (Professor, Chemistry, Dr. BAMU, Ch. Sambhajinagar)

Dr. Bapu Shingte (Professor, Dr. BAMU, Ch. Sambhajinagar)

Dr. Bhaskar Sathe (Professor, Dr. BAMU, Ch. Sambhajinagar)

Dr. Anusaya Chavan (Asso. Prof. Dr. BAMU, Ch. Sambhajinagar)

Dr. S. P. Hangirgekar (Sr. Professor, Shivaji University, Kolhapur)

Dr. Anant Kapadi (Professor, ICT, Mumbai)

Dr. Dinesh Sawant (Scientist, NCL, Pune)

Dr. Kushal Bhatte (Scientist, NCL, Pune)

Dr. Sunita Salunke (Professor, SPPU, Pune)

Dr. Shubhangi Umberkar (Scientist, Catalysis Division, NCL, Pune)

Dr. S. R. Bhusare (Professor, DSM College, Parbhani)

Dr. S. D. Deosarkar (Professor, SRTMU, Nanded)

Dr. A. L. Puyad (Asso. Professor, SRTMU, Nanded)

Dr. Naresh Nalajala (Scientist, PPISR, Bengaluru)

Dr. Mazahar Farooqui (Principal, Azad College, Ch. Sambhajinagar)

Dr. G. K. Kakade (Principal, ACS college, Kille Dharur)

Dr. Santosh Undare (Principal, Balbhim College, Beed)

Dr. K. P. Hawal (Asso. Professor, Dr. BAMU Sub-campus, Dharashiv)  
Dr. R. M. Tigote (Asso. Professor, Dr. BAMU Sub-campus, Dharashiv)  
Dr. A. S. Munde (HOD, Chemistry, Milind College, Ch. Sambhainagar)  
Dr. B. C. Khade (HOD, Chemistry, D.S.M. College, Parbhani)  
Dr. D. R. Munde (Professor, N.E.S. Science College, Nanded)  
Dr. Sudhakar Patil (HOD, Chemistry, M. U. Mahavidyalaya, Udgir)  
Dr. Haridas Tirpude (HOD, Chemistry, Shivaji Mahavidyalaya, Udgir)  
Dr. Sambhaji Wartale (Professor, Yashwant College, Nanded)  
Dr. Arvind Aghao (Professor, Balbhim College, Beed)  
Dr. B. V. Kendre (HOD, Chemistry, Vaidyanathe College, Parali)  
Dr. Y. P. Sarnikar (HOD, Chemistry, Dayanand Sci. College, Latur)  
Dr. R. G. Momale (HOD, Chemistry, SGG ASC college, Dharmapuri)  
Dr. V. S. Suryawanshi (HOD, Chemistry, Ch. Shivaji College, Omerga)  
Dr. V. G. Deshpande (HOD, Chemistry, LD Mahavidyalaya, Parali)  
Dr. S. N. Ipper (HOD, Chemistry, SS Mahavidyalaya, Mazalgaon)  
Dr. V. V. Borgaonkar (HOD, Chemistry, S. Mahavidyalaya, Majalgaon)  
Dr. A.S. Kirdant (HOD, Chemistry, Baburaoji Adaskar Mahavidyalaya, Kaij)

## **SCOPE AND OBJECTIVE OF CONFERENCE**

The conference aims to sensitize and stimulate the young minds to bring out the best among the various frontiers of Chemical Sciences by providing a common platform to researchers working in the various sub disciplines of the themes. This conference would generate awareness amongst the researcher scholars, undergraduate and postgraduate students particularly in the local region.

### **The objectives of the conference are as follows:**

- To allow students, researchers, scientists and academicians for fruitful discussions and presentation of new results within the theme of the conference.
- To provide premier scientific forum for students, researchers, scientists and academicians to navigate the future research for betterment of society at large.
- To discuss and promote the recent findings and new emerging trends in the Chemical Sciences.

## THEMES

**Organic Chemistry** : Synthetic and Structural Organic Chemistry Natural Products, Applications of Spectroscopic Techniques, Bio organic Chemistry, Drug Design and development, Medicinal Chemistry, Green Chemistry etc.

**Physical Chemistry** : Physicochemical properties of drugs/Ionic Liquids/Surfactants, Electrochemistry, Quantum Chemistry, Nuclear Chemistry, Solution Thermodynamics, Thermodynamics of Biological Systems, Surface Chemistry, Colloid and Interface etc.

**Inorganic Chemistry**: Coordination Chemistry, Industrial Pollution, Bio-inorganic Chemistry, Organometallics, Metallurgy, etc. Polymer Chemistry, Analytical Chemistry, Industrial Chemistry, Agrochemicals and Pesticides, Petrochemicals, Soil Chemistry, Nano – Technology, Pharmaceutical Chemistry, Nano - Chemistry, Material Chemistry and any other topic related to the theme of the symposium.

## ABOUT THE COLLEGE

It was in 1935, when the great sanyasi, freedom fighter and the prime leader of Hyderabad Mukti Sangram, an MP, Swami Ramanand Teerth came over to Ambajogai and officially established and started this institution with two objectives – to strengthen the Indian freedom movement and educate the poor Marathwada students. The main objective of this institution has been, since then Patriotism, Nation building, Education, Democracy, Secularism and Upliftment of the poor sections of the society. The institution has grown into a large banyan tree during the last ninety years due to the honest, sincere and tireless striving of these Society authorities (Rev. Babasaheb Paranjape, Hon. Purshottam alias Bhausaheb Chousalkar, Hon. Shridhar Soman, Hon. Shivajirao Chousalkar, Hon. Adv. Trimbakrao Khursale, Dr. Vyankatrao Deshpande, Rajarampant Sonwalkar, Hon. R.D. Deshpande, Bethuji Guruji, Hon. Balirampant Kamkhedkar, Hon. E.M. Kulkarni, Dr. S.T. Khursale Adv. V.K.Chousalkar and the existing Mr. Chandrashekhar Bardapurkar, K. Chausalkar, Mr. G. B. Vyas, Dr. Shailesh Vaidya, Mr. Bhimashanker Shete and Adv. Jagdish Chausalkar ).

# CONTENT

SR. NO	ARTICLE/PAPER	PAGE NO
1	<b>Design, Synthesis, and Biological Evolution of New Chromen-2-one Derivatives as Antituberculosis Agents</b> Siddheshwar B. Lonari, Anil S. Kirdant, Suresh C. Jadhavar	01-09
2	<b>Microwave Dielectric Study of Micronutrients of Soil at X Band</b> Manisha D. Dhiware	10-15
3	<b>A Review Article on Microwave-Assisted Multicomponent Reactions in Heterocyclic Chemistry</b> Nilesh P. Tale	16-20
4	<b>Synthesis, Characterization and Biological Studies of Imino- Pyrazol Schiff Base and Transition Metal Complexes</b> Vishvas Ganpat Choudhari, Netaji Keru Desai, Mahesh Bajarang Gurame, Anil Shivaji Kirdant	21-32
5	<b><math>\alpha</math> -Amino phosphonates: Synthesis and Biomedical Application</b> Ganesh V. Shitre, Mahadev B. Suwarnkar	33-39
6	<b>Comparative Study of Corrosion in Metals in Acidic media</b> Bhagyashree Chari	40-44
7	<b>Green Synthesis of Flavanones By L-Glycine</b> Arshia Parveen	45-50
8	<b>Sustainable Practices in Chemical Synthesis : A Comprehensive Review</b> Sanghratna L. Kasare	51-57
9	<b>Complexation of Zinc Metal with Medicinal Drugs in Mixed Solvent Media</b> Ramesh Ware, Rajpal Jadhav, Hansaraj Joshi, Shailendrasingh Thakur	58-63
10	<b>Tailoring and Characterization of Copper Oxide Nanoparticles by Sol-Gel Route</b> Sangita Shinde, Pallavi Nalle, N. D. Chaudhari	64-67
11	<b>Eco-Friendly Adsorption Technology: Efficient Removal of Heavy Metals Chromium and Lead Ions by using Terminalia catalpa Leaves</b> Harshal Madhukar Bachhav, Kulbhushan Ashru Sasane	68-73
12	<b>Electronic Spectral Solvent Coefficient and Electronic Transition of Eriochrome Black T. Indicator and Its Cobalt, Nickel and Copper Complexes</b> Pandit Khakre, Dr. Sonaji Gayakwad, Mr. Atul Chavan	74-78
13	<b>Facile Synthesis of rGO decorated on NiMn<sub>2</sub>O<sub>4</sub> &amp; CoMn<sub>2</sub>O<sub>4</sub> Nanocomposite Electrode for Responsive their Ammonia Sensors</b> Saurabh V. Helavi-Reddy, Navnath K. Chavan, Nilesh V. Sankpal, Mohan D. Jamdar, Vishal W. Banewar	79-88

14	<b>Theoretical Study of Catechol and Hydroquinone with Solvent Molecule</b> Chandrakant S. Aher	89-94
15	<b>Development &amp; Studies of Effective Plant Based Laboratory Hand Sanitizers &amp; Their Effect on Pathogenic Bacteria</b> Narsinge A.P, Kadam A.S, Didwani R.D, Ghatol L.S, Gutte D.K, Shinde A.S, Chavan A.N, Waghmare A.V, Sanghai S.P, Dongahu A.D	95-99
16	<b>One Pot Procedure for Green Synthesis of Benzylidenethiazolidine-2,4-Diones Using Catalytic Amount of Anhydrous Aluminium Chloride in Ethanol Solvent Via Knoevenagel Condensation Reaction</b> Sayas K Lad, Babasaheb V Kendre	100-105
17	<b>Synthesis of Nanoparticles by Green Synthesis Method</b> H. A. Tirpude, P. S. Reddy	106-113
18	<b>Zinc Triflet : A Highly Effective Catalyst for the One-Pot Synthesis of 3,4-Dihydropyrimidine-2(1H)-ones and Thiones</b> Hanmant M. Kasralikar, Nitish S. Kaminwar, Shrinivas L. Nakkalwar	114-119
19	<b>Thickness Dependent Physical Properties of SILAR Deposited Nanostructured MgSe Thin Films</b> K. C Shinde, Y. S. Sakhare, R. J. Topare	120-123
20	<b>A Review on Biogenic Synthesis of Silver Nanoparticles</b> Mahadev B Suwarnkar, Ganesh V Shitre, Suresh A Kamble, Madhav J Hebade	124-128
21	<b>Analysis of Physico-Chemical Properties of Kayadhu River</b> Gajanan G. Kadam, Kishor Dawane, Rameshwar M. More	129-132
22	<b>Cobalt(II) Schiff Base Complexes: Synthesis, Characterization, and Comprehensive Spectral Analysis</b> Bhagawat R. Gurme	133-137
23	<b>Advances in HPTLC-based Phytochemical Profiling: A critical review of Semecarpusanacardium marker compounds</b> Gurpreet Singh Bhullar, Dr. Ranjeet Kaur Bajwa, Dr. Prafullachandra Tekale, Gaganjyot Kaur	138-148
24	<b>Complexation of Samarium With Schiff Bases : Thermodynamic Study</b> Hansaraj Joshi, Rajpal Jadhav, Ramesh Ware, Shailendrasingh Thakur	149-155
25	<b>Graphene-TiO<sub>2</sub>-Polyaniline Nanocomposite: An Efficient and Sustainable Catalyst for Visible-Light-Driven Hydrogen Generation</b> Kalpana B. Gawande, Vivek R. Mate, Sanjay R. Thakare, Sandeep B. Gawande	156-164
26	<b>Study of Structural Characterization of Co<sub>3</sub>M<sub>2</sub>O<sub>4</sub>/Activated Carbon for Supercapacitor Application</b> Digambar M. Sapkal	165-169
27	<b>Novel Co(II), Ni(II) Schiff Base Metal Complexes Derived From 1- Hydroxy-2-acetonaphthone And Phenylethyl Amine: Synthesis, Spectral Characterization And Antimicrobial Evaluation</b> Dhananjay V. Bondar	170-181



28	<b>Exploring the Chemistry of 1, 3, 4-Thiadiazole Derivatives and Their Metal Complexes: A Concise Study</b>	182-199
	Rajpal Jadhav, Hansaraj Joshi, Vishal Naiknaware, Ramesh Ware	
29	<b>Magnetically Active Silica Sulfuric Acid: An Efficient, Heterogeneous and Reusable catalyst for Synthesis of Quinoxalines at Room-Temperature</b>	200-209
	Pankaj V. Patale, Jaishri L. Somawanshi, Sushil R. Mathapati	
30	<b>Machine Learning for Predictive Materials Discovery and Design</b>	210-213
	Rajeshwar G. Joshi	
31	<b>Study of Acoustic Parameters for Binary Liquid Mixture Using Ultrasonic Interferometer</b>	214-218
	Pallavi B. Nalle, S. U. Shinde, K. M. Jadhav	
32	<b>Study of Structural, Morphological and Magnetic Properties of Magnesium Doped Zinc Nanoferrites</b>	219-223
	Vyankati Jadhav, Ramesh Bhise, Manisha Dhiware	
33	<b>[Hmim]H<sub>2</sub>SO<sub>4</sub> Catalyzed an Eco-Friendly Synthesis of 3-Substituted Indole Derivatives Using Indole, Aryl Aldehydes, and Acetophenone</b>	224-227
	Ramdas N. Katapalle	
34	<b>Assessing the Impact of Seasonal Changes on Water Quality Index in Khudawadi Dam, Maharashtra : A Case Study Approach</b>	228-235
	D. N. Gatilewar, V. G. Mane, G. T. Rathod	
35	<b>Phytochemical Profiling of Leucas Aspera Using HPTLC Standardized Method</b>	236-246
	Vrushita Hegde, Dr. Manjiri Bhawe, Dr. Gaganjyot Kaur, Abhishek Suryawanshi, Dr. Prafullachandra Tekale, Chandrakant Khairnar	
36	<b>Advancing Green Chemistry: Novel Approaches to Peptide Cleavage from Resin Without Ethers as Solvent</b>	247-268
	Chandrakant Kulkarni, Yogeshwar Suryawanshi, Sujatha Parmeswaran	
37	<b>Photocatalysis in Environmental Chemistry : A Comprehensive Literature Review</b>	269-273
	Rajkumar G. Momle, Gopal K. Kakade	
38	<b>Synthesis of Quinoline-3-Carbonitrile Derivatives Via One Pot Ecofriendly Protocol</b>	274-278
	Kadam Shuddhodan Narhari, Rahul D. Kamble, Khatke Tukaram Eknathrao	
39	<b>Synthesis, Characterization and Biological Relevance of Cu(II) and Mn(II) Complexes of The NOON Donor Schiff Base Ligand</b>	279-286
	Bhagwat T. Vhanale, Dhananjay V. Bondar And Yogesh G. Mugale	
40	<b>PTC: An Efficient One Pot Multicomponent Synthesis of 2 Amino 4H Chromenes under Mild Reaction Conditions</b>	287-292
	Asghar Jafar Khan, A. R. Shaikh, Abdul Rahim Abdul Sami	
41	<b>Ultrasound Synthesis and Spectral Study of Transition Metal Complexes</b>	293-297
	D. D. Suryawanshi, A. D. Suryawanshi, V. S. Suryawanshi	
42	<b>Application of Computer Technology in Material Science and Data Processing</b>	298-301

	Dr. U. V. Thete	
43	<b>Room Temperature Alkaline Gas Detection Using NiFe<sub>2</sub>O<sub>4</sub>/rGO Nanocomposites as Electrodes</b> P. R. Birmule, V. D. Bhirde, R. K. Patil, R.B. Patil, V. B. Helavi-Reddy	302-314
44	<b>Synthesis and Biological Evaluation of 1H-Indole Condensed Thiazolidin-4-Ones As Mycobacterium Tuberculosis Protein Tyrosine Phosphatase B (Ptpb) Inhibitors</b> Pawan S Hardas, Babasaheb V Kendre, Rushikesh B Kendre, Mahadev G Landge	315-332
45	<b>Removal of Heavy Metal Ions from Wastewater Using Selected Bioadsorbents: A Focus on Chromium, Arsenic, and Lead</b> Shriram Pathak, Dr. Vishwas Mane	333-341
46	<b>Novel Derivatives of 1H-Imidazole -2-Carboxylic Acid Hydrazide: Synthesis and Antimicrobial Activity Screening</b> Satish V. Gaikwad, Kailash R. Borude	342-347
47	<b>Electron Spin Resonance Studies of Cu(II) Complex of Novel Schiff Base Prepared From 3-Formylchromone and 3-Aminoquinoline</b> Sushil K. Ghumbre	348-350
48	<b>Deciphering Atorvastatin Calcium Degradation Paradigms : A Review of HPTLC- Facilitated Analytical Methodologies</b> Ankita Singh, Dr. Ranjeet Kaur Bajwa, Dr. Prafullachandra Tekale, Dr. Gaganjyot Kaur	351-358
49	<b>Approaches to Quinoline Derivative Synthesis : A Comprehensive Review</b> A. S. Patki, P. R. Pande	359-364
50	<b>A Preliminary Checklist of Marine Algae found in Mumbai's selected Marine Regions</b> Priti Dhamal, Babita Rana	365-372
51	<b>Density, Viscosity and Ultrasound velocity measurement of bioactive Schiff base: N-((2-chloro-6-methylquinolin-3-yl)methylene)-4-(5-methyl-1H-tetrazol-1-yl)benzenamine in Chloroform and DMF solvents</b> S. A. Kamble, A. S. Kirdant, S. G. Vedpathak, S. H. Quadri	373-380
52	<b>Security Databases : A Comprehensive Overview</b> Mahendra D. Acharya	381-385
53	<b>One Pot Procedure for Green Synthesis of Benzylidenethiazolidine-2,4-Diones Using Catalytic Amount of Anhydrous Aluminium Chloride in Ethanol Solvent Via Knoevenagel Condensation Reaction</b> Sayas K Lad, Babasaheb V Kendre	386-391
54	<b><math>\beta</math>-Ammonium Metavanadate Catalyzed One-pot Synthesis of <math>\alpha</math>-Amidoalkyl <math>\beta</math>-Naphthols</b> Shaikh Alfiya Sadaf Atique, Pathan Rumina Munawar Khan, Shrikant S. Pandalwar, Sudhakar R. Bhusare	392-395

55	<b>[Hmim]HSO<sub>4</sub> Catalyzed an Eco-friendly Synthesis of 3-Substituted Indole Derivatives</b> Miss V. N. Aiwale, Jivan M. Kondre, Dr. Pradeep B. Lasonkar, Dr. Maruti V. Kanetkar, Tukaram E. Khatke, Dr. Suresh C. Jadhavar	396-399
56	<b>Synthesis of Spiro-fused Heterocycles under Aerobic Conditions by using Polymer Gel Entrapped Catalyst</b> Shital Shinde, Rajashri Salunkhe	400-405
57	<b>Isolation And Screening of Dye Degrading Actinomycetes from Textile Effluent Contaminated Soil</b> Mr. Warbhuvan P.G, Dr. Narsinge A. P, Mr. Kadam A. S, Mr. Karpude T. N	406-414

# Design, Synthesis, and Biological Evolution of New Chromen-2-one Derivatives as Antituberculosis Agents

Siddheshwar B. Lonari, Anil S. Kirdant\*, Suresh C. Jadhavar\*

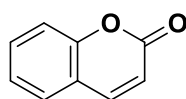
Department of Chemistry, Yogeshwari Mahavidyalay Ambajogai, Dist – Beed. Pin – 431517, Maharashtra, India

## ABSTRACT

The most commonly faced disease is tuberculosis. It is mainly caused by a bacterium called Mycobacterium tuberculosis and primarily affects the lungs. It is a preventable and curable disease. It may spread through the air when the affected person directly coughs, sneezes, or spit in public places. So many drugs and vaccines are available in the market for TB. We aim to synthesize the molecule which is more active toward antituberculosis. It would be better if they get good IC<sub>50</sub> than marketed available drugs. Sometimes, it would be beneficial if the drug dosage is decreased with more effectiveness. As a part of this, we synthesized the derivative of a naturally occurring coumarin, Umbelliferone (7-hydroxy coumarin), as an antituberculosis agent. For that, Synthesis of phenyl acetamide Derivatives (Compound 3a – 3e). These amides are then purified using silica gel column chromatography and dried using rotary evaporator, and then check the NMR for these amides. Once we get the pure form of the compound, then we go for coupling of Umbelliferone with these amides to get effective molecules that act as antituberculosis agents. After coupling, we have to test the biological activities of these molecules (Compound 4a-4e). If it shows better activity towards antituberculosis, we go for further in silico studies such as molecular docking, SAR, molecular simulation, ADMET, etc.

**Keywords:** - Tuberculosis, Anticancer, Antidiabetic activities, Invitro, Umbelliferone (7-Hydroxy coumarin), N- Phenyl Acetamide Derivatives.

## INTRODUCTION



**Coumarin(1)**

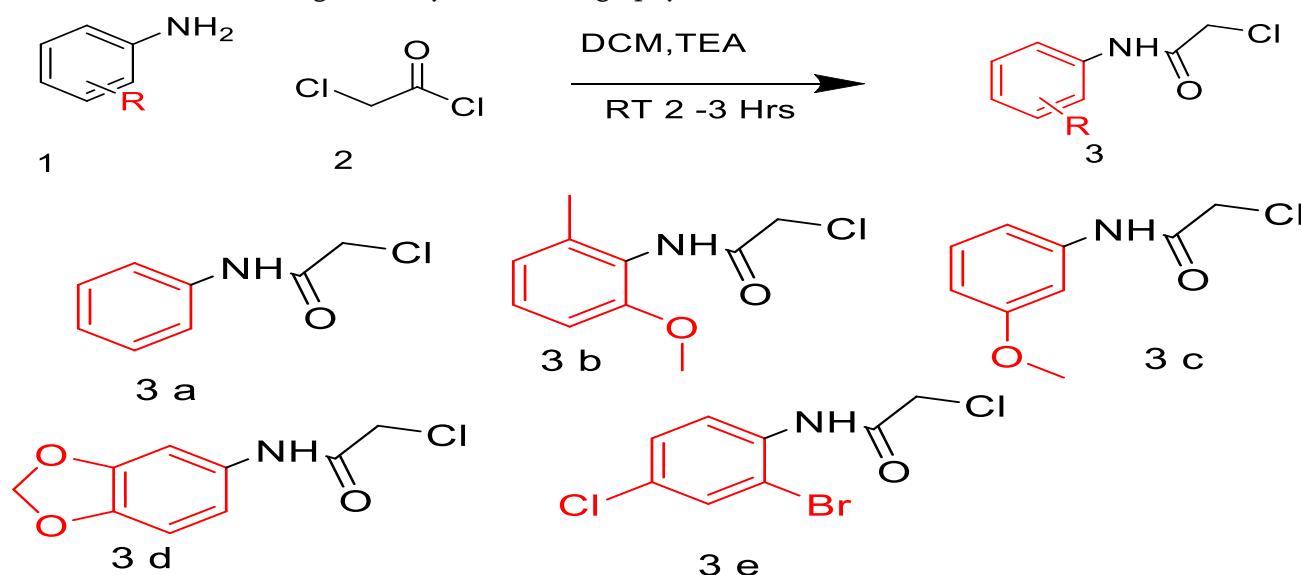
For the millennia, human civilizations have relied on nature and its products as medicine, with traditional healing practices across cultures drawing on the therapeutic properties of plants, animals, fungi, and microorganisms (Fokunang CN et.al,2011). The diverse array of natural products they produce contains biologically active compounds that have been harnessed for treating various ailments and enhancing overall health and wellness (Ekiz E et.al,2023). Plants have been a primary source of medicinal compounds. Plant species contain chemical compounds known as phytochemicals (Altemimi et.al, 2017). More than a thousand

phytochemicals have been identified to date, and they can be obtained from a variety of sources including whole grains, fruits, vegetables, nuts, and herbs. They are plant-derived chemical with bioactive properties for example quinones, flavonoids, polyphenols, tannins, terpenoids, alkaloids, polypeptides, steroids, saponins, coumarins. These phytochemicals display antibacterial, antidiarrheal, anthelmintic, antiallergic, antispasmodic, and antiviral properties as well as significant antioxidant activity( Kumar A et al,2023). Of these phytochemicals mentioned coumarin is widespread in nature and more than 1300 coumarins have been identified as secondary metabolites from plants, bacteria, and fungi (Tsivileva et.al,2022). Coumarin is a colorless, crystalline substance that tastes bitter and has a sweet, vanilla-like aroma. It is utilized as a flavoring agent in food products such baked goods, alcoholic beverages, and tobacco as well as in the fragrance industry (Lončar et.al, 2020). It has wide range of pharmacological properties such as anti-inflammatory, anticoagulant, antibacterial, antifungal, antiviral, anticancer, antihypertensive, antitubercular, anticonvulsant, antiadipogenic, antihyperglycemic, antioxidant, and neuroprotective properties (Venugopala et.al,2013). 'Coumarin', the name is derived from the plant Coumarouna odorata and was isolated by Vogal in 1820 (Lončar et.al, 2020). Coumarins belong to the benzopyrone family commonly found in many medicinal plants.

## EXPERIMENTAL ANALYSIS

### Synthesis of N-PhenylAcetamide Derivatives.

**General Reaction:-** Respective Diff Aniline/pyridine is taken as starting material , the reagent used is chloroacetyl chloride, Triethyl amine and the solvent used is Dichloromethane(DCM).The progress of the reaction is checked through thin layer chromatography



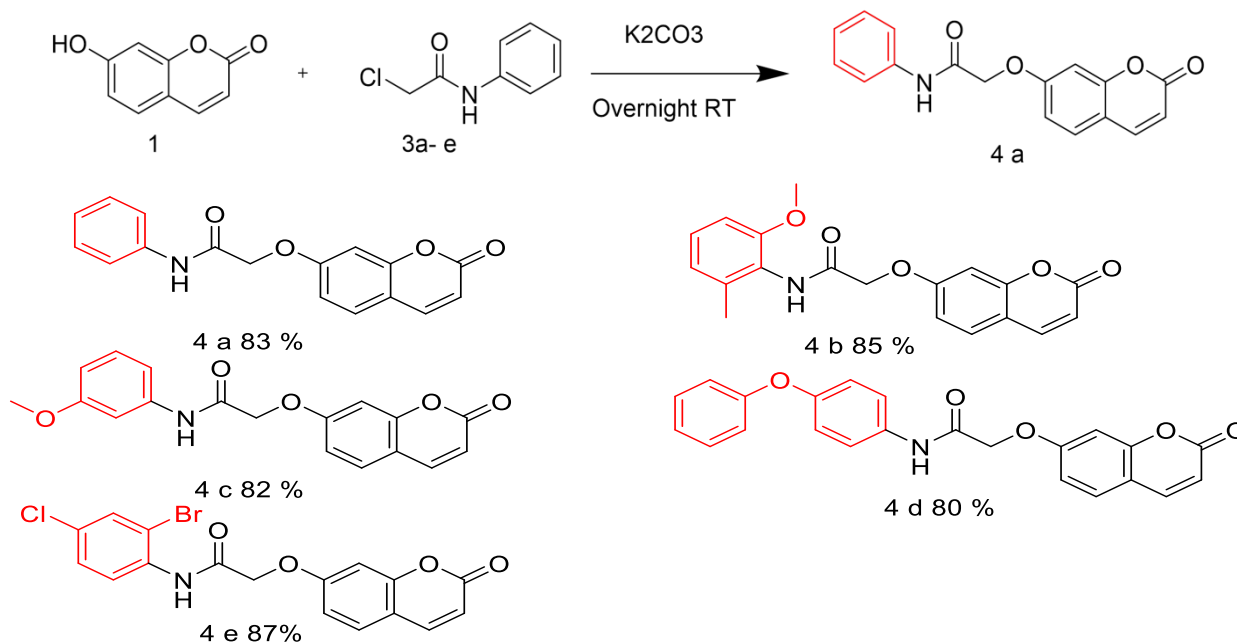
Scheme 1:- Synthesis of N-PhenylAcetamide Derivatives.

### Scheme 2.

Coupling Reaction of 7-hydroxy -2H-chromen-2-one Molecule N-Phenylacetamide.

**General Procedure :-**

1 equivalent 7-hydroxycoumarin is taken as starting material. Add 1.3 equivalent of phenyl acetamides and 2 equivalent of potassium carbonate as base and add DMF as solvent under room temperature overnight. After the reaction is completed, wash the reaction mixture with crushed ice and ethyl acetate. The upper layer is collected and dried the excess solvent using rotary evaporator



**Scheme 2- 7-hydroxy -2H-chromen-2-one molecule N-Phenylacetamide**

**MOLECULAR DOCKING AND PHARMOKINETIC STUDIES**

Molecular docking analysis of compounds with TB receptor protein Mycobacterium tuberculosis DNA gyrase (PDB ID: 3IG0) Docking is a good approach to performing in silico screening of a large compound library and hypothesizing how the ligands inhibit the target receptors structurally. This method is invaluable for lead optimization. The molecular docking studies of the synthesized molecules were carried out to evaluate their binding pattern against Mycobacterium tuberculosis DNA gyrase (Fig 1-4). The compounds synthesized in the present study shows good binding affinities ranging from -6 to -7 kcal/mol. The binding affinities of the synthesized compounds along with their hydrogen bonding and amino acid interactions against targeted protein were summarized in Table 1. The Ribbon model shows the binding pocket structure of Mycobacterium tuberculosis DNA gyrase with synthesized compounds. Hydrogen bonds between compounds and amino acids are shown as green dashed lines, hydrophobic interaction are shown as pink lines.

COMPOUND	3-D INTERACTION WITH RECEPTOR	2-D INTERACTION
----------	-------------------------------	-----------------

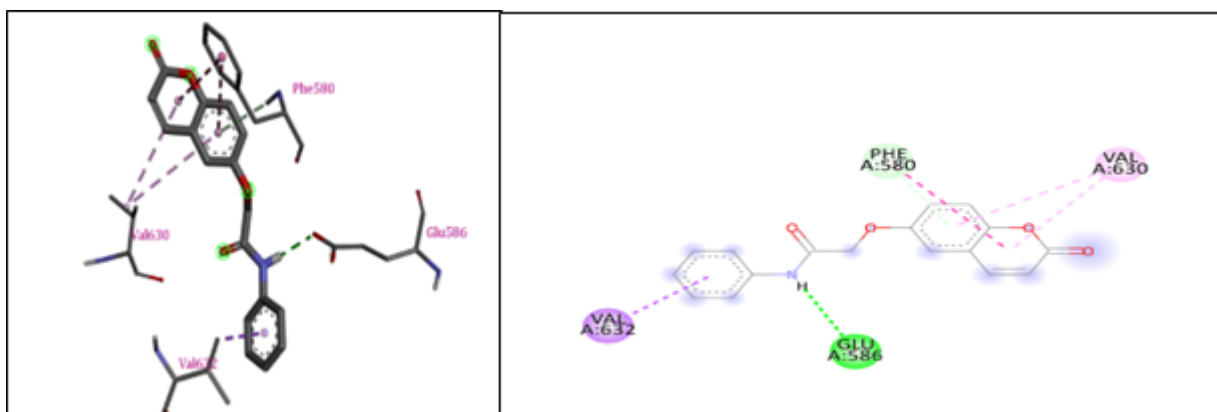


Fig.1: Interaction of compound 4-A with Mycobacterium tuberculosis DNA gyrase

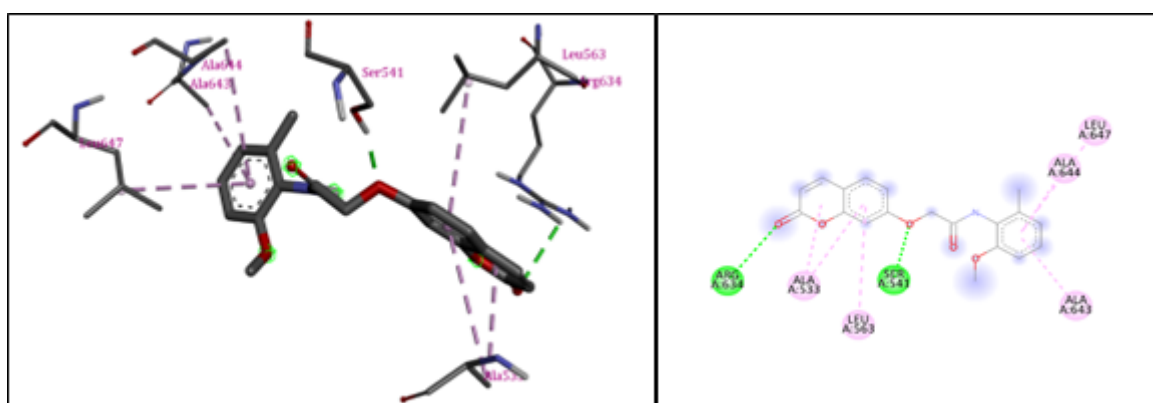


Fig.2: Interaction of compound 4-B with Mycobacterium tuberculosis DNA gyrase

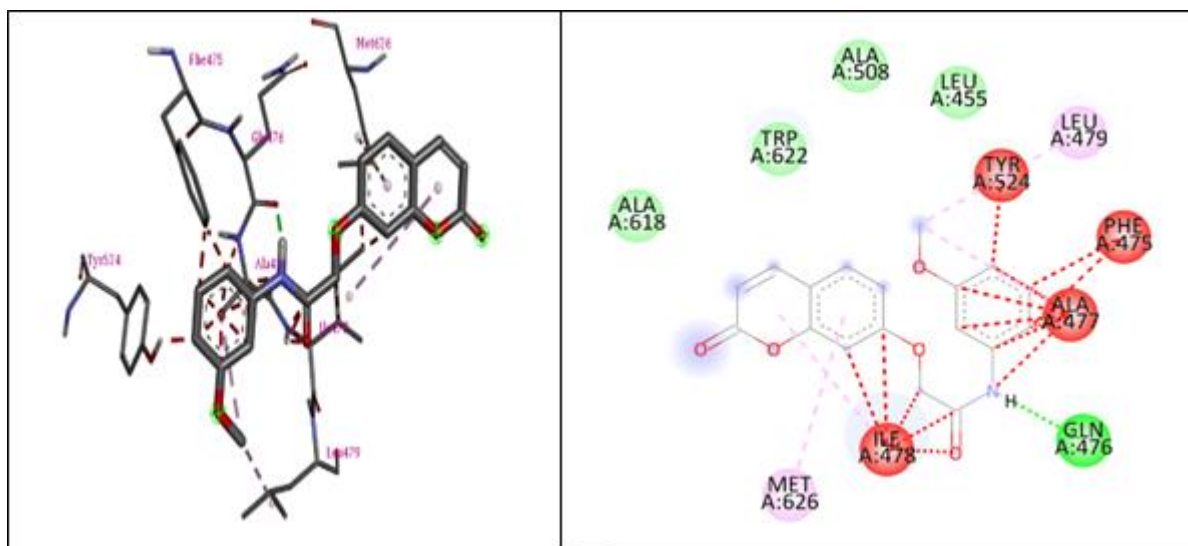


Fig.3: Interaction of compound 4-C with Mycobacterium tuberculosis DNA gyrase

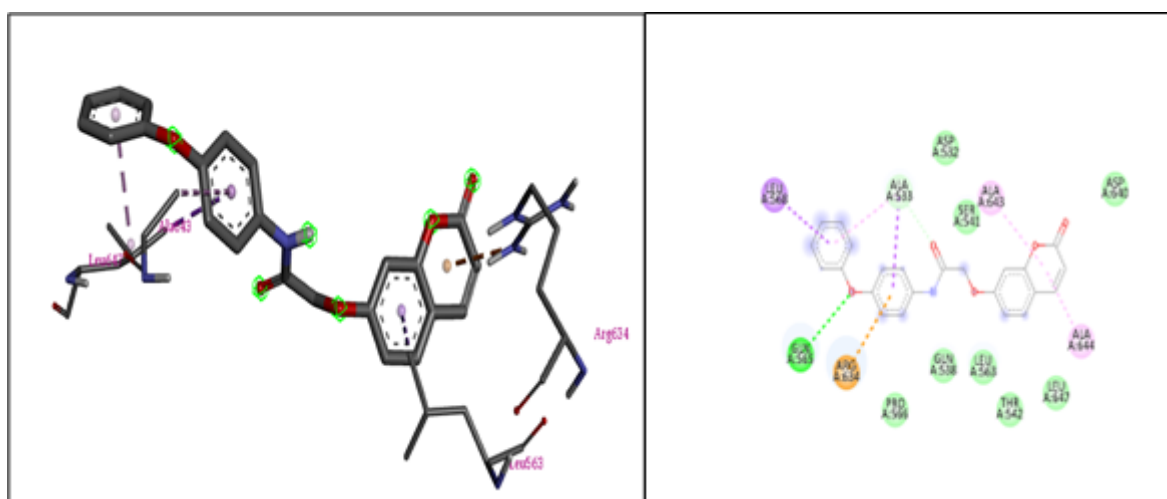


Fig.4: Interaction of compound 4-D with Mycobacterium tuberculosis DNA gyrase

Table 1. Molecular docking analysis of synthesized molecule with Mycobacterium tuberculosis DNA gyrase

Compounds	Affinity (kcal/mol)	H-bonds	Amino acid interactions	
			Hydrophobic/Pi-citation/Pi-anion/Pi-alkyl interactions	Van der Waals interactions
4-a	-6.8	Glu-586	Val-632, Phe-580, Val-630	-----
4-b	-6.4	Ser-541, Arg-634	Ala-533, Leu-563, Ala-643, Ala-644, Leu-647	-----
4-c	-6.7	Gln-476	Tyr-524, Leu-479, Phe-475, Ala-477, Ile-478, Met-626	Ala-618, Trp-622, Ala-508, Leu-455
4-d	-6.8	Gln-565	Leu-568, Ala-533, Ala-643, Ala-644, Arg-634	Asp-532, Ser-541, Asp-640, Leu-647, Thr-542, Leu-563, Gln-538, Pro-566

## PHARMACOKINETIC STUDY

### ADMET

The pharmacokinetic properties of compounds can be analyzed using computer assisted in silico screenings methods. In the course of this work, the compounds synthesized were analyzed for their drug likeness properties using Swiss ADME predictions. SWISSADME predictions show that all synthesized molecules obey Lipinski's rule of five with 0 violation (Table 2). The results were analyzed using Lipinski's rule of five. Lipinski defines these compounds as drug like; having sufficiently acceptable ADMET properties. Toxicity of the molecules were analyzed and predicted (Table 3). The brain or intestine estimated permeation graph prediction model (BOILED-Egg) shows that the relation between the prediction of gastrointestinal (GI) absorption and Blood-brain barrier (BBB) penetration (Fig 1-5).



**Table 2: Drug-likeness predictions of compounds by SwissADME**

Molecule	Formula	Mol.wt (g/mol)	NRB	NHA	NHD	TPSA (A <sup>2</sup> )	LogP (cLogP)	Lipinski's rule of five violation
4-a	C17H13NO4	295.29	5	4	1	68.54	2.45	0
4-b	C19H17NO5	339.34	6	5	1	77.77	2.82	0
4-c	C18H15NO5	325.32	6	5	1	77.77	2.48	0
4-d	C23H17NO5	387.38	7	5	1	77.77	3.71	0
4-e	C17H11BrClNO4	408.63	5	4	1	68.54	3.71	0

**Table 3: Pharmacokinetic properties and toxicity prediction of compounds.**

Molecule	Formula	Skin permeation value (log <sub>kp</sub> ) cm/s	GI absorption	BBB permeability	Inhibitor interaction (SwissADME/ PreADMET)					
					P-gp substrate	CYP1A2	CYP2C19	CYP2C9	CYP2D6	CYP3A4
4-a	C17H13NO4	-6.13	High	Yes	No	Yes	Yes	Yes	Yes	No
4-b	C19H17NO5	-6.15	High	Yes	No	Yes	Yes	Yes	Yes	Yes
4-c	C18H15NO5	-6.43	High	Yes	No	Yes	Yes	Yes	Yes	Yes
4-d	C23H17NO5	-5.70	High	No	No	Yes	Yes	Yes	Yes	Yes
4-e	C17H11BrClNO4	-5.88	High	Yes	No	Yes	Yes	Yes	No	Yes

## RESULTS AND CONCLUSION

- The main molecule used for the reaction is umbelliferone(7-hydroxycoumarin), which are chromen-2-one derivatives .
- Different derivatives of N- Phenyl Acetamide were synthesized Compound (3a – 3e)
- These amides were coupled with chromen-2-one derivate molecule.
- Biological activity tests of coupled molecules should be conducted.( 4a-4e)
- The more active molecules should be taken for the further studies such as insilico, etc.

### Author Contribution

**Siddheshwar B. Lonari:** Conceptualization, Experiment, Analysis, Manuscript draft preparation, editing.

**Anil S. Kirdant:** Conceptualization and Guidance.

**Suresh C. Jadhavar:** Conceptualization, formal editing, and guidance.

#### **Acknowledgement:**

Student Funding Agencies :- (MJPRF 2022, Nagpur)

Siddheshwar B. Lonari Thanks to Mahatma Jyotiba Phule Research Fellowship Mahajyoti Nagpur (MJPRF 2022)

## **EXPERIMENTAL DATA**

### **<sup>1</sup>H and <sup>13</sup>C NMR**

#### **EXPERIMENTAL ANALYSIS (<sup>1</sup>H NMR, <sup>13</sup>C NMR, HPLC)**

##### **2-((2-oxo-2H-chromen-7-yl)oxy)-N-phenylacetamide (4a):**

HPLC: 98. <sup>1</sup>H NMR (400 MHz, DMSO)  $\delta$  10.17 (s, 1H), 7.98 (d, J = 9.5 Hz, 1H), 7.68 – 7.60 (m, 3H), 7.37 – 7.28 (m, 2H), 7.12, – 7.00 (m, 3H), 6.31 (d, J = 9.5 Hz, 1H), 4.86 (s, 2H).

**N-(2-methoxy-6-methylphenyl)-2-((2-oxo-2H-chromen-7-yl)oxy)acetamide(4b):** HPLC:98%. <sup>1</sup>H NMR (400 MHz, DMSO)  $\delta$  9.45 (s, 1H), 8.02 (d, J = 9.5 Hz, 1H), 7.70 – 7.65 (m, 1H), 7.17 (t, J = 7.9 Hz, 1H), 7.06 (dd, J = 6.5, 2.5 Hz, 2H), 6.92 – 6.87 (m, 1H), 6.83 (d, J = 7.6 Hz, 1H), 6.33 (d, J = 9.5 Hz, 1H), 4.85 (s, 2H), 3.76 (s, 3H), 2.12 (s, 3H). <sup>13</sup>C NMR (100 MHz, DMSO)  $\delta$  166.45, 161.38, 160.71, 155.63, 155.37, 144.77, 137.15, 129.91, 127.93, 124.43, 122.39, 113.52, 113.32, 113.28, 109.57, 102.15, 67.64, 55.96, 18.28.

**N-(3-methoxyphenyl)-2-((2-oxo-2H-chromen-7-yl)oxy)acetamide (4c):** HPLC: 97%. <sup>1</sup>H NMR (400 MHz, DMSO)  $\delta$  10.15 (s, 1H), 8.01 (d, J = 9.5 Hz, 1H), 7.69 – 7.65 (m, 1H), 7.32 (t, J = 2.2 Hz, 1H), 7.26 – 7.16 (m, 2H), 7.06 – 7.02 (m, 2H), 6.69 – 6.66 (m, 1H), 6.32 (d, J = 9.5 Hz, 1H), 4.84 (s, 2H), 3.73 (s, 3H). <sup>13</sup>C NMR (101 MHz, DMSO)  $\delta$  166.33, 161.40, 160.67, 159.98, 155.64, 144.73, 139.95, 130.07, 130.02, 113.35, 113.32, 113.20, 112.32, 109.68, 105.86, 102.09, 67.73, 55.47.

**2-((2-oxo-2H-chromen-7-yl)oxy)-N-(4-phenoxyphenyl)acetamide (4d):** HPLC: 98%. <sup>1</sup>H NMR (400 MHz, DMSO)  $\delta$  10.20 (s, 1H), 8.01 (d, J = 9.5 Hz, 1H), 7.67 (dd, J = 10.7, 8.3 Hz, 3H), 7.41 – 7.34 (m, 2H), 7.14 – 6.94 (m, 8H), 6.32 (d, J = 9.5 Hz, 1H), 4.85 (s, 2H). <sup>13</sup>C NMR (101 MHz, DMSO)  $\delta$  166.13, 161.39, 160.67, 157.70, 155.64, 152.67, 144.73, 134.60, 130.46(2C), 130.02, 123.55, 121.93(2C), 119.88(2C), 118.44(2C), 113.35(2C), 113.22, 102.11, 67.77.

**N-(2-bromo-4-chlorophenyl)-2-((2-oxo-2H-chromen-7-yl)oxy)acetamide (4e):** HPLC: 84%. <sup>1</sup>H NMR (400 MHz, DMSO)  $\delta$  9.77 (s, 1H), 8.02 (d, J = 9.5 Hz, 1H), 7.85 (d, J = 2.4 Hz, 1H), 7.78 (d, J = 8.7 Hz, 1H), 7.69 (d, J = 8.7 Hz, 1H), 7.50 (dd, J = 8.7, 2.4 Hz, 1H), 7.08 (d, J = 7.4 Hz, 2H), 6.34 (d, J = 9.5 Hz, 1H), 4.92 (s, 2H).

## **REFERENCES**

- [1] Beloor Suresh, A., Rosani, A., Wadhwa, R., 2023. Rifampin, in: StatPearls. StatPearls Publishing, Treasure Island (FL).
- [2] Jilani, T.N., Avula, A., Zafar Gondal, A., Siddiqui, A.H., 2023. Active Tuberculosis, in: StatPearls. StatPearls Publishing, Treasure Island (FL).
- [3] Kiazzyk, S., Ball, T., 2017. Latent tuberculosis infection: An overview. *Can Commun Dis Rep* 43, 62–66.
- [4] Kumari, S., Carmona, A.V., Tiwari, A.K., Trippier, P.C., 2020. Amide Bond Bioisosteres: Strategies, Synthesis, and Successes. *J. Med. Chem.* 63, 12290–12358. <https://doi.org/10.1021/acs.jmedchem.0c00530>
- [5] Kumari, S., Sharma, A., Yadav, S., 2023. Pharmacological Potential of CoumarinBased Derivatives: (A Comprehensive Brief Review). *Orient. J. Chem* 39, 568–576. <https://doi.org/10.13005/ojc/390304>
- [6] LUCA, S., MIHAESCU, T., 2013. History of BCG Vaccine. *Maedica (Bucur)* 8, 53–58.
- [7] Mazimba, O., 2017. Umbelliferone: Sources, chemistry and bioactivities review. *Bulletin of Faculty of Pharmacy, Cairo University* 55, 223–232. <https://doi.org/10.1016/j.bfopcu.2017.05.001>
- [8] Musa, M.A., Cooperwood, J.S., Khan, M.O.F., 2008. A Review of Coumarin Derivatives in Pharmacotherapy of Breast Cancer. *Curr Med Chem* 15, 2664–2679.
- [9] Sharifi-Rad, J., Cruz-Martins, N., López-Jornet, P., Lopez, E.P.-F., Harun, N., Yeskaliyeva, B., Beyatli, A., Sytar, O., Shaheen, S., Sharopov, F., Taheri, Y., Docea, A.O., Calina, D., Cho, W.C., 2021. Natural Coumarins: Exploring the Pharmacological Complexity and Underlying Molecular Mechanisms. *Oxid Med Cell Longev* 2021, 6492346. <https://doi.org/10.1155/2021/6492346>
- [10] <https://www.nationaljewish.org/conditions/tuberculosis-tb/types>
- [11] Mary Liang, Tyler B. Tarr,§ Karla Bravo-Altamirano, Guillermo Valdomir, Gabriel Rensch, Lauren Swanson, Nicholas R. DeStefino, Cara M. Mazzarisi, Rachel A. Olszewski, Gabriela Mustata Wilson, Stephen D. Meriney, and Peter Wipf, 2023, Synthesis and Biological Evaluation of a Selective N- and P/Q-Type Calcium Channel Agonist 49
- [12] Sandip B. Bharate, Vikas Kumar, Shreyans K. Jain, Mubashir J. Mintoo, Santosh K. Guru, Vijay K. Nuthakki, Mohit Sharma, Sonali S. Bharate, Sumit G. Gandhi, Dilip M. Mondhe, Shashi Bhushan, and Ram A. Vishwakarma, 2023., Discovery and Preclinical Development of IIIM-290, an Orally Active Potent Cyclin-Dependent Kinase Inhibitor
- [13] <https://en.wikipedia.org/wiki/Isoniazid>
- [14] Kapil M. Agrawal & Gokul S. Talele , 2012., Synthesis and antibacterial, antimycobacterial and docking studies of novel N-piperazinyl fluoroquinolones
- [15] Xiaodong Yao , Hongmei Hu, Shibin Wang , Wenhao Zhao, Mingxia Song, and Qiugui Zhou, 2020., Synthesis, Antimicrobial Activity, and Molecular Docking Studies of Aminoguanidine Derivatives Containing an Acylhydrazone Moiety
- [16] Bin Jia , Yang-min Ma, Bin Liu, Pu Chen , Yan Hu and Rui Zhang, 2019., Synthesis, Antimicrobial Activity, Structure-Activity Relationship, and Molecular Docking Studies of Indole Diketopiperazine Alkaloids
- [17] Sujit Kumar Mohanty, Dr. Anindya Bose , Pabbala Veeresh , Uppari Ramanjaneyulu , M. Venu Gopal, P. Bhargavi, Y. Harshitha and V. Sirisha, 2016., Design, Synthesis, Molecular Docking of Novel 4-methyl quinolone derivatives; Evaluation of antimicrobial, anti-tubercular activities.

- [18] Lourenço AM, Ferreira LM, Branco PS. Molecules of natural origin, semi-synthesis and synthesis with anti-inflammatory and anticancer utilities. *Curr Pharm Des.* 2012;18 (26):3979-4046. doi: 10.2174/138161212802083644. PMID: 22632756
- [19] R. D. H. Murray, J. Mendez and S. A. Brown, *the Natural Coumarins: Occurance, Chemistry and Biochemistry*, Wiley & Sons, New York, 1982.
- [20] Xiaodong Yao , Hongmei Hu, Shibin Wang , Wenhao Zhao, Mingxia Song, and Qiugui Zhou, 2020., *Synthesis, Antimicrobial Activity, and Molecular Docking Studies of Aminoguanidine Derivatives Containing an Acylhydrazone Moiety*
- [21] Sujit Kumar Mohanty, Dr. Anindya Bose , Pabbala Veeresh , Uppari Ramanjaneyulu , M. Venu Gopal, P. Bhargavi , Y. Harshitha and V. Sirisha, 2016., *Design, Synthesis, Molecular Docking of Novel 4-methyl quinolone derivatives; Evaluation of antimicrobial, anti-tubercular activities*

# Microwave Dielectric Study of Micronutrients of Soil at X Band

Dr. Manisha D. Dhiware

Department of Physics, K. V. N. Naik Arts, Commerce & Science College, Nashik, 422002, Maharashtra, India  
manishasalunke73@gmail.com

## ABSTRACT

The naturally available macronutrients of soil show variation in dielectric properties. Inorganic matter in soil appreciably affects its dielectric properties. In this work we have concluded that the dielectric constant of soils depends on many factors like frequency, moisture, and its physical and chemical compositions. In the interpretation of various remote sensing data, the dielectric constant and dielectric loss of soil samples measured at X band microwave frequency plays important role. By knowing the correlation coefficient of various soil properties and nutrients with dielectric constant, it is easy to understand and analyze the satellite data. Results will be helpful for the prediction of soil texture, nutrients type and their concentrations present in the soil.

**Keywords:** microwave, soil, moisture content, dielectric, soil texture.

## INTRODUCTION

Soil plays a very crucial role in supporting ecosystems and human civilization. Besides being a non-renewable and valuable resource, it has high variability in its properties and behavior all over the World. Non-judicious exploitation of resources by mankind has not only resulted in the depletion of finite land resources but also deteriorated their performance. All the production systems have their base in soil, so it is very much important for us to know its properties, extent and spatial distribution. Sustenance of the ecosystem depends on soil [1]. Thus, characterization and mapping of soils and their interpretation is of great significance. For this, one has to evaluate the quantity as well as quality of resources based on accurate baseline information and methods [2]. Soil survey helps to prepare inventory of different kinds of soils and extent of distribution for the prediction of their characteristics and potentialities [3]. Such knowledge is required for making better utilization of soils in a sustainable way. Traditional soil survey techniques are time consuming, labor intensive and costly. Recent advancements in computer and information technology have brought new techniques of soil resource mapping. RS, GIS and GPS are such techniques for analyzing the different features of soils over space and time [4]. These geospatial tools are very valuable for preparation of soil resource inventory at local to global scales. RS provides spatially explicit, digital data representing the surface features of earth that can be pooled with digitized maps in GIS for efficient characterization and analysis of vast amounts of data. In natural resource management, satellite RS along with GIS can be very much useful. According to Karla et al. (2010)[5], RS integrated with GIS database can enhance data collection

and interpretation for soil survey in much less time and with lesser expenses as compared to conventional methods. The high precision and synoptic coverage of RS data and GIS analysis protocols have made soil mapping a very effective tool in managing the soil resource and environment [6]. The soil is a life supporting system upon which human beings have been dependent from the dawn of civilization. Therefore, comprehensive information on soil resources, its potential / limitations / capabilities, is required for a variety of purposes such as command area development, soil conservation in catchment areas, sustainable agriculture, watershed management, reclamation of degraded lands etc. In this context, characterization and mapping of different types of soils, developing rational / scientific criteria for land evaluation and interpretation of soils for multifarious land uses attains greater importance. In this paper an attempt has been made to review as well as analyze the microwave remote sensing behavior of soil in India Soil and dielectric constant Knowledge of dielectric constant of soil at microwave frequencies is valuable in microwave remote sensing. It determines the response of the soil to an incident electromagnetic wave. This response is composed of two parts, which determine the wave velocity and energy losses respectively. In a non-homogeneous medium such as soil the dielectric properties have a strong impact and its microwave emission. However, the relationship between soil dielectric constant and the soil physical properties is not straightforward. Soil plays a key role in various hydrological and meteorological applications. In microwave remote sensing, for the study of soil, the dielectric constant is the most important parameter. In active microwave remote sensing the sensors measure the back scatter coefficient of the soil and in passive microwave remote sensing the sensors are sensitive to the emissivity parameter of the soil. The backscatter coefficient and emissivity depend on the dielectric constant of the soil. The moisture content in the soil has an effect on the dielectric constant of the soil. The value of dielectric constant depends upon the percentage of moisture content in the soil. Soils are composed of solids, liquids and gases mixed together in variable proportions. Study of physical properties, chemical properties, dielectric properties of soil with varied organic and inorganic matter is useful in agriculture to predict quality and fertility of soil. Also it is useful for the researchers working in the field of microwave remote sensing. When microwaves are directed towards a material, energy gets reflected or transmitted through the surface or absorbed by it. The proportions of energy, which fall into these three categories, have been defined in terms of material proportions. Permittivity and permeability are the key parameters describing the interactions of materials with electromagnetic fields (1973). Really soil texture has a remarkable effect in the dielectric properties. Soil characterization of a region is an important aspect in relation to sustainable agricultural productions.

## EXPERIMENTAL METHOD

### A. Soil Sampling

**The soil samples collected during the fieldwork are processed after air drying of the soils. They are pounded and grinded so that the soil sample passes through a 2 mm sieve. These soil samples are analyzed for various physical and chemical properties like pH, EC, texture, organic carbon, and exchangeable cations, CEC etc. that aid in the taxonomic classification of soils and also to identify any salinity or alkalinity like problems.**

## B. Measurement of Dielectric Constant of dry Soil Samples

The waveguide cell method is used to determine the dielectric properties of the dry soil samples. An X-band microwave set-up in the TE<sub>10</sub> mode with Gunn source operating at frequency 9.85 GHz, is used for this purpose. The solid dielectric cell with soil sample is connected to the opposite end of the source. The signal generated from the microwave source is allowed to incident on the soil sample. The sample reflects part of the incident signal from its front surface. The reflected wave combined with incident wave standing wave pattern. These standing wave patterns are then used in determining the values of shift in minima results due to before and after inserting the sample.

Experiments were performed at room temperatures.

## RESULT AND DISCUSSION

### Relationship of electrical conductivity and dielectric constant with status of Macronutrients in the soil:

Our result shows strong positive correlations of electrical conductivity of soil samples with available macronutrients such as nitrogen ( $R^2 = 0.953$ ), phosphorus ( $R^2=0.835$ ), potassium ( $R^2=0.545$ ) content. Fig. 1 shows variation of electrical conductivity with macronutrient N of soil samples. Fig. 2 shows variation of electrical conductivity with macronutrient P of soil samples and Fig. 3 shows variation of electrical conductivity with macronutrient K of soil samples.

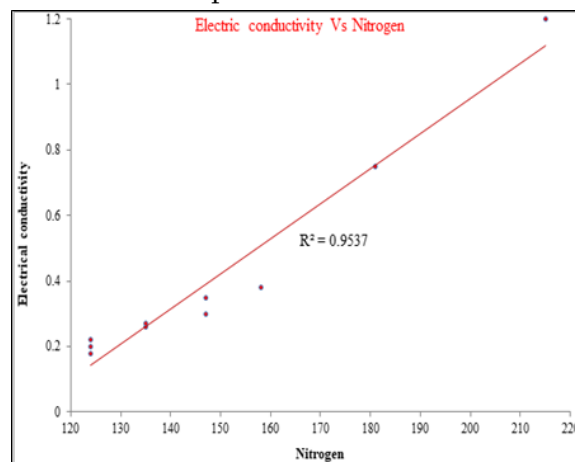
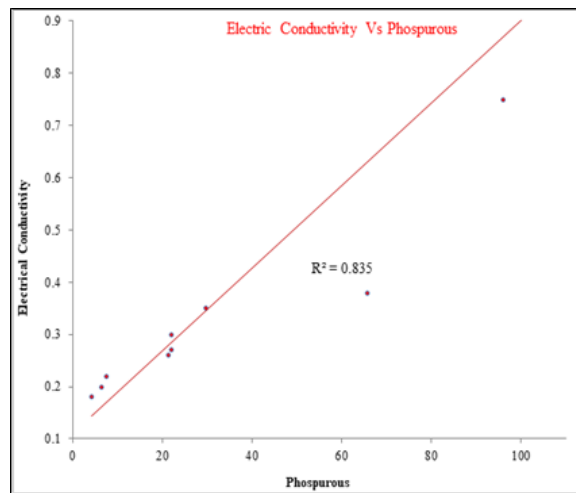
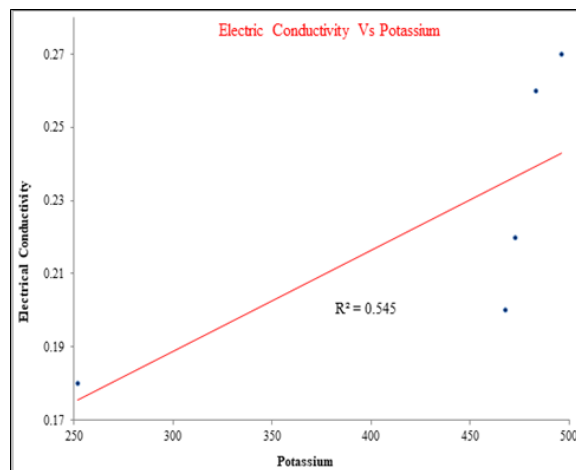


Fig .1 Variation of Electrical Conductivity with macronutrient N of soil samples



**Fig .2 Variation of Electrical Conductivity with macronutrients P of soil samples**



**Fig 3: Variation of Electrical Conductivity with macronutrients K of soil samples**

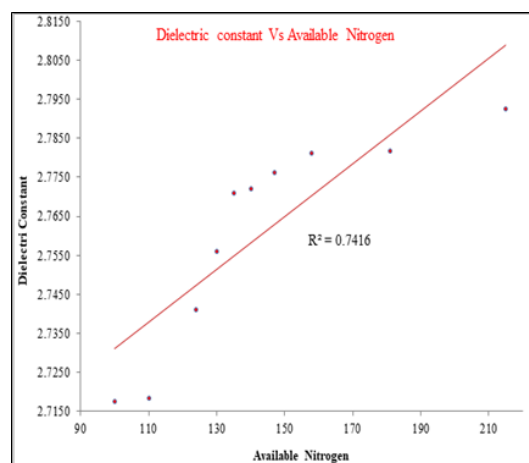


**Fig 4 Variation of Dielectric constant with macronutrients N of soil samples**



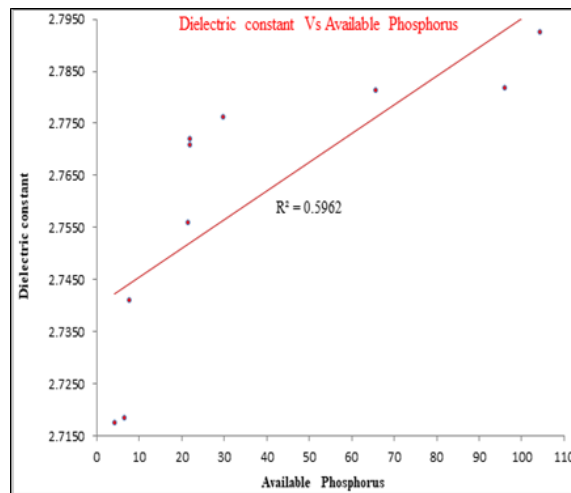


**Fig 5 Variation of Dielectric constant with macronutrients P of soil samples**

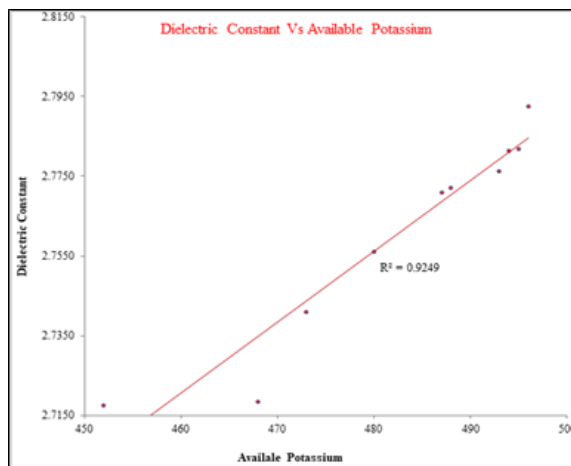


**Fig .6 Variation of Dielectric constant with macronutrients K of soil samples**

Also our results from fig (4, 5 and 6) shows strong positive correlations of dielectric constant of soil samples with available macronutrients such as nitrogen ( $R^2=0.741$ ), phosphorus ( $R^2=0.5962$ ), potassium ( $R^2=0.9249$ ) content.

## CONCLUSIONS

From the above results and discussion we have concluded that the dielectric constant of soils depends on many factors like frequency, moisture, and its physical and chemical compositions. In the interpretation of various remote sensing data, the dielectric constant and dielectric loss of soil samples measured at X band microwave frequency plays an important role. . By knowing the correlation coefficient of various soil properties and nutrients with dielectric constant, it is easy to understand and analyze the satellite data. Results will be helpful for the prediction of soil texture, nutrients type and their concentrations present in the soil.

## REFERENCES

- [1] Gessler, P. E. (1996). Statistical soil–landscape modelling for environmental management. Doctoral Dissertation, The Australian National University, Canberra, Australia.
- [2] Laake, P. E. (2000), Spatial tools for Laymen, Natural Resource Management by experts. *International Archives of Photogrammetry and Remote Sensing* 33, 1593-1600.
- [3] Mandal, A.K. and R.C. Sharma, (2005), Computerization database on salt affected soils of Haryana state. *Journal of the Indian Society of Remote Sensing* 33, 447-455.
- [4] Yeung, A.K.W. and C.P. Lo, (2002), Concepts and Techniques of Geographic Information Systems. *International Journal of Geographical Information Science* 17, 819-820.
- [5] Kalra, N.K., L. Singh, R. Kachhwah, and D.C. Joshi, (2010), remote sensing and GIS in identification of soil constraints for sustainable development in Bhilwara district, Rajasthan. *Journal of the Indian Society of Remote Sensing* 38, 279-29
- [6] Srinivasan, P. (1988), Use of RS techniques for detail hydro morphological investigation in part of Narmadasagar command area. M.P. *Journal of the Indian Society of Remote Sensing* 16, 55-62
- [7] Ali, R.R. (2008), Digital Soil Mapping for Optimum Land Uses in some Newly Reclaimed Areas West of the Nile Delta, Egypt. *Australian Journal of Basic and Applied Sciences* 2, 165-173.
- [8] Aly, Z., F. J. Bonn, and R. Magagi (2007), Analysis of the Backscattering Coefficient of Salt-Affected Soils Using Modeling and RADARSAT-1 SAR Data. *Geoscience and Remote Sensing, IEEE Transactions on* 45, 332-341.
- [9] Anderson, K. and H. Croft, (2009), Remote sensing of soil surface properties. *Progress in Physical Geography* 33, 16.
- [10] Apan, A., R. Kelly, T. Jensen, D. Butler, W. Strong, and B. Basnet (2002), Spectral discrimination and separability analysis of agricultural crops and soil attributes using ASTER imagery., in 11th ARSPC, edited, Brisbane, Australia.
- [11] Asadi, S.S., B.V.T. Vasantha Rao, and S. Sekar, (2012), Creation of physical characteristics information for Natural Resources Management Using Remote sensing and GIS: A Model study. *International Journal of Modern Engineering Research* 2, 226-232.
- [12] Baldridge, A.M., S.J. Hook, C. I. Grove, and G. Rivera (2008), The ASTER Spectral Library Version 2.0 Rep., 1-18 pp, Jet Propulsion Laboratory.
- [13] Barnes, G.B., D. Chaplin, D. Moyer, E. Des Roche, M. Eckl, and M. Santori, (1998), GPS methodology for cadastral surveying and mapping in Albania, working paper no.17, Albania Series, Land Tenure Centre, University of Wisconsin- Madison.
- [14] Bastiaanssen, W. G. M., E.J.M. Noordman, H. Pelgrum, G. Davids, B. P. Thoreson, and R. G. Allen (2005), SEBAL Model with Remotely Sensed Data to Improve WaterResources Management under Actual Field Conditions. *Journal of Irrigation and Drainage Engineering* 131, 85-93.
- [15] Bedini, E., F. van der Meer, and F. van Ruitenbeek (2009), Use of HyMap imaging spectrometer data to map mineralogy in the Rodalquilar caldera, southeast Spain. *International Journal of Remote Sensing* 30, 327-348.

# A Review Article on Microwave-Assisted Multicomponent Reactions in Heterocyclic Chemistry

Nilesh P. Tale \*

Department of Chemistry, Late B. S. Arts, Prof. N.G. Science and A. G. Commerce college Sakharkherda Tq. Sindkhed Raja Dist. Buldhana, Maharashtra, India

\*E-mail: [nileshtale23@gmail.com](mailto:nileshtale23@gmail.com)

## ABSTRACT

Microwave-assisted multicomponent reactions (MCRs) have gained prominence in heterocyclic chemistry, offering an efficient approach to synthesize complex heterocyclic compounds. This review highlights the advantages of microwave irradiation in accelerating reaction rates, improving yields, and promoting green chemistry practices. We discuss key MCR methodologies, their applications in synthesizing heterocycles, and future directions in this rapidly evolving field.

**Keywords:** Microwave irradiation, Multicomponent reactions (MCRs), Reaction acceleration.

## INTRODUCTION

Heterocycles are fundamental structures in numerous pharmaceuticals, agrochemicals, and materials. Traditional synthetic routes to heterocycles often involve multiple steps, leading to increased time and resource consumption. MCRs streamline this process by combining three or more reactants in a single step, facilitating the rapid generation of diverse heterocyclic frameworks. Microwave-assisted MCRs have emerged as a powerful tool for the synthesis of heterocycles, offering several advantages over traditional synthetic methods and has been applied to the synthesis of a wide variety of complex compounds.<sup>1,2</sup> Reviews (REFS) on microwave-assisted synthesis of heterocycles show case the advancements in the total synthesis of such compounds, emphasizing the role of microwave irradiation in the efficient construction of complex heterocyclic frameworks. Furthermore, the synthesis of medium-sized heterocycles has been a focus of microwave-assisted techniques and also show cases the progress made in this area together with emphasis on the use of dedicated microwave synthesizers for the synthesis of these compounds.<sup>3,4</sup> Microwave-assisted MCRs not only make the synthesis of complex molecules more efficient and sustainable, MCR. But in addition to pharmaceuticals, agrochemicals, and materials, researchers have also been able to obtain biologically active molecules using microwave-assisted MCRs. In particular, microwave-assisted synthesis also shows great promise for the rapid and selective synthesis of spiroheterocycles, as demonstrated by several recent studies.<sup>5-15</sup>

## ADVANTAGES OF MICROWAVE IRRADIATION

Microwave irradiation offers several benefits over conventional heating methods:

- **Enhanced Reaction Rates:** Microwaves provide uniform heating, leading to improved energy transfer and significantly faster reaction times.
- **Higher Yields:** Many MCRs exhibit increased yields under microwave conditions due to reduced side reactions and better reaction kinetics.
- **Reduced Solvent Usage:** Microwave synthesis often allows for solvent-free reactions or the use of minimal solvents, aligning with green chemistry principles.

## KEY MULTICOMPONENT REACTIONS

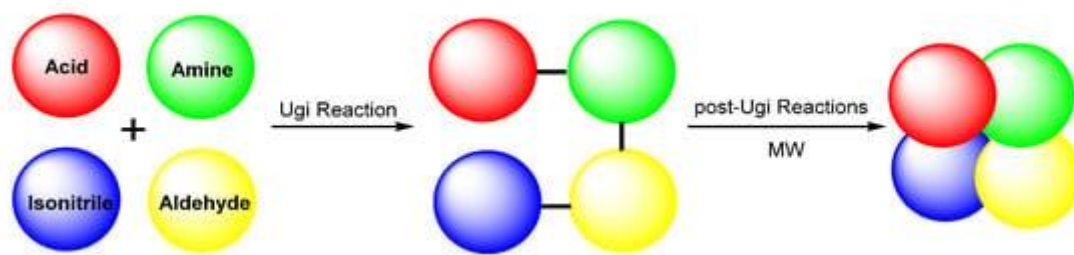
Several prominent MCRs have been adapted for microwave-assisted synthesis of heterocycles:

- **Biginelli Reaction:** This reaction allows for the synthesis of dihydropyrimidinones from aldehydes,  $\beta$ -keto esters, and urea. Microwave conditions enhance reaction rates and yields, making it a valuable method for generating pyrimidine derivatives.



- **Ugi Reaction:** The Ugi reaction involves the condensation of an amine, carboxylic acid, isocyanide, and carbonyl compound. Microwave assistance has facilitated the rapid formation of diverse  $\alpha$ -amino acid derivatives, expanding its utility in heterocyclic synthesis.

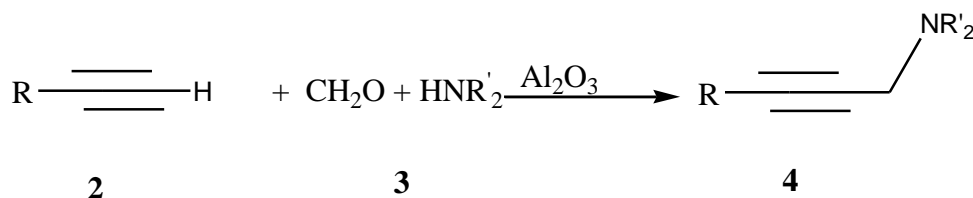
As microwave irradiation and post-Ugi reactions possess their respective advantages over other protocols, merging strategies show high value in synthetic chemistry. Through the combination of microwave irradiation and post-Ugi reactions, various polycycles have been efficiently and sustainably synthesized. In this minireview, we wish to highlight the recent advances of microwave-assisted post-Ugi reactions for the synthesis of polycycles



Scheme 1. Synthesis of polycycles through microwave-assisted post-Ugi reactions.

- **Mannich Reaction:** This three-component reaction forms  $\beta$ -amino carbonyl compounds. Under microwave conditions, the Mannich reaction has been optimized to produce a variety of substituted piperidines and pyrrolidines efficiently. Mannich reaction is one of the most important multicomponent reaction in organic chemistry. <sup>16</sup>

Here one report on environmental benign preparation of propargylamines via a mannich reaction on  $\text{Al}_2\text{O}_3$ ; without any organic solvent as reaction medium.

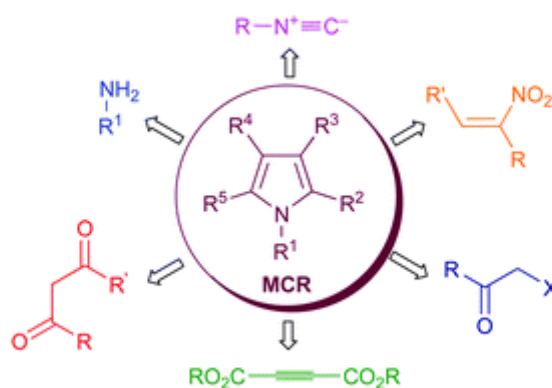


- **Preparation of propargylamines via a mannich reaction**

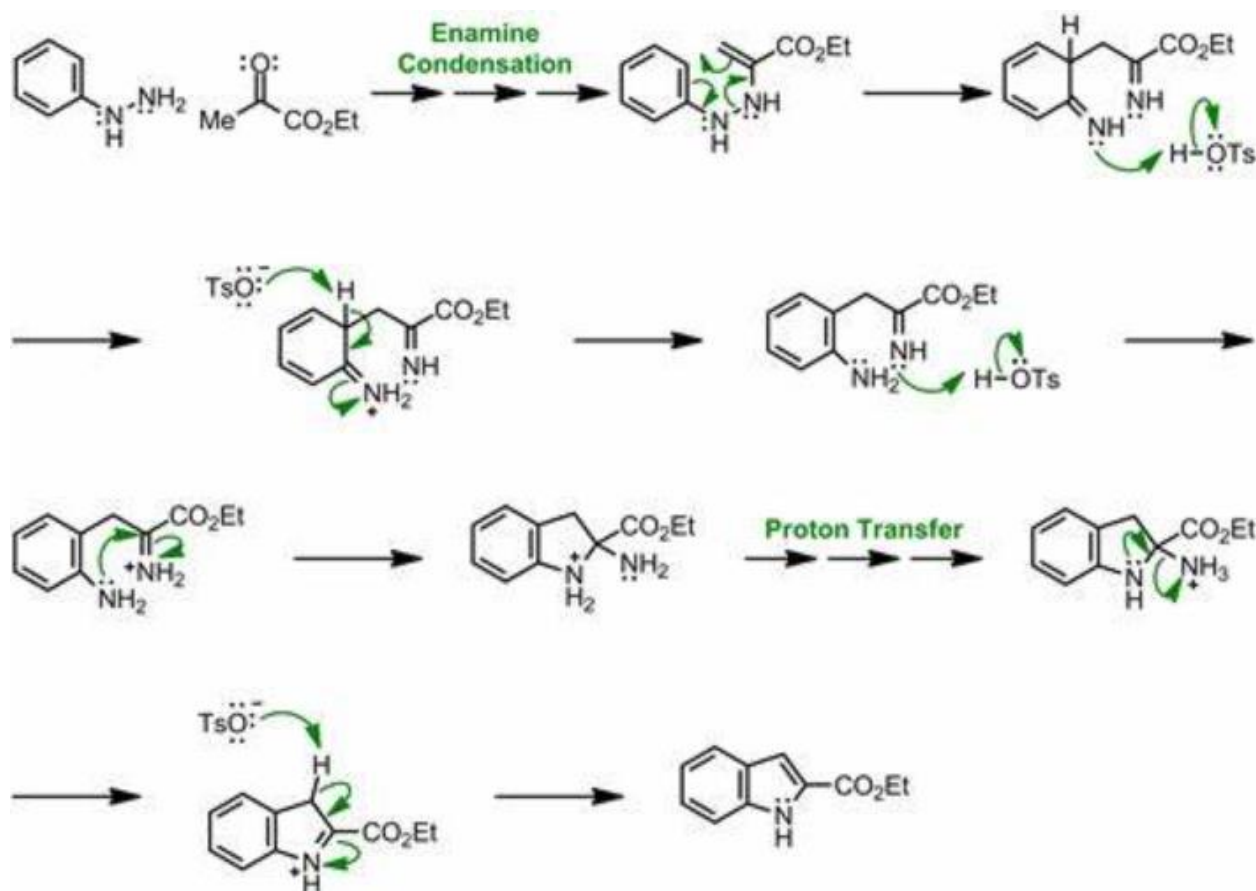
## APPLICATIONS IN HETEROCYCLIC CHEMISTRY

The applications of microwave-assisted MCRs extend to the synthesis of various heterocycles, including:

- **Pyrroles and Indoles:** MCRs have been effectively employed to synthesize these important building blocks for pharmaceuticals and natural products. Pyrrole is one of the most important one-ring heterocycles. The ready availability of suitably substituted and functionalized pyrrole derivatives is essential for the progress of many branches of science, including biology and materials science.



Scheme 2. Pyrrole Derivatives.



Scheme. 3 Fischer indolesynthesis.

## FUTURE DIRECTIONS

The field of microwave-assisted MCRs in heterocyclic chemistry is evolving, with potential future advancements including:

- **Automation and Parallel Synthesis:** Integration of microwave technology with robotic systems for high-throughput screening of compounds.
- **Diversity-Oriented Synthesis:** Continued exploration of novel reaction conditions to expand the range of accessible heterocycles.
- **Green Chemistry Innovations:** Development of more sustainable methodologies, such as using biodegradable solvents or conducting reactions under solvent-free conditions.

## CONCLUSION

Microwave-assisted multicomponent reactions represent a transformative approach in heterocyclic chemistry, combining efficiency with sustainability. As research in this area progresses, the potential for innovative synthetic strategies and novel compound development continues to grow, promising significant impacts on medicinal chemistry and beyond.

**REFERENCES**

- [1] M. Henary, C. Kananda, L. Rotolo, B. Savino, E. Owens and G. Cravotto, *RSC Adv.*, 2020, 10, 14170.
- [2] G. Singh and Z. Desta, *Chem. Rev.*, 2012, 112, 6104.
- [3] J. Soni, S. Joshi, K. Chemitikanti and N. Shankaraiah, *Eur. J. Inorg. Chem.*, 2021, 10, 1476.
- [4] M. Kamboj, S. Bajpai, M. Yadav and S. Singh, *Curr. Green Chem.*, 2023, 10, 57.
- [5] K. Kamanna and Y. Amaregouda, *Curr. Organocatal.*, 2023, 10, 160.
- [6] D. Amariuca-Mantu, V. Mangalagiu, R. Danac and I. I. Mangalagiu, *Molecules*, 2020, 25, 716.
- [7] T. Sengoku, A. Shirai, A. Takano, T. Inuzuka, M. Sakamoto, M. Takahashi and H. Yoda, *J. Org. Chem.*, 2019, 84, 12532.
- [8] G. Meera, K. R. Rohit, S. Saranya and G. Anilkumar, *RSC Adv.*, 2020, 10, 36031.
- [9] N. Z. Kiss, E. B' alint and G. Keglevich, *Microwave-Assisted Syntheses in Organic Chemistry*, ed. G. Keglevich, *Milestones in Microwave Chemistry*, SpringerBriefs in Green Chemistry for Sustainability, Springer International Publishing, Switzerland, 2016, ch. 2, DOI: 10.1007/978-3 319-30632-2\_2.
- [10] A. Kumar, Y. Kuang, Z. Liang and X. Sun, *Mater. Today Nano*, 2020, 11, 100076.
- [11] D. Garella, E. Borretto, A. Di Stilo, K. Martina, G. Cravotto and P. Cintas, *MedChemComm*, 2013, 4, 1323.
- [12] J. Fairsoosa, S. Saranya, S. Radhika and G. Anilkumar, *ChemistrySelect*, 2020, 5, 5180.
- [13] G. Tiwari, A. Khanna, V. K. Mishra and R. Sagar, *RSC Adv.*, 2023, 13, 32858.
- [14] S. Das, *Synth. Commun.*, 2022, 52, 637.
- [15] N. Sharma, U. K. Sharma and E. V. Van der Eycken, *Microwave-Assisted Organic Synthesis: Overview of Recent Applications*, *Green Techniques for Organic Synthesis and Medicinal Chemistry*, ed. W. Zhang and W. Berkeley Cue, John Wiley & Sons Ltd, 2nd edn, 2018, ch. 17.
- [16] Volkmann R.A.(1991) In Trost B.M., Fleming I (eds) *Comprehensive organic synthesis*, vol.1 pergamon press.

# Synthesis, Characterization and Biological Studies of Imino-Pyrazol Schiff Base and Transition Metal Complexes

Vishvas Ganpat Choudhari<sup>1\*</sup>, Netaji Keru Desai<sup>1</sup>, Mahesh Bajarang Gurame<sup>1</sup>, Anil Shivaji Kirdant<sup>2</sup>

<sup>1</sup>Department of Chemistry Karamveer Mamasahab Jagadale Mahavidyalaya, Washi, District -Dharashiv, Maharashtra, India

<sup>2</sup>Department of Chemistry, Baburaoji Adaskar Mahavidyalaya Kaij Dist -Beed, Maharashtra, India

## ABSTRACT

In By refluxing 3-aminopyrazole and 3, 5-dichloro-2-hydroxybenzaldehyde in a 1:1 M composition in ethanol, a novel Schiff base known 2-(((1H-pyrazol-3-yl) imino) methyl)-4, 6-dichlorophenol (PBSB) was synthesized. The synthesized Schiff base was analyzed by thin layer chromatography, <sup>1</sup>HNMR and IR spectroscopy. However using thin layer chromatography, IR spectroscopy, thermal and elemental analysis, the cobalt, nickel and copper complexes with PBSB were characterized. IR spectral analysis show that the Schiff base is a bidentate ligand that binds to the metal ions via protonated phenolic O and imine N. The coordination of water molecules in complexes is confirmed by thermal analysis. Findings proposes octahedral geometry to cobalt and nickel complexes and square planar to copper complex. Moreover, the Schiff base PBSB and metal complexes were screened for antibiotic, antifungal, antioxidant and antimalarial activities. All the synthesized complexes show improved biological activities compared to ligand.

**Keywords:** 3-aminopyrazole, Schiff base complexes, antifungal, antibiotic, antioxidant

## INTRODUCTION

Schiff bases that use nitrogen and oxygen as donor atoms are very interesting and have many uses in the field of pharmaceutical chemistry [1]. Recent developments in spectroscopy, along with their exceptional antibacterial, antifungal, and anticancer properties, have given Schiff base ligands and their complexes a well-earned and significant significance [2]. The metal complexes of pyrazole-based Schiff bases have attracted a lot of attention in a variety of fields due to their structural characteristics and unquestionably beneficial biologic applications. These ligands have always been relevant to a bonding occurrence with the transition metal ions [3]. These structures were primarily formed by the Schiff base's structure, the coordinating sites' flexibility, and the geometry surrounding the metal ion [4]. Because of its unique structural characteristics, pyrazole is one of the main and most attractive azole drugs against bacterial infections [5]. Schiff bases based on pyrazoles are one type of asymmetric N-containing heterocyclic ligand that has garnered a lot of attention in catalysis and medicinal chemistry at the moment [6]. The organic moiety in the five-membered ring with two N on the neighboring site is known as a pyrazole. The pyrazole moiety of metal complexes has garnered significant attention in the biological area because of their wide

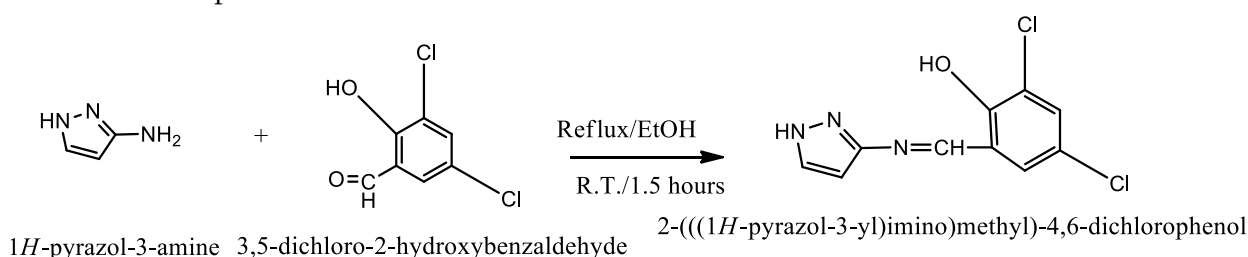


range of properties, including antiviral, antitumoral, antibacterial, and antimalarial activity [7]. The class of ligands known as pyrazoles with aldehydes is capable of working as excellent antifungal, anticancer, antibacterial, and anti-tubercular agents. When pyrazoles are chelated with transition metal, this property is enhanced. Because they necessitate the presence of an imine group, Schiff base type ligands are the structural analogs of biological compounds. These ligands smoothly form stable compounds with the metal ions and are synthetically flexible [8]. The core metal ions and the surrounding Schiff base group both influence how effective a medication is. A small alteration to the Schiff base's structure can result in the creation of a new medication. Therefore, choosing a Schiff base requires special consideration. Because of their hydrophobic nature and capacity to coordinate, ligands are an excellent choice.

## EXPERIMENTAL

### 2.1 Synthesis of Schiff base 2-(((1H-pyrazol-3-yl) imino) methyl)-4,6-dichlorophenol (PBSB)

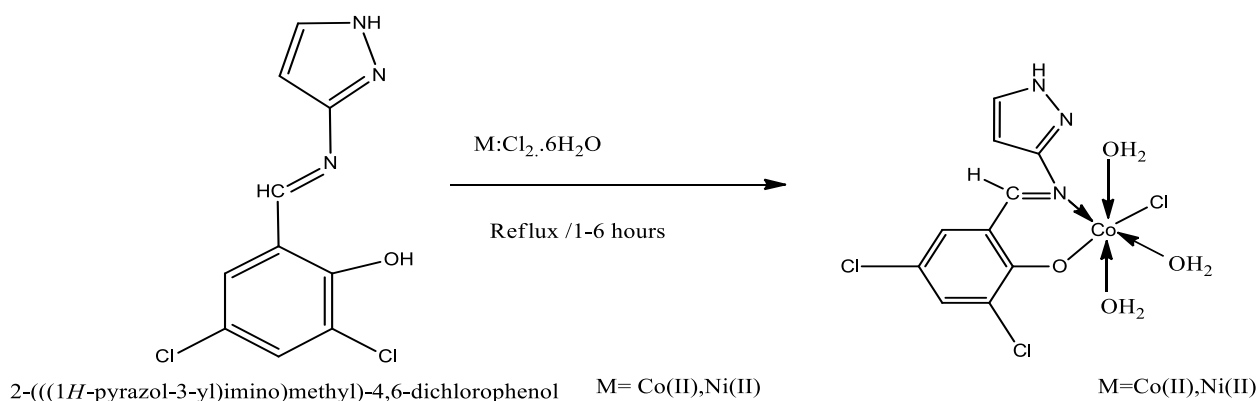
Condensing the ethanolic solutions of (0.01M) 3-aminopyrazole and (0.01M) 3, 5-dichloro-2-hydroxybenzaldehyde heating mental for 1.5 hours produced the PBSB. Thin layer chromatography was used to verify the product's formation. The yellow precipitate was then filtered off and dried. The PBSB synthesis scheme is provided below.



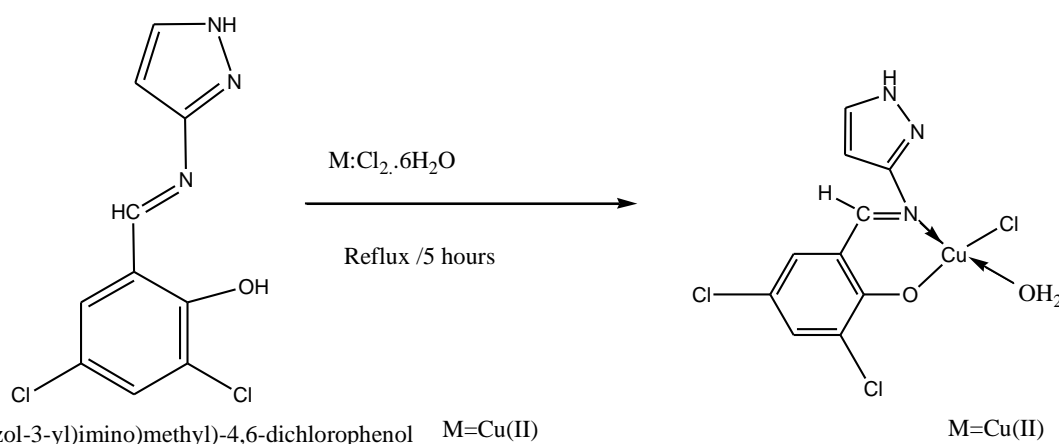
**Scheme 1** Synthesis of Schiff base (PBSB).

### 2.2 Synthesis of Schiff base Co, Ni and Cu complexes

Metal complexes were synthesized by refluxing 0.01M metal halide solution in ethanol with 0.01M Schiff base PBSB for 1-6 hours at room temperature. The completion of reaction was checked with thin layer chromatography. Solid precipitate formed were filtered off and dried.



**Scheme 2** Synthesis of Schiff base Co (II) and Ni (II) complexes.



**Scheme 3** Synthesis of Schiff base Cu (II) complexes.

## RESULTS AND DISCUSSION

IR, <sup>1</sup>HNMR, elemental analysis, and thermogravimetric analysis, were used to characterize these compounds.

### 3.1. Elemental analysis:

The elemental analysis of ligands and metal complexes is shown in Table No. 1.

**Table No. 1.** Elemental analysis of ligands and metal complexes.

Compounds	Molecular Formula	%C (% Calc.)	%H (Calc.)	%O (Calc.)	%N (Calc.)	%Metal (Calc.)
PBSB	C <sub>10</sub> H <sub>7</sub> ON <sub>3</sub> Cl <sub>2</sub>	46.5 (47.05)	2.71 (2.74)	6.1 (6.27)	16.2 (16.47)	-
Co: PBSB	C <sub>10</sub> H <sub>12</sub> O <sub>4</sub> N <sub>3</sub> Cl <sub>3</sub> Co	29.2 (29.85)	2.3 (2.98)	15.5 (15.92)	10.2 (10.44)	14.2 (14.66)
Ni: PBSB	C <sub>10</sub> H <sub>12</sub> O <sub>4</sub> N <sub>3</sub> Cl <sub>3</sub> Ni	29.3 (29.85)	2.80 (2.98)	15.5 (15.92)	10.2 (10.44)	14.2 (14.60)
Cu: PBSB	C <sub>10</sub> H <sub>8</sub> O <sub>2</sub> N <sub>3</sub> Cl <sub>2</sub> Cu	33.2 (33.75)	2.1 (2.25)	8.5 (9.0)	11.2 (11.81)	17.5 (17.87)

### 3.2. IR Spectra:

By comparing the infrared spectra of the novel Schiff base with the metal complexes, the bonding mode of PBSB with metal ions was tabulated in table No. 1. Fig. 1, 2, 3 and 4 show IR spectra of Schiff base, Co, Ni and Cu complexes respectively. The development of a strong signal at 1624 cm<sup>-1</sup> (Fig. 1) owing to the imine group  $\nu$  (-CH = N) moiety and the absence of stretching frequencies due to the pyrazole's  $\nu$ (-NH<sub>2</sub>) and aldehyde  $\nu$ (-CHO) moiety substantiated the synthesis of Schiff base [9]. A second band at 3441 cm<sup>-1</sup> resulting from the aldehyde moiety's hydroxy group emerged in the Schiff base and vanished in the complexes as a result of the metal ions' interaction with the oxygen of the Schiff base [10]. The band that developed in the region 1460- 1485 cm<sup>-1</sup> region as a result of the  $\nu$  (C - O) further supports this bonding. The characteristic

band of Schiff base for  $\nu$  ( $-\text{CH}=\text{N}$ ) occurs in the region of  $1415\text{--}1425\text{ cm}^{-1}$  shifts to lower values by  $10\text{--}15\text{ cm}^{-1}$  after complexation, signifying the binding of azomethine nitrogen to the metal ions [11]. Due to the  $\nu(\text{M}\text{--}\text{N})$  and  $\nu(\text{M}\text{--}\text{O})$  bonds, two new bands in the regions  $420\text{--}430$  and  $470\text{--}490\text{ cm}^{-1}$  emerged in the metal complexes [12]. Coordination of the water molecules produced a broad signal in the spectra of metal complexes  $3340\text{--}3380\text{ cm}^{-1}$ [13].

**Table No. 2** IR spectral data of Schiff base and its metal complexes.

Compound	$\nu$ ( $-\text{CH}=\text{N}-$ ) $\text{cm}^{-1}$	$\nu$ (OH) $\text{cm}^{-1}$	$\nu(\text{H}_2\text{O}/\text{OH})$ $\text{cm}^{-1}$	$\nu$ (M-O) $\text{cm}^{-1}$	$\nu$ (M-N) $\text{cm}^{-1}$	$\nu$ (C-O) $\text{cm}^{-1}$
PBSB	1624	3441				1485
Co: PBSB	1615		3380	489	425	1480
Ni: PBSB	1616		3417	503	420	1480
Cu: PBSB	1618		3344	473	429	1462

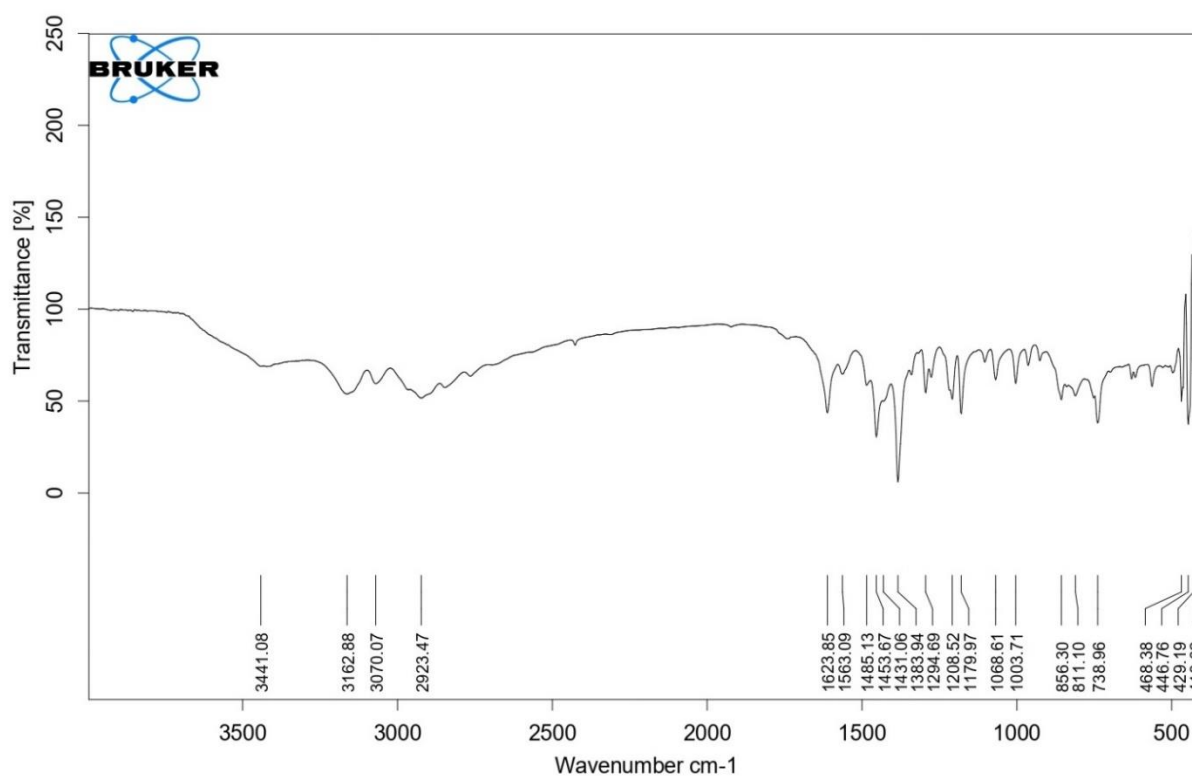


**Figure 1** IR of Schiff base PBSB.

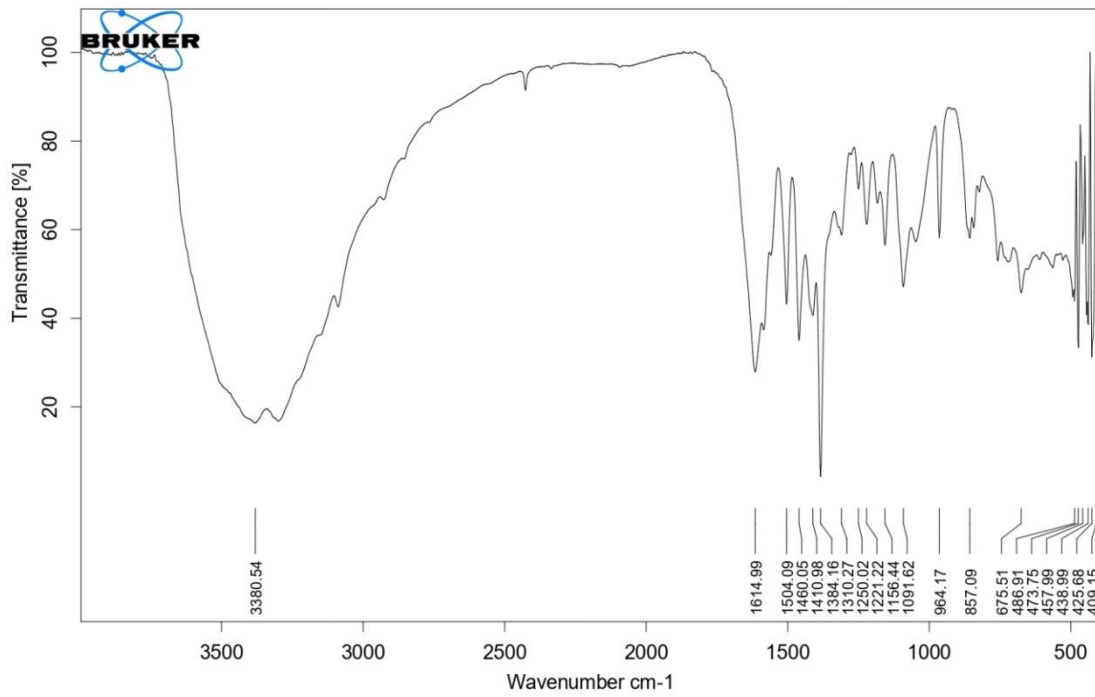


Figure 2 IR of Co: PBSB complex.

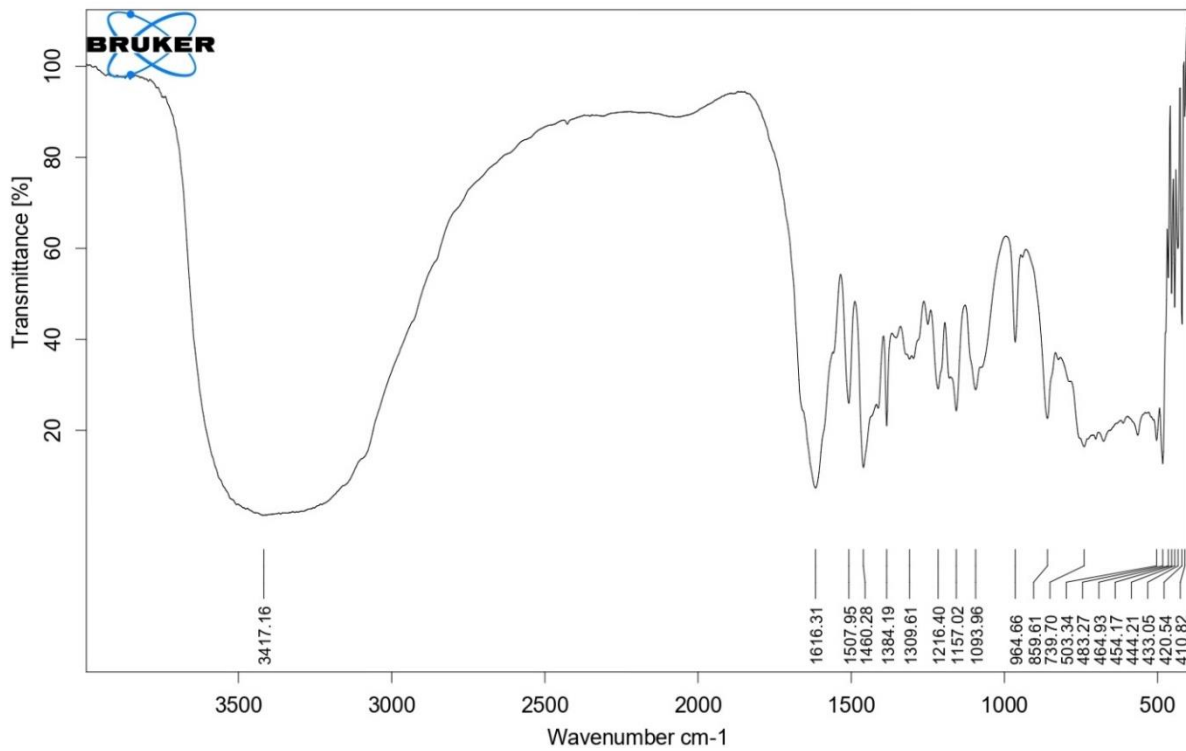
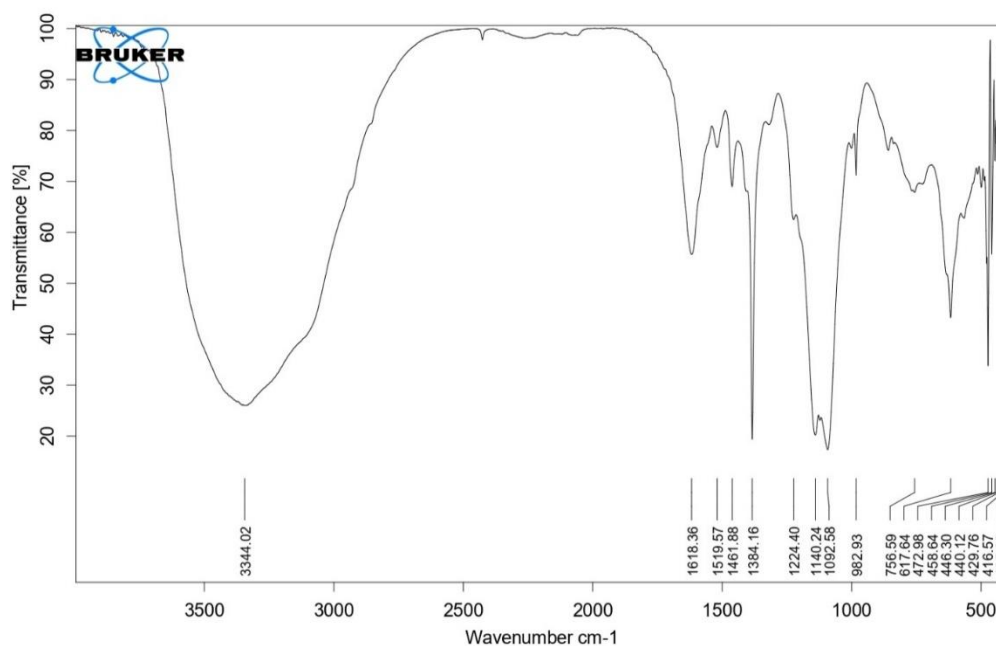


Figure 3 IR of Ni: PBSB complex.



**Figure 4** IR of complex Cu: PBSB.

### 3.3. $^1\text{H}$ NMR spectra:

Using TMS as the standard, the  $^1\text{H}$ NMR spectra of the PBSB in  $\text{CDCl}_3$  is shown in Fig. 5. The appearance of two singlets' at  $\delta$  13.12 and  $\delta$  8.97 ppm, caused by the hydroxy proton and proton of  $-\text{C}=\text{NH}-$  group of imine, verified the formation of PBSB. A singlet was observed by the PBSB at  $\delta$  6.16 ppm due to the pyrazole's  $-\text{CH}$  proton. The proton of pyrazole's  $-\text{NH}$  caused a singlet to form at  $\delta$  12.57 ppm. The aromatic protons produced a signal between  $\delta$  6.87 and  $\delta$  7.79 ppm.

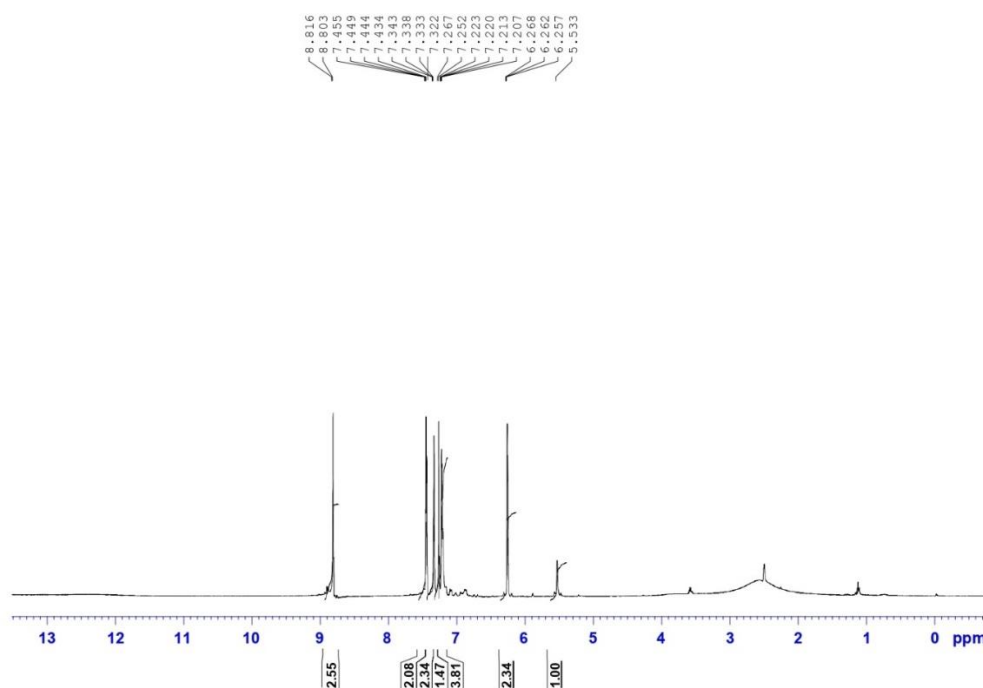


**Figure 5**  $^1\text{H}$ NMR spectrum of 2-(((1H-pyrazol-3-yl) imino) methyl)-4,6-dichlorophenol (PBSB).

### 3.4. Thermal analysis:

The thermal analysis of cobalt, nickel and copper complexes are shown in Fig. 6, 7 and 8. Three phases are involved in Co: PBSB (1:1)'s heat deterioration (in Fig. 6). Three coordinated H<sub>2</sub>O molecules break down in the first step within the range of 70-290°C, with a mass loss percentage of 12.9 % (cal. 13.43%). The very next stage is the breakdown of the pyrazole moiety in a temperature range of 290-450 °C, with a mass loss of 10.5% (cal. 9.7%). The final stage is the breakdown of the organic moiety in a temperature range of 450-550 °C, with a mass loss of 53.5% (calculated to 55.2%). The residue left is the oxide of cobalt with a mass 20.2% (calculated to 18.62%).

Likewise, three steps are involved in Ni: PBSB (1:1)'s thermal breakdown (in Fig. 7). Three coordinated H<sub>2</sub>O molecules break down in the first step at a temperature range of 70-290°C, with a mass loss percentage of 13.80% (calc. 13.44 %). In the second step, the pyrazole moiety is broken down between 290 °C and 450 °C degrees Celsius, with a mass loss of 9.8% (calculated to be 9.2%). The final stage involves the breakdown of pyrazole moiety occurs at the temperature range of 450–550 °C, with a mass loss of 54.2% (calculated 55.2%). The residue left is 21.6% (calculated 20.27 % as Ni O).

The thermal degradation of Cu: PBSB (1:1) occurs in three main stages (in Fig. 8). One coordinated H<sub>2</sub>O molecule decomposes in the first step at a temperature between 80 and 210 °C, with a mass loss percentage of 4.9 % (calculated 4.7%). In the second step, the pyrazole moiety is broken down in the temperature range of 211-410 °C, resulting in a mass loss of 9.5 % (calcd.10.2 %). The organic moiety decomposes in the final stage at a temperature range of 410-550 °C, with a mass loss of 23% (calculated to be 20.97 %). There is 25.4% residue left (calculated 26.0 % Cu O).

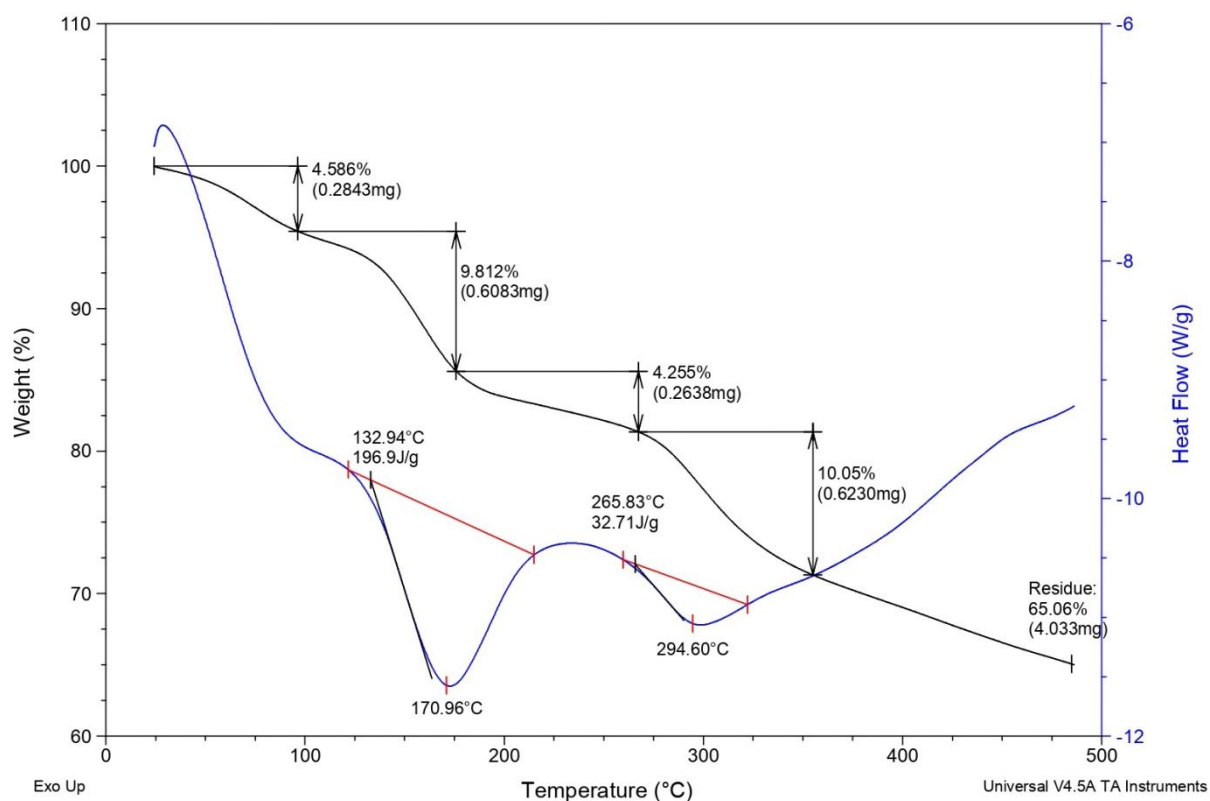


Figure 6 TGA-DSC spectra of Co: PBSB complex.

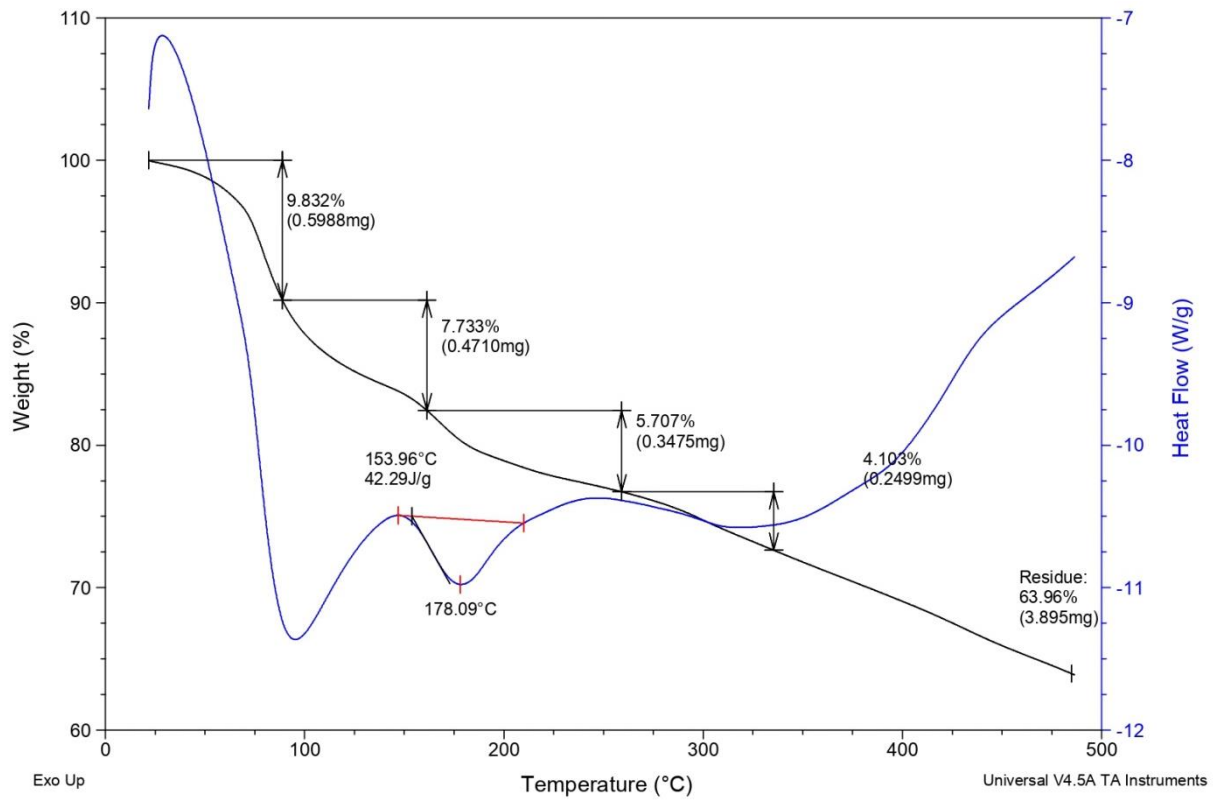


Figure 7 TGA-DSC spectra of Ni: PBSB complex.

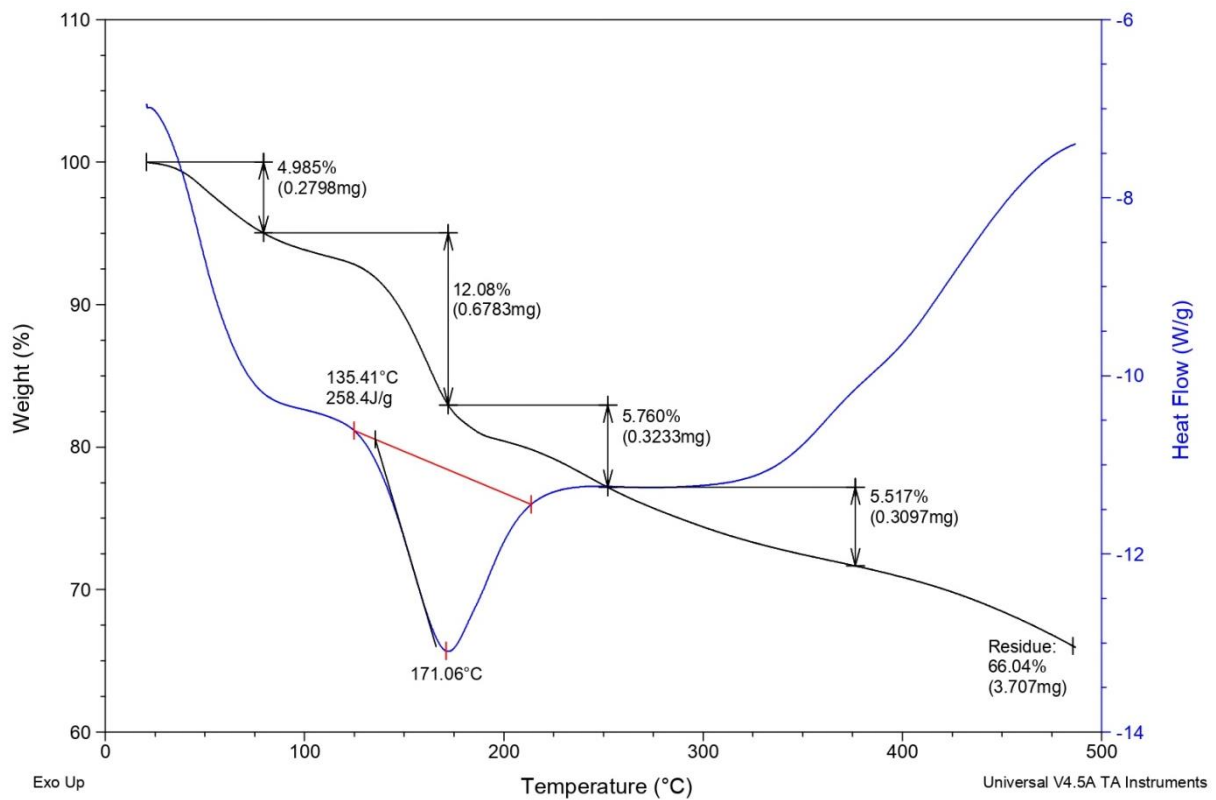


Figure 7 TGA-DSC spectra of Cu: PBSB complex.

### 3.5. Biological activities:

All the compounds were screened for biological activities such as antibiotic, antifungal and antioxidant as shown in table no. 2, 3 and 4. All these complexes show moderate to high antibiotic activities. At the concentration of 1000 µg/ml Co: PBSB exhibits excellent antibiotic activity and antifungal activity. Likewise, all Schiff base metal complexes have significant antioxidant and antimalarial activity, among them Co: PBSB shows better antioxidant while Cu: PBSB shows significant antimalarial activity as compared to other substances.

**Table No.2 % Zone of inhibition (Antibiotic) of Schiff base (PBSB) and its metal complexes.**

Sr. No	Sample	Concentration	Zone of Inhibition (mm)	
			<i>E. coli</i>	<i>S. aureus</i>
1.	Control		-	-
2.	Standard Streptomycin	1000µg/ml	31	38
3	Co: PBSB	500µg	19	25
		1000µg	29	32
4.	Ni: PBSB	500µg	11	16
		1000µg	21	28
5	Cu: PBSB	500µg	17	15
		1000µg	24	21
6	PBSB	500µg	Nil	04
		1000µg	01	06

**Table No. 3 Zone of inhibition (Antifungal) of Schiff base (PBSB) and its metal complexes.**

Sr. No.	Sample	Concentration	Zone of Inhibition (mm)	
			<i>C.albicans</i>	<i>A. niger</i>
1.	Control		-	-
2.	Standard Fluconazole	1000µg/ml	26	22
3.	Sample (Co: PBSB)	500µg	18	16
		1000µg	29	23
4.	Sample (Ni: PBSB)	500µg	01	12
		1000µg	04	17
5.	Sample (Cu: PBSB)	500µg	08	04
		1000µg	22	12
6.	PBSB	500µg	02	Nil
		1000µg	08	Nil



Table No. 4 % zone of inhibition (Antioxidant) of Schiff base (PBSB) and its metal complexes.

Antioxidant activity by DPPH (96 well method)						
Sample code	Concentration	Absorbance			Mean	% inhibition
Control	-	1.356	1.355	1.356	1.355	-
STD (Ascorbic Acid)	100µg/ml	0.356	0.350	0.352	0.352	73.98
	200µg/ml	0.342	0.340	0.344	0.342	74.77
	400 µg/ml	0.288	0.28	0.285	0.284	79.02
	600µg/ml	0.274	0.270	0.269	0.271	80.00
	800 µg/ml	0.256	0.255	0.243	0.251	81.46
	<b>1000µg/ml</b>	<b>0.235</b>	<b>0.230</b>	<b>0.212</b>	<b>0.225</b>	<b>83.35</b>
PBSB	100µg/ml	0.956	0.952	0.954	0.954	29.62
	200µg/ml	0.945	0.935	0.940	0.940	30.66
	400 µg/ml	0.935	0.932	0.931	0.932	31.20
	600µg/ml	0.925	0.921	0.923	0.923	31.91
	800 µg/ml	0.886	0.895	0.896	0.892	34.17
	<b>1000 µg/ml</b>	<b>0.856</b>	<b>0.855</b>	<b>0.845</b>	<b>0.852</b>	<b>37.15</b>
Co: PBSB	100µg/ml	0.742	0.741	0.744	0.742	45.24
	200µg/ml	0.732	0.730	0.725	0.729	46.22
	400 µg/ml	0.712	0.715	0.710	0.712	47.45
	600µg/ml	0.685	0.688	0.682	0.685	49.47
	800 µg/ml	0.675	0.665	0.664	0.668	50.72
	<b>1000 µg/ml</b>	<b>0.615</b>	<b>0.611</b>	<b>0.602</b>	<b>0.609</b>	<b>55.05</b>
Ni: PBSB	100µg/ml	0.845	0.841	0.832	0.839	38.08
	200µg/ml	0.825	0.833	0.823	0.827	38.99
	400 µg/ml	0.812	0.801	0.789	0.800	40.93
	600µg/ml	0.786	0.775	0.765	0.775	42.80
	800 µg/ml	0.755	0.756	0.777	0.762	43.74
	<b>1000 µg/ml</b>	<b>0.673</b>	<b>0.670</b>	<b>0.672</b>	<b>0.671</b>	<b>50.45</b>
Cu: PBSB	100µg/ml	0.820	0.835	0.832	0.829	38.84
	200µg/ml	0.812	0.801	0.796	0.803	40.76
	400 µg/ml	0.788	0.785	0.776	0.783	42.24
	600µg/ml	0.776	0.772	0.752	0.766	43.44
	800 µg/ml	0.720	0.722	0.685	0.709	47.70
	<b>1000 µg/ml</b>	<b>0.686</b>	<b>0.688</b>	<b>0.682</b>	<b>0.685</b>	<b>49.44</b>

**Table No 5** % zone of inhibition (Antimalarial) of Schiff base and its complexes

Compound	Concentration ( $\mu\text{g/mL}$ )	Absorbance				mean	% inhibition
Control	-	0.808	0.926	0.932	0.888		
Standard (chloroquine diphosphate)	250	0.281	0.272	0.241	0.264	70.2175	
	500	0.156	0.163	0.166	0.161	81.8079	
	1000	0.112	0.101	0.103	0.105	<b>88.1470</b>	
PBSB	250	0.763	0.763	0.763	0.763	14.1410	
	500	0.675	0.637	0.675	0.662	25.4688	
	1000	0.586	0.588	0.473	0.549	<b>38.2220</b>	
Co: PBSB	250	0.658	0.556	0.645	0.619	30.2700	
	500	0.565	0.568	0.565	0.566	36.3090	
	1000	0.478	0.489	0.467	0.478	<b>46.2115</b>	
Ni: PBSB	250	0.650	0.635	0.653	0.646	27.2522	
	500	0.540	0.543	0.535	0.540	39.1891	
	1000	0.460	0.455	0.445	0.453	<b>48.9864</b>	
Cu: PBSB	250	0.550	0.545	0.535	0.545	38.6261	
	500	0.450	0.435	0.438	0.441	50.3378	
	1000	0.350	0.372	0.360	0.360	<b>59.4594</b>	

## CONCLUSION:

Novel Schiff base was synthesized by condensing 3-aminopyrazole with 3, 5-dichloro-2-benzaldehyde to create metal complexes. The formation of metal complexes was confirmed by elemental analysis, thin layer chromatography and IR spectroscopy. The mechanism of ligand coordination with the metal ions was elucidated through the application of infrared spectroscopy. The oxygen (O) of the hydroxyl group and the nitrogen (N) of the imine moiety of the metal ions, in particular, create a bidentate bond with the Schiff base. Thermogravimetric analysis revealed the existence of coordinated water within or outside of the coordination sphere. The cobalt and nickel metal complexes are suggested to have an octahedral geometry and square planar to copper complex. The biological assay was examined to evaluate all the compounds (antibiotic, antifungal, and antioxidant). The findings indicated that the metal complexes showed superior biological properties compared to their corresponding ligands. Among the synthesized complexes, Co: PBSB exhibits highest above activities.

## REFERENCES

- [1] N. Ramadan, B. Rasayan, J. Chem., 2010, 3(4), 660-670.
- [2] N. Prajapati, S. Chaturvedi, J. Sci. Technol, 2023, 16(12), 931-940.

- [3] A. Prakash, D. Adhikari, *Int. J. Chemtech Res.*, 2011, 3(4), 1891-1896.
- [4] E. Raczuk, B. Dmochowska, J. S.Fiertek, J. Madaj, *Mol.*, 2022, 27(3), 787.
- [5] J. V. Faria, P. F. Vegi, A. G. C. Miguita, M.S. d. Santos, N. Boechat, A. M. R. Bernardino, *Bioorg. Med. Chem.*, 2017, 25(21), 5891-5903.
- [6] M.S.More, P.G.Joshi, Y.K.Mishra, P.K. Khanna, *Mater Today Chem.*, 2019, 14: 100195
- [7] M. J. Naim, O. Alam, F. Nawaz, M. J. Alam, P. Alam, *J. Pharm. Bioallied Sci.*, 2016, 8(1), 2-17.
- [8] P. A. Vigato, S. Tamburini, *Chem. Rev.*, 2004, 248, 17(20), 1717-2128.
- [9] V. Kumar, K. Kaur, G. K. Gupta, A. K. Sharma, *Eur. J. Med. Chem.*, 2013, 69, 735-753.
- [10] Neelofar, N. Ali, S. Ahmad, N. M AbdEl-Salam, R. Ullah, R. Nawaz, Sohail Ahmad, *Trop. J. Pharm. Res.* 2016, 15(12), 2693-2700.
- [11] E. Raczuk, B. Dmochowska, J. Samaszko-Fiertek, J. Madaj, *Mol.*, 2022, 27(3), 787.
- [12] S. Sepehrfar, M. Salehi, S. Parvarinezhad, A. M. Grześkiewicz, M. Kubicki, *J. Mol. Struct.*, 2023, 15, 1278, 134857.
- [13] P. Devi, K. Singh, B. Kubavat, 2023, 5, 100813.

# $\alpha$ -Amino phosphonates: Synthesis and Biomedical Application

Dr. Ganesh V. Shitre<sup>1</sup>, Dr. Mahadev B. Suwarnkar<sup>2</sup>

<sup>1</sup>Department of Chemistry, Vaishnavi Mahavidyalaya Wadwani, Dist. Beed, (Maharashtra), India  
ganeshdrugchem@gmail.com

<sup>2</sup>Department of Chemistry, Baburauji Adaskar Mahavidyalaya, Kaij, Dist. Beed, Maharashtra, India

## ABSTRACT

Due to their biological and physical characteristics,  $\alpha$ -aminophosphonates are a significant class of amino acid analogues with numerous uses in industrial, agricultural, and pharmaceutical chemistry. This article begins with general introduction, synthetic process, and its applications in medicinal chemistry, including antitumor, antibacterial, antiviral, antioxidant, and antimicrobial drugs, are covered first. In conclusion, we offer our viewpoints regarding the potential of  $\alpha$ -aminophosphonate for upcoming scientific endeavors.

**Keywords:** Antitumor drug activity, Antibacterial drug activity, Antiviral drug activity, Antioxidant drug etc.

## INTRODUCTION

$\alpha$ -aminophosphonic acids are amino acid analogues that have a phosphonic acid or similar group (typically phosphonous or phosphinic acids) in place of the carboxylic group. Because of their structural similarity to  $\alpha$ -amino acids,  $\alpha$ -aminophosphonates have garnered a lot of attention nowadays. In the fields of medical chemistry and pharmaceutical sciences,  $\alpha$ -amino phosphonates are essential substances that function as R-amino acid analogs<sup>1</sup>. Compounds containing this structural unit display a broad variety of biological action, making the  $\alpha$ -aminophosphonate moiety a versatile and new pharmacophore<sup>2</sup>.

For a long time, it has been known that phosphonates can be used as phosphate mimics. These compounds are desirable as phosphate mimics in many applications because the phosphonate linkage is not easily hydrolyzed in a biological environment, unlike a phosphate group. Put another way, systematic chemical and biological research of phosphonic acids and their derivatives have been made possible by the structural connection between C-C-P bonds and C-O-P bonds, despite the fact that these two types of bonds differ greatly in their chemical properties.

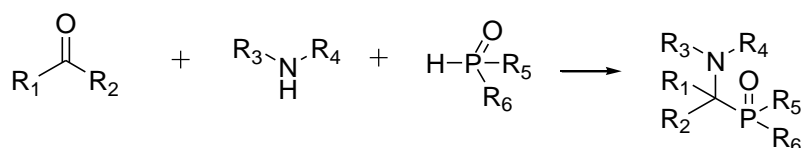
## GENERAL SYNTHETIC METHODS

There are several methods for preparing  $\alpha$ -aminophosphonates, depending on the type of organic moiety. Phosphorus nucleophiles are typically added to imines in the presence of an acid or base to create  $\alpha$ -aminophosphonates.  $\text{BF}_3 \cdot \text{OEt}_2$ ,  $\text{ZnCl}_2$ ,  $\text{MgBr}_2$ ,  $\text{SnCl}_4$ , and other reagents have all been used in this reaction<sup>3</sup>.

4. However, because the amines and water present during imine synthesis can break down or deactivate the Lewis acids, these reactions cannot be performed in a one-pot operation with a carbonyl compound, amine, and diethyl phosphite.

Numerous research groups have presented a straightforward and effective technique for producing  $\alpha$ -Aminophosphonates. Some of these are multicomponent syntheses that begin with an aldehyde, an amine, and diethyl or triethyl phosphite. Lewis acids<sup>5-14</sup> such as SnCl<sub>4</sub>, SnCl<sub>2</sub>, MgBr<sub>2</sub>, ZnCl<sub>2</sub>, Cu(OTf)<sup>15</sup>, FeCl<sub>3</sub>.8H<sub>2</sub>O<sup>16</sup>, and Bronsted acids<sup>17-19</sup>, have been described in the presence of these compounds.

The most typical process for producing  $\alpha$ -aminophosphonates involves hydrophosphonylating imines. In 1952, Kabachnik and Fields discovered the three-component synthesis of  $\alpha$ -aminophosphonates (scheme 1).



**Scheme 1: Kabachnik- Fields Reaction**

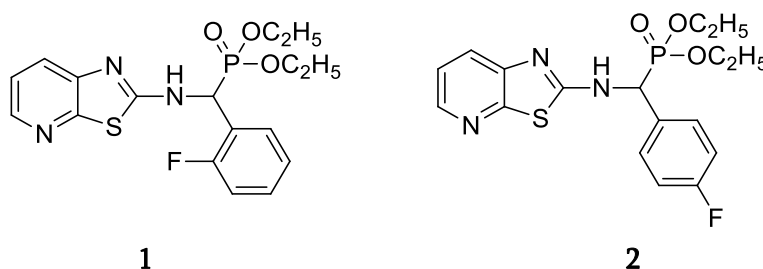
The  $\alpha$ -aminophosphonic acid and their corresponding derivatives have received much interest in organic<sup>20-23</sup> as well as in medicinal chemistry<sup>24</sup>.

## IMPORTANCE OF $\alpha$ -AMINOPHOSPHONATES IN MEDICINAL CHEMISTRY.

The N-C-P group is present in the structure of  $\alpha$ -aminophosphonates, and because of their biological and physical characteristics, they are useful in a variety of industries and agricultural domains. They are also important in organic reactions.  $\alpha$ -Aminophosphonates have several medicinal chemistry applications such as acting as HIV protease inhibitors, catalytic antibody haptens, anticancer drugs, and enzyme inhibitors.  $\alpha$ -aminophosphonates function as pesticides, herbicides, insecticides, and regulators of plant growth in agrochemistry. In addition, they function as pharmacological agents, herbicides, peptide mimics<sup>25</sup>, enzyme inhibitors<sup>26</sup>, herbicides<sup>27</sup>, and pharmacological agent<sup>28</sup>.

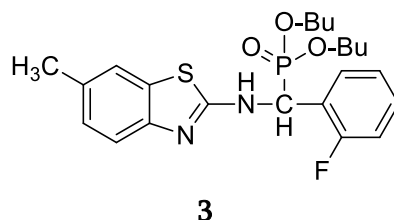
### 3.1. Antitumor drug

The synthesis and biological activity of a pyridine derivative were described by Gu<sup>29</sup> and colleagues. Three human cancer cell lines, including PC-3, Bcap-37, and H460, were used to examine the anticancer properties of those produced compounds. With IC<sub>50</sub> ( $\mu$ M) values of 0.84 and 1.04, respectively, diethyl ((2-fluorophenyl)(thiazolo[5,4-b]pyridin-2-ylamino)methyl)phosphonate **1** and diethyl ((4-fluorophenyl)(thiazolo[5,4-b]pyridin-2-ylamino)methyl)phosphonate **2** exhibit strong antitumor activity (figure 1).



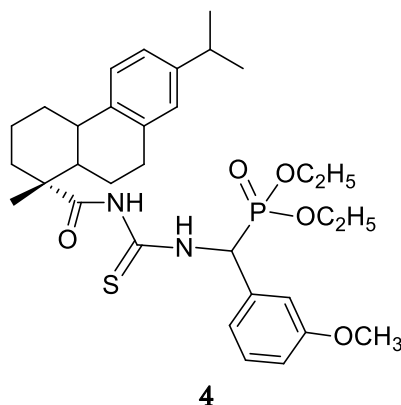
**Figure-1:** Molecular structure of  $\alpha$ -aminophosphonates compound **1** and **2**.

Jin<sup>30</sup> and co-workers synthesized  $\alpha$ -aminophosphonates of benzothiazole compounds & evaluated for anticancer activities against PC3, A431, A375, and Bcap37 cells in vitro by the MTT method. The compound dibutyl ((2-fluorophenyl)((6-methylbenzo[d]thiazol-2-yl)amino)methyl)phosphonate **3** shows strong activity against PC3 cell line with varying concentration such as 1 $\mu$ M (52.1), 5 $\mu$ M (86.0), 10  $\mu$ M (89.1) (figure-2).



**Figure- 2:** Molecular structure of dibutyl ((2-fluorophenyl)((6-methylbenzo[d]thiazol-2-yl)amino)methyl)phosphonate **3**.

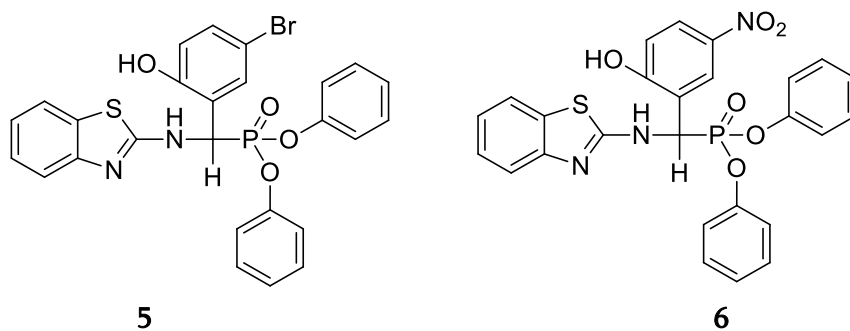
Huang<sup>31</sup> and his research team have reported seventeen substances that are  $\alpha$ -aminophosphonates. Those reported compounds were tested as antitumor against SKOV3 cells. Specially the compound diethyl ((3-((1R)-7-isopropyl-1-methyl-1,2,3,4,4a,9,10,10a-octahydro-phenanthrene-1-carbonyl) thioureido) (3-methoxy-phenyl)methyl)phosphonate **4** exhibit better antitumor activity with IC<sub>50</sub> of 9.96  $\mu$ M (figure-3).



**Figure-3:** Molecular structure of diethyl ((3-((1R)-7-isopropyl-1-methyl-1,2,3,4,4a, 9, 10, 10a-octahydrophenanthrene-1-carbonyl)thioureido)(3-methoxy- phenyl)methyl) phos-phonate **4**.

### 3.2. Antibacterial drug

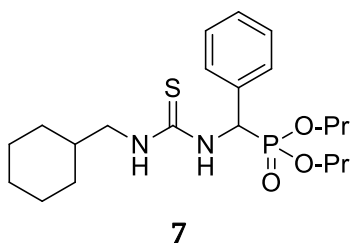
The antibacterial activity and synthesis of (R)-diphenyl ((benzo[d]thiazol-2-ylamino)(5-bromo-2-hydroxyphenyl) methyl) phosphonate **5** and (R)-diphenyl ((benzo[d]thiazol-2-ylamino)(2-hydroxy-5-nitrophenyl)methyl) phosphonate **6** were reported by Rao<sup>32</sup> and colleagues. The disc diffusion method (figure 4) to demonstrate superior antibacterial efficacy against Gram positive bacteria, *Staphylococcus aureus* (13 and 13  $\mu$ g/mL), *Bacillus subtilis* (10 and 12  $\mu$ g/mL), and Gram negative bacteria, *Escherichia coli* (11 and 13  $\mu$ g/mL), *Klebsiella pneumoniae* (13 and 12  $\mu$ g/mL).



**Figure-4:** Molecular structure of compound **5** and **6**.

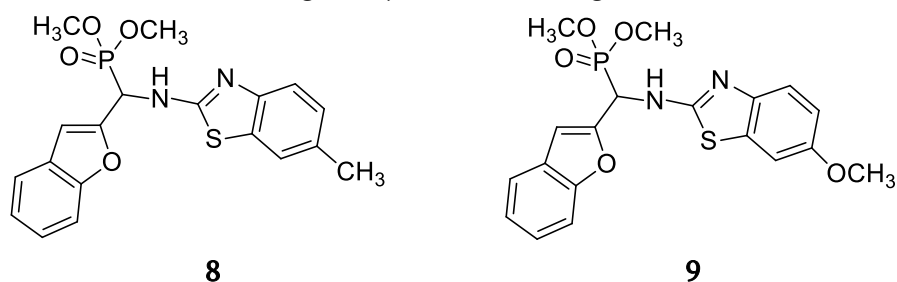
### 3.3. Antiviral drug

Chen<sup>33</sup> *et al.* found that  $\alpha$ -aminophosphonate had antiviral efficacy against TMV. With EC<sub>50</sub> values of 239.8  $\mu$ g/mL of TMV, the compound dipropyl ((3-(cyclohexylmethyl)thioureido)(phenyl)methyl)phosphonate **7** has good antiviral activity (figure-5).



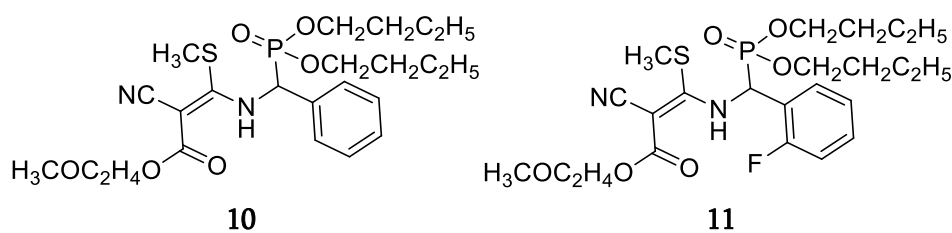
**Figure-5:** Molecular structure of dipropyl ((3-(cyclohexylmethyl)thioureido)(phenyl)methyl)phosphonate **7**.

The production and antiviral activity of furan containing  $\alpha$ -aminophosphonate were demonstrated by Tang<sup>34</sup> and colleagues. The antiviral activity of the synthesized compounds was evaluated against the tobacco mosaic virus (TMV). With an inhibition rate of 57.64% and 58.92%, respectively, the compounds dimethyl (benzofuran-2-yl((6-methylbenzo[d]thiazol-2-yl)amino)methyl)phosphonate **8** and dimethyl (benzofuran-2-yl((6-methoxybenzo[d]thiazol-2-yl)amino)methyl)phosphonate **9** exhibit superior *in vivo* protective effect over the commercial reference Ningnanmycin (54.12%) (figure-6).



**Figure-6:** Molecular structure of compound **8** and **9**.

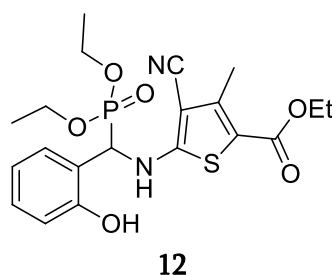
Yang<sup>35</sup> and colleagues looked on the production and antiviral properties of compounds with thiomethyl functional groups that contain  $\alpha$ -aminophosphonate. The synthetic drugs' antiviral efficacy against TMV was evaluated. Compound **10** and **11** were illustrates the remarkable antiviral activities of compounds (E)-2-methoxyethyl 2-cyano-3-(((dibutoxyphosphoryl)(phenyl)methyl)amino)-3-(methylthio)acrylate **10** and (E)-2-methoxyethyl 2-cyano-3-(((dibutoxyphosphoryl)(2-fluorophenyl) methyl)amino)-3-(methylthio)acrylate **11** (figure-7).



**Figure-7:** Molecular structure of compound **10** and **11**.

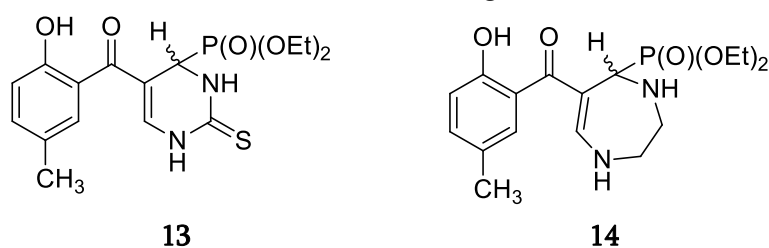
### 3.4. Antioxidant drug

The synthesis of  $\alpha$ -aminophosphonate compounds based on thiophene was reported by Rao<sup>36</sup> and colleagues. Using DPPH, NO, and H<sub>2</sub>O<sub>2</sub> techniques, the antioxidant activity of the produced compounds was evaluated. A molecule with good action (IC<sub>50</sub> value of 30.2) is ethyl 4-cyano-5-((diethoxyphosphoryl)(2-hydroxyphenyl)methyl)amino)-3-methylthiophene-2-carboxylate **12** (figure 8).



**Figure-8:** Molecular structure of compound **12**.

Ali<sup>37</sup> and *et al* reported synthesis and antioxidant activity of pyrimidines & diazepin derivatives. All synthesized compounds were tested as antioxidant activity. The compound diethyl (5-(2-hydroxy-5-methylbenzoyl)-2-thioxo-1,2,3,4-tetrahydropyrimidin-4-yl)phosphonate **13** and diethyl (6-(2-hydroxy-5-methylbenzoyl)-2,3,4,5-tetrahydro-1H-1,4-diazepin-5-yl)phosphonate **14** shows better antioxidant activities in range 37.81-78.35% at different concentration (figure-9).

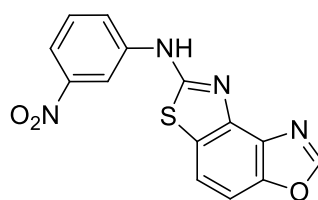


**Figure-9:** Molecular structure of compound **13** and **14**.

### 3.5. Antimicrobial drug

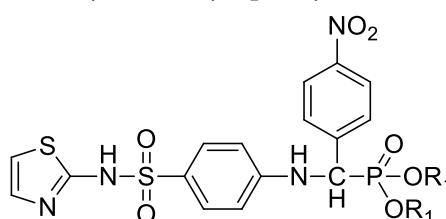
The antibacterial activity of heterocycles containing nitrogen, sulfur, and oxygen was described by Vodela<sup>38</sup> and study group. Using a nutrient agar medium, compound 15 exhibits good activity against gram-positive bacteria and gram-negative bacteria, including *Escherichia coli* 18 (0.94), *Proteus mirabilis* 17 (0.85), and *Salmonella typhi* 15 (0.93). Gram-positive bacteria include *Staphylococcus aureus* 22 (10.4), *Staphylococcus albus* 25 (1.13), and *Streptococcus faecalis* 29 (1.03) (figure-10).



**15**

**Figure- 10:** Molecular structure of N-(3-nitrophenyl)thiazolo[5',4':5,6]benzo[1,2-d]oxazol-7-amine **15**.

Chinnam<sup>39</sup> and *et al* reported thiazole derivatives. Using the disc diffusion method, the compounds were tested against both Gram positive and Gram negative bacteria. Figure 12 illustrates the good activity of Dimethyl (4-nitrophenyl)(4-(N-thiazol-2-ylsulfamoyl) phenylamino) methyl phosphonate **16** (figure-11).

**16**

**Figure-11:** Molecular structure of Dimethyl (4-nitrophenyl)(4-(N-thiazol-2-ylsulfamoyl) phenylamino)methylphosphonate **16**.

## CONCLUSION

The biological and pharmacological characteristics of these organophosphorus compounds, which are natural counterparts of amino acids, have drawn attention in organic and medicinal chemistry recently. A growing amount of interest has been paid to "bioisosterism," or structure analogues of amino acids, because of their strong biological activity.

## REFERENCES

- [1] Kafarski, P.; Lejczak, B. In Aminophosphonic and Aminophosphinic Acids; Kukhar, V. P., Hudson, H. R., Eds.; John Wiley and Sons: 2000; Chapter 12, 407.
- [2] (a) S. C. Fields, Tetrahedron, 1999, 55, 12237; (b) E. K. Fields, J. Am. Chem. Soc., 1952, 74, 1528.
- [3] (a) S. Lashat and H. Kunz, Synthesis, 1992, 90; (b) J. S. Yadav, B. V. S. Reddy, K. Sarita Raj and K. Bhaskar Reddy, Synthesis, 2001, 2277.
- [4] J. Zon, Pol. J. Chem, 1981, 55, 643.
- [5] M. R. Saidi, N. Azizi, Synlett. 2002, 8, 1347-1349.
- [6] A. Heydari, A. Javidan, M. Shaffie, Tetrahedron. Lett. 2001, 42, 8071-8073.
- [7] K. Manabe, S. Kobayashi, Chem. Commun. 2000, 669-670.
- [8] B. C. Ranu, A. Hajra, U. Jana, Org. Lett. 1999, 1, 1141-1143.
- [9] C. Qian, T. Huang, J. Org. Chem. 1998, 63, 4125-4128.
- [10] S. Chandrasekhar, S. J. Prakash, V. Jagadeshwar, C. Narsihmulu, Tetrahedron Lett. 2001, 42, 5561-5563.
- [11] J. S. Yadav, B. V. S. Reddy, C. Madan, Synlett. 2001, 7, 1131-1133.

- [12] K. R. Reddy, K. S. Reddy, C. V. Reddy, M. Mahesh, P. V. K. Raju, V. V. N. Reddy, *Chem. Lett.* 2005, 34, 444-445.
- [13] B. Kaboudin, R. Nazari, *Tetrahedron Lett.* 2001, 42, 8211-8213.
- [14] K.A. Petrov, V.A. Chauzov, T.S. Erokhina, *Usp. Khim.* 1974, 43, 2045-2087.
- [15] A. S. Paraskar, A. Sudalai, *Arkivoc.* 2006, x, 183-189.
- [16] Z. Rezaei, S. Khabnadideh, K. Zomorodian, K. Pakshir, S. Nadali, N. Mohtashami, E. F. Mirzaei, *Int. J. Med. Chem.* 2011, 54, 1-11.
- [17] T. Akiyama, M. Sanada, K. Fuchibe, *Synlett*, 2003, 10, 1463-1464.
- [18] G. D. Joly, E. N. Jacobsen, *J. Am. Chem. Soc.* 2004, 126.
- [19] F. G. Whitelaw.; L. A. Bruce.; J. M. Eadie.; W. J. Shand, *App. Env. Micro.*, 1983, 46, 951-953.
- [20] R. Engel, *Chem Rev.*, 1977, 77, 349-367.
- [21] J. Hiratake.; L. Oda, Biasci. *Biotech. Biochem.*, 1997, 61, 211-218.
- [22] K. Moonen.; I. Laureyn.; C. V. Stevens, *Chem. Rev.*, 2004, 104, 6177-6215.
- [23] K. A. Schug.; W. Lindner, *Chem. Rev.*, 2005, 105, 67-113.
- [24] A. Mucha.; P. Kafarski.; Y. Berlicki, *J. Med. Chem.*, 2011, 54, 5955-5980.
- [25] P. Kafarski and B. Lejczak, *Phosphorus, Sulfur, Silicon Relat. Elem.*, 1991, 63, 1993.
- [26] (a) M. C. Allen, W. Fuhrer, B. Tuck, R. Wade and J. M. Wood, *J. Med. Chem.*, 1989, 32, 1652; (b) P. P. Giannousis and P. A. Bartlett, *J. Med. Chem.*, 1987, 30, 1603.
- [27] A. Barder, *Aldrichim. Acta*, 1988, 21, 15.
- [28] (a) F. R. Atherton, C. H. Hassal and R. W. Lambert, *J. Med. Chem.*, 1986, 29, 29; (b) E. K. Baylis, C. D. Campbell and J. G. Dingwall, *J. Chem. Soc., Perkin Trans. 1*, 1984, 2845.
- [29] L. Gu.; C. Jin, *Org. Biomol. Chem.*, 2012, 10, 7098-7102.
- [30] L. Jin.; B. Song.; G. Zhang.; R. Xu.; S. Zhang.; X. Gao.; D. Hu.; S. Yang *Bioorg. Med. Chem. Lett.*, 2006, 16, 1537-1543.
- [31] X. Chao Huang.; M. Wang.; Y. M. Pan.; X. Y. Tian.; H. S. Wang.; Y. Z. Bioorg. *Med. Chem. Lett.*, 2013, 23, 5283-5289.
- [32] A. Janardhan Ra.; P. V. Rao.; V. K. Rao.; C. Mohan.; C. N. Raju.; C. S. Reddy, *Bull. Korean Chem. Soc.*, 2010, 31, 1863-1868.
- [33] M. H. Chen.; Z. Chen.; B. A. Song.; Pinaki S. Bhadury.; S. Yang.; X. J. Cai.; D. Y. Hu.; W. Xue.; S. Zeng, *J. Agric. Food Chem.*, 2009, 57, 1383-1388.
- [34] C. Tang.; Z. Chen.; H. Xiao.; X. Wang.; G. Zhang.; D. Hu, *Phosphorus, Sulfur Relat. Elem.*, 2015, 190, 585-595.
- [35] J. Q. Yang.; B. Song.; P. S. Bhadury.; Z. Chen.; Song Yang.; X. J. Cai.; D. Y. Hu, *J. Agric. Food Chem.*, 2010, 58, 2730-2735.
- [36] S. Rao. Da.; R. Sa.; T. Basha. S Ka.; N. Raju. Ca.; Naresh, *Der Pharma Chemica.*, 2013, 5, 61-74.
- [37] T. E. Ali.; S. A. A. Aziz.; S. M. E. Edfawy.; E. H. A. Mohamed.; S. M. A. Kariem *Syn. Org. Chem.*, 1-9.
- [38] S. Vodela.; R. V. R. Mekala.; H. Gadegoni, *IJRPC.*, 2014, 4, 148-153.
- [39] S. Chinnam.; C. Potturi.; S. Maddila.; V. B. R. Muttana.; A. Ediga.; V. Chinnam.; *Der Pharma Chemica.*, 2013, 5, 327-333.

# Comparative Study of Corrosion in Metals in Acidic media

Dr. Bhagyashree Chari

Xavier Institute of Engineering, Mumbai 400 016, Maharashtra, India

Email: [bhagyashree.c@xavier.ac.in](mailto:bhagyashree.c@xavier.ac.in)

## ABSTRACT

Metallic corrosion is of immense importance in industry. Present study involves a comparison on corrosion reaction between iron, copper and zinc in various acidic media at constant room temperature for a given period of time exposure. Nitric acid is found to be more corrosive than sulphuric acid under similar conditions of temperature and exposure time. Also, the severity of corrosion depends upon the position of metal in galvanic series. The weight loss method was used to check the severity of corrosion.

**Keywords:** corrosion, exposure time, galvanic series, weight loss

## INTRODUCTION

Metal industries extensively work with different types of metals in various conditions and these find enormous applications in engineering field. Corrosion Science is of interest since many years due to its impact on the environment.<sup>[1][2][3]</sup> It is not only confined to metals and alloys but also to the nanomaterials and microscopic materials. Corrosion is a kind of man – made destruction that can be prevented to some extent unlike natural hazards like volcanoes, earthquakes, etc. Most of the modern day industrial as well as domestic applications involves the use of metals and alloys and corrosion causes a heavy loss to industries and impairs the economic status of a society in general. Several industries such as automobile industry, petroleum industry, electroplating industry, paper and pulp industry, alloy manufacturing industry and chemical industry largely contribute to the phenomena of corrosion. Degradation of metals results in the reduction of their useful properties such as ductility and malleability and causes loss of cross sectional area and increase in the roughness of the surface. Corrosion is exactly reverse of metallurgy, a process of extraction of metals<sup>[4]</sup>. Some d – block elements including Iron, Copper, Cobalt, Zinc, Chromium are extensively used in industry for the engineering purposes<sup>[5][6][7]</sup>. It is essential to predict the corrosion behavior of these metals to prevent from any type of severe hazard<sup>[8]</sup>.

Present paper describes a comparative study on the corrosion reaction of three metals, viz, iron, copper and zinc in acidic media. To avoid any ambiguity, the procedures are done under similar experimental condition such as temperature, exposure time and concentration and volumes of acids. The surface areas of metals under investigation are also uniform. Previously, enormous research<sup>[9][10][11]</sup> is being conducted on behavior of metals when exposed to different corroding media. Weight loss method<sup>[12]</sup> is used for analyzing the behavior of the three metals. Profoundly, nitric acid is observed as more corrosive than sulphuric acid in all

the three cases. Further, rate of corrosion also depends upon position of zinc (on the top side), iron (medial position) and copper (towards the bottom side) in the galvanic series<sup>[13][14]</sup>. The corrosion tendency amongst the three follows the order  $Zn > Fe > Cu$ .

## METHODS AND MATERIAL

The metal sheets were procured from Jindal Company. Sulphuric acid and nitric acid were of analytical grade Merck make. All the glasswares used were made of borosilicate glass. Distilled water was obtained from water distillation plant used in lab. Acetone, used for washing was obtained from SD Fine Chemicals. Thermostatic water bath from LABPRO was used to maintain the constant temperature. All diluted acid samples were prepared as per standard procedure<sup>[15]</sup>.

Iron metal specimen 3cm X 3cm was cleaned with acetone and its initial weight was noted. Then it was immersed for 20 min. in 0.5 N sulphuric acid solution. Then, it was washed with distilled water, dried and cleaned with acetone and final weight noted. The procedure was repeated using the same iron specimen with three other sulphuric acid samples with concentrations 1.0 N, 1.5 N and 2 N respectively at room temperature 23.5°C. The weight loss was calculated after each exposure.

In another set – up, copper specimen 3cm X 3cm was immersed in 0.5 N sulphuric acid at room temperature and weight loss was noted after 20 minutes. The process was repeated by using Sulphuric acids of various concentrations, 1.0 N, 1.5 N and 2 N respectively at room temperature.

Similarly, Zinc specimen was also tested for corrosion in these acidic media.

To have a comparative study, the whole procedure was repeated by using 0.5 N, 1N, 1.5 N and 2 N Nitric acid solutions on the three metals.

## RESULTS AND DISCUSSION

According to the corrosion theory, metals have a strong tendency to displace hydrogen in acidic medium. Their electropositive nature is responsible for oxidation tendency. In the present study, when the three metals were investigated for corrosion behavior, it was observed that, zinc undergoes faster reaction as compared to iron and copper. This may be due to its higher position in galvanic series owing to its higher standard oxidation potential 0.76 V than the other two metals iron and copper with S. O. P values, 0.44 V and – 0.34 V respectively. As shown in the table 1, the weight loss is significant in zinc when exposed to nitric acid of higher concentration. Similarly, table II and III depicts the corrosion behavior in iron and copper respectively. In general, the weight loss is maximum in higher in nitric acid than in sulphuric acid as shown in the Fig 1 and Fig. 2. Nitric acid has strong oxidizing power than sulphuric acid. Therefore, rate of corrosion is maximum in the former than the latter. Corrosion continues till all the metal is oxidized, there occurs the formation of corrosion products on the surface, which make the surface rough and brownish deposits are observed as shown in Fig. 3.

TABLE I  
CORROSION IN ZINC

Concentration of Acid	Initial Weight (g)	Final weight (g) after dipping in Sulphuric acid	Final weight (g) after dipping in Nitric acid
0.5 N	2.5	2.2	1.7
1 N	2.5	1.8	1.5
1.5 N	2.5	1.5	0.9
2 N	2.5	1.1	0.8

TABLE II  
CORROSION IN IRON

Concentration of Acid	Initial Weight (g)	Final weight (g) after dipping in Sulphuric acid	Final weight (g) after dipping in Nitric acid
0.5 N	2.5	2.4	2.2
1 N	2.5	2.2	2.0
1.5 N	2.5	2.1	1.9
2 N	2.5	1.9	1.0

TABLE III  
CORROSION IN COPPER

Concentration of Acid	Initial Weight (g)	Final weight (g) after dipping in Sulphuric acid	Final weight (g) after dipping in Nitric acid
0.5 N	2.5	2.3	2.2
1 N	2.5	2.2	1.9
1.5 N	2.5	1.7	1.5
2 N	2.5	1.1	1.0

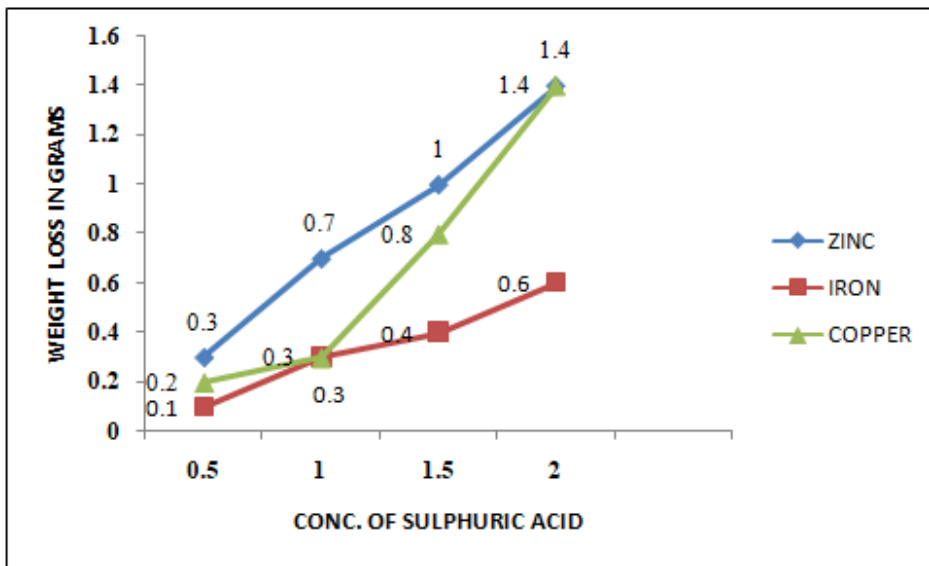


FIG 1: Effect of sulphuric acid concentrations on weight loss of metals

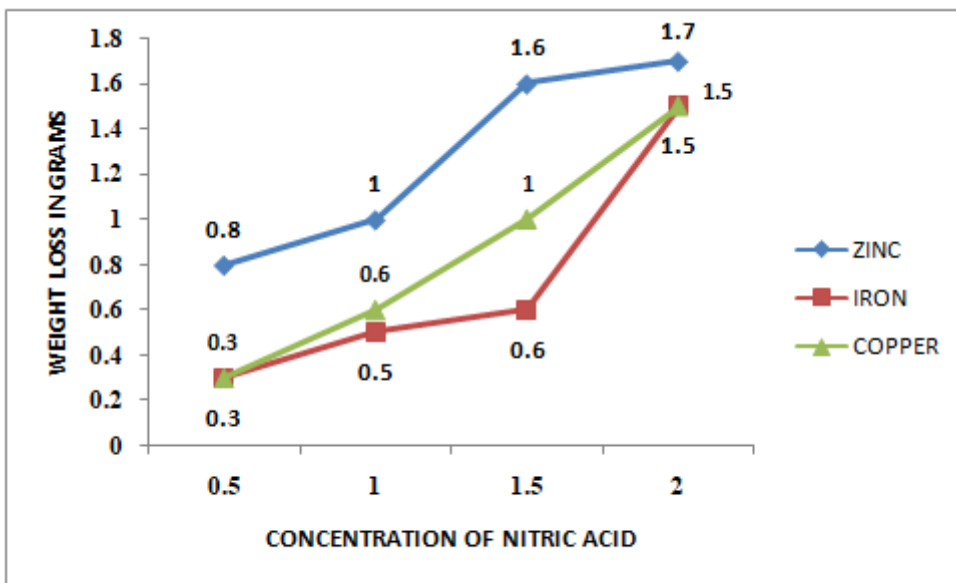


FIG 2: Effect of Nitric Acid concentrations on weight loss of metals



Fig 3. Appearance of Metal coupons after corrosion

## CONCLUSION

The metals under investigation are of enormous importance in engineering purposes such as in metallurgy, electrical industry, electroplating industry and many more. It is essential to examine the corrosion of these metals prior to use, so that, necessary measures can be adopted to prevent from any type of industrial hazard. Their corrosion behavior is in accordance with the positions in galvanic series. Higher the electrode potential value, higher is the tendency of the metal to undergo corrosion. In present study, corrosion is clearly visible in the form of blisters, and it is basically oxidation of the metal by the respective acid. The research can be further conducted to pursue chemical kinetic study of the reactions at various temperatures and time exposure.

## REFERENCES

- [1] P. R. Roberge, Handbook of Corrosion Engineering, Mc-Graw Hill Publishers, 1999.
- [2] M. G. Fontana, Corrosion Engineering, New York, Mc – Graw Hill Publishers, 1986.
- [3] W. H. Ailor, Handbook on Corrosion Testing and Evaluation, New York, John Wiley and sons 1971, pp 697.
- [4] B. Sivasankar, Engineering Chemistry, Tata McGraw Hill publishing company, New Delhi, 2008, pp 467.
- [5] Edwin C. Constable. 2019. Royal Society of Chemistry, March 2019, DOI: 10.1039/c9dt00765B
- [6] P. Pal, J. M. Ting et. al. 2021. Reactions. , September 2021, <https://doi.org/10.3390/reactions2030022>
- [7] M. Weller, J. Rourke, T. Overton and F. Armstrong, “The d-block elements”, in the book Inorganic Chemistry, (August 2023) DOI:10.1093/hesc/9780198768128.003.0021
- [8] D. A. Jones, Principles and Prevention of Corrosion, 2nd edition, Prentice Hall, Upper Saddle River, NJ.
- [9] S. A. Farooq, A. Raina, M. I. Ul Haq and Ankush Anand. 2022. Journal of the Institution of Engineers (India): Series D, Review Paper, June 2022, Volume 103, pages 639 – 661.
- [10] Ming Liu. 2023. Materials, Jan 2023, <https://doi.org/10.3390/ma16030973>.
- [11] D. B. Patil and A. Sharma, “Study on Corrosion Kinetics of Iron in Acid and Base medium”, E – Journal of Chemistry, April 2011, page 358 – 362.
- [12] Brahim El Ibrahimi and Elyor B., “Weight Loss Technique for Corrosion Measurements”, in Electrochemical and Analytical Technique for Sustainable Corrosion Monitoring: Advances, Challenges & Opportunities, Elsevier, Saudi Arabia, 2023, pages 81 – 90. <https://doi.org/10.1016/C2021-0-03502-1>
- [13] S. S. Dara and S. S. Umare, “Corrosion” in Text Book of Engineering Chemistry, S. Chand, New Delhi, 12th Edition, page 198 – 199.
- [14] P. Jain and M. Jain, T. B. of Engineering Chemistry, 16th Edition, Dhanpat Rai Publishing Co., New Delhi, 2016.
- [15] P. B. Joshi, Experiments in Engineering Chemistry, I. K. International Publishing House Ltd., New Delhi, 2016.

# Green Synthesis of Flavanones By L-Glycine

Dr. Arshia Parveen

Department of Chemistry, B. Raghunath ACS College, Parbhani, Maharashtra, India

[arshiairfanmalik@gmail.com](mailto:arshiairfanmalik@gmail.com)

## ABSTRACT

An efficient and one pot method for smooth conversion of substituted  $\alpha$ - $\beta$ -unsaturated carbonyl compounds into a range of flavanones have been synthesized in very good yield under solvent-free conditions by grinding  $\alpha$ - $\beta$ -unsaturated carbonyl compounds in the presence of L-Glycine as a catalyst and KOH. The short reaction time, clean reaction, and easy workup make this protocol green.

## INTRODUCTION

Flavanones are pharmacologically important naturally occurring compounds possessing a wide range of biological activities<sup>1</sup> as hypertensive, antibacterial, antitumor, antifungal, and anti-inflammatory agents and also used in the treatment of various diseases<sup>2</sup>. Different methods are used for the synthesis of flavones, includes Allan- Robinson synthesis<sup>3</sup>, synthesis from chalcones<sup>4</sup> and via intramolecular witting reaction<sup>5</sup>. The most common method used involves Baker- Venkatramn arrangement. In this method 2- hydroxy acetophenone are converted to benzoyl ester, which in presence of base (pyridine/KOH) form 1,3 diketones. The diketones are further cyclized under strong acidic condition to afford the flavones<sup>6</sup>. In recent development of such dehydrative cyclization it includes the use of Amberlyst-15<sup>7</sup>, CoIII(sulpr)OH<sup>8</sup>, FeCl<sub>3</sub><sup>9</sup>, Br<sub>2</sub>/CHCl<sub>3</sub><sup>10</sup>, EtOH/HCl<sup>11</sup>, clay<sup>12</sup>, NaOAc/AcOH<sup>13</sup> and H<sub>2</sub>SO<sub>4</sub> under microwave irradiation<sup>14</sup>. Prenylated flavanone is a unique class of naturally occurring flavonoids characterized by the presence of a Prenylated side chain in the flavonoid skeleton. It was reported that one phenolic group and certain degree of lipophilicity are required for the activity of the flavonoids.<sup>10</sup> Substitution of the flavonoid ring system with phenyl groups would increase their lipophilicity and consequently enhance their interaction with cellular membranes<sup>15</sup>. 4',5,7-Trihydroxy-3'-prenylflavanone (1) has been isolated for the first time in 1989 from the chloroform extract of the stem bark of *Erythrina eriotriocha*<sup>16</sup>. The chemical and pharmaceutical industries are always under the pressure to find out environmental friendly organic reaction methodologies. Microwave irradiation is used for a variety of organic reactions due to their use in a rapid and cleaner synthesis of organic compounds<sup>17-18</sup>. Ionic liquids are possible green catalyst acts as alternatives for several catalytic reactions. Ionic liquids attracted attention of researchers due to their mild reaction conditions, short reaction times and better yield, solvating ability and easy recyclibility<sup>19</sup>. Various reactions have been reported recently using ionic liquids as a catalyst, reaction media<sup>20</sup> and as rate enhancers<sup>21</sup>.



**RESULT AND DISCUSSION:**

L-Alanine, the amino acid additive in the presence of KOH and NaOH described previously<sup>22</sup>. Herein we wish to report for the synthesis of flavanone (**2**) promoted by L-Glycine as a catalyst, at room temperature in presence of base KOH and Water in excellent yield with shorter reaction time (**Scheme 1**). Comparison of the alkali hydroxides as bases showed that catalytic activities increase in the order of KOH > NaOH > LiOH Table 1. In a typical reaction, the  $\alpha$ - $\beta$ -unsaturated carbonyl compounds (**1**) in L-Glycine was grind in a motor for a specified time. The progress of the reaction was monitor by TLC. After completion of the reaction, reaction mixture was directly extracted with 50% ethyl acetate in petroleum ether. Compound comes in organic layer, was washed with water, brine & dried over MgSO<sub>4</sub>. Organic solvent is evaporated to afford pure flavanones (**2**).

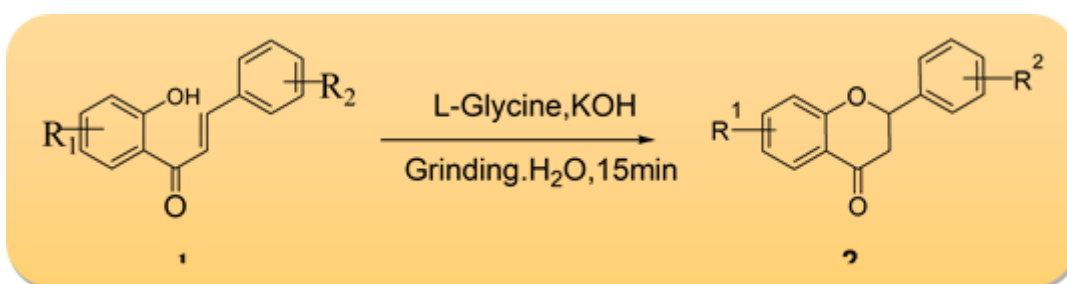
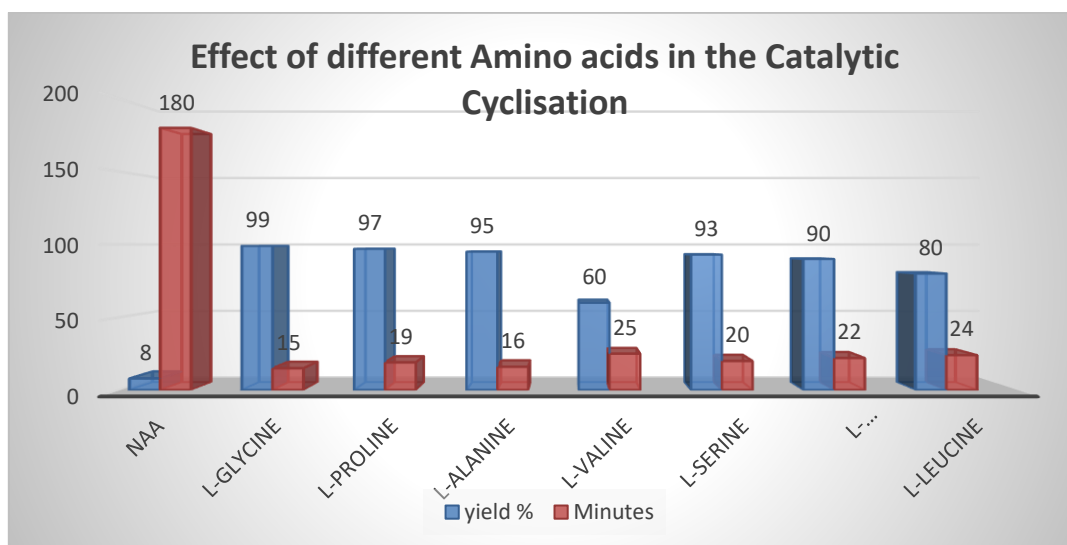
**Table1:- Effect of different bases in the catalytic cyclisation**

Sr. No	Base	Yield % (2)
1.	KOH	99%
2.	NaOH	98%
3.	LiOH	60%
4.	Ca(OH) <sub>2</sub>	40%
5.	Na <sub>2</sub> CO <sub>3</sub>	10%

We further extended our study of Different amino acid additives were examined to further enhance the catalytic activities in the presence of KOH. **Table 2** shows that (1) can be converted to (2) in just 8% yield in 180 min in the absence of amino acid. However, (1) can be completely converted to (2) very easily in the presence of most amino acids in 15-25min. This reaction time is comparable to that of microwave irradiation assisted catalysis<sup>23</sup>. It is observed that L-Proline, L-Alanine and L-Phenylalanine found to be good yield but prolong reaction time was required for completion of reaction and L-Leucine and L-Serine gives poor yield as compare to other amino acids. Therefore, we select L-Glycine because the yield is maximum in minimum reaction time.

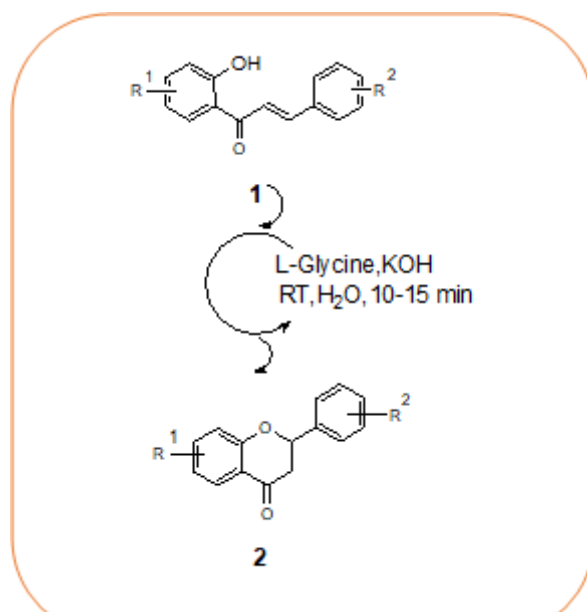
**Table 2 Effect of different amino acids in the catalytic cyclisation**

Entry	Amino Acid	Yield% (2)	Reaction Time in Minutes
1.	No Amino acid	8%	180 min
2.	L-Glycine	99%	15min
3.	L-proline	97%	19min
4.	L-Alanine	95%	16min
5.	L-Valine	60%	25min
6.	L-Serine	93%	20min
7.	L-Phenylalanine	90%	22min
8.	L-Leucine	80%	24min



**Scheme-1: Synthesis of flavanones(2-phenyl-4-H-chroman-4-one)**

In a typical reaction, the  $\alpha$ - $\beta$ -unsaturated carbonyl compounds **1** in L-Glycine was grind into motor in a specified time. The progress of the reaction was monitor by TLC. After completion of the reaction, reaction mixture was directly extracted with 50% ethyl acetate in petroleum ether. Compound comes in organic layer, was washed with water, brine & dried over MgSO<sub>4</sub>. Organic solvent is evaporated to afford pure flavanones **2**. The IR spectra of **2** shows absorption at 1690 cm<sup>-1</sup> confirms C=O and absence of peaks corresponding to chalcone and other values are identical with the known compound. To evaluate the synthetic utility of the process, various substituted chalcones were prepared by the established procedure and subjected to the reaction under rt grinding. The results are shown in Table-3. The reaction proceeds cleanly without formation of any side product except water. The protocol of the process offers advantages in terms of simple procedure and work up, mild reaction conditions and excellent yields.



**Scheme-2 Possible mechanism of (2) flavanone**

It is assumed that Amino acid with the carbonyl oxygen increasing the reactivity of the parent carbonyl of chalcone by virtue of its inherent acidity. The traditional method for synthesis of flavanone is intramolecular conjugation addition of o-hydroxychalcone **1** to the corresponding cyclic carbonylic system. However, in most of the traditional methods the conversion of chalcones to flavanone **2** is incomplete and very slow, and generally proceeds with only moderate yields. Herein we afford the method in which the L-Glycine is acting as a catalyst and water is acting reaction medium therefore, we report a simple and clean mechanism for the synthesis of the flavanone **2**.

#### EXPERIMENTAL:

The  $\alpha$ - $\beta$ -unsaturated carbonyl compounds **1** (1 mmol), KOH (8M, 0.1ml) was added L-Glycine (2 mmol) in water 10 ml and grind into mortar for 10-15 min. The reaction was monitored on TLC. After completion on the reaction, the mixture was extracted 5 X 20 ml. of ethyl acetate: petroleum ether (50%+50%). Compound comes in organic layer, was again treated with water, brine & dried over MgSO<sub>4</sub>. Organic solvent is evaporated to afford pure flavanones **2**. The obtained products **2a-j** were identified by comparison with authentic samples <sup>1</sup>H NMR and their melting points.

**Spectral Data:** Melting points were determined in open glass capillaries and uncorrected. <sup>1</sup>H NMR and <sup>13</sup>C NMR spectra were recorded at room temperature on a Varian Inova Spectrometer in CDCl<sub>3</sub> using TMS as internal standard. The spectral data of some selected compounds:

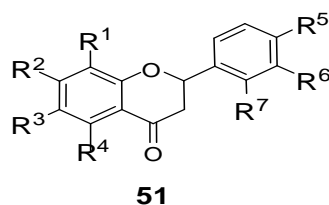


**Table-3** Synthesis of Flavanone **2** derivatives by using L-Glycine, KOH and H<sub>2</sub>O at RT.

Product	R <sup>1</sup>	R <sup>2</sup>	R <sup>3</sup>	R <sup>4</sup>	R <sup>5</sup>	R <sup>6</sup>	R <sup>7</sup>	Time (min)	Yield (%)
<b>2a</b>	H	H	H	H	H	H	H	10	85
<b>2b</b>	H	H	H	H	Cl	H	H	15	88
<b>2c</b>	H	H	H	H	OMe	H	H	14	89
<b>2d</b>	H	H	Me	H	OMe	H	H	17	84
<b>2e</b>	H	H	H	H	OMe	OMe	H	16	85
<b>2f</b>	H	OH	H	H	H	H	H	18	87
<b>2g</b>	H	H	H	H	H	H	Cl	20	86
<b>2h</b>	H	H	H	H	H	OMe	H	22	87
<b>2i</b>	H	H	H	H	Br	H	H	20	85
<b>2j</b>	H	H	H	H	H	H	NO <sub>2</sub>	15	88

**Compound 2b:** <sup>1</sup>H NMR (300 MHz, CDCl<sub>3</sub>) δ 2.44 (s, 3H), 7.22 (s, 1H), 7.69 (dd, 1H, J = 8.9, 2.1 Hz), 7.74 (d, 1H, J = 8.6 Hz), 7.85 (m, 1H), 8.38 (s, 4H); <sup>13</sup>C NMR (125 MHz, CDCl<sub>3</sub>) 21.5, 109.9, 119.6, 125.1, 125.3, 128.8, 136.5, 136.8, 138.3, 149.7, 154.8, 160.6, 177.2. **Compound 2e:** <sup>1</sup>H NMR (300 MHz, CDCl<sub>3</sub>) δ 3.95 (s, 3H), 3.98 (s, 3H), 6.72 (s, 1H), 6.96 (d, 1H, J = 8.1 Hz), 7.36 (d, 1H, J = 1.8 Hz), 7.40 (dd, 1H, J = 7.2 Hz, J = 7.5 Hz), 7.51 (dd, 1H, J = 1.8 Hz, J = 8.1 Hz), 7.53 (d, 1H, J = 7.5 Hz), 7.67 (ddd, 1H, J = 1.5 Hz, J = 7.2, J = 7.8 Hz), 8.20 (dd, 1H, J = 1.5 Hz, J = 7.8 Hz); <sup>13</sup>C NMR (125 MHz, CDCl<sub>3</sub>) 56.1, 106.4, 108.8, 111.2, 118.0, 120.0, 123.9, 124.2, 125.6, 133.6, 149.3, 152.1, 156.1, 163.3, 178.3.

**Compound 2f:** <sup>1</sup>H NMR (300 MHz, CDCl<sub>3</sub>) δ 6.91 (s, 1H), 7.95 (dd, 1H, J = 1.8, J = 9.0 Hz), 7.02 (d, 1H, J = 1.8 Hz), 7.57-7.29 (m, 3H), 7.91 (d, 4H, J = 9.0 Hz), 8.05-8.08 (m, 2H); 10.8 (s, 1H); <sup>13</sup>C NMR (125 MHz, CDCl<sub>3</sub>) 102.6, 106.6, 115.1, 116.2, 126.2, 126.5, 129.1, 131.3, 131.5, 157.5, 161.2, 162.8, 176.4.

## CONCLUSION:

In summary we have demonstrated an efficient and mild protocol for the dehydrative cyclization of α-β-unsaturated carbonyl compounds to flavanones in presence of L-Glycine as a catalyst by grinding. Shorter reaction time, simple reaction conditions and higher yield render this grinding method superior. The method is clean and simple, which can be used as an alternative to the existing methods.

**Acknowledgement:** The author is Thankful to the Department of Chemistry, B. Raghunath ACS college Parbhani.

## REFERENCES

- [1] A.F. Welton, L.D. Tobias, C. Fiedler-Nagy, W. Anderson, W. Hope, K. Middleton Jr; J.B. Harbirne and A.R. Liss, New York; 1986, 231.
- [2] Havsteen, Biochem. Pharmacol., 1983, 32,1141.

- [3] A. Banerji and N. Goomer, *Synthesis*, 1980, 874.
- [4] Y. Hoshino, T. Oohinata and N. Takeno, *Bull. Chem. Soc. Jpn*; 1986, 59, 2351.
- [5] Y. LeFloch'h and M. LeFeuvre, *Tetrahedron Lett*; 1986, 27, 2751.
- [6] M. Balogh and P. Laszlo, *Organic Chemistry Using Clays*, Springer, Berlin, 1993, J. Chisen, I. C. Chisen, J. S. Rafelt, D. J. Macquarrie and J. H. Clark, *Chem. Commun.*, 1997, 2203.
- [7] Y. Hoshino and N. Takino, *Bull. Chem. Soc. Jpn.* 1987, 60, 1919-1920.
- [8] A Nishinaga, H. Ando, K. Maruyama and T. Mashino, *Synthesis* 1982, 839.
- [9] P.K. Zubaidha, A.M Hashmi and R.S. Bhosale, *Heterocyclic Commun.* 2005, 11, 9100.
- [10] S. Garg, M. P. S. Ishar, R. Sarin, R.P. Gandhi, *Indian J. Chem. Soc.* 1994, 33B, 1123- 1128.
- [11] J.C. Jung, J. P Min and O. S. Park, *Synth. Commun.* 2001, 31(12), 1837-
- [12] R.S. Verma, R. K Saini and D. Kumar, *J. Chem. Res. (S)*. 1998, 348- 349.
- [13] P.E. Kumar and K.J.R. Prashad, *Indian J. Chem.* 1999, 38B, 1277- 1279.
- [14] M. Tsukayama, Y. Kawamura, T. Ishizuka, S. Hayas and F. Torii, *Heterocycles*, 2003, 60 (12), 2775.
- [15] Baron D , Ragai K I. *Phytochemistry* 1989, 27 87
- [16] Nkengfack A E, Sanson D R , Tempesta M S J. *Nat. Prod.* 1989, 52 320
- [17] R.S. Varma, M. Varma and A.K. Chatterjee, *J. Chem. Soc., Perkin Trans.* 1993, 1, 999; R.S. Varma, A. K. Chatterjee, and M. Varma, *Tetrahedron Lett.*, 1993, 34, 3207; R.S. Varma, J. B. Lamture and M. Varma, *Tetrahedron Lett.*, 1993, 34, 3029; R.S. Varma, A.K. Chatterjee, and M. Varma, *Tetrahedron Lett.*, 1993, 34, 4603.
- [18] J.M. Lerestif, L. Toupet, S. Sinbandhit, F. Tonnerd, J.P. Bazureau and J. Hanelin, *Tetrahedron*, 1997, 53, 6351; A.L. Marrero-Terrero and A. Loupy, *Synlett*, 1996, 245; A. Benalloum, B. Labiad and D. Villemin, *Chem. Commun.*, 1998, 386.
- [19] T. Welton, *Chem. Rev.* 1999, 99, 2071. P. Wassercheid and W. Keim, *Angew. Chem. Int. Ed.* 2000, 39, 3772; R. Sheldon, *Chem. Commun.* 2001, 2399; D. Zhao, M. Wu, Y. Kou and K. Min, *Catal. Today*. 2002, 1, 2654.
- [20] R. Rajgopal, D.V. Jarikote, R.J. Lahoti, D.Thomas, K.V. Srinivasan, *Tetrahedron Lett.* 2003, 44, 1615; D.V. Jarikote, S.A. Siddiqui, R. Rajgopal, D.Thomas, R.J. Lahoti and K.V. Srinivasan, *Tetrahedron Lett.* 2003, 44, 1835; A.R. Gholap, K. Venkatesan, D. Thomas, R.J. Lahoti and K. V. Srinivasan, *Green Chem.* 2004, 6, 147-150; S.P. Panchgalle, U.R. Kalkote, P.S. Nipahadkar, P.N. Joshi, S.P. Chavan and G.M. Chaphekar, *Green Chem.* 2004, 6, 308-309.
- [21] B.R. Madje, S.S. Shindalkar and M.S. Shingare, *Indian Journal of Heterocyclic Chem.* 2004, 14, 87-88. [22] T. Walton, *Chem. Rev.* 1999, 99, 2071; P. Walden, *Bull. Acad. Imper. Sci. (St. Petersburg)*
- [22] a) Heyan Jiang, Xuxu Zheng\*, Zhongyi Yin and Jingjing Xie, *Journal of Chemical Research*, 2011, 220-221. b) K. Tanaka and T. Sugino, *Green Chem.*, 2001, 3, 133.
- [23] D. Kumar, G. Patel, A. Kumar, R.K. Roy, *J. Heterocyclic Chem.*, 2009, 46, 791.

# Sustainable Practices in Chemical Synthesis : A Comprehensive Review

Dr. Sanghratna L. Kasare

Late Shankarrao Gutte Gramin Arts, Commerce, and Science College Dharmapuri, Dist- Beed 431515, Maharashtra, India

## ABSTRACT

Sustainability in chemical synthesis has emerged as a vital focus of research and industry, driven by the need to mitigate the environmental impact of chemical processes. Sustainable practices in chemical synthesis involve the efficient use of resources, minimizing waste, and reducing harmful emissions. This review discusses the core principles of sustainable chemistry, highlights innovative technologies, and provides examples from academic and industrial settings. Key topics include atom economy, catalysis, renewable feedstocks, and energy-efficient processes. Case studies from the pharmaceutical, polymer, and agrochemical industries illustrate the practical implementation of sustainable chemistry.

**Keywords:** Sustainable chemistry, green chemistry, atom economy, catalysis, renewable feedstocks, energy efficiency

## INTRODUCTION

The environmental impact of industrial chemical processes has prompted a shift toward sustainable practices in chemical synthesis. Traditional chemical processes often rely on hazardous reagents, generate significant waste, and consume large amounts of energy, leading to negative environmental consequences. In response, sustainable chemistry, also known as green chemistry, has emerged as a framework to minimize the ecological footprint of chemical manufacturing.

Green chemistry emphasizes the design of products and processes that reduce or eliminate the generation of hazardous substances. This review explores sustainable practices in chemical synthesis, focusing on advances in atom economy, catalysis, the use of renewable feedstocks, and energy-efficient technologies. Real-world examples from various sectors demonstrate the benefits of adopting sustainable practices.

## PRINCIPLES OF SUSTAINABLE CHEMISTRY

Sustainable chemistry is guided by 12 principles, first outlined by Anastas and Warner in 1998. These principles are designed to reduce the environmental impact of chemical processes and promote sustainability.

Key principles include:

1. **Waste Prevention:** Processes should be designed to minimize waste production.

2. **Atom Economy:** Chemical reactions should maximize the incorporation of starting materials into the final product.
3. **Less Hazardous Chemical Syntheses:** Reactions should use and generate substances with minimal toxicity to human health and the environment.
4. **Designing Safer Chemicals:** Chemical products should be designed to be effective while minimizing toxicity.
5. **Use of Renewable Feedstocks:** Raw materials should be renewable whenever technically and economically viable.
6. **Energy Efficiency:** Energy use should be minimized, and processes should ideally occur at ambient temperature and pressure.

These principles serve as a blueprint for sustainable chemical synthesis, guiding the development of new methods and technologies.

## ATOM ECONOMY IN SUSTAINABLE CHEMICAL SYNTHESIS

### 3.1 Definition and Importance

Atom economy, introduced by Barry Trost in 1995, is a metric for measuring the efficiency of a chemical reaction based on how much of the reactants are incorporated into the final product. In contrast to traditional yield-based metrics, atom economy accounts for the generation of waste byproducts. Reactions with high atom economy are more sustainable because they reduce the amount of raw materials and energy required, and they minimize waste production.

### 3.2 Examples of Atom-Efficient Reactions

One example of a highly atom-efficient reaction is the **Diels-Alder reaction**, a pericyclic reaction between a diene and a dienophile that forms a six-membered ring without generating byproducts. The Diels-Alder reaction is widely used in organic synthesis and industrial applications because of its 100% atom economy. Another notable example is the **hydroamination of alkenes**, a reaction that adds an amine to an alkene without the need for activating reagents. This reaction is atom-efficient because it avoids the formation of side products and utilizes both reactants entirely in the final product.

In the pharmaceutical industry, atom economy has been applied to optimize drug synthesis. For example, the **synthesis of ibuprofen** was traditionally a six-step process with low atom economy, generating significant waste. A newer method, developed by BHC Company, reduces the process to just three steps, improving atom economy and reducing waste production by 70% [1].

## CATALYSIS: A CORNERSTONE OF SUSTAINABLE SYNTHESIS

### 4.1 Role of Catalysts in Sustainability

Catalysts play a crucial role in sustainable chemical synthesis by lowering the activation energy of reactions, increasing reaction rates, and reducing the energy required for chemical transformations. Catalysts also allow reactions to proceed with fewer byproducts, improving both yield and atom economy. The use of

catalysts is essential for making chemical processes more sustainable, as they enable more efficient and selective reactions.

#### 4.2 Types of Catalysts

Catalysts used in sustainable chemistry include homogeneous, heterogeneous, and biocatalysts:

**Homogeneous Catalysts:** These catalysts are in the same phase as the reactants, typically in a liquid solution. Transition metal catalysts, such as palladium or rhodium complexes, are widely used in homogeneous catalysis. For example, the **Suzuki-Miyaura coupling reaction**, which forms carbon-carbon bonds, is catalyzed by palladium complexes and is essential in the synthesis of pharmaceuticals and agrochemicals [2].

**Heterogeneous Catalysts:** In heterogeneous catalysis, the catalyst is in a different phase (usually solid) than the reactants. Heterogeneous catalysts are easily separated from the reaction mixture and reused, making them ideal for large-scale industrial applications. For instance, **hydrogenation reactions** commonly use solid metal catalysts like platinum or nickel to reduce alkenes to alkanes with high efficiency.

**Biocatalysts:** Enzymes and whole-cell catalysts are used in biocatalysis, which often operates under mild conditions (ambient temperature and pressure) and in water. Biocatalysis is particularly useful for asymmetric synthesis, where it produces enantiomerically pure products. The synthesis of **pregabalin**, a drug used to treat neuropathic pain, utilizes an enzyme-catalyzed step to introduce chirality, making the process both efficient and environmentally friendly [3].

#### 4.3 Case Study: Catalysis in the Pharmaceutical Industry

In the synthesis of the anti-inflammatory drug celecoxib, Pfizer implemented a palladium-catalyzed coupling reaction to replace a traditional stoichiometric method that produced significant waste. The catalytic process reduced the environmental impact of the synthesis and improved the overall efficiency by increasing yield and atom economy [4].

### RENEWABLE FEEDSTOCKS: REDUCING RELIANCE ON FOSSIL FUELS

#### 5.1 Introduction to Renewable Feedstocks

A key aspect of sustainable chemical synthesis is the shift from fossil-derived feedstocks to renewable resources. Renewable feedstocks, such as biomass, provide a sustainable source of carbon and other elements for chemical production. These feedstocks are derived from biological materials like plants, algae, and agricultural waste, and they offer an alternative to petrochemical-based starting materials.

#### 5.2 Examples of Renewable Feedstocks in Chemical Synthesis

One prominent example of a renewable feedstock is **lignocellulosic biomass**, which consists of cellulose, hemicellulose, and lignin. This biomass can be converted into valuable chemicals such as ethanol, furfural, and levulinic acid through fermentation and catalytic processes. **Bioethanol**, produced from sugarcane or corn, is used as a renewable fuel and a feedstock for the production of chemicals like ethylene, which is a key building block in the manufacture of plastics [5].

**Polylactic acid (PLA)**, a biodegradable polymer, is another example of a product derived from renewable feedstocks. PLA is synthesized from lactic acid, which can be produced via the fermentation of corn starch. PLA has applications in packaging, textiles, and medical devices, providing an eco-friendly alternative to traditional plastics derived from fossil fuels.



### 5.3 Challenges in Implementing Renewable Feedstocks

While renewable feedstocks offer significant environmental benefits, there are challenges associated with their use. The processing of biomass often requires harsh conditions, and the separation of desired chemicals from complex mixtures can be energy-intensive. Additionally, the large-scale implementation of renewable feedstocks may compete with food production, raising concerns about land use and food security.

Despite these challenges, advancements in biotechnology and catalysis are improving the efficiency of converting biomass into valuable chemicals. For example, the use of **biorefineries**, which integrate biomass processing with chemical production, offers a promising solution for producing renewable chemicals on an industrial scale [6].

## GREEN SOLVENTS: REDUCING ENVIRONMENTAL IMPACT

### 6.1 Introduction to Green Solvents

Traditional solvents, such as chlorinated hydrocarbons and volatile organic compounds (VOCs), are often toxic and environmentally damaging. Green chemistry promotes the use of solvents that are safer for both human health and the environment. Green solvents are non-toxic, biodegradable, and derived from renewable sources.

### 6.2 Examples of Green Solvents

**Water** is the most sustainable solvent available, as it is non-toxic, abundant, and inexpensive. Water is increasingly being used as a solvent in chemical reactions, especially in biocatalysis and environmental applications. For instance, water-based oxidation reactions have been developed to replace traditional solvent-based processes, reducing the overall toxicity and environmental impact of the reaction [7].

**Supercritical carbon dioxide (scCO<sub>2</sub>)** is another example of a green solvent. In its supercritical state, CO<sub>2</sub> exhibits properties of both a gas and a liquid, making it an effective solvent for extractions and reactions. Supercritical CO<sub>2</sub> is non-toxic and can be easily recycled, making it an ideal solvent for applications such as the decaffeination of coffee and the extraction of essential oils [8].

**Ionic liquids** are salts that are liquid at low temperatures and are considered green solvents because they have low volatility and can be designed for specific reactions. Ionic liquids have been used in various applications, including catalysis, electrochemistry, and separations. Their tunable properties make them versatile solvents for sustainable chemical processes [9].

### 6.3 Case Study: Green Solvents in the Agrochemical Industry

In the synthesis of crop protection agents, Bayer developed a process using supercritical CO<sub>2</sub> as a solvent for the production of an insecticide. The use of scCO<sub>2</sub> reduced the need for toxic organic solvents and improved the overall environmental profile of the synthesis [10].

## ENERGY EFFICIENCY IN CHEMICAL SYNTHESIS

### 7.1 Importance of Energy Efficiency

Energy consumption is a major contributor to the environmental impact of chemical processes. Traditional chemical reactions often require high temperatures and pressures, leading to significant energy use and

greenhouse gas emissions. Energy-efficient chemical processes are essential for reducing the carbon footprint of chemical manufacturing.

### 7.2 Energy-Efficient Technologies

One approach to improving energy efficiency is the use of **microwave-assisted synthesis**, which uses microwave radiation to heat the reaction mixture directly, reducing reaction times and energy consumption. Microwave-assisted reactions have been widely adopted in organic synthesis and have been shown to improve both yield and selectivity [11].

Another energy-efficient technology is **flow chemistry**, where reactions are conducted in a continuous flow system rather than in batch reactors. Flow chemistry offers better control over reaction conditions, leading to improved efficiency and scalability. Flow reactors are also more energy-efficient because they allow for precise temperature control and heat transfer [12].

### 7.3 Case Study: Energy Efficiency in Polymer Synthesis

The production of polymers, such as polyethylene and polypropylene, is energy-intensive due to the high temperatures and pressures required for polymerization. Dow Chemical developed a new catalyst system that allows for the polymerization of ethylene at lower temperatures and pressures, reducing energy consumption by 30% compared to traditional methods. This innovation has significantly improved the sustainability of polymer production [13].

## CASE STUDIES OF SUSTAINABLE PRACTICES IN INDUSTRY

### 8.1 Pharmaceutical Industry

The pharmaceutical industry has been a leader in adopting sustainable practices in chemical synthesis. Companies like Pfizer, Merck, and GlaxoSmithKline have developed green synthetic routes for drug production, reducing waste and improving process efficiency. One notable example is the synthesis of the antiretroviral drug efavirenz, where a new catalytic process reduced the use of hazardous reagents and improved atom economy [14].

### 8.2 Agrochemical Industry

In the agrochemical industry, sustainable practices have been implemented in the synthesis of pesticides and herbicides. BASF developed a process for the production of a fungicide using renewable feedstocks and a catalytic hydrogenation step, reducing the environmental impact of the synthesis by 40% [15].

### 8.3 Polymer Industry

The polymer industry has made significant strides in adopting sustainable practices, particularly in the development of biodegradable and bio-based polymers. The production of **polyhydroxyalkanoates (PHAs)**, a biodegradable polymer derived from bacterial fermentation, offers a sustainable alternative to traditional plastics. PHAs are used in applications such as packaging, agriculture, and medical devices, providing a greener solution to plastic waste [16].

## CHALLENGES AND FUTURE DIRECTIONS

While significant progress has been made in sustainable chemical synthesis, challenges remain. The scalability of green processes, the economic viability of renewable feedstocks, and the development of new catalysts are areas that require further research and innovation. Collaboration between academia, industry, and government will be essential for overcoming these challenges and promoting the widespread adoption of sustainable practices.

Future research should focus on the development of more efficient catalysts, the discovery of new renewable feedstocks, and the integration of green chemistry principles into existing industrial processes. Additionally, advances in artificial intelligence and machine learning offer promising opportunities for optimizing chemical processes and accelerating the development of sustainable technologies.

## CONCLUSION

Sustainable practices in chemical synthesis are critical for reducing the environmental impact of chemical manufacturing. Advances in atom economy, catalysis, renewable feedstocks, green solvents, and energy-efficient technologies have paved the way for more sustainable chemical processes. Real-world examples from the pharmaceutical, agrochemical, and polymer industries demonstrate the successful implementation of these practices.

As the demand for environmentally friendly products and processes continues to grow, the principles of green chemistry will play an increasingly important role in shaping the future of chemical synthesis. By adopting sustainable practices, the chemical industry can reduce its ecological footprint and contribute to a more sustainable world.

## REFERENCES

- [1] Trost, B. M. (1995). Atom Economy—A Challenge for Organic Synthesis: Homogeneous Catalysis Leads the Way. *Angew. Chem. Int. Ed. Engl.*, 34(3), 259-281.
- [2] Miyaura, N., & Suzuki, A. (1995). Palladium-Catalyzed Cross-Coupling Reactions of Organoboron Compounds. *Chem. Rev.*, 95(7), 2457-2483.
- [3] Sheldon, R. A., & Woodley, J. M. (2018). Role of Biocatalysis in Sustainable Chemistry. *Chem. Rev.*, 118(2), 801-838.
- [4] Hays, P. J., & Adams, A. (2012). Green Chemistry in the Pharmaceutical Industry. *Green Chem.*, 14(1), 96-100.
- [5] Zhang, Y. H. P., & Lynd, L. R. (2010). Toward an Integrated Biorefinery. *Biotechnol. Bioeng.*, 105(1), 71-83.
- [6] Clark, J. H., & Luque, R. (2010). Green Chemistry for Sustainable Biofuel Production. *Energy Environ. Sci.*, 3(3), 292-301.
- [7] Anastas, P. T., & Zimmerman, J. B. (2003). Design through the 12 Principles of Green Engineering. *Environ. Sci. Technol.*, 37(5), 94A-101A.

- [8] Jessop, P. G., Leitner, W., & Leitner, W. (2000). Supercritical Fluids as Green Solvents: Progress and Prospects. *Chem. Rev.*, 100(2), 3649-3665.
- [9] Welton, T. (1999). Room-Temperature Ionic Liquids: Solvents for Synthesis and Catalysis. *Chem. Rev.*, 99(8), 2071-2083.
- [10] Ritter, S. K. (2007). Going Green with Bayer CropScience. *Chem. Eng. News*, 85(3), 38-41.
- [11] Varma, R. S. (2016). Microwave-Assisted Organic Synthesis: A Green Chemical Approach. *Green Chem.*, 18(1), 122-139.
- [12] Plutschack, M. B., Pieber, B., Gilmore, K., & Seeberger, P. H. (2017). The Hitchhiker's Guide to Flow Chemistry. *Chem. Rev.*, 117(18), 11796-11893.
- [13] Matyjaszewski, K. (2008). Atom Transfer Radical Polymerization (ATRP): Current Status and Future Perspectives. *Macromolecules*, 41(19), 6757-6765.
- [14] Snee, L. W. (2010). Green Chemistry in the Pharmaceutical Industry. *Green Chem.*, 12(5), 751-756.
- [15] Dearden, J. C., & Cronin, M. T. D. (2016). Green Chemistry in Agrochemical Synthesis. *Green Chem.*, 18(1), 75-92.
- [16] Sudesh, K., Abe, H., & Doi, Y. (2000). Synthesis, Structure and Properties of Polyhydroxyalkanoates: Biological Polyesters. *Prog. Polym. Sci.*, 25(10), 1503-1555.

# Complexation of Zinc Metal with Medicinal Drugs in Mixed Solvent Media

Ramesh Ware<sup>1</sup>, Rajpal Jadhav<sup>2</sup>, Hansaraj Joshi<sup>2</sup>, Shailendrasingh Thakur<sup>1</sup>

<sup>1</sup>Department of Chemistry, Milliya Art's, Science & Management Science College, Beed, Maharashtra, India

<sup>2</sup>Department of Chemistry, Swa. Sawarkar College, Beed, Maharashtra, India

## ABSTRACT

The stability constant of seven medicinal drugs with Zn (II) metal ion were investigate using pH metric titration technique in 20%(v/v) ethanol-water mixture at 300 K temperature and at an ionic strength of 0.1M NaClO<sub>4</sub>. {Metal to ligand ratio = 1:5 and 1:1} The method of Calvin and Bjerrum as adopted by Irving and Rossotti has been employed to determine proton- ligand pK<sub>a</sub> and metal-ligand stability constant logK values. It is observed that copper metal ion forms 1:1 and 1:2 complexes.

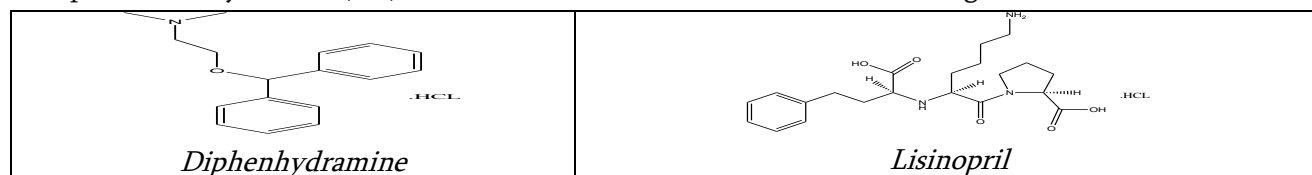
**Keywords:** Stability Constant, zinc metal, medicinal drugs, pH metry.

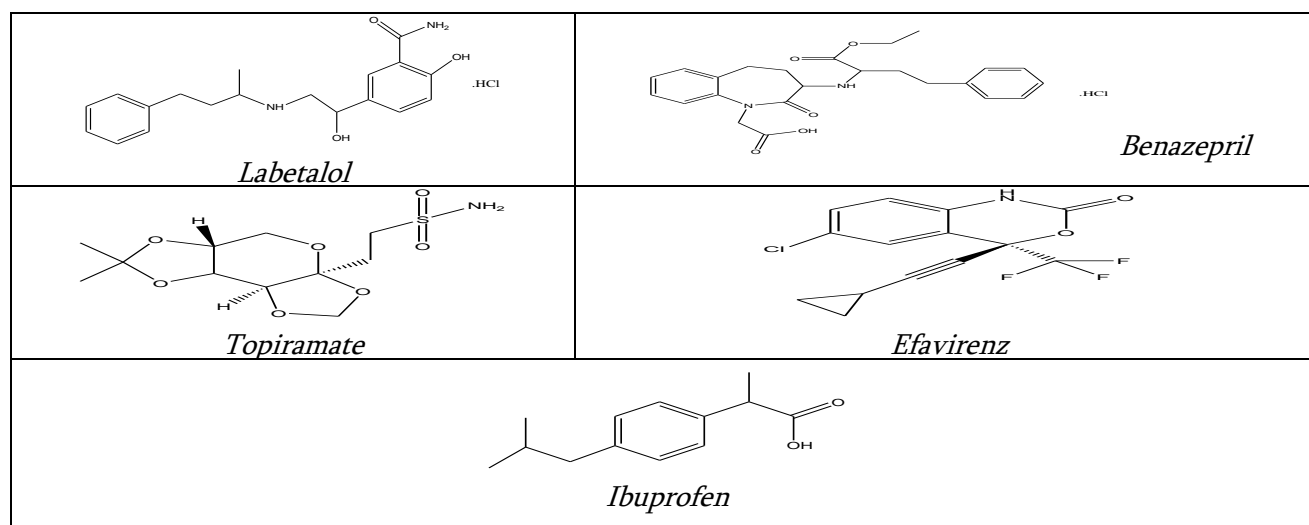
## INTRODUCTION

Metal complexes with various ligand shows their contribution in the field of pollution control, medicine, industries, analytical chemistry, pharmacology, pathology biochemistry, metallurgy etc. These metal complexes like cisplatin and auranofin are used as drugs on the treatment of genitourinary, head and neck tumours and rheumatoid arthritis respectively. Jannik Bjerrum developed the general method for determination and calculation of stability constants of metal amine complexes. Further studies were carried by Neil Bjerrum on kinetics and equilibrium study to explain stepwise formation constants. Martell et.al carried work on stability constant of metal complexes of inorganic, organic, biological ligands and significantly contributed towards coordination chemistry.

Most of the d-block elements form complexes. For the present investigation, we selected seven medicinal drugs as Diphenhydramine (L<sub>1</sub>), Lisinopril (L<sub>2</sub>), Labetalol (L<sub>3</sub>), Benazepril (L<sub>4</sub>), Topiramate (L<sub>5</sub>), Efavirenz (L<sub>6</sub>) and Ibuprofen(L<sub>7</sub>)

In continuation of our earlier work with complexation of medicinal drugs<sup>01-16</sup> and after literature survey we have carried out a solution study on the complexation of seven medicinal drugs with transition metal ion Zn<sup>2+</sup> pH metrically in 20% (v/v) ethanol-water mixture at constant ionic strength of 0.1M NaClO<sub>4</sub>.





## METHODS AND MATERIAL

NaOH, NaClO<sub>4</sub>, HClO<sub>4</sub>, Zinc metal salt were of AR grade. All medicinal drugs are soluble in 20% (v/v) ethanol-water mixture. The solutions used in the pH metric titration were prepared in double distilled water. NaOH solution was standardized against oxalic acid solution and standard alkali solution was again used for standardization of HClO<sub>4</sub>. The measurements were made at temperature 300K in 20% (v/v) ethanol-water mixture at ionic strength 0.1M NaClO<sub>4</sub>. Water thermostat is used to maintain the temperature constant. pH measurement was made using Elico L<sub>1</sub>-120 pH meter in conjunction with glass and reference calomel electrode. The instrument was calibrated at pH 7.00 and 4.00 using standard buffer solutions.

For evaluating the protonation constant of

the ligand and the formation constant of the complexes in 20 % (v/v) ethanol-water mixture with Zinc metal ion we prepare the following sets of solutions.

- (A) HClO<sub>4</sub> (A)
- (B) HClO<sub>4</sub>+ medicinal drug (A+ L)
- (C) HClO<sub>4</sub>+ medicinal drug + Zinc Metal (A+ L+ M)

Above mentioned sets prepared by keeping M: L ratio, concentration of perchloric acid and sodium perchlorate were kept constant for all sets. The volume of every mixture was made up to 50ml with double distilled water and the reaction solution were pH meterically titrated against the standard alkali at temperature 300K.

**Table. 1** PROTON-LIGAND STABILITY CONSTANT OF MEDICINAL DRUGS IN 20% (V/V) ETHANOL-WATER MEDIUM

Sr. No.	Ligands (Drug)	Proton-ligand stability constant	
		pK <sub>1</sub>	pK <sub>2</sub>
1	Diphenhydramine Hydrochloride(L <sub>1</sub> )	.....	9.3814
2	Lisinopril Hydrochloride(L <sub>2</sub> )	3.3231	7.5482
3	Labetalol Hydrochloride(L <sub>3</sub> )	---	7.7424
4	Benazepril Hydrochloride(L <sub>4</sub> )	---	3.6486

5	Topiramate (L <sub>5</sub> )	---	8.9864
6	Efavirenz (L <sub>6</sub> )	---	10.7206
7	Ibuprofen (L <sub>7</sub> )	---	5.2366

**Table. 2** METAL-LIGAND STABILITY CONSTANT OF MEDICINAL DRUGS IN 20% (V/V) ETHANOL-WATER MEDIUM  
{METAL TO LIGAND RATIO =1:5}

Sr. No.	Ligands (Drug)	Metal-ligand stability constant		
		logK <sub>1</sub>	logK <sub>2</sub>	logβ
1	Diphenhydramine Hydrochloride(L <sub>1</sub> )	5.7804	4.3653	10.145
2	Lisinopril Hydrochloride(L <sub>2</sub> )	3.4064	2.8612	6.2676
3	Labetalol Hydrochloride(L <sub>3</sub> )	3.2344	2.9832	6.2176
4	Benazepril Hydrochloride(L <sub>4</sub> )	2.8581	2.7614	5.6195
5	Topiramate (L <sub>5</sub> )	3.9083	3.8072	7.7155
6	Efavirenz (L <sub>6</sub> )	6.3522	5.8070	12.1592
7	Ibuprofen (L <sub>7</sub> )	3.0769	2.8843	5.9612

**Table. 3** METAL -LIGAND STABILITY CONSTANT OF MEDICINAL DRUGS IN 20% (V/V) ETHANOL-WATER MEDIUM  
{METAL TO LIGAND RATIO =1:1}

Sr. No.	Ligands (Drug)	Metal-ligand stability constant		
		logK <sub>1</sub>	logK <sub>2</sub>	logβ
1	Diphenhydramine Hydrochloride(L <sub>1</sub> )	5.5167	--	5.5167
2	Lisinopril Hydrochloride(L <sub>2</sub> )	4.1102	--	4.1102
3	Labetalol Hydrochloride(L <sub>3</sub> )	3.7286	--	3.7286
4	Benazepril Hydrochloride(L <sub>4</sub> )	3.8440	--	3.8440
5	Topiramate (L <sub>5</sub> )	4.4424	--	4.4424
6	Efavirenz (L <sub>6</sub> )	7.4636	--	7.4636
7	Ibuprofen (L <sub>7</sub> )	3.7082	--	3.7082

## RESULT AND DISCUSSION

The proton ligand stability constants of all seven drugs were determined in 20% (v/v) ethanol-water medium at 27 °C temperature and at 0.1M ionic strength (NaClO<sub>4</sub>). The proton-ligand stability constants of all the drugs are presented in Table 1. The drug L<sub>2</sub> have two pK values where as L<sub>1</sub>, L<sub>3</sub>, L<sub>4</sub>, L<sub>5</sub>, L<sub>6</sub> and L<sub>7</sub> has only one pK value. The  $\bar{n}_A$  value ranges between 0.2 to 1.8 indicates the presence of two pK values whereas the range of  $\bar{n}_A$  is in between 0.2 to 0.8 shows one pK value. In the present investigation drugs selected contains amino group(s), carboxyl or hydroxyl groups as bonding sites.

The order of pK<sub>a</sub> values of seven drugs is as follows.

$$L_2 > L_6 > L_1 > L_5 > L_3 > L_7 > L_4$$

The above order indicates that L<sub>4</sub> (benazepril) has lowest basicity whereas L<sub>2</sub> (lisinopril) has highest basicity. The present drugs are diverse in nature hence it is difficult to correlate pK<sub>a</sub> values of one drug with other. The experimentally calculated values of logK<sub>1</sub>, logK<sub>2</sub> and logβ of the complexes of drugs with Zn (II) metal ion are presented in **Table 2**. An examination of titration curve indicates that complex formation takes place in solution on following grounds. The metal titration curve of solution shows displacement with respect to ligand titration curve of solution along volume axis. This indicates affinity of ligand to metal ions which release proton and produce volume difference. In another words on addition of metal ion to free ligand solution shifted the buffer region of ligand to lower pH value. A large decrease in pH for metal titration curves relative to ligand titration curve might be attributed to strong metal-ligand interactions. In all the systems studied, the deviation of metal titration curve from ligand titration curve lies in the region where hydrolysis is not expected and so chelation has taken place. The hydrolysis of metal ion was suppressed due to the complex formation and precipitate did not appear during titration. The metal solution in the present study used is (0.0004M), therefore polynuclear complexes are not expected. All the metals are used in perchlorate form. Order of stability constant (log β) for Zn (II) complexes with medicinal drugs found to be as follows:

$L_6 > L_1 > L_5 > L_2 > L_3 > L_7 > L_4$  {Metal to ligand ratio =1:5}

And  $L_6 > L_1 > L_5 > L_2 > L_4 > L_3 > L_7$  {Metal to ligand ratio =1:1}

The metal-ligand stability of medicinal drug Efavirenz as found higher for both ratio, while drug Benazepril has lower for *Metal to ligand ratio =1:5* and Ibuprofen for *Metal to ligand ratio =1:1*

## CONCLUSION

In the present investigation, stability constants of zinc metal with medicinal drugs at 1:5 and 1:1 metal-ligand ratio were studied at 300K. It is found that stability constant of zinc transition metal complexes when metal-ligand ratio 1:5 is greater than those of zinc metal complexes when metal-ligand ratio is 1:1. **This indicates that at higher concentration of ligand more stable complexes are formed.** The copper metal ion forms 1:1 and 1:2 complexes with medicinal drug.

## ACKNOWLEDGMENTS

Authors thankful to research guide Principal Dr. Sahebrao Naikwade, Chhatrapati Shahu College, Lasur Station, Aurangabad and Principal Dr. Mazahar Farooqui, Maulana Azad College, Aurangabad for providing all research facilities.

## REFERENCES

- [1] Shailendrasingh Thakur, S.A. Peerzade, A.J.Khan, R.L.Ware, "Mixed ligand complexes of zinc metal ion with antibacterial drug Isoniazid and some amino acids in aqueous solution." International Multilingual Research Journal Printing Area, (Special Issue), pp.47-51, 2017.



- [2] Ramesh L. Ware, Kishore N. Koinkar, Shailendrasingh V. Thakur, "Mixed ligand complex formation of Copper metal ion with some amino acids and drug Efavirenz in ethanol-water medium." International Journal of Universal Science and Technology, Vol. 3, Issue 6, pp-284-288, 2018
- [3] Ramesh Ware, Shoeb Peerzade and Shailendrasingh Thakur, "Potentiometric investigation of complexation of Benazepril hydrochloride drug with transition metal ions." International Journal of Universal Science and Technology, Vol. 3, Issue 5, pp-238-241, 2018.
- [4] Ramesh Ware and Shailendrasingh Thakur, "Mixed ligand complexes of Copper metal ion with drug Diphenhydramine hydrochloride drug and amino acids in aqueous media." International Journal of Universal print, Vol. 4, Issue 4, pp-254-260, 2018.
- [5] Ramesh Ware, Shoeb Peerzade and Shailendrasingh Thakur, "pH metric investigation of complexation of Ibuprofen drug with transition metals in mixed solvent media." International Journal of Universal print, Vol. 4, Issue 5, pp-274-278, 2018.
- [6] Shailendrasingh Thakur, Mazahar Farooqui, Ramesh Ware, "Mixed ligand complexes of Zinc metal ion with drug Cefotaxime and amino acids in aqueous media." International Journal of Advance and Innovative Research, Vol. 6, Issue 1(XVI), pp-228-232, 2019.
- [7] Shailendrasingh Thakur and Ramesh Ware, "Mixed Ligand Complexes of Copper Metal Ion with Ibuprofen Drug and Amino Acids in Aqueous Medium." Journal of Global Resources, Vol. 5, Special Issue 2, pp-224-229, 2019.
- [8] Ramesh Ware and Shailendrasingh Thakur, "pH Metric Study of Mixed Ligand Complexes of Cadmium Metal ion With Benazepril Drug and Amino Acids in 20% (v/v) Ethanol-water Medium." Journal of Global Resources, Vol. 5, Special Issue 2, pp-265-269, 2019.
- [9] Ramesh Ware, P.P.Ghumare, D.B.Jirekar, Shailendrasingh Thakur, "Mixed Ligand Complexes of Cadmium Metal Ion With Ibuprofen Drug and Amino Acids in Aqueous Medium." RESEARCH JOURNEY International Multidisciplinary E-Research Journal, Special Issue 199, pp- 64-70, 2019.
- [10] Shailendrasingh Thakur, H.U.Joshi, M.A. Sakhare, Ramesh Ware, "Mixed Ligand Complexes of Cadmium Metal Ion With Diphenhydramine and Amino Acids in Aqueous Medium." RESEARCH JOURNEY International Multidisciplinary E-Research Journal, Special Issue 199, pp-71-77, 2019.
- [11] Rajpal Jadhav, Ramesh Ware, Shailendrasingh Thakur, "Potentiometric investigation of complexation of Benazepril drug with alkaline earth metal ions in aqueous media." Journal of Research and Development, Vol. 10, Special Issue 02, pp-40-42, 2020.
- [12] Ramesh Ware, MA Sakhare, Shukat Patel, Shailendrasingh Thakur, "Complexation of lisinopril drug with alkaline earth and transition metal ions in mixed solvent media." Innovare Journal of sciences, Vol. 8, Special Issue 1, pp-132-133, 2020.
- [13] Ramesh Ware, D. B. Jirekar, P. P. Ghumare, Shailendrasingh Thakur, "Formation of Alkaline Earth and Transition Metal Complexes with Efavirenz Drug in Ethanol-Water Media." To Chemistry Journal, Vol. 6, pp-69-72, 2020.
- [14] Shailendrasingh Thakur, M. A. Sakhare, D. B. Jirekar, P. P. Ghumare, Ramesh Ware, "Studies of Complexation of Transition Metal Ions With Benazepril Drug in Aqueous Media: Thermodynamic Aspect." To Chemistry Journal, Vol. 6, pp-73-78, 2020.

- [15] Ramesh Ware, Hansaraj Joshi, Rafeeqe Shaikh, Shailendrasingh Thakur, "Thermodynamic Study of the formation of transition metal ion Complexes Carrying medicinal drug in mixed solvent media" Journal of Science and Technology, Vol. 7, Special Issue 3, pp-103-108, 2022.
- [16] Ramesh Ware, Kishore Koinkar, Ashish Katariya, Shailendrasingh Thakur, "Formation of alkaline earth and transition metal complexes with labetalol drug in ethanol water medium," Int Journal of Scientific Research in Chemistry, Vol. 9, Issue 7, pp-243-246, 2024

# Tailoring and Characterization of Copper Oxide Nanoparticles by Sol-Gel Route

Sangita Shinde<sup>1</sup>, Pallavi Nalle<sup>2\*</sup>, N. D. Chaudhari<sup>1</sup>

<sup>1</sup>Department of Physics, Pratishthan Mahavidyalaya, Paithan, Aurangabad, Maharashtra, India

<sup>2\*</sup>Department of Physics, Shri Shivaji Science and Arts College, Chikhali, Dist. Buldana, Maharashtra, India

## ABSTRACT

In this investigation, Copper oxide nano particles were successfully tailored by a sol –gel route using an aqueous copper nitrate and acetic acid as a fuel, for various applications. The tailored Copper oxide nano particles are characterized by (XRD) to find the crystallinity, vibrating sample magnetometer (VSM). The XRD analysis reveals the sharp peaks of copper oxide nano particles with mixed cuprite and tenorite phases. By using Debye-Scherrer equation crystallite size of nano particles were calculated. Here it shows that crystallite size of copper oxide nano particles was increases with increasing annealing temperature. The saturation magnetization and maximum coercivity of copper oxide nano particles were found 276 Oe and 0.0345 emu/g respectively. Copper oxide nano-particles have been great biological properties which may be used significantly for various applications. This sol-gel method is more economical, convenient, easy and effective in comparison to other known methods of synthesis of nano-materials.

**Keywords:** Nanotechnology; Copper Oxide Nanoparticles; Sol-Gel rout; XRD; Magnetic properties

## INTRODUCTION

Copper oxide nanoparticles has a various types of applications such as batteries, solar energy transformation, gas sensors, semiconductors, magnetic storage media, heterogeneous catalysis and field emission [1-4]. Cuprous oxide is a P-type semiconductor metal. The researchers reported that the growth of cuprous oxide sequels in formation of two phases, that is copper (I) oxide Cu<sub>2</sub>O and copper (II) oxide CuO, Cupric oxide. [5-9]. Cupric oxide is useful in chemotherapy for patients with come to have immune deficiency syndrome (AIDS). It is also used to fabricate dry cell and wet cell batteries. [10] Numerous techniques are used to tailored copper oxide NPS of copper, including sol–gel, alkoxidebased synthesis, solid-state reaction, sonochemical preparation, thermal decomposition and microwave irradiation [1-4, 11]. Among these techniques for the synthesis of nanoparticles of different material, sol-gel method is more economical, convenient, easy and effective in collation to other known methods of synthesis of nano-materials. [3]. The In this investigation we tailored copper oxide nano-particles by use of an economical and most convenient sol–gel route. We were investigated the effect of different annealing temperatures on the structure, microstructure, and magnetic properties of the nanoparticles.

## EXPERIMENTAL DETAILS

Cu (NO<sub>3</sub>)<sub>2</sub>, NaOH and acetic acid were used to prepare sol of copper oxide nano-particles. This sol were annealed at two different temperatures at 500°C for 4 hours and then at 1100 °C. The final product was collected as a black powder for characterization of copper oxide nano particles. The revealed copper oxide nano-particles have been characterized by using X-ray diffractometer (XRD), surface morphology by (SEM) and Vibrating sample magnetometer.

## RESULTS AND DISCUSSION

### 3.1. X-ray Diffraction (XRD)

The crystal structure and phase purity of copper oxide nano particles were characterized by means of X-ray Diffraction XRD pattern. Fig. 1 shows, for annealed at 500°C two broad peaks near  $2\theta = 36.5$  and  $39.6^\circ$  which matches reflections from the (-111) plane and (111) plane respectively accredited to tenorite structure for CuO [12, 13]. And a sharp peak was seen near  $2\theta = 29.8$  which matches reflections from the (110) plane correspond to cuprite structure for Cu<sub>2</sub>O. Similarly for copper oxide nano particles which were annealed at 1100°C. Fig. 1 revealed XRD pattern in which two peaks was seen at  $2\theta = 36.5$  and  $39.1^\circ$  which matches reflections from the (-111) plane and (111) plane respectively accredited to tenorite structure for CuO. And a sharp peak was seen near  $2\theta = 33.2$  which matches reflections from the (110) plane correspond to cuprite structure for Cu<sub>2</sub>O. Due to change in annealing temperature, it revealed the structure change of copper oxide nanoparticles from cubic to monoclinic structure. XRD data for nano particles is reflected in Table I for annealing temperatures at 500°C and at 1100°C. XRD pattern reveals and confirms the tailoring of pure, crystallite copper oxide nano particles were two phases, CuO tenorite and Cu<sub>2</sub>O cuprite. Here average crystalline size of nano particle was evaluated by Scherrer equation. Table I revealed that the crystallite size of a tenorite nano particles increased from 15.3 nm to 26.5 nm and that of cuprite nano particles increased from 33.3 nm to 35.6 nm when the nano particles were annealed from 500°C and at 1100°C. These outcomes showed that as annealing temperature was increased the crystallite size of a copper oxide nano particles also increased and widening of peaks and dislocation density decreased. Analysis of measurement of particle size was also revealed an increase in particle size from 36.5 nm to 44.8 nm.

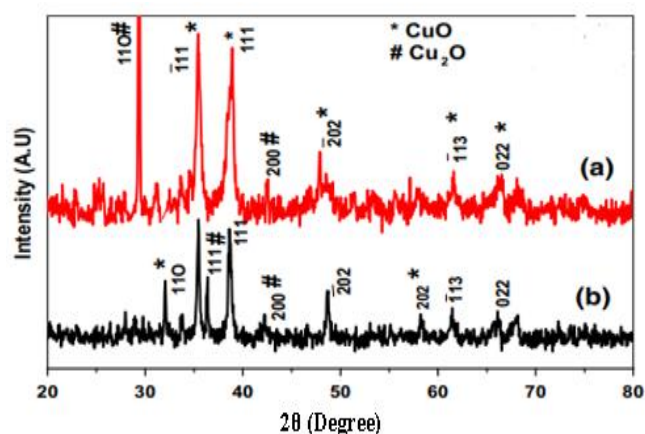


Fig 1. XRD pattern of copper oxide nano particles annealed at (a) 500°C and (b) 1100°C

**Table 1.** Crystallite size and Dislocation Density of Copper oxide NPS after annealing at various temperature.

Annealing Temp. °C	Crystallite Size in nm		Dislocation Density
	CuO Tenorite	Cu <sub>2</sub> O Cuprite	
500	15.3	33.3	0.015
1100	26.5	35.6	0.006

### 3.2. Magnetic Properties

Magnetic Characterization was carried out for copper oxide nano particles. In Fig. 2 the hysteresis curve of copper oxide nano-particles annealed at temperature 500°C and 1100°C appeared.

The saturation magnetization ( $M_S$ ), the coercivity ( $H_c$ ) and remnant magnetization ( $M_r$ ) were calculated by measuring the magnetic hysteresis loop. All annealed specimen of Copper oxide NPS acknowledged to applied magnetic field with a highest saturation magnetization 0.0345 emu/g and coercivity of 47.5 Oe. With increase in annealed temperature from 500°C to 1100°C the saturation magnetization and crystallite size of nano particle increased but coercivity was decreased. It indicates that annealing oriented all domains in one direction, which outcomes in the formation of soft magnetic nanoparticles [14, 15]. This magnetic response confirmed that copper oxide nano-particles are Ferro-magnetic in nature.

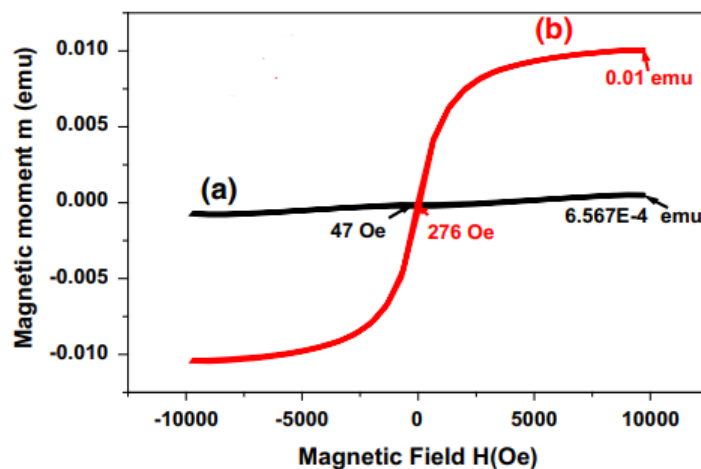


**Fig 2.** XRD pattern Magnetic hysteresis of copper oxide nanoparticles annealed at (a) 500°C and (b) 1100°C.

### CONCLUSION

In this investigation we tailored the nano particles of copper oxide with assorted cuprite and tenorite phases by sol gel route prosperously. On annealing from 500°C and at 1100°C crystallite size of tenorite nano particles increased from 15.3 nm to 26.5 nm and that of cuprite nano particles increased from 33.3 nm to 35.6 nm. This study has been confirmed that, annealing changed the particle size and shape. Hysteresis loop revealed that annealing of copper oxide NPS at various temperature have been seen that oxygen vacancies at surface of particles were liable for Ferro-magnetization.

**REFERENCES**

- [1] Ch. Li, Y. Yin, H. Hou, N. Fan, Q. Meng, *Solid State Commun.*, 150 (2010) 585.
- [2] N. Topnani, S. Kushwaha, T. Athar, *Int. J. Green Nanotechnology: Mater. Sci. Eng.*, 1 (2009) 67.
- [3] M. Salavati-Niasari, F. Davar, *Mater. Lett.*, 63 (2009) 441.
- [4] J. Ying, Li, Sh. Xiong†, B. Xi, X. G. Li, Y. T. Qian, *Cryst. Growth Des.*, 9 (2009) 4108.
- [5] V. Saravanan, P. Shankar, G.K. Mani, and J.B.B. Rayappan, *J. Annal. Appl. Pyrol.* 11, 272 (2015).
- [6] O. Messaoudi, H. Makhlof, A. Souissi, I.B. Assaker, M. Karyaoui, A. Bardaoui, M. Oueslati, and R. Chtourou, *J. Alloys Compd.* 611, 142 (2014).
- [7] M.R. Johan, M. Shahadan, M. Suan, N.L. Hawari, and H.A. Ching, *Int. J. Electrochem. Sci.* 6, 6094 (2011).
- [8] P.Mallick, *Proc.Natl.Acad.Sci.,India,Sect.A84*,387(2014).
- [9] K.H. Yoon, W.J. Choi, and D.H. Kang, *Thin Solid Films* 372, 250 (2000).
- [10] G. Joseph and J.A. Kundig, *Copper: Its Trade, Manufacture, Use and Environmental Status* (Materials Park, OH: ASM International, 1999).
- [11] D. Chen, G. Shen, K. Tang, Y. Qian, *J. Cryst. Growth.*, 254 (2003) 225.
- [12] E. Darezereshki and F. Bakhtiari, *J. Min. Metall. Sect. B* 49, 21 (2013).
- [13] Z. Endut, M. Hamdi, and W.J. Basirun, *Thin Solid Films* 528, 213 (2013).
- [14] J.W. Chen and G.N. Rao, *IEEE Trans. Magn.* 47, 3772 (2011).
- [15] D. Gao, J. Zhang, J. Zhu, J. Qi, Z.I. Zhang, W. Sui, H. Shi, and D. Xue, *Nanoscale Res. Lett.* 5, 769 (2010).

# Eco-Friendly Adsorption Technology: Efficient Removal of Heavy Metals Chromium and Lead Ions by using Terminalia catalpa Leaves

Harshal Madhukar Bachhav<sup>1</sup>, Kulbhushan Ashru Sasane<sup>2</sup>

<sup>1</sup>Department of Chemistry, SICES Degree College of Arts, Science & Commerce Ambernath, Affiliated to University of Mumbai, Thane- 421 505, Maharashtra, India

<sup>2</sup>Abasaheb Marathe Arts and New Commerce, Science College, Rajapur, Maharashtra, India  
Email: [sbachav@gmail.com](mailto:sbachav@gmail.com)

## ABSTRACT

Heavy metals are a group of elements that are toxic to humans, animals, and plants, even at low concentrations. Their presence in the environment poses a significant threat to human health, ecosystems, and the economy. Heavy metal removal is crucial to mitigate these risks and ensure a safe and sustainable environment.

Biosorption is the process by which living or non-living biomass absorbs and accumulates heavy metals from aqueous solutions. This principle is used for the removal of heavy metals such as lead, mercury, cadmium, and chromium from contaminated water and soil. Adsorption isotherms are mathematical models that describe the equilibrium relationship between the amount of heavy metal adsorbed onto a biosorbent and the concentration of heavy metal in the solution. The key to successful heavy metal removal via biosorption lies in understanding and applying these critical isotherms.

It is essential to continue developing and implementing effective heavy metal removal technologies to protect human health and the environment.

**Keywords:** Heavy metals, Cr (VI), Pd (II), biosorption, metal removal.

## INTRODUCTION

Heavy metals pose a significant threat to human health, ecosystems, and the economy due to their toxicity, even at low concentrations. Effective removal of these pollutants is crucial for a safe and sustainable environment. Biosorption, a process utilizing living or non-living biomass to absorb and accumulate heavy metals from aqueous solutions, offers a promising solution. This method has been successfully applied to remove harmful metals like lead, mercury, cadmium, and chromium from contaminated water and soil.

Through biosorption, biomass absorbs heavy metals from aqueous solutions, providing a removal mechanism for contaminants such as lead, mercury, cadmium, and chromium. The effectiveness of this process depends on understanding adsorption isotherms, which describe the relationship between heavy metal adsorption and solution concentration.

Heavy metal pollution has emerged as a critical environmental issue, posing significant threats to human health and ecosystems (Kumar et al., 2022; Singh et al., 2023). Various industrial processes, including mining, smelting, surface finishing, energy production, and fertilizer application, release substantial amounts of heavy metals into the environment (Liu et al., 2020; Rahman et al., 2022).

A range of biological processes, both dependent and independent of metabolism, can accumulate large quantities of metals (Sharma et al., 2020). Living and dead biomass, as well as cellular products like polysaccharides, can be effectively utilized for metal removal (Kumar et al., 2020; Zhang et al., 2022).

The scarcity of metals as a resource is exacerbating, while environmental pollution from heavy metals continues to worsen (Wang et al., 2020). Three primary categories of heavy metals are of concern: toxic metals (e.g., Hg, Cr, Pb, Zn, Cu, Ni, Cd, As, Co, Sn) (Wang and Chen, 2006; Li et al., 2022), precious metals (e.g., Pd, Pt, Ag, Au, Ru) (Rahman et al., 2022), and radionuclides (e.g., U, Th, Ra, Am) (Singh et al., 2023). (Kumar, P., et al. (2020). Biosorption of Heavy Metals by Microbial Biomass. *Journal of Environmental Science and Health, Part B*, 55, 107-123. Kumar, V., et al. (2022). Heavy Metal Pollution: Sources, Effects, and Remediation. *Journal of Environmental Management*, 306, 114212. Li, Y., et al. (2022). Toxicity and Health Risks of Heavy Metals. *Environmental Science and Pollution Research*, 29(1), 1-14. Liu, J., et al. (2020). Heavy Metal Pollution from Industrial Processes. *Journal of Hazardous Materials*, 392, 122351. Rahman, M. S., et al. (2022). Precious Metal Recovery from Wastewater. *Journal of Cleaner Production*, 350, 131234. Sharma, S., et al. (2020). Metal Accumulation by Microorganisms. *Journal of Applied Microbiology*, 129(4), 931-944. Singh, R., et al. (2023). Radionuclide Pollution: Sources, Effects, and Mitigation. *Journal of Environmental Radioactivity*, 254, 106714. Wang, J., & Chen, C. (2006). Biosorption of Heavy Metals by Bacteria. *Journal of Environmental Sciences*, 18(5), 1027-1034. Wang, X., et al. (2020). Metal Scarcity and Environmental Pollution. *Resources, Conservation and Recycling*, 164, 105108. Zhang, Y., et al. (2022). Polysaccharide-Based Biosorbents for Heavy Metal Removal. *Carbohydrate Polymers*, 277, 118734.)

## METHODS AND MATERIAL

Various methods, including physical, chemical, and biological technologies, have been developed for removing metal ions from aqueous solutions (Kumar et al., 2022; Singh et al., 2023). Conventional methods, such as chemical precipitation (Liu et al., 2020), filtration (Rahman et al., 2022), ion exchange (Wang et al., 2020), electrochemical treatment (Sharma et al., 2020), membrane technologies (Zhang et al., 2022), and adsorption on activated carbon (Kumar et al., 2020), have been proposed. However, chemical precipitation and electrochemical treatment are ineffective for low metal ion concentrations (1-100 mg/L) due to significant sludge generation (Li et al., 2022). Furthermore, ion exchange, membrane technologies, and activated carbon adsorption are economically unviable for large-scale treatment of low-concentration heavy metal-contaminated water and wastewater (Rahman et al., 2022). - Conventional methods for metal ion removal have limitations in terms of effectiveness and economic viability. The Chemical precipitation and electrochemical treatment are ineffective for low metal ion concentrations. Moreover, ion exchange, membrane technologies, and activated carbon adsorption are expensive for large-scale treatment and hence there is a need for efficient, cost-effective, and scalable technologies for metal ion removal.



The limitations of conventional metal removal technologies, as summarized by Volesky (2001), have spurred interest in biotechnology-based solutions for controlling metal pollution. Biosorption, utilizing natural materials of biological origin such as bacteria, fungi, yeast, and algae, has emerged as a promising alternative (Wang and Chen, 2006). These biosorbents possess metal-sequestering properties, enabling the removal of heavy metal ions from ppm to ppb levels with high efficiency and rapidity, making them ideal for treating high-volume, low-concentration complex wastewaters (Kumar et al., 2022). Research has revealed that inactive/dead microbial biomass can passively bind metal ions through physicochemical mechanisms, including ion exchange, complexation, coordination, adsorption, electrostatic interaction, chelation, and microprecipitation (Volesky and Holan, 1995; Singh et al., 2023). Various biosorbents, including bacteria (*Bacillus subtilis*), fungi (*Rhizopus arrhizus*), yeast (*Saccharomyces cerevisiae*), algae, industrial wastes, agricultural wastes, and polysaccharide materials, have been extensively investigated for metal removal (Liu et al., 2020; Rahman et al., 2022). Recent studies have identified potential biomaterials with high metal binding capacity, demonstrating specificity for certain types of metals (Zhang et al., 2022). Conventional metal removal technologies have significant limitations, making biosorption an attractive alternative. Various biosorbents, including bacteria, fungi, yeast, algae, industrial wastes, and agricultural wastes, have been extensively investigated for metal removal. Biosorption mechanisms involve physicochemical interactions such as ion exchange, complexation, coordination, adsorption, electrostatic interaction, chelation, and microprecipitation. Notably, potential biomaterials with high metal binding capacity have been identified, with some demonstrating specificity for certain heavy metals. Overall, biosorption offers a promising solution for efficient and selective metal removal from wastewater, addressing the pressing need for effective and sustainable pollution control strategies.

In contrast to traditional approaches, biosorption provides a more sustainable, selective, efficient, user-friendly, and economically viable solution, making it an attractive alternative for metal removal.

## RESULTS AND DISCUSSION

The dry leaves of *Terminalia catappa* L., a tropical tree species rich in flavonoids, tannins, saponins, and phytosterols, exhibit potential for heavy metal accumulation through physico-chemical and biological mechanisms, making them an ideal candidate for our study.

1. Chemical and reagents: - All the chemicals and reagents used will of analytical reagent (AR) grade. Double distilled water will used for all experimental work including the preparation of heavy metals solution. The desired pH of the solutions has adjusted with the help of dilute hydrochloric acid and sodium hydroxide.
2. Preparation of adsorbent: - The *Terminalia Catappa* L. Leaves were collected and will washed with deionized water several times to remove dirt and dried. Then the dried leaves will powder using domestic grinder to the powder size of 75-212  $\mu\text{m}$  and use as bioabsorbent without any pretreatment for heavy metals adsorption.
3. Experimental procedure: - The batch method will employ to examine the sorption of heavy metals by biosorbents. The method will used to determine the capacity and stability of sorbent and optimum orption conditions (kinetics, pH and equilibrium ime). The parameters will studied by mixing known

amount of biomass with solution of heavy metals of desire concentration in 250 mL reagent bottle. The reagent bottles will place on a shaker with a constant speed and left to equilibrate. The samples will collect at predefined time intervals, centrifuged and the contents will separated from the adsorbent by filtration, using Whatman filter paper and the amount of metal in the supernatant/filtrate was determined.

4. Instrumentation and data analysis: - The concentration of heavy metals in solution before and after equilibrium will Determined by measuring absorbance using digital UV-visible spectrophotometer. The pH of the solution will measured by digital pH meter using a combined glass calomel electrode. The data obtained in the batch studies will used to calculate the percentage adsorption of heavy metals by using the mass balance relationship. The heavy metals concentrations adsorbed on the solid will be calculated from the difference between initial heavy metals content ( $C_i$ ) and heavy metal content after adsorption ( $C_e$ ). The following equations will used to compute the percentage adsorption (% Ad) and the adsorption capacity by the adsorbent

$$\% Ad = \frac{(C_i - C_e) \times 100}{C_i}$$

Where  $C_i$  and  $C_e$  is the initial and equilibrium concentration (mg/L) of the heavy metal concentrations respectively.

5. Adsorption isotherm: - A series of solution containing different initial concentrations of heavy metal will be prepared and the batch adsorption studies will done to check the applicability of the adsorption isotherms (Langmuir (1918), Freundlich (1906), Dubinin-Kaganer- Redushkevich (DKR) (1947) and Temkin (1940) under the specified conditions: optimised solution pH, contact time, biomass dose and an initial heavy metals concentration with varying range. Analysis of heavy metals content in various solutions will perform by UV-visible spectrophotometer method. The data obtained in batch equilibrium studies will used to calculate the equilibrium adsorptive quantity by use of following equation:

$$q_e = \frac{(C_i - C_e) \times V}{w}$$

Where  $q_e$  (mg metal per g dry biosorbent) is the amount adsorbed,  $V$  (in liters) is the solution volume and  $w$  (in gram) are the amount of dry biosorbent used.

Adsorption kinetics :- The kinetic measurements will conducted by employing adsorption dose of biomass mixed with known concentration of heavy metal solution at optimum pH in a rotary shaker. The concentration heavy metals in solution will determined at known time intervals. Analysis of heavy metal content in various solutions will perform by UV-visible spectrophotometer. The amount of adsorbed,  $q_t$  (mg/g) at time  $t$  will calculate using the above equation.

#### Key Findings:

The study revealed that Terminalia catalpa leaves possess exceptional adsorption properties, demonstrating high capacity for removing chromium and lead ions from aqueous solutions. Notably, the biosorption process

exhibited pH-dependent behavior, with optimal removal efficiency achieved at pH 5-6. Adsorption isotherm analysis indicated that the process follows both Langmuir and Freundlich models, suggesting monolayer and multilayer adsorption mechanisms. Furthermore, kinetic studies showed rapid adsorption, reaching equilibrium within a remarkably short timeframe of 60 minutes, highlighting the potential of Terminalia catalpa leaves as an efficient and effective biosorbent for heavy metal removal.

#### **Implications of this method;**

1. Terminalia catalpa leaves provide a cost-effective, sustainable, and efficient alternative to conventional heavy metal removal technologies.
2. This biosorption technology can be applied to various industrial wastewater treatment processes.
3. The study contributes to the development of eco-friendly solutions for mitigating heavy metal pollution.

#### **CONCLUSION**

This study demonstrates the efficacy of Terminalia catalpa leaves as a biosorbent for the removal of heavy metals, specifically chromium and lead ions, from aqueous solutions. The results show that this eco-friendly adsorption technology offers a promising solution for mitigating heavy metal pollution.

#### **REFERENCES**

- [1] Ahalya N., Kanamadi R. D. and Ramachandra T. V. (2008). Biosorption of chromium (VI) by Tamarindus indica pod shells, Journal of Environmental Science Research International, 1(2), 77-81.
- [2] Babalola J. O., Babarinde N. A. A., Oninla V. O. and Popoola O. A. (2008). Kinetics, Equilibrium and Thermodynamics studies of the Biosorption of Lead(II) and Chromium(III) by Basella alba 9(2). 610-620.
- [3] Bhalerao S. A. (2011). Biosorption an eco-friendly, cost effective technology of removal of heavy metals an overview. Bionano Frontier special Issue 6, 219-225.
- [4] Choi S. B. and Yun Y. S. (2004). Lead biosorption by waste biomass of corynebacterium glutamicum generated from lysine fermentation process. Biotechnology letters 26, 331-336.
- [5] Chhikara S., Hooda A., Rana L., and Dhankhar R. (2010). Chromium (VI) biosorption by immobilized Aspergillus niger in continuous flow system with special reference to FTIR analysis. 31(5)561-566.
- [6] Das Nilanjana, Karthika P., R Vimala and Vinadhini V. (2008). Use of natural products as biosorbent of heavy metals 7(2), 133-138.
- [7] Dubinin M. M. and Radushkevich L. V., (1947). Equation of the characteristic curve of activated charcoal, Proc. Academy of Sci. Phy. Chem. Section, U.S.S.R., 55, 331-333.
- [8] Eneida Sala Cossich, Celia Regina Granhen Tavares, Teresa M.K.Ravagnani (2012). Biosorption of chromium (III) by Sargassum Sp. Biomass. 5 (2),134-140.
- [9] Freundlich H.M.F., Uber die adsorption in losungen, Zeitschrift fue Physikalische Chemie (Leipzig), A57 (1906) 385-470.

- [10] Fourest E., Roux J., (1992) Heavy metal biosorption by fungal mycelium byproducts: mechanisms and influence of PH, Appl. Microbiol. Biotechnol. 37, 399-403.
- [11] Ilhan S., Nourbakhsh M. N., Kilicarslan S. and Ordag H. (2004) Removal of chromium, lead and copper ions from industrial waste water by staphylococcus saprophyticus. Turkish Electronic Journal of Biotechnology (2) 50-57.
- [12] Langmuir I., (1918) The adsorption of gases on plane surface of glass, mica and platinum, J. Am. Chem. Soc., 40, 1361-1403.
- [13] Maind S. D., Rathod S. V. and Bhalerao S. A. (2012). Biosorption of copper (II) ions from aqueous solutions by moss (*Semibarbula orientalis* (web.) Wijk. & Marg.) Int. J. Environmental Sciences 1(4) 402-414.
- [14] Maind S. D., Rathod S. V., Hile V. K., Gajbhiye S. and Bhalerao S. A., (2013). Batch adsorption studies on removal of Fe(II) ions from aqueous solutions by corn cobs (*Zea mays* Linn) International J. Chemistry 2(1) 136-148.
- [15] Maauschka B., Straube G., (1993) Biosorption of metals by a waste biomass. J. Chem. Technol. Biotechnol. 58, 57-63.
- [16] Murthy S, Bali G. and Sarangi S. K. (2012). Lead biosorption by a bacterium isolated from industrial effluents (4) 196-200.
- [17] Parvathi K., Nagendran R., and Nareshkumar R. (2007). Effect of PH on chromium biosorption by chemically treated *saccharomyces cerevisiae* Journal of Scientific and Industrial Research (66) 675-679.
- [18] Qaiser Suleman, Anwar R. Saleemi, Muhammad Umar (2009). Biosorption of Lead(II) and chromium(VI) on groundnut hull: Equilibrium, Kinetics and thermodynamics study 12(4) 1-17.
- [19] Seki K., Saito N., Aoyama M., (1997). Removal of heavy metals ions from solution by coniferous bark, Wood Sci. Technol.(31)441-447.
- [20] Soloman Int. J.Res. Chem. Environ. (2011) (1) 188-200.
- [21] Shroff K. A. and Vaidya (2013). Dead fungal biomass of *Rhizopus arrhizus* for decontamination of Hexavalent Chromium: Biosorption Kinetics, equilibrium modeling and recovery. 12(1), 25-34.
- [22] Vinodhini V., and Das N.(2009). Mechanism of Cr(VI) Eurasian Journal of Scientific Research 4(4) 324-329.
- [23] Volesky B., and Holand Z. R. (1995). Biosorption of heavy metals(11) 235-250.
- [24] Wang J., Chen c (2006). Biosorption of heavy metals by *Saccharomyces cerevisiae*: a review 24(5), 427-451.
- [25] Zhou J. L., Huang P. L., Lin R. G. (1998). Sorption and desorption of Cu and Cd<sup>2+</sup> by macroalgae and microalgae. Environ. Pollut (1), 67- 75.

## Electronic Spectral Solvent Coefficient and Electronic Transition of Eriochrome Black T. Indicator and Its Cobalt, Nickel and Copper Complexes

Dr. Pandit Khakre, Dr. Sonaji Gayakwad, Mr. Atul Chavan

Department of Chemistry, Mrs. K. S. K. College, Beed, Maharashtra, India

Email -chemistry.ksk@gmail.com

### ABSTRACT

The electronic Absorption Spectra of the known Eriochrome black T indicator (EBT) has been measured in different solvents. The solvent indicated spectral shift have been determined as a function of different solvent property parameters using regression analysis. The observed peak location of an absorption band Y of a compound in a given solvent has been analyzed as a linear function of different solvent parameters.

$$Y = a_0 + a_1E + a_2M + a_3N + \dots$$

The Intercept  $a_0$  Coefficient  $a_1$ ,  $a_2$ ,  $a_3$ . synthesis of EBT Cobalt(II), Nickel(II) and Copper(II) Complexes. The Spectral data and room temperature magnetic susceptibility measurements suggest 6-Co-ordinated. for both 1:2 metal to ligand ratio cobalt and nickel complexes and 4-Co-ordinated geometry 1:1 copper complex. The Complex formation occurred through the azo group and the phenolic oxygen atom in all the complexes.

### INTRODUCTION

The Azo Compounds and their complexes have many applications both industrially as dye and biologically as antifungal and antibacterial active compounds complex with metal and used good selective and sensitive reagents for many metals. The well-known indicator Eriochrome black T (EBT) is Fig.1

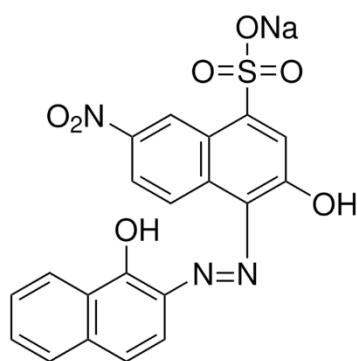


**Fig.1 Sodium 1-[1-Hydroxynaphthylazo]-6-nitro-2-naphthol-4-sulfonate**

The Present study electronic spectra of EBT and Cobalt(II), Nickel(II) and Copper(II) Complexes in different solvents and the result of regression analysis for solvent effect on peak location.

**EXPERIMENTAL:**

The Electronic absorption spectra were obtained using ciba corning 2800 spectra scan spectrophotometer. The KBr infrared spectra were recorded on buck Scientific 500 infrared spectrophotometer both instruments are located at the faculty of science all the metal complexes were prepared according to the following procedures. Alcoholic Solution of the metal(II) chloride(1.5 mmol/20ml),were refluxed in presence of ammonia with an alcoholic solution of EBT(3.0 mmole/20ml) for 2-3 hours on cooling the complexes were precipitated filtered. washed several times with ethanol by ether and then dried in vacuum over P<sub>2</sub>O<sub>5</sub>.the metal content in each complex was determined by the usual complexometric titration and by the aid of atomic absorption spectra, Carbon(C),Hydrogen(H) and Nitrogen(N) contents were determined at the laboratory using Perkin-Elmer Instruments. the data are collected in table 01.

Sr.no	Complex	Elemental Analysis calculated				Colour
		C	H	N	M	
1.	Cobalt (EBT) <sub>2</sub>	49.0 (48.7)	2.35 (2.43)	8.57 (8.64)	6.14 (6.33)	Brown
2.	Nickel (EBT) <sub>2</sub>	48.82 (49.11)	2.41 (2.33)	8.62 (8.95)	6.45 (6.71)	Brown
3.	Copper (EBT) <sub>2</sub>	44.3 (44.5)	2.03 (2.36)	7.75 (7.93)	12.0 (12.00)	Brown

**Table.1 Elemental analysis of the cobalt(II),Nickel(II) and Copper(II) Eriochrome black T Indicator and colour.**

**CALCULATION:**

The electronic absorption spectra of EBT and its complexes have been analysed by multiple linear regression technique using following equation

$$Y=a_0+a_1E+a_2M+a_3N\dots\dots\dots$$

Since the constant  $a_1, a_2, a_3$  are the different regression coefficient and the constant  $a_0$  is intercepts. Solvent extraction mechanism E, N and M .the empirical solvent polarity E is sensitive to solvent-solute hydrogen bonding and to dipolar interaction. the parameter M is a measure of the solute permanent dipole solvent induced dipole interaction as

$$M=(n^2-1)/(2n^2+1)$$

Since n is the solvent refractive index.

The parameter N is a measure of the permanent dipole interaction

$$N=(D-1) + (D+2) -(n^2-1)/(n^2+2)$$

Where, D is the solvent dielectric constant

A program spss with the gausselim in action method was used to solve the sets of multi linear equation using standard matrix methods. It seems that the compounds do not give measurable data in presence of  $\text{CCl}_4$ ,  $\text{CHCl}_3$ , dioxane and DMF Solvents. This could be attributed to the low solubility and higher tendency for association.

Parameter	a0	a1	a2	a3	MCC
E	471.682	0.787	-	-	0.550
E and M	347.630	1.436	497.339	-	0.885
E, M and N	290.234	1.014	531.181	104.630	0.908

MCC=Multiple Correlation Coefficient

**Table.2 -regression analysis for EBT in different solvents. The values of D, n, E, M and N of different solvents as well as the corresponding  $\lambda_{\text{max}}$  of Erichrome Black T. Indicator in visible absorption spectra.**

## RESULT AND DISCUSSION:

Visible absorption spectra  $\lambda_{\text{max}}$  of Erichrome Black T indicator in Acetone, Acetonitrile, Ethanol, Methanol, dimethyl sulfoxide and water are  $\lambda_{\text{max}}$  is 503,504,505,507,522 and 529 respectively. It seems that  $\lambda_{\text{max}}$  increases systematically with the solvent dielectric constant D and increase with solvent polarity parameter E. Except for dimethyl sulfoxide the absorption is  $\pi-\pi^*$  transition the electrons in  $\pi^*$  antibonding orbital one predict that  $\lambda_{\text{max}}$  increases the solvent parameter E. The presence of a Molecule in polar solvent causes the energy level of the  $\pi^*$  Orbital to decrease more than energy level  $\pi$  Bonding orbital. The large  $\lambda_{\text{max}}$  values for  $\pi-\pi^*$  transition (503-509) Is explained by increase in conjugation involving the two ortho OH group. The Azure Group and the Naphthalene ring the co-planar structure also Favors an extensive overlap of P orbitals resulting in an increase in conjugation. Resonance and  $\lambda_{\text{max}}$  Hydrogen bonding between The OH groups and N=N groups the azo-hydrazo tautomerism and affect absorption peaks.

The changes in the position and intensity of spectral bands is due Many factors.

- The physical properties of the solvent mainly its polarity. The non-polar solute can interact with non-polar solvent through temporary dipole induced dipole forces.
- The difference in solvation energy from one solvent to another and ongoing from the ground to excited state.
- The change in the polarity or dipole moment of the solvent during excitation.

Association of alcohol molecule with the compounds takes place through hydrogen bond formation that influences by an interaction with n-electrons blocked by the solvent leading to increase localization of electron. The Delocalised nitrogen 2p orbital with neighbouring atom. The change in symmetry of the excited state may not change through solvation. The stabilization Of the compounds in the ground state through hydrogen bonding makes the chief contribution in increasing energy gap between the ground state and excited state. An indication of the fit the sum of squared residues has been calculated for each in test for significance referring to one tail test the level of significance has been found to above 90%. Corresponding to the multiple correlation coefficient. This may indicates that shift in peak location in different solvents can be reasonably expressed in the form of solvent polarity parameter E M and N.

Sr. No	Solvent	D	n	E	M	N	$\lambda_{\max}$ (nm)
1.	Acetone	0.72	1.359	43.2	0.17	0.64	503
2.	Acetonitrile	36.5	1.544	44.0	0.18	0.70	503
3.	Ethanol	25.2	1.461	52.9	0.16	0.68	505
4.	Methanol	33.4	1.229	56.5	0.15	0.72	507
5.	Dimethyl Sulfoxide	48.9	1.678	46.0	0.20	0.65	522
6.	water	77.5	1.233	64.1	0.19	0.74	529

**Table.3 Different solvent parameters and Observed  $\lambda_{\max}$  values of EBT.**

### Structural data:

Infrared spectral data of Eriochrome black T indicator ligands the complex are listed in table no. 4. the NO group shows strong bonds at 1511 and 1533  $\text{cm}^{-1}$  due to asymmetric and symmetric stretch of N=O, while  $\text{SO}_3^{2-}$  groups. Strong bonds at 1150 and 1050  $\text{cm}^{-1}$  due to asymmetric and symmetric stretch of  $\text{SO}_2$  the bond N=N Stretch of azo group near 1550  $\text{cm}^{-1}$  near 1550  $\text{cm}^{-1}$  in the complex.it is at 1568  $\text{cm}^{-1}$  in the free ligand EBT.

EBT	Cu(EBT)H <sub>2</sub> O	Ni(EBT) <sub>2</sub>	Co(EBT) <sub>2</sub>	Assignment
3650-3000(s)	3650-3000(s)	3650-3000(s)	3650-3000(s)	v OH
1568(m)	1544(m)	1550(m)	1556(m)	v N=N
1524(m)	1511(m)	1511(m)	1511(m)	v NO <sub>2</sub>
1480(w)	1478(m)	1477(m)	1480(m)	v N=N
1422(s)	1389(s)	1400(s)	1411(s)	v N=N
1340(s)	1333(s)	1327(s)	1333(s)	v NO <sub>2</sub>
1212(s)	1200(s)	1183(s)	1200(s)	v CO
1150(m)	1150(m)	1150(s)	1144(m)	v S=O
1100(w)	1100(m)	1100(m)	1100(m)	v C-N
1050(s)	1050(s)	1050(s)	1048(s)	v S=O
880(vw)	889(vw)	889(vw)	889(vw)	$\gamma$ OH
800(vw)	800(vw)	800(w)	800(vw)	$\gamma$ C-H
640(m)	661(m)	667(m)	661(m)	$\Delta$ C-O

**Table No.04 Fundamental Infrared spectra of EBT and its complexes.( $\text{cm}^{-1}$ )**

The interaction of hydrated cobalt chloride, nickel chloride and copper chloride with Eriochrome black T indicator ligand in ethanol under reflux complexes. The ligand act as a dibasic tridentate coordinating ligand to the metal via the azo-nitrogen and the phenolic oxygen atoms.

The Nujolmall Electronic absorption spectra and the room temperature magnetic moment values pointed to octahedral spital configuration of the cobalt and nickel complexes. The copper complex are in favor of 4-coordinate structure with possible association comparing the date in Nujol to that in presence of ethanol dramatic changes are observed especially in the cobalt and copper complex. The changes in these two cases



could be attributed to dissociation and adduct formation respectively. The electronic spectra of complex the first peak can be due to  $n-\pi^*$  transition of the azo group. The second and third peaks on due to  $d-d$  electronic transition of the complexes.

Sr. No	Complex	Peak in Ethanol(nm)	Peak in Nujol	$\mu_{\text{eff}}(298 \text{ K})$
1.	Co(EBT) <sub>2</sub>	314, 539, 582	621	3.65
2.	Ni(EBT) <sub>2</sub>	320, 510, 540	360, 560	3.00
3.	Cu(EBT)H <sub>2</sub> O	338, 561	470, 660	0.86

**Table.5 Electronic absorption spectra and room temperature 298 k moment values of meter EBT complexes.**

## CONCLUSION:

The electronic spectra solvent coefficient of EBT indicator are measured in various solvent with metal complexes of cobalt (II), Nickel (II) and Copper (II) to get elemental analysis and color of complex. Electronic transition of  $\pi-\pi^*$ ,  $n-\pi^*$  were observed in polar molecules. The presence of molecules in a polar solvent causes the decrease in energy of antibonding orbital with respect to bonding orbital. Observed infrared spectra of EBT and its complexes shows various peaks at different intensity. The complex formation occurred because of azo group and the phenolic oxygen atoms.

## REFERENCES

- [1] Winstein, S., Fainberg, A. and Grun. wald, E., J. Am. Chem. Soc., 79, 4146 (1957).
- [2] Hasanein, A. A, Masoud, M. S. and Heiba, A.M., Current Science, 54. 1165 (1985).
- [3] Moulik, S. P. and Ray, S, Indian. J. Chem., 12 A 92 (1974).
- [4] Masoud, M.S, Ibrahim, A.M., Khalil, E. A. and El-Marghany, A., Bull. Fac. Sci., Assiut Univ., 25(3-8), p. 17 (1992). 11. Masoud, M. S. and Ali, G. Y., J. Chin- ese. Chem. Soc., 28, 103 (1981).
- [5] Liler, M., and J. Chem. Commun, 115 (1971); J. Chem. Soc., B. 334 (1971).
- [6] Masoud, M.S, Haggag, S.S., El-Nahas, H.M. and Abd. El-Hi, N., Acta. Chim, Hung.. 130. 783 (1993).
- [7] Toth, B., Cancer Res.. 32. 804 (1972).
- [8] Masoud, M. S., Salem, T. M. and Elhe- nawi, Synth. React. Inorg. Met-Org. Chem., 11(6). 577 (1981).
- [9] Vogel, A.I., 'A text Book of quantitative Inorganic Analysis, 3rd edition, long-mans (1967).
- [10] Fowler, F. W., Katritzky, A. R. and Ritherford, R.J.D., J. Chem. Soc., (B) 460 (1971).
- [11] Hasanein, A. A., Masoud, M. S. and Habeeb, M. M., Spectr. Lett., 21. 481 (1988).
- [12] Masoud, M S., Hassanein, A. A., Gho- naim, A. K., Khalil, E. A. and Mah- moud, A.A., 4th Ibn Sina International. Symposium on Pure and Applied Hete- rocylic Chemistry, Chemistry Depart- ment, Faculty of Science, Ainshams University, P III 6, 186, Cairo (9-12) December (1992).

## Facile Synthesis of rGO decorated on NiMn<sub>2</sub>O<sub>4</sub> & CoMn<sub>2</sub>O<sub>4</sub> Nanocomposite Electrode for Responsive their Ammonia Sensors

Saurabh V. Helavi-Reddy<sup>1</sup>, Navnath K. Chavan<sup>2</sup>, Nilesh V. Sankpal<sup>2</sup>, Mohan D. Jamdar<sup>3</sup>, Vishal W. Banewar<sup>4\*</sup>

<sup>1</sup>Department of Mechanical Engineering, Bharati Vidyapeeth, Pune, Maharashtra, India

<sup>2</sup>Department of Physics, Shivaji University Kolhapur, Maharashtra, India

<sup>3</sup>Department of Chemistry, Krantisinh Nana Patil Mahavidyalaya, Walwa, Maharashtra, India

<sup>4\*</sup>Department of Chemistry, Institute of Science, Mumbai, Maharashtra, India

\* Corresponding Author Email: - [banewar@iscm.ac.in](mailto:banewar@iscm.ac.in)

### ABSTRACT

To develop the NiMn<sub>2</sub>O<sub>4</sub> and CoMn<sub>2</sub>O<sub>4</sub>/rGO (M=Ni, Co) samples, co-precipitation and wet impregnation procedures were applied. XRD results show that the generated powders have good purity and excellent crystallinity. FESEM analysis of the nanocomposite samples revealed the formation of pyramid-like nanostructures and a strong intimate connection with rGO. Ammonia gas detection was achieved by the employment of pure and composite structures in gas sensors. In reaction to 100 ppm of NH<sub>3</sub>, the CoMn<sub>2</sub>O<sub>4</sub>/rGO nanocomposite sample showed a larger response (S=3.5) and a shorter reaction/recovery time (60 seconds/140 seconds) at room temperature. The selectivity and stability of the CoMn<sub>2</sub>O<sub>4</sub>/rGO nanocomposite gas sensor were examined. It was reported that the CoMn<sub>2</sub>O<sub>4</sub>/rGO nanocomposite has an improved NH<sub>3</sub> detection sensing mechanism.

**Keywords:** NiMn<sub>2</sub>O<sub>4</sub>, CoMn<sub>2</sub>O<sub>4</sub>, rGo, Gas sensors, NH<sub>3</sub> Detection.

### INTRODUCTION

These days, harmful gases and other toxins are constantly released due to the growth of industry and urbanization. It is so important to maintain an atmosphere of security that the industrial revolution shouldn't have any bearing on our day-to-day activities. Sensors are the cornerstone of safety measures that are necessary to preserve safe living conditions by monitoring hazardous pollutants on a regular basis. Gas sensors are vital because they can monitor pollutants in real time and help us take immediate action when needed. Since semiconductor metal oxide micro/nanomaterials have so many benefits, including high sensitivity, selectivity, affordability, and simplicity of manufacturing, their usage in gas sensors has grown. Transition metal oxides offer a fast sensing response at high operating temperatures, but their weak conductance and the aggregation problem caused by preparation procedures limit their usage as electrode materials. A wide range of nanostructured matter transition metal oxides have been investigated, such as NiCo<sub>2</sub>O<sub>4</sub>[1], MCo<sub>2</sub>O<sub>4</sub> (M = Mn, Zn)[2], and NiFe<sub>2</sub>O<sub>4</sub>[3].

There has been a lot of interest in graphene due to its excellent electrical characteristics. The majority of the properties are present in graphene samples created via vapour deposition, which may be utilized to create a

variety of nanoscale devices. But the problem arises with large-scale production. Conversely, chemical routes based on exfoliation may be able to produce large volume synthesis with little damage to the carbon graphite skeleton. Stated differently, improper exfoliation can result in chemically synthesized graphene samples with many layers and various graphitic carbon structural defects. The chemical removed graphene sample, also known as graphene oxide, can have its defects restored or removed using post-synthesis reduction techniques. There is a strong similarity between these reduced samples, frequently referred to as reduced graphene oxide (rGO), and graphene samples produced in the vapour phase. It's also critical to remember that samples of chemically manufactured graphene always include many functional groups at their borders, which can have differing degrees of beneficial and detrimental effects. Throughout the construction of the composite, these functional groups might act as anchors for their compositing equivalents.

According to previous research, Ying Yang et al.[4] synthesized NiCo<sub>2</sub>O<sub>4</sub>/rGO nanocomposites as and reported their fast (3.51) H<sub>2</sub>S sensing response at 100 ppm. Xiao-Feng Wang et al. have proposed that NiFe<sub>2</sub>O<sub>4</sub> hexagonal bipyramids, which are metal-organic frameworks with tuneable compositions, might be helpful for n-propanol sensing at low temperatures (120°C). In a similar vein, [5] combined CuFe<sub>2</sub>O<sub>4</sub> with rGO to increase the ammonia (NH<sub>3</sub>) smelling sensitivities by 25% for 200 ppm and 2% for 5 ppm.

We successfully generated pure MMn<sub>2</sub>O<sub>4</sub> and MMn<sub>2</sub>O<sub>4</sub>/rGO (M=Ni, Co) shaped like a nanocomposites by employing the co-precipitation and wet impregnation techniques. A detailed investigation was conducted into the gas-sensing capabilities of MMn<sub>2</sub>O<sub>4</sub>/rGO (M = Ni, Co) composites against ammonia gas. For gas sensing applications, the NiMn<sub>2</sub>O<sub>4</sub> and CoMn<sub>2</sub>O<sub>4</sub> pyramids can offer a large specific surface area. In addition to offering electron-conductive pathways, the composite structure made of rGO sheets keeps the active components from aggregating.

## EXPERIMENT SECTION

### 1.2.1 Chemicals

Merck provided sodium hydroxide (NaOH), manganese nitrate tetrahydrate (Mn(NO<sub>3</sub>)<sub>2</sub>.4H<sub>2</sub>O), nickel nitrate hexahydrate (Ni(NO<sub>3</sub>)<sub>2</sub>.6H<sub>2</sub>O), and cobalt nitrate hexahydrate (Co(NO<sub>3</sub>)<sub>2</sub>.4H<sub>2</sub>O) without performing any further purification processes. The enhanced Hummers' method was used to create graphite oxide, and double-distilled water (DDW) was used as the solvent.

### 1.2.2 Preparation of rGO

Typically, to make rGO, 25 mg of graphene oxide (GO) are dissolved in 50 ml of water, the mixture is sonicated for an hour, and then 20 ml of ammonia solution is added dropwise to the mixture to produce a smooth, brown graphene oxide distribution. The aqueous solution was then moved to a Teflon-lined autoclave and heated to 180°C for six hours. Following autoclave cooling to room temperature, the resulting material underwent centrifugation, comprehensive cleaning, and a 12-hour drying process at 60 °C[6].

### 1.2.3 Preparation of NiMn<sub>2</sub>O<sub>4</sub>, CoMn<sub>2</sub>O<sub>4</sub>, NiMn<sub>2</sub>O<sub>4</sub>/rGO and CoMn<sub>2</sub>O<sub>4</sub>/rGO

In this study, NiMn<sub>2</sub>O<sub>4</sub> was produced via the co-precipitation process. To dissolve 10.92 g of Mn(NO<sub>3</sub>)<sub>2</sub>.4H<sub>2</sub>O, it was first agitated in 80 mL of distilled water for 30 minutes. To begin, 5.68 g of Ni (NO<sub>3</sub>)<sub>2</sub>.6H<sub>2</sub>O. The solution above was heated to 6 °C in order to produce a homogeneous mixture. After then, the temperature was increased to 90 °C. The pH of the resultant aqueous solution was adjusted to 12 by adding sodium hydroxide

(NaOH, 2M) drop-wise. After 90 minutes, the precipitates were centrifuged, washed with double-distilled water, and dried at 100°C for 24 hours. The end product was baked at 900 °C for three hours after being dried and ground into a fine powder. Using, pure  $\text{CoMn}_2\text{O}_4$  was created[7].

#### Gas-sensing device fabrication and measurements

To generate the gas detecting material, the annealed powder samples were stirred in ultrapure water using ultrasonic vibrations for 30 minutes. Subsequently, the solution was spread onto a glass substrate that had been coated with FTO, and it was dried at 80 °C for three hours. The gas-detecting capabilities of the sensor were measured using a pico ammeter that is connected to it and kept inside a chamber [8]. A sealed testing box with varying quantities of the target gas was used to house the associated sensors. The reaction of the  $\text{MMn}_2\text{O}_4/\text{rGO}$  (M = Ni, Co) gas sensors was given by the value of  $S = I_g / I_a$ , where  $I_g$  was the sensor current for different target gas levels and  $I_a$  was the sensor current for an open-air environment [9].

## RESULTS AND DISCUSSION

### 1.4.1 XRD analysis

Figs. 1.1 & 1.2 display the XRD patterns of the rGO,  $\text{NiMn}_2\text{O}_4$ ,  $\text{NiMn}_2\text{O}_4/\text{rGO}$ ,  $\text{CoMn}_2\text{O}_4$ , and  $\text{CoMn}_2\text{O}_4/\text{rGO}$  samples. The (002), (110), and (004) planes of rGO contributed to the peaks in the rGO sample (Fig. 1.1) at 25.6°, 44.55°, and 55.2°, respectively, according to JCPDS card No. 75-2078 [10]. The observed peak broadness at 25.6° may be due to the presence of oxygen-containing functional groups such as epoxy, hydroxyl, and carbonyl on the surface/edges of rGO, which serve as anchoring sites for metal oxides. The (111), (220), (311), (222), (400), (422), (511), and (440) crystals are represented by the  $\text{NiMn}_2\text{O}_4$  diffraction peaks at 18.1°, 30.8°, 35.4°, 37.4°, 53.03°, 43.03°, 56.9°, and 62.4°, as shown in Fig. 1.2 (a, b).

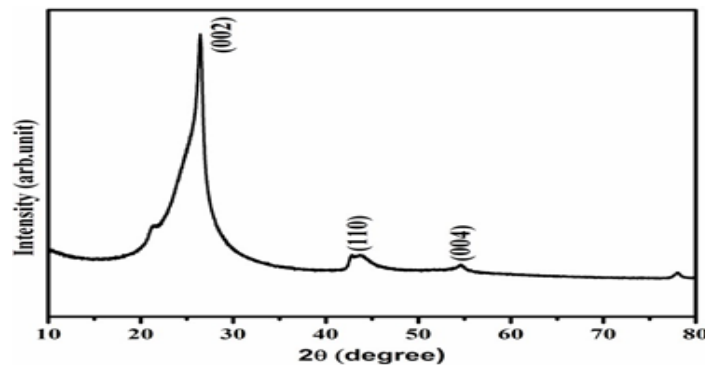


Fig. 1.1 XRD pattern of rGO

The  $\text{NiMn}_2\text{O}_4/\text{rGO}$  composite sample (Fig. 1.2b) also had the diffraction peak of rGO and the distinctive peaks of  $\text{NiMn}_2\text{O}_4$ , indicating the formation of the  $\text{NiMn}_2\text{O}_4/\text{rGO}$  composite [11]. The cubic  $\text{CoMn}_2\text{O}_4$  crystal planes (101), (112), (103), (211), (004), (220), (105), (321), (215), (323), and (413) coincide with the  $\text{CoMn}_2\text{O}_4$  diffraction peaks in Fig. 6.2(c) at 18.1°, 29.3°, 30.8°, 33.3°, 36.7°, 36.8°, 44.2°, 51.07°, 52.7°, 53.9°, and 60.8°. In the case of the  $\text{CoMn}_2\text{O}_4/\text{rGO}$  sample (Fig. 1.2 d), the identification of diffraction peaks corresponding to both  $\text{CoMn}_2\text{O}_4$  and rGO confirms the successful formation of the nanocomposite[12].

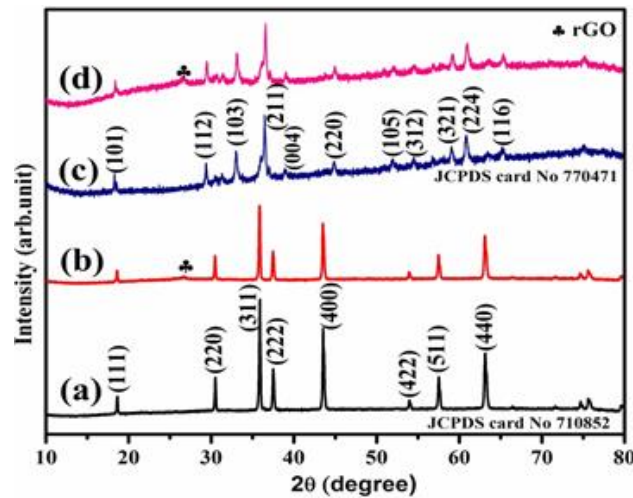


Fig. 1.2 XRD patterns of (a)  $\text{NiMn}_2\text{O}_4$ , (b)  $\text{NiMn}_2\text{O}_4/\text{rGO}$ , (c)  $\text{CoMn}_2\text{O}_4$ , and (d)  $\text{CoMn}_2\text{O}_4/\text{rGO}$  nanocomposite

#### 1.4.2 FTIR analysis

The FTIR spectra of the rGO,  $\text{NiMn}_2\text{O}_4$ ,  $\text{NiMn}_2\text{O}_4/\text{rGO}$ ,  $\text{CoMn}_2\text{O}_4$ , and  $\text{CoMn}_2\text{O}_4/\text{rGO}$  samples are shown in Fig. 1.3. The peak at  $1190\text{ cm}^{-1}$  in the FTIR spectra of rGO (Fig. 1.3a) was attributed to C-OH stretching, whereas the peak at  $1560\text{ cm}^{-1}$  originated from the C=C structure of graphene sheets. The  $\text{Ni}^{2+}$  and  $\text{Mn}^{3+}/\text{Mn}^{4+}$  at around  $531\text{ cm}^{-1}$  and  $621\text{ cm}^{-1}$  caused the two strong bands that were observed in the  $\text{NiMn}_2\text{O}_4$  and  $\text{NiMn}_2\text{O}_4/\text{rGO}$  samples (Fig. 1.3(b, c)). [13]. The observed reduction in the intensity of the C=O stretching vibrational band at  $1737\text{ cm}^{-1}$  in the  $\text{NiMn}_2\text{O}_4/\text{rGO}$  sample (Fig. 1.3(c)) [14] confirms the formation of the nanocomposite. Similarly, two peaks in the lower wavenumber range ( $451\text{ cm}^{-1}$  and  $598\text{ cm}^{-1}$ ) of the FTIR spectra of the  $\text{CoMn}_2\text{O}_4$  and  $\text{CoMn}_2\text{O}_4/\text{rGO}$  samples, as shown in Fig. 1.3(d, e), verified the presence of metal-oxygen stretching vibrations. These peaks were associated with  $\text{Mn}^{3+}/\text{Mn}^{4+}\text{O}^{2-}$  and  $\text{Co}^{2+}$ . Furthermore, each sample showed a few distinct peaks. The signal seen at  $2922\text{ cm}^{-1}$  can be attributed to the  $\text{CO}_2$  molecule that was deposited on the surface from the surrounding environment [15]. The OH stretching vibrations of  $\text{H}_2\text{O}$  molecules are linked to the big peak at around  $3421\text{ cm}^{-1}$ .

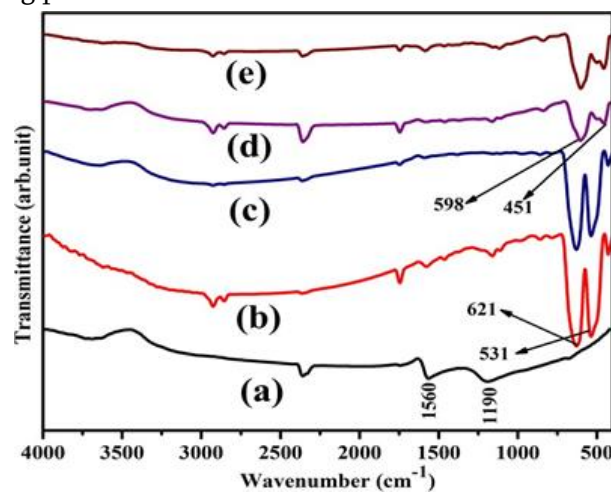


Fig. 1.3 FTIR transmittance spectrum of (a) rGO (b)  $\text{NiMn}_2\text{O}_4$ , (c)  $\text{NiMn}_2\text{O}_4/\text{rGO}$ , (d)  $\text{CoMn}_2\text{O}_4$  and (e)  $\text{CoMn}_2\text{O}_4/\text{rGO}$  nanocomposite

### 1.4.3 Morphological characterization

A FESEM was used to analyse the morphology of the pure and rGO composited metal oxide samples. Fig. 6.4 (a-d) displays the FESEM images of pure  $\text{NiMn}_2\text{O}_4$  and  $\text{CoMn}_2\text{O}_4$ , which demonstrate the creation of regularly-shaped particles. The  $\text{NiMn}_2\text{O}_4$  samples (Fig. 1.4(a, b)) have an irregular thickness and a three-dimensional hexagonal form. The  $\text{CoMn}_2\text{O}_4$  sample exhibits a well-grown pyramid-like structure, as seen in Fig. 1.4(c, d) [16]. As previously reported [17], the wet impregnation method is among the simplest and most efficient techniques to produce graphene-based composites.

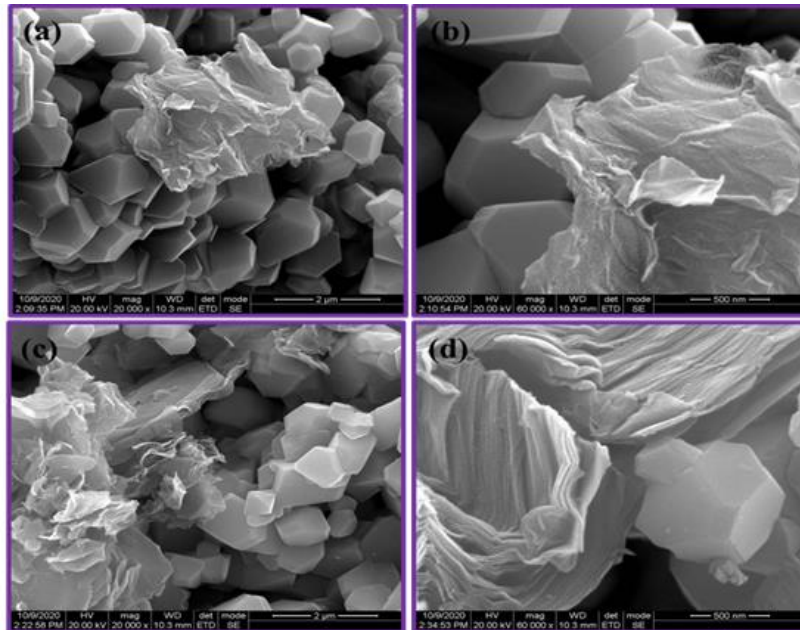


Fig. 1.4 FESEM images of (a, b)  $\text{NiMn}_2\text{O}_4$ , and (c, d)  $\text{CoMn}_2\text{O}_4$

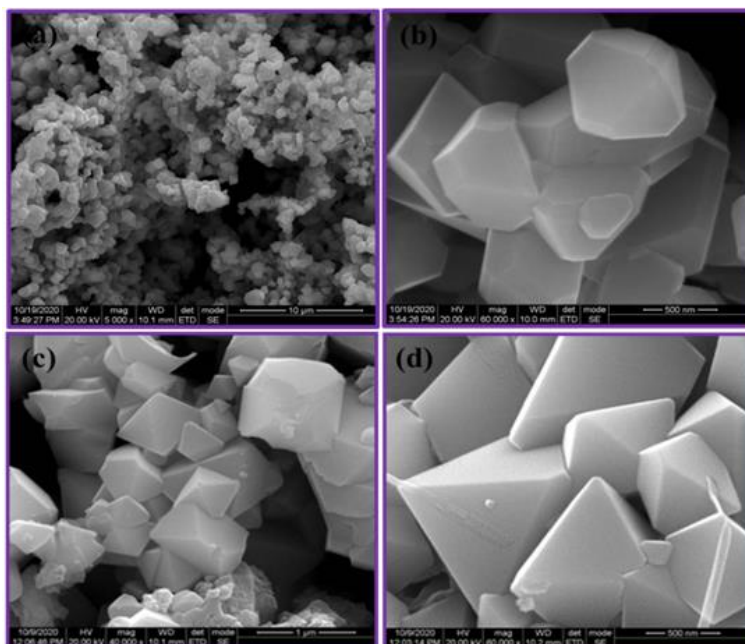


Fig. 1.5 FESEM images of (a, b)  $\text{NiMn}_2\text{O}_4/\text{rGO}$ , and (c, d)  $\text{CoMn}_2\text{O}_4/\text{rGO}$  nanocomposite

Here, the wet impregnation approach was used to fix the NiMn<sub>2</sub>O<sub>4</sub> and CoMn<sub>2</sub>O<sub>4</sub> nanoparticles over the rGO layers, which was expected to help improve the resultant samples' gas sensing abilities. Exfoliating rGO sheets coated with MMn<sub>2</sub>O<sub>4</sub> (M=Ni, Co) are shown in Fig. 1.5. In the NiMn<sub>2</sub>O<sub>4</sub>/rGO (Fig. 1.5(a, b)) and CoMn<sub>2</sub>O<sub>4</sub> (Fig. 1.5(c, d)) samples, MMn<sub>2</sub>O<sub>4</sub> has been integrated with rGO.

## GAS SENSING PERFORMANCE

Sensing materials having suitable nanostructures, such nanoparticles, nanowires, nanoflowers, etc., are frequently used to create better gas sensors[18]. Researchers have hypothesized that creating distinctive morphology or shapes and structures on the sensing surface might be one approach to get favourable results[19]. For example, Yi Zeng et al. demonstrated that CoFe<sub>2</sub>O<sub>4</sub> double-shelled hollow spheres exhibited a sensing response of 0.6 to ammonia at room temperature[20].

The gas sensing performance (current against time) of the samples was evaluated (at 30°C) by equally adding 100 ppm of NH<sub>3</sub> into the gas sensing chamber for each generated sample. The sensing response was then determined by measuring the current value. As shown in Figure 1.6(a), the sensitivity values for the pure NiMn<sub>2</sub>O<sub>4</sub> and CoMn<sub>2</sub>O<sub>4</sub> samples were found to be 1.03 and 1.5, respectively. The calculated sensitivity values for NiMn<sub>2</sub>O<sub>4</sub>/rGO and CoMn<sub>2</sub>O<sub>4</sub>/rGO rose to 1.55 and 3.5, respectively, in the case of composite samples. The CoMn<sub>2</sub>O<sub>4</sub>/rGO sample showed an unusually higher sensitivity value in comparison to the other samples. This is explained by the fact that in addition to the charge, there are additional active sites for oxygen adsorption.

The CoMn<sub>2</sub>O<sub>4</sub>/rGO gas sensor's selectivity was evaluated by subjecting it to 100 ppm concentrations of several gases, including acetone (CH<sub>3</sub>COCH<sub>3</sub>), ethanol (CH<sub>3</sub>CH<sub>2</sub>OH), and ammonia (NH<sub>3</sub>). The selectivity characteristic data for the CoMn<sub>2</sub>O<sub>4</sub>/rGO sample are shown in Fig. 1.6(c). It has been demonstrated that the sensor is selective for ammonia gas at room temperature and has a maximum sensitivity value of 3.5. Ten exposure cycles later, the sensing test was repeated to further investigate the long-term stability of the CoMn<sub>2</sub>O<sub>4</sub>/rGO sensor. The findings are shown in Fig. 1.6 (d). It was found that there had been just a minor reduction in the sensor's detecting response. The obtained results show that the CoMn<sub>2</sub>O<sub>4</sub>/rGO gas sensor displays long-term stability for repeated cycle detections. Fig. 1.7 shows the CoMn<sub>2</sub>O<sub>4</sub>/rGO gas sensor's response and recovery times to various NH<sub>3</sub> concentrations (10 ppm - 100 ppm). The response time increased from 60 seconds to around 140 seconds as the gas concentration increased. The recuperation time increased from 120 to around 150 seconds at initially. On the other hand, the recovery time decreased to 60 seconds above 50 ppm at an ammonia concentration of 100 ppm.

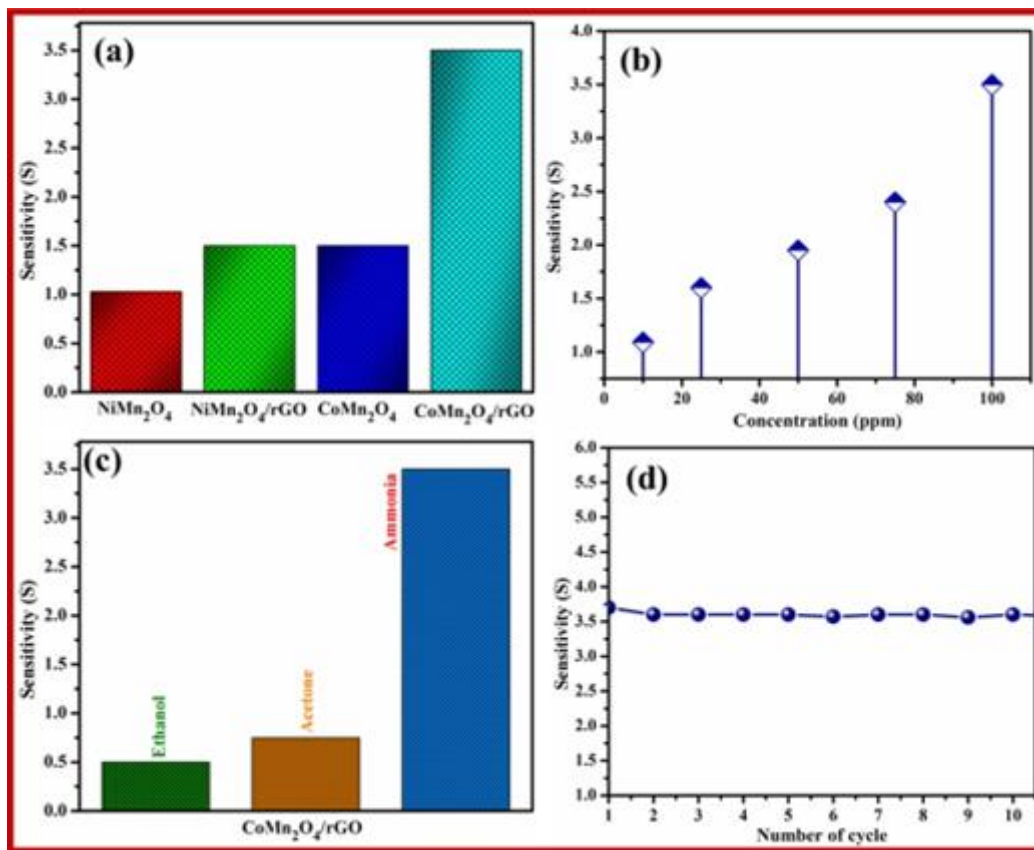


Fig. 1.6 (a) Comparison of sensitivity of MMn<sub>2</sub>O<sub>4</sub> (M= Ni, Co), and MMn<sub>2</sub>O<sub>4</sub>/rGO (M=Ni, Co)/rGO, to 100 ppm NH<sub>3</sub> gas. (b) Gas sensing response of the CoMn<sub>2</sub>O<sub>4</sub>/rGO to different concentrations of NH<sub>3</sub>. (c) Comparison of gas sensing response of the CoMn<sub>2</sub>O<sub>4</sub>/rGO towards different gases. (d) Stability of the CoMn<sub>2</sub>O<sub>4</sub>/rGO sensor to NH<sub>3</sub> up to 10 cycles

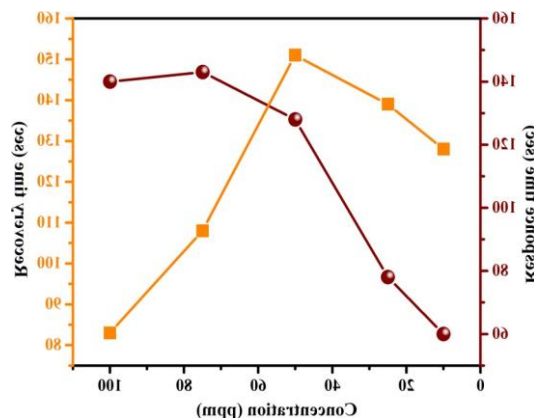


Fig. 1.7 Response and recovery time curve of CoMn<sub>2</sub>O<sub>4</sub>/rGO sample

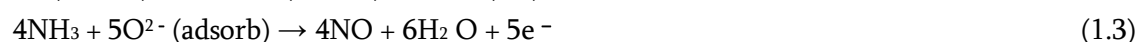
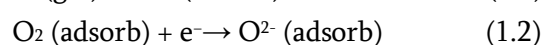
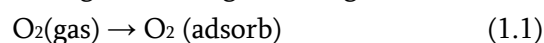
### SENSING MECHANISM

It is well known that the fundamental mechanism for gas detection is molecules adhering and desorbing on the sensor surface [21]. Several published articles have shown how beneficial these types of sensors may be.



In this case, the surface of CoMn<sub>2</sub>O<sub>4</sub>/rGO is composed of several hetero-Nano grains, on which the adsorbed O<sub>2</sub> molecules from the surrounding air result in a change in current. More specifically, the oxygen molecules adsorbed on the surface of the CoMn<sub>2</sub>O<sub>4</sub>/rGO nanocomposite arrest free electrons from the conduction band, generating O<sup>2-</sup> oxygen ions [22]. This causes a free-electron deficit, which restricts the amount of current that may flow. As of right now, the primary factor affecting the current produced by the CoMn<sub>2</sub>O<sub>4</sub>/rGO nanocomposite is the production of oxygen ions.

The production of oxygen ions on the sensor surface may be controlled by adjusting the operating temperature. In particular, at very low temperatures, only the O<sup>2-</sup> (< 100 °C) and O<sup>-</sup> (100-300 °C) ions may be chemically generated[23].The following equations show the general potential response in CoMn<sub>2</sub>O<sub>4</sub>/rGO during ammonia gas sensing.



Ammonia gas becomes oxidized when it combines with oxygen ions, according to equation (1.3). Numerous studies on selective oxidation-based ammonia sensing have been published. For example, Lihua Hub et al. [24] reported the use of coral-shaped Dy<sub>2</sub>O<sub>3</sub> that was hydrothermally generated for ammonia sensing at ambient temperature. By acting as a catalyst, the sensor converted the ammonia gas into NO and H<sub>2</sub>O. Researchers have explored a wide range of catalysts, but in particular, transition metal oxides that form hydrazinium-type intermediate during the oxidation of ammonia, such as Ag/Al<sub>2</sub>O<sub>3</sub>, MnOx/CeO<sub>2</sub>, La-hexaaluminates (La-M, where M = Fe, Cu, Co, and Mn) catalysts [25], etc. By passing the reducing gas (NH<sub>3</sub>) past the sensor (CoMn<sub>2</sub>O<sub>4</sub>/rGO), where it interacts with the adsorbed oxygen anions, oxygen is extracted from the sample in this experiment.

## CONCLUSION

An extremely sensitive gas sensor for ammonia (NH<sub>3</sub>) was developed utilizing a rGO nanosheet sample that had a CoMn<sub>2</sub>O<sub>4</sub> pyramid on it. The surface of reduced graphene oxide (rGO) was consistently anchored by CoMn<sub>2</sub>O<sub>4</sub> pyramid micro/nano networks. The NH<sub>3</sub> sensing capabilities of the synthesized materials were evaluated at different gas concentrations. With a 3.5 for 100 ppm at room temperature, the CoMn<sub>2</sub>O<sub>4</sub>/rGO nanocomposite sample performed better than the NiMn<sub>2</sub>O<sub>4</sub> (1.03), CoMn<sub>2</sub>O<sub>4</sub> (1.5), and NiMn<sub>2</sub>O<sub>4</sub>/rGO (1.55) samples. The observed results indicate that the pyramid-shaped CoMn<sub>2</sub>O<sub>4</sub> nanostructure with rGO has potential applications in high-performance gas sensor systems.

## REFERENCES

- [1] A. Umar, M.S. Akhtar, S. Ameen, M. Imran, R. Kumar, Y. Wang, A.A. Ibrahim, H. Albargi, M. Jalalah, M.A. Alsaiari, M.S. Al-Assiri, Colloidal synthesis of NiMn<sub>2</sub>O<sub>4</sub> nanodisks decorated reduced graphene oxide for electrochemical applications, *Microchem. J.* 160 (2021) 105630. <https://doi.org/10.1016/j.microc.2020.105630>.

- [2] T. Larbi, L. Ben Said, A. Ben Daly, B. Ouni, A. Labidi, M. Amlouk, Ethanol sensing properties and photocatalytic degradation of methylene blue by  $Mn_3O_4$ ,  $NiMn_2O_4$  and alloys of Ni-manganates thin films, *J. Alloys Compd.* 686 (2016) 168–175. <https://doi.org/10.1016/j.jallcom.2016.06.001>.
- [3] T. Zone, L. Among, *Us Pt Us Pt*, *Biomed. Mater.* *Accept.* (2020) 0–16.
- [4] Y. Guan, C. Yin, X. Cheng, X. Liang, Q. Diao, H. Zhang, G. Lu, Sub-ppm  $H_2S$  sensor based on YSZ and hollow balls  $NiMn_2O_4$  sensing electrode, *Sensors Actuators, B Chem.* 193 (2014) 501–508. <https://doi.org/10.1016/j.snb.2013.11.072>.
- [5] Y. Gawli, S. Badadhe, A. Basu, D. Guin, M. V. Shelke, S. Ogale, Evaluation of n-type ternary metal oxide  $NiMn_2O_4$  nanomaterial for humidity sensing, *Sensors Actuators, B Chem.* 191 (2014) 837–843. <https://doi.org/10.1016/j.snb.2013.10.071>.
- [6] J. Deng, H. Lu, B. Xu, Y. Cao, W. Yang, J. Liu,  $NiMn_2O_4$ -based Ni-Mn bimetallic oxides as electrocatalysts for the oxygen reduction reaction in Al–air batteries, *Chem. Eng. J.* 413 (2021) 127439. <https://doi.org/10.1016/j.cej.2020.127439>.
- [7] Z. Zhao, Y. He, X. Qi, N. Li, Z. He, B. Liu, H. Lai, Y. Chen, T. Jin, Synthesis of nanoflower-like  $NiMnO_3$  combined with MWCNTs for the electrochemical determination of fentanyl, *Electrochim. Acta* 462 (2023) 142747. <https://doi.org/10.1016/j.electacta.2023.142747>.
- [8] X. Zhou, X. Cheng, Y. Zhu, A.A. Elzatahry, A. Alghamdi, Y. Deng, D. Zhao, Ordered porous metal oxide semiconductors for gas sensing, *Chinese Chem. Lett.* 29 (2018) 405–416. <https://doi.org/10.1016/j.ccllet.2017.06.021>.
- [9] T. Zhou, T. Zhang, Recent Progress of Nanostructured Sensing Materials from 0D to 3D: Overview of Structure–Property–Application Relationship for Gas Sensors, *Small Methods* 5 (2021) 1–32. <https://doi.org/10.1002/smtd.202100515>.
- [10] T. Zhou, T. Zhang, J. Deng, R. Zhang, Z. Lou, L. Wang, P-type  $Co_3O_4$  nanomaterials-based gas sensor: Preparation and acetone sensing performance, *Sensors Actuators, B Chem.* 242 (2017) 369–377. <https://doi.org/10.1016/j.snb.2016.11.067>.
- [11] H.J. Zhang, L.Z. Liu, X.R. Zhang, S. Zhang, F.N. Meng, Microwave-assisted solvothermal synthesis of shape-controlled  $CoFe_2O_4$  nanoparticles for acetone sensor, *J. Alloys Compd.* 788 (2019) 1103–1112. <https://doi.org/10.1016/j.jallcom.2019.03.009>.
- [12] H.T. Zhang, X.H. Chen, Size-dependent x-ray photoelectron spectroscopy and complex magnetic properties of  $CoMn_2O_4$  spinel nanocrystals, *Nanotechnology* 17 (2006) 1384–1390. <https://doi.org/10.1088/0957-4484/17/5/037>.
- [13] Z. Zanolli, R. Leghrib, A. Felten, J.J. Pireaux, E. Llobet, J.C. Charlier, Gas sensing with au-decorated carbon nanotubes, *ACS Nano* 5 (2011) 4592–4599. <https://doi.org/10.1021/nn200294h>.
- [14] W. Yu-De, C. Zhan-Xian, L. Yan-Feng, Z. Zhen-Lai, W. Xing-Hui, Electrical and gas-sensing properties of  $WO_3$  semiconductor material, *Solid. State. Electron.* 45 (2001) 639–644. [https://doi.org/10.1016/S0038-1101\(01\)00126-5](https://doi.org/10.1016/S0038-1101(01)00126-5).
- [15] Z. Li, Y. Gao, P. An, F. Lan, Y. Wu, Abstract : Pr ep pe er re v iew Pr ep er ed, (2000).
- [16] Q. Wu, H. Zhang, L. Zhou, C. Bao, H. Zhu, Y. Zhang, Synthesis and application of rGO/ $CoFe_2O_4$  composite for catalytic degradation of methylene blue on heterogeneous Fenton-like oxidation, *J. Taiwan Inst. Chem. Eng.* 67 (2016) 484–494. <https://doi.org/10.1016/j.jtice.2016.08.004>.

- [17] S.D. Waghmare, S.D. Raut, B.G. Ghule, V. V. Jadhav, S.F. Shaikh, A.M. Al-Enizi, M. Ubaidullah, A. Nafady, B.M. Thamer, R.S. Mane, Pristine and palladium-doped perovskite bismuth ferrites and their nitrogen dioxide gas sensor studies, *J. King Saud Univ. - Sci.* 32 (2020) 3125–3130. <https://doi.org/10.1016/j.jksus.2020.08.024>.
- [18] T. Van Tran, H.T.T. Nguyen, H.H. Dang, D.T.C. Nguyen, D.H. Nguyen, T. Van Pham, L. Van Tan, Central composite design for optimizing the organic dyes remediation utilizing novel graphene oxide@CoFe<sub>2</sub>O<sub>4</sub> nanocomposite, *Surfaces and Interfaces* 21 (2020) 100687. <https://doi.org/10.1016/j.surfin.2020.100687>.
- [19] W. Ren, Y.C. Zhang, N.N. Zhu, A.L. Feng, S.G. Shang, Synthesis of NiMn<sub>2</sub>O<sub>4</sub> thin films via a simple solid-state reaction route, *Ceram. Int.* 46 (2020) 11675–11679. <https://doi.org/10.1016/j.ceramint.2020.01.198>.
- [20] M. Zong, Y. Huang, N. Zhang, Reduced graphene oxide-CoFe<sub>2</sub>O<sub>4</sub> composite: Synthesis and electromagnetic absorption properties, *Appl. Surf. Sci.* 345 (2015) 272–278. <https://doi.org/10.1016/j.apsusc.2015.03.203>.
- [21] M.E. Hassan Amrani, R.M. Dowdeswell, P.A. Payne, K.C. Persaud, An intelligent gas sensing system, *Sensors Actuators, B Chem.* 44 (1997) 512–516. [https://doi.org/10.1016/s0925-4005\(97\)00240-2](https://doi.org/10.1016/s0925-4005(97)00240-2).
- [22] S. Acharyya, S. Nag, S. Kimbahun, A. Ghose, A. Pal, P.K. Guha, Selective Discrimination of VOCs Applying Gas Sensing Kinetic Analysis over a Metal Oxide-Based Chemiresistive Gas Sensor, *ACS Sensors* 6 (2021) 2218–2224. <https://doi.org/10.1021/acssensors.1c00115>.
- [23] S. Basu, P. Bhattacharyya, Recent developments on graphene and graphene oxide based solid state gas sensors, *Sensors Actuators, B Chem.* 173 (2012) 1–21. <https://doi.org/10.1016/j.snb.2012.07.092>.
- [24] Y. Dan, Y. Cao, T.E. Mallouk, A.T. Johnson, S. Evoy, Dielectrophoretically assembled polymer nanowires for gas sensing, *Sensors Actuators, B Chem.* 125 (2007) 55–59. <https://doi.org/10.1016/j.snb.2007.01.042>.
- [25] E. Comini, A. Cristalli, G. Faglia, G. Sberveglieri, Light enhanced gas sensing properties of indium oxide and tin dioxide sensors, *Sensors Actuators, B Chem.* 65 (2000) 260–263. [https://doi.org/10.1016/S0925-4005\(99\)00350-0](https://doi.org/10.1016/S0925-4005(99)00350-0).

# Theoretical Study of Catechol and Hydroquinone with Solvent Molecule

Dr. Chandrakant S. Aher

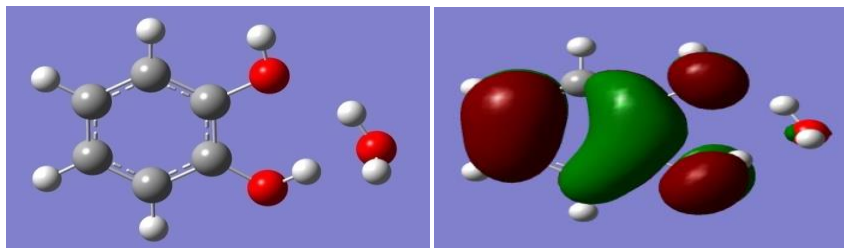
Department of Chemistry, M.S.G. College Malegaon Camp, Pin 423105. India.

Email: [chandsaher55555@gmail.com](mailto:chandsaher55555@gmail.com)

## ABSTRACT

Computational study using Gaussian 09W software, DFT method, B3LYP 6-31(G)d as basis set was performed on Window-7, Intel core i5 system. Theoretical study of experimental molecules and their combinations were optimized to understand the fundamental interactions between Catechol and hydroquinone with water. Data obtained is applicable in the field of solution chemistry.

**Keyword:** DFT, Gaussian, Catechol, Hydroquinone.



## INTRODUCTION

Gaussian software is now very important tool in theoretical chemistry for interpretation of structure of various organic molecules [1, 2]. Hence we used this software for explaining interactions between molecules. Phenolic compounds were reported as antibacterial activity in various plants. Catechol and pyrogallol are allelochemicals which belong to phenolic compounds synthesized in plants [3]. In synthetic organic chemistry Catechol is use as precursor, polymer and dyes industries [4]. The antimicrobial property of arbutin and hydroquinone as the active metabolite is responsible for antimicrobial activity [5, 6]. Solvent-solvent and solvent-solute interactions of electrolytes are extremely important for the synthesis, design of processes and simulations of unit operations [7, 8].

The HOMO-LUMO energy gap shown in Table-1 and Fig.1 are calculated by equation:

$$\text{Energy Gap} = E. \text{ LUMO} - E. \text{ HOMO} \quad \dots(1)$$

Where E. LUMO is energy of LUMO in eV and E. HOMO is energy of LUMO in eV.

Electrochemical properties: EHOMO describes the charge density i.e. higher the EHOMO energy the greater the ability of the molecule to donate electrons. Large EHOMO-LUMO energy difference means electronic excitation required high energy i.e. electron have less tendency to move to the excited state and such molecules are chemically more inert. [9, 10]

According to Koopman's theorem, global reactivity descriptor such as:

$$\text{Electronegativity } (\chi) = -1/2 (\text{EHOMO} + \text{ELUMO})$$

$$\text{Chemical potential } (\mu) = 1/2 (\text{EHOMO} + \text{ELUMO})$$

$$\text{Global hardness } (\eta) = 1/2 (\text{ELUMO} - \text{EHOMO})$$

$$\text{Electrophilicity index } (\omega) = \mu^2 / 2\eta$$

$$\text{Ionization energy } (I) = - \text{ELUMO}$$

$$\text{Electron affinity } (A) = - \text{EHOMO}$$

All these values are summarised in Table-2.

## EXPERIMENTAL SECTIONS

**2.1 Material:** -Triple distilled water was used in all experiments. Other chemicals was supplied by

Name of Chemical	Name of supplier	Percentage purity	Standard
Catechol	Sigma-Aldrich co.	≥99%	Reagent Grade
Hydroquinone	Sigma-Aldrich co.	99%	Reagent Grade

**2.2 Procedure:** -Theoretical study of experimental molecules and their combinations were optimized on Window-7, Intel core i5 system. Computational study using Gaussian 09W software, DFT method, B3LYP 6-31(G)d as basis set was performed to understand the fundamental interactions between solvent-solvent and solute-solvent molecules.[11-13]

**Table 1-HOMO, LUMO energies and Energy Gap between LUMO-HOMO Calculated by DFT method at B3LYP level (d) using 6-31G basis set.**

System	Phase/ Media	HOMO (eV)	LUMO (eV)	LUMO-HOMO Energy gap (eV)
C	Gas	-5.624	0.219	5.843
	Water	-8.179	-4.047	4.132
H	Gas	-5.412	-0.062	5.350
	Water	-5.536	-0.174	5.361
W	Gas	-7.924	1.704	9.628
	Water	-8.035	2.062	10.097
WC	Gas	-5.540	0.235	5.775
	Water	-5.695	0.114	5.809
WH	Gas	-4.926	0.365	5.290
	Water	-5.316	-0.036	5.280

**Figure1-HOMO, LUMO structures with LUMO-HOMO Energy Gap.**

Molecule	HOMO	L-H E.G.(eV)	LUMO
C		Gas 5.843	
		Water 4.132	
H		Gas 5.350	
		Water 5.361	
W		Gas 9.628	
		Water 10.097	
WC		Gas 5.775	
		Water 5.809	
WH		Gas 5.290	
		Water 5.280	

**Table 2- Global chemical reactivity indices. [Chemical Hardness ( $\eta$ ), Chemical Softness ( $\delta$ ), Electronegativity ( $\chi$ ), Electrochemical potential ( $\mu$ ), Global electrophilicity index ( $\omega$ ), Electron affinity (A), Ionization energy (I)]**

Molecule	Phase/ Media	$\eta$ (eV)	$\delta$ (eV)	$\chi$ (eV)	$\mu$ (eV)	$\omega$ (eV)	A (eV)	I (eV)
C	Gas	2.92	0.34	2.70	-2.70	1.25	-0.22	5.62
	Water	2.07	0.48	6.11	-6.11	9.04	4.05	8.18
H	Gas	2.68	0.37	2.74	-2.74	1.40	0.06	5.41
	Water	2.68	0.37	2.86	-2.86	1.52	0.17	5.54
W	Gas	4.81	0.21	3.11	-3.11	1.00	-1.70	7.92
	Water	5.05	0.20	2.99	-2.99	0.88	-2.06	8.04
WC	Gas	2.89	0.35	2.65	-2.65	1.22	-0.23	5.54
	Water	2.90	0.34	2.79	-2.79	1.34	-0.11	5.70
WH	Gas	2.65	0.38	2.28	-2.28	0.98	-0.36	4.93
	Water	2.64	0.38	2.68	-2.68	1.36	0.04	5.32

**Figure 2-Optimized structures of solute, solvents combinations by DFT method at B3LYP level using 6-31G(d) basis set.**

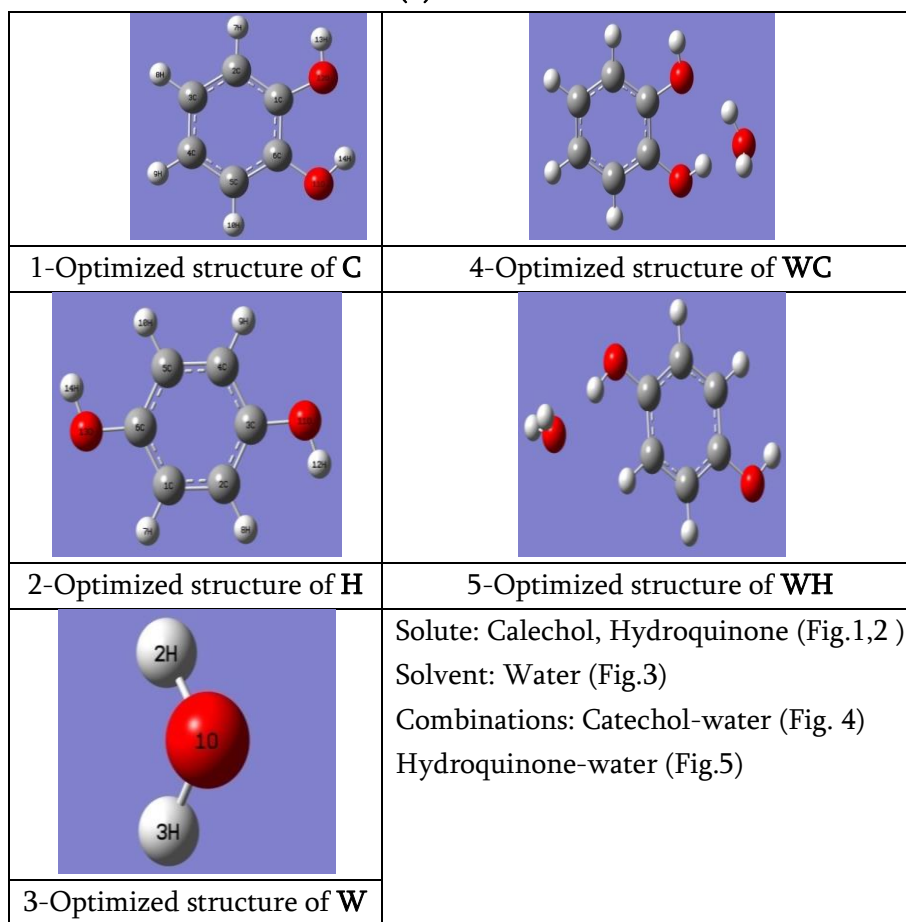


**Table 3- Theoretical Thermodynamic functions calculated by DFT/B3LYP method at 6-31G (d) basis set**

Molecule	Phase/Media	E (RB3LYP) a.u.	Zero point vibrational energy Kcal/mol.	Nuclear Repulsion Energy Hartrees	Total Energy(a.u.)		
					E(Thermal) Kcal/mol.	C <sub>v</sub> cal/mol.Kel v.	S cal/mol.Kel v.
C	Gas	-382.68162	68.29475	350.698	72.536	26.54	80.44
	Water	-382.68967	68.16156	350.5293	72.399	26.57	80.39
H	Gas	-382.678	68.1481	343.8718	72.406	26.712	80.57
	Water	-382.688	67.9844	343.6457	72.251	26.775	80.631
W	Gas	-76.40895	13.2834	9.088237	15.062	5.997	45.14
	Water	-76.41630	13.25463	9.079528	15.033	5.997	45.15
WC	Gas	-459.10680	83.88594	438.1257	89.974	35.759	99.51
	Water	-459.12005	83.69986	438.7085	89.709	35.738	95.65
WH	Gas	-459.102	83.3329	421.6249	89.842	36.817	100.96
	Water	-459.119	83.3464	423.0705	89.662	36.467	98.159

## RESULTS AND DISCUSSIONS

Computational study using Gaussian 09 software, with DFT, B3LYP, 6-31(G)d method was performed to understand the fundamental interactions between solvent-solvent and solute-solvent molecules. First, the structures of the solvent were optimized and stable conformers were obtained. The optimized structure of water then interacted with solute molecule as shown in Fig.2. Total energy, heat capacity at constant volume, entropy, zero-point vibrational energy and nuclear repulsion energy are given in Table 3. This data is used for the selection of proper solvent for the solute.

HOMO-LUMO energy gap gives information of reactivity of molecules. When the energy gap is more molecule is less reactive/may be inert for electronic excitation and vice versa less energy gap shows more reactivity.

## CONCLUSION

Thermochemical parameters as given in Table-3, shows solute molecule increases energy in combination with solvent molecules and hence increase of reactivity. Same result is observed in HOMO-LUMO energy gap decrease hence reactivity increase as shown in Table-1 and Fig.1. These thermochemical parameters are total energy, heat capacity at constant volume, entropy, zero-point vibrational energy and nuclear repulsion energy can provide valuable information about these molecules for further study when these compounds consider as starting materials in new reactions.

## ACKNOWLEDGMENTS

The authors express their sincere thanks to the general secretary M. G. Vidyamandir and Principal M.S.G. College, Malegaon Camp for providing laboratory facility and encouragement.

## REFERENCES

- [1] Mahdir S, Computational Methods for Study of Hydrogen Bonding Between Phenol Derivatives with Ethanol, 2009, Asian Journal of Chemistry, Vol. 21, No. 2 , (2009)879-884
- [2] Zhang F, Comparative theoretical study of three C56 fullerenes, their chlorinated derivatives, and chlorofullerene oxides, Computational and Theoretical Chemistry, 1117,(2017)81-86.
- [3] Hye-Kyoung Song, Jeong-In Oh, Mu-Yong Kim, Yong-Zu Kim, In-Chull Kim and Jin-Hwan Kwak, 1996, Journal of Antimicrobial Chemotherapy, 37, (1996)711-726.
- [4] Barner B. A, "Catechol" in Encyclopedia of Reagents for Organic Synthesis (Ed: L.Paquette), J. Wiley & Sons, New(2004) York. doi:10.1002/047084289
- [5] Jurica K, Gobin I, Kremer D, Cepo D. V, Grubescic R. J, Karaconji I. B, Kosalec I, Arbutin and its metabolite hydroquinone as the main factors in the antimicrobial effect of strawberry tree (Arbutus unedo L.) leaves, Journal of Herbal Medicine-172, (2017)S2210-8033(17)30020-9, DOI: <http://dx.doi.org/doi:10.1016/j.hermed.2017.03.006>.



- [6] Aher C. S, 'Hydroquinone solubility in pure and binary solvent mixtures at various temperatures with FTIR' Research J. pharm. and Tech. 15(1): (January 2022), 40-46.
- [7] Aher C. S, Solubility, Density and Thermodynamic Functions of Catechol in Pure Water, Ethanol and Their Binary Solvent Mixtures at Various Temperatures, International Journal of Research and Analytical Reviews (IJRAR), (May 2019), Volume 6, Issue 2, 640-647. (E-ISSN: 2348-1269, P- ISSN: 2349-5138)
- [8] Mydlarz J, Jones, A. G, Solubility and Density Isotherms for Magnesium Sulfate Heptahydrate-Water-Propan-1-ol, J. Chem. Eng. Data, 36, (1991)119-121.
- [9] Li F.Y and Zhao J. J, At Mol Sci, 1, (2012) 8.
- [10] Mohammad E and Kanaani A, The effect of solvent polarity on solubility of HMX and FOX-7: A DFT study, Indian J. of pure & applied physics, Vol. 55, pp. (July 2017)490-496.
- [11] Aher C. S, Excess molar volume of aqueous 1-propanol and apparent molar volume of 2-Naphthol in water, 1-propanol and their binary mixtures at various temperatures with DFT study, Journal of Applicable Chemistry, 7 (1), (2018), 151-164. (ISSN: 2278-1862)
- [12] Pawar R. R, Aher C. S, Molecular interactions of 2-Naphthol in binary solvent mixtures of water+methanol and water+ethanol with DFT study, International Journal of Chemical and Physical Sciences, 7 (1) (Jan-Feb 2018), 78-88. (ISSN: 2319-6602).
- [13] Aher C. S, DFT study of interaction between 2-naphthol with water, methanol and their binary solvent system' Asian Journal of organic and medicinal chemistry, Vol.7, Issue 2, (2022) 142-156.

# Development & Studies of Effective Plant Based Laboratory Hand Sanitizers & Their Effect on Pathogenic Bacteria

Narsinge A.P, Kadam A.S, Didwani R.D, Ghatol L.S, Gutte D.K, Shinde A.S, Chavan A.N, Waghmare A.V, Sanghai S.P, Dongahu A.D

Department of Microbiology, Yogeshwari Mahavidyalaya, Ambajogai, Dist. Beed (M.S.)-431517, Maharashtra, India

e-mail ID- [narsingeanil@gmail.com](mailto:narsingeanil@gmail.com)

## ABSTRACT

The COVID-19 pandemic highlighted the importance of hand sanitizers in preventing virus transmission, especially when soap and water are unavailable (Tien tran et.al). Background-Many studies have shown that understaffing and increased workload is risk factor for health care-associated epidemics and the goal of hand hygiene is to obtain sufficient reduction of microbial counts on the skin to prevent cross-transmission of pathogens among patients (Ravi kumar seth et. al) There are also studies showing herbal hand sanitizers having significant bacteriostatic effect on hands. The WHO recommended alcohol-based sanitizers with at least 60% alcohol, often combined with plant-based antimicrobials like aloe vera (Ali Khumaeni et.al). While effective in killing the virus, prolonged use of high-alcohol sanitizers (80-95%) can cause skin irritation and tissue damage, potentially allowing bacteria to enter. Post-pandemic, the rise of MDR (Multiple Drug Resisting) bacteria has been linked to poor hand hygiene and contact with contaminated surfaces (Carlos Lopera et.al). Hand sanitizer usage has proven to be a common and practical method for reducing the spread of infectious diseases which can be caused by many harmful pathogens. There is a need for alcohol-free hand sanitizers because most hand sanitizers on the market are alcohol-based, and regular use of them can damage the skin and can be hazardous (J Verma et.al) There is a growing need for sanitizers with less alcohol and more plant-based antimicrobials which can effectively suppress the growth of MDR bacteria & also eco-friendly.

**Key Words:** Eco-friendly, antimicrobial, Sanitizer, Aloe vera

## INTRODUCTION

The pandemic era of corona virus has shown the importance of hand sanitizers in preventing the exposure to the covid virus & also an important alternative to hand hygiene. The hand sanitizer provides a handy option to reduce the chance of covid infection & its spread (Jerikias maramure *et.al*). WHO recommended using alcohol-based hand sanitizers that has at least 60% alcohol along with some natural antimicrobial substances (mainly plant based) such as aloe vera (WHO Guidelines). Post covid pandemic era is shocked with the uprise of antibiotic-resistant bacteria & fatality rate due to the MDR (Multiple Drug Resisting)

bacteria all over the world (Mousami Shah *et.al*). Recent studies have found that the major source of outbreak of such bacteria is been touching to the inanimate objects & negligence towards the hand hygiene leading to the entry of such pathogens into human body. To tackle such situations its now a need to reintroduce hand sanitizers in public areas. The alcohol-based hand sanitizers (60-95 %) are most effective but continuous use of high quantity alcohol sanitizers (80-95%) are causing irritation to the hands leading to the damage to the tissue which possibly makes an entry gate for the bacteria (Amani Alhalwani *et.al*). It is a need of a time to create sanitizers which are less with alcohol content, high with plant based antimicrobial substances but must be as effective. We have created a laboratory-based hand sanitizer using plant-based extracts & minimizing the use of alcohol. The variable concentrations of alcohol (decreasing concentration) & plant-based extracts (increasing concentration) such as aloe vera gel, waste lemon was used to create laboratory-based hand sanitizers (J Verma *et.al*). Aloe Vera is well-known for its natural ability to hydrate the skin, and its gel-like texture makes it a perfect ingredient for hand sanitizers (Ali Khumaeni *et.al*). However, many are unaware that Aloe Vera also provides protection against viral and bacterial infections, as it contains polyphenols that inhibit bacterial growth (Lewelyn Christine H. Palmero *et. al*)

The aloe vera have different types of antimicrobial substances such as anthraquinones, saponins, salicylic acid, aloctin which were found to be effective in suppressing the growth of several pathogenic. The lemon extract also contains vitamins, flavonoids, essential oils, citric acid which are known to be antimicrobial. These laboratory-based hand sanitizers were further tested & found to be effective against suppressing the growth of gram positive as well as gram negative bacteria mainly isolated from sewage samples in local area. In upcoming future, the use of hand sanitizers will be a useful weapon to fight against outbreak of MDR bacteria.

## MATERIALS & METHODS

Eco friendly sanitizers were created with variable concentrations using alcohol & herbal extracts mainly obtained from aloe vera & lemon extract. The aloe vera was handpicked from the Yogeshwari college campus. Then it was washed & was peeled off. Then it was subjected to blending to obtain the pure slurry. Similarly, the used waste lemon pieces were filled in a bottle with 10% alcohol & 90% D/W & kept in a dark for 1 week to extract the lime contents. The alcohol was taken in decreasing concentrations while the aloe vera gel & lemon extract were used in increasing concentrations & eco friendly sanitizers were made accordingly as shown in the table below (Juhui lee *et.al*)

**Table 1:** Indicating differential percentage of alcohol & herbal extracts used for preparation of sanitizers

Aloe vera sanitizer		Lemon extract sanitizer	
% Alcohol	% Aloe vera	% Alcohol	% Lemon extract
80	20	80	20
70	30	70	30
60	40	60	40
50	50	50	50
40	60	40	60

**Note:** Rose water (Less than 1%) was used for smell

These varying concentration sanitizers were kept in different bottles. Dettol sanitizer available in market was taken as a control.



**Fig 1.** Eco friendly sanitizers with variable concentrations of alcohol & herbal extracts

### Methodology to check the effect of eco friendly sanitizers on bacterial strains

These sanitizers were further subjected to check their efficacy on bacterial samples mainly *E. coli* & *Bacillus species* obtained from domestic sewage & soil respectively. These samples were then isolated in pure form & further inoculated on nutrient agar plate by spread plate method in standard concentration. Such plates were made for each varying concentration of sanitizers. Now from each sanitizer prepared earlier, a paper disc was dipped into the sanitizer (Ecofriendly & Dettol) & placed in the middle of the plate aseptically. ([M. Chojnacki](#) et al) These plates were then incubated at 37° Celsius in an incubator for 24 hours.



**Fig 2.** Indicating clear zone of inhibition around the paper disc of laboratory made hand sanitizers placed at centre of petri dish inoculated with bacterial samples

### OBSERVATION & RESULTS

After 24 hours, a clear visible zone of inhibition was seen & results were recorded as follows indicating efficacy of ecofriendly sanitizers.

**Table 2:** Indicating diameter of zone of inhibitions formed on agar plates indicating efficacy of laboratory made hand sanitizers

Aloe vera sanitizer		Lemon extract sanitizer			Market sanitizer (Dettol)		
% Alcohol	% Aloe vera	Diameter of zone of inhibition (in cm)	% Alcohol	% Lemon extract	Diameter of zone of inhibition (in cm)	% Alcohol	Diameter of zone of inhibition (in cm)
80	20	1.7	80	20	1.3	78%	1.2
70	30	1.9	70	30	1.6	-	-
60	40	1.8	60	40	1.5	-	-
50	50	1.7	50	50	0.5	-	-
40	60	1.5	40	60	0.7	-	-

It clearly shows that there is very slight change in diameter of zone of inhibition although alcohol concentration in sanitizer is decreased. This clearly may be due to the antimicrobial substances present in the herbal extracts such as aloe vera which contains anthraquinones, salicylic acid, aloctin while lemon extract containing vit c, citric acid, essential oils & flavonoids which disturbs the chemiosmotic balance of bacterial plasma membrane as well as can carry out oxidative stress & kills the bacterial cell.

## CONCLUSION

Sanitizers having 40% alcohol & 60% herbal extracts when tested, shown clear zone of inhibition indicating efficacy of ecofriendly sanitizer. The control sanitizer (Dettol hand sanitizer) having 78% alcohol has shown a zone of inhibition around 1.2 cm while the sanitizer prepared by our research team having 40% (nearly 1.5 times less alcohol) shows a zone of inhibition of around 1.5cm. From the present study it may conclude that the sanitizers which are less in content with alcohol & more in content with herbal extract (Aloe vera & Lemon extract) showing similar results to the market sanitizer but the main advantage is being an ecofriendly & even more effective (based upon the observations & results)

In future this type of approach will be a great preventive major to stop the spread of multiple drug resisting bacteria. The further challenge in front of our researchers will be to check the efficacy of this sanitizer against other multiple drug resisting bacteria & modify the content accordingly.

## REFERENCES

- [1] Aiello AE, Cimiotti J, Della-Latta P, Larson EL. 2003. A comparison of the bacteria found on the hands of 'homemakers' and neonatal intensive care unit nurses. *J Hosp Infect* 54:310–315.
- [2] Ain V, Karibasappa G, Dodamani A, Prashanth VK, Mali G. 2016. Comparative assessment of antimicrobial efficacy of different hand sanitizers: an in vitro study. *Dent Res J* 13:424–431.

DEVELOPMENT OF ALOE VERA HAND SANITIZER Lewelyn Christine H. Palmero Laguna State Polytechnic University Sta. Cruz, Philippine

- [3] Design of Automatic Hand Sanitizer System Compatible with Various Containers. Juhui Lee,1,2,3 Jin-Young Lee,2 Sung-Min Cho,2 Ki-Cheol Yoon,2,3 Young Jae Kim,1,2,3 and Kwang Gi Kim 1,2,3,4
- [4] Development and Evaluation of an Eco-Friendly Hand Sanitizer Formulation Valorised from Fruit Peels. J. Verma, 1 R. Mishra, 1 A. Mazumdar, 2 R. Singh, 3 and N. Sh. El-Gendy 4 , 5
- [5] Effectiveness of hand sanitizers in the prevention of COVID-19 and related public health concerns: A review Jerikias maramure, Zakio makuvara, Richwell Alufasi
- [6] Evaluating the Antimicrobial Properties of Commercial Hand Sanitizers M. Chojnacki, C. Dobrotka, R. Osborn, W. Johnson, M. Young, B. Meyer, E. Laskey, R. A. F. Wozniak, S. Dewhurst, P. M. Dunman
- [7] [https://www.researchgate.net/publication/370939140\\_FORMULATION\\_AND\\_EVALUATION\\_OF\\_A\\_LCOHOL\\_BASED\\_HERBAL\\_HAND\\_SANITIZER](https://www.researchgate.net/publication/370939140_FORMULATION_AND_EVALUATION_OF_A_LCOHOL_BASED_HERBAL_HAND_SANITIZER)
- [8] [https://www.researchgate.net/publication/374941115\\_Formulation\\_of\\_antibacterial\\_hand\\_sanitizer\\_gel\\_supplemented\\_with\\_moisturizers\\_from\\_Aloe\\_vera](https://www.researchgate.net/publication/374941115_Formulation_of_antibacterial_hand_sanitizer_gel_supplemented_with_moisturizers_from_Aloe_vera)
- [9] <https://eprajournals.com/IJMR/article/12529#:~:text=Aloe%20Vera%20is%20widely%20known,polyp henols%20that%20stop%20bacterial%20growth>
- [10] [https://www.researchgate.net/publication/370939140\\_FORMULATION\\_AND\\_EVALUATION\\_OF\\_A\\_LCOHOL\\_BASED\\_HERBAL\\_HAND\\_SANITIZER](https://www.researchgate.net/publication/370939140_FORMULATION_AND_EVALUATION_OF_A_LCOHOL_BASED_HERBAL_HAND_SANITIZER)
- [11] [https://www.researchgate.net/publication/353072469\\_Formulation\\_of\\_herbal\\_hand\\_sanitizer\\_from\\_Indian\\_herbs](https://www.researchgate.net/publication/353072469_Formulation_of_herbal_hand_sanitizer_from_Indian_herbs)
- [12] Multidrug Resistant Bacteria in the Community: Trends and Lessons Learned. David van Duin1\* and David Paterson2
- [13] Production Of Hand Sanitizer Using Aloe Vera and Silver Nanoparticles as An Active Agent Ali Khumaeni1 Ana Qona'ah2, Syifa Avicenna3, Iis Nurhasanah4 Department of Physics, Faculty of Science and Mathematics, Diponegoro University, Jl. Prof. Soedharto, S.H., Tembalang, Semarang 50275, Indonesia
- [14] Prevalence and impact of multidrug-resistant bacteria in solid cancer patients with bloodstream infection: a 25-year trend analysis. Carlos Lopera, Patricia Monzó, Tommaso Francesco Aiello <https://orcid.org/0000-0003-4441-6318>, Mariana Chumbita <https://orcid.org/0000-0001-5372-6444>, Olivier Peyrony, Antonio Gallardo-Pizarro,
- [15] Review on Multiple Facets of Drug Resistance: A Rising Challenge in the 21st Century Mousumi Saha1, \* and Agniswar Sarkar2
- [16] The impact of alcohol hand sanitizer uses on skin health between healthcare worker: Cross-sectional study. Amani Alhalwani, Amal Husain, Amjad Saemaldahar, Faizah Makhdoum, Montaha Alhakami, Rana Ashi, Razaz Wali, Sarah Alsharif, Muhammad Anwar Khan, Nisreen Jastaniah, Ismail Fasfous

# One Pot Procedure for Green Synthesis of Benzylidenethiazolidine-2,4-Diones Using Catalytic Amount of Anhydrous Aluminium Chloride in Ethanol Solvent Via Knoevenagel Condensation Reaction

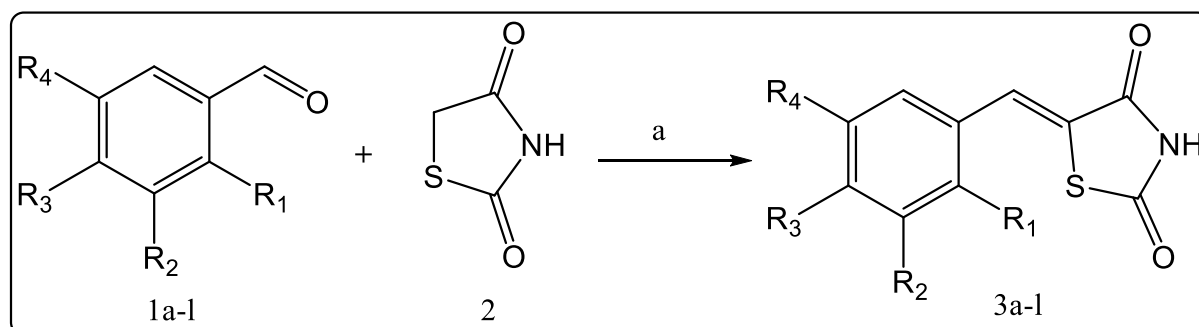
Sayas K Lad, Babasaheb V Kendre\*

Post Graduate Research Centre in Chemistry, Vaidyanath College, (Affiliated to Dr. Babasaheb Ambedkar Marathwada University, Chh. Sambhajinagar), Parli-Vajinath Dist. Beed, Maharashtra, India

Email: [bvkendre71@gmail.com](mailto:bvkendre71@gmail.com)

## ABSTRACT

A new series of benzylidenethiazolidine-2,4-diones (**3a-j**) has been synthesized *via* the condensation reaction of substituted aromatic aldehydes with active methylene compound (thiazolidin-2,4-dione) in the presence of catalytic amount of anhydrous AlCl<sub>3</sub> in freshly distilled out ethanol under refluxing conditions for 1.5-2h. The transformation of reactants to the products was supported by functional group tests and melting points. The structures of synthesized compounds were confirmed by IR, <sup>1</sup>HNMR, <sup>13</sup>CNMR and mass spectral analysis. This simplified procedure is environmentally sustainable and cost effective that gives target compounds in excellent yields (87-92%) with high selectivity in short reaction time.



**Reagents and reaction conditions:** a) AlCl<sub>3</sub>, Ethanol, Reflux, 1.5-2h, (87-92%)

**Keywords:** Thiazolidin-2,4-dione, benzylidenethiazolidine-2,4-dione, Green synthesis, Anhydrous aluminium chloride, conventional heating.

## INTRODUCTION

The set of concepts called as “green chemistry” has been become extremely popular since discovery by Paul Anastas and John C Warner in the 1990s<sup>1</sup> and provided insight on developing new chemicals and chemical processes to achieve the function of ecofriendly environment. Nowadays, it is a creative challenge for the researchers, technologists and engineers to put twelve principles into action to achieve the goal of green

chemistry<sup>2</sup>. Knoevenagel condensation reaction is one of the important name reactions in chemistry which has gained tremendous attraction of researchers for synthesizing a variety of heterocyclic compounds having medicinal values<sup>3</sup>. Knoevenagel condensation reaction has played significant role in synthesizing a wide range of naturally occurring medicinally active heterocyclic compounds<sup>4</sup>. This reaction finds application in synthesizing a number of heterocyclic compounds for medicinal applicability<sup>5</sup>.

Benzylidenethiazolidine-2,4-diones are biologically active heterocyclic compounds contain five and six member rings condensed through a  $\pi$  bond, five membered ring contains N, S and O as bioactive hetero atoms and six membered aromatic ring is substituted by a variety of functional groups. Due to these unique features, benzylidenethiazolidine-2,4-diones possess multiple broad spectrum of biological activities including antimicrobial<sup>6</sup>, antidiabetic<sup>7</sup>, anticancer<sup>8</sup>, anti-inflammatory<sup>9</sup>, antiproliferative<sup>10</sup> antitumor<sup>11</sup> and inhibitors of protein tyrosine phosphatases<sup>12</sup> activity. Aluminum chloride ( $\text{AlCl}_3$ ) is regarded as a versatile inorganic substance, and therefore finds applications in many fields, particularly in chemical reactions and organic synthesis<sup>13</sup>. It is inexpensive, highly reactive and selective Lewis acid catalyst. Notably,  $\text{AlCl}_3$  is used as a catalyst in both Friedel-Crafts acylation and alkylation reactions<sup>14</sup>. It is also used widely in manufacturing of rubber, lubricants, wood preservatives and paints. It is used in pesticides and pharmaceuticals.

Benzylidenethiazolidine-2, 4-diones were synthesized by several methods such as, sodium acetate in acetic acid under reflux conditions<sup>15</sup>, sodium acetate in acetic acid under microwave irradiation<sup>16</sup>, piperidine in ethanol under reflux conditions<sup>17</sup>, piperidine in acetic acid<sup>18</sup>, grinding with ammonium acetate in the absence of solvents<sup>19</sup>, baker's yeast<sup>20</sup> and polyethylene glycol-300 at 100-120°C<sup>21</sup>. However, these literature methods are associated with certain drawbacks such as long reaction time, create harmful wastes, organic solvents, low product yields and difficult isolation procedures. To the best of our knowledge,  $\text{AlCl}_3$  has not been used as a catalyst in Knoevenagel condensation reaction, especially in the synthesis of benzylidenethiazolidine-2, 4-diones, therefore received our attention for synthesizing benzylidenethiazolidine-2, 4-diones as biologically active molecules. Ethyl alcohol is second widely used solvent after water in industrial field. It is one of the important green solvents mostly manufactured from the natural sources<sup>22</sup>. Herein, we attempt to explore the significance of present investigation under the category of green synthesis for synthesizing new heterocyclic compounds possessing biological properties.

## MATERIAL AND METHODS

All chemicals were obtained from Spectrochem and S.D. Fine Chem. Co. and used without further purification. Melting points of the compounds were determined by open capillary method and were uncorrected. IR spectra were recorded on a Bruker made spectrophotometer.  $^1\text{H}$  and  $^{13}\text{C}$  NMR spectra were recorded using a Bruker instrument ( $^1\text{H}$  at 400 MHz and  $^{13}\text{C}$  at 300 MHz) in  $\text{DMSO-d}_6$  solvent and TMS as internal standard. Chemical shifts were reported in ppm. Mass spectra for the compounds were recorded on Shimadzu GC-MS-QP-2010 model using Direct Injection Probe technique. Reactions have been monitored by thin layer chromatography on 0.2-mm precoated plates of silica gel G60 F254 (Merck).

### General procedure for the synthesis of Benzylidenethiazolidine-2, 4-diones



Place aromatic aldehydes **1a-1** (0.01mol), thiazolidine-2,4-dione **2** (0.01mol), freshly distilled out ethyl alcohol (5ml) and 10 mole% anhydrous  $\text{AlCl}_3$  in RB flask (100mL). The reaction mixture was refluxed for 1.5-2h on water bath and progress of reaction was monitored by TLC. After the completion of reaction as indicated by TLC, the reaction mixture was cooled and poured into 100gm ice crystals and stirred by glass rod till the solid separates out. The solid product was filtered, washed 4-5 times with cold water and recrystallized from ethanol to obtain pure benzylidenethiazolidine-2, 4-diones in (87-92%) yields.

**Table 1: Synthesis of benzylidenethiazolidine-2, 4-diones (3a-j)**

Entry	R <sub>1</sub>	R <sub>2</sub>	R <sub>3</sub>	R <sub>4</sub>	Reaction Time (h)	Yield(%) <sup>a</sup>	Mp (°C) <sup>b</sup>
<b>3a</b>	H	H	H	H	1.5	92	85-87
<b>3b</b>	H	H	-OH	H	2.0	87	104-105
<b>3c</b>	H	H	-F	H	2.0	88	77-79
<b>3d</b>	H	H	-Cl	H	2.0	88	97-98
<b>3e</b>	H	-OCH <sub>3</sub>	-OH	C <sub>4</sub> H <sub>9</sub> N <sub>2</sub>	1.5	90	162-164
<b>3f</b>	H	-OCH <sub>3</sub>	-OH	C <sub>4</sub> H <sub>8</sub> NO	1.5	90	145-146
<b>3g</b>	H	H	-NO <sub>2</sub>	H	1.5	91	96-98
<b>3h</b>	H	H	-Br	H	2.0	87	107-108
<b>3i</b>	H	-OH	H	H	2.0	92	99-100
<b>3j</b>	H	NO <sub>2</sub>	H	H	1.5	92	89-93

Bold signifies the Isolated Yield.

<sup>a</sup> Isolated yields

<sup>b</sup>Physical constants

**Table 2: Solvent optimization for model reaction**

Sr. No.	Solvent	Time (h)	Yield (%) <sup>a</sup>
1	Ethanol (EtOH)	2.5	92
2	Ethylene glycol (EG)	2.5	91
3	Dimethyl formamide (DMF)	3h	72
4	Tetrahydrofuran (THF)	3h	70
5	No solvent	5h	65

<sup>a</sup>Isolated yields

## RESULTS AND DISCUSSION:

The present investigation describes synthesis of benzylidenethiazolidine-2, 4-dione derivatives (3a-l) from substituted aromatic aldehydes **1a-1** and heterocyclic compound thiazolidine-2,4-dione **2** via Knoevenagel condensation reaction under refluxing conditions on water bath in the presence of anhydrous aluminum chloride ( $\text{AlCl}_3$ ) as catalyst in ethanol for 3-4 hours. Earlier, thiazolidine-2, 4-dione was prepared following our previously reported literature procedure. In the beginning, we attempted to synthesize

benzylidenethiazolidine-2, 4-dione from benzaldehyde and thiazolidine-2,4-dione using molecular iodine as catalyst in water under conventional heating conditions for 8-10h, but could not afford product. The above reaction was also attempted in ethanol using  $I_2-K_2CO_3$  catalyst under conventional heating conditions for 7-8 hours. The reaction gave product formation in 40% yield. Improvement in the yield did not observe even after changing solvents. Anhydrous aluminum chloride ( $AlCl_3$ ) was extensively used catalyst in number of chemical transformation therefore, we thought worthwhile to use this catalyst in above chemical reaction. Surprisingly, the reactants started to convert into products after 1.5 hours in ethylene glycol and afforded desired product in 85% yield after 2.5 hours. The product formation was confirmed by TLC, functional group test and melting point. The target compound was selectively obtained without side products. We attempted to carry out above model reaction in ethanol using 10 mole percent catalytic amount of anhydrous aluminum chloride to maintain eco-friendly environment. The reaction was completed in 2.5 hours with little improvement in yield (Table 1). In order to optimize the reaction conditions, we performed this model reaction at higher temperature by increasing the catalytic amount in ethanol and in other solvents on refluxing into oil bath for 4-5 hours, no significant improvement in yield was observed. Therefore, the quantity of aromatic aldehyde (0.01mole), thiazolidine-2,4-dione (0.01mole) and ethanol (5-6mL) was fixed for all condensation reactions. The percentage yield, time and physical constant for all target compounds are entered into table-1. The structures of compounds were confirmed by IR,  $^1H$ NMR,  $^{13}C$ NMR and mass spectral methods.

### 3.1. The spectral data for new compounds 3e and 3f is given below.

#### (a). (Z)-5-(4-hydroxy-3-methoxy-5-(piperazin-1-yl)benzylidene)thiazolidine-2,4-dione 3e

IR (KBr,  $\nu$   $cm^{-1}$ ): 3392 (NH str.), 1705, 1782 (C=O str.), 1590 (C=C str.), 772 (C-S-C str.), 3465 (O-H str.).  $^1H$  NMR (400 MHz, DMSO- $d_6$ ):  $\delta$ = 11.15 (s, 1H, NH), 8.71(s,1H, OH), 7.01- 6.54 (d, 2H, aromatic), 3.73(s, 3H,  $OCH_3$ ), 7.75 (s, 1H, CH) ppm;  $^{13}C$  NMR (100 MHz, DMSO- $d_6$ ):  $\delta$ =166.37, 164.63, 148.15, 144.07, 140.37, 128.75, 128.21, 115.31, 99.73, 99.13, 54.56 ppm; EI-MS (m/z): 335.09 [ $M^+$ ].

#### (b). (Z)-5-(4-hydroxy-3-methoxy-5-morpholinobenzylidene)thiazolidine-2,4-dione 3f

IR (KBr,  $\nu$   $cm^{-1}$ ): 3321 (NH str.), 1735, 1797 (C=O str.), 1595 (C=C str.), 767 (C-S-C str.), 3445 (O-H str.).  $^1H$  NMR (400 MHz, DMSO- $d_6$ ):  $\delta$ = 11.16 (s, 1H, NH), 8.69(s,1H, OH), 7.02- 6.61 (d, 2H, aromatic), 3.71(s, 3H,  $OCH_3$ ), 7.77 (s, 1H, CH) ppm;  $^{13}C$  NMR (100 MHz, DMSO- $d_6$ ):  $\delta$ =166.34, 164.68, 148.15, 145.00, 140.35, 128.79, 128.12, 115.31, 100.03, 99.15, 63.21, 54.52 ppm; EI-MS (m/z): 336.08 [ $M^+$ ].

## CONCLUSION

In conclusion, we have developed an efficient procedure for the synthesis of benzylidenethiazolidine-2, 4-diones using anhydrous  $AlCl_3$  as catalyst under refluxing conditions in ethanol. We attempt to synthesize target compounds under ecofriendly conditions to minimize environmental pollution. The final products were easily isolated without complications and purified by recrystallization technique. The current methodology has the advantages of operational simplicity, mild reaction conditions and good to high yields of the products (87-92%). The present technique reduces reaction time with improved yield. The substituents on aromatic ring did not show strongly effects in terms of reaction time and yield of products.

## ACKNOWLEDGEMENTS:

Authors are thankful to Principal, Vaidyanath College Parli-Vajinath for providing research facilities.

## REFERENCES

- [1] Emil Knoevenagel (1898). "Condensation von Malonsäure mit aromatischen Aldehyden durch Ammoniak und Amine" [Condensation of malonic acid with aromatic aldehydes via ammonia and amines]. *Berichte der deutschen chemischen Gesellschaft*. 31 (3): 2596-2619. doi:10.1002/cber.18980310308.
- [2] Chen TL, Kim H, Pan SY, Tseng PC, Lin YP, Chiang PC. Implementation of green chemistry principles in circular economy system towards sustainable development goals: Challenges and perspectives. *Science of the Total Environment*. 2020;716(1):136998. DOI: 10.1016/j.scitotenv.2020.136998
- [3] a) B. C. Ranu, R. Jana, Ionic Liquid as Catalyst and Reaction Medium - A Simple, Efficient and Green Procedure for Knoevenagel Condensation of Aliphatic and Aromatic Carbonyl Compounds Using a Task-Specific Basic Ionic Liquid, *Eur. J. Org. Chem.*, 2006, 3767-3770. b) Dr. Ramya Tokala, Darshana Bora, Dr. Nagula Shankaraiah Contribution of Knoevenagel Condensation Products toward the Development of Anticancer Agents: An Updated Review, *ChemMedChem*, 2022, 17(8), e202100736, <https://doi.org/10.1002/cmdc.202100736>
- [4] Heravi, M.M., Janati, F. & Zadsirjan, V. Applications of Knoevenagel condensation reaction in the total synthesis of natural products. *Monatsh Chem* 151, 439-482 (2020). <https://doi.org/10.1007/s00706-020-02586-6>.
- [5] van Beurden, K., de Koning, S., Molendijk, D., & van Schijndel, J. (2020). The Knoevenagel reaction: a review of the unfinished treasure map to forming carbon-carbon bonds. *Green Chemistry Letters and Reviews*, 13(4), 349-364. <https://doi.org/10.1080/17518253.2020.1851398>
- [6] Kumar, H., Deep, A. & Marwaha, R.K. Design, synthesis, in silico studies and biological evaluation of 5-((E)-4-((E)-(substituted aryl/alkyl)methyl)benzylidene)thiazolidine-2,4-dione derivatives. *BMC Chemistry* 14, 25 (2020). <https://doi.org/10.1186/s13065-020-00678-2>.
- [7] Najmi, A., Alam, M.S., Thangavel, N. et al. Synthesis, molecular docking, and in vivo antidiabetic evaluation of new benzylidene-2,4-thiazolidinediones as partial PPAR- $\gamma$  agonists. *Sci Rep* 13, 19869 (2023). <https://doi.org/10.1038/s41598-023-47157-x>
- [8] Khaled El-Adl, Abdel-Ghany A. El-Helby, Helmy Sakr, Ibrahim H. Eissa, Sanadelaslam S.A. El-Hddad, Fatma M.I.A. Shoman, Design, synthesis, molecular docking and anticancer evaluations of 5-benzylidenethiazolidine-2,4-dione derivatives targeting VEGFR-2 enzyme, *Bioorganic Chemistry*, 102, 2020, 104059, ISSN 0045-2068, <https://doi.org/10.1016/j.bioorg.2020.104059>.
- [9] Ma L, Xie C, Ma Y, Liu J, Xiang M, Ye X, Zheng H, Chen Z, Xu Q, Chen T, Chen J, Yang J, Qiu N, Wang G, Liang X, Peng A, Yang S, Wei Y, Chen L. Synthesis and biological evaluation of novel 5-benzylidenethiazolidine-2,4-dione derivatives for the treatment of inflammatory diseases. *J Med Chem*. 2011 Apr 14;54(7):2060-8. doi: 10.1021/jm1011534.
- [10] Patil, V., Tilekar, K., Mehendale-Munj, S., Mohan, R., Ramaa, C.S. *Eur. J. Med. Chem.* 45 (2010) 4539-44.

- [11] Iqbal Singh, Richa Rani, Vijay Luxami, Kamaldeep Paul, Synthesis of 5-(4-(1H-phenanthro[9,10-d]imidazol-2-yl)benzylidene)thiazolidine-2,4-dione as promising DNA and serum albumin-binding agents and evaluation of antitumor activity, *European Journal of Medicinal Chemistry*, 166, 2019, 267-280, 0223-5234, <https://doi.org/10.1016/j.ejmech.2019.01.053>.
- [12] Maccari R, Paoli P, Ottanà R, Jacomelli M, Ciurleo R, Manao G, Steindl T, Langer T, Vigorita MG, Camici G (2007) 5-Arylidene-2,4-thiazolidinediones as inhibitors of protein tyrosine phosphatases. *Bioorg Med Chem* 15:5137–5149.
- [13] Galatsis P (1999). "Aluminum Chloride". In Reich HJ, Rigby JH (eds.). *Acidic and Basic Reagents. Handbook of Reagents for Organic Synthesis*. New York City: Wiley. pp. 12–15. ISBN 978-0-471-97925-8.
- [14] Olah GA, ed. (1963). *Friedel-Crafts and Related Reactions*. Vol. 1. New York City: Interscience.
- [15] V. Patil, K. Tilekar, S.M. Munj, R. Mohan, C.S. Ramaa, Synthesis and primary cytotoxicity evaluation of new 5-benzylidene-2,4-thiazolidinedione derivatives, *Eur. J. Med. Chem.* 45 (2010) 4539–4544.
- [16] Ajmal R. Bhat, Mohd H. Najar, Rajendra S. Dongre, Mohammad S. Akhter, Microwave assisted synthesis of Knoevenagel Derivatives using water as green solvent, *Current Research in Green and Sustainable Chemistry*, 3, 2020, 100008, ISSN 2666-0865, <https://doi.org/10.1016/j.crgsc.2020.06.001>.
- [17] M.A. Ibrahim, M.A.M. Abde-Hamed, N.M. El-Gohary, A new approach for the synthesis of bioactive heteroaryl thiazolidine-2,4-diones, *J. Brazilian Chem. Soci* 6 (2011) 1130–1139.
- [18] Yang D-H, Chen Z-C, Chen S-Y, Zheng Q-G. A Convenient Synthesis of 5-Benzylidenethiazolidine-2,4-Diones under Microwave Irradiation without Solvent. *Journal of Chemical Research*. 2003;2003(6):330-331. doi:10.3184/030823403103174272.
- [19] Metwally, Nadia Hanafy et al. "A simple and green procedure for the synthesis of 5-arylidene-4-thiazolidinones by grinding." *Green Chemistry Letters and Reviews* 4 (2011): 225 – 228.
- [20] Umesh R. Pratap, Dhanaji V. Jawale, Manisha R. Bhosle, Ramrao A. Mane, *Saccharomyces cerevisiae* catalyzed one-pot three component synthesis of 2,3-diaryl-4-thiazolidinones, *Tetrahedron Letters*, Volume 52, Issue 14, 2011, Pages 1689-1691, ISSN 0040-4039, <https://doi.org/10.1016/j.tetlet.2011.01.143>.
- [21] Mahalle, S. R., Netankar, P. D., Bondge, S. P., & Mane, R. A. (2008). An efficient method for Knoevenagel condensation: a facile synthesis of 5-arylidene 2,4-thiazolidinedione. *Green Chemistry Letters and Reviews*, 1(2), 103–106. <https://doi.org/10.1080/17518250802139881>
- [22] "Your Guide to Ethanol Extraction". *Cannabis Business Times*. Retrieved 9 April 2019.

# Synthesis of Nanoparticles by Green Synthesis Method

H. A. Tirpude, P. S. Reddy

P.G. Department of Chemistry, Shivaji Mahavidyalaya, Udgir (MS) – 413517, Maharashtra, India

Email: [tirpudeha@gmail.com](mailto:tirpudeha@gmail.com)

## ABSTRACT

As an emphasis on the synergistic interaction of nanotechnology and Nano biotechnology, nanoparticles need to develop environmentally benign technologies in the synthesis of biosynthesis and nanomaterial's. Microorganisms, plants and fungi can be used as biodegradable agents material in this field work. Thus, it was possible to develop a simple, fast and green method for the synthesis of nanoparticles. Various strategies are used for the synthesis of nanoparticles. Traditionally, physicochemical techniques have increased environmental concerns due to the reduction of metal ions followed by surface modification, toxic compounds added for stability, and dangerous byproducts formed. At the time of nanoparticle synthesis by adding chemical and physical methods at high temperature and pressure, reducing and stabilizing agents; nanoparticle synthesis by biological methods; room temperature and pressure, reducing and stabilizing agents are needed. Green synthesis method; provides a faster metallic nanoparticle production by offering an environmentally friendly, simple, economical and reproducible approach. Given the wide range of applications of metallic nanoparticles produced, biological methods play a major role in the synthesis of metallic nanoparticles.

**Keywords:** green approaches, green chemistry, organic synthesis, green solvent, green catalyst

## INTRODUCTION

Nano is a metric measure of one billionth of a meter and covers a width of 10 atoms. In terms of comparison with real objects, an example that hair is 150,000 nanometers may be given. The rapidly developing nanotechnology is the inter-disciplinary research and development field of biology, chemistry, physics, food, medicine, electronics, aerospace, medicine, etc., which examines the design, manufacture, assembly, characterization of materials that are smaller than 100 nanometers in scale, as well as the application of miniature functional systems derived from these materials. It represents the whole of development activities. As for the nano-biotechnology, on the other hand, it is the result of a combination of biotechnology and nanotechnology branches with a common combined functioning.

### 1.1. Nanoparticles and their properties:

The process of removing toxic and waste metals in the environment includes microorganisms, plants and other biological structures; achieved by means of oxidation, reduction or catalysis of metals with metallic nanoparticles. Metallic nanoparticles produced by biological methods; are used in the biomedical field for

purposes such as protection from harmful microorganisms, bio-imaging, drug transport, cancer treatment, medical diagnosis and sensor construction because of their unique properties such as being insulator, optics, antimicrobial, antioxidant, anti-metastasis, biocompatibility, stability and manipulability. Metallic nanoparticles, which can be used in the industrial field due to their catalytic activity, are of great importance nowadays. Figure 1 shows in detail where metallic nanoparticles obtained by biological methods are used.

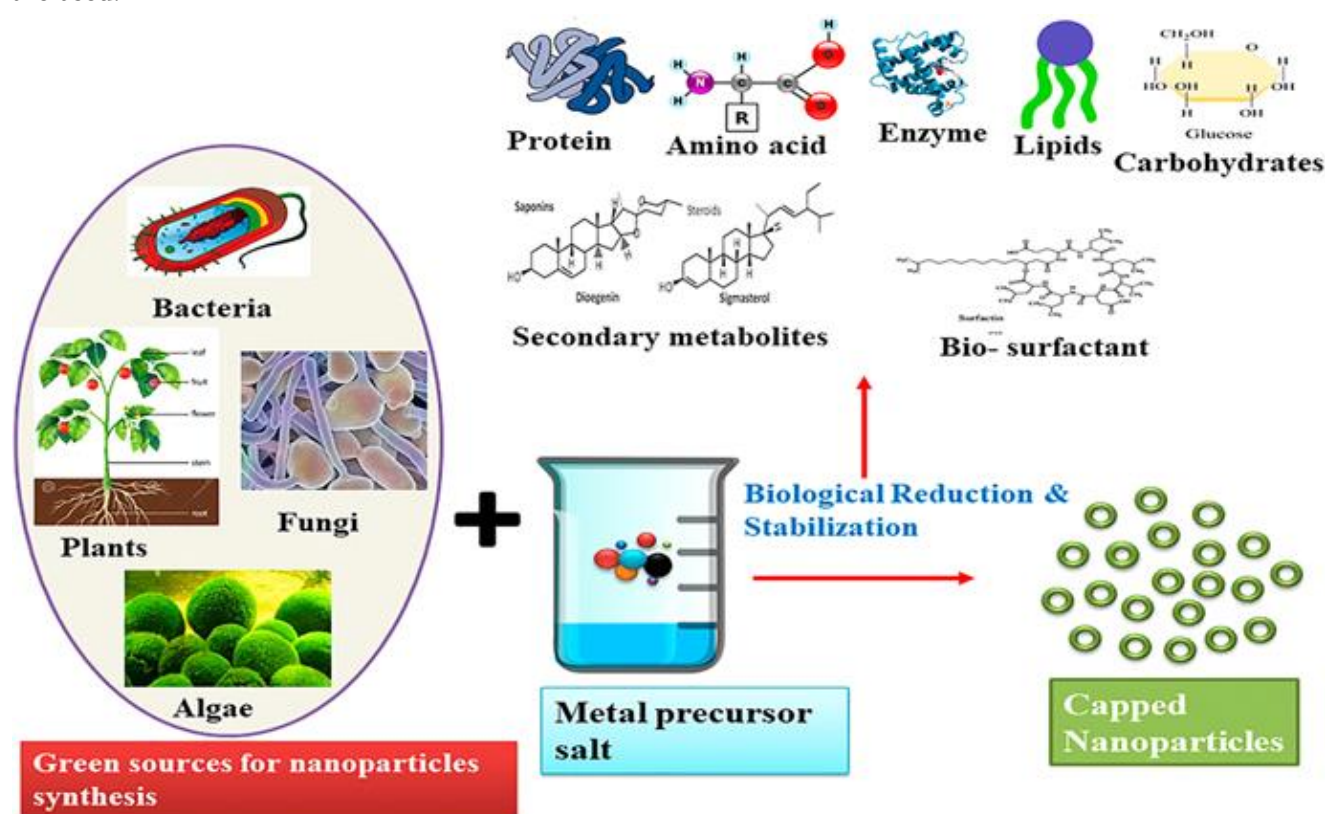


**Figure 1 Application areas of metallic nanoparticles synthesized by biological methods.**

Nanomaterials, which are the mainstay of nanotechnology that serve our lives for many years thanks to the contributions of many sciences, can be classified according to their origins, dimensions and structural configurations. According to their origin; nanomaterials are classified into two main groups: natural nanomaterials that are found in nature such as viruses, proteins, enzymes and minerals, and artificial nanomaterials which are not found in nature and require some processes for their production. According to their dimensions, nanomaterials are examined under four classes: - nano-sized nanocrystals -also known as zero dimensions- which includes metallic and semiconductor nanoparticles. - one-dimensional nanomaterials include nanowires, nano-bots, and nanotubes. - two-dimensional nanomaterials such as nanocomposites and nanoplates; - three-dimensional nanomaterials, bulkers. According to their structural configurations, nanomaterials are studied under four main groups as metallic nanomaterials, carbon based nanomaterials, dendrimers and composites.

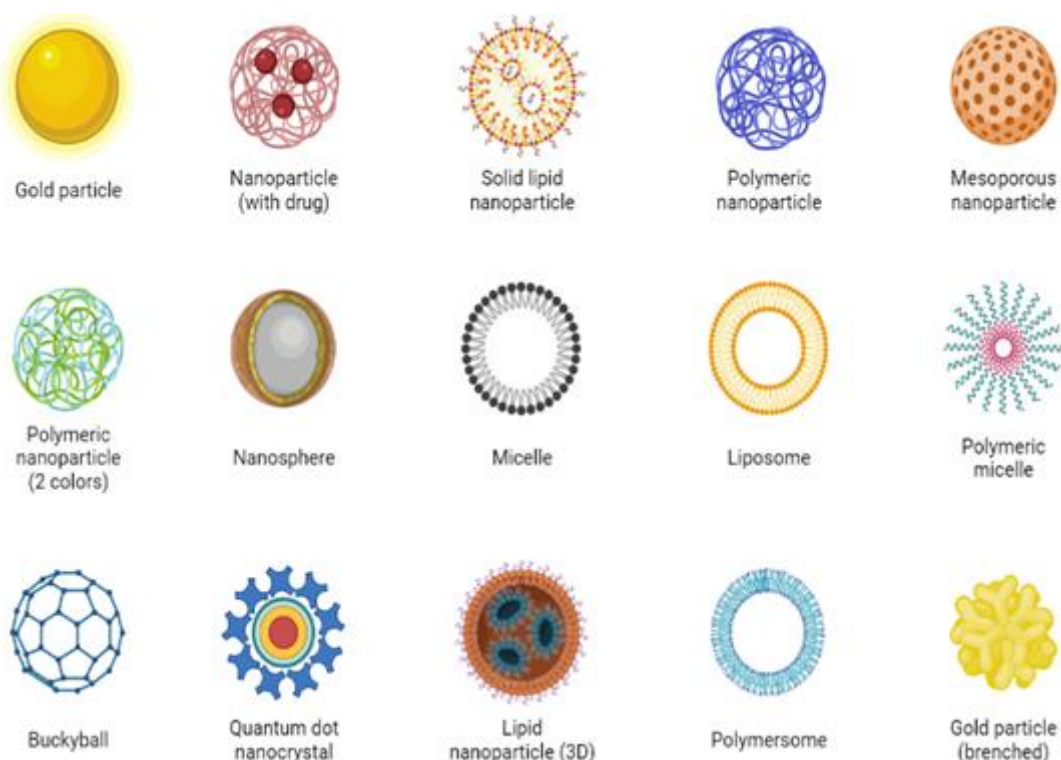


**Figure 2 shows some types of nanoparticles used in nano-technology.**

The reason for the intense interest of scientists nowadays in nanoparticles is that nanoparticles can exhibit different properties and functions than normal bulk materials. The most important factor that enables production of nanostructures in desired size, shape and properties and provides their usage in various fields is that the effects of classical physics are reduced and the quantum physics becomes active. Other reasons for the different behavior of nanoparticles in physical, chemical, optical, electrical and magnetic behavior include the limitation of load carriers, size dependent electronic structures, increased surface / volume ratio, and other factors incurred by the unique properties of atoms.

### **1.2. Synthesis methods of nanoparticles:**

In the synthesis of nanoparticles, which can be natural or synthetic origin and exhibit unique properties at the nanoscale, two basic approaches that include various preparation methods and are known from early times are used. The first approach is the "top-down" method which calls for breaking down of solid materials into small pieces by applying external force. In this approach, many physical, chemical and thermal techniques are used to provide the necessary energy for nanoparticle formation. The second approach, known as "bottom-up", is based on gathering and combining gas or liquid atoms or molecules. These two approaches have advantages and disadvantages relative to each other. In the top-down approach, which is costlier to implement, it is impossible to obtain perfect surfaces and edges due to cavities and roughness that can occur in nanoparticles; whereas excellent nanoparticle synthesis results can be obtained by bottom-up approach. In addition, with the bottom up approach, no waste materials that need to be removed are formed, and nanoparticles having smaller size can be obtained thanks to the better control of sizes of the nanoparticles. The classification of synthesis methods of nanoparticles is given in Figure.

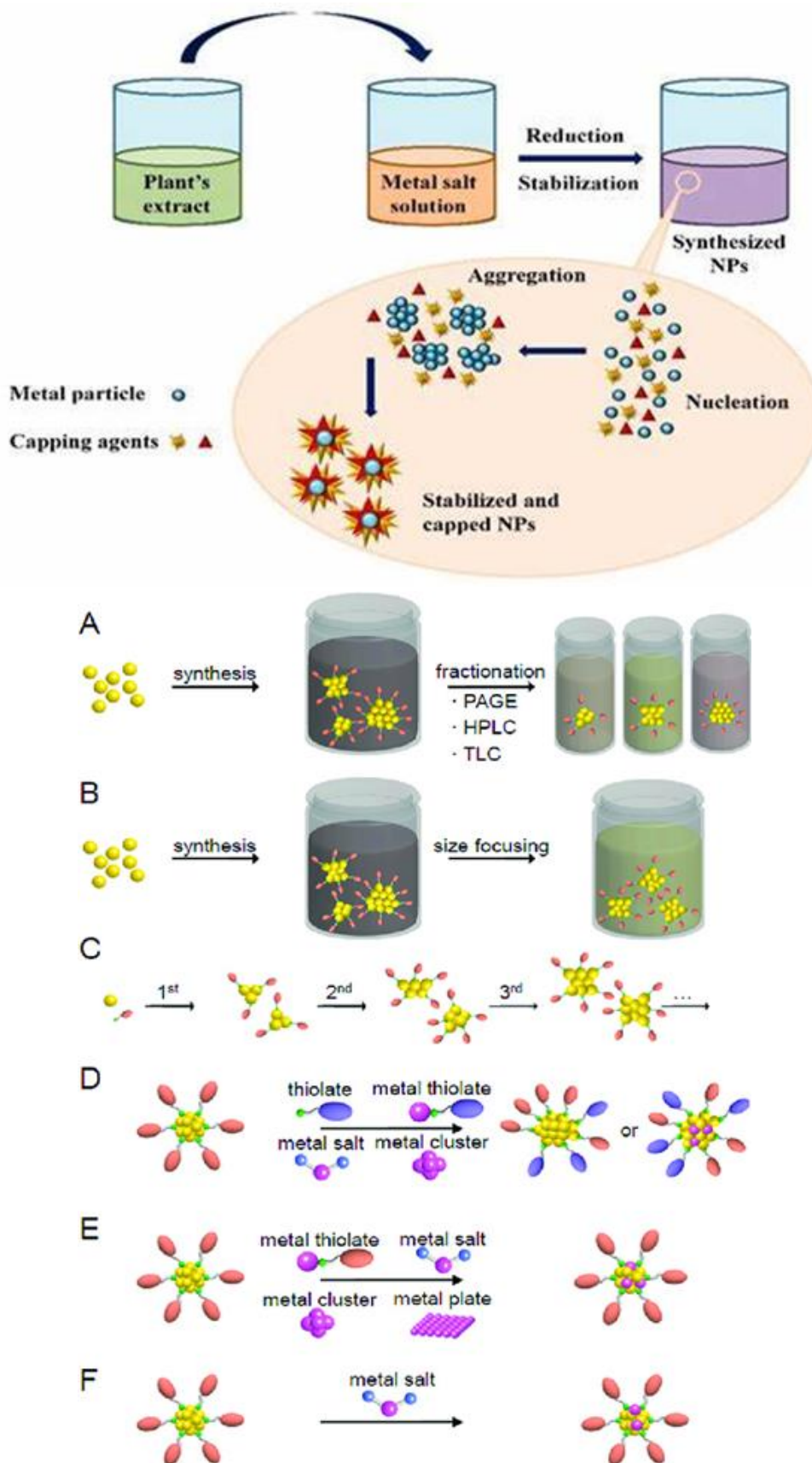


Figure 3 shows the synthesis of nanoparticles used in nano-technology.



The mechanical abrasion method, which is listed under the top-down approach, uses various ball mills to break down the material into particles and provides the production of nano-sized alloys, composites and semi-crystalline structures. Although this method is inexpensive, efficient and simple, it is susceptible to contamination caused by the balls

### GREEN SYNTHESIS METHOD:

The biological method, which is represented as an alternative to chemical and physical methods, provides an environmentally friendly way of synthesizing nanoparticles. Moreover, this method does not require expensive, harmful and toxic chemicals. Metallic nanoparticles with various shapes, sizes, contents and physicochemical properties can be synthesized thanks to the biological method actively used in recent years. Synthesis can be done in one step using biological organisms such as bacteria, actinobacteria, yeasts, molds, algae and plants, or their products. Molecules in plants and microorganisms, such as proteins, enzymes, phenolic compounds, amines, alkaloids and pigments perform nanoparticle synthesis by reduction. In traditional chemical and physical methods; reducing agents involved in the reduction of metal ions, and stabilizing agents used to prevent undesired agglomeration of the produced nanoparticles carry a risk of toxicity to the environment and to the cell. Besides, the contents of the produced nanoparticles are thought to be toxic in terms of shape, size and surface chemistry. In the green synthesis method in which nanoparticles with biocompatibility are produced, these agents are naturally present in the employed biological organisms.

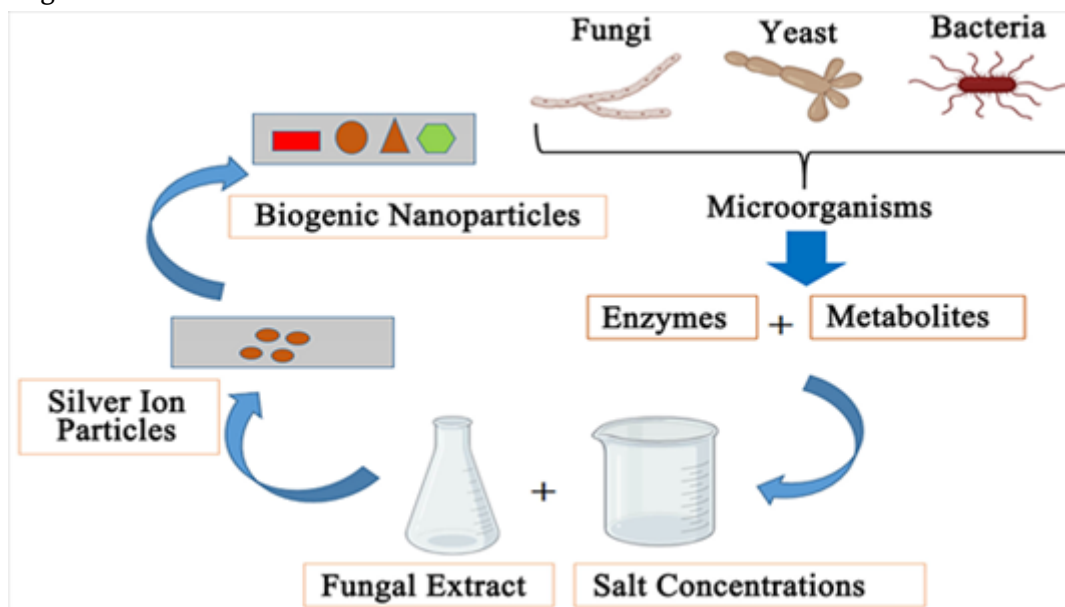


**Figure 4 summarizes how nanoparticles are produced by biological methods.**

Biological synthesis of nanoparticles Because of rapid development, affordable culturing costs and easy control and manipulation of growth environment, bacteria are clearly targets in the production of nanoparticles. At the same time, it is known that some species of bacteria have special mechanisms to suppress the toxicity of metals or heavy metals. Bacteria preferred for these properties, can perform nanoparticle synthesis in-situ and ex-situ. Through the use of biochemical pathways and reducing agents

such as proteins, enzymes, etc. which present in the bacteria, metal ions can be reduced and precipitated for nanoparticle production. Actinobacteria, which performs the production of secondary metabolites such as antibiotics, are aerobic, immobile, and mostly filamentous gram-positive bacteria. They are resistant to the most toxic heavy metals owing to their detoxification property. Soluble toxic metal ions are detoxified by either being degraded by intracellular or extracellular reduction or precipitation. Thus, nanoparticles being antibacterial, antifungal, anticancer, antioxidant, antibiotic-contamination and having catalytic activity can be produced. Synthesis of nanoparticles can be done as extra-cellular or intra-cellular with enzymes by employing simply-cultured and fast-breeding eukaryotic yeasts and molds with easy biomass design, as. The incubation conditions and the metallic ion solutions used influence the size of the nanoparticles produced. Being pathogenic for humans limits the use of some molds in nanoparticle production. Algae are eukaryotic aquatic photosites and they break down metallic salts into nanoparticles thanks to the pigments, proteins, carbohydrates, fat, nucleic acid and secondary metabolites they contain. The algae extract that exists in an aqueous medium at a certain temperature is supplemented with metal solutions of the corresponding pH and concentration, and hence the synthesis of nanoparticles is achieved which may have antimicrobial properties without producing any toxic by-products during the synthesis. Size of nanoparticles is determined by certain parameters such as the incubation time of the solution, the ambient temperature, the pH of the mixture used and the metal ion concentration. Algae also provide an advantage to this synthesis method by virtue of their easy availability and usefulness. In addition, effective biomolecules in the reaction medium in the use of bacteria and plant extracts are less extinguished by the nanoparticles formed. Plants, which have great potential for detoxification, reduction and accumulation of metals, are promising, fast and economical in removing metal-borne pollutants. Metallic nanoparticles having various morphological characteristics can be produced intracellularly and extracellularly. Synthesis process; is initiated by addition of extracts obtained from plant parts such as leaves, roots and fruits into the aqueous solution of metal ions. With the materials present in the plant extract, such as sugar, flavonoid, protein, enzyme, polymer and organic acid, acting as a reducing agent, takes charge in bioinduction of metal ions into nanoparticles.

## CONCLUSION

Recently, a variety of microorganisms and plant extracts have been used to efficiently synthesize metal nanoparticles for green synthesis. Thus, the synthesis of nanoparticles by green synthesis is the most convenient, easy, environmentally friendly way and minimizes the side effects of chemical and physical methods by preventing the use of toxic chemicals and formation of harmful/dangerous by-products. Nanoparticles have widespread use for their superior properties and are being studied intensively in recent years. The physical and clinical effects of antimicrobial, antioxidative and non-toxic nanoparticles obtained by green synthesis are becoming increasingly important. Future studies will probably focus on obtaining nanoparticles with antimicrobial effects at its maximum level and toxicity at minimum. Because of this reason, synthesizing metallic nanoparticles, especially by non-toxic green synthesis method-, which are used in many application fields such as cancer treatment, drug transport, biosensor construction is of great importance to-day.

**REFERENCES**

- [1] Pearce JM. Make nanotechnology research open-source. *Nature* (2012) 491:519–21. doi:10.1038/491519a.
- [2] Schrofel A, Kratosova G, Safarik I, Safarikova M, Raska I, Shor LM. Applications of biosynthesized metallic nanoparticles - A re-view. *Acta Biomaterialia* (2014) 10:4023–42. doi:10.1016/j.actbio.2014.05.022.
- [3] Singh P, Kim YJ, Zhang DB, Yang DC. Biological Synthesis of Na-nanoparticles from Plants and Microorganisms. *Trends in Biotechnol-ogy* (2016) 34:588–99. doi:10.1016/j.tibtech.2016.02.006.
- [4] Byrappa K, Ohara S, Adschiri T. Nanoparticles synthesis using su-percritical fluid technology - towards biomedical applications. *Ad-vanced Drug Delivery Reviews* (2008) 60:299–327. doi:10.1016/j.addr.2007.09.001.
- [5] Li XQ, Xu HZ, Chen ZS, Chen GF. Biosynthesis of Nanoparticles by Microorganisms and Their Applications. *Journal of Nanomateri-als* (2011). doi:10.1155/2011/270974.
- [6] Ince S. Determination of retention, characterization and antimicro-bial properties of Ag, Au and Pt nanoparticles by green synthesis method using yolks of quail eggs. Master Thesis. Erzurum (2017).
- [7] Shah M, Fawcett D, Sharma S, Tripathy SK, Poinern GE. Green Synthesis of Metallic Nanoparticles via Biological Entities. *Materi-als* (2015) 8:7278–308. doi:10.3390/ma8115377.
- [8] Iravani S. Green synthesis of metal nanoparticles using plants. *Green Chemistry* (2011) 13:2638–50. doi:10.1039/c1gc15386b.
- [9] Cerjak H. Book note: introductions to nanoparticles and nanomateri-als. *Powder Metallurgy* (2014) 57:82.
- [10] Makarov VV, Love AJ, Sinitsyna OV, Makarova SS, Yaminsky IV, Taliansky ME, et al. "Green" Nanotechnologies: Synthesis of Metal Nanoparticles Using Plants. *Acta Naturae* (2014) 6:35–44.
- [11] Geonmonond RS, Da Silva, AGM, Camargo PH. Controlled synthe-sis of noble metal nanomaterials: motivation, principles, and oppor-tunities in nanocatalysis. *Anais Da Academia Brasileira De Ciencias* (2018) 90:719–44. doi:10.1590/0001-3765201820170561.
- [12] Nadaroglu H, Onem H, Gungor AA. Green synthesis of Ce2O3 NPs and determination of its antioxidant activity. *Iet Nanobiotechnology* (2017) 11:411–9. doi:10.1049/iet-nbt.2016.0138.
- [13] Nadaroglu H, Gungor AA, Ince S, Babagil A. Green synthesis and characterisation of platinum nanoparticles using quail egg yolk. *Spectrochimica Acta Part a-Molecular and Biomolecular Spectros-copy* (2017) 172:43–7. doi:10.1016/j.saa.2016.05.023.
- [14] Cicek S, Gungor AA, Adiguzel A, Nadaroglu H. Biochemical Eval-uation and Green Synthesis of Nano Silver Using Peroxidase from Euphorbia (*Euphorbia amygdaloides*) and Its Antibacterial Activity. *Journal of Chemistry* (2015). doi:10.1155/2015/486948.
- [15] Narayanan KB, Sakthivel N. Biological synthesis of metal nanopar-ticles by microbes. *Advances in Colloid and Interface Science* (2010) 156:1–13. doi:10.1016/j.cis.2010.02.001.
- [16] Mukhopadhyay NK, Yadav TP. Some Aspects of Stability and Nanophase Formation in Quasicrystals during Mechanical Milling. *Israel Journal of Chemistry* (2011) 51:1185–96. doi:10.1002/ijch.201100145.

- [17] Hussain I, Singh NB, Singh A, Singh H, Singh SC. Green synthesis of nanoparticles and its potential application. *Biotechnology Letters* (2016) 38:545–60. doi:10.1007/s10529-015-2026-7.
- [18] Korbekandi H, Iravani S, Abbasi S. Production of nanoparticles using organisms. *Critical Reviews in Biotechnology* (2009) 29:279–306. doi:10.3109/07388550903062462.
- [19] Gao Y, Wei Z, Li F, Yang ZM, Chen YM, Zrinyi M, et al. Synthesis of a morphology controllable Fe<sub>3</sub>O<sub>4</sub> nanoparticle/hydrogel magnetic nanocomposite inspired by magnetotactic bacteria and its application in H<sub>2</sub>O<sub>2</sub> detection. *Green Chemistry* (2014) 16:1255–61. doi:10.1039/c3gc41535j.
- [20] Manivasagan P, Venkatesan J, Sivakumar K, Kim SK. Actinobacteria mediated synthesis of nanoparticles and their biological properties: A review. *Critical Reviews in Microbiology* (2016) 42:209–21. doi:10.3109/1040841x.2014.917069.
- [21] Moghaddam AB, Namvar F, Moniri M, Tahir PM, Azizi S, Mo-hamad R. Nanoparticles Biosynthesized by Fungi and Yeast: A Review of Their Preparation, Properties, and Medical Applications. *Molecules* (2015) 20:16540–65. doi:10.3390/molecules200916540.
- [22] Siddiqi KS, Husen A. Fabrication of Metal and Metal Oxide Nanoparticles by Algae and their Toxic Effects. *Nanoscale Research Letters* (2016) 11. doi:10.1186/s11671-016-1580-9.
- [23] Karaduman I, Gungor AA, Nadaroglu H, Altundas A, Acar S. Green synthesis of gamma-Fe<sub>2</sub>O<sub>3</sub> nanoparticles for methane gas sensing. *Journal of Materials Science-Materials in Electronics* (2017) 28:16094–105. doi:10.1007/s10854-017-7510-5.
- [24] Park S, Sung HK, Kim Y. Green Synthesis of Metal Nanoparticles Using Sprout Plants: Pros and Cons. *Journal of Nanoscience and Nanotechnology* (2016) 16:4444–9. doi:10.1166/jnn.2016.10970.

# Zinc Triflet : A Highly Effective Catalyst for the One-Pot Synthesis of 3,4-Dihydropyrimidine-2(1H)-ones and Thiones

Hanmant M. Kasralikar, Nitish S. Kaminwar, Shrinivas L. Nakkalwar\*

Lal Bahadur Shastri Mahavidyalaya, Dharmabad-431809, Maharashtra, India

[snakkalwar@rediffmail.com](mailto:snakkalwar@rediffmail.com)

## ABSTRACT

We present a straightforward and efficient method for the one-pot Biginelli condensation of aldehydes,  $\beta$ -ketoesters, and urea or thiourea using copper (II) sulfamate as a novel catalyst. This approach offers several advantages over traditional Biginelli reaction conditions, including higher yields, reduced reaction times, and enhanced experimental simplicity.

**Keywords:** Zinc Triflet, Biginelli Reaction, Dihydropyrimidinones.

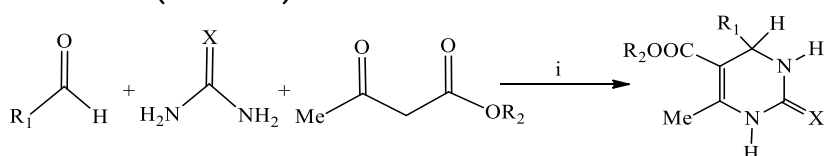
## INTRODUCTION

Dihydropyrimidinones (DHPMs) and their derivatives are prominent heterocyclic compounds in both natural and synthetic organic chemistry, valued for their diverse biological and therapeutic activities, including antibacterial, antiviral, antitumor, and anti-inflammatory properties [1-3]. Recently, DHPM analogs with specific functional groups have become crucial in the development of calcium channel blockers, antihypertensive agents, and  $\alpha$ -adrenergic receptor antagonists [4-5]. Additionally, marine-sourced alkaloids featuring the dihydropyrimidine core, such as batzelladine alkaloids, have demonstrated significant biological activities, including potent HIV gp-120-CD4 inhibition [6-7].

The most straight forward method for synthesizing DHPMs was first described by Italian chemist Pietro-Biginelli over a century ago. This method involves a one-pot, three-component condensation of benzaldehyde, ethyl acetoacetate, and urea under strongly acidic conditions [8]. Despite its simplicity, this reaction often requires harsh conditions, extended reaction times, and yields that can be low, especially when using substituted aromatic or aliphatic aldehydes.

Recent advancements have introduced various techniques to enhance and modify the Biginelli reaction, including microwave irradiation [9], ultrasound irradiation [10], and the use of ionic liquids [11], as well as Lewis and protic acid promoters such as lanthanide triflate [12],  $H_3BO_3$  [13],  $VCl_3$  [14],  $Sr(OTf)_2$  [15],  $PPh_3$  [16], Indium(III) halides [17],  $KAl(SO_4)_2 \cdot 12H_2O$  supported on silica [18], Silicasulfuric acid [19],  $Mn(OAc)_3 \cdot 2H_2O$  [20],  $Y(NO_3)_3 \cdot 6H_2O$  [21],  $In(OTf)_3$  [22],  $TaBr_5$  [23],  $Ce(NO_3)_3 \cdot 6H_2O$  [24], silica chloride [25],  $HCOOH$  [26] others. Despite these improvements, many of these methods still face challenges, such as the use of costly reagents, strong acidic conditions, and prolonged reaction times.

To address these issues, there is a need for milder and more efficient methods that offer higher yields. Notably, copper (II) sulfamate and its derivatives have not been explored as catalysts for these reactions. Building on our interest in Lewis acid catalysis for the Biginelli reaction [27-28], we present a novel, simple, and efficient approach for synthesizing 3,4-dihydropyrimidin-2(1H)-ones and thione analogs. This method utilizes copper (II) sulfamate as a catalyst, achieving moderate to good yields in the reaction of aldehydes,  $\beta$ -ketoesters, and urea or thiourea (**Scheme 1**).



**Reaction conditions and reagents:** i) 1mol%, Zn(OTf)<sub>2</sub>, ACOH, reflux, 90-98% yield

## RESULTS AND DISCUSSION:

To evaluate the catalyst's effectiveness under various conditions, we selected the reaction of benzaldehyde, ethyl acetoacetate, and urea as a model system. The results are summarized in Table 1. Initially, we investigated the impact of different solvents on the reaction (Table 1, entries 1–5) and found that glacial acetic acid was the most effective. Next, we examined the effect of varying the amount of Zn(OTF)<sub>2</sub> (Table 1, entries 5, 7–12). The optimal result was achieved with 1mole% of Zn(OTF)<sub>2</sub> (Table 1, entry 10). In contrast, in the absence of Zinc Triflate and under the same conditions, the yield of product 4a was only 33% (Table 1, entry 6). We also explored the influence of reaction time on the yield (Table 1, entries 10, 13–18). The highest yield was observed with a reaction time of 5 hours. Therefore, the optimal conditions for the reaction are 0.01:1:1:1.5 mole ratios of Zn(OTF)<sub>2</sub>, benzaldehyde, ethyl acetoacetate, and urea, at 100 °C for 5 hours, using glacial acetic acid as the solvent.

**Table 1 : Effect of catalyst Zn(OTF)<sub>2</sub>, under different reaction conditions for condensation of benzaldehyde, ethyl acetoacetate and urea<sup>a</sup>**

Entry	Solvent	Zn(OTF) <sub>2</sub> (mol%)	Time (h)	Yield (%)
1	EtOH	2.5	6	62
2	CH <sub>3</sub> CN	2.5	6	62
3	H <sub>2</sub> O	2.5	6	30
4	Toluene	2.5	6	35
5	ACOH	2.5	6	60
6	ACOH	None	6	30
7	ACOH	0.1	6	40
8	ACOH	0.3	6	61
9	ACOH	0.5	6	72
10	ACOH	1.0	6	75
11	ACOH	1.0	6	76
12	ACOH	2.0	6	73

13	ACOH	1.0	1	60
14	ACOH	1.0	2	65
15	ACOH	1.0	5	80

<sup>a</sup> Isolated yield.

In order to study the scope of the procedure, a series of DHPMs were synthesized using the new reaction set-up. The results are listed in Table 2. In all cases studied, the three-component reaction proceeded smoothly to give the corresponding DHPMs in satisfactory yields. Most importantly, aromatic aldehydes carrying either electron donating or electron withdrawing substituents reacted very well to give the corresponding DHPMs with high purity in moderate to good yields. Another important feature of this procedure is the tolerance of various functional groups such as methoxy, halides, nitro, hydroxy, etc. to the reaction conditions, as well as the compatibility without formation of side products of acid sensitive aldehydes such as furfural and cinnamaldehyde. Thiourea has been used with similar success to provide corresponding S-dihydropyrimidinones analogues, which are also of interest due to their biological activities (Table 2, entries 4n–4p). The use of methyl acetoacetate as 1,3-dicarbonyl moiety in place of ethyl acetoacetate also gave similar results, as shown in Table 2 (entries 4q–4t).

**Table 2. Synthesis of 3,4-Dihydropyrimidin-2(1H)-ones/Thiones derivatives:**

Entry	R <sub>1</sub>	R <sub>2</sub>	X	Yields (%) <sup>b</sup>	Mp (°C) <sup>c</sup>	Found Reported (Lit.)
4a	C <sub>6</sub> H <sub>5</sub>	EtO	O	79	201-204	202-203[22]
4b	4-CH <sub>3</sub> O-C <sub>6</sub> H <sub>4</sub>	EtO	O	69	204-206	203-204[22]
4c	C <sub>6</sub> H <sub>5</sub> -CH=CH	EtO	O	84	234-236	234-236[22]
4d	4-F-C <sub>6</sub> H <sub>4</sub>	EtO	O	68	183-185	175-177[8]
4e	3-Br-C <sub>6</sub> H <sub>4</sub>	EtO	O	84	190-192	185-186[21]
4f	4-CH <sub>3</sub> -C <sub>6</sub> H <sub>4</sub>	EtO	O	79	212-213	216-217[12]
4g	4-Cl-C <sub>6</sub> H <sub>4</sub>	EtO	O	75	212-214	212-214[6]
4h	3-NO <sub>2</sub> -C <sub>6</sub> H <sub>4</sub>	EtO	O	89	224-226	226-228[22]
4i	3-CH <sub>3</sub> O,4-HO-C <sub>6</sub> H <sub>3</sub>	EtO	O	75	233-235	233-235[22]

Reaction conditions: Aldehyde (2 mmol), β-ketoester (2 mmol), urea (3 mmol), Zn(OTF)<sub>2</sub>·22 (0.02 mmol), ACOH (10 mL), 100 °C;

<sup>b</sup> Isolated yield; <sup>c</sup> Melting points are uncorrected.

**Experimental Details:** All compounds were characterized by IR, <sup>1</sup>H NMR spectroscopy, and elemental analysis. IR spectra were recorded as potassium bromide pellets using a FTS-40 spectrometer (Bio-Rad, U.S.A.). <sup>1</sup>H NMR spectra were obtained on a Varian Inova-400 spectrometer with CDCl<sub>3</sub> or DMSO-d<sub>6</sub> as solvents and TMS as the internal standard; chemical shifts are reported in ppm. Elemental analysis (C, H, and N) was conducted using a Perkin-Elmer Analyzer 2400. Melting points were determined with a Büchi B-540 instrument and are reported uncorrected.

**General Procedure for the Synthesis of 3,4-Dihydropyrimidin-2(1H)-(Thio)ones:**

A mixture of aldehyde (2 mmol), ethyl acetoacetate (2 mmol), urea or thiourea (3 mmol), and  $Zn(OTf)_2$  (0.02 mmol) was refluxed at 100°C in glacial acetic acid (10 mL) for 5 hours without stirring. The progress of the reaction was monitored by TLC. After cooling, the reaction mixture was poured onto crushed ice (50 g) and stirred for 5 minutes. The resulting solid was filtered under suction, washed with cold water (50 mL), and recrystallized from ethanol to obtain the pure product. The results are summarized in Table 2. All products (except 4p) are known compounds and were characterized by melting point, IR,  $^1H$  NMR spectroscopy, and elemental analysis.

**5-Ethoxycarbonyl-6-methyl-4-(3-bromophenyl)-3,4-dihydropyrimidin-2(1H)-thione(4p):** Mp 182-184 °C;  $^1H$  NMR (DMSO- $d_6$ )  $\delta$ : 1.12 (t, 3H,  $J = 7.2$  Hz,  $OCH_2CH_3$ ), 2.30 (s, 3H,  $CH_3$ ), 4.03 (q, 2H,  $J = 7.2$  Hz,  $OCH_2$ ), 5.17 (s, 1H, CH), 7.20-7.50 (m, 4H, Ar-H), 9.68 (s, 1H, NH), 10.41 (s, 1H, NH);  $^{13}C$  NMR (DMSO- $d_6$ )  $\delta$ : 14.64, 17.85, 54.21, 60.35, 100.75, 122.32, 126.04, 129.92, 131.22, 131.64, 146.22, 146.67, 165.59, 174.99; IR ( $\nu$  max; KBr,  $cm^{-1}$ ): 3228, 3099, 2976, 1707, 1652, 1589, 1284, 1225, 1090, 767; Anal. calcd. (%) for  $C_{14}H_{15}N_2O_2S$ : C 61.07, H 5.49, N 10.17. Found: C 61.21, H 5.45, N 10.28.

**CONCLUSIONS:**

In conclusion, we have demonstrated the first use of  $Zn(OTf)_2$  as an efficient catalyst for the synthesis of 3,4-dihydropyrimidin-2(1H)-ones and thione analogs via multicomponent Biginelli reactions. This protocol offers several advantages, including mild reaction conditions, short reaction times, easy isolation, and good yields. Future work will focus on expanding the catalytic activity of  $Zn(OTf)_2$  to other organic transformations.

**ACKNOWLEDGEMENTS**

We are grateful to the Principal of Lal Bahadur Shastri Mahavidyalaya, Dharmabad for Providing specialized research facilities.

**REFERENCES**

- [1] Kappe, C.O. 100 Years of the Biginelli Dihydropyridine Synthesis. *Tetrahedron* 1993, 49, 6937–6963.
- [2] Kappe, C.O.; Fabian, W.M.F.; Semones, M.A. Conformational Analysis of 4-Aryl Dihydropyrimidine Calcium Channel Modulators: A Comparison of Ab Initio, Semiempirical, and X-Ray Crystallographic Studies. *Tetrahedron* 1997, 53, 2803–2816.
- [3] Kappe, C.O. Recent Advances in the Biginelli Dihydropyrimidine Synthesis: New Tricks from an Old Dog. *Acc. Chem. Res.* 2000, 33, 879–888.
- [4] Atwal, K.S.; Rovnyak, G.C.; Kimball, S.D.; Floyd, D.M.; Moreland, S.; Swanson, B.N.; Gougoutas, D.Z.; Schwartz, J.; Smillie, K.M.; Malley, M.F. Dihydropyrimidine Calcium Channel Blockers. II. 3-Substituted-4-aryl-1,4-dihydro-6-methyl-5-pyrimidinecarboxylic Acid Esters as Potent Mimics of Dihydropyridines. *J. Med. Chem.* 1990, 33, 2629–2635.



- [5] Nagarathnam, D.; Miao, S.W.; Lagu, B.; Chiu, G.; Fang, J.; Murali Dhar, T.G.; Zhang, J.; Tyagarajan, S.; Marzabadi, M.R.; Zhang, F.; Wong, W.C.; Sun, W.; Tian, D.; Zhang, J.; Wetzel, J.M.; Forray, C.; Chang, R.S.L.; Broten, T.P.; Schorn, T.W.; Chen, T.B.; O'Malley, S.; Ransom, R.W.; Schneck, K.; Bendesky, R.; Harrell, C.M.; Gluchowski, C. Design and Synthesis of Novel  $\alpha$ 1a Adrenoceptor-Selective Antagonists. 1. Structure-Activity Relationship in Dihydropyrimidinones. *J. Med. Chem.* 1999, 42, 4764–4777.
- [6] Patil, A.D.; Kumar, N.V.; Kokke, W.C.; Bean, M.F.; Freyer, A.J.; Brossi, C.D.; Mai, S.; Truneh, A.; Faulkner, D.J.; Carte, B.; Breen, A.L.; Hertzberg, R.P.; Johnson, R.K.; Westly, J.W.; Potts, B.C.M. Novel Alkaloids from the Sponge *Batzella* sp.: Inhibitors of HIV gp120-Human CD4 Binding. *J. Org. Chem.* 1995, 60, 1182–1188.
- [7] Snider, B.B.; Chen, J.; Patil, A.D.; Freyer, A. Synthesis of the Tricyclic Portions of Batzelladines A, B, and D. Revision of the Stereochemistry of Batzelladines A and D. *Tetrahedron Lett.* 1996, 37, 6977–6980.
- [8] Biginelli, P. *Gazz. Chim. Ital.* 1893, 23, 360–413.
- [9] Banik, B.K.; Reddy, A.T.; Datta, A.; Mukhopadhyay, C. Microwave-Induced Bismuth Nitrate-Catalyzed Synthesis of Dihydropyrimidinones via Biginelli Condensation under Solventless Conditions. *Tetrahedron Lett.* 2007, 48, 7392–7394.
- [10] Li, J.T.; Han, J.F.; Yang, J.H.; Li, T.S. An Efficient Synthesis of 3,4-Dihydropyrimidin-2-ones Catalyzed by  $\text{NH}_2\text{SO}_3\text{H}$  under Ultrasound Irradiation. *Ultrason. Sonochem.* 2003, 10, 119–122.
- [11] Peng, J.J.; Deng, Y.Q. Ionic Liquids Catalyzed Biginelli Reaction under Solvent-Free Conditions. *Tetrahedron Lett.* 2001, 42, 5917–5919.
- [12] Ma, Y.; Qian, C.; Wang, L.; Yang, M. Lanthanide Triflate Catalyzed Biginelli Reaction: One-Pot Synthesis of Dihydropyrimidinones under Solvent-Free Conditions. *J. Org. Chem.* 2000, 65, 3864–3868.
- [13] Tu, S.J.; Fang, F.; Miao, C.B.; Jiang, H.; Feng, Y.J.; Shi, D.Q.; Wang, X.S. One-Pot Synthesis of 3,4-Dihydropyrimidin-2(1H)-ones Using Boric Acid as Catalyst. *Tetrahedron Lett.* 2003, 44, 6153–6155.
- [14] Sabitha, G.; Reddy, G.S.K.K.; Reddy, K.B.; Yadav, J.S. Vanadium(III) Chloride Catalyzed Biginelli Condensation: Solution Phase Library Generation of Dihydropyrimidin-(2H)-ones. *Tetrahedron Lett.* 2003, 44, 6497–6499.
- [15] Su, W.K.; Li, J.J.; Zheng, Z.G.; Shen, Y.C. One-Pot Synthesis of Dihydropyrimidinones Catalyzed by Strontium (II) Triflate under Solvent-Free Conditions. *Tetrahedron Lett.* 2005, 46, 6037–6040.
- [16] Debache, A.; Amimour, M.; Belfaitah, A.; Rhouati, S.; Carboni, B. A One-Pot Biginelli Synthesis of 3,4-Dihydropyrimidin-2(1H)-ones/thiones Catalyzed by Triphenylphosphine as Lewis Base. *Tetrahedron Lett.* 2008, 49, 6119–6121.
- [17] Fu, N.Y.; Yuan, Y.F.; Pang, M.L.; Wang, J.T.; Peppe, C. Indium(III) Halides-Catalyzed Preparation of Ferrocenedihydropyrimidinones. *J. Organomet. Chem.* 2003, 672, 52–57.
- [18] Azizian, J.; Mohammadi, A.A.; Karimi, A.R.; Mohammadzadeh, M.R.  $\text{KAl}(\text{SO}_4)_2 \cdot 12\text{H}_2\text{O}$  Supported on Silica Gel as a Novel Heterogeneous System Catalyzed Biginelli Reaction: One-Pot Synthesis of Dihydropyrimidinones under Solvent-Free Conditions. *Appl. Catal. A Gen.* 2006, 300, 85–88.
- [19] Salehi, P.; Dabiri, M.; Zolfigol, M.A.; Fard, M.A.B. Silica Sulfuric Acid: An Efficient and Reusable Catalyst for the One-Pot Synthesis of 3,4-Dihydropyrimidin-2(1H)-ones. *Tetrahedron Lett.* 2003, 44, 2889–2891.

- [20] Kumar, K.A.; Kasthuraiah, M.; Reddy, C.S.; Reddy, C.D. Mn(OAc)<sub>3</sub>·2H<sub>2</sub>O-Mediated Three-Component, One-Pot Condensation Reaction: An Efficient Synthesis of 4-Aryl-Substituted 3,4-Dihydropyrimidin-2-ones. *Tetrahedron Lett.* 2001, 42, 7873–7875.
- [21] Nandurkar, N.S.; Bhanushali, M.J.; Bhor, M.D.; Bhanage, B.M. Y(NO<sub>3</sub>)<sub>3</sub>·6H<sub>2</sub>O: A Novel and Reusable Catalyst for One-Pot Synthesis of 3,4-Dihydropyrimidin-2(1H)-ones under Solvent-Free Conditions. *J. Mol. Catal. A Chem.* 2007, 271, 14–17.
- [22] Ghosh, R.; Maiti, S.; Chakraborty, A. In(OTf)<sub>3</sub>-Catalyzed One-Pot Synthesis of 3,4-Dihydropyrimidin-2(1H)-ones. *J. Mol. Catal. A Chem.* 2004, 217, 47–50.
- [23] Ahmed, N.; Lier, J.E.V. TaBr<sub>5</sub>-Catalyzed Biginelli Reaction: One-Pot Synthesis of 3,4-Dihydropyrimidin-2-(1H)-ones/thiones under Solvent-Free Conditions. *Tetrahedron Lett.* 2007, 48, 5407–5409.
- [24] Adib, M.; Ghanbary, K.; Mostofi, M.; Ganjali, M.R. Efficient Ce(NO<sub>3</sub>)<sub>3</sub>·6H<sub>2</sub>O-Catalyzed Solvent-Free Synthesis of 3,4-Dihydropyrimidin-2(1H)-ones. *Molecules* 2006, 11, 649–654.
- [25] Karade, H.N.; Sathe, M.; Kaushik, M.P. Synthesis of 4-Aryl Substituted 3,4-Di hydro- pyrimidinones Using Silica-chloride Under Solvent Free Conditions. *Molecules* 2007, 12, 13411351.
- [26] Cheng, J.; Qi, D.Y. An Efficient and Solvent-Free One-Pot Synthesis of Dihydropyrimidinones under Microwave Irradiation. *Chin. Chem. Lett.* 2007, 18, 647–650.
- [27] Liu, C.J.; Wang, J.D.; Li, Y.P. One-Pot Synthesis of 3,4-Dihydropyrimidin-2(1H)-ones Using b Strontium (II) Nitrate as a Catalyst. *J. Mol. Catal. A Chem.* 2006, 258, 367–370.
- [28] Zhang, X.L.; Li, Y.P.; Liu, C.J.; Wang, J.D. An Efficient Synthesis of 4-Substituted pyrazoly1,3,4-Dihydropyrimidin-2(1H)-(thio) ones Catalyzed by Mg(ClO<sub>4</sub>)<sub>2</sub> under Ultrasound Irradiation. *J. Mol. Catal. A Chem.* 2006, 253, 207–211.

# Thickness Dependent Physical Properties of SILAR Deposited Nanostructured MgSe Thin Films

K. C Shinde<sup>1</sup>, Y.S. Sakhare<sup>2\*</sup>, R.J. Topare<sup>1</sup>

<sup>1</sup>Department of physics, Yogeshwari Mahavidyalaya, Ambajogai, Maharashtra, India

<sup>2</sup>Department of Physics, Late Pundalikrao Gawali Arts and Science College, Shirpur (Jain), Maharashtra, India

\*Email: [-sakhare.yogesh@gmail.com](mailto:-sakhare.yogesh@gmail.com)

## ABSTRACT

The preparation of nanostructured MgSe thin films onto amorphous glass substrate by SILAR method is discussed. The characterization techniques such as X-ray diffraction (XRD), Scanning Electron Microscopy (SEM), Optical absorption and Electrical resistivity measurements were used to investigate size dependent physical properties of MgSe thin films. The SILAR grown MgSe material exhibits hexagonal structure. The electrical studies revealed that the resistivity and activation energy is found to be thickness dependent. The thermo-emf measurements confirmed that SILAR grown MgSe films are of n-type.

**Keywords:** Thin film; MgSe; SILAR method; Electrical properties

## INTRODUCTION

Metal chalcogenide structures have newly attracted unlimited consideration due to the fact that they possessed exceptional physical and chemical properties which open space for countless applications. Their supreme optical and electrical properties contributed to them being extensively used in solar energy conversion, optoelectronics industries [1, 2]. In recent years, magnesium selenide (MgSe) has gained significant attention as a semiconducting thin film material due to its intriguing electronic properties, including tunable bandgap, excellent charge carrier mobility, and compatibility with various substrates [3-5]. MgSe primarily demonstrates two crystalline structures: a tetragonal phase and a hexagonal phase [6]. Investigated how deposition potential influences the properties of chemically grown iron selenide thin films, revealing a hexagonal wurtzite structure with well-defined morphology. The aim of this work is to present results of MgSe thin films obtained by the SILAR method.

## MATERIAL AND METHOD

SILAR method, to develop thin film the substrate is immersed repeatedly into separately placed cationic and anionic precursor alternately. To eliminate freely bound variety, after each precursor immersion, the substrate is rinsed in de-ionized water. For the current work the glass slides of size 75×25×1 mm was used as substrates. Before actual deposition cleaning of the substrate is very important as it affects the development

system. Initially, the slides were washed with liquid detergent, then boiled in concentrated acid for 2 hour, and then kept in it for next 48 hours. The substrates were then washed with double distilled water and cleaned in ultrasonic cleaner for 10 min. Finally, the substrates were dried using AR grade acetone. The  $\text{SeO}_2$  solution was prepared by dissolving 1g of selenium powder (99% purity, Merck) with 10 ml nitric acid ( $\text{HNO}_3$ ). It was then boiled for few minutes to get white residual powder. To it 100 ml of distilled water was added to prepare 0.13 M  $\text{SeO}_2$  solution. The deposition of MgSe films was done at room temperature in a reactive solution prepared in a beaker. Glass substrates were immersed in the 80 ml of  $\text{MgCl}_2$  solution for 10 s. It was then to immersed in 80 ml of freshly prepared  $\text{SeO}_2$  solution for 10 s. This forms one SILAR deposition cycle. Deposition cycles were varied from 50 to 250 cycles in the steps of 25 cycles. All the prepared samples were annealed for 48 h for the complete transformation. The X-ray diffraction was used to study the structure of the film. X-ray diffraction patterns of the films were taken with a PANalytical X'Pert PRO MRD X-ray diffractometer with  $\text{CuK}\alpha$  radiation in the  $2\theta$  range from  $20^\circ$  to  $90^\circ$ . The morphological study of the film was carried out using scanning electron microscopy (SEM) with a Park Scientific Instruments and SEM/EDAX with JOEL's JSM -7600F.

## RESULT AND DISCUSSION

### 3.1 X-ray Diffraction and Morphology

The XRD patterns of the MgSe films of various thicknesses deposited on glass substrates. The crystallographic data of these films compared with standard JCPDS data file. The analysis showed that the films are nano crystalline in nature with hexagonal structure. The (111), (200), (220) and (400) XRD peaks confirms nature with cubic structure of MgSe in accordance with JCPDS card. The average crystallite size of the film material was determined by using Debye - Scherrer formula

$$D = \frac{K \lambda}{\beta \cos \theta} \quad (1)$$

where  $\lambda$  is the wavelength used (0.154 nm), K is constant,  $\beta$  is the angular line width at half maximum intensity in radians;  $\theta$  is the Bragg's angle. The SEM micrographs of MgSe films having thicknesses are shown in Figure 2. It is observed that the MgSe thin films are uniform, homogeneous and well covered to the glass substrate.

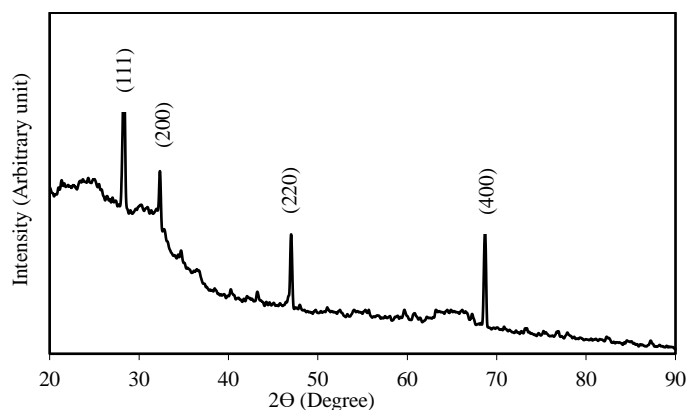


**Fig:1** The XRD patterns of the MgSe films

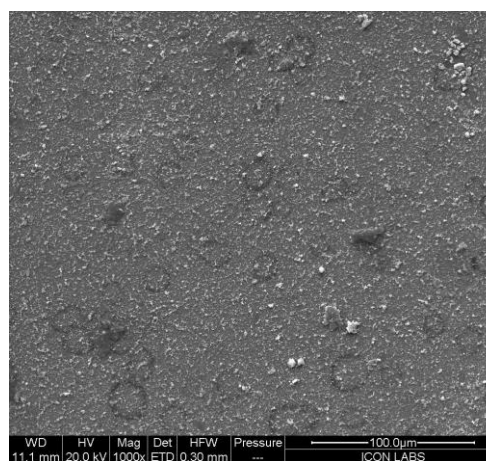


**Fig:2** The SEM micrographs of MgSe films

### 3.2 Optical Properties and Electrical Characterizations

The optical properties of MgSe thin films deposited by SILAR technique on glass substrate were investigated by measuring optical absorbance in the wavelength range 300 to 900 nm is as shown in figure 3. The nature of the transition involved can be determined on the basis of the dependence of absorption coefficient ' $\alpha$ ' on photo energy  $h\nu$ . For allowed direct transition,  $\alpha$  is by

$$\alpha = \frac{A(Eg - h\nu)^n}{h\nu} \quad (2)$$

Where A is the constant which is related to the effective masses associate with the valance and conduction bands, Eg is the energy between the bottom of the conduction band and top of the valance band at the same value of wave vector k. The electrical resistivity of MgSe thin films was measured by conventional dc two-probe method in the range of temperature from 300 to 500 K. The resistivity of the films is of the order of  $10^3 \Omega\text{-cm}$  and follows the relation,

$$\rho = \rho_0 \left( \frac{E_a}{KT} \right) \quad (3)$$

Where  $\rho$  is the resistivity at temperature T,  $\rho_0$  is constant; K is Boltzmann constant and  $E_a$  is activation energy. Resistivity decreases with increase in temperature indicating semiconducting nature of MgSe.

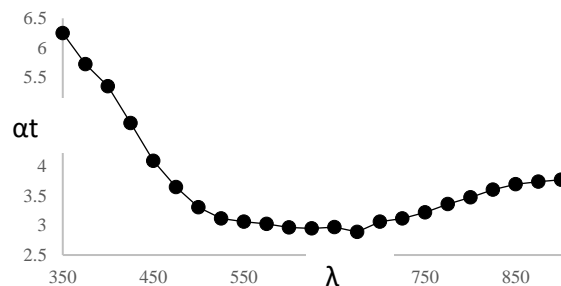


Fig:3 MgSe thin film optical absorbance in the wavelength range 300 to 900 nm.

### CONCLUSION

MgSe thin films were prepared onto glass substrates using simple and economic SILAR technique. The X-ray diffraction study revealed that the films are nanocrystalline in nature with hexagonal structure. Electrical resistivity measurements indicate semiconducting nature of MgSe thin films. In conclusion it was observed that physical properties of MgSe can be engineered by film thickness.

### REFERENCES

- [1] P.E. Agbo, P.A. Nwofe, R.A. Chikwenze, and D.A. Famuyibo, 8 (3): (2016) 152 – 156.
- [2] A.M. Kwiecińska, D. Kutyła, K. Kołczyk-Siedlecka, K. Skibińska, P. Żabiński, and R. Kowalik, Journal of Electroanalytical Chemistry, 848, (2019), 113278.
- [3] Ubale A.U., Sakhare Y.S., Bhute M.V., Belkhedkar M.R., Singh A. Solid State Sci.,16 (2013)134.
- [4] Qasrawi A.F., Toubasi A.J. Optik, 287, (2023)171173.

- [5] NM S.S.B., Chandra Mohan R., Saravana Kumar S., Ayeshamariam A., Jayachandran M. Fluid Mech Open Acc, 4 (2017) 6.
- [6] Piperno L., Celentano G., Sotgiu G. Coatings,13 (2023)1905.

# A Review on Biogenic Synthesis of Silver Nanoparticles

Mahadev B Suwarnkar<sup>1</sup>, Ganesh V Shitre<sup>2</sup>, Suresh A Kamble<sup>1</sup>, Madhav J Hebade<sup>3\*</sup>

<sup>1</sup>Department of Chemistry, Baburaoji Adaskar Mahavidyalaya, Kaij, Dist. Beed, Maharashtra, India

<sup>2</sup>Department of Chemistry, Vaishnavi Mahavidyalaya, Wadvani, Dist. Beed, Maharashtra, India

<sup>3</sup>Department of Chemistry, Badrinarayan Barwale Mahavidyalaya, Dist. Jalna, Maharashtra, India

Email: [msuwarnkar@gmail.com](mailto:msuwarnkar@gmail.com)

## ABSTRACT

Silver nanoparticles (Ag NPs) have attracted significant interest due to their unique optical, electronic, and antimicrobial properties. The traditional methods of synthesis of Ag NPs often involve hazardous chemicals and high energy consumption. In contrast to this biotical approach for the synthesis of Ag NPs utilizes biological agents such as microorganisms, plants, and enzymes, offers a greener and more sustainable approach. This review delves into the biogenic synthesis of Ag NPs, discussing the biological agents involved, mechanisms of nanoparticle formation, advantages, limitations, and emerging applications.

## INTRODUCTION

In the past few decades, nanotechnology has been empowered as a new and developing interdisciplinary area of science and innovation that coordinates material science and biology. The small-sized nanoparticles (1–100 nm) dominate the entire research globally, due to its surprising applications in physical, chemical, and biological sciences [1]. Due to intensive and extensive research by the research fraternity, nanotechnology has successfully knocked on the door and a common man at present scenario experiencing the feature of nanotechnology [2]. Nanoscience and nanotechnology open up new streets of examination that is helpful in synthesizing novel nanomaterials with incredible applications.

There are various physical methods and chemical mediated synthesis methods were used for the preparation of nanomaterials. The physical methods involves deposition, sputtering, ball milling, and plasma based techniques [3]. The rate of synthesis of metal nanoparticles is very slow in most of these methods. Extensive size distribution, slow production rate, and waste by-products and high consumption of energy make most of the physical methods extremely expensive which cannot be adopted for practical commercial applications [4]. A variety of chemical methods for nanoparticle synthesis has been put forward and most of them are widely used to synthesize nanostructured materials (e.g., chemical reduction, pyrolysis, sol-gel method, microemulsion, polyol synthesis, hydrothermal synthesis, chemical vapor deposition) [5]. Moreover, employing hazardous chemicals and reagents during the synthesis process and generation of byproducts is lethal to humans and the environment also [6]. Therefore, specifically such kind of NPs is limited for biological applications.

Green nanotechnology is an emerging field to design novel NPs using a green chemistry approach. Biological methods of NPs synthesis provide a new possibility of synthesizing NPs using natural reducing and stabilizing agents. It is an economical and environmentally friendly alternative to chemical and physical approaches with no usage of energy and toxic chemicals. Among various metal nanomaterials, silver nanoparticles (AgNPs) paying attention to the researchers due to their versatile antibacterial characteristics and biological properties. Biogenically synthesizing AgNPs from plants and microorganisms seems to be an extremely capable substitute for developing a technology that is both environmentally benign and fast.

## FUNDAMENTALS OF BIOGENIC SYNTHESIS:

Biogenic synthesis of Ag NPs involves the use of biological systems, such as microorganisms, plants, and fungi, to reduce silver ions ( $\text{Ag}^+$ ) to metallic silver ( $\text{Ag}^0$ ) nanoparticles. The process can be broadly categorized into three approaches:

### Microbial Synthesis:

The synthesis of silver nanoparticles (Ag NPs) using microorganisms is an innovative and environmentally friendly approach. This biogenic method exploits the unique capabilities of bacteria, fungi, and algae to convert silver ions into nanoparticles with specific properties, which are valuable in various applications [7]. The microbial synthesis involved microorganisms like bacteria, fungi, and algae. Commonly used bacteria include *Escherichia coli*, *Bacillus subtilis*, and *Pseudomonas aeruginosa*. These organisms can reduce silver ions extracellularly or intracellularly. Fungal species like *Fusarium* and *Aspergillus* are known for their ability to synthesize Ag NPs through enzymatic pathways. Green algae, such as *Chlorella* and *Spirulina*, also participate in nanoparticle synthesis. **The** reduction of silver ions carried out in the synthesis mechanism. Microorganisms reduce  $\text{Ag}^+$  ions to metallic silver ( $\text{Ag}^0$ ) through metabolic processes. This can occur through extracellular and intracellular reduction. Extracellular reduction releases the enzymes or metabolite into the surrounding medium facilitates the reduction of silver ions. In intracellular reduction: Silver ions are taken up by microbial cells and reduced inside, where they aggregate to form nanoparticles. The microbial synthesis is eco-friendly, cost effective and biocompatible [8-9]. Microbial synthesis of silver nanoparticles offers a sustainable and innovative approach to nanoparticle production. As research continues to advance, this method has the potential to contribute significantly to fields such as medicine, environmental science, and nanotechnology.

### Plant-Based Synthesis:

Plant-based synthesis of silver nanoparticles (Ag NPs) is an eco-friendly and sustainable approach that utilizes various plants extracts to reduce silver ions to nanoparticles. This method leverages the natural metabolites present in plants, making it a promising alternative to traditional chemical synthesis. Various plant sources were used i.e. leaf, fruit and root extracts. Commonly used **leaf extracts** include *Aloe vera*, *Neem* (*Azadirachta indica*), *Basil* (*Ocimum basilicum*), and *Mint* (*Mentha* spp.) [10-14]. Extracts from fruits like *Papaya* and *Pomegranate* have also shown potential for nanoparticle synthesis [15-16]. Roots of plants such as *Ginger* and *Turmeric* can be used to produce Ag NPs. Plant extracts contain various phytochemicals, such as flavonoids, tannins, and alkaloids, that can reduce silver ions ( $\text{Ag}^+$ ) to metallic silver ( $\text{Ag}^0$ ). These phytochemicals also help stabilize the nanoparticles, preventing agglomeration and maintaining their size



and shape. Plant-based synthesis of silver nanoparticles represents a promising field that combines the principles of green chemistry with nanotechnology. As research progresses, this method is likely to find increasing applications in medicine, environmental science, and materials development, providing a sustainable path for nanoparticles production.

#### **Enzyme-Mediated Synthesis:**

Enzyme-mediated synthesis of silver nanoparticles (Ag NPs) is a biotechnological approach that harnesses the catalytic properties of enzymes to reduce silver ions ( $\text{Ag}^+$ ) into metallic silver ( $\text{Ag}^0$ ). This method offers several advantages, including specificity, mild reaction conditions, and potential for large-scale production. Commonly used enzymes include dehydrogenases, reductases, and laccases, which can efficiently reduce silver ions ( $\text{Ag}^+$ ) to silver nanoparticles ( $\text{Ag}^0$ ). The synthesis typically occurs in an aqueous solution, where silver salts (like  $\text{AgNO}_3$ ) are mixed with the enzyme. Conditions such as pH, temperature, and ionic strength can influence nanoparticle size and morphology. Enzymes facilitate the transfer of electrons to silver ions, reducing them to their metallic state. The reaction may also involve co-factors or substrates that participate in the electron transfer. After the initial reduction, nanoparticles nucleate and grow. The enzyme may stabilize the particles, preventing agglomeration through steric or electrostatic effects [17-18]. Enzyme-mediated synthesis of silver nanoparticles represents a promising approach for producing AgNPs with desirable properties for various applications. By harnessing biological catalysts, this method not only enhances sustainability but also opens new avenues for research and development in nanotechnology. Continued exploration of enzyme interactions and optimization of synthesis conditions will further advance this field.

#### **Advantages of Biogenic Synthesis:**

- ❖ The Biogenic Synthesis methods are eco-friendly. These produces less polluting and use non-toxic substances, making them environmentally benign compared to traditional chemical methods.
- ❖ Utilizing biological systems can be more economical as it reduces the need for expensive reagents and complex equipment. Hence these methods are Cost-Effective.
- ❖ The Scalability of these methods are high. Biogenic synthesis processes can be scaled up with relative ease, making them suitable for large-scale production.

#### **Limitations and Challenges:**

- ❖ *Reproducibility:* The synthesis process can be affected by variations in biological sources, leading to inconsistencies in nanoparticles size and morphology.
- ❖ *Purity:* Isolating pure nanoparticles can be challenging due to the presence of residual biological materials.
- ❖ *Optimization:* The synthesis conditions, such as pH, temperature, and concentration, need to be optimized for each biological system, which can be time-consuming.

#### **Applications of Biogenically Synthesized Ag NPs:**

- ❖ *Biomedical Applications:* Ag NPs are used in drug delivery, imaging, and as antimicrobial agents. Their biogenic synthesis enhances their biocompatibility and reduces toxicity.
- ❖ *Environmental Remediation:* Ag NPs can be employed for removing pollutants from water and air. Their biogenic synthesis contributes to their effectiveness in these applications.

- ❖ *Catalysis*: Due to their high surface area and unique properties, Ag NPs are used as catalysts in various chemical reactions. Biogenic synthesis can tailor these properties for specific catalytic applications.

## CONCLUSION:

The biogenic synthesis of silver nanoparticles represents a promising and sustainable approach to nanoparticles production. Utilizing biological systems for the synthesis of Ag NPs not only aligns with green chemistry principles but also offers potential advantages in terms of cost, scalability, and environmental impact. However, challenges related to reproducibility, purity, and optimization must be addressed to fully harness the potential of this approach. Continued research and development in this field will likely enhance the practical applications of biogenically synthesized Ag NPs, contributing to advancements in medicine, environmental science, and industrial processes.

## REFERENCES

- [1] Jeevanandam J, Barhoum A, Chan YS, Dufresne A, Danquah MK; Review on nanoparticles and nanostructured materials: history, sources, toxicity and regulations. *Beilstein J. Nanotechnol.* 9(2018):1050–1074.
- [2] Chandrasekaran R, Yadav SA, Sivaperumal S; Phytosynthesis and characterization of copper oxide nanoparticles using the aqueous extract of *Beta vulgaris* L and evaluation of their antibacterial and anticancer activities. *J Clust Sci* 6 (2019).
- [3] Dhand C, Dwivedi N, Loh XJ, Jie Ying AN, Verma NK, Beurman RW, Lakshminarayanan R, Ramakrishna S; Methods and strategies for the synthesis of diverse nanoparticles and their applications: a comprehensive overview. *RSC Adv* 5 (2015) 105003–105037.
- [4] Seetharaman PK, Chandrasekaran R, Gnanasekar S, Chandrakasan G, Gupta M, Manikandan DB, Sivaperumal S; antimicrobial and larvicidal activity of eco-friendly silver nanoparticles synthesized from endophytic fungi *Phomopsis liquidambaris*. *Biocatal Agric Biotechnol*, 16 (2018) 22–30.
- [5] Darroudi M, Sabouri Z, Kazemi R, Oskuee, Khorsand Zak A, Kargar H, Hamid MHNA; Sol–gel synthesis, characterization, and neurotoxicity effect of zinc oxide nanoparticles using gum tragacanth. *Ceram Int*, 39 (2013) 9195–9199.
- [6] Zhang M, Yang J, Cai Z, Feng Y, Wang Y, Zhang D, Pan X (2019) Detection of engineered nanoparticles in aquatic environments: current status and challenges in enrichment, separation, and analysis, *Environ Sci Nano* 6 (2019) 709–735.
- [7] E.-S.R. El-Sayed, H.K. Abdelhakim, Z. Zakaria, Extracellular biosynthesis of cobalt ferrite nanoparticles by *Monascus purpureus* and their antioxidant, anticancer and antimicrobial activities: yield enhancement by gamma irradiation, *Mater. Sci. Eng. C* 107 (2020) 110318.
- [8] Hakim, L.F., Portman, J.L., Casper, M.D., Weimer, A.W., 2005. Aggregation behavior of nanoparticles in fluidized beds. *Powder Technol.* 160 (3), 149–160.
- [9] Tripp, S.L., Pusztay, S.V., Ribbe, A.E., Wei, A., 2002. Self-assembly of cobalt nanoparticle rings. *J. Am. Chem. Soc.* 124 (27), 7914–7915.

- [10] B. Ajitha, Y. Ashok Kumar Reddy, K.M. Rajesh, P. Sreedhara Reddy; *Sesbania grandiflora* leaf extract assisted green synthesis of silver nanoparticles: antimicrobial activity, *Mater. Today Proc.* 3 (2016) 1977-1984.
- [11] O. Azizian-Shermeh, A. Einali, A. Ghasemi; Rapid biologically one-step synthesis of stable bioactive silver nanoparticles using Osage orange (*Maclura pomifera*) leaf extract and their antimicrobial activities, *Adv. Powder Technol.* 28 (2017) 3164-3171.
- [12] F.Ö. K p, S.  os, kun ay, F. Duman; Biosynthesis of silver nanoparticles using leaf extract of *Aesculus hippocastanum* (horse chestnut): evaluation of their antibacterial, antioxidant and drug release system activities, *Mater. Sci. Eng. C* 107 (2020) 110207.
- [13] M. Asimuddin, M.R. Shaik, S.F. Adil, M.R.H. Siddiqui, A. Alwarthan, K. Jamil, M. Khan, *Azadirachta indica* based biosynthesis of silver nanoparticles and evaluation of their antibacterial and cytotoxic effects, *J. King Saud Univ. Sci.* 32 (2020) 648-656.
- [14] S.S. Royji Albeladi, M.A. Malik, S.A. Al-thabaiti, Facile biofabrication of silver nanoparticles using *Salvia officinalis* leaf extract and its catalytic activity towards Congo red dye degradation, *J. Mater. Res. Technol.* 9 (2020) 10031-10044.
- [15] R. Renuka, K.R. Devi, M. Sivakami, T. Thilagavathi, R. Uthrakumar, K. Kaviyarasu, Biosynthesis of silver nanoparticles using *Phyllanthus emblica* fruit extract for antimicrobial application, *Biocatal. Agric. Biotechnol.* 24 (2020) 101567.
- [16] M.A. Odeniyi, V.C. Okumah, B.C. Adebayo-Tayo, O.A. Odeniyi, Green synthesis and cream formulations of silver nanoparticles of *Nauclea latifolia* (African peach) fruit extracts and evaluation of antimicrobial and antioxidant activities, *Sustain. Chem. Pharm.* 15 (2020) 100197.
- [17] Mukherjee, P., Ahmad, A., Mandal, D., Senapati, S., Sainkar, S.R., Khan, M.I., Parishcha, R., Ajaykumar, P.V., Alam, M., Kumar, R., Sastry, M.; Fungus-mediated synthesis of silver nanoparticles and their immobilization in the mycelial matrix: a novel biological approach to nanoparticle synthesis. *Nano Lett.* 1 -10, (2001), 515-519.
- [18] Riddin, T., Gericke, M., Whiteley, C.G.; Biological synthesis of platinum nanoparticles: effect of initial metal concentration. *Enzyme Microbial. Technol.* 46-6, (2010), 501-505.

# Analysis of Physico-Chemical Properties of Kayadhu River

Dr. Gajanan G. Kadam\*, Kishor Dawane, Dr. Rameshwar M. More

Department of Chemistry, Shri Datta Arts, Commerce and Science College Hadgaon, Dist-Nanded, Maharashtra, India

## ABSTRACT

The present water study deals with the physicochemical characteristics of water of the Kayadhu River, Hadgaon. Parameters like pH, conductivity, Total dissolved solid (TDS), sulphates, nitrates, and phosphates showed distinct variations in the river. The pH in the Kayadhu River was found to be moderate.

## INTRODUCTION

Water is a fundamental natural resource and most essential necessity to both natural ecosystem and human life. The natural water bodies are strength of plant and a source of energy for living organisms, healthy aquatic life is also depends on the quality of water. [1]. In general water pollution occurs due to the city sewage and manmade waste discharge into water bodies which affects on aquatic ecosystem and human beings. The condition for the ecology of living organisms provides significant information about the available water resource supporting the aquatic life or not supporting due to manmade pollution.[2]

The water pollution occurred due to human activities like idol immersion, which releases non-biodegradable pop, toxic paints into the water body and get poisonous. The human activity of immersing such material into water bodies results in the oxygen level of water to 50%.[3] The water of Kayadhu river is utilised for agriculture and also as a drinking water source for Hadgaon town. Therefore, it is essential to monitor physico-chemical parameters to check the magnitude and source of any pollution load and to suggest appropriate conservative measures.[4-5] For this study we reviewed some work, information in relation to physico-chemical analysis of water in the Kayadhu is not extensively studied, thus study was conducted in the months of November and December 2023.[6]

Therefore, present study is carried out to reveal the status of pollution of Kayadhu in terms of Physico-chemical analysis.

## MATERIALS AND METHOD

**Study Area :** The water samples were collected from three stations namely S1 (Gojegaon village side),S2 (Marlegaon village side) and S3 (Dhanora village side) in the months of November and December 2023.The sampling spot were chosen considering the location of nearby villages, domestic and agricultural areas.

The water samples (1L) were collected in clean polyethylene bottles in the morning between 8.00 am to 9.00 am. Some parameters were recorded at the sampling points and other physico-chemical parameters checked in the Research Laboratory of Chemistry, Shri Datta Arts, Commerce and Science College Hadgaon, followed by the method prescribed by APHA (2005). The climatic condition of the study area was cool winter, temperature range a minimum 12.7°C and a maximum of 30.4°C.

## RESULT AND DISCUSSION

The Physico-chemical parameters such as temperature, pH, turbidity, phosphate, chloride, nitrate, dissolve oxygen (DO), biological oxygen demand (BOD), total suspended solids (TDS), total hardness (Ca and Mg salts) were analyzed for the water samples collected from the Kayadhu River. The findings are organized through statistical analysis, including the highest, lowest, and average values for Stations 1, 2, and 3.

- 1) **Temperature:** Water temperature spans from 13.7°C to 31.4°C across various locations. Changes in water temperature are noted due to changes in water depth and air quality.
- 2) **pH:** The value of pH is very important for plankton growth. During this study, pH is ranging from 6.2 to 9.9. These pH values indicate alkaline nature of water and high values may be due to sewage discharge and agricultural fields.
- 3) **Turbidity:** Turbidity of water was ranging from 0.3 to 11.8 NTU. During winter season silt, clay and other suspended particles settle down and result in low turbidity value.
- 4) **Phosphate:** Phosphate group is the most important limiting factor for the maintenance of reservoir fertility as it acts as insecticidal agents. During this study the phosphate concentration ranged from 0.003 to 0.097 mg/l at different sites.
- 5) **Chloride :** Chloride found to be high ranging from 32.21 mg/l to 43.44 mg/l revealed the increased level of pollution.
- 6) **Nitrate :** The high concentration of nitrate in water turned to be toxic to aquatic life. The Nitrate values range between 0.01 to 0.07mg/l.
- 7) **Dissolved Oxygen :** Dissolved oxygen is an essential parameter for aquatic life. The DO values were found between 2.92 to 9.7 mg/l. high values of DO in winter due to low rate of decomposition of organic matter and high flow of water.
- 8) **Biochemical Oxygen Demand:** Biological oxygen demand (BOD) is an important parameter to the oxygen required for degradation of organic matter. During the study period BOD recorded from 1.98 to 6.90 mg/l which is within the permissible range.
- 9) **Total Dissolved Solids:** Total dissolved solids (TDS) values were ranging from 246.5 to 293.2 mg/l at all different stations. TDS analysis has great implications in the control of physical wastes in the water treatment process.
- 10) **Total Hardness:** The overall hardness is caused by calcium and magnesium salts, while the temporary hardness is a result of bicarbonates in the water. The hardness levels varied from 238 to 208 parts per million. The rise in hardness can be linked to a reduction in water volume and a faster evaporation rate at higher temperatures.

Water quality parameters	Station 1 (Golegaon village)			Station 2 (Mardagaon village)			Station 3 (Dhanora Village)		
	Max	Min	Mean	Max	Min	Mean	Max	Min	Mean
(unit)									
Water temperature (°C)	29.5	12.7	21.1	30.4	14.1	22.25	12.9	22.7	17.8
pH	9.9	6.9	8.4	9.7	7.7	8.7	7.7	6.2	6.95
Turbidity (NTU)	11.8	0.5	6.15	10.5	0.5	5.5	9.5	0.3	4.9
Phosphate (mg/l)	0.097	0.015	0.056	0.09	0.012	0.051	0.087	0.003	0.045
Chloride (mg/l)	43.44	36.39	39.91	42.0	34.0	38	38.20	32.21	35.20
Nitrate (mg/l)	0.06	0.02	0.04	0.07	0.02	0.045	0.04	0.01	0.025
Dissolved oxygen (DO) (mg/l)	9.7	5.60	7.65	8.40	4.36	6.38	7.13	2.92	5.025
Biological oxygen demand (BOD) (mg/l)	5.93	2.62	4.27	6.90	2.50	4.7	5.20	1.98	3.59
Total dissolved solids (TDS) (mg/l)	277.2	261.5	269.3	293.2	252.0	272.6	271.2	246.5	258.8
Total Hardness (ppm)	238.0	211.6	224.8	235.2	214	224.6	230.9	208.1	219.5
Concern	Marginal Concern			Marginal Concern			-		

**Table-1 Water quality parameters and sampling stations from Kayadhu River**

## CONCLUSION:

The physico-chemical parameters are generally within desirable limits, with only slight concern at specific sites. The analysis indicates that the water from Kayadhu River is safe for drinking and irrigation. The findings from this study will be valuable for ensuring the water remains potable and for future water management.

## REFERENCES

- [1] Magarde V., Iqbal S.A., Malik S. Pollution parameters including toxic and heavy metals contamination studies of upper Lake Bhopal. *Curr. World Environ*; 1(2), 2005
- [2] Watkar A. M. and Barbate M. P., Impact of idol immersion activities on the water quality of Kellar river, *Int., Research J. Environmental Science*, 3(3), 2014.

- [3] Jadhao P. and Dongare M., Evaluation of dissolved oxygen in ex situ Ganesh idol immersion, *Nature Environ and Pollution Technology*, 8(3), 2009.
- [4] Damotharan P., Permal N. V., Perumal P., Seasonal variation of physico-chemical characteristics of Point Calimere coastal waters, *Middle-East Journal of scientific research*, 6(4), 2010.
- [5] Prasanna M. and Ranjan P. C., Physico-chemical properties of water collected from Dhamra estuary, *International Journal of Environmental Science*, 1(3), 2010.
- [6] Dhawale P.G. and Ghyare B. P., Assessment of Physico-Chemical Status of Water in Pus Dam of Pusad Tahsil, *Journal of Natural Sciences Research*, 5 (9), 2015.

# Cobalt(II) Schiff Base Complexes: Synthesis, Characterization, and Comprehensive Spectral Analysis

Bhagawat R. Gurme

Late Shankarrao Gutte Gramin Arts, Commerce and Science College Dharmapuri, tq- Parli dist- Beed, Maharashtra, India

## ABSTRACT

Schiff base ligands and their metal complexes have gained significant attention due to their versatile coordination properties and wide range of applications in catalysis, biological systems, and materials science. This review focuses on the synthesis and characterization of Cobalt(II) Schiff base complexes, highlighting the detailed methodologies used for their preparation and the various spectral techniques employed for their structural elucidation. The Schiff bases are typically derived from the condensation of primary amines with carbonyl compounds, followed by coordination with cobalt to form stable complexes. Commonly used characterization techniques include UV-Vis, IR, NMR, and X-ray diffraction, providing comprehensive insight into the geometry and bonding patterns of the complexes. Spectral data is presented to confirm the coordination environment, while the applications of these complexes in catalytic, antimicrobial, and electrochemical processes are discussed. This review offers a clear synthesis pathway, standard characterization procedures, and valuable insights into the practical applications of Cobalt(II) Schiff base complexes, paving the way for further research in this field.

**KEYWORDS:** Schiff base, Cobalt(II) complexes, synthesis, characterization, spectral analysis, catalysis, applications.

## INTRODUCTION

### Introduction:

Cobalt(II) Schiff base complexes have been widely studied due to their versatility in coordination chemistry and applications in fields such as catalysis, biological activity, and materials science. This section provides detailed examples of synthesized cobalt(II) Schiff base complexes, their characterization methods, and the spectral data associated with each complex.

### 1. Cobalt(II)Salicylaldehyde-EthylenediamineComplex:

The synthesis of the cobalt(II) Schiff base complex with salicylaldehyde and ethylenediamine is one of the most well-documented examples. Salicylaldehyde acts as the aldehyde component, and ethylenediamine serves as the amine, forming the Schiff base ligand upon condensation.



**Synthesis:****Step1: Formation of Schiff Base Ligand**

A solution of salicylaldehyde (2 mmol) in ethanol (20 mL) is slowly added to a solution of ethylenediamine (1 mmol) in ethanol (20 mL) with constant stirring. The reaction mixture is refluxed for 1–2 hours, and the resulting Schiff base ligand is obtained as a yellow precipitate upon cooling.

**Step2: Complexation with Cobalt(II)**

Cobalt(II) acetate tetrahydrate (1 mmol) is dissolved in ethanol (20 mL) and added dropwise to the Schiff base solution. The mixture is refluxed for an additional 2–3 hours, resulting in the formation of a dark-colored complex. The complex is isolated by filtration and washed with cold ethanol. The product is air-dried to yield a cobalt(II) Schiff base complex.

**Characterization:****1. UV-Visible Spectroscopy:**

The UV-Vis spectrum of the cobalt(II) Schiff base complex shows characteristic absorption bands at 310–340 nm due to  $\pi$ - $\pi^*$  transitions of the conjugated Schiff base ligand and at 410–450 nm corresponding to metal-ligand charge transfer (MLCT).

A weak d-d transition band is observed at around 560–580 nm, which is typical for cobalt(II) in a distorted octahedral geometry.

**2. FTIR Spectroscopy:**

The IR spectrum of the free Schiff base ligand shows a sharp band at  $1610\text{ cm}^{-1}$ , corresponding to the imine (C=N) stretching. Upon coordination with the cobalt(II) ion, this band shifts to a lower wavenumber (around  $1590\text{ cm}^{-1}$ ), indicating the involvement of the nitrogen atom in coordination.

Additional bands at  $440\text{ cm}^{-1}$  and  $515\text{ cm}^{-1}$  are observed, which are attributed to Co-N and Co-O vibrations, confirming the metal coordination.

**3.  $^1\text{H-NMR}$  Spectroscopy:**

In the Schiff base ligand, the imine proton ( $-\text{CH}=\text{N}$ ) shows a singlet around  $\delta$  8.5 ppm. Upon complexation with cobalt(II), the chemical shift of the imine proton moves slightly downfield, indicating interaction with the metal center.

**4. X-ray Diffraction (XRD):**

Single-crystal X-ray analysis reveals that the cobalt(II) complex adopts a distorted octahedral geometry, with two nitrogen atoms and two oxygen atoms from the Schiff base ligand coordinating to the central cobalt ion.

**Spectral Data:**

**UV-Vis:**  $\lambda_{\text{max}} = 320\text{ nm}$  ( $\pi$ - $\pi^*$  transition),  $430\text{ nm}$  (MLCT),  $570\text{ nm}$  (d-d transition).

**FTIR:**  $\nu(\text{C}=\text{N}) = 1590\text{ cm}^{-1}$  (shifted from  $1610\text{ cm}^{-1}$  in the free ligand),  $\nu(\text{Co-N}) = 440\text{ cm}^{-1}$ ,  $\nu(\text{Co-O}) = 515\text{ cm}^{-1}$ .

**$^1\text{H-NMR}$ :**  $\delta(\text{CH}=\text{N}) = 8.5\text{ ppm}$  (free ligand),  $8.7\text{ ppm}$  (complex).

**XRD:** Distorted octahedral geometry confirmed by bond lengths and angles.

## 2. Cobalt(II) Schiff Base Complex with N,N'-Bis(salicylidene)ethylenediamine (Salen):

The Schiff base ligand N,N'-Bis(salicylidene)ethylenediamine (commonly known as Salen) is formed by the reaction of two equivalents of salicylaldehyde with ethylenediamine. The cobalt(II) Salen complex is a widely studied compound due to its catalytic and magnetic properties.

### Synthesis:

#### Step 1: Formation of Salen Ligand

Ethylenediamine (1 mmol) is added to salicylaldehyde (2 mmol) in ethanol (30 mL) under stirring. The mixture is refluxed for 2 hours, forming the yellow Salen ligand.

#### Step 2: Complexation with Cobalt(II)

The Salen ligand is dissolved in ethanol (20 mL), and cobalt(II) acetate (1 mmol) is added to the solution under reflux. The reaction is continued for 3 hours, resulting in the formation of a brown precipitate. The product is filtered and washed with cold ethanol.

### Characterization:

#### 1. UV-Visible Spectroscopy:

The UV-Vis spectrum of the cobalt(II) Salen complex shows a strong absorption band at 320 nm, corresponding to the  $\pi-\pi^*$  transition of the Salen ligand, and an MLCT band at 410 nm.

A weak d-d transition band at 580 nm suggests a square-planar geometry around the cobalt(II) center.

#### 2. FTIR Spectroscopy:

The IR spectrum of the Salen ligand shows a prominent C=N stretching vibration at  $1620\text{ cm}^{-1}$ , which shifts to  $1605\text{ cm}^{-1}$  upon complexation with cobalt(II).

Co-N and Co-O bands appear at  $450\text{ cm}^{-1}$  and  $520\text{ cm}^{-1}$ , respectively, confirming coordination of the ligand to the cobalt ion.

#### 3. Magnetic Susceptibility:

The cobalt(II) Salen complex exhibits paramagnetic behavior, consistent with a square-planar geometry and an unpaired electron in the d7 configuration of cobalt(II).

#### 4. X-ray Diffraction (XRD):

Single-crystal XRD analysis shows a square-planar geometry with two nitrogen and two oxygen atoms coordinating to the cobalt(II) ion. The Co-N and Co-O bond distances are consistent with coordination complexes of cobalt.

### Spectral Data:

**UV-Vis:**  $\lambda_{\text{max}} = 320\text{ nm}$  ( $\pi-\pi^*$  transition),  $410\text{ nm}$  (MLCT),  $580\text{ nm}$  (d-d transition).

**FTIR:**  $\nu(\text{C}=\text{N}) = 1605\text{ cm}^{-1}$  (shifted from  $1620\text{ cm}^{-1}$  in free Salen),  $\nu(\text{Co}-\text{N}) = 450\text{ cm}^{-1}$ ,  $\nu(\text{Co}-\text{O}) = 520\text{ cm}^{-1}$ .

**Magnetic Susceptibility:**  $\mu_{\text{eff}} = 2.1\text{ BM}$  (indicative of paramagnetism).

**XRD:** Square-planar geometry confirmed by bond lengths and angles.

### 3. Cobalt(II) Schiff Base Complex with o-Vanillin and Ethylenediamine:

A Schiff base ligand derived from o-vanillin and ethylenediamine forms an interesting complex with cobalt(II). This complex has been explored for its antimicrobial properties.

#### Synthesis:

##### Step 1: Formation of Schiff Base Ligand

A solution of o-vanillin (2 mmol) in methanol (20 mL) is added to a solution of ethylenediamine (1 mmol) in methanol (20 mL). The mixture is stirred and heated under reflux for 1 hour to obtain the Schiff base ligand.

##### Step 2: Complexation with Cobalt(II)

Cobalt(II) chloride (1 mmol) is dissolved in methanol (20 mL) and added to the Schiff base solution. The reaction is refluxed for an additional 2 hours, and the complex is obtained as a dark green precipitate, which is filtered and washed with methanol.

#### Characterization:

##### 1. UV-Visible Spectroscopy:

The complex shows a strong absorption band at 330 nm due to  $\pi$ - $\pi^*$  transitions of the Schiff base and an MLCT band at 450 nm.

The d-d transition band at 580 nm suggests an octahedral geometry around the cobalt ion.

##### 2. FTIR Spectroscopy:

The C=N stretching frequency of the Schiff base ligand shifts from  $1635\text{ cm}^{-1}$  to  $1615\text{ cm}^{-1}$  upon complexation with cobalt.

Co-O and Co-N vibrations are observed at  $450\text{ cm}^{-1}$  and  $525\text{ cm}^{-1}$ .

##### 3. $^1\text{H-NMR}$ Spectroscopy:

The imine proton signal at  $\delta$  8.3 ppm (in the free ligand) shifts to  $\delta$  8.6 ppm in the complex, suggesting coordination of the imine nitrogen to cobalt.

#### Spectral Data:

**UV-Vis:**  $\lambda_{\text{max}} = 330\text{ nm}$  ( $\pi$ - $\pi^*$  transition),  $450\text{ nm}$  (MLCT),  $580\text{ nm}$  (d-d transition).

**FTIR:**  $\nu(\text{C}=\text{N}) = 1615\text{ cm}^{-1}$  (shifted from  $1635\text{ cm}^{-1}$ ),  $\nu(\text{Co-N}) = 450\text{ cm}^{-1}$ ,  $\nu(\text{Co-O}) = 525\text{ cm}^{-1}$ .

**$^1\text{H-NMR}$ :**  $\delta(\text{CH}=\text{N}) = 8.6\text{ ppm}$  (complex).

#### CONCLUSION:

Cobalt(II) Schiff base complexes exhibit diverse structures and significant chemical properties, making them versatile for various applications. The complexes synthesized using Schiff base ligands, such as those derived from salicylaldehyde, o-vanillin, and ethylenediamine, show distinct spectral features, including UV-Vis, FTIR,  $^1\text{H-NMR}$ , and X-ray diffraction, confirming their coordination geometries and bonding characteristics. These well-characterized complexes are promising candidates for applications in catalysis, biological activity, and material science.

**REFERENCES**

- [1] Vogel, A. I., "Vogel's Textbook of Practical Organic Chemistry," Longman Group UK Ltd., 5th edition, 1989.
- [2] Nakamoto, K., "Infrared and Raman Spectra of Inorganic and Coordination Compounds," John Wiley & Sons, 2009.
- [3] Lever, A. B. P., "Inorganic Electronic Spectroscopy," Elsevier, 1984.
- [4] Cotton, F. A., Wilkinson, G., "Advanced Inorganic Chemistry," John Wiley & Sons, 6th edition, 1999.
- [5] Pavia, D. L., Lampman, G. M., Kriz, G. S., "Introduction to Spectroscopy," Brooks/Cole, 4th edition, 2008.
- [6] Sheldrick, G. M., "A short history of SHELX," *Acta Cryst. A*64, 2008, 112–122.
- [7] Gupta, K. C., Sutar, A. K., "Schiff base complexes in catalysis," *Coordination Chemistry Reviews*, 2008.
- [8] Sharma, V. K., "Cobalt Schiff base complexes in oxidation reactions," *Journal of Catalysis*, 2010.
- [9] Haiduc, I., and Sowerby, D. B., "The Chemistry of Cobalt Complexes," Elsevier, 1989.

# Advances in HPTLC-based Phytochemical Profiling: A critical review of *Semecarpus anacardium* marker compounds

Gurpreet Singh Bhullar, Dr. Ranjeet Kaur Bajwa, Dr. Prafullachandra Tekale, Dr. Gaganjyot Kaur  
GNIRD, Guru Nanak Khalsa College of Arts, Science & Commerce (Autonomous), Matunga, Mumbai-19,  
Maharashtra, India  
Email: [gurpreetsbhullar26@gmail.com](mailto:gurpreetsbhullar26@gmail.com)

## ABSTRACT

*Semecarpus anacardium*, a highly valued medicinal plant is frequently used in a large number of traditional herbal preparations, contains a diverse array of phytochemicals that require detailed analysis. The nut of this plant is utilized in traditional medicine for its therapeutic benefits, containing biflavonoids, phenolic compounds, stilbenoids, minerals, vitamins, and amino acids. Advances in High-Performance Thin-Layer Chromatography (HPTLC) have revolutionized phytochemical profiling, allowing for precise identification and quantification of bioactive marker compounds. This review provides a thorough, evidence-based evaluation of HPTLC-based phytochemical profiling of *Semecarpus anacardium*, emphasizing marker compounds, method optimization, and validation protocols. A comprehensive literature review demonstrates HPTLC's outstanding capability in resolving complex phytochemical matrices, ensuring high precision, accuracy, and reproducibility. Additionally, this review highlights key instrumental benefits, innovative applications like the isolation of an antimicrobial compound from *Semecarpus anacardium* seeds validates the use of this plant in the treatment of infections and emerging trends in HPTLC-based phytochemical analysis, showcasing its potential for standardizing *Semecarpus anacardium*-based herbal products.

**Keywords:** *Semecarpus anacardium*; HPTLC (High-Performance Thin-Layer Chromatography); Phytochemical Profiling; Antimicrobial compound; Bioactive marker compounds; Phytochemical analysis.

## INTRODUCTION

*Semecarpus anacardium*, commonly known as the “marking nut tree,” is a medicinal plant with significant therapeutic potential in traditional Ayurvedic medicine. It has been widely used for its anti-inflammatory, antimicrobial, anticancer, and antioxidant properties. The bioactive compounds present in its fruits and seeds, including phenolic acids, flavonoids, and other secondary metabolites, contribute to its pharmacological actions. To ensure the quality, efficacy, and safety of herbal formulations containing *Semecarpus anacardium*, it is crucial to develop reliable analytical methods for the identification and quantification of its bioactive constituents. [10]

High-Performance Thin Layer Chromatography (HPTLC) has emerged as a powerful and versatile technique for this purpose due to its simplicity, cost-effectiveness, and capability to analyze multiple

samples simultaneously. HPTLC allows for the separation, detection, and quantification of phytochemicals in complex plant matrices, making it a preferred method for quality control and standardization of herbal products. In recent years, several studies have focused on the development and validation of HPTLC methods for analyzing the chemical constituents of *Semecarpus anacardium*. These methods have been optimized for various markers, providing essential data on the composition and concentration of active compounds. Method validation is a crucial aspect to ensure the reliability, reproducibility, and precision of the analytical technique in accordance with International Conference on Harmonization (ICH) guidelines. [12]

This paper aims to review and summarize the development and validation of HPTLC methods for the analysis of *Semecarpus anacardium*, aiming to provide a robust analytical approach for the standardization of herbal formulation containing this medical plant, we seek to provide an efficient analytical framework for future pharmacological and phytochemical studies involving this medicinal plant.



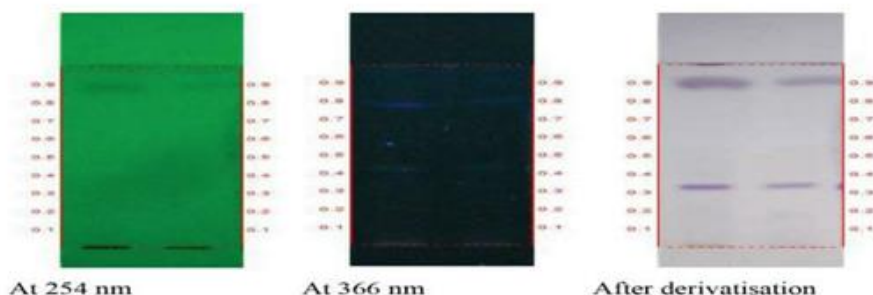
#### EXPERIMENTAL REVIEW: -

2.1.G Senthilvel, developed a HPTLC method in which the unsaponifiable matter of *Serankottainei* (a siddha drug from milk extract of *Semecarpus anacardium* nut) which was dissolved in 10 ml of chloroform and 3 and 6 ul of the above sample was applied on to a pre-coated silica plate to a band width of 7 mm using Linomat 5 TLC applicator. The plate was developed in toluene: ethyl acetate (9.0:1.0). The developed plates were visualized in UV 254, 366, 540 (White light) and scanned under UV, 366 nm, 540 nm and 620 nm post derivatization. R<sub>f</sub>, colour of the spots and densitometric scan were recorded. On photo documentation at 254 nm, 366 nm and under white light (post derivatization with vanillin sulphuric acid), *serankottainei* showed one spot (R<sub>f</sub> 0.90), three spots (R<sub>f</sub> 0.21, 0.44, 0.80) and two spots (R<sub>f</sub> 0.33, 0.90) respectively (Figure 1, Table 2). On densitometric scan at 254 nm, *serankottainei* showed 13 peaks: peak with R<sub>f</sub> 0.76 and 0.89 being the major spots contributing to 29.38% and 19.72% area (Figure 2). At 366 nm, drug showed 5 peaks: peaks with R<sub>f</sub> 0.02, 0.33 and 0.05 being the major spots of 39.27%, 35.16% and 15.08% area (Figure 3). Thus, this protocol could be useful for fingerprinting the *serankottainei* (a siddha drug from milk extract of *Semecarpus anacardium* nut). [2]

254 nm	366 nm	Post derivatisation
-	0.21 (FL. blue)	-
-	-	0.33 (D. purple)
-	0.44 (FL. blue)	-
-	0.80 (FD. blue)	-
0.90 (L. green)	-	0.90 (D. purple)
-	-	-

\*L:Light, D:Dark; F:Fluorescent

Drug name	Minimum inhibitory concentration (MIC)
Pyrazinamide	3.125 µg/ml
Ciprofloxacin	3.125 µg/ml
Streptomycin	6.25 µg/ml
<i>Serankottai nei</i>	1.6 µg/ml



At 254 nm                      At 366 nm                      After derivatisation  
 Track 1-*Semecarpus anacardium*-3 µl  
 Track 2-*Semecarpus anacardium*-6 µl  
 Solvent system: Toluene: Ethyl acetate (9.0:1.0)

Figure 1: HPTLC photo documentation of ethanol extract of *Serankottai nei*.

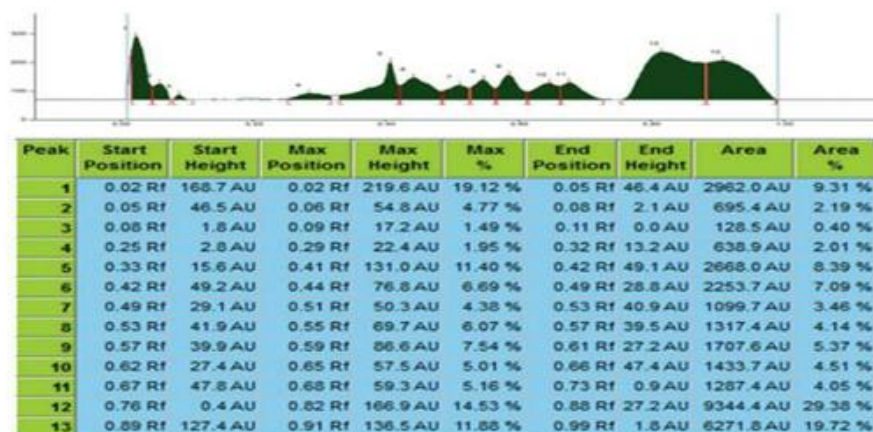


Figure 2: Densitometric scan of *Serankottai nei* (6 µl) at 254 nm.

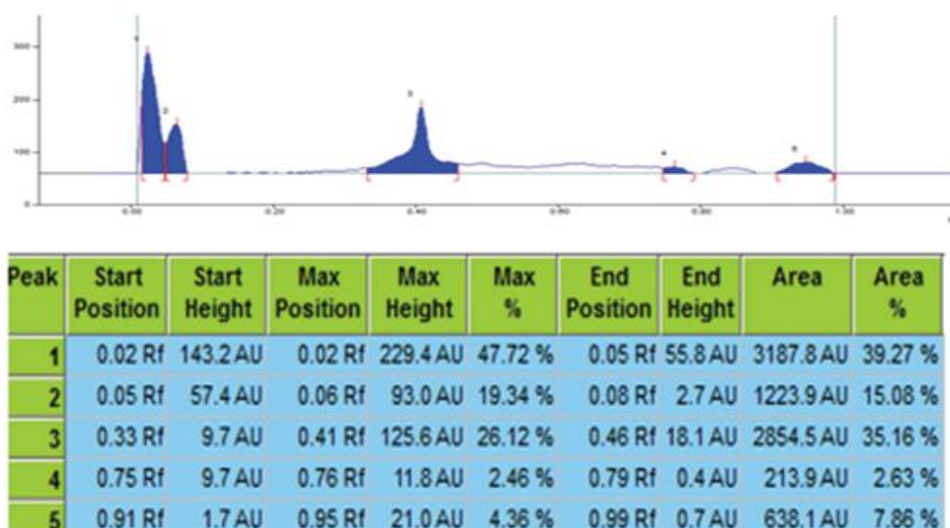


Figure 3: Densitometric scan of *Serankottai nei* (6 µl) at 366 nm.

2.2. Shashi Shankar Tiwari, developed a method in which densitometry HPTLC analysis was performed for the development of characteristic fingerprint profile, which may be used as marker for quality evaluation and standardization of the drug. In which the powder sample of *Semecarpus anacardium* fruit was

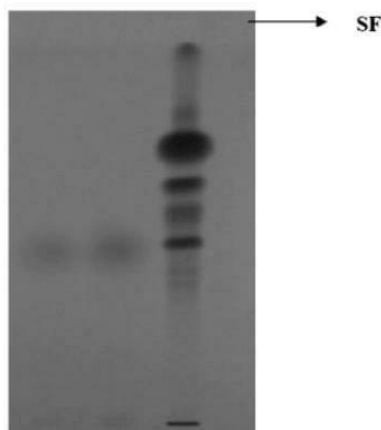


Fig. 3. HPTLC profile under UV-254 nm.

extracted with methanol under reflux, filtered and concentrated on rotavapor. A solution of 10 mg/ml solution was prepared using methanol and a catechol standard of 1 mg/ml. 10 µl of the standard solution and test solution were applied on a pre-coated silica gel 60 F<sub>254</sub> TLC plate (E. Merck). The plate was developed in the solvent system of Toluene: ethyl acetate: formic acid (8:2: 0.1 v/v) catechol was simultaneously quantified by using CAMAG TLC Scanner model-3 equipped with winCATS [version 3.2.1] Software. Shown in figure 4 and 5 below:

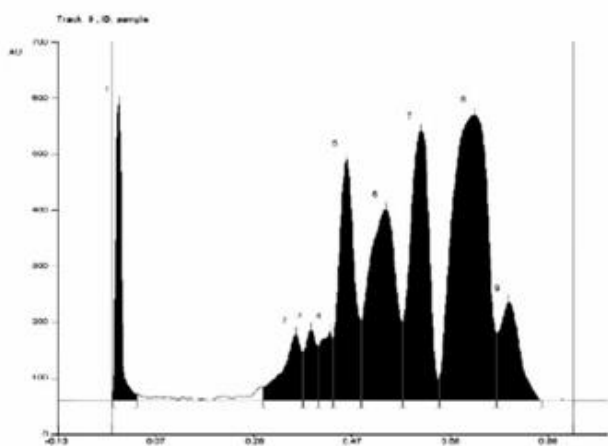


Fig. 5. HPTLC densitometric scan (at 254 nm) of *Semecarpus anacardium* fruit.

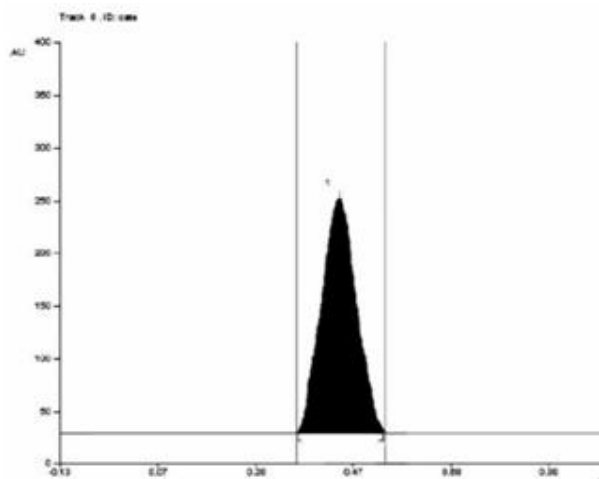


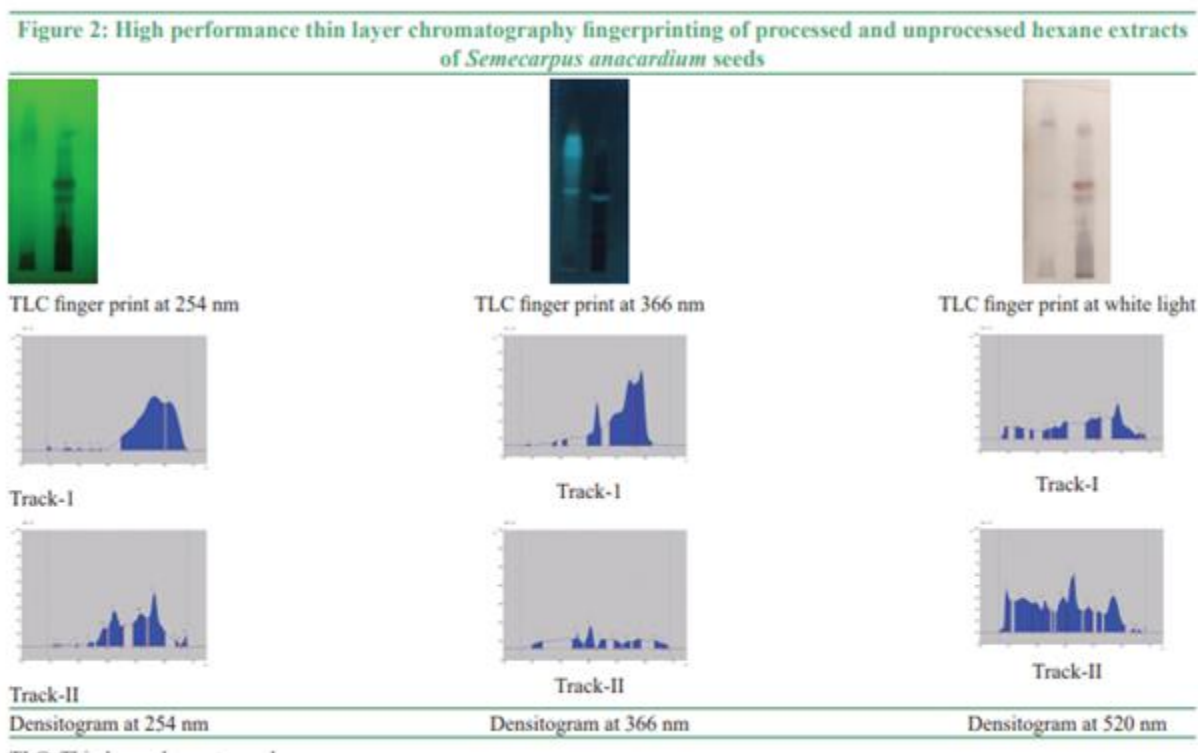
Fig. 4. HPTLC densitometric scan (at 254 nm) of catechol as marker compound

On quantitative HPTLC analysis showed that catechol was present in *Semecarpus anacardium* fruit is 0.082% (w/w) concentration. [3]

2.3. ManasRanjanSahoo, developed a TLC method in which a sample of *Semecarpus anacardium* seeds was extracted using petroleum ether under reflux followed by filtration. The test solution is applied on a pre-coated TLC plate with silica gel 60 F<sub>254</sub> and run through the solvent system of Toluene: Ethyl acetate (8:2)



(v/v). After the development, the plate was sprayed with anisaldehydesulfuric acid and heated at 105°C for 5 min. The plate was visualized in CAMAG UV cabinet under 254 and 366 nm. CAMAG Scanner III equipped with winCATS software version 1.4.3 was used to scan the plates. The HPTLC fingerprint profile of petroleum ether extracts of *Semecarpus anacardium* at 254, 366, and 520 nm is presented in Figure 2. The SA extracts showed 8 bands after Shodhana process while unprocessed extracts showed 14 bands under 254 nm. These components were removed after the purification of *Semecarpus anacardium* seeds. Similarly, the area of the many bands at different R<sub>f</sub> was reduced after their purification process, indicating a decrease in their concentration in the processed or purified *Semecarpus anacardium* seeds. This was further substantiated from the observed lower extractive values from alcohol and petroleum ether extractions of purified *Semecarpus anacardium* seeds as compared to its corresponding raw *Semecarpus anacardium* seeds.[4]



2.4. Sanjeeb Kumar Mishra, developed a TLC method in which the extraction of pre shodhit and shodhitnut was subjected to Maceration in methanol solvent followed by evaporation to dryness. The sample is applied on the TLC plate using TLC sampler followed by dipping in the mobile phase of Chloroform: Methanol (9.8:0.2 v/v). The calibration parameters consist of mode of single level, calibration curve with area and peak height. The percentage was calculated as per the following formula:

$$\text{Percentage of constituent} = \frac{\text{Sample area} \times \text{Standard dilution} \times \text{Purity}}{\text{Standard area} \times \text{Sample dilution}} \times 100$$

The PSM (Tracks 1, 3 and 5) and SM (Tracks 2, 4 and 6) of methanolic extracts showed well resolved spots on HPTLC plates [Table 2 and Figures 1, 2]. The maximum height and area were decreased in SM.

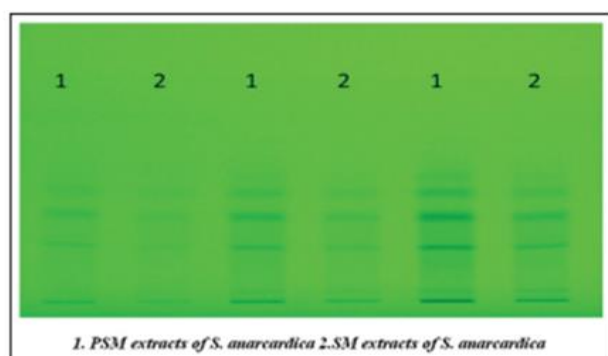


**Figure 1:** High performance thin layer chromatography of pre-shodhit methanolic (PSM) and shodhit methanolic extract (SM) of *Semecarpus anacardium* before derivatization in short Ultraviolet (254 nm). 1 – PSM extracts of SA, 2 – SM extracts of SA

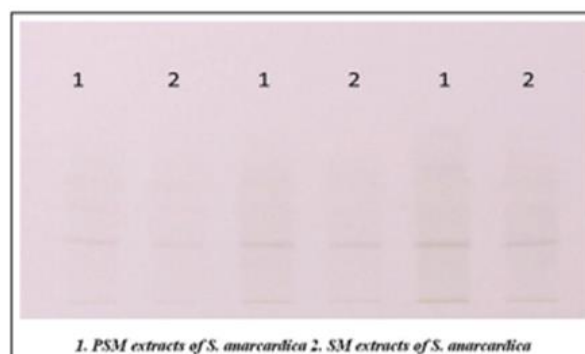


**Figure 2:** High performance thin layer chromatography of pre-shodhit methanolic (PSM) and shodhit methanolic extract (SM) of *Semecarpus anacardium* after derivatization in white light. 1 – PSM extracts of SA, 2 – SM extracts of SA

**Table 2:** HPTLC analysis of PSM and SM extract of SA

Track No	Details of standard and sample	R <sub>f</sub>	Maximum height	Area
1	PSM extract 0.5 µg/L	0.37	133.3	3867.6
2	SM extract 0.5 µg/L	0.36	72.8	1899.9
3	PSM extract 1 µg/L	0.36	209.2	6522.0
4	SM extract 1 µg/L	0.35	122.2	3432.3
5	PSM extract 2 µg/L	0.36	308.2	10589.3
6	SM extract 2 µg/L	0.36	200	6147.3

PSM: Pre-shodhit methanolic, SM: Shodhit methanolic extract, SA: *Semecarpus anacardium*, HPTLC: High performance thin layer chromatography

It has been put forth that none of the phytochemical analysis has been found to complete without the progress of HPTLC. In this study, they have conducted HPTLC of both PSM and SM extract of SA to evaluate the effects of Shodhana on phytoconstituents present. However, maximum height and areas were found to be decreased in both PSM as well as SM which were noticed on observing the concentrations values. [5]

**2.5** Mohamed Fawzy Ramadan, developed a method in which a seed of *Semecarpus anacardium* were finely grounded and Soxhlet extracted with n-hexane for 12 hrs followed by column chromatography using Chloroform to get a neutral lipid. By means of thin layer chromatography (TLC) on SilicaGel F<sub>254</sub> a further characterization of the neutral lipid subclasses was carried out using a solvent system of n-hexane: Diethyl ether: acetic acid (60:40:1)(v/v/v). For detection, the TLC plates were sprayed with sulphuric acid (40%). Each spot was identified with lipid reference compounds as well as their reported retention factor (R<sub>f</sub>) values. For the quantitative determination of neutral lipids subclasses, individual bands were scraped from the plate and recovered by extraction with 10% methanol in diethyl ether. Data presented are the average of three gravimetric determinations. The R<sub>f</sub> values of neutral lipid subclasses are shown in Table 1: [6]

**Table 1** Lipid classes (g/kg TL) in *S. anacardium* crude seed oil

Lipid class	R <sub>f</sub> values × 100 <sup>a</sup>	g/kg TL	Glycolipid class	g/kg TL	Phospholipid class	g/kg TL
MAG	14	5.67 ± 0.23	SQD	0.35 ± 0.03	PS	0.25 ± 0.03
DAG	39	7.86 ± 0.33	DGD	0.64 ± 0.04	PI	0.74 ± 0.04
FFA	56	6.66 ± 0.21	CER	1.12 ± 0.04	PC	2.55 ± 0.09
TAG	79	885 ± 3.13	SG	1.55 ± 0.07	PE	1.22 ± 0.07
STE	95	5.43 ± 0.26	MGD	0.16 ± 0.02		
			ESG	1.32 ± 0.03		
Total glycolipids		5.14				
Total phospholipids		4.76				

Results are given as the average of triplicate determinations ± standard deviation

TL total lipids, MAG monoacylglycerols, DAG diacylglycerols, TAG triacylglycerols, FFA free fatty acids, STE sterol esters, SQD sulphoquinovosyldiacylglycerol, DGD digalactosyldiacylglycerol, CER cerebrosides, SG steryl glucoside, MGD monogalactosyldiacylglycerol, ESG esterified steryl glucoside, PS phosphatidylserine, PI phosphatidylinositol, PC phosphatidylcholine, PE phosphatidylethanolamine

<sup>a</sup> Solvent system used in TLC development: *n*-hexane/diethyl ether/acetic acid (60:40:1, v/v/v)

2.6.D. K. Tiwari and N. Upmanyu, developed a HPLC method as 1 gram of hydro-alcoholic extract prepared using ethanol:water (1:1), filtered and dried using water bath further with vacuum and was mixed with silica gel for column chromatography and extracted by maceration with ethanol. The extract was made up to 50 ml in a volumetric flask. 5 and 10 µl of the isolated ethanolic extract was applied on a pre-coated Silica gel F<sub>254</sub> on aluminium plates to a band width of 7 mm using CAMAG Linomat 5 TLC applicator. The plate was then developed in CAMAG twin-trough chamber using Ethyl Acetate: Water: Formic Acid: Acetic acid (100:26:11:11) (v/v/v/v) as mobile phase. The R<sub>f</sub> values were determined by photodocumentation performed using CAMAG photo

Track 1- *S. anacardium*– 5 µl; Track 2- *S. anacardium*– 10 µl Solvent system: Ethyl Acetate: Water: Formic Acid: Acetic acid (100:26:11:11) v/v/v/v

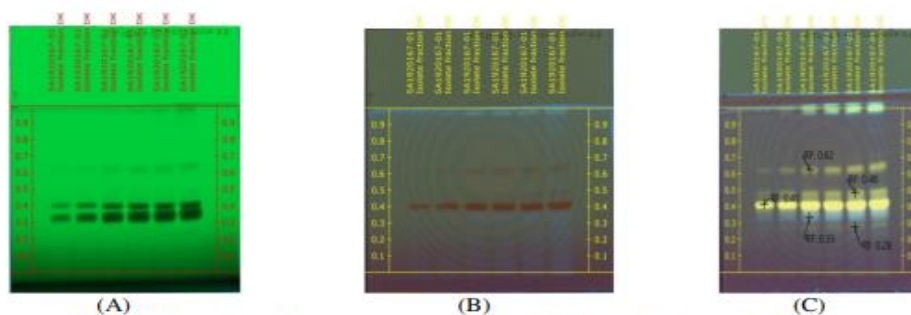


**Fig. 3:** HPTLC photo documentation of isolated ethyl acetate fraction of leaves of *S. anacardium*

**Table 4:** R<sub>f</sub> values of ethanol extract of nuts of *S. anacardium*

Name	Track no.	No.	Colour	Intensity	R <sub>f</sub> Value
DKT-SA-01	1	1	Yellow	High	0.41
	3	2	Blue	Low	0.33
			Yellow	Medium	0.62
	5	2	yellow	Medium	0.48
			yellow	Low	0.28

documentation chamber and the plates were scanned under 254 nm, 366 nm and 620 nm which gives 06 spots in fig 3(a), 3(b) after derivatisation using CAMAG Scanner (Sethi 1996). Post derivatisation using 10% methanolic sulfuric acid spray reagent. HPTLC is still increasingly finding its way in pharmaceutical analysis and with the advancements in the stationary phases and the introduction of densitometers as detection equipment, the technique achieves for given applications, a precision and trueness when compared to High Performance Liquid Chromatography (Shivatara et al., 2013). [7]

2.7. Ilanchezhian R, developed a TLC method in which a TLC plate coated with a stationary phase, typically silica gel, a methanolic extract of *Semecarpus anacardium* Linn. fruit was applied as a spot near the bottom of the plate using a capillary tube. The plate is then placed vertically in a developing chamber containing a benzene: ethyl acetate (6:1) (v/v) solvent system, ensuring the sample spot is above the solvent level. Once the solvent front hits the plate is removed, dried, and the spots are visualized under UV long wavelength i.e. 366 nm and by staining using Iodine vapour. Similar TLC analysis was done using toluene: ethyl acetate (9.3:0.7) solvent system. The results with Rf values of *Semecarpus anacardium* Linn. fruit are mentioned in the Table 3. [8]

**Table 3: Showing Rf values of *Semecarpus anacardium* Linn. - Fruit**

Extractives	Solvent system	Viewing reagent	Rf values
Methanol	Toluene: Ethylacetate (9.3:0.7)	Iodine vapour	0.29, 0.50, 0.56, 0.69, 0.90
Methanol	Benzene: Ethylacetate (6:1)	Iodine vapour	0.40, 0.64, 0.74, 0.96

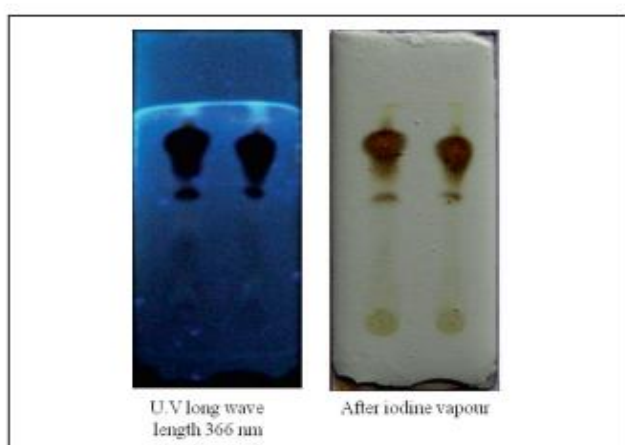


**Figure 10: TLC – Benzene: Ethylacetate**

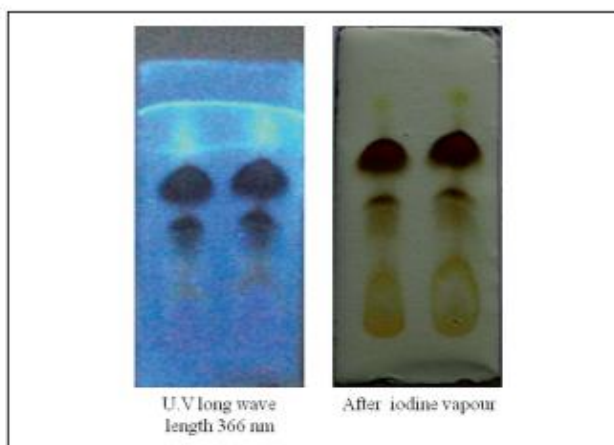


**Figure 11: TLC – Toluene: Ethylacetate**

2.8. Alka Sharma and R. A. Sharma, developed a TLC method in which a 1 gram powdered nuts of *Semecarpus anacardium* were extracted with 10 ml methanol on water bath (60 C/5min). The filtrate was condensed by evaporation, added a mixture of water and EtOAc(10:1 ml), mixed thoroughly. The EtOAc phase retained is used for further analysis. The flavonoids spots were separated using chloroform: methanol (19:1) solvent system. The colour and Rf values of these spots were recorded under U.V light (Wagner and Bladt 1996). The data of TLC for flavonoids in *Semecarpus anacardium* is shown in the Table 1. It has revealed the presence of flavonoids in the nuts as shown below:

**Table 1.** Qualitative separation of flavonoids of *S.anacardium*.

S. no.	Colour of the spots	Rf values of Free flavonoids	Rf value of Bound flavonoids
1	Dark brown	0.23	0.34
2	Light brown	0.40	-
3	Yellow	0.82	0.82
4	Light yellow	0.91	-
5	blue	0.98	0.98

Similarly, the powdered sample of nuts were lixiviated in methanol on rotary shaker for 24h. The condensed filtrate was used for chromatography. Phenols were separated using chloroform:methanol(27:03)(v/v) solvent system. The colour and Rf values of these phenols were recorded under visible light after spraying the plates with Folin-Ciocalteu's reagent heating at 70 C/10min (Harborne 1998). The data of TLC for Phenols in *Semecarpus anacardium* is shown in the Table 2. Five phenolic spots with different colour and Rf values were observed.[9]

**Table 2.** Qualitative separation of phenols of *S.anacardium*

S.No.	Plant part (Nuts) Colour of spots	Rf values
1.	Blue	6.68
2	Dark blue	16.07
3	Intense blue	41.01
4	Blue	55.05
5	Blue	66.64

## CONCLUSION

This review highlights the significant advancements in HPTLC-based phytochemical profiling of *Semecarpus anacardium*, underscoring its crucial role in the identification and quantification of bioactive marker compounds. The diverse methodologies discussed demonstrate HPTLC's effectiveness in resolving complex phytochemical matrices, ensuring high precision, accuracy, and reproducibility in analytical outcomes. The ability to standardize herbal products derived from *Semecarpus anacardium* is essential for ensuring their quality, safety, and efficacy in traditional medicine.

The evidence presented in various studies showcases HPTLC's versatility and reliability, reinforcing its position as a preferred analytical technique in phytochemical research. As the field evolves, continued exploration and optimization of HPTLC methods will further enhance our understanding of *Semecarpus anacardium*'s therapeutic potential and facilitate the development of standardized herbal formulations. Future research should focus on validation of the above methods, integrating HPTLC with other analytical

techniques to provide a comprehensive profile of the phytochemicals present, ultimately contributing to the effective utilization of this valuable medicinal plant in modern healthcare.

## REFERENCES

- [1] Anonymous, "Medicinal Plants of India", Indian Council of Medical Research; 1976; p. 87-89.
- [2] G Senthilvel, Arul Amuthan, KN Sunil Kumar; Phytochemical Standardization of Serankottainei (a Siddha drug from milk extract of *Semecarpus anacardium* nuts) and its in-vitro antitubercular activity against H37Rv strain; International Journal of Pharmacology and Clinical Sciences; Mar 2016; Vol 5; Issue 1; p. 17-24.
- [3] Shashi Shankar Tiwari, Ram Saji wan Singhaand Ajay Kumar Singh Rawatb, Phytochemical, heavy metals and antioxidant studies on *Semecarpus anacardium* (fruit); J. Indian Chem.Soc., Vol. 92. January 2015, p. 1-7.
- [4] ManasRanjanSahoo, Ramesh RaghavaVarier, O. P. Baburaj, AnithaKumariRajendran, Bala Guru, S. Srikrishan, Comparative Phytochemical Evaluation of Ashodhit and ShodhitBhallataka (*Semecarpus anacardium* L.f.) Using HPTLC and TLC Chromatographic Profiling, UV Vis Spectroscopy Study and <sup>1</sup>H NMR Based Fingerprinting; Journal of Ayurveda; Vol. 18; Issue 1; January-March 2024.
- [5] Sanjeeb Kumar Mishra, Gaurav Mahesh Doshi, Pratap Kumar Sahu, Phytochemical analysis of nuts of *Semecarpus anacardium* using gas chromatography-mass spectrometry and high-performance thin layer chromatography: Effect of Shodhana; International Journal of Green Pharmacy; Jan-Mar 2017 (Suppl); 11 (1); S106.
- [6] Mohamed Fawzy Ramadan, S. G. Kinni, M. Seshagiri · Jorg-Thomas Morsel; Fat-Soluble Bioactives, Fatty Acid Profile and Radical Scavenging Activity of *Semecarpus anacardium* Seed Oil; J Am Oil Chem Soc 2010 87: p. 885–894.
- [7] D. K. Tiwari \* and N. Upmanyu; Phytochemical Analysis for Bio-Active Potential of *Semecarpus anacardium* leaves; Plant Archives Vol. 21; Supplement 1; 2021, p. 635–642.
- [8] Ilanchezhian R\*, Roshy Joseph C, Acharya RN, Harisha CR, Shukla VJ; Pharmacognostical and Physicochemical Analysis of Bhallataka (*Semecarpus anacardium* Linn.) – Fruit; Pharmacognosy Journal; February 2011; Vol 3; Issue 20: 09-16.
- [9] Alka Sharma and R. A. Sharma; Qualitative and Quantitative Estimation of Flavonoids and Phenolic Compounds of *Semecarpus anacardium* Nuts; J. Indian bot. Soc.; Vol. 98 (3&4) 2019: p. 194-200.
- [10] Mohan, M., & Sharma, S.; Phytochemical analysis of *Semecarpus anacardium* : An overview; Asian Journal of Pharmaceutical and Clinical Research; 13(1), 2020p. 45-50.
- [11] Kumar, V., & Dutta, S. (2022).; HPTLC and its applications in herbal medicine: A review. International Journal of Green Pharmacy; 16(1), p. 1-10.
- [12] Sethi PD.; High Performance Thin Layer Chromatography. 1st ed., New Delhi: CBS Publishers and Distributors; 1996; p. 1-56.
- [13] Ilanchezhian R, Roshy JC, Acharya R.; Importance of media in Shodhana (purification/processing) of poisonous herbal drugs. AncSci Life 2010; 30; p:54 7.

- [14] Harmorne JB. *Phytochemical Methods. A Guide to Modern Techniques of Plant Analysis*. 3rd ed. New York, NY: Chapman and Hall; 1984. p. 291-93.
- [15] Sahu, P., & Gupta, R.; Recent advancements in the extraction and analysis of phytochemicals from medicinal plants. *Analytical Methods*, 14(7);p. 885-900.
- [16] Chang C, Yang M, Wen H, Chern J ; Estimation of Total Flavonoid Content in Propolis by Two Complementary Colorimetric Methods.; *J Food & Drug Analysis*; 10(3); 2002; p. 178- 182.
- [17] Harborne J B 1998; *Phytochemical methods*, 3 edition Chapman and Hall;Madras; 1998.
- [18] Nair PKR, Melnick SJ, Wnuk SF, Rapp M, Escalon E, Ramachandran C; Isolation and characterization of an anticancer catechol compound from *Semecarpus anacardium* . *J Ethnopharm* 122 2009: p. 450–456.
- [19] Sunil, K.K.N. and Ravishankar, B.; Amalgamation of Chemistry and Biology to overcome bottlenecks in standardization of ayurvedic medicines. *J Tradi Med ClinNatur.*; 5(1) 2016: p. 119.
- [20] Kunle, O.F.; Egharevba, H.O. and Ahmadu, P.O.; Standardization of herbal medicines a review. *Int. J. Biodivers. Conserv.* 4: 2012; p. 101-112.

# Complexation of Samarium With Schiff Bases : Thermodynamic Study

Hansaraj Joshi<sup>\*1</sup>, Rajpal Jadhav<sup>1</sup>, Ramesh Ware<sup>2</sup>, Shailendrasingh Thakur<sup>2</sup>

<sup>\*1</sup>Department of Chemistry, Swa Sawarkar Mahavidyalaya, Beed, Maharashtra, India

<sup>2</sup>Department of Chemistry, Milliya College, Beed, Maharashtra, India

## ABSTRACT

We have used a pH metric titration technique in an 80% (v/v) ethanol-water mixture at three different temperatures (298K, 308K and 318K) at an ionic strength of 0.1M NaClO<sub>4</sub> to measure the proton-ligand and metal-ligand stability constants of new Schiff bases containing lanthanide metal ions. The logK values of the metal-ligand stability constant have been determined using the modified Irving-Rossotti version of the Calvin-Bjerrum method. The thermodynamic parameters, including Gibb's free energy change ( $\Delta G$ ), entropy change ( $\Delta S$ ) and enthalpy change ( $\Delta H$ ), related to the complexation reactions were quantitatively determined.

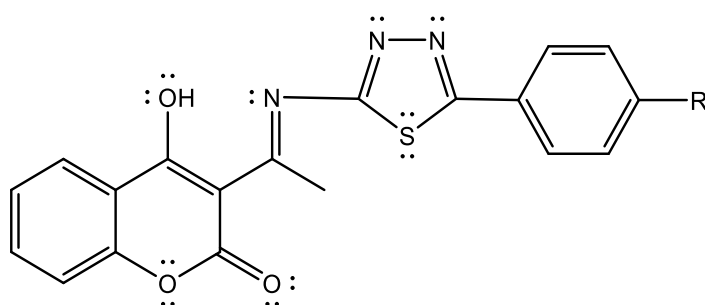
**Keywords:** Rareearth metal ions, Schiff bases, Stability constants, pHmetry, Thermodynamic parameters, etc.

## INTRODUCTION

Schiff base metal complexes significantly contribute in the evolution of coordination chemistry. Proton transfer is crucial in complexation reactions like other acid base catalyzing enzymatic reactions taking place in aqueous medium. Understanding the behavior of ligands and how they interact with metal ions in aqueous solutions requires an accurate estimate of stability constant values. pH metric titration technique is a powerful, simple electro analytical technique for determination of stability constants. For the present investigation, we have selected a series of seven Schiff bases. Synthesis of all seven Schiff bases was done by reported methods. Series of seven Schiff bases were synthesized by reported method and were employed for the present investigation.

In continuation of our earlier work regarding complexation of Schiff bases<sup>1-7</sup> and going through the in depth study of literature<sup>8-15</sup>, it was thought to be fascinating to look at how temperature may affect thermodynamic parameters such as Gibb's free energy change  $\Delta G$ , enthalpy change  $\Delta H$  and entropy change  $\Delta S$  of complexes of seven Schiff bases with rare earth metal ion Sm<sup>3+</sup> by pH metric measurement technique in 80% (v/v) ethanol-water mixture.





R= -H, -CH<sub>3</sub>, NO<sub>2</sub>, -F, -Cl, -Br, -I

Figure: Schiff base ligand

(Molecular formula C<sub>19</sub>H<sub>12</sub> O<sub>3</sub>N<sub>3</sub>SR)

## EXPERIMENTAL

**Materials and Solution:** All chemicals used viz. Samarium metal salt, NaOH, NaClO<sub>4</sub>, HClO<sub>4</sub> used were of AR grade. The solutions used in the pH metric titration were prepared in CO<sub>2</sub> free double distilled water. The NaOH solution was standardized against oxalic acid solution, standard alkali solution was again used for standardization of HClO<sub>4</sub>. The measurements were made at temperatures 298K, 308K and 318K in 80% (v/v) ethanol-water mixture at constant ionic strength (0.1M NaClO<sub>4</sub>). The thermostat is used to maintain the temperature constant and the solutions were equilibrated in the thermostat for about 10-15 minutes before titration. The pH measurement was made using a digital Spectra lab potentiometric titrator AT 38°C with combined glass electrode consisting of glass and reference electrodes in the single entity. This digital potentiometric titrator has built in voltage stabilizer for ± 10% fluctuations in voltage supply. Provision of in built three way valves and gas tight burette with Teflon piston with an accuracy of 0.001 ml enabled the required precision during the titration particularly near the equivalence point. The instrument was calibrated at pH 4.00, 7.00 and 9.18 using the standard buffer solutions.

**pH metric procedures:** For evaluating the protonation constant of the ligand and the formation constant of the complexes with Samarium metal ion, the following sets of solutions were prepared in 80% (v/v) ethanol-water mixture (total volume 50 ml) and titrated pH metrically against standard NaOH solution at three different temperatures 298K, 308K and 318K.

- i. HClO<sub>4</sub> (A)
- ii. HClO<sub>4</sub> + Schiff base (A+L)
- iii. HClO<sub>4</sub> + Schiff base + Metal (A+L+M)

The above mentioned sets were prepared by keeping M:L ratio, the concentration of perchloric acid and sodium perchlorate (0.1M) were kept constant for all sets.

**Determination of the thermodynamic parameters:** Thermodynamic parameters such as Gibb's free energy change, entropy change and enthalpy change for formation of complexes were determined. The change in Gibb's free energy ( $\Delta G$ ) of the ligands was calculated by using the equation.

$$\Delta G = -2.303RT \log K$$

Where R (ideal gas constant) = 8.314 JK<sup>-1</sup>mol<sup>-1</sup>,

K is the dissociation constant for the ligand or the stability constant of the complex and

T is absolute temperature in Kelvin.

The change in enthalpy ( $\Delta H$ ) is calculated by plotting  $\log K$  vs  $1/T$

The equation utilized for the calculation of changes in enthalpy is as

$$\text{Slope} = - \frac{\Delta H}{2.303R}$$

The evaluation of changes in entropy ( $\Delta S$ ) is given by the equation:

$$\Delta S = \frac{(\Delta H - \Delta G)}{T}$$

**Table 1: Proton-ligand stability constant of Schiff bases**

Temperature	Proton-ligand stability constant	Schiff bases						
		S <sub>1</sub>	S <sub>2</sub>	S <sub>3</sub>	S <sub>4</sub>	S <sub>5</sub>	S <sub>6</sub>	S <sub>7</sub>
298K	pK <sub>1</sub>	3.2234	3.3961	3.0385	2.9744	3.6355	3.4792	--
	pK <sub>2</sub>	4.4968	5.1755	4.7142	3.6138	4.8790	5.3457	4.0972
308K	pK <sub>1</sub>	3.0782	3.2750	2.9374	2.8893	3.4614	3.3438	--
	pK <sub>2</sub>	4.3749	5.0532	4.5991	3.487	4.7013	5.1946	3.9860
318K	pK <sub>1</sub>	2.9303	3.1228	2.826	2.8061	3.3052	3.1451	--
	pK <sub>2</sub>	4.2027	4.8810	4.4339	3.3352	4.5062	5.0035	3.8637

**Table 2: Sm (III)-ligand stability constant of Schiff bases**

Temperature	298K			308K			318K		
	logK <sub>1</sub>	logK <sub>2</sub>	log $\beta$	logK <sub>1</sub>	logK <sub>2</sub>	log $\beta$	logK <sub>1</sub>	logK <sub>2</sub>	log $\beta$
Nd(III)-ligand stability constant → Schiff Bases↓									
S <sub>1</sub>	3.7784	3.5491	7.3275	3.6902	3.4698	7.1600	3.6041	3.3865	6.9906
S <sub>2</sub>	4.1893	3.8344	8.0237	4.0525	3.7268	7.7793	3.9110	3.6222	7.5332
S <sub>3</sub>	4.2285	3.8360	8.0645	4.1412	3.7373	7.8785	4.0475	3.6452	7.6927
S <sub>4</sub>	3.5717	3.2586	6.8303	3.4895	3.2110	6.7005	3.4170	3.1685	6.5855
S <sub>5</sub>	4.9062	4.1902	9.0964	4.7107	4.0482	8.7589	4.5280	3.8992	8.4272
S <sub>6</sub>	5.4230	5.2398	10.6628	5.1920	5.0425	10.2345	4.9784	4.8335	9.8119
S <sub>7</sub>	3.7310	3.5045	7.2355	3.6510	3.4414	7.0924	3.5696	3.3736	6.9432

**Table 3: Thermodynamic parameters of Schiff base complex formation with Sm (III) at 298K**

Schiff Bases	- $\Delta G_1$	- $\Delta G_2$	- $\Delta H_1$	- $\Delta H_2$	$\Delta S_1$	$\Delta S_2$
	(KJmol <sup>-1</sup> )		(KJmol <sup>-1</sup> )		(KJK <sup>-1</sup> mol <sup>-1</sup> )	
S <sub>1</sub>	21.559	20.251	15.813	14.746	19.30	18.50
S <sub>2</sub>	23.904	21.871	25.240	19.252	- 04.50	08.80
S <sub>3</sub>	24.127	21.888	16.412	17.314	25.90	15.30

S <sub>4</sub>	20.380	18.593	14.043	8.178	21.30	34.90
S <sub>5</sub>	27.994	23.909	34.320	26.390	-21.20	-08.30
S <sub>6</sub>	30.943	29.898	40.348	36.844	-31.60	-23.30
S <sub>7</sub>	21.289	19.996	14.639	11.869	22.30	27.30

**Table 4: Thermodynamic parameters of Schiff base complex formation with Sm (III) at 308K**

Schiff Bases	- ΔG <sub>1</sub> (KJmol <sup>-1</sup> )	- ΔG <sub>2</sub> (KJmol <sup>-1</sup> )	- ΔH <sub>1</sub> (KJmol <sup>-1</sup> )	- ΔH <sub>2</sub> (KJmol <sup>-1</sup> )	ΔS <sub>1</sub> (KJK <sup>-1</sup> mol <sup>-1</sup> )	ΔS <sub>2</sub> (KJK <sup>-1</sup> mol <sup>-1</sup> )
S <sub>1</sub>	21.762	20.463	15.813	14.746	19.30	18.60
S <sub>2</sub>	23.899	21.978	25.240	19.252	-04.40	08.90
S <sub>3</sub>	23.629	21.324	16.412	17.314	24.20	13.50
S <sub>4</sub>	19.911	18.321	14.043	08.178	19.70	34.00
S <sub>5</sub>	26.879	23.098	34.320	26.390	-25.00	-11.00
S <sub>6</sub>	29.625	28.772	40.348	36.844	-36.00	-27.10
S <sub>7</sub>	20.832	19.636	14.639	11.869	20.80	26.10

**Table 5: Thermodynamic parameters of Schiff base complex formation with Sm (III) at 318K**

Schiff Bases	- ΔG <sub>1</sub> (KJmol <sup>-1</sup> )	- ΔG <sub>2</sub> (KJmol <sup>-1</sup> )	- ΔH <sub>1</sub> (KJmol <sup>-1</sup> )	- ΔH <sub>2</sub> (KJmol <sup>-1</sup> )	ΔS <sub>1</sub> (KJK <sup>-1</sup> mol <sup>-1</sup> )	ΔS <sub>2</sub> (KJK <sup>-1</sup> mol <sup>-1</sup> )
S <sub>1</sub>	21.945	20.620	15.813	14.746	19.30	18.50
S <sub>2</sub>	23.813	22.055	25.240	19.252	-04.50	08.80
S <sub>3</sub>	23.094	20.799	16.412	17.314	22.40	11.70
S <sub>4</sub>	19.497	18.079	14.043	8.178	18.30	33.20
S <sub>5</sub>	25.836	22.248	34.320	26.390	-28.50	-13.90
S <sub>6</sub>	28.406	27.579	40.348	36.844	-40.10	-31.10
S <sub>7</sub>	20.368	19.249	14.639	11.869	19.20	24.80

## RESULTS AND DISCUSSION

The results obtained are analysed by computer programme and stability constant values were calculated. The proton-ligand stability constant was determined by point wise calculation method as suggested by Irving and Rossoti. The proton ligand stability constant pK<sub>a</sub> of all seven Schiff bases were determined in aqueous medium at three different temperatures 298K, 308K, 318K at 0.1M NaClO<sub>4</sub> ionic strength. The proton- ligand stability constants of all the Schiff bases are presented in **TABLE 1**. The Schiff base S<sub>7</sub> has only one pK value where as S<sub>1</sub>, S<sub>2</sub>, S<sub>3</sub>, S<sub>4</sub>, S<sub>5</sub> and S<sub>6</sub> have two pK values. The  $\bar{n}_A$  value ranges between 0.2 to 1.8 indicates the presence of two pK values whereas the range of  $\bar{n}_A$  is in between 0.2 to 0.8 shows only one pK value. In the present investigation Schiff base selected contains hydroxyl group and azomethine nitrogen as bonding sites. The order of pK<sub>a</sub> values of seven ligands is as:

**S<sub>6</sub> > S<sub>2</sub> > S<sub>5</sub> > S<sub>3</sub> > S<sub>1</sub> > S<sub>4</sub> > S<sub>7</sub>**

The above order indicates that S<sub>7</sub> has lowest basicity whereas S<sub>6</sub> has highest basicity. Metal ligand stability constant logK of Sm(III) metal ion with Schiff bases are calculated by point wise and half integral method of Calvin-Bjerrum as adopted by Irving-Rossotti. The logK<sub>1</sub> values calculated by point wise calculation method and half integral method, indicates simultaneous formation of 1:1 complex. We got values of proton-ligand formation number ( $\bar{n}_A$ ) between 0.2 to 0.8 and 1.2 to 1.8 indicating 1:1 and 1:2 complex formations. The proton-ligand stability constant pK<sub>a</sub> values decrease with increase in temperature i.e. the acidity of the ligands increases<sup>12</sup>, it suggests that the liberation of proton becomes easier at higher temperature. Order of stability constants for Sm(III) complexes with Schiff bases (**Table 2**) found to be as follows:

**S<sub>6</sub> > S<sub>5</sub> > S<sub>3</sub> > S<sub>2</sub> > S<sub>1</sub> > S<sub>7</sub> > S<sub>4</sub>**

The metal-ligand stability of bromo (Br) substituted Schiff base was found higher, while fluoro (F) substituted Schiff base lower {S<sub>6</sub> > S<sub>5</sub> > S<sub>7</sub> > S<sub>4</sub>} and the metal-ligand stability of nitro substituted Schiff base was found higher, while unsubstituted Schiff base lower. {S<sub>3</sub> > S<sub>2</sub> > S<sub>1</sub>}

The negative  $\Delta G$  values indicates that both dissociation of the ligand and the complexation process are spontaneous<sup>15</sup>. A decrease in metal-ligand stability constant logK with an increase in temperature and the negative values of enthalpy change  $\Delta H$  for the complexation suggests that all the complexation reactions are exothermic, favorable at lower temperature and the metal-ligand binding process is enthalpy driven<sup>11</sup> and metal-ligand bonds are fairly strong.

The positive entropy changes  $\Delta S$  accompanying a given reaction are due to the release of bound water molecules from the metal chelates. The positive value of  $\Delta S$  is considered to be the principal driving force for the formation of respective complex species. According to Martell -Calvin positive entropy effects was predicted towards an increase in the number of particles after the reaction and positive  $\Delta S$  is responsible to give more negative  $\Delta G$ . The positive values of  $\Delta S$  in some cases indicate that the entropy effect is predominant over enthalpy effect. The positive  $\Delta S$  values for metal complexes indicated that the formation of these complexes was entropy favored, while negative  $\Delta S$  values (**Table 3 - 5**) for metal complexes suggesting a highly solvated metal complexes<sup>15</sup>.

## CONCLUSION

Samarium metal ion forms 1:1 and 1:2 complexes with all Schiff Bases. The metal-ligand stability constant logK decreases with an increase in temperature. The negative values of change in enthalpy  $\Delta H$  for the complexation suggest that all the complexation reactions are exothermic, favourable at lower temperature. The negative change in free energy  $\Delta G$  values indicates that both dissociation of the ligand and the complexation process are spontaneous. The positive  $\Delta S$  values for some metal complexes indicated that the formation of these complexes was entropy favoured, while negative  $\Delta S$  values indicated a highly solvated metal complex.

**REFERENCES**

- [1] Hansaraj Joshi, RajpalJadhav, GopalDhond, Ramesh Ware, Shailendrasingh Thakur, "Complexation of Gadolinium with novel Schiff bases: Thermodynamic Study" *Int. J. Scientific Research in Chemistry*, 9(7), 70-75, (2024)
- [2] Hansaraj Joshi, RajpalJadhav, MazaharFarooqui, Shailendrasingh Thakur, "Thermodynamics study of formation of zinc complexes carrying novel Schiff bases in mixed solvent media." *J. Adv. Applied Sci,Tech.*,8(1), 91-96, (2022)
- [3] Jadhav R. L., Joshi H. U., Dr. S. B. Ubale, "Synthesis, characterization and biological activities of some novel Schiff bases derived from 3-acetyl-4-hydroxy-2H-chromen-2-one and 2-amino 5-(4-halosubstituted phynyl)-1-3-4-thiadiazole" *Int. J. Ana. Exp. Modal Analysis*, XIII(XI), 452-464, (2021)
- [4] Jadhav R. L., Joshi H. U., Ubale S. B., "Synthesis, characterization and biological activities of some novel Schiff bases derived from 3-acetyl-4-hydroxy-2H-chromen-2-one and 5-(4-substituted phenyl)-1,3,4-thiadiazol-2-amine," *J. Interdisc. Cycle Res.*, XIII(X), 414-424, (2021)
- [5] Hansaraj U. Joshi, Rajpal L. Jadhav, Mazahar N. Farooqui, Shailendrasingh V. Thakur, "Complexation of La(III) metal ion with novel schiff bases: Thermodynamic Study." *J. Advanced Scientific Research*,12(2), 133-136, (2021)
- [6] Hansaraj Joshi, RajpalJadhav, MazaharFarooqui, Shailendrasingh Thakur, "Thermodynamics of the formation of divalent Copper complexes carrying novel Schiff bases in mixed solvent media." *J. Interdisc. Cycle Res.*,13(04),53-61, (2021)
- [7] Hansaraj Joshi, RajpalJadhav, MazaharFarooqui, Shailendrasingh Thakur, "Studies of complexation of trivalentrare earth metal ion Cerium with novel Schiff bases: Thermodynamic Aspect." *Int. J. Ana. Exp. Modal Analysis*, 13(04),74-80, (2021)
- [8] Hansaraj Joshi, M.A. Sakhare, S.D.Naikwade and Shailendrasingh Thakur, "Study of complexation of divalent transition and trivalent Lanthanide metal ions with Schiff base 2-hydroxy-5-bromo acetophenone-n-(2-chloro-5-nitrophenyl) imine: Thermodynamic aspect." *J. Global Res*, 5(02), 87-89, (2019).
- [9] Shailendrasingh Thakur, SahebraoNaikwade, MazaharFarooqui "Thermodynamics of the formation trivalent Lanthanide complexes carrying Adenosine drug in mixed solvent media." *Int. J. Chem. Stud.*, 1(3), 88-92, (2013)
- [10] ShailendrasinghVirendrasingh Thakur, MazaharFarooqui, M.A. Sakhare, S.D. Naikwade, "Thermodynamic studies of Oxytetracycline with some transition and rare earth metal ions in mixed solvent media." *American Int. J. Res. Formal, Appl.& Nat. Sci.*, 3(1),123-127, (2013).
- [11] Shailendrasingh Thakur, MazaharFarooqui, SahebraoNaikwade "Thermodynamics of the complexation of ImipramineHydrochloride drug with Lanthanide." *Int. J. Emer. Tech. Comp. and Appl. Sci.*, 4(4), 342-346, (2013).
- [12] S. V.Thakur, MazaharFarooqui, S. D. Naikwade "Thermodynamic studies of rare earth metal complexes with Metformin Hydrochloride drug in mixed solvent system." *J. Adv. Sci. Res.*, 4(1):31-33, (2013).

- [13] Thangjam PD, Lonibala R. "Potentiometric Studies on the Complexation reactions of N-(2,2-[1- (3-Aminophenyl)ethylidene] hydrazine-2- oxoethyl)benzamide with Ni<sup>2+</sup>, Cu<sup>2+</sup> and Cd<sup>2+</sup> ions in aqueous dioxane and micellar media". J. Chem. Eng. Data, 55(3): 1166- 1172, (2010).
- [14] Sharmeli Y, Lonibala R. "Thermodynamics of the complexation of N-(Pyridin-2-ylmethylene) Isonicotinohydrazide with lighter lanthanides". J. Chem. Eng. Data, 54(1): 28-34, (2009).
- [15] El-Sherbiny MF. "Potentiometric and Thermodynamic Studies of 2-Thioxothiazolidi-4-one and its Metal Complexes". Chem Paper 59(5): 332-335, (2005).

# Graphene-TiO<sub>2</sub>-Polyaniline Nanocomposite: An Efficient and Sustainable Catalyst for Visible-Light-Driven Hydrogen Generation

Kalpana B. Gawande<sup>1</sup>, Vivek R. Mate<sup>2</sup>, Sanjay R. Thakare<sup>1</sup>, Sandeep B. Gawande<sup>1</sup>

<sup>1</sup>Department of Chemistry, Institute of Forensic Science, Civil Lines, Nagpur, 440001, Maharashtra, India

<sup>2</sup>Department of Chemistry, Yashwantrao Chavan Arts and Science College, Mangrulpir, Dist. Washim 444 403, Maharashtra, India

## ABSTRACT

This study investigates the photocatalytic hydrogen production capabilities of a graphene-TiO<sub>2</sub>-PANI (GP-TiO<sub>2</sub>-PANI) nanocomposite under visible light. The composite, with an optimal band gap of 3.05 eV, exhibited significant hydrogen generation when varying the ratios of GP, TiO<sub>2</sub>, and PANI. The composition of 0.2:1:0.2 achieved the highest hydrogen generation rate of 830  $\mu\text{mol h}^{-1}$ . The enhanced performance is attributed to graphene's superior electron mobility, preventing recombination, and PANI's role as a co-catalyst, improving charge separation. Stability tests confirmed that the catalyst maintained its activity over multiple cycles, indicating its potential for long-term use. Analytical techniques like XRD, FTIR, and UVDRS confirmed successful synthesis. The study highlights the critical importance of fine-tuning the GP-TiO<sub>2</sub>-PANI composition for maximizing hydrogen production efficiency, making it a promising candidate for sustainable hydrogen generation applications.

## INTRODUCTION

The need for sustainable and clean energy sources has accelerated research in hydrogen generation, particularly via photocatalytic water splitting using solar energy. Hydrogen, a clean fuel, is a crucial alternative to fossil fuels due to its high energy content and its role in reducing greenhouse gas emissions. Among various photocatalysts[1-5], titanium dioxide (TiO<sub>2</sub>) has been extensively studied due to its chemical stability, non-toxicity, and low cost. However, the primary challenge with TiO<sub>2</sub> is its wide bandgap ( $\sim 3.2$  eV), limiting its photocatalytic activity to the ultraviolet (UV) region, which accounts for only 5% of the solar spectrum[6-7]. To address this limitation, several modifications of TiO<sub>2</sub> have been explored,[8-15] aiming to extend its absorption into the visible light region, which constitutes a much larger portion of sunlight.

Graphene, with its high electrical conductivity, large surface area, and excellent electron mobility, has emerged as a powerful additive to improve the photocatalytic performance of TiO<sub>2</sub>. [1-7] By coupling TiO<sub>2</sub> with graphene, electron-hole recombination is significantly reduced, enhancing photocatalytic efficiency.

Moreover, the hybridization of TiO<sub>2</sub> with conductive polymers like polyaniline (PANI) further extends the light absorption capacity into the visible range, thereby improving hydrogen generation[6-7].

The incorporation of graphene into TiO<sub>2</sub> matrices enables effective charge separation due to graphene's ability to act as an electron acceptor and transporter.[2-6] Studies have shown that graphene-based TiO<sub>2</sub> composites exhibit enhanced photocatalytic properties, with increased photocurrent response and prolonged lifetime of photogenerated electrons. For instance, Kamat et al. (2010) demonstrated that the addition of graphene to TiO<sub>2</sub> significantly enhances the rate of photocatalytic hydrogen generation under visible light. Furthermore, Cao and Yu (2014) reported that the integration of PANI into TiO<sub>2</sub>-graphene composites improves visible light absorption and electron transport, resulting in higher hydrogen yields[3-6].

Despite these advancements, visible light-driven photocatalysts still face significant challenges. One major limitation is the insufficient absorption of visible light by most photocatalysts. Even with graphene and PANI modification, the efficiency of visible light photocatalysis remains lower than desired for commercial-scale hydrogen production. Additionally, the long-term stability of these photocatalysts, especially under real-world conditions, is another concern[1-14]. Over time, TiO<sub>2</sub>-based catalysts may suffer from deactivation due to surface poisoning or photocorrosion, which reduces their efficiency. Moreover, the scalability of synthesizing these composites at a low cost is yet another challenge[14-15].

Several reports have indicated varying levels of success in addressing these limitations. For example, Li et al. (2015) explored different heterostructures to improve charge transfer but observed issues related to long-term stability during photocatalysis[6]. Wang et al. (2018) reported that N-doped TiO<sub>2</sub> composites could enhance visible light absorption; however, the catalytic activity still declined after several cycles [16]. The Graphene-TiO<sub>2</sub>-PANI (GP-TiO<sub>2</sub>-PANI) composite offers a promising solution to these limitations by combining the strengths of all three components. Graphene acts as an efficient electron acceptor and transporter, preventing recombination of photogenerated electron-hole pairs, while PANI extends the light absorption into the visible spectrum. Additionally, the TiO<sub>2</sub> component serves as the primary photocatalyst, driving the water-splitting reaction under solar irradiation. Together, these components create a robust and efficient photocatalyst that enhances hydrogen generation under visible light, as reported by Cui et al. (2014),[5] where GP-TiO<sub>2</sub>-PANI composites demonstrated higher photocatalytic efficiency than TiO<sub>2</sub> alone.

This work aims to explore the photocatalytic performance of GP-TiO<sub>2</sub>-PANI under visible light irradiation, focusing on its hydrogen generation capacity. By addressing the limitations associated with visible light photocatalysis and exploring the structural, optical, and catalytic properties of this ternary composite, this study contributes to the development of more efficient and stable photocatalysts for sustainable hydrogen production.

## EXPERIMENTAL

Graphene oxide (GO) was prepared using the well-known Hummers method from graphite powder [19]. In our procedure, TiCl<sub>3</sub> (0.9 mol) and the synthesized GO were mixed in 60 mL of distilled water, and the solution was ultrasonicated for one hour. After ultrasonication, the solution was treated with the required



amount of HNO<sub>3</sub> and refluxed for one hour. Once cooled to room temperature, aniline (0.1 mol) was added with constant stirring, followed by the dropwise addition of ammonium persulfate (0.1 mol) solution. During the addition, the solution underwent a color change, ultimately resulting in a dark brown precipitate. The precipitate was collected by centrifugation at 2000 rpm, thoroughly washed with water, dried, and used for further reactions. Photocatalytic water splitting under visible light was carried out as per our previous work [8,16,19].

### Photocatalytic activity

In a typical photocatalytic experiment, 0.1 g of the GP-TiO<sub>2</sub>-PANI photocatalyst (S1 sample) was dispersed in 200 mL of deionized water. The reaction was conducted in a custom cylindrical quartz photochemical reactor. Before irradiation, the solution was thoroughly purged with argon (Delux, India) to eliminate all oxygen from the reactor headspace and the dissolved oxygen in the water. A 300 W Xe lamp (LOT ORIEL GRUPPE, EUROPA, LSH302) was used as the visible light source to irradiate the sample, with constant stirring. The amount of hydrogen gas produced was collected in a 500 mL graduated glass cylinder. All prepared samples were tested for catalytic activity under identical conditions. The evolved gas was analyzed using gas chromatography. The apparent quantum yield (AQE) was determined by measuring the light intensity with a Lux meter (Lutron LX-107HA), which was placed in front of the 300 W Xe light source to obtain the correct wavelength. The AQE was calculated using the following equation:

$$\text{AQE Number} = \frac{\text{Number of H}_2 \text{ and O}_2 \text{ molecules evolved} \times 2}{\text{Number of incident photon}} \times 100$$

## RESULTS AND DISCUSSION

### 3.1. Characterization

The XRD spectrum of the material, as shown in Figure 1, exhibits characteristic peaks at 2θ values of 25.1°, 37.6°, 48.1°, 53.5°, and 55.2°, corresponding to the (101), (004), (200), (105), and (211) crystal planes of anatase TiO<sub>2</sub>, as referenced by JCPDS No. 76-1940. This suggests that the sol-gel treatment of TiCl<sub>3</sub> in a solution containing Graphene (GP) and PANI successfully results in the formation of anatase TiO<sub>2</sub>. Notably, no distinct diffraction peaks corresponding to GP or PANI were detected in the binary or ternary samples. This absence could be due to the small quantities of GP and PANI present in the samples or the possibility that their peaks overlap with those of TiO<sub>2</sub>.

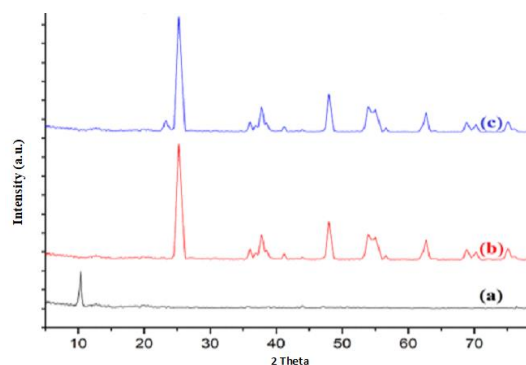


Figure 1. XRD patterns of (a) GO, (b) TiO<sub>2</sub>-PANI and (c) GP-TiO<sub>2</sub>-PANI composite.

The SEM images in Figure 2 depict the typical morphologies and microstructures of the GP-TiO<sub>2</sub>-PANI composite. The graphene sheets exhibit a wavy, thin-layered structure with wrinkled, abundant surface areas, indicating successful support of TiO<sub>2</sub> on reduced graphene. This structure provides ample surface area for the deposition of PANI. The SEM image of the GP-TiO<sub>2</sub>-PANI composite reveals corrugated and curly graphene nanosheets interconnected by PANI and coated with TiO<sub>2</sub> nanoparticles.

Figure 2 also displays the morphological TEM images of the samples. The TiO<sub>2</sub>-PANI hybrid shows a uniform distribution of spherical TiO<sub>2</sub> particles with sizes ranging from 50 to 70 nm (Figure 2A). After successful PANI coating on the TiO<sub>2</sub> surface, the binary TiO<sub>2</sub>-PANI hybrid exhibits a smoother surface morphology (Figure 2A), suggesting that the bare TiO<sub>2</sub> particles were fully enveloped by PANI nanosheets. This controlled the morphology and nucleation of TiO<sub>2</sub>-PANI, maintaining particle sizes between 50 and 70 nm (Figure 2A). As reported in previous studies [20-24], the optimal TiO<sub>2</sub> to PANI mass fraction (9:1) was used to fabricate the GP-TiO<sub>2</sub>-PANI ternary hybrid composite. Figures 2B and 2B1 illustrate that graphene sheets were clearly dispersed throughout the ternary GP-TiO<sub>2</sub>-PANI composite, with an overall composite size ranging from 110 to 130 nm.

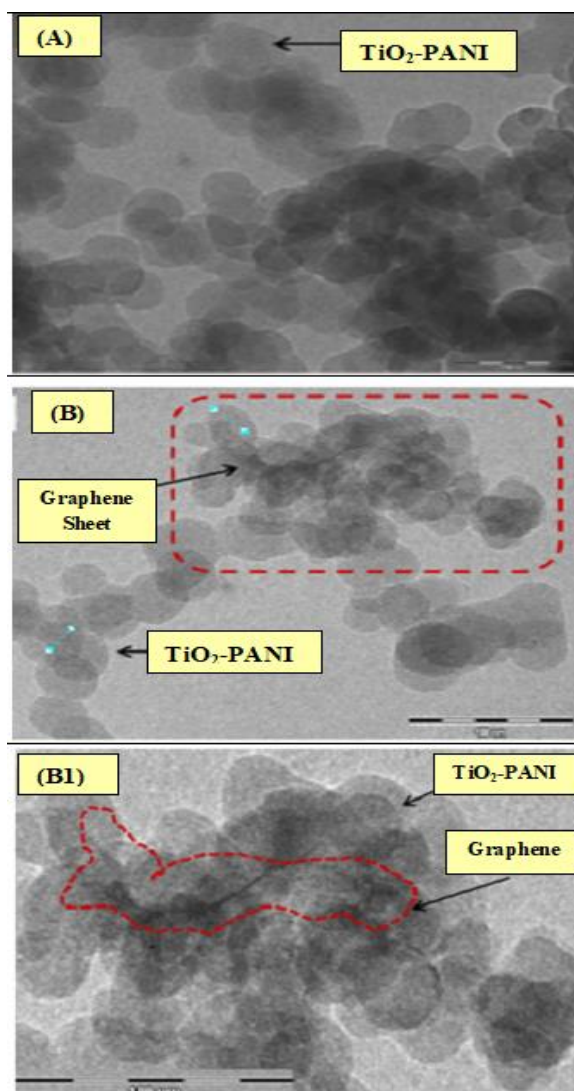
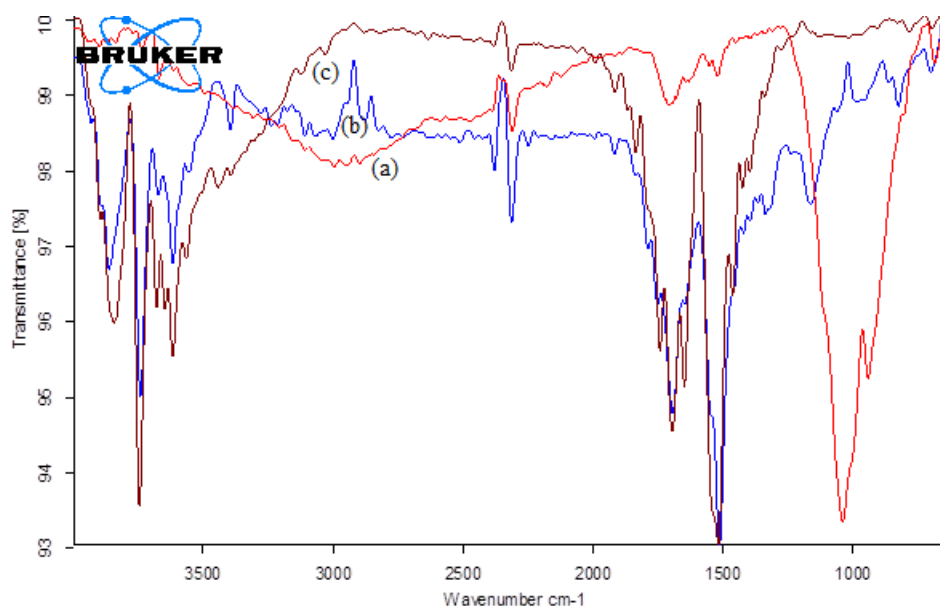


Figure 2. TEM images of (A) TiO<sub>2</sub>-PANI, (B) GP-TiO<sub>2</sub>-PANI composite.

The FTIR spectra of GO, TiO<sub>2</sub>-PANI, and the GP-TiO<sub>2</sub>-PANI composite are presented in Figure 3(a, b, and c). The characteristic absorption peak of GO around 1600 cm<sup>-1</sup> significantly decreases in intensity or even disappears after combining with TiO<sub>2</sub>-PANI. This suggests the reduction of GO to graphene during the initial stage of composite formation, which aligns with the XRD results. Additionally, the vibrational bands corresponding to PANI and TiO<sub>2</sub> are clearly observed and represented in Figure 3.



**Figure 3. Comparative studies of FTIR spectrum of (a) GO, (b) TiO<sub>2</sub>-PANI and (c) GP-TiO<sub>2</sub>-PANI composite.**

To investigate the interaction within the GP-TiO<sub>2</sub>-PANI composite, Raman analysis was conducted. The Raman spectrum, shown in Figure 4, spans the range of 100–5000 cm<sup>-1</sup>. The broad, low-intensity band at 217 cm<sup>-1</sup> corresponds to the symmetric bending mode of O–Ti–O. The bands at 532 and 537 cm<sup>-1</sup> are attributed to the bending modes of the TiO<sub>2</sub> component, while the broad bands at 1075 and 1125 cm<sup>-1</sup> are recognized as the  $\nu_1$  symmetric and  $\nu_3$  antisymmetric stretching modes of TiO<sub>2</sub>, respectively. Additionally, the D (1610 cm<sup>-1</sup>) and G (1340 cm<sup>-1</sup>) bands, characteristic of graphene, align closely with previously reported spectra of graphene [2, 23]. The slight red shift observed in the D band likely results from strong electrostatic interactions between the TiO<sub>2</sub>, PANI, and the ring current of graphene. Notably, no peaks corresponding to GO were observed in the Raman spectra, supporting the complete reduction of GO to graphene. These results confirm that graphene, PANI, and TiO<sub>2</sub> are strongly interacting, further validating the formation of the GP-TiO<sub>2</sub>-PANI composite.

40

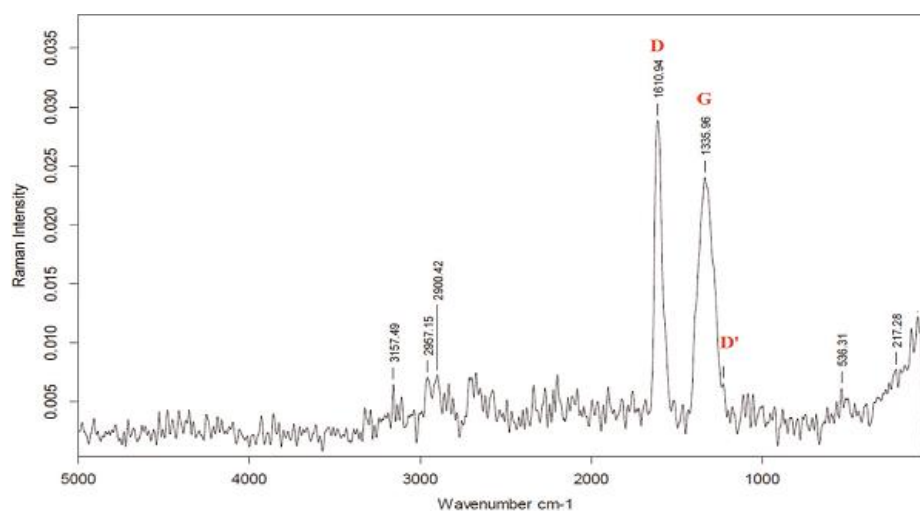


**Figure 4. Raman spectrum of GP-TiO<sub>2</sub>- PANI composite material, viewing both the D and G bands belongs to the graphene.**

The formation of the composite material was examined using UV-visible diffuse reflectance spectroscopy (DRS), a reliable method for analyzing optical behavior. The DRS spectra of GP, TiO<sub>2</sub>, and PANI composites are shown in Figure 4a. The absorption edges of GP, TiO<sub>2</sub>, and PANI appear at approximately 426, 452, and 478 nm, respectively [10, 24]. The corresponding band gaps were calculated to be 2.75 eV for GP, 2.95 eV for TiO<sub>2</sub>-PANI, and 3.05 eV for the GP-TiO<sub>2</sub>-PANI composite, with a slight red shift observed due to the incorporation of TiO<sub>2</sub> in GP. The energy band gap between these features suggests the formation of a mid-gap (deep-level acceptor) state.

The optical properties of the semiconductor nanocomposite materials were further investigated using photoluminescence (PL), a valuable technique that provides insights into surface oxygen defects and the separation and recombination of photo-induced charge carriers. The PL spectra of GP, TiO<sub>2</sub>-PANI, and GP-TiO<sub>2</sub>-PANI samples were obtained at ambient temperature with excitation wavelengths of 425, 480, and 450 nm, respectively, as shown in Figure 4b. A broad green emission band at 510 nm, attributed to oxygen defects, was observed in all samples [25-29]. This confirms the successful formation of the GP-TiO<sub>2</sub>-PANI composite.

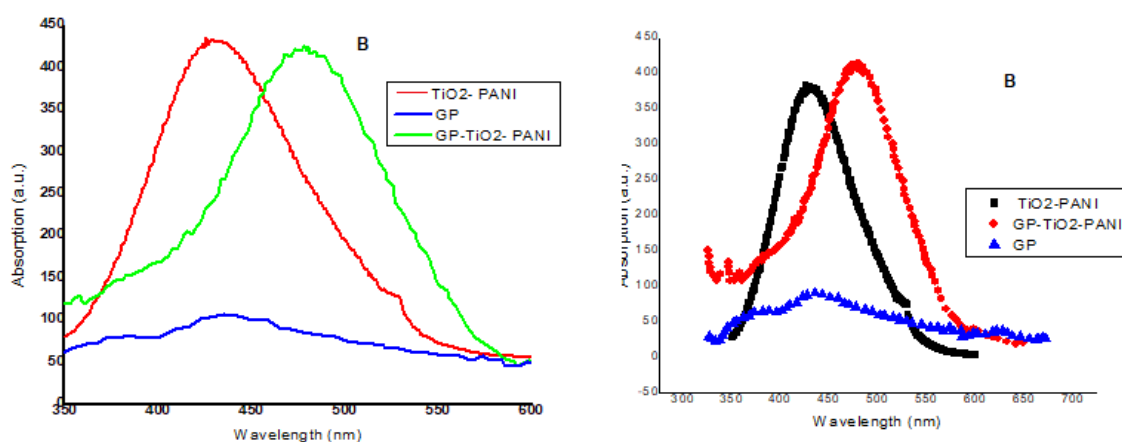


**Figure 6:- (a) UV-DRS spectra of GP, TiO<sub>2</sub>-PANI and GP-TiO<sub>2</sub>-PANI samples. (b) PL spectra of GP, TiO<sub>2</sub>-PANI and GP-TiO<sub>2</sub>-PANI samples.**

### Catalytic Activity

Considering the band gap of the graphene-TiO<sub>2</sub>-PANI (GP-TiO<sub>2</sub>-PANI) nanocomposite 3.05 eV, which falls in the visible light region, the photocatalytic hydrogen generation experiments were conducted under visible light. The photocatalytic performance of the prepared samples, with varying compositions of GP, TiO<sub>2</sub>, and PANI, is summarized in Table 1. The catalytic activity for hydrogen production over different compositions of GP-TiO<sub>2</sub>-PANI (Table 1) shows that the hydrogen generation increases with specific adjustments in the GP, TiO<sub>2</sub>, and PANI ratios. The sample with a composition of 1:1:1 (GP-TiO<sub>2</sub>-PANI) exhibited a hydrogen generation rate of 542  $\mu\text{mol h}^{-1}$  and an apparent quantum yield of 16.61%. This activity increment is attributed to the effective charge separation and better electron-hole generation in the visible light spectrum. As the composition shifted from 1:1:1 to 0.8:2:0.8, the hydrogen production increased to 578  $\mu\text{mol h}^{-1}$  with a corresponding quantum yield of 17.71%. This slight modification in the GP-TiO<sub>2</sub>-PANI ratio significantly enhances the photocatalytic performance. Further optimization led to a composition of 0.6:1:0.6, achieving a hydrogen generation of 614  $\mu\text{mol h}^{-1}$  with a quantum yield of 18.82%, indicating that a reduction in GP and PANI content still enhances electron-hole separation. This might be due to the presence of graphene facilitates superior electron mobility, preventing recombination and enhancing hydrogen generation[10]. PANI serves as a co-catalyst, contributing to enhanced charge separation and reducing electron-hole recombination[10]. The best performance was observed for the composition of 0.2:1:0.2, where the hydrogen generation reached 830  $\mu\text{mol h}^{-1}$ , and the apparent quantum yield increased to 25.44%. This substantial improvement in catalytic activity is likely due to the optimal electron transport properties of graphene, combined with the efficient charge carrier separation in the TiO<sub>2</sub>-PANI matrix. Thus, the result clearly shows that the modification of the GP-TiO<sub>2</sub>-PANI composition plays a critical role in enhancing photocatalytic efficiency. Increasing the amount of graphene beyond an optimal point leads to recombination of electron-hole pairs, reducing activity. Therefore, the 0.2:1:0.2 composition represents the optimal balance for maximizing hydrogen generation. Overall, the results indicate that the composite structure and composition play a crucial role in maximizing photocatalytic efficiency, leading to superior hydrogen production under visible light irradiation.

The repeatability of the hydrogen production using catalyst GP-TiO<sub>2</sub>-PANI (0.2:1:0.2) was observed with excellent accuracy (standard deviation 0.917 and 0.018 in the case of volume of hydrogen generated and quantum yield). The sample GP-TiO<sub>2</sub>-PANI (0.2:1:0.2) was established to keep hold of its activity after the third recycle, which proves the stability of the catalyst (Table 1, Entry 10). Auxiliary study with comprehensive investigations is in evolution. It is quite motivating and curious that sample GP-TiO<sub>2</sub>-PANI (0.2:1:0.2) confers hydrogen production.

**Table 1. Photocatalytic activity for water splitting using nano structured GP-TiO<sub>2</sub>-PANI visible photocatalysts <sup>a</sup>**

Sr. No	Catalysts	Composition	<sup>b</sup> Average H <sub>2</sub> generation ( $\mu\text{mol h}^{-1}$ )	<sup>b</sup> Apparent quantum yield
1	GP/TiO <sub>2</sub> /PANI	1:1:1	542	16.6
2	GP/TiO <sub>2</sub> /PANI	0.8:1:0.8	578	17.7
3	GP/TiO <sub>2</sub> /PANI	0.6:1:0.6	614	18.8

4	GP/TiO <sub>2</sub> /PANI	0.4:1:0.4	690	21.1
5	GP/TiO <sub>2</sub> /PANI	0.2:1:0.2	830	25.4
6	GP/TiO <sub>2</sub> /PANI	0.1:1:0.1	810	24.8
7	TiO <sub>2</sub>	-	210	6.4
8	<sup>c</sup> TiO <sub>2</sub> -PANI	1:0.2	263	8.0
9	<sup>d</sup> GP/TiO <sub>2</sub>	0.2:1	650	19.9
10	<sup>e</sup> GP/TiO <sub>2</sub> /PANI	0.2:1:0.2	801	24.5

<sup>a</sup> Reaction conditions: catalyst, 0.1 g; water, 250 ml; Xe lamp, 300 W (Oriel). <sup>b</sup> Standard deviation is 0.957 and 0.019, in the case of volume of hydrogen generated and apparent quantum yield, respectively. <sup>c</sup> Physical mixture of commercial graphene and TiO<sub>2</sub> catalysts. <sup>d</sup>Physically mixture TiO<sub>2</sub> and PANI. <sup>e</sup> Indicates the activity of catalyst after the third recycle.

## CONCLUSION:

In this study, the photocatalytic performance of the graphene-TiO<sub>2</sub>-PANI (GP-TiO<sub>2</sub>-PANI) nanocomposite was successfully optimized for hydrogen production under visible light irradiation. The photocatalyst GP-TiO<sub>2</sub>-PANI has been synthesized successfully confirms the incorporation of PANI, TiO<sub>2</sub> and graphene in a composite by various analytical tools namely XRD, FTIR, Raman spectroscopy, UVDRS and PL spectroscopy. The results demonstrate that the band gap of 3.05 eV for the GP-TiO<sub>2</sub>-PANI composite material, which allows absorption in the visible light region, contributes significantly to the photocatalytic hydrogen generation process. The optimal photocatalytic activity was achieved with a GP-TiO<sub>2</sub>-PANI composition ratio of 0.2:1:0.2, resulting in a hydrogen generation rate of 830  $\mu\text{mol h}^{-1}$  and an apparent quantum yield of 25.44%. This enhanced activity can be attributed to the superior electron mobility provided by graphene, which prevents recombination, as well as the role of PANI as a co-catalyst. PANI enhances charge separation, reduces electron-hole recombination, and promotes efficient charge transfer, ultimately improving the overall photocatalytic activity. Additionally, the reduced content of graphene and PANI still maintained high efficiency, suggesting that the precise composition balance plays a critical role in optimizing the photocatalyst's performance. The stability of the catalyst was confirmed through repeatability tests, showing negligible loss in activity after three cycles, with a standard deviation of 0.917 for the volume of hydrogen generated. This indicates that the GP-TiO<sub>2</sub>-PANI (0.2:1:0.2) nanocomposite is stable and efficient for repeated use in hydrogen generation. Overall, the study underscores the importance of tuning the composition of the GP-TiO<sub>2</sub>-PANI nanocomposite to enhance photocatalytic hydrogen production. Further investigations are ongoing to explore the full potential of this promising catalyst for water splitting and other applications.

## REFERENCES

- [1] Chen X. & Mao S. S. Chemical Reviews, 107(7), (2007) 2891-2959.
- [2] Geim A. K. & Novoselov K. S. Nature Materials, 6(3), (2007)183-191.

- [3] Kamat P. V. *Journal of Physical Chemistry Letters*, 1(2), (2010) 520-527.
- [4] Cao S. & Yu J. *Journal of Physical Chemistry Letters*, 5(12), (2014) 2101-2107.
- [5] Cui W., An W., Liu L., Liang Y., & Hu J. *Journal of Materials Chemistry A*, 2(13), (2014). 4302-4309.
- [6] Li X., Yu J., Low J., Fang Y., Xiao J., & Chen X. *Journal of Materials Chemistry A*, 3(6), (2015) 2485-2534.
- [7] Fujishima, K. Honda, *Nature* 238 (1972) 37.
- [8] S.B. Gawande, K.B. Gawande, S.R. Thakare, N.R. Manwar, V.R. Mate, *J. Phys. Chem. Solids* 85 (2015) 132.
- [9] A. Tayyebi, T. Soltani, B. Lee, M. Outokesh, *J. Alloys Compd.* 723 (2017) 1001.
- [10] Y. Chen, K. Katsumata, Y. Chiu, K. Okada, N. Matsushita, Y. Hsu, "*Applied Catal. A, Gen.* 490 (2015) 1.
- [11] T. Wang, C. Li, J. Ji, Y. Wei, P. Zhang, S. Wang, (2014) 1.
- [12] Y. Chen, X. Ma, D. Li, H. Wang, C. Huang, *RSC Adv.* 7 (2017) 4395.
- [13] Y.P. Zhang, J.J. Xu, Z.H. Sun, C.Z. Li, C.X. Pan, *Prog. Nat. Sci. Mater. Int.* 21 (2011) 467.
- [14] Zhang N., Zhang Y., & Xu Y. J. (2014). *Nanoscale*, 6(15), 8676-8684.
- [15] Wang Z., Luan D., Lou X. W., & Xi S. *Advanced Energy Materials*, 8(11), (2018) 1702880.
- [16] K. Urkude, Sanjay R. Thakare, S. Gawande, *J. Environ. Chem. Eng.* 2 (2014) 759-764.
- [17] Jai Prakash, *Photochem* 2022, 2(3), 651-671.
- [18] W.S. Hummers, R.E. Offeman, *J. Am. Chem. Soc.* 80 (1958) 1339-1339.
- [19] Kalpana B. Gawande, Sanjay R. Thakare, Vivek R. Mate and Sandeep B. Gawande, *Multilogic in Science Vol. 8*, (2018) ISSUE 27.
- [20] S. G. Kumar, K. S. R. K. Rao, *Catalysis Today*, 2016, 260, 134-142.
- [21] J. Zhang, Y. Peng, X. Jiang, *Journal of Physical Chemistry C*, 2017, 121(2), 1287-1297. .
- [22] Z. H. Ibupoto, K. Khun, *Materials Science in Semiconductor Processing*, 2018, 80, 80-88.
- [23] H. Yu, G. Zhao, *Journal of Applied Polymer Science*, 2019, 136(47), 48291.
- [24] N. Thanh Tung, M. Nguyen, *Applied Catalysis B: Environmental*, 2020, 266, 118642.
- [25] Li, G., & Zhang, D. (2013). Enhanced photocatalytic activity of graphene-TiO<sub>2</sub> hybrid material for hydrogen evolution by visible light. *Journal of Materials Science*, 48(11), 4207-4213.
- [26] Zhang, H., Chen, G., & Bahnemann, D. W. (2009). Photoelectrocatalytic materials for energy and environment. *ChemSusChem*, 2(1), 36-58.
- [27] Sun, Y., Wang, W., Zhang, L., & Zhang, W. (2011). Defect-related photoluminescence and photocatalytic properties of TiO<sub>2</sub> nanoparticles prepared by mechanochemical processing. *Journal of Applied Physics*, 109(8), 084303.
- [28] Yu, J. G., Zhou, M. H., & Cheng, B. (2006). Effects of hydrothermal temperature and time on the photocatalytic activity and microstructures of bimodal mesoporous titania. *Applied Catalysis B: Environmental*, 69(3-4), 171-180.
- [29] Cui, W., An, W., Liu, L., Liang, Y., & Hu, J. (2014). PANI/TiO<sub>2</sub>/graphene ternary nanocomposites with enhanced photocatalytic activity for the degradation of methylene blue under visible light irradiation. *Journal of Materials Chemistry A*, 2(13), 4302-4309.

# Study of Structural Characterization of $\text{CoMoO}_4$ /Activated Carbon for Supercapacitor Application

Dr. Digambar M. Sapkal

Department of Physics, S.I.C.E.S. Degree College of Arts, Science & Commerce, Ambarnath(W)- 421501,  
Maharashtra, India

Email: [dmsapkal@yahoo.co.in](mailto:dmsapkal@yahoo.co.in)

## ABSTRACT

Supercapacitors are among the most promising options for large-scale energy storage because of their high energy and power density, which find use in everything from everyday electronic gadgets to satellites. One important way to improve energy storage device performance is through the creation of hybrid materials. The synthesis techniques used to produce the hybrid material of activated carbon and  $\text{CoMoO}_4$ , a viable option for advanced supercapacitor applications. The synthesis techniques used to produce the hybrid material of activated carbon and  $\text{CoMoO}_4$ , a viable option for cutting-edge supercapacitor applications. The addition of activated carbon modifies the  $\text{CoMoO}_4$  crystal structure in the AC-CMO hybrid. Although  $\text{CoMoO}_4$  maintains its monoclinic structure, the addition of activated carbon creates a new amorphous component. Because of this dual phase structure, the well-ordered crystalline domains of  $\text{CoMoO}_4$  coexist with the porous, disordered structure of activated carbon, resulting in a heterogeneous material architecture.  $\text{CoMoO}_4$  (CMO) and activated carbon- $\text{CoMoO}_4$ (AC-CMO) were synthesized at room temperature using a simple co-precipitation method. This process produced monoclinic-phase cobalt molybdate, which was confirmed by extensive analysis using XRD and Raman investigations. Both the CMO and AC-CMO XRD spectra demonstrate the presence of polycrystalline cobalt molybdenum oxide with a monoclinic crystal structure.

**Keywords:** activated carbon,  $\text{CoMoO}_4$ , AC-CMO, hybrid material, monoclinic etc.

## INTRODUCTION

Since the late 19th century, energy demand from the world is increasing rapidly. Industrialization being one of the major factors behind this tremendous energy consumption. To withstand this tremendous demand for energy generation, it is important to have capable energy storage devices and infrastructure. Supercapacitors are one of the most promising candidates of large-scale energy storage and they provide high energy and power density with wide range use from satellites to daily life electronic devices. On the contrary, while single phase nanomaterials can be used for above mentioned applications, they often come with certain drawbacks. To address these limitations, scientists have turned to hybrid materials, which are composed of two or more nanoscale materials, such as combinations of metals with



semiconductors or organic with inorganic components. These hybrid materials have been employed for the same applications, not only overcoming the drawbacks of single nanomaterials but also significantly enhancing overall application efficiency. As a result, there is a significant focus on developing energy conversion and storage devices based on hybrid nanomaterials. We embarked on the synthesis of CoMoO<sub>4</sub>(CMO) and activated carbon-CoMoO<sub>4</sub>(AC-CMO) employing a straightforward co-precipitation technique at ambient temperature. This method led to the creation of monoclinic-phase Cobalt Molybdate, a fact ratified through thorough examination via XRD, Raman studies

## EXPERIMENTAL:

In the pursuit of tailored nanomaterials with advanced energy storage capabilities, our experimental journey commences with the co-precipitation method, a top-down approach renowned for its precision. Within this methodology, we craft two distinct nanomaterials, beginning with the creation of CoMoO<sub>4</sub> (CMO) as the foundation. Subsequently, we elevate this synthesis by infusing activated carbon, culminating in the birth of the activated carbon-CoMoO<sub>4</sub> hybrid (AC-CMO), a potent union poised to unlock new energy storage horizons. The co-precipitation method was judiciously chosen as our synthesis approach due to its exceptional versatility, allowing precise control over material composition and properties. Its capacity for homogeneous integration of activated carbon within the CoMoO<sub>4</sub> matrix ensures a harmonious synergy of components. Moreover, the method's scalability, practicality, and room temperature operation align seamlessly with our goal of crafting an efficient and feasible energy storage solution. This method stands as the ideal conduit to engineer the activated carbon-CoMoO<sub>4</sub> hybrid, empowering us to unlock its full potential for enhanced supercapacitor performance. Chemicals used for the synthesis of both CMO and AC-CMO are as follows Ammonium Molybdate (NH<sub>4</sub>)<sub>2</sub>MoO<sub>4</sub>, Cobalt Chloride CoCl<sub>2</sub>, Sodium Boro-hydrate NaBH<sub>4</sub>, NMP/ N-Methyl-2-Pyrrolidone (C<sub>5</sub>H<sub>9</sub>NO), PVDF/Polyvinylidene Fluoride (C<sub>2</sub>H<sub>2</sub>F<sub>2</sub>).

The synthesis of CoMoO<sub>4</sub>(CMO) and the activated carbon-CoMoO<sub>4</sub> hybrid (AC-CMO) was achieved through a facile co-precipitation method, meticulously executed to ensure the precise creation of these materials. Beginning with CMO, the synthesis involved a sequential process.

Initially, 1 mmol of ammonium molybdate (NH<sub>4</sub>)<sub>2</sub>MoO<sub>4</sub>, was introduced into 50 ml of distilled water, followed by continuous stirring at room temperature for 30 minutes using a magnetic stirrer. Subsequently, 1 mmol of Cobalt Chloride CoCl<sub>2</sub>, was introduced into the same solution, with consistent stirring maintained under identical conditions. Finally, the addition of 30 mmol of NaBH<sub>4</sub> into a 50 ml mixture of ammonium molybdate and cobalt chloride completed the chemical reaction. This resultant aqueous solution was further subjected to continuous stirring for an additional 30 minutes. The synthesis process for AC-CMO mirrored that of CMO, with the inclusion of 200 mg of activated carbon into 50 ml of distilled water as the initial step.

After each variant's three-step synthesis process, the reaction solutions were left undisturbed for 12 hours, facilitating the formation of precipitates. Following this, the separation of supernatant and precipitate was

achieved through a decanting process, meticulously repeated six times for both material variants. Material Characterization Techniques

### X-RAY DIFFRACTION (XRD) :

XRD is a widely used and most famous technique to obtain information about the crystal structure of solid materials, such as the lattice parameter, orientation of single crystals, phase, and composition [ 7]. The XRD pattern of a material is like its fingerprint which can identify the material under observation. The XRD pattern from a material can be used for determining lattice stress, strain and structural and phase confirmation [8, 9]. It is also important to note that this technique more useful for crystalline solid phase materials.

The XRD technique is based on scattering of monochromatic X-ray reflection from the crystallographic phase of lattice [10]. The interplanar distance (d) can be determined using the Bragg's diffraction equation [11].

$$2d\sin\theta = n\lambda$$

Where,  $\lambda$  = wavelength of monochromatic x-rays,  $n$  = order of diffraction and  $\theta$  = diffraction angle Using this relation, the 'd' values are computed for known values of  $\lambda$ ,  $\theta$  and  $n$ . This data is then compared with a standard data set either from Joint Committee Powder Diffraction Standards (JCPDS). The crystallite size for the sample can also be calculated using the XRD data and using Scherrer formula [12]. By determining the full width at half maxima (FWHM) of the most intense peak from the data, we can employ it in the following formula and obtain the crystallite size.

$$k\lambda$$

$$D = \frac{k\lambda}{\beta \cos\theta}$$

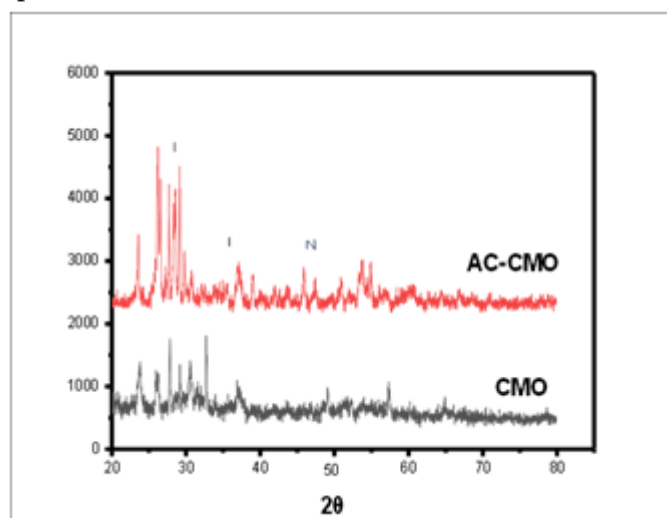
Where,  $D$  = crystallite size,  $\beta$  = FWHM in radians and  $k$  = constant (0.89-1.39, mostly 1)

### X-RAY DIFFRACTION (XRD) PATTERN :

XRD unveils the concealed structural nuances of four synthesized materials, providing insights into their crystalline arrangements at the atomic scale. Through XRD, we decode distinctive fingerprint patterns that shed light on the crystallographic essence and phase composition, enriching our understanding and seamlessly aligning with our comprehensive analysis [13]. Fig. .2 depicts the XRD patterns of CMO and AC-CMO. It is clear from the XRD pattern that both materials contain polycrystalline cobalt molybdenum oxide with monoclinic crystal structure. The sharp diffraction peak at  $26.58^\circ$  corresponds to the reflection of (012) plane. The other diffraction peak at  $23.45^\circ, 28.58^\circ, 36.49^\circ, 38.58^\circ, 45.04^\circ, 47.04^\circ, 53.8^\circ$  can be assigned to (0 2 1), (0 1 2), ( $\bar{2}$  2 0), ( $\bar{1}$  1 3), (2 0 2), (1 4 1), ( $\bar{1}$  4 2), (1 1 3) planes respectively

The diffraction peaks of the samples can be ascribed to cobalt molybdate and are well matched in concordance with the standard JCPDS (card no. 26-0477). No peaks due to impurities or other residuals was observed for CMO, indicating high purity of synthesized nanostructure. Further, the crystallinity of the hybrid material (AC-CMO) was comparatively higher than the CMO. The broad

and weak diffraction peaks pattern evidenced small crystallite size and poor crystallization nature of the samples. In present work, the crystal structures of thin films were analyzed by using X-ray diffraction (XRD) patterns recorded with the Bruker D8 X-ray diffractometer in the  $2\theta = 20^\circ - 80^\circ$  range. X-ray tube with Cu anode ( $\lambda = 1.5406 \text{ \AA}$ ) was operated at 30 kV and 20 mA.



## CONCLUSION:

Material characterization techniques such as XRD, Raman spectroscopy have provided invaluable insights into the structural nuances of the synthesized materials, XRD reveals the crystalline structure of both materials, confirming their composition. The broad and weak diffraction peaks pattern evidenced small crystallite size and poor crystallization nature of the samples. Raman Spectroscopy identifies vibrational modes, CMO exhibits a uniform and well-defined nanostructure with an average particle size of around 20 nanometers.

## REFERENCES

- [1] Monshi, A., et al., Modified Scherrer equation to estimate more accurately nano-crystallite size using XRD. 2012. 2(3): p. 154-160.
- [2] Lyon, L.A., et al., Raman spectroscopy. 1998. 70(12): p. 341-362.
- [3] Villa, P., et al., Study of the interaction between  $\text{CoMoO}_4$  and  $\text{Al}_2\text{O}_3$  by Raman spectroscopy. 1974. 1(3): p. 341-344.
- [4] Pawley, J.J.S.-N.Y. and B.B.T. MAHWAH-, The development of field-emissions scanning electron microscopy for imaging biological surfaces. 1997. 19: p. 324-336.
- [5] Veerasubramani, G.K., et al., Synthesis, characterization, and electrochemical properties of  $\text{CoMoO}_4$  nanostructures. 2014. 39(10): p. 5186-5193.
- [6] Kissinger, P.T. and W.R.J.J.o.c.e. Heineman, Cyclic voltammetry. 1983. 60(9): p. 702.
- [7] Cullity, B.D., Elements of X-ray Diffraction. 1956: Addison-Wesley Publishing.
- [8] Zak, A.K., et al., X-ray analysis of ZnO nanoparticles by Williamson-Hall and size-strain plot methods. 2011. 13(1): p. 251-256.

- [9] Mote, V., et al., Williamson-Hall analysis in estimation of lattice strain in nanometer-sized ZnO particles. 2012. 6: p. 1-8.
- [10] Li, J. and J. A. o. c. r. Sun, Application of X-ray diffraction and electron crystallography for solving complex structure problems. 2017. 50(11): p. 2737-2745.
- [11] Nath, D., et al., X-ray diffraction analysis by Williamson-Hall, Halder-Wagner and size-strain plot methods of CdSe nanoparticles - a comparative study. 2020. 239: p. 122021.
- [12] Vorokh, A. S. J. H. ф., химия, математика, Scherrer formula: estimation of error in determining small nanoparticle size. 2018. 9(3): p. 364-369.
- [13] Monshi, A., et al., Modified Scherrer equation to estimate more accurately nano-crystallite size using XRD. 2012. 2(3): p. 154-160.
- [14] Lyon, L. A., et al., Raman spectroscopy. 1998. 70(12): p. 341-362.
- [15] Villa, P., et al., Study of the interaction between  $\text{CoMoO}_4$  and  $341-1341-1-\text{Al}_2\text{O}_3$  by Raman spectroscopy. 1974. 1(3): p. 341-344.

# Novel Co(II), Ni(II) Schiff Base Metal Complexes Derived From 1-Hydroxy-2-acetonaphthone And Phenylethyl Amine: Synthesis, Spectral Characterization And Antimicrobial Evaluation

Dr. Dhananjay V. Bondar

Department of Chemistry, Shri Chhatrapati Shivaji College, Omerga, Dist. Dharashiv-413606, Maharashtra, India

E-mail- [dvbondar21@gmail.com](mailto:dvbondar21@gmail.com)

## ABSTRACT

Herein, two novel Co(II) and Ni(II) Schiff base metal complexes have been synthesized, characterized and their antimicrobial activity reported. The metal complexes have been investigated using UV-Vis., FT-IR, NMR, LCMS and powder X-ray diffraction. UV-Vis. spectra revealed a more than 400 nm transition peak, confirming the occurrence of metal-ligand charge transfer. FT-IR reveals the production of an unsymmetrical Schiff base ligand and its complex including naphthol -OH and azomethine -C=N- groups. <sup>1</sup>H-NMR spectra confirm the production of the Schiff base ligand and its complexes. The XRD results confirm that the produced Co(II) and Ni(II) complexes have an Orthorombic crystal structure. The antimicrobial activity of Schiff bases and their metal complexes were detected against two gram-negative bacterial strains, *E. coli* and *P. aeruginosa*, as well as two gram-positive strains, *S. aureus* and *B. subtilis*. Schiff bases and metal complexes provide antifungal action against two fungus, *C. albicans* and *A. niger*. It was found that the generated complexes are more active than the comparable Schiff base.

**Keywords:** Schiff base, 1-Hydroxy-2-acetonaphthone, phenylethyl amine, antimicrobial.

## INTRODUCTION

Nowadays, Schiff bases and subsequent metal ion complexes are currently gaining popularity due to their numerous advantages. The introduction of Schiff bases has considerably aided the progress of coordination chemistry, as they provide a diversity of effects and steric interactions with various geometries.<sup>[1]</sup> They are recognized as a valuable class of extensively investigated compounds due to their various catalytic, chemical, biological, and electrochemical properties.<sup>[2,3]</sup> Schiff bases can coordinate numerous transition metal ions by interacting with some or all of the donor atoms in the chemical structure. They were monodentate, bidentate, or polydentate systems with several donor sites.<sup>[4,5]</sup> Because of their popularity, transition metal complexes containing Schiff base ligands have begun to dominate modern research.

The usage of naphthalene scaffold pharmaceuticals benefits a wide range of pathophysiological illnesses, including antibacterial, antidepressant, anti-inflammatory, anticancer, and antiviral conditions.<sup>16</sup> Additionally, Naphthalene ring-based Schiff base compounds shown anti-COVID activity.<sup>[7]</sup> The

naphthalene moiety performs a wide range of biological roles depending on its structural modifications.<sup>[8]</sup> The literature describes Schiff base metal complexes containing 1-hydroxy-2-acetonaphthone (HAN). HAN Schiff base molecules had a major role in the development of food products.<sup>[9]</sup> The HAN has focused significantly more on activities linked to catalysis,<sup>[10]</sup> dyes and pigments,<sup>[11]</sup> antimicrobial,<sup>[12]</sup> antiviral,<sup>[13]</sup> anti-HIV,<sup>[14]</sup> antioxidant,<sup>[15]</sup> anticancer,<sup>[16]</sup> and anti-inflammatory.<sup>[17]</sup>

Nickel's redox activity contributes significantly to catalytic reactions, particularly alkynes effectively hydrosilylation.<sup>[18]</sup> Schiff base complexes with Ni(II) metals have also been shown to have catalytic activity.<sup>[19]</sup> As a result, to our knowledge, there is no literature describing the use of these Schiff base compounds as primary precursors to ensure complexation with Co(II) and Ni(II) metals.

We present the synthesis and characterisation of Schiff base generated from HAN and phenylethyl amine (PEA) and its transition metal complexes Co(II) and Ni(II). The reported Schiff base and its metal complexes of Co(II) and Ni(II) were lighted utilizing spectroscopic techniques such as UV-Vis, FT-IR, <sup>1</sup>H-NMR, LCMS, Powder XRD studies. Biological evaluation of Schiff base and its metal complexes of Co(II), Ni(II) were taken as an antibacterial activity against *E. coli*, *P. aeruginosa*, and *S. aureus*, *B. subtilis* microorganisms, and antifungal activity against *C. albicans* and *A. niger* fungus. and has reached alarming levels in terms of its negative effects on living things.<sup>[5]</sup> The higher concentration of heavy metals causes adverse changes in color, test, odor of water and it also stains clothes and utensils. The Overload of heavy metals may cause severe health problems such as liver cancer, diabetes, cirrhosis of liver, disease related to heart and central nervous systems, infertility, etc.<sup>[10]</sup>

## MATERIAL AND METHODS

### 2.1. Materials

Sigma Aldrich provided all analytical reagent grade chemicals, including 1-hydroxy-2-acetonaphthone, phenylethyl amine, Co(II)(OAc)<sub>2</sub>·4H<sub>2</sub>O, and Ni(II)(OAc)<sub>2</sub>·4H<sub>2</sub>O. We acquired HPLC grade methanol, 100% ethanol, and other solvents from local sources and did not purify them. Thin layer chromatography (TLC) was utilized in laboratories to determine the purity of items. TLC was performed on 0.25-mm E Merck gel plates (60F-254), and the spots were detected using iodine vapours. Melting points were measured using the Kofler bench, a computerized equipment. The elements analysis was performed using a Perkin-Elmer 240 elemental analysers. A Shimadzu UV-1800 series spectrophotometer with a 340 nm light source was used to record UV-visible spectra in methanol at 200-600 nm wavelengths. FT-IR spectroscopy was used to examine the functional groups present in compounds. FT-IR spectra were taken with a KBr disc on a Bruker Alpha II analyzer in the infrared spectrum between 650 and 4000 cm<sup>-1</sup>. <sup>1</sup>H-NMR spectral data were collected using a Bruker AVANCE NEO 400 MHz spectrometer and CDCl<sub>3</sub> solvent with tetramethyl silane (TMS) as an internal reference standard. LCMS mass spectra of synthesized compounds were obtained using a single quadrupole Agilent 1290 G7104A, model LCMSD G6125B MSD with a scan range of 100 m/z to 1400 m/z. The Powder XRD of ligand and metal complexes was recorded using a Desktop X-ray Diffractometer MiniFlex II with a range of 10 - 80o target Cu and a wavelength of 1.540598 Å.

### 2.2 Antibacterial activity

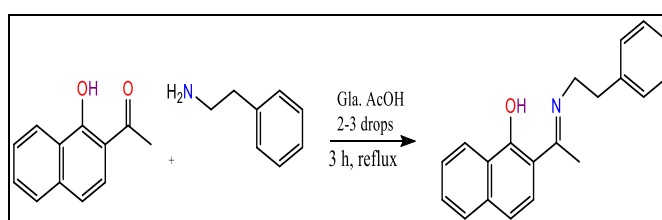
The Zone Inhibition Method was utilized to determine antibacterial activity. Bacteria such as gram-negative *Escherichia coli*, *Pseudomonas aeruginosa* and gram-positive *Staphylococcus aureus*, as well as *Bacillus subtilis* were used to assess the antibacterial capabilities of the newly synthesized compounds. The Mueller Hinton Agar (MHA) plates were spread and inoculated with 100  $\mu$ l of log cultures of each bacterium (adjusted to 0.5 McFarland Unit), followed by a disc containing 10  $\mu$ l of varied concentrations (0 to 1000 mg/ml). As a vehicle control, one disk in each plate was loaded with DMSO solvent alone, and Ciprofloxacin (2 mg/ml, 20  $\mu$ g) was utilized as the positive control. The clear zones surrounding the disc were measured and recorded after the test organism plates had been incubated at 37°C for 24 hours.

### 2.3 Antifungal activity

The Zone Inhibition Method was performed to assess the antifungal activity. The newly synthesized Schiff base and its metal complexes molecules were tested for antifungal activities against the fungus *Candida albicans* and *Aspergillus niger*. The Zone Inhibition Method was performed to assess the antifungal activity. 100  $\mu$ l of log cultures from each fungus strain were inoculated into Mueller Hinton Agar (MHA) and Potato Dextrose Agar (PDA) plates. The disk contains 10  $\mu$ l of *C. albicans* and *A. niger* at varying concentrations (0 to 1000 g/ml, adjusted to 0.5 McFarland Unit). As the vehicle control, each plate included a single disc loaded with DMSO solvent. The *C. albicans* plates were incubated for 24 hours at 37°C, whereas the *A. Niger* plates were treated for 24 to 74 hours at 32°C. We measured and documented the size of the disc in the clear zone.

### 2.4 Synthesis of Schiff base ligand (HL)

According to the modified classical procedure given in the literature, the Schiff base was produced by dissolving HAN (0.186 g, 1 mmol) in absolute ethanol (10 ml) and adding 2-3 drops of glacial acetic acid. To this heated solution, an ethanolic solution of PEA (0.120 g, 1 mmol) was added dropwise while swirling constantly. The yellow reaction mixture was refluxed for approximately 3 hours and the progress of the reaction was monitored by TLC. To achieve the optimum results, the reaction solution was left at room temperature overnight. Yellow fine needle-shaped crystals (HL) were filtered and recrystallised using absolute ethanol.



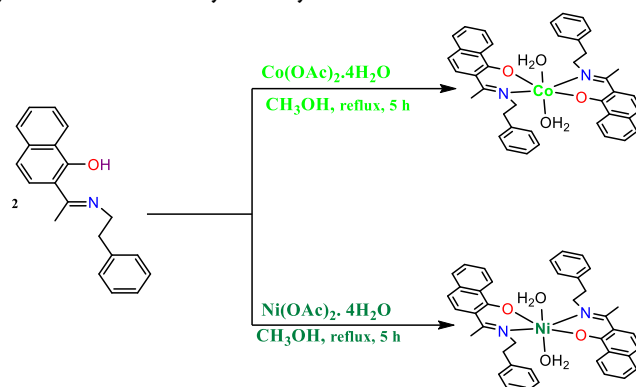
**Scheme 1** Synthesis of Schiff base ligand (HL)

### 2-(1-(phenethylimino)ethyl)naphthalen-1-ol (HL)

Molecular formula: [C<sub>20</sub>H<sub>19</sub>NO], Molecular weight: 289.38, Yield: 271.46 mg (87%), Colour: Yellow, m. p. 122-124 °C. Elemental Analysis: C, 83.01; H, 6.62; N, 4.84; O, 5.53 FT-IR (KBr, cm<sup>-1</sup>): 3424.01( $\nu$  -OH), 1703.14 ( $\nu$  -C=N), 1591.53- 1452.91 ( $\nu$  -C=C-), 1271.38 ( $\nu$  -C-O), 1022.21( $\nu$  C-N-C). <sup>1</sup>H NMR (400 CDCl<sub>3</sub>),  $\delta$  (ppm): 2.255 (s, -CH<sub>3</sub>, 3H), 3.107 (t, -CH<sub>2</sub>-, 2H), 3.820 (t, N-CH<sub>2</sub>, 2H), 6.774- 8.539 (m, Ar-H, 11H), 16.414 (s, Ar-OH, 1H). ESIMS(m/z): 290.2

### 2.5 Synthesis of metal complexes [M(L)<sub>2</sub>]

According to the published literature, a generic technique for synthesizing Co(II) and Ni(II) complexes was discovered. Metal salts (1 mmol, 0.249 g for Co(II)(OAc)<sub>2</sub>·4H<sub>2</sub>O and 0.248 g for Ni(II)(OAc)<sub>2</sub>·4H<sub>2</sub>O) were dissolved in methanol and added to a Schiff base (HL) hot methanolic solution. The colour of the solution instantly changed, indicating ligand metal complexation. The reaction mixture was then refluxed for 5 hours, after which the solution was cooled to room temperature. The resulting solid was filtered and thoroughly cleaned with dry diethyl ether and a small amount of methanol.



**Scheme 2** Synthesized Metal complexes M(L)<sub>2</sub>

#### Co<sup>II</sup>(L)<sub>2</sub> complex [Co(L)<sub>2</sub>(H<sub>2</sub>O)<sub>2</sub>]

Molecular formula: C<sub>40</sub>H<sub>40</sub>CoN<sub>2</sub>O<sub>4</sub>, Molecular weight: 671.70, Yield: 562 mg (67%), Colour: Brown, m. p. 274- 276°C. Elemental Analysis: C, 71.53; H, 6.00; Co, 8.77; N, 4.17; O, 9.53

FT-IR (KBr, cm<sup>-1</sup>): 1616.92 (ν C=N), 1577.72- 1452.02 (ν C=C), 1250.38 (ν C-O), 1024.19 (ν C-N-C). <sup>1</sup>H NMR (400, CDCl<sub>3</sub>), δ (ppm): 2.709 (s, -CH<sub>3</sub>, 3H), 3.499 (t, -CH<sub>2</sub>, 2H), 3.527 (t, N-CH<sub>2</sub>, 2H), 7.260- 8.475 (m, Ar-H, 11H). *ESIMS* (m/z): 671.23 (100.0%).

#### Ni<sup>II</sup>(L)<sub>2</sub> complex [Ni(L)<sub>2</sub>(H<sub>2</sub>O)<sub>2</sub>]

Molecular formula: C<sub>40</sub>H<sub>40</sub>N<sub>2</sub>NiO<sub>4</sub>, Molecular weight: 671.46, Yield: 593 mg (71%), Colour: Olive, m. p. 300<°C. Elemental Analysis: C, 71.55; H, 6.00; N, 4.17; Ni, 8.74; O, 9.53

FT-IR (KBr, cm<sup>-1</sup>): 1591.50 (ν C=N), 1526.55- 1452.88 (ν C=C), 1270.98 (ν C-O), 1022.10 (ν C-N-C). <sup>1</sup>H NMR (400, CDCl<sub>3</sub>), δ (ppm): 2.288 (s, -CH<sub>3</sub>, 3H), 3.106 (t, -CH<sub>2</sub>, 2H), 3.827 (t, N-CH<sub>2</sub>, 2H), 6.786- 8.536 (m, Ar-H, 11H). *ESIMS* (m/z): 670.23 (100.0%).

Sr.no.	Compound	Colour	Yield %	m.pt.(°C)	Elemental Analysis found (Cal.) %				
					C	H	N	O	M
1	HL, C <sub>20</sub> H <sub>19</sub> NO	Yellow	87	122-124	83.01 (82.97)	6.62 (6.59)	4.84 (4.81)	5.53 (5.49)	-
2	Fe(L) <sub>2</sub> ·(H <sub>2</sub> O) <sub>2</sub>	Brown	65	251- 253	71.86 (71.81)	6.03 (5.97)	4.19 (4.13)	9.57 (9.49)	8.35 (8.27)
3	Mn(L) <sub>2</sub> ·(H <sub>2</sub> O) <sub>2</sub>	Olive	59	176- 178	71.95 (71.92)	6.04 (5.97)	4.20 (4.17)	9.58 (9.51)	8.23 (8.19)

**Table 1** Analytical and physical data of ligand and its metal complexes

## RESULTS AND DISCUSSION



The synthesized Schiff base and metal complexes have a range of colors and are stable at room temperature in both air and moisture. They dissolve in chloroform, dichloromethane, dimethyl sulfoxide, dimethylformamide, tetrahydrofuran, ethyl acetate, and acetone, but are insoluble in petroleum ether and n-hexane. UV-Vis, FT-IR,  $^1\text{H}$  NMR, Powder XRD and LCMS proved their structural integrity.

### 3.1 UV-Vis. Analysis

The UV-Visible absorption spectra of the Schiff base ligand (HL) and its metal complexes were obtained in a methanol solvent. The Schiff base contains five main peaks, which are located at 225.50, 271.50, 322.50, and 409.00 nm. The bands are caused by an aromatic ligand ring change occurring between 225 and 300 nm. The bands between 300 and 350 nm were caused by the ligand chromophore ( $-\text{C}=\text{N}-$ )  $\pi \rightarrow \pi^*$  transition. The Schiff base compound's  $n \rightarrow \pi^*$  transition of non-bonding electrons caused the expanded wavelength bands to approach 400 nm.<sup>[20]</sup> Also, in the Co(II) and Ni(II) metal complexes, wavelengths greater than 400 nm were observed, pushing the electronic absorption band due to metal ligand charge transfer (MLCT) transitions.

### 3.2 FT-IR analysis

Using FT-IR analysis of the newly synthesized Schiff base and its complexes (Figures 1, 2), we can determine how the coordination between the metal ion and ligand was achieved. The ligand has a distinct band with a strong core at  $3424.01\text{ cm}^{-1}$ , showing the existence of a phenolic (Ph-OH) group with substantial intramolecular hydrogen bonding. Schiff base ligand imine peak ( $-\text{C}=\text{N}-$ ) was observed at  $1703.14\text{ cm}^{-1}$ . Aromatic ( $-\text{C}=\text{C}-$ ) peaks ranged from  $1591.53$  to  $1452.91\text{ cm}^{-1}$ , while aromatic (Ar-H) peaks were minor in intensity and spanned  $3029.89$  to  $2866.55\text{ cm}^{-1}$ . When compared to metal complexes, the broad peak Phenolic -OH disappeared, indicating deprotonation of the ligand's phenolic -OH group. When the imine ( $-\text{C}=\text{N}-$ ) group bonds with metal ions, it shifts to a lower frequency at  $1616.92\text{ cm}^{-1}$  for Co(II) and  $1591.50\text{ cm}^{-1}$  for Ni(II) metal complexes,<sup>[21]</sup> respectively.

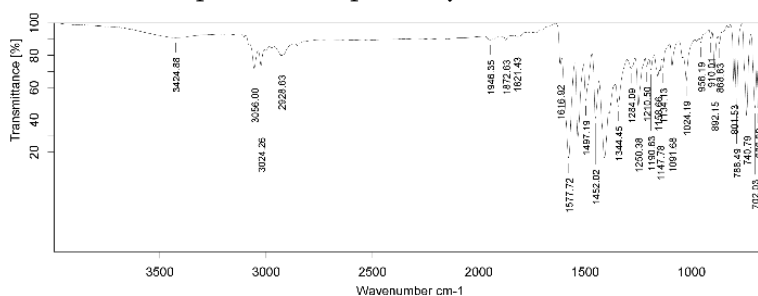


Figure1. IR spectra of  $[\text{Co}(\text{L})_2(\text{H}_2\text{O})_2]$  complex

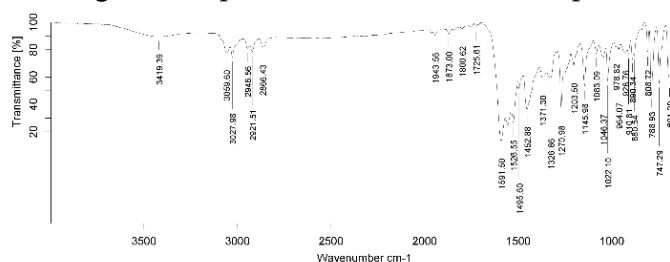


Figure2. IR spectra of  $[\text{Ni}(\text{L})_2(\text{H}_2\text{O})_2]$  complex

Table 2 FT-IR spectral data of Schiff base and its complexes

Compound	$\nu(-OH)$	$\nu(H_2O)$	$\nu(C=C-H)$	$\nu(C=N-)$	$\nu(C-O)$	$\nu(C-N-C)$
HL	3424.01	-	3059.89	1591.53	1271.38	1022.21
Co(L) <sub>2</sub> (H <sub>2</sub> O) <sub>2</sub>	-	3424.88	3056.00	1616.92	1250.38	1024.19
Ni(L) <sub>2</sub> (H <sub>2</sub> O) <sub>2</sub>	-	3419.39	3059.60	1591.50	1270.98	1022.10

### 3.3 <sup>1</sup>H NMR analysis

In the <sup>1</sup>H NMR spectra of the ligand HL (Figure 3), the proton of phenolic -OH was detected as a singlet at 16.414 ppm. Aromatic proton signals resonate in the 6.786-8.536 ppm range for Schiff base ligands and metal complexes. Two triplet signals of the ethylene chain =N-CH<sub>2</sub>-CH<sub>2</sub>-Ar were observed in the ligand at 3.827 and 3.106 ppm, respectively, while these triplet signals were detected downfield in the metal chelates. The peak at 2.288 was created by the ligand's methyl protons with the formula -N=C-CH<sub>3</sub>, and it was barely influenced by metal chelates.<sup>[22]</sup> In contrast to the <sup>1</sup>H NMR spectra of the ligand and its metal complexes, the protons signals have been moved to the downfield, indicating that the metal ion has complexed with the ligand.

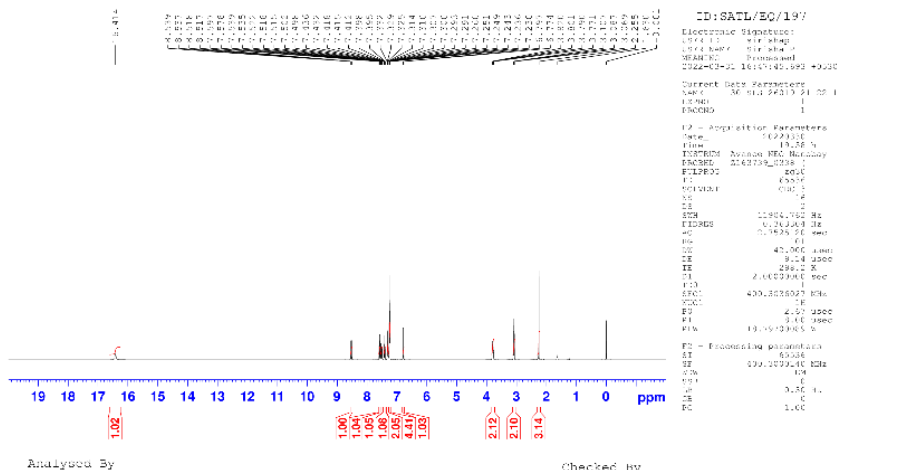


Figure3. <sup>1</sup>H NMR spectra of Schiff base ligand (HL)

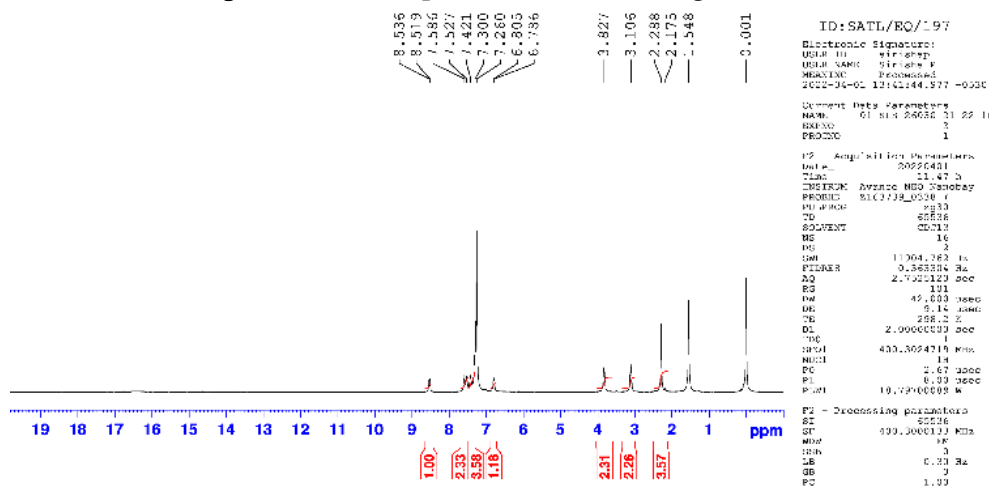


Figure4. <sup>1</sup>H NMR spectra of [Ni(L)<sub>2</sub>(H<sub>2</sub>O)<sub>2</sub>] complex

### 3.4 LCMS

The ESI-MS analysis confirmed the molecular weights of the Schiff base ligand and associated metal complexes, as illustrated in Figures 5, 6. The Schiff base ligand HL exhibited a molecular ion peak at  $m/z$  290.2, which corresponds to its molecular weight. A similar molecular ion peak was detected in related metal complexes, confirming the ligand-metal ion interaction and fragmentation when mass spectra were taken. Metal complexes  $[\text{Co}(\text{L})_2(\text{H}_2\text{O})_2]$  and  $[\text{Ni}(\text{L})_2(\text{H}_2\text{O})_2]$  were associated with molecular ion peaks at  $m/z$  671.23 and 670.23, respectively.

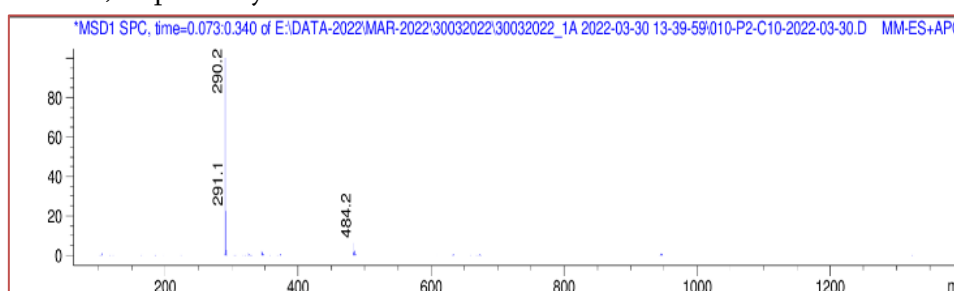


Figure 5. Mass spectra Schiff base ligand (HL)

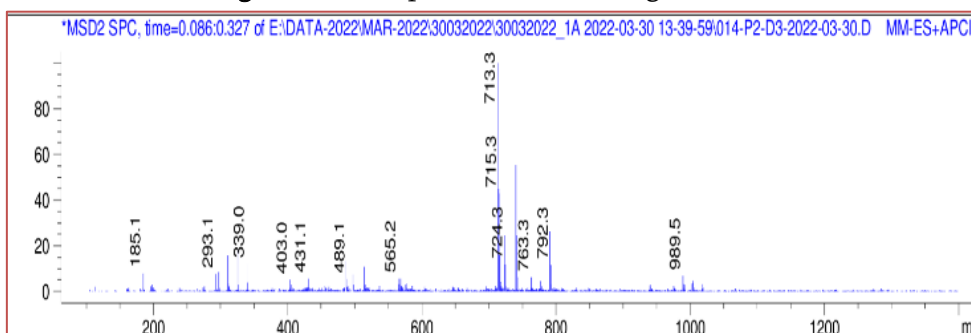


Figure 6. Mass spectra of  $[\text{Co}(\text{L})_2(\text{H}_2\text{O})_2]$  complex

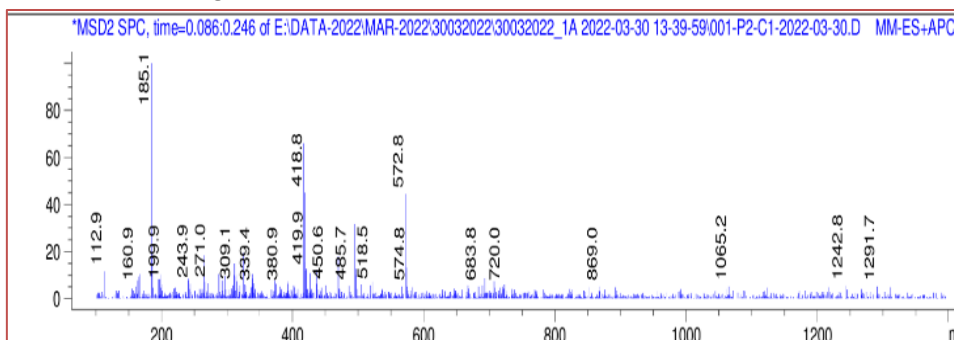


Figure 7. Mass spectra of  $[\text{Ni}(\text{L})_2(\text{H}_2\text{O})_2]$  complex

### 3.5 Powder XRD

The analysis was conducted using a powder X-ray diffractometer with the following settings: scanning mode:  $2\theta/\theta$ , scanning type: continuous, and scan speed: 5.000 degrees per minute. Fine X-ray peaks, as shown in Fig. 8, 9, were assigned to the synthesized ligand and its complexes, allowing for comparison and the formation of metal complexes with the Schiff base ligand. XRD plots show that the strength of ligand peaks dropped in metal complexes while peak broadness rose in metal chelates, indicating the presence of ligand-metal chelation.<sup>[23]</sup> We discovered the ligand and complexes using XRD analysis, as well as the crystal system, space group, and unit cell volume parameters presented in Table 3.

Table 3 Powder-XRD data of Schiff base and its metal complexes

Compound	HL	[Co(L) <sub>2</sub> (H <sub>2</sub> O) <sub>2</sub> ]	[Ni(L) <sub>2</sub> (H <sub>2</sub> O) <sub>2</sub> ]
Empirical formula	C <sub>20</sub> H <sub>19</sub> NO	C <sub>40</sub> H <sub>40</sub> CoN <sub>2</sub> O <sub>4</sub>	C <sub>40</sub> H <sub>40</sub> N <sub>2</sub> NiO <sub>4</sub>
Formula weight	289.38	671.23	670.23
Temperature, K	298	298	298
Crystal system	Tetragonal	Orthorombic	Orthorombic
Lattice type	P1	<i>P mmm</i>	<i>P mmm</i>
a/Å	5.250244	15.11380	8.430661
b/Å	5.250244	12.67799	6.383021
c/Å	25.42294	4.843458	6.258832
α/°	90.00000	90.00000	90.000000
β/°	90.00000	90.00000	90.00000
γ/°	90.00000	90.00000	90.000000
Unit cell volume, Å <sup>3</sup>	700.78494	928.06764	336.80707

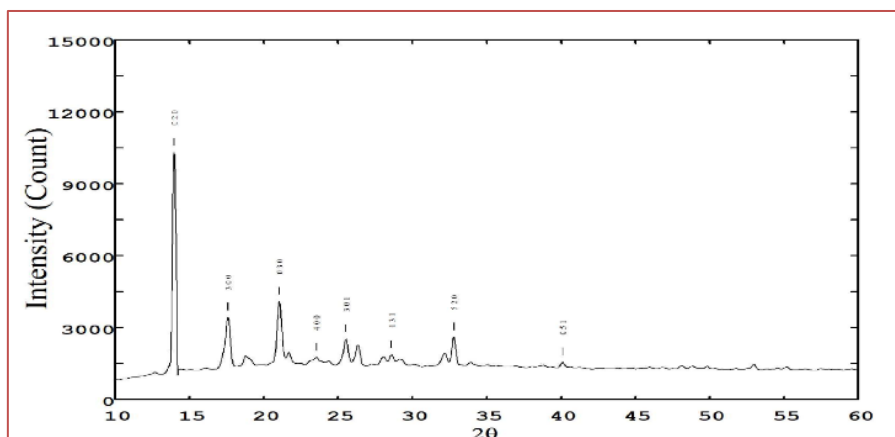


Figure 8. XRD spectra of [Co(L)<sub>2</sub>(H<sub>2</sub>O)<sub>2</sub>] complex

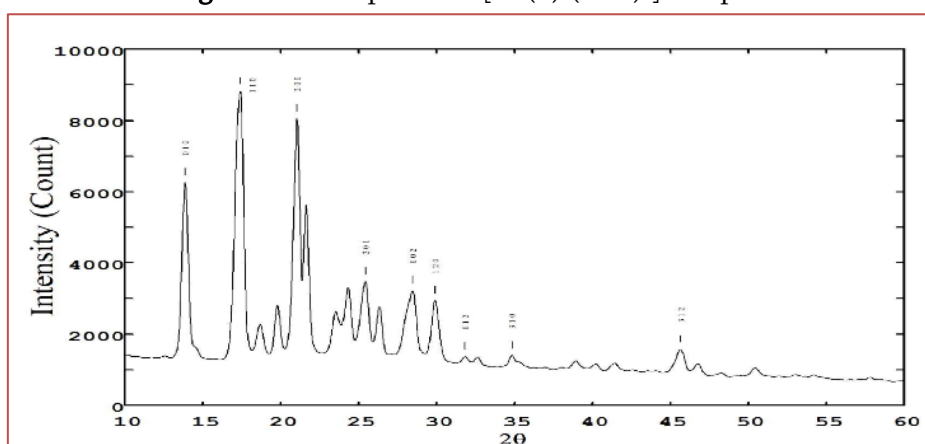


Figure 9. XRD spectra of [Ni(L)<sub>2</sub>(H<sub>2</sub>O)<sub>2</sub>] complex

### 3.6 Antimicrobial activity

The *in vitro* antibacterial activity of Schiff base ligands and complexes was investigated, as indicated in Table 4. To improve bioinorganic chemistry, the antibacterial capabilities of the synthesized Schiff base ligands and metal complexes were tested *in vitro* against certain pathogens. These specific microorganisms

were found in standard strains of two gram-negative *Escherichia coli*, *Pseudomonas aeruginosa*, and the gram-positive bacteria *Staphylococcus aureus* and *Bacillus subtilis*. Tweedy's chelation hypothesis and Overtone's idea [25] both state that metal complexes have greater antibacterial activity than free ligands.

The *in vitro* antifungal activity of Schiff base ligands and complexes was examined, as indicated in Table 4. *Candida albicans* and *Aspergillus niger* were cultivated on Mueller Hinton Agar and Potato dextrose agar, respectively. Both antifungal assays for Schiff base ligand and metal complexes show higher activity than *Ciprofloxacin*, the reference drug. Furthermore, when HL ligands are chelated with metals, their antifungal bioactivity rises. As a result, metal complexes suppress the growth of the microorganisms being studied more effectively.

**Table 4.** *In vitro* Antibacterial and Antifungal activity data of Schiff base and its metal complexes (in mm)

Compound	Concentration µg/ml	Antibacterial activity				Antifungal activity	
		<i>E. coli</i>	<i>P. aeruginosa</i>	<i>S. aureus</i>	<i>B. subtilis</i>	<i>C. albicans</i>	<i>A. niger</i>
HL	1000	9	10	12	8	6	8
	500	9	8	9	8	6	6
	250	7	7	7	7	5	6
	125	6	7	6	-	-	5
	50	-	6	-	-	-	-
[Co(L) <sub>2</sub> (H <sub>2</sub> O)]	1000	13	14	12	12	9	10
	500	10	10	9	11	8	9
	250	9	9	8	8	7	7
	125	6	7	7	6	6	6
	50	-	-	-	-	-	-
[Ni(L) <sub>2</sub> (H <sub>2</sub> O)]	1000	15	15	13	14	11	11
	500	13	12	11	13	10	10
	250	8	9	9	12	7	7
	125	6	7	7	8	6	-
	50	-	-	-	-	-	-
<i>Ciprofloxacin</i> *	20	39	31	33	28	5	5

\*- reference drug

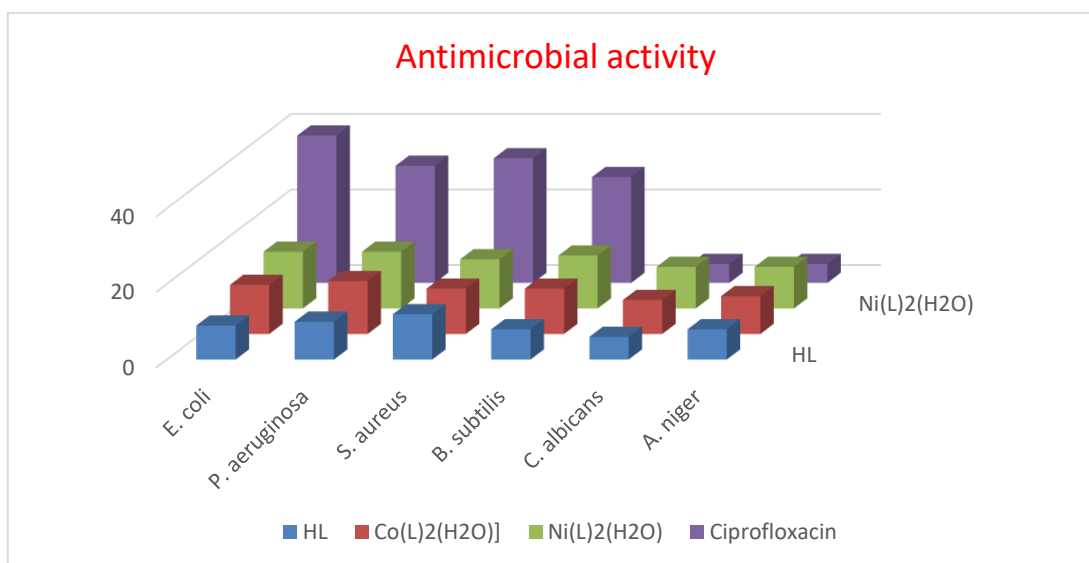


**Figure 10.** Graphical representation of Schiff base and their metal complexes antimicrobial activity (at 1000  $\mu\text{g/ml}$ )

## CONCLUSION

In light of the aforementioned work, a novel Schiffbase 2-(1-(phenethylimino)ethyl)naphthalen-1-ol (HL) was synthesized by condensation of 1-Hydroxy-2-acetonaphthone and Phenylethyl amine. UV-Vis, FT-IR and  $^1\text{H}$  NMR spectroscopy were used to suggest the formation of the ligand and its complexes. The bidentate ligand HL contains N and O donor atoms and binds to metal ions. It was also demonstrated using LCMS mass spectra, powder XRD. Metal complexes were observed to have an octahedral geometry. When the ligand was absent, Schiff bases had poor bioactivity; however, when coupled with metal atoms, they have outstanding antibacterial bioactivity. As a result, naphthalene-based chemicals and their complexes have high biological activity.

## REFERENCES

- [1] Khorshidifard M.; Rudbari H.A.; Kazemi-Delikani Z.; Mirkhani V.; Azadbakht R. Synthesis, characterization and X-ray crystal structures of Vanadium(IV), Cobalt(III), Copper(II) and Zinc(II) complexes derived from an asymmetric bidentate Schiff-base ligand at ambient temperature, *J. Mol. Str.*, 2014, 1081, 494-505. doi: <http://dx.doi.org/10.1016/j.molstruc.2014.10.071>
- [2] Dholakiya P. P.; Patel M. N. Preparation, Characterization, and Antimicrobial Activities of Some Mixed - Ligand Complexes of Mn(II), Co(II), Ni(II), Cu(II), and Cd(II) with Monobasic Bidentate (ON) Schiff Base and Neutral Bidentate (NN) Ligands. *Synthesis and Reactivity in Inorganic and Metal-Organic Chemistry*, 2004, 34, 383-395. <http://dx.doi.org/10.1081/SIM-120028308>
- [3] Ourari A.; Khelafi M.; Aggoun D.; Bouet G.; Khan M. A. Synthesis, Characterization, and Electrochemical Study of Tetradentate Ruthenium-Schiff Base Complexes: Dioxygen Activation with

- a Cytochrome P450 Model Using 1- or 2-Methylimidazole as Axial Bases. *Adv. Phy. Chem.*, 2011, 2011, 1-11. <https://doi.org/10.1155/2011/157484>
- [4] Messasma Z.; Ourari A.; Mahdadi R.; Houchi S.; Aggoun D.; Kherbache A.; Bentouhami E. Synthesis, spectral characterization, DFT computational studies and inhibitory activity of novel N2S2 tetradentates Schiff bases on metallo-beta-lactamases of *Acinetobacter baumannii*. *J. Mol. Str.*, 2018, 1171, 672-681. <https://doi.org/10.1016/j.molstruc.2018.06.044>
- [5] Daniel V. P.; Murukan B.; Kumari B. S.; Mohanan K. Synthesis, spectroscopic characterization, electrochemical behaviour, reactivity and antibacterial activity of some transition metal complexes with 2-(N-salicylideneamino)-3-carboxyethyl-4,5-dimethylthiophene. *Spectrochim. Acta-A: Mol. Biomol. Spectrosc.*, 2008, 70, 403-410. <https://doi.org/10.1016/j.saa.2007.11.003>
- [6] Makar S.; Saha T.; Singh S. K. Naphthalene, a versatile platform in medicinal chemistry: Sky-high perspective. *Eur. J. Med. Chem.*, 2019, 161 252-276. <https://doi.org/10.1016/j.ejmech.2018.10.018>
- [7] Bhati S. Structure-based drug designing of naphthalene based SARS-CoVPLpro inhibitors for the treatment of COVID-19. *Heliyon*, 2020, 6, e05558. <https://doi.org/10.1016/j.heliyon.2020.e05558>
- [8] Maher K. Schiff Bases Derived from 2-Hydroxynaphthalene-1-carbaldehyde and their Metal Complexes. *Asian J. Chem.*; 2018, 30,1171-1182. <https://doi.org/10.14233/ajchem.2018.21286>
- [9] Pandey P.; Verma A.; Bretosh K.; Sutter J.P.; Sunkari S. S. Template directed synthesis of half condensed Schiff base complexes of Cu(II) and Co(III): Structural and magnetic studie. *Polyhedron*, 2019,164, 80-89. <https://doi.org/10.1016/j.poly.2019.02.037>
- [10] Lashanizadegan M.; Ashari H. A.; Sarkheil M.; Anafcheh M.; Jahangiry S. New Cu(II), Co(II) and Ni(II) azo-Schiff base complexes: Synthesis, characterization, catalytic oxidation of alkenes and DFT study. *Polyhedron*, 2021, 200, 115148. <https://doi.org/10.1016/j.poly.2021.115148>
- [11] Freitas V. L. S.; Ribeiro da Silva M. D. M. C. Structural and Energetic Insights on Two Dye Compounds: 1-Acetyl-2-Naphthol and 2-Acetyl-1-Naphthol. *Molecules*, 2020, 25, 3827. <http://dx.doi.org/10.3390/molecules25173827>
- [12] Vhanale B.; Kadam D.; Shinde A. Synthesis, spectral studies, antioxidant and antibacterial evaluation of aromatic nitro and halogenated tetradentate Schiff bases. *Heliyon*, 2022, 8, e09650. <https://doi.org/10.1016/j.heliyon.2022.e09650>
- [13] da Silva C. M.; da Silva D. L.; Modolo L. V.; Alves R. B.; de Resende M. A.; Martins C. V.B.; de Fa'tima A. Schiff bases: A short review of their antimicrobial activities. *J. Adv. Res.*, 2011, 2, 1-8. <http://dx.doi.org/10.1016/j.jare.2010.05.004>
- [14] More M. S.; Joshi P. G.; Mishra Y. K.; Khanna P. K. Metal complexes driven from Schiff bases and semicarbazones for biomedical and allied applications: a review. *Mater.TodayChem.*, 2019, 14, 100195. <https://doi.org/10.1016/j.mtchem.2019.100195>
- [15] Vhanale B. T.; Shinde A. T. Synthesis, characterization and biological relevance of Ni(II) and Fe(III) complexes of the halogenated 2,2' ((pentane 1,3 diylbis(azanylylide ne))bis(ethan 1 yl 1 ylidene))bis(naphthalen 1 ol) Schiff base ligand. 2022, 19, 2641- 2653. <https://doi.org/10.1007/s13738-021-02486-4>
- [16] Lee J. M.; Shin S. Y.; Yoon H.; Lee M. S.; Lee Y. R.; Koh D.; Le Y. H. Synthesis and Biological Evaluation of a Novel Pyrazolecarbothioamide Derivative (DK115) Inducing Cell Cycle Arrest at the

- G1 Phase in HCT116 Human Colon Cancer Cells. *J. Korean Soc. Appl. Biol. Chem.*, 2013, 56, 343–347. <https://doi.org/10.1007/s13765-013-3065-1>
- [17] Ibrahim S. R. M.; Mohamed G. A. Naturally occurring naphthalenes: chemistry, biosynthesis, structural elucidation, and biological activities. *PhytochemRev* ., 2016, 15, 279–295. <https://doi.org/10.1007/s11101-015-9413-5>
- [18] Skrodzki M.; Patroniak V.; Pawluc P. Schiff Base Cobalt(II) Complex-Catalyzed Highly Markovnikov-Selective Hydrosilylation of Alkynes. *Org. Lett.*, 2021, 23, 663–667. <https://dx.doi.org/10.1021/acs.orglett.0c03721>
- [19] Kuchtanin V.; Klešč'íková L.; Šoral M.; Fischer R.; Ru° z'ic'kováZ.;Rakovsky' E.;Moncol' J.;Segl' P. Nickel(II) Schiff base complexes: Synthesis, characterization and catalytic activity in Kumada–Corriu cross-coupling reactions. *Polyhedron*, 2016, 117, 90–96. <http://dx.doi.org/10.1016/j.poly.2016.05.037>
- [20] Gutiérrez K. J.; Pedreira W. M.; Piñero Cruz D. M. Synthesis, structural, electrochemical and spectroscopic characterization, and theoretical calculations of two new Cu(II) and Ni(II) complexes from 2-(1-((pyridine-2-ylmethyl)imino)ethyl)naphthalen-1-ol,*J. Coord. Chem.*,2019, 72, 2654–2668. <https://doi.org/10.1080/00958972.2019.1670348>
- [21] Abdel-Rahman L. H.; Abu-Dief A. M.; El-Khatib R. M.; Abdel-Fatah S. M. Some new nano-sized Fe(II), Cd(II) and Zn(II) Schiff base complexes as precursor for metal oxides: Sonochemical synthesis, characterization, DNA interaction, in vitro antimicrobial and anticancer activities. *Bioorg. Chem.*, 2016, 69, 140–152. <http://dx.doi.org/10.1016/j.bioorg.2016.10.009>
- [22] Kumar A.; Agarwal M.; Singh A. K. Schiff bases of 1-hydroxy-2-acetonaphthone containing chalcogen functionalities and their complexes with and (p-cymene)Ru(II), Pd(II), Pt(II) and Hg(II): Synthesis, structures and applications in C–C coupling reactions. *J.Organomet. Chem.*, 2008, 693, 3533–3545. <https://doi.org/10.1016/j.jorganchem.2008.07.024>
- [23] Chaves S.; Pérez Redondo A.; Quevedo R. Solid State Structure and Intermolecular Interactions of two N Benzylidenephénylethylamines. *J. Chem. Crystallogr.*, 2020, 50, 206– 211. <https://doi.org/10.1007/s10870-019-00792-7>
- [24] Kargar H.; Behjatmanesh-Ardakani R.; Torabi V.; Sarvian A.; Kazemi Z.; Chavoshpour-Natanzi Z.; Mirkhani V.; Sahraei A.; Tahir M. N.; Ashfaq M. Novel copper(II) and zinc(II) complexes of halogenated bidentate N,O-donor Schiff base ligands: Synthesis, characterization, crystal structures, DNA binding, molecular docking, DFT and TD-DFT computational studies, *Inorg. Chim. Acta*, 2020, 514, 120004. <https://doi.org/10.1016/j.ica.2020.120004>



# Exploring the Chemistry of 1, 3, 4-Thiadiazole Derivatives and Their Metal Complexes: A Concise Study

Rajpal Jadhav<sup>1\*</sup>, Hansaraj Joshi<sup>1</sup>, Vishal Naiknaware<sup>1</sup>, Ramesh Ware<sup>2</sup>

<sup>1</sup>Department Chemistry, Swa Sawarkar Mahavidyalaya, Beed, Maharashtra, India

<sup>2</sup>Department Chemistry, Milliya College, Beed, Maharashtra, India

## ABSTRACT

1, 3, 4-Thiadiazole derivatives and their metal complexes have gained attention due to their diverse biological activities, such as antibacterial, antifungal, anti-tubercular, and antiulcer properties. Key drugs like methazolamide and acetazolamide, containing the 4-thiazolidinone nucleus, showcase this scaffold's therapeutic potential. Thiadiazole derivatives have also demonstrated significant effects against breast cancer cell lines. While antibacterial and anti-tubercular properties have been well-explored, other therapeutic areas remain under-researched. Schiff bases, particularly in metal complexes, enhance the biological activity of these derivatives, with promising applications in organic synthesis and catalysis. This review highlights the versatility of 1, 3, 4-thiadiazole and stresses the importance of further research into its antimicrobial and therapeutic potential.

**Keywords:** 1, 3, 4-Thiadiazole, biological activities, antibacterial, antifungal, antitubercular, methazolamide and acetazolamide etc.

## INTRODUCTION

Throughout history, humanity has faced numerous outbreaks of contagious diseases, leading scientists to develop a variety of antimicrobial medicines. However, microbes continuously evolve, increasing their resistance and turning this into a serious problem [1]. In this context, bioinorganic chemistry plays a crucial role in addressing these emerging health issues, serving as a bridge between inorganic chemistry and biochemistry. This discipline investigates the interactions between inorganic substances and living systems, focusing on the transport, speciation, and mineralization of inorganic materials. It examines the role of essential elements, including metal ions (e.g.,  $K^+$ ,  $Fe^{2+}$ ), coordination compounds (e.g., cisplatin, technetium carbonyl), and inorganic molecules (e.g.,  $CO$ ,  $O_2$ ) in biological processes. Given the persistent emergence of new diseases, there is an urgent need to explore advanced antimicrobial agents and develop effective drugs that are vital to medicinal chemistry [2-5]. Recent advancements in bioinorganic chemistry have generated keen interest in Schiff bases and thiol derivative complexes, which may serve as models for biologically significant species [6, 7].

Nitrogen-containing heterocycles are particularly important in medicinal chemistry, with five-membered aromatic rings, such as 1, 3, 4-thiadiazoles, being notable for their pharmacological activities. [8]

Thiadiazoles, characterized by a five-membered ring structure containing two nitrogen atoms and one sulphur atom, has various isomers, including 1,2,3-thiadiazole, 1,2,5-thiadiazole, 1,2,4-thiadiazole, and 1,3,4-thiadiazole. Among these, 1, 3, 4-thiadiazole (Figure-1) is recognized as the most bioactive isomer [6, 7]. Compounds like 5-Phenyl-1, 3, 4-thiadiazole demonstrate a range of bioactivity, with many pharmacological actions [9]. The azole group in the 1, 3, 4-thiadiazole structure functions as a versatile pharmacophore, displaying diverse biological activities, [10-14] thus making it a focal point for new drug development.

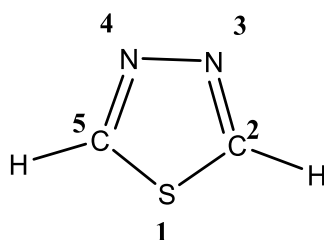


**Figure-1: Structure of 1,3,4-Thiadiazole**

The 1,3,4-thiadiazole scaffold is essential for developing drugs with various biological activities, including antibacterial, antitubercular, and antiulcer properties. Medically significant compounds like methazolamide, megazol, and acetazolamide derive their efficacy from the 4-thiazolidinone nucleus in their structures. While antibacterial and antitubercular applications have been widely studied, additional therapeutic targets for 1,3,4-thiadiazole remain underexplored. The versatility of this framework is crucial for designing biologically active molecules with broad-spectrum medical applications.

Recent advancements in Schiff base coordination chemistry highlight its importance across multiple fields, including organic synthesis, analytical chemistry, metallurgy, electroplating, and photography.[15-17] Schiff bases are utilized in the dye industry, catalysis, and agrochemicals. [18, 19] Many of these compounds exhibit remarkable antibacterial, antifungal, and anticancer properties, underscoring their critical role in coordination compound chemistry.[20] Schiff bases, which are derived from amino and carbonyl compounds, are essential ligands that coordinate with metal ions through azomethine nitrogen and have been extensively studied. The C=N linkage in these azomethine derivatives is vital for their biological activity, with numerous examples showing impressive antibacterial, antifungal, anticancer, and antimalarial properties. [7] The chemistry and applications of new Schiff base thiadiazole derivatives need thorough investigation, particularly in their coordination with various metal ion moieties. Consequently, research on the structure-activity relationship of 1, 3, 4-thiadiazoles should be prioritized in the near future [21].

## REVIEW OF LITERATURE

The biological activity of 1,3,4-thiadiazole derivatives has attracted considerable interest due to their diverse pharmacological properties. These compounds are known to exhibit various biological activities, including antibacterial, antifungal, anticancer, and anti-inflammatory effects. Research indicates that structural modifications in 1,3,4-thiadiazole derivatives can enhance their biological efficacy. For instance, the incorporation of different substituents or coordination with metal ions can significantly influence their

activity and selectivity against specific biological targets. The azole group within the 1,3,4-thiadiazole framework serves as a versatile pharmacophore, allowing for the development of compounds with a wide range of therapeutic applications. Ongoing studies aim to explore the structure-activity relationships of these derivatives, paving the way for discovering new and effective drugs.

**Profire L.** (2007), *et. al.* presented the preparations and antibacterial activities of new 1,3,4-thiadiazole compounds 5a-e (Figure-2). The possible antimicrobial properties of the synthesized compounds were examined using the *S. aureus* ATCC 25923, *B. anthracis* ATCC 8705, *B. cereus* ATCC 10987, *Sarcinalutea* ATCC 9341 and *E. coli* ATCC 25922 strains. These compounds displayed encouraging activities against *B. anthracis* and *B. cereus* [22].

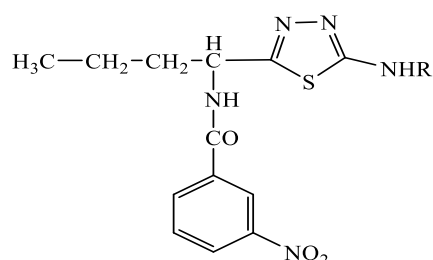


**Figure-2 : New 1,3,4-thiadiazole compounds 5a-e**

**Ashutosh et. al.** (2009) synthesized a series of dichlorides (Ia-h), followed by 1, 3, 4-thiadiazol-2-amine derivatives (IIa-h), using various dicarboxylic acids (a-h). The reaction of compound (I) with thiosemicarbazide in the presence of sulfuric acid resulted in the formation of the corresponding 1, 3, 4-thiadiazol-2-amines (IIa-h). (Figure-3) The structures of these compounds were confirmed through IR, NMR, and mass spectral analysis. The newly synthesized compounds were then evaluated for their antibacterial and antifungal activities. The results showed that compounds (IIa), (IIe), (IIf), and (IIh) exhibited moderate to good antibacterial and antifungal activity at concentrations of 5-100 mcg/mL [23].

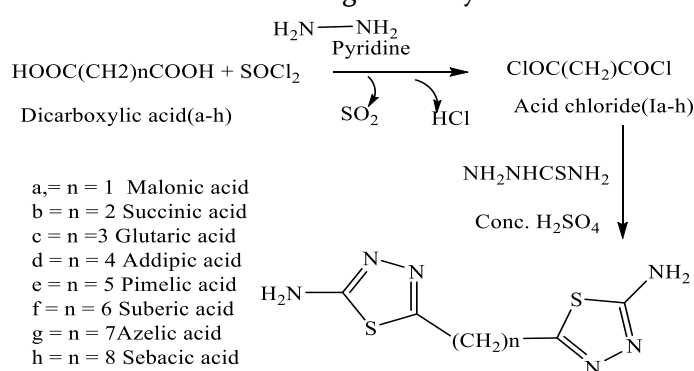


**Figure-3: Synthesis of Thiadiazole derivatives(IIa-h)**

**Pandey et al.** (2012) illustrated synthesized novel Schiff bases from 2-amino-5-aryl-1,3,4-thiadiazole derivatives (Figure-4) condensed with different aromatic aldehydes and structures of the compounds characterized from first to last by IR and <sup>1</sup>H NMR spectral measurements. The synthesized Schiff bases have been screening intended for activities like antimicrobial, analgesic and anti-inflammatory. The compounds 4a, 4d, 4e and 4j proved fine antibacterial activity against gram-positive bacteria, whereas compounds 4b, 4d, 4e and 4j proved excellent antibacterial activity against gram-negative bacteria. [24]

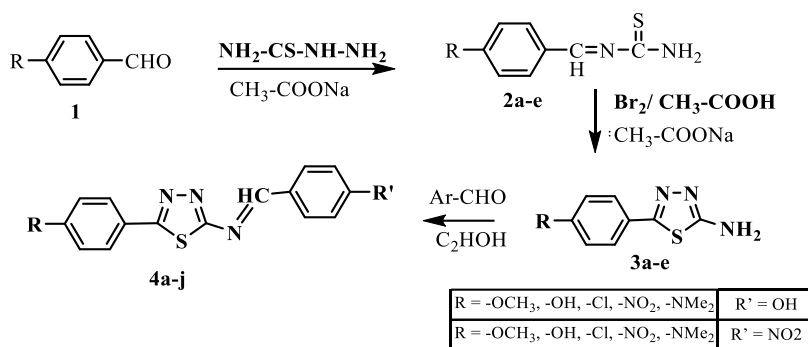


Figure-4: Synthesis of Schiff bases of 1, 3, 4-thiadiazoles derivatives

M. Sugumaran (2012) *et.al.* synthesized series of from fluorenbenthiazole incorporated 1, 3, 4 - thiadiazole derivative compounds (SH<sub>1</sub>-SH<sub>11</sub>). (Figure-5) The newly structure of the synthesized compounds was confirmed by UV, IR, <sup>1</sup>H NMR, Mass spectral analysis and appraised for their antimicrobial and anti-inflammatory activity. Growth inhibition activities shown by compounds SH<sub>6</sub> -SH<sub>11</sub> against discovered significant good quality bacterial activity. Compound SH<sub>11</sub> has been found to have better anti-inflammatory activity in the inhibition compared to compound SH<sub>6</sub>. [25]

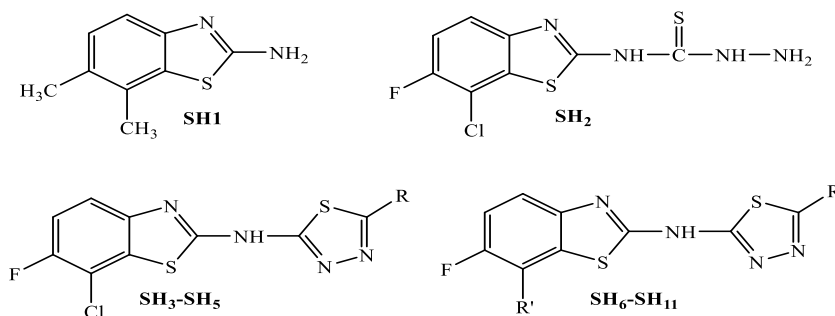


Figure-5: Fluorenbenthiazole incorporated 1, 3, 4 - thiadiazole derivative compounds (SH<sub>1</sub>-SH<sub>11</sub>).

Al-Shammary (2012) a series of compounds of Schiff bases (Figure-6) synthesized from 1,3,4-thiadiazole (2,5-di(N-substitutedbenzylideneamino) 1,3,4-thiadiazole and benzaldehyde and substituted benzaldehydes. The chemical structure of the synthesized compounds was examined by using analytical and spectral means. The entire compounds were screened for their antioxidant activity. The compound 5 reveals the highest antioxidant activity [26].

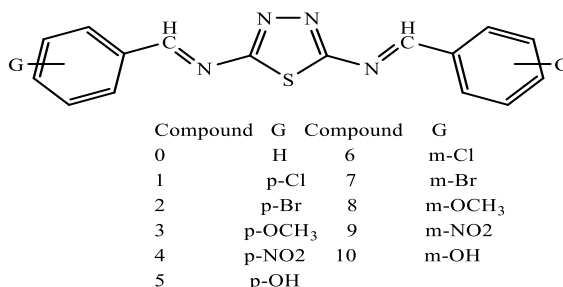


Figure-6: Series of Schiff bases

M. Narayana Babu *et. al.* (2012) synthesized a novel of 3-chloro-4-(substituted)-1-(5-phenyl-1, 3, 4-thiadiazol -2-yl) azetidin-2-ones and their antimicrobial activity is described. The synthesis of the final compounds, (Figure-7) involves four steps. First step involves the synthesis of 2-amino-5-aryl-1,3,4-

thiadiazole which is accomplished by cyclization of thiosemicarbazide in the presence of ferric chloride which is further converted into imines by the treatment with various substituted aldehydes. The final compounds were synthesized by Staudinger imine reaction of Schiff's bases [27].

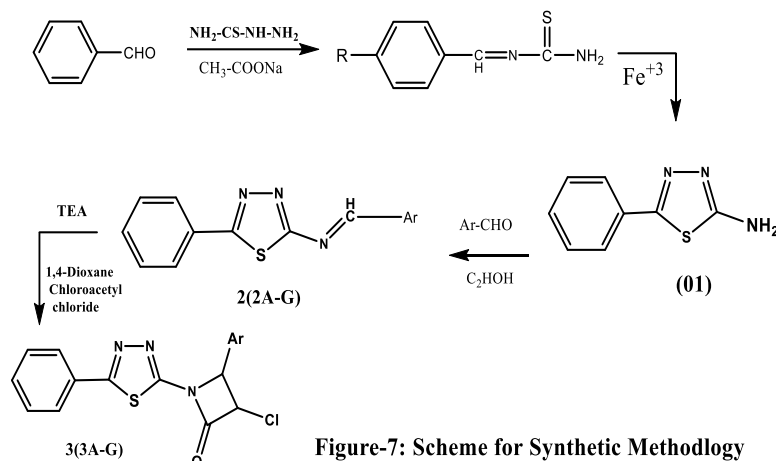


Figure-7: Scheme for Synthetic Methodology

Sunny *et al.* (2012) reviewed the synthesis and biological activities of Schiff bases of imidazo-[2,1b]-1,3,4-thiadiazole derivatives. (Figure-8) Schiff bases, containing a carbon-nitrogen double bond, were synthesized by condensing 1,3-benzodioxole-5-carboxylic acid with thiosemicarbazide, followed by further reactions to obtain imidazo-thiadiazole derivatives. These derivatives were used to produce Schiff bases, which were characterized by IR, NMR, and mass spectroscopy. The synthesized compounds exhibited moderate to good antimicrobial activity, particularly when compared to the standard antibiotic ampicillin. Schiff bases are known for their diverse biological activities, including antimicrobial properties [28].

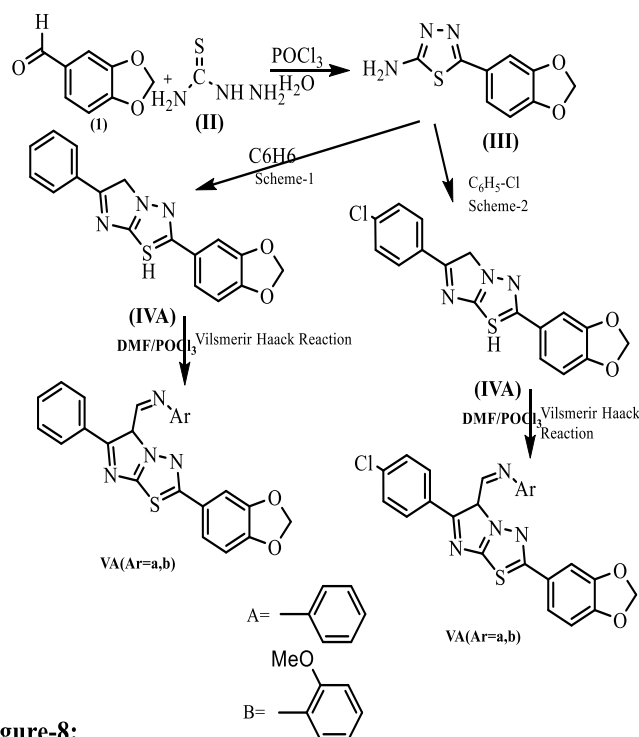
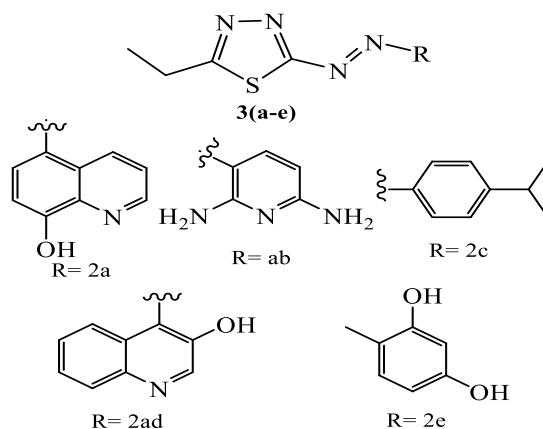


Figure-8: Some Schiff bases of imidazo-[2, 1b]-1, 3, 4-thiadiazole derivatives

**Kumar, C.T** (2013) *et. al.* synthesized a series of heterocyclic azodyes of 5-Ethyl-1,3,4-thiadiazole-2-amine **3 (a- e)** by coupling 8-hydroxyquinoline, 2,6-diaminopyridine, *N,N*-dimethyl aniline, 2-naphthol and resorcinol with diazotized 5-ethyl-1,3,4-thiadiazol-2-amine in nitrosylsulphuric acid. These dyes (Figure-9) were described by UV, IR,  $^1\text{H}$  NMR,  $^{13}\text{C}$  NMR, elemental analysis and mass spectrometry for selected dyes. These were assessed for antibacterial activity against gram (+ve) *B. megaterium*, *B. subtilis* and gram (-ve) *E. coli* and *A. aerogenes* and antifungal activity against *A. Flavus*, *C. Keratinophilum* and *C. Albicans*. Compound **3a** and **3b** illustrated good antimicrobial activities than other compounds. But, compounds **3a** was established to show good antifungal activity [29].



**Figur-9: Synthesized a series of heterocyclic azodyes of 5-Ethyl-1,3,4-thiadiazole-2-amine 3 (a- e)**

**Mahendrasinh et.al.** (2013) synthesized a novel series of 1,3,4-thiadiazole derivatives ( $\text{C}_1$ - $\text{C}_5$ ) (Figure-10) from novel thiadiazoles derived from 4-hydroxybenzoic acid and thiosemicarbazide.

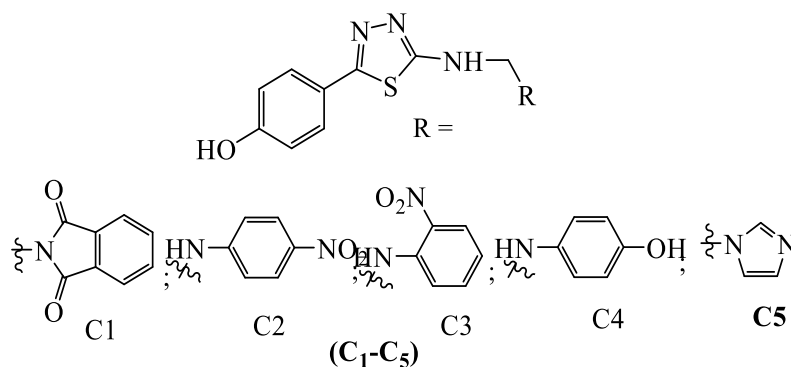


**Figure-10: Synthesis of a novel series of 1,3,4-thiadiazole derivatives**

The structures established by using IR,  $^1\text{H}$  NMR and nitrogen estimation. All these compounds were screened for antibacterial activity against the (*S. aureus* ATCC 9144, *B. Cereus* ATCC 11778, *E. coli* ATCC 25922, *P. aeruginosa* ATCC 2853 and anti-fungal (*A. niger* ATCC 9029 and *A. fumigatus* ATCC 46645) by paper disc diffusion method. In vitro antibacterial activity against tested organisms displayed considerable activity with a broad scale of difference. It has been found that compound  $\text{C}_1$ ,  $\text{C}_4$  exhibits important antibacterial activity remaining has exhibited considerable activity against the same strain. Whereas derivatives  $\text{C}_1$ ,  $\text{C}_2$ , and  $\text{C}_4$  have revealed higher activity against *A. fumigatus* [30].

**Naveen K. et. al.** (2014) synthesized Schiff bases (Figure-11) by a reaction of primary amine, 5-ethyl-1,3,4-thiadiazol-2-amine (1) with substituted aldehydes, obtained a new class of imine group holding

compounds (3, 5 & 7). The prepared compounds were characterized by using spectroscopic techniques viz.,  $^1\text{H-NMR}$ ,  $^{13}\text{C-NMR}$  and mass spectral studies. Antimicrobial activity was done using disc diffusion technique using *B. subtilis*, *E. coli*, *S. aureus* and *R. solanacearum* and antifungal activity against *A. niger*, *A. flavus* and *A. solani*. All the synthesized compounds exhibited potent antimicrobial activities [31].

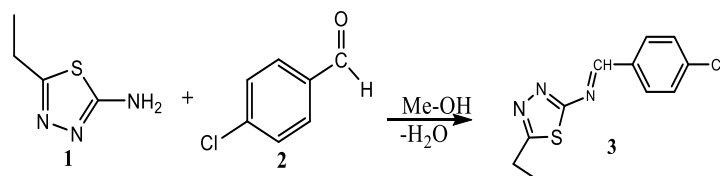


Figure-11' : Synthesis of Schiff base (-Cl Substituted)

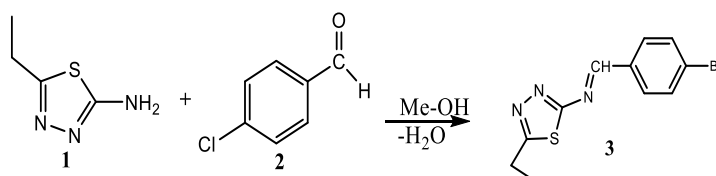


Figure-11 : Synthesis of Schiff base (-Br Substituted)

**Siddhanadham et al.** (2016) highlighted that thiadiazoles and their derivatives exhibit various biological activities, including antibacterial, antifungal, and anti-tubercular effects. In this study, 1,3,4-thiadiazole Schiff bases (Figure-12) were synthesized from benzoic acid and thiosemicarbazide, followed by modification with aromatic aldehydes. The compounds purity was confirmed by TLC and purified by recrystallization and column chromatography, with their structures verified by IR,  $^1\text{H NMR}$ , and mass spectrometry. These Schiff bases showed significant antimicrobial, antifungal, and anti-tubercular activity, likely due to cell wall disruption or inhibition of mycolic acid synthesis. [32]

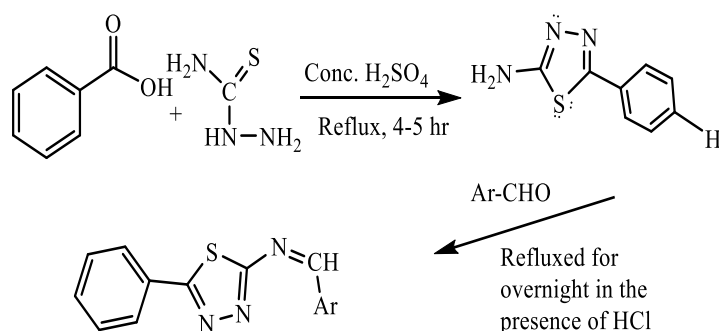
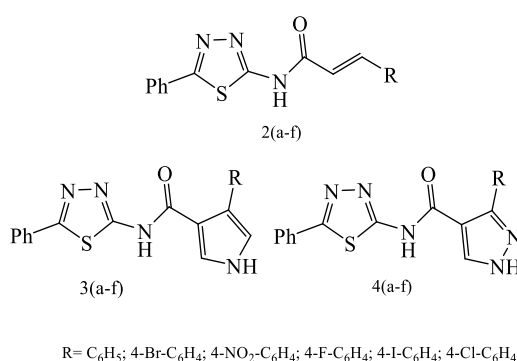


Figure-12: Synthesis of 2-amino-5-phenyl-1,3,4-thiadiazole Schiff base

**Maddila, S.et.al.** (2016) synthesized three new series of (E)-3-(4-substitutedphenyl)-N-(5-phenyl-1,3,4-thiadiazol-2-yl) acrylamide (2a-f), 4-(4-substitutedphenyl)-N-(5-phenyl-1,3,4-thiadiazol-2-yl)-1Hpyrazole-3-carboxamides(3a-f) and 4-(4-substitutedphenyl)-N-(5-phenyl-1,3,4-thiadiazol-2-yl)-1Hpyrrole-3-carboxamide(4a-f) compounds. (Figure-13) The newly synthesized structures were confirmed by using  $^1\text{H NMR}$ ,  $^{13}\text{C NMR}$ , LCMS mass, FT-IR and elemental analysis. All these compounds were screened for their anti-inflammatory activity in which compounds 3c, 3d, and 4c proved effective anti-inflammatory activities as compared to the standard drugs [33].



**Figure-13: Synthesized three new series of (E)-3-(4-substitutedphenyl)-N-(5-phenyl-1,3,4-thiadiazol-2-yl) acrylamide (2a-f)**

**Lingareddy et al. (2016)** described synthesis, spectroscopical characterization and biological studies of Co(II), Ni(II), Cu(II) and Zn(II) complexes of 2-amino-5-hydroxyphenyl-1,3,4-thiadiazoles. (Figure-14) The characterization involved elemental analysis, molar conductance, IR, <sup>1</sup>H NMR, electronic, magnetic susceptibilities, ESR, FAB-mass and thermal studies. The ligand coordinates through nitrogen at 4th position of thiadiazole moiety and phenolic oxygen of salicylic acid moiety via deprotonation. From the above studies it is concluded that the ligands act as a bidentate molecule with stoichiometry being 1:2 (metal: ligand) obeying the general formula [ML<sub>2</sub>.2H<sub>2</sub>O]. Co(II), Ni(II) and Zn(II) complexes possessing an octahedral geometry while Cu(II) complexes have exhibited distorted octahedral geometry. The compounds were tested in vitro to evaluate their antibacterial and antifungal properties. Those that showed activity were further analyzed for their MIC (Minimum Inhibitory Concentration) values. Additionally, the antitubercular activity of the compounds was assessed against the H37Rv strain using the Middlebrook method. The brine shrimp bioassay was also carried out to study the in vitro cytotoxicity properties for the ligands and their corresponding complexes [34].

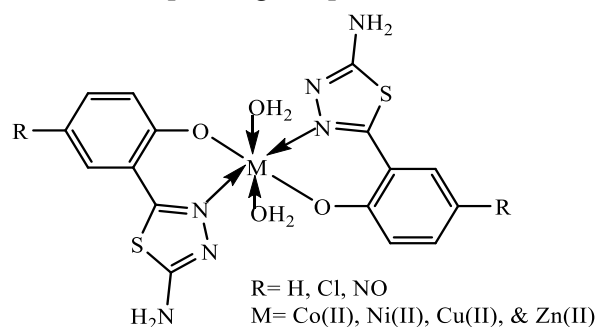


**Figure-14: Complexes of Co(II), Ni(II), Cu(II) and Zn(II) with 2-amino-5-hydroxyphenyl-1,3,4-thiadiazoles**

**Mousa (2017)** synthesized six new Schiff bases (5a-5f) from 5-parachlorophenyl-1,3,4-thiadiazole-2-amine and benzaldehyde derivatives. (Figure-15) Their structures were confirmed using FT-IR, <sup>1</sup>H-NMR, and CHNS elemental analysis. The compounds were tested for antimicrobial activity against gram-positive (*S. aureus*, *B. cereus*) and gram-negative bacteria (*E. coli*, *P. aeruginosa*). Compound 5b showed the least bacterial inhibition, while 5f demonstrated the highest activity, surpassing the standard drug cefuroxime. The antimicrobial effects are attributed to the synergistic action of the Schiff base and 1,3,4-thiadiazole groups, making these compounds promising candidates for antimicrobial applications [35].



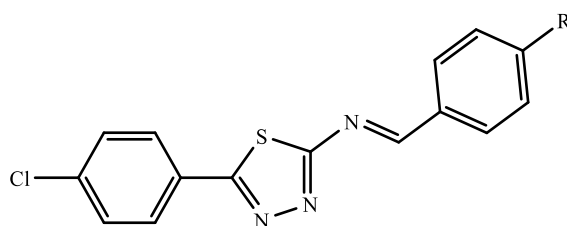


**Figure-15: Schiff bases 5 (a-f); R a=H; b=CH<sub>3</sub>; c=OH; d=NO<sub>2</sub>; e=Cl; f=Br**

**Emad Yousif et al.** (2017) synthesized five novel metal complex derivatives of 2N-salicylidene-5-(p-nitrophenyl)-1,3,4-thiadiazole (HL)(Figure-16) using the metal ions Vo(II), Co(II), Rh(III), Pd(II), and Au(III) in analcoholic medium. The complexes were characterized by micro elemental analysis, FTIR, UV-Vis, mass spectroscopy, <sup>1</sup>H & <sup>13</sup>C NMR, magnetic susceptibility, and conductivity measurements. All the complexes were four-coordinated with square planar geometry, except for VO(II) (complex 1) and Co(II) (complex 2), which exhibited square pyramidal and tetrahedral geometries, respectively. Antibacterial screening revealed moderate activity for complexes 1–5, slightly higher than the ligand HL [36].

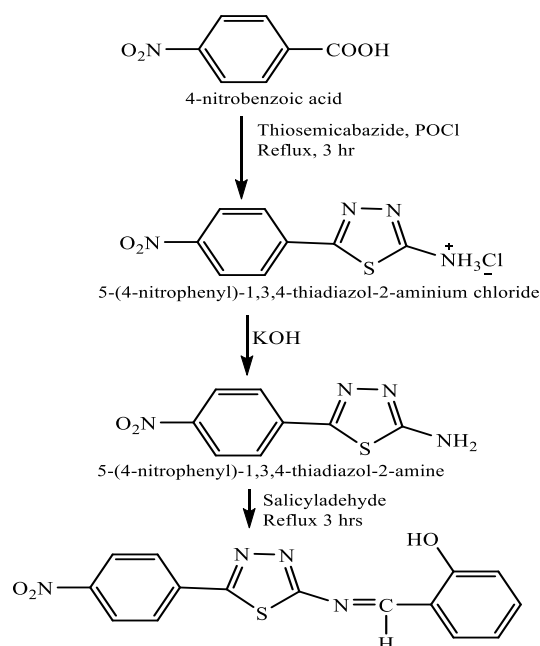


**Figure-16: Ligand HL**  
2-([5-(4-nitrophenyl)-1,3,4-thiadiazol-2-ylidene]methyl)phenol

**Hassan et al.** (2017) synthesized Schiff bases (Figure-17) from 5-(4-aminophenyl)-2-amino-1,3,4-thiadiazole and 4-(Di-methylamino) benzaldehyde under reflux condition for 6 hours. These compounds were described by FTIR and evaluated for their anticancer activity against breast cancer (MCF7) and human prostate cancer (DU 145). It was found that anticancer outcomes revealed that thiazole derivative exhibited additional effect in the case of breast cancer than in prostate cell line [37].

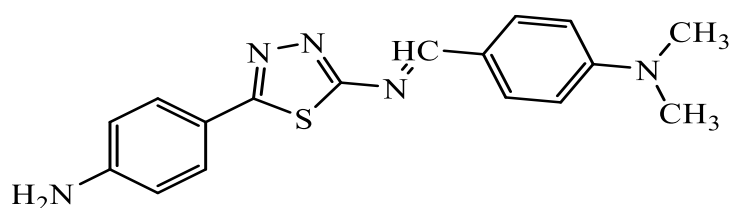
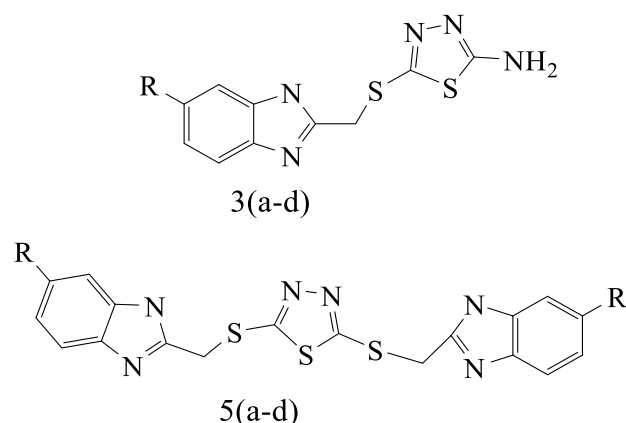


**Figure-17: Synthesis of Schiff base from 5-(4-aminophenyl)-2-amino-1,3,4-thiadiazole and 4-(Dimethylamino) benzaldehyde**

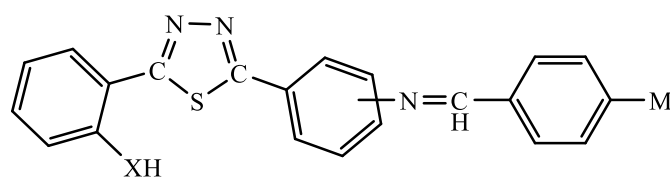
**Muayed Redayan, et. al.** (2017) synthesized a sequence of novel 5-amino-1,3,4-thiadiazole-2-thiol and 1,3,4-thiadiazole-2,5-dithiol derivatives of benzimidazole. (Figure-18) The structures of the synthesized compounds were confirmed by spectral methods of analysis (FT-IR,  $^1\text{H}$  and  $^{13}\text{C}$  NMR). All of the target compounds were tested for their antibacterial activity against Gram(-) bacteria like *E. coli*, *P. aeruginosa*, and Gram(+) bacteria as *B. subtilis*, *S. aureus*. Most of the synthesized derivatives demonstrated well to moderate activity against both bacteria Gram- (+) both *B. subtilis*, *S. aureus* and Gram(-) both *E. coli*, *P. aeruginosa* bacteria [38].



Comp. No.	R
1a, 3a, 5a	H
1b, 3b, 5b	CH <sub>3</sub>
1c, 3c, 5c,	COOH
1d, 3d, 5d	NO <sub>2</sub>

**Figure-18: 5-amino-1,3,4-thiadiazole-2-thiol and 1,3,4-thiadiazole-2,5-dithiol derivatives of benzimidazole**

**Ajit Pandey** (2018) synthesized novel Schiff bases (Figure-19) of 2,5-disubstituted-1,3,4-thiadiazole, confirming their structures using IR,  $^1\text{H}$  NMR, and elemental analysis. The compounds were tested in vivo for analgesic and anti-inflammatory activities. Notably, compound 6f (5-(2-Mercaptophenyl)-2-{N-(4-methoxybenzylidene)-4-aminophenyl}-1,3,4-thiadiazole) exhibited superior analgesic and anti-inflammatory effects with minimal gastric ulceration. This study successfully introduced a series of compounds with promising pharmacological properties, with compound 6f standing out for its therapeutic potential [39].



X=O,S ; R= 2-NH<sub>2</sub>, 3-NH<sub>2</sub>, 4-NH<sub>2</sub> and M= 4-OCH<sub>3</sub>

**Figure-19: Different Schiff bases of 2,5-Disubstituted-1,3,4-thiadiazole (6a-f), (7a-f)**

**Naeem Basher** (2020) prepared a new ligand (L<sub>1</sub>) (Figure-20) from thiadiazole derivatives by reacting 1,2,5-dihydrazine, 1,3,4-thiadiazole, and 4-Dimethyl amino benzaldehyde. Transition metal complexes of Co(III) and Cu(II) with this ligand were synthesized and characterized using various techniques such as elemental analysis, FTIR, <sup>1</sup>H-NMR, mass spectroscopy, magnetic sensitivity, and molar conductivity. The study found that [L<sub>1</sub>CoCl<sub>3</sub>] has an octahedral geometry, while [L<sub>1</sub>CuCl<sub>2</sub>] adopts a square planar shape. The Co(III) complex is electrolytic, while the Cu(II) complex is non-electrolytic. Biological activity tests revealed that the ligand and complexes showed strong activity against *Escherichia coli* but no activity against *Staphylococcus aureus* [40].

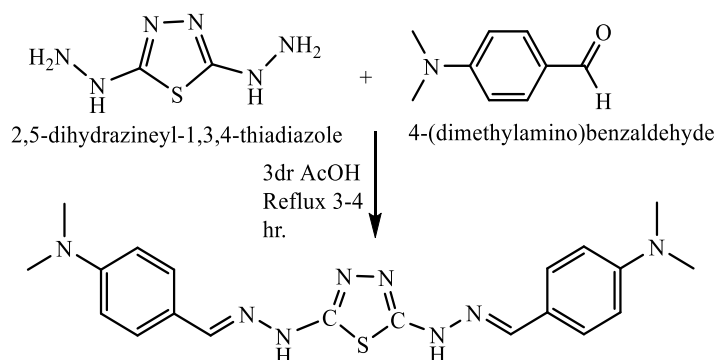
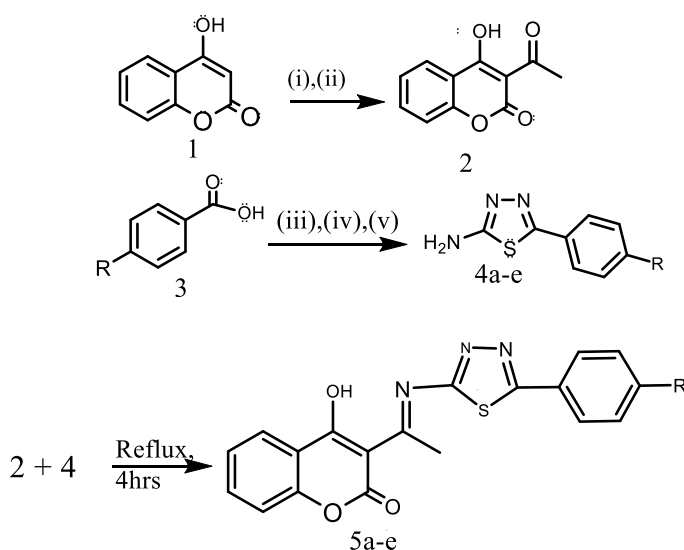


**Figure-20: Synthesis of ligand**

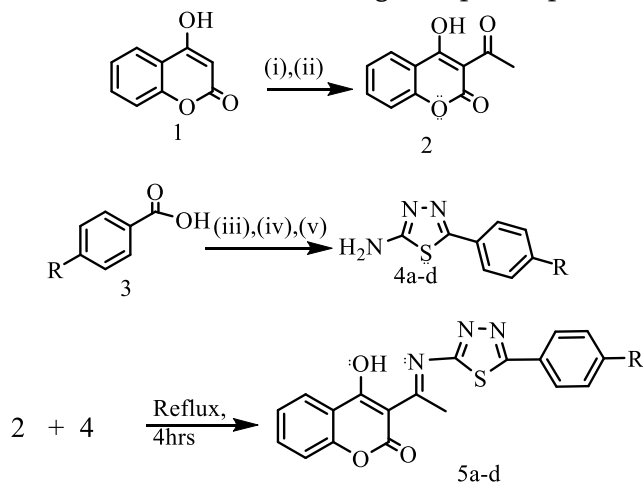
**Jadhav R.L. et al.** (2021) emphasize the significance of 2H-Chromen-2-one derivatives as intermediates in pharmaceuticals and agrochemicals. The study involves synthesizing Schiff bases (Figure-21) from 3-acetyl-4-hydroxy-2H-chromen-2-one and 5-(4-substituted phenyl)-1,3,4-thiadiazol-2-amine, known for their biological activity. These compounds were tested for antibacterial and antifungal properties, showing notable activity against various species. The presence of a phenolic hydroxyl group likely enhances their effectiveness, especially in gram-negative bacteria. Electron-withdrawing groups on the aromatic ring were particularly effective in increasing antifungal activity [41].



(i) Ac-OH, (ii) POCl<sub>3</sub>, (iii) Thiosemicarbazide, (iv) Et-OH, (v) Conc.H<sub>2</sub>SO<sub>4</sub>  
 R=(a)-H, (b)-CH<sub>3</sub>, (c) -OH, (d) -OCH<sub>3</sub>,(e)-NO<sub>2</sub>

**Figure-21: Reaction for synthesis of Novel Schiff's Bases (5a-5e)**

J. Rajpa *et.al.*(2021) synthesized four novel Schiff's bases (SB 5a-d), incorporating coumarin and 1,3,4-thiadiazole derivatives,(Figure-22) were synthesized by reacting 3-acetyl-4-hydroxy chromen-2-one with substituted 2-amino 5-(4-halo phenyl)-1,3,4-thiadiazoles. The structures of these synthesized compounds were confirmed through elemental analysis and spectral data. Antimicrobial activity was evaluated against bacterial species (*S. aureus*, *E. coli*, *S. typhi*, *B. subtilis*) using the Agar cup method, and fungal species (*A. niger*, *P. chrysogenum*, *F. moniliforme*, *A. flavus*) through the poison plate method.



(i) Ac-OH, (ii) POCl<sub>3</sub>, (iii) Thiosemicarbazide, (iv) Et-OH, (v) Conc.H<sub>2</sub>SO<sub>4</sub>  
 R=(a)-F, (b)-Cl, (c) -Br, (d) -I

**Figure-22: Synthesis of Novel Schiff's Bases(SB 5a-d)**

All compounds demonstrated notable antimicrobial activity and hold promise for future applications in drug development, with potential uses in fields like antioxidant research, dyeing, and corrosion prevention [42].

**JoshiHansaraj***et.al.* also studied the complexation tendencies of these Schiff bases (Figure-21 and Figure-22) by pH metric study and found promising results in this regard[43-47].

**Aamer** *et. al.* (2023) synthesized five derivatives of 1,3,4-thiadiazole linked to Schiff bases, (Figure-23)

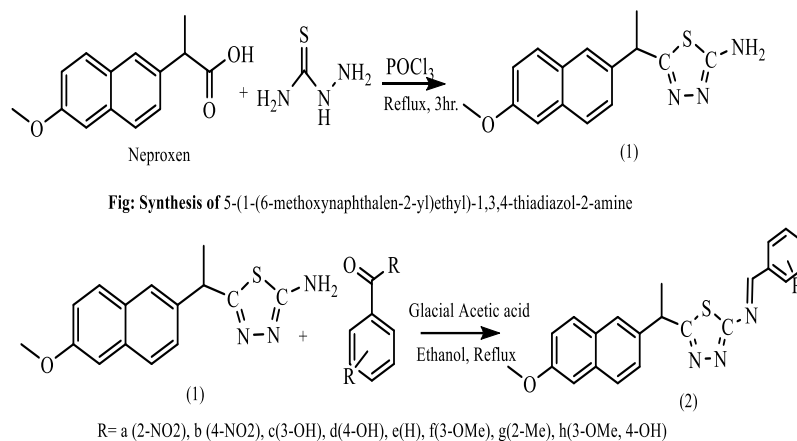


**Figure-23: Synthesis of compounds Schiff bases (a-h) derivatives**

aiming for anti-cancer properties. These compounds were prepared through a cyclization reaction involving Naproxen and thiosemicarbazide, followed by structural confirmation via <sup>1</sup>H-NMR, <sup>13</sup>C-NMR, FT-IR, and elemental analysis. The new compounds demonstrated promising anti-cancer activity in MTT assays, showing potential for future cancer treatments. Further research is needed to validate their clinical effectiveness [46].

In **Sajid**,*et. al.* (2023) study, ten Schiff bases (Figure-24) of 1,3,4-thiadiazole were synthesized and characterized using advanced techniques like FT-IR, NMR, and mass spectroscopy. The Schiff bases demonstrated notable antimicrobial activity against various bacterial and fungal strains. However, their effectiveness was lower than conventional antibiotics, highlighting the need for further optimization. This research contributes to the potential use of 1,3,4-thiadiazole derivatives in developing new antimicrobial agents [47].

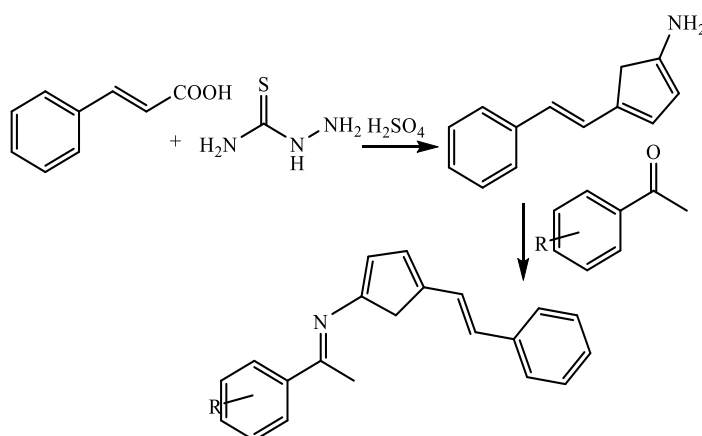


**Figure-24: Synthesis of Schiff bases with a moiety of 1,3,4-thiadiazoles**

**Al-araj***et. al.* (2024) were synthesized several The target compounds, including 1,3,4-oxadiazoles, 1,3,4-thiadiazoles, 1,2,4-triazoles, and Schiff bases, using cholic acid as a starting material. The structures of the synthesized compounds were confirmed through FTIR and <sup>1</sup>H, <sup>13</sup>C-NMR spectroscopy. The biological

activity of the compounds was tested against Gram-positive and Gram-negative bacteria, showing significant results for certain chemicals. The synthesized compounds hold potential for further bio-application studies [48].

**M. Pervaiz** (2024) discusses the significance of metal complexes of Schiff base ligands (Figure-25) derived from thiosemicarbazide and 1,3,4-thiadiazole, which feature the imine ( $-C=N-$ ) functional group. These compounds have gained considerable interest due to their broad applications across material and biological sciences. Their unique properties stem from the involvement of N, S, and O donor atoms, as well as their chelating abilities, low toxicity linked to the  $-N-C=S$  bond, and structural versatility. The Schiff base ligands, typically synthesized from aromatic aldehydes and primary amines, form metal chelates that exhibit remarkable chemical and pharmacological potential [49].

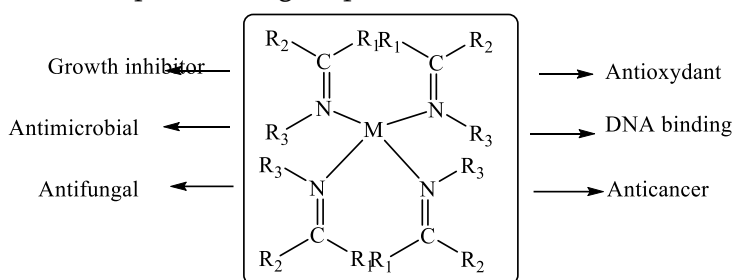


**Figure-25: Schiff base ligands derived from thiosemicarbazide and 1,3,4 thiadiazole and their metal chelation with transition metals, non-metals and f-block metals and their Applications**

## CONCLUSION

In conclusion, 1,3,4-thiadiazole derivatives and their metal complexes have emerged as valuable compounds due to their wide range of biological activities, including antibacterial, antifungal, anti-tubercular, and antiulcer effects. Drugs like methazolamide and acetazolamide highlight the therapeutic potential of this scaffold. While significant progress has been made in exploring their antibacterial and anti-tubercular properties, other therapeutic areas, such as cancer treatment, require more in-depth research. Schiff bases, particularly in metal complexes, further enhance their biological activity, suggesting promising applications in both medicine and catalysis. Continued research is essential to fully uncover the potential of these versatile compounds.

## REFERENCES

- [1] M. M. Imran, Abida1 & A. J. Alsaman "Synthesis and Evaluation of Antimicrobial Activity of Some 2-Morpholinomethylamino-4-(7-Unsubstituted/Substituted Coumarin-3-yl)-6-Chlorosubstitutedphenyl Pyrimidines", Trop. J. Pharm. Res., 15(2),15 (2): 393-404, (2016).
- [2] Cowan, J. A. "Inorganic Biochemistry an Introduction" 2nd. Ed., VCH, New York, (1997).
- [3] Bertini, I.; Gray, H. B.; Stiefel E. I. and Valentine, J. S. " Biological Inorganic Chemistry", University Science Books,( 2007).

- [4] Rehder, D. "Introduction to Bioinorganic Chemistry", University of Lund, May/June Lecture Notes, (2008).
- [5] S. J. Gilani, S. A. Khan, N. Siddiqui, S. P. Verma, P. Mullick and O. Alam, *J. Enzyme Inhib. Med.Chem.*, 26(3), 332 (2011).
- [6] Rosette M. and Malone R. "Bioinorganic Chemistry": A Short Course, John Wiley & Sons,(2002).
- [7] Annapoorani, S., Krishnan, C. J., "Synthesis and spectroscopic studies of trinuclear N4 Schiff base complexes", *Int. J. ChemTech Res.*; 5 (1): 180–185, (2013).
- [8] P. Mullick, S. A. Khan, S. P. Verma and O. Alam, *Bull. Korean Chem. Soc.*, 31(8), 2345, (2010).
- [9] V. Padmavathi, A.V. Nagendra Mohan, P. Thriveni and V. Shazia, *Eur. J. Med. Chem.*, 44(4), 2313, (2009).
- [10] Talesara, G. L.; Kumawat, M., "Synthesis of ethoxyphthalimido derivatized thiadizole assembled imidazolidinone and chloroazetidione systems from common intermediate Schiff's bases and evaluation of their antibacterial activity", *J. Applicable Chem.*, 2, 754, (2013).
- [11] Singh, A. K.; Mishra, G.; Jyoti, K., "Review on biological activities of 1, 3, 4-thiadiazole derivatives", *J. Applied Pharmaceutical Sci.*, 1, 44, (2011).
- [12] Mehta, D.; Taya, P. A review on the various biological activities of thiadiazole. *Int. J. Pharm.&Pharmaceut. Sci.*, 7, 39, (2015).
- [13] Kamal, M.; Shakya, A. K.; Jawaid, T., "1, 3, 4- thiadiazole as antimicrobial agent: A review", *Int. J. Biomedical Res.*, 2, 41, (2011).
- [14] Jain, A. K.; Sharma, S.; Vaidya, A.; Ravichandran, V.; Agrawal, R. K. 1, 3, 4- thiadiazole and its derivatives: A review on recent progress in biological activities. *Chemical Biology & Drug Design* 81, 557, (2013).
- [15] P. Pfeiffer, E. Bucholz, O. Bouer, *J. Prakt. Chem.*; 129, 163, (1931).
- [16] P. Pfeiffer, E. Brieith, E. Lubbe, T. Tsumaki, Leibigs; *J. Ann. Chem.*, 84, 503, (1933).
- [17] P. Pfeiffer, H. Pfitzinger ; *J. Prakt. Chem.*; 145, 243, (1936).
- [18] S. Gaur, *Asian J. Chem.*; (15) 1, 250,(2003).
- [19] M.J. Gemi, C. Biles, B.J. Keiser, S.M. Poppe, S.M. Swaney, W.G. Tarapley, D.L. Romeso, Y. Yage ; *J. Med. Chem.* 43, 1034,(2000).
- [20] (a) C.T. Supuran, M. Barboiu, C. Luca, E. Pop, M.E. Brewster, A. Dinculescu, *Eur. J. Med. Chem.*; 31, 597 (1996). (b) L.H. Abdel-Rahman, R.M. El-Khatib, L.A.E. Nassr, A.M. Abu-Dief, M. Ismael; *Spectrochim. Acta, Part A.*; 117, 366–378 (2014). (c) M. Abu-Dief, L.A.E. Nassr; *J. Iran. Chem. Soc.*; 12, 943–955,(2015). (d) L.H. Abdel-Rahman, A.M. Abu-Dief, R.M. El-Khatib, S.M. Abdel-Fatah; *Bioorg. Chem.*; 69, 140–152 (2016). (e) L.H. Abdel-Rahman, A.M. Abu-Dief, M.O. Aboelez, A.A.H. Abdel-Mawgoud; *J. Photochem. Photobiol., B.*; 170:271–285,( 2017). (f) L.H. Abdel-Rahman, M.S. Adam, A.M. Abu-Dief, H. Moustafa, M. Basha, A.H. Aboria, B. Saad Al-Farhan, H. El-Sayed Ahmed; *Appl. Organomet. Chem.*;32, e4527,(2018). (g) L.H. Abdel-Rahman, A.M. Abu-Dief, M.R. Shehata, F.M. Atlam, A.A. Hassan Abdel-Mawgoud; *Appl. Organomet. Chem.*; e4699 (2019).
- [21] Salimon, J.; Salih, N.; Ibraheem, H.;Yousif, E., "Synthesis of 2-N-Salicylidene-5-(substituted)-1,3,4-thiadiazole as Potential Antimicrobial Agents" *Asian J. Chem*; 22 (7): 5289–5296, (2010).

- [22] Profire,L., Pintilie,O., Sunel,V., Popa,M., Pui,A., Synthesis and Antimicrobial Activity of Some New 1,3,4-Thiadiazole and 1,2,4-Triazole Compounds Having a D,L-Methionine Moiety. *Molecules*, 12(1), 103-113, (2007).
- [23] Ashutosh, B., Ankur,J., Kumar,N.R., Sonia,G. Synthesis, characterization and antimicrobial activity of azol substituted derivatives. *Int J Pharm Sci Drug Res.*, 1(3), 207-210, (2009).
- [24] Pandey,A.; Rajavel, R.; Chandraker, R.; Dash,D. "Synthesis of Schiff Bases of 2-amino-5-aryl-1,3,4 thiadiazole and Its Analgesic, Anti-Inflammatory & Anti-Bacterial Activity",*E-J. Chem.*; 9(4): 2524-2531, (2012).
- [25] Sugumaran, M. and Hemachander, R. Synthesis, Spectral Analysis and Biological Evaluation OF Some Novel Flurobenzothiazole Incorporated 1, 3, 4 - Thiadiazole . *IJPSR*; 3 (6): 1809- 1816, (2012).
- [26] Al-Shammary Kahlan M. A. Synthesis of Some Schiff'sBases Containing 1,3,4-Thiadiazole Ring and TheirProperties as Antioxidants ,*J. Al-Nahrain University*;5(3):49-53, (2012).
- [27] M. Narayana Babu, Bidya Bhushan, V. Madhavan, "Synthesis and Biological activity of some Novel 1, 3, 4-Thiadiazole derivatives", *Int. J. ChemTech Res.*, CODEN (USA): IJCRGG ISSN: 0974-4290, Vol.4, No.1, pp 74-78, (2012).
- [28] Sunny Jalhan, Anil Jindal, Avneet Gupta, Hemraj, "Synthesis, Biological Activities and Chemistry of Thiadiazole Derivatives and Schiffs Bases", *Asian J Pharm Clin Res*, Vol 5, Issue 3, 199-208, (2012).
- [29] Kumar,C.T.; Keshavayya,J.; Rajesh, T. ; Peethambarb, S. K.,Shoukatt Ali, R. A.,"Synthesis, Characterization andAntimicrobial Activity of Heterocyclic Azodyes Derivedfrom Thiadiazole",*ChemSci Trans.*; 2(4):1346-1351, (2013).
- [30] Mahendrasinh M Raj, Hemul V Patel, Lata M Raj, and Naynika K Patel; Synthesis, Characterization and Antimicrobial Evaluation of Some 5-(Substituted)-2-Amino-Thiadiazoles; *RJPBCS Vol.4 Issue 3*, Pp. 721, (2013).
- [31] Naveen Kumar R. M., Shiva Prasad K., Chandan S. and Prasad N., 'Synthesis and characterization of thiadiazole containing Schiff base:Antimicrobial activity', *Scholars Research Library*, ISSN 0975-413X, CODEN (USA): PCHHAXDer *Pharma Chemica*, 6(4):10-14, (2014).
- [32] Siddhanadham Arun Satyadev, "Synthesis, charectrization and biological evaluation of some 1,3,4-thiadiazols Schiff's baese", *Int. J. Current Res.*; Vol. 8, Issue, 08, pp.36100-36106, August, (2016).
- [33] Maddila, S., Gorle,S., Sampath,Ch., Lavanya,P., "Synthesis and anti-inflammatory activity of some new 1,3,4-thiadiazoles containing pyrazole and pyrrole nucleus"*J. Saudi Chem. Society*; 20:S306–S312, (2016).
- [34] Lingareddy C., Phaniband M.A., Asma Tatagar., Shashikant Pattan and Javed Moodi; New metal based antimicrobial and antitubercular agents with their cytotoxicity evaluation derived from 2-amino-5-hydroxyphenyl-1, 3, 4-thiadiazoles; *Int. J. Recent Scientific Res.*; Vol. 7, Issue, 4, pp. 10132-10139, April, (2016).
- [35] Mousa M.N., "Synthesis, Characterization and Evaluation of Antibacterial Activity Of 1,3,4-Thiadiazole Derivatives Containing Schiff Bases", *IJPCBS*; 7(1), 71-76, (2017).
- [36] Emad Yousif , Ahmed Majeed, Khulood Al-Sammarrae, Nadia Salih, Jumat Salimon, Bashar Abdullah, "Metal complexes of Schiff base: Preparation, characterization and antibacterial activity", *Arabian J. Chem.*: 10, S1639–S1644, (2017). [www.ksu.edu.sawww.sciencedirect.com](http://www.ksu.edu.sawww.sciencedirect.com)



- [37] Hassan, F., Hairunisa,N., Mohammed S.A., Yousif,E., A Study on Antitumor Effect of 1,3,4-Thiadiazole Derivatives in Prostate and Breast Cancer Cell Lines (In Vitro)Preprints,; 1-8, (2017).
- [38] Muayed Ahmed Redayan, Wassan Baqir Ali, And Ahmed Mudhafar Mohammed; Synthesis, Characterization and Antibacterial Evaluation of some Novel Benzimidazole Derivatives Containing 1,3,4-thiadiazole moiety; Oriental J. Of Chem.; Vol. 33, No (6): Pg. 3138-3143, (2017).
- [39] Ajit Kumar Pandey, Pranita P Kashyap, Chanchal Deep Kaur, Hemant A Sawarkar, Hemant J Dhongade and Mukesh Kumar Singh, "New 1,3,4-thiadiazole Derivatives Endowed with Analgesic and Anti-inflammatory Activities", Chiang Mai J. Sci.; 45(2), (2018).
- [40] Naeem A. Basher, Ibrahim A. Flifel, Abdulateef A. Mashaf, "Synthesis, Characterization and antibacterial Study of some Complexes Derivatives from 1,3,4-Thiadiazole Schiff base", IOP Conf. Series: Materials Science and Engineering 928,(2020) 052009, y (ISCAU-2020).
- [41] Jadhav R.L., Joshi H.U., Ubale S.B., "Synthesis, characterization &biological activities of some novel Schiff bases derived from 3-acetyl-4-hydroxy-2H-chromen-2-one and 5-(4-substituted phenyl)-1,3,4-thiadiazol-2-amine", J. Interdis. Cyclic Res.; Vol. XIII, Issue X, pp.414-24, 10(2021).
- [42] Jadhav R.L., Joshi H.U., Dr.S.B.Ubale; "Synthesis, characterization &biological activities of some novel Schiff bases derived from 3-acetyl-4-hydroxy-2H-chromen-2-one and 2- amino 5-(4-halo substituted phenyl)-1, 3, 4-thiadiazole", The Int.j. ana. &experi. modal ana., Vol. XIII, Issue XI, pp. 452-64,(2021).
- [43] Hansaraj Joshi, Rajpal Jadhav, Mazahar Farooqui, Shailendrasingh Thakur; "Thermodynamics of the formation of divalent Copper complexes carrying novel Schiff bases in mixed solvent media", J. Interdis. Cycle Res., Vol. XIII, Issue IV, pp.53-61, 4 (2021),
- [44] Hansaraj Joshi, Rajpal Jadhav, Mazahar Farooqui, Shailendrasingh Thakur, "Studies of complexation of trivalent rare earth metal ion Cerium with novel Schiff bases: Thermodynamic Aspect", The Inter. J. ana.& experi. modal ana., Vol. XIII, Issue IV,pp.74-80 4(2021).
- [45] Hansaraj U. Joshi, Rajpal L. Jadhav, Mazahar N. Farooqui, Shailendrasingh V. Thakur, "Complexation of lanthanide metal ions with novel €schiff bases: Thermodynanamic study", J. Advanced Scientific Res. Vol. XIII, Issue IV, pp.133-136, 4/(2021).
- [46] Hansaraj Joshi, Rajpal Jadhav, Mazahar Farooqui, Shailendrasingh Thakur, "Thermodynamics Study of Formation of Zinc Complexes Carrying Novel Schiff Bases In Mixed Solvant Media", J. Advances in Applied Sci.& Tech., Vol. 8|Issue 1| Pp. 91-96, (2022).
- [47] Hansaraj Joshi, Rajpal Jadhav , Gopal Dhond, Ramesh Ware, Shailendrasingh Thakur, "Complexation of Gadolinium with Novel Schiff Bases: Thermodynamic Study", Int J Sci Res Chemi.; 9 (7) : 70-75, (2024).
- [48] Aamer A. Chaab, Mazin N. Mousa, "Synthesis and characterization of new 1, 3, 4-thiadiazole derivatives of naproxen as a potential antineoplastic agent", Oncology and Radiotherapy © 17(8): 274-277 · Research Article, (2023).
- [49] Sajid Ajit Malak, Jamatsing Darbarsing Rajput, & Mustakim Sharifl, "Design, synthesis, spectral analysis, and biological evaluation of Schiff bases with a 1,3,4-thiadiazole moiety as an effective inhibitor against bacterial and fungal strains", Eur. J. Chem. 14 (4) ,466-472, (2023).

- [50] I. Q. Mahmood Al-araj, Rana A. Saeed , Linda R. Abdul-Raheem , Amena A. Ahmed, “Synthesis of Some New 1,3,4-Thiadiazole Derivatives Derived from Cholic Acid and Evaluation of their Biological Activity”, Al-araj IQM et al. JOTCSA.;11(2):425-432, (2024).
- [51] M. Pervaiz, R. Quratulain, A. Ejaz, M. Shahin, Z. Saeed, S. Nasir, R. R. M.Khan, A. Ashraf, S. Ullah, U. Younas,, “Thiosemicarbazides, 1,3,4 thiadiazole Schiff base derivatives of transition metal complexes as antimicrobial agents, Inorg. Chem. Commu., Vol.160, 111856, ISSN 1387-7003,(2024). <https://doi.org/10.1016/j.inoche.2023.111856>,

## Magnetically Active Silica Sulfuric Acid: An Efficient, Heterogeneous and Reusable catalyst for Synthesis of Quinoxalines at Room-Temperature

Pankaj V. Patale, Jaishri L. Somawanshi, Sushil R. Mathapati\*

Department of Chemistry, Shri Madhavrao Patil Mahavidyalaya, Murum-413605, Affiliated to Dr. B. A. M. University, Aurangabad, Dist.- Osmanabad, Maharashtra, India

E-mail: [sushilrswami@gmail.com](mailto:sushilrswami@gmail.com)

### ABSTRACT

In presented work, we have reported highly proficient, environmental benign, Fe<sub>3</sub>O<sub>4</sub>@silica sulfuric acid catalyzed protocol for the synthesis 2, 3-diphenyl quinoxalines via condensation of o-phenylenediamine with  $\alpha$ -diketones. Surface modified silica with sulfuric acid and magnetically activated it through the adsorption of Fe<sub>3</sub>O<sub>4</sub> nanoparticles offered outstanding catalytic efficiency at room temperature and it sustained up to six cycles. The methodology boasts a hassle-free catalyst preparation and separation process, operates under energy-conserving conditions, yields a commendable (96-86%) output of the targeted moieties, and exhibits catalyst recyclability. These appealing features position it as a superior and eco-friendly alternative to traditional methods for synthesizing quinoxalines.

**Keywords:** Diamine, Diketones, Quinoxaline, Fe<sub>3</sub>O<sub>4</sub>@silica sulfuric acid catalyst, Room temperature, Recyclability.

### INTRODUCTION

It is widely recognized that a broad spectrum of synthetic compounds, natural products, agrochemicals, and medicinal medications includes heterocyclic moieties. Considering the varied array of heterocyclic units, quinoxalines stand out as a pivotal scaffold found in a multitude of biologically and pharmaceutically significant compounds. [1]. Quinoxaline derivatives have broad spectrum of therapeutical activities similar to antiviral [2], antibacterial and antifungal [3], antioxidant and antiproliferative [4], antineoplastic [5], antitumor [6-8], antitubercular agent [9,10], antimicrobial [11] and anticancer [12,13]. These hetero moieties have been also used in electroluminescent devices [14] and organic semiconductors [15].

Owing to such diverse applications, synthesis of quinoxaline has grabbed attention of researchers. Several synthetic routes for quinoxalines have been established. Primarily, quinoxalines were prepared through cyclo-condensation of 1,2-diaminobenzene with several organic moieties such as  $\alpha$ -ketoesters or  $\alpha$ -ketoacids [16],  $\alpha$ -hydroxy ketone [17], vicinal diols [18], dimethyl and diethyl acetylene dicarboxylate [19],  $\alpha$ -haloketone [20], epoxides [21], 1,2-diketones [22] etc.

Among these approaches, condensation of 1,2-diaminobenzene with 1,2-diketones is the most attractive and frequently used route. This synthetic approach of quinoxaline has included numbers of catalysts like silica-bonded S-sulfonic acid (SSA), ceric ammonium nitrate (CAN), Ga(OTf)<sub>3</sub>, nano-TiO<sub>2</sub>, ionic liquid such as ([Hbim]BF<sub>4</sub>), Ga(ClO<sub>4</sub>)<sub>3</sub>, CeCl<sub>3</sub>·7H<sub>2</sub>O, DABCO, graphite, manganese ferrite (MnFe<sub>2</sub>O<sub>4</sub>) nanoparticles, cerium-oxide nanoparticles [23-25]. Furthermore, solid phase and microwave assisted protocols are also described for quinoxaline synthesis [26, 27].

On the other hand, among these methods several catalytic processes were comes with one or more limitations resemble to rough reaction parameters, inadequate yields, required toxic and expensive catalysts or components, use of polar solvent leading to tedious work-up processes. To overcome such shortcomings, researchers diverted towards eco-friendly reactions, use of greener solvents or applying efficient and easy available reactants and catalysts, process under mild circumstances. Accordingly, the invention of resourceful and eco-friendly approach for the production of quinoxalines is quite exceedingly preferred. Recently, solid-supported reagents have been developed by many researchers and exploited them in plenty of organic transformations. Usually, acid functionality supported over the surface of silica gel such as silica sulfuric acid, SiO<sub>2</sub>-HClO<sub>4</sub>, SiO<sub>2</sub>-NaHSO<sub>4</sub> [28-30] etc. has significant contribution in organic synthesis owing to their notable benefits such as high surface area, outstanding efficiency, stability, recyclability, nontoxic and effortless preparation and safe handling.

Owing to this, recently we have reported polyphosphoric acid functionalized silica (SiO<sub>2</sub>@PPA) for quinoxalines synthesis [31]. We have extended our work in the direction of design the efficient protocols for the production of organic moieties using magnetically active and heterogeneous catalyst [32-35]. Herein, we have prepared magnetically active silica sulfuric acid (Fe<sub>3</sub>O<sub>4</sub>@SiO<sub>2</sub>-SO<sub>3</sub>H) and investigated the catalytic efficiency for quinoxalines synthesis from diamine and diketones. Literature revealed that Fe<sub>3</sub>O<sub>4</sub>@SiO<sub>2</sub>-SO<sub>3</sub>H catalyst has performed as heterogeneous, recyclable solid catalyst and it produced high yield of products under ambient conditions [36]. Additionally, it is very easy to prepare from silica powder and sulfuric acid under normal reaction parameters and it transferred in to magnetically active by adoption of Fe<sub>3</sub>O<sub>4</sub> nano particles. As per my best knowledge, described methodology has not reported earlier. It is observed that prepared catalyst showed remarkable efficiency for current transformation and reported 96-86% yield of target molecule and it sustain catalytic efficiency up to 6th cycle. Effect of solvent, effect of temperature and amount of catalyst have been well illustrated along with confirmation of role of catalyst through probable mechanism.

## METHODS AND MATERIAL

### A. Materials

Silica powder (70-230 mesh) and H<sub>2</sub>SO<sub>4</sub> were procured from Sigma Aldrich. All reactants (Diamines/Diketones) and solvents (CHCl<sub>3</sub>, ethyl acetate, ethanol, double distilled water) were sourced from a commercial chemical supplier and employed without recrystallization and distillation.

### B. Preparation of Fe<sub>3</sub>O<sub>4</sub> Nanoparticles [37]

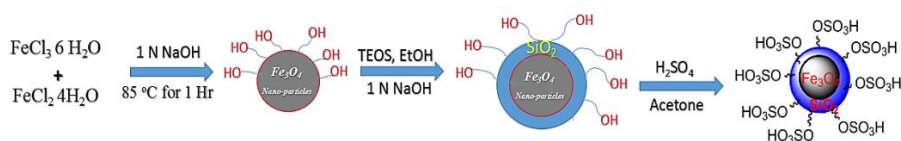
Fe<sub>3</sub>O<sub>4</sub> nano-particles were prepared via improved chemical co-precipitation method. According to this method, Add FeCl<sub>3</sub> 6 H<sub>2</sub>O (6.66gm) and FeCl<sub>2</sub> 4H<sub>2</sub>O (3.66gm) conical flask containing 30 ml of distilled water and heating at 85 oC for 1 Hr. Then add 20 ml of 1 N solution of NaOH drop wise and vigorous mechanical stirring for 1 hr. After the 1 hr stirring color of bulk solution turned to black. The precipitated particles were washed five times with hot water and separated by magnetic decantation. Finally, magnetic NPs of Fe<sub>3</sub>O<sub>4</sub> were dried under vacuum at 60 °C for 12 h.

### C. Preparation of Silica Coated Magnetic Nanoparticles, Fe<sub>3</sub>O<sub>4</sub>@Silica [38]

The synthesized Fe<sub>3</sub>O<sub>4</sub> nanoparticles (2 gm) were diluted with 120 mL water and 450 mL ethanol. The suspension was dispersed under vigorous mechanical stirring for 4 hr at room temperature. Meanwhile add sodium hydroxide 1 N solution (10 mL) was added to the suspension. Then, 2 mL Tetraethyl orthosilicate (TEOS) was slowly added to this dispersion and continue the stirring for 12 hr. The silica was formed on the surface of magnetite nanoparticles through hydrolysis and condensation of TEOS. The coated particles were finally separated from the liquid by a magnetic decantation and washed several times with deionized water. Then dried under vacuum at 60°C overnight.

### D. Preparation of Fe<sub>3</sub>O<sub>4</sub>@Silica Sulfuric Acid [39]

Fe<sub>3</sub>O<sub>4</sub>@Silica Sulfuric Acid were prepared by adding 20 mL of acetone containing 2 mL of H<sub>2</sub>SO<sub>4</sub> dropwise to a solution of 10 gm Fe<sub>3</sub>O<sub>4</sub>@SiO<sub>2</sub> in 60 mL acetone, then stirring for four hours at 30 °C. The paste was dried in the oven at 100 °C for 24 h to remove the solvent. The dried solid was washed several times with water to get rid of the excess acid which was not adsorbed on the surface.



Scheme 1. Preparation of Fe<sub>3</sub>O<sub>4</sub>@silica sulfuric Acid catalyst.

### E. Optimized procedure for quinoxalines synthesis using Fe<sub>3</sub>O<sub>4</sub>@SiO<sub>2</sub>-SO<sub>3</sub>H

In a 100 mL round bottom flask, diamine (1 mmol) and  $\alpha$ diketones (1 mmol) were combined in 10 mL EtOH in presence of 10 wt. % Fe<sub>3</sub>O<sub>4</sub>@SiO<sub>2</sub>-SO<sub>3</sub>H, was magnetically stirred at room temperature. Reaction progress was monitored by TLC, and upon completion, the vessel was extracted with ethyl acetate. The catalyst was separated through simply using external strong magnet, catalyst washed thrice with 10 mL of ethyl acetate each time, and the combined washings were added to the ethyl acetate extract. Evaporation under vacuum on a rotary evaporator yielded the crude solid product, which was purified into a pure quinoxaline derivative through recrystallization and column chromatography.

### F. Spectral analysis of some reprehensive compounds [22, 40-44].

#### 2,3-Diphenylquinoxaline (3a, Scheme 2)

White solid; mp 128–129 oC; IR (KBr in cm<sup>-1</sup>) 3057, 1602, 1442, 1346, 1246, 852, 767, 698; <sup>1</sup>HNMR (CDCl<sub>3</sub>, in  $\delta$  ppm): 8.19 (m, 2H), 7.76 (m, 2H), 7.45 (m, 4H), 7.35 (m, 6H); <sup>13</sup>C NMR (100 MHz, CDCl<sub>3</sub>, in ppm): 154.6, 142.4, 141.3, 132.1, 130.4, 129.7, 129.1, 128.8. MS (m/z): 284.09.

#### 6-Methyl-2,3-diphenylquinoxaline (3b, Scheme 2)

Cream solid; mp 132–133 oC; IR (KBr in  $\text{cm}^{-1}$ ) : 3057, 2941, 1618, 1446, 1342,1246, 817, 773, 702;  $^1\text{H}$ NMR ( $\text{CDCl}_3$ , in  $\delta$  ppm): 8.09 (d, 1H), 8.00 (s, 1H), 7.69 (d, 1H), 7.52 (m, 4H), 7.31 (m, 6H), 2.65 (s, 3H);  $^{13}\text{C}$  NMR (100 MHz,  $\text{CDCl}_3$ , in PPM ): 163.6, 157.8, 155.9, 154.5, 153.2, 148.1, 145.3, 144.6, 142.2, 141.4, 140.1, 139.5,137.1, 135.4, 133.2, 130.6, 129.3, 128.7, 128.1, 127.8, 23.8. MS (m/z): 296.53.

*6-Chloro-2,3-diphenylquinoxaline (3e, Scheme 2)*

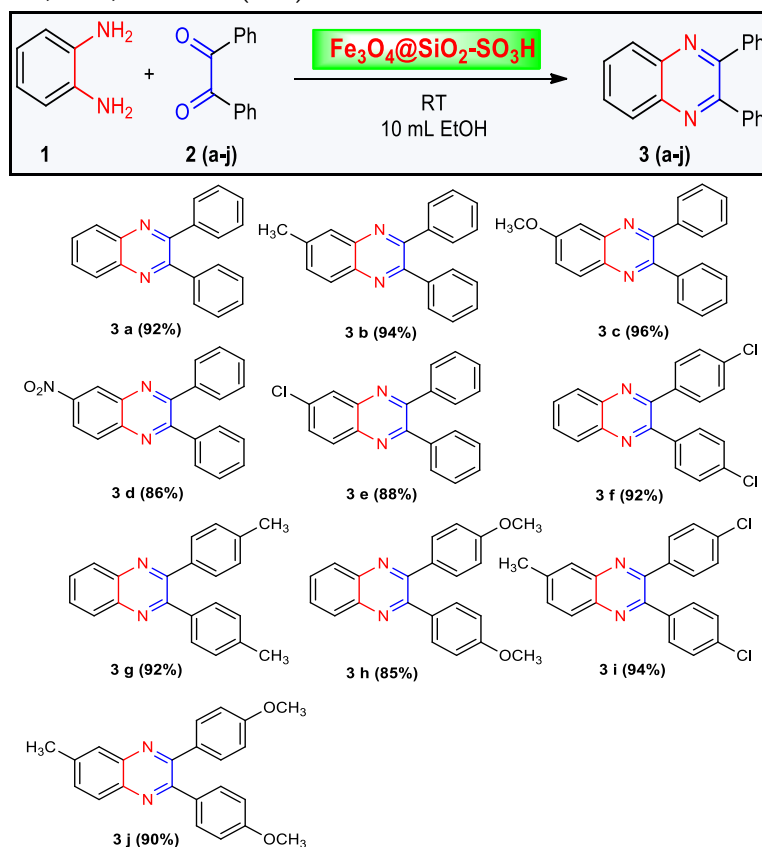
Pale yellow solid; mp 118–119 oC; IR (KBr in  $\text{cm}^{-1}$ ) : 3059, 1602, 1450, 1340, 1246,804, 763, 696;  $^1\text{H}$ NMR ( $\text{CDCl}_3$ , in  $\delta$  ppm): 8.17 (s, 1H), 8.11 (d,1H), 7.98 (d, 1H), 7.68 (m, 4H), 7.51 (m, 4H), 7.34 (m, 2H);  $^{13}\text{C}$ NMR (100 MHz,  $\text{CDCl}_3$ , in PPM) 154.4, 153.7, 142.2, 139.1, 139.0, 138.8, 136.1, 136.0, 135.3, 130.6, 130.1, 129.8. MS (m/z): 316.08.

*2,3-Bis(4-methoxyphenyl)quinoxaline (3h, Scheme 2)*

Yellow solid; mp 145–148 oC; IR (KBr in  $\text{cm}^{-1}$ ) : 2958, 1602, 1458, 1394, 1344, 1294, 1174, 835, 759, 698;  $^1\text{H}$ NMR ( $\text{CDCl}_3$ , in  $\delta$  ppm): 8.13 (m,2H), 7.72 (m, 2H), 7.47(d, 4H), 6.94(m, 4H), 3.85 (s, 6H);  $^{13}\text{C}$  NMR (100 MHz,  $\text{CDCl}_3$ , in PPM): 159.7, 153.1, 141.2, 132.2, 130.4, 128.7, 126.5, 114.6, 55.8, 55.4; MS (m/z): 341.09.

*2,3-bis(4-Methoxyphenyl)-6-methylquinoxaline (3j, Scheme 2)*

White solid; mp 124–127 oC; FT-IR (KBr, in  $\text{cm}^{-1}$ ): 2939, 1681, 1599, 1160, 839;  $^1\text{H}$ NMR ( $\text{CDCl}_3$ , in  $\delta$  ppm): 7.91 (m, 1H), 7.65–7.45 (m, 6H), 6.90–6.80 (m, 4H), 3.85 (s, 6H), 2.84 (s, 3H);  $^{13}\text{C}$ NMR (100 MHz,  $\text{CDCl}_3$ , in PPM): 160.6, 160.3, 152.4, 151.3, 141.0, 140.3, 137.3, 132.1, 131.4, 131.1, 129.4, 129.0, 126.8, 114.0, 113.4, 55.4, 55.3, 22.0. MS (m/z): 356.16



**Scheme 2:  $\text{Fe}_3\text{O}_4@\text{SiO}_2\text{-SO}_3\text{H}$  catalyzed synthesis of quinoxalines at room temperature.**

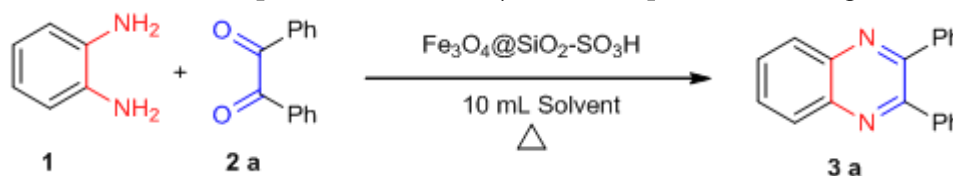
## RESULTS AND DISCUSSION

We have planned to evaluate catalytic efficiency of magnetically active silica sulfuric acid. Our research started with preparation of catalyst, it was synthesized followed by procedure reported in literature. After the successful synthesis of catalyst, we have evaluated the catalytic efficiency of Fe<sub>3</sub>O<sub>4</sub>@SiO<sub>2</sub>-SO<sub>3</sub>H for the quinoxalines production. Initially, we have optimized reaction parameters to set the most appropriate reaction conditions. This was done over the model reaction as ortho-phenyldiamine (1 mmol) stirred with benzil (1 mmol) and catalyst in 10 mL solvent. The obtained outcomes are précised in table 1.

To attain standard reaction parameter, analysis of solvents, temperature and amount of catalyst were important aspects. We have evaluated all these parameters and observed outcomes are displayed in table 1. Primarily, we have checked the effect of solvent on the model reaction conducted in presence of 10 wt. % Fe<sub>3</sub>O<sub>4</sub>@SiO<sub>2</sub>-SO<sub>3</sub>H catalyst at room temperature. The obtained results indicated that ethanol has been appropriate solvent for the planned reaction. It reported 92 % yield of quinoxaline within 2 h (Table 1, entry 1) stirring at room temperature, while other solvents like acetonitrile (CH<sub>3</sub>CN), methanol, THF, DCM and water (Table 1, entries 1-6) were failed to compete the result of ethanol (EtOH) under prescribed reaction parameter. Furthermore, to study the role of temperature we have carried out same reaction at varying temperature from room temperature to 40 oC, 60 oC and 80 0C. Entries 7 to 9 showed that increasing the temperature up to 40 oC and 60 oC was suitable for current transformation while negative impact on outcome of reaction were observed on rising the temperature at 80 0C. It may due to the decomposition of reactants or evaporation of solvent at higher temperature. By means of energy economy, we preferred to carry out reaction at room temperature rather than at 40 oC or 60 oC.

Meanwhile, the amount of catalyst is also an important phase to outline optimized conditions and achieve most appropriate scheme for quinoxaline synthesis from diamine and benzil at room temperature. The proposed reaction was accompanied with loading of altering amount of Fe<sub>3</sub>O<sub>4</sub>@SiO<sub>2</sub>-SO<sub>3</sub>H catalyst. Results expressed that the lower amounts like 7.5 wt. % and 5 wt. % (Table 1, entries 12 and 13) of catalyst was insufficient to produce remarkable yield of target molecule while higher amount as 12 wt. % of Fe<sub>3</sub>O<sub>4</sub>@SiO<sub>2</sub>-SO<sub>3</sub>H has not displayed enhancement in outcome of studied transformation (Table 1, entries 10). Similarly, further addition in catalytic amount (15 wt. %) lead to negative impact that produced only 82% yield (Table 1, entry 11). After the investigation of these factors, we finalized as 10 wt. % was appropriate amount of Fe<sub>3</sub>O<sub>4</sub>@SiO<sub>2</sub>-SO<sub>3</sub>H to produce outstanding yield (92%) of quinoxaline, via 2 h stirring of reactants in 10 mL ethanol at room temperature.

**Table 1. Optimization of reaction parameters for the synthesis of quinoxaline using Fe<sub>3</sub>O<sub>4</sub>@SiO<sub>2</sub>-SO<sub>3</sub>H.**



Entry	Fe <sub>3</sub> O <sub>4</sub> @SiO <sub>2</sub> -SO <sub>3</sub> H amount	Solvent	Temperature (°C)	Reaction Time <sup>(b)</sup> (h)	Yield <sup>(c)</sup> (%)
1	10 wt.%	Ethanol	RT	2	92
2	10 wt.%	CH <sub>3</sub> CN	RT	3	80
3	10 wt.%	Methanol	RT	3	82
4	10 wt.%	THF	RT	10	62
5	10 wt.%	DCM	RT	10	60
6	10 wt.%	Water	RT	15	55
7	10 wt.%	Ethanol	40	2	92
8	10 wt.%	Ethanol	60	2	92
9	10 wt.%	Ethanol	80	2	80
10	12 wt.%	Ethanol	RT	2	92
11	15 wt.%	Ethanol	RT	2	82
12	7.5 wt.%	Ethanol	RT	4	80
13	5 wt.%	Ethanol	RT	6	65

<sup>a</sup>Reaction conditions:Diamine (1 mmol), benzil (1 mmol), solvent 10 mL, Fe<sub>3</sub>O<sub>4</sub>@SiO<sub>2</sub>-SO<sub>3</sub>H catalyst.  
<sup>b</sup>monitored by TLC; <sup>c</sup>Isolated yield.

Having the finest conditions for the model reaction, we examined the scope using different substrates and synthesised ten derivatives of quinoxaline, the results are shown in scheme 2. We found that the procedure has been applied to quinoxalines, which yields uniformly in the very good to excellent range (96-86%) of target molecule. A variety of structural types and functional groups were well-tolerated. Electron donating and electron withdrawing moieties were accelerated to the reaction and conserved throughout the reaction. All synthesized compounds are reported. We hope designed protocol may be quite fit to large production of quinoxaline derivatives. The structural conformation of prepared quinoxalines was done through spectral analysis (IR, NMR, Mass) and analytical data that over and done via compared with literature data [22, 40-44].

#### A. Probable mechanism for the quinoxaline synthesis

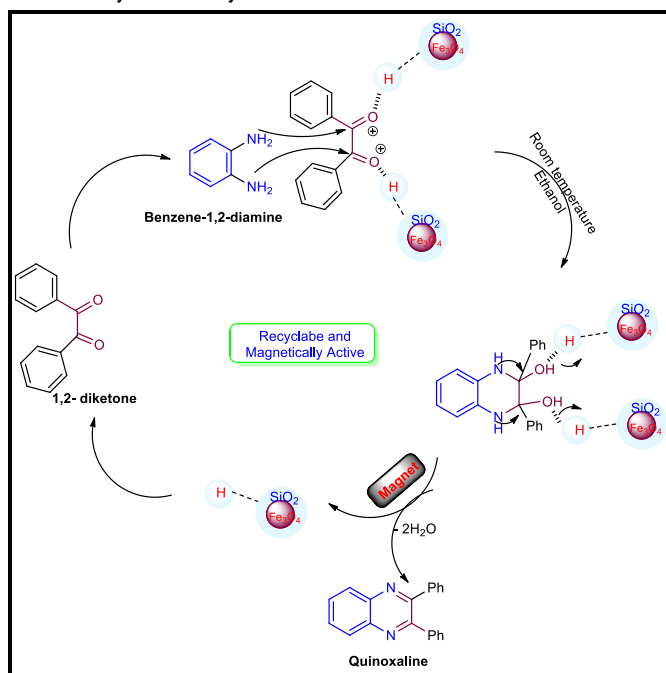
The catalytic action can be illustrated through mechanism. Herein, we dispatched the probable mechanism for quinoxaline production attending with Fe<sub>3</sub>O<sub>4</sub>@SiO<sub>2</sub>-SO<sub>3</sub>H catalyst in scheme 3. The reaction was expected to follow the acid-catalyzed condensation reaction and corresponding to mechanism reported in literature [22]. From this, we clearly concluded that, reported catalyst has played vial role in activation of carbonyl groups of benzil, which fascinated attack of diamine, again catalyst supported to dehydration and cyclisation to get final product.

#### B. Recyclability test of Fe<sub>3</sub>O<sub>4</sub>@SiO<sub>2</sub>-SO<sub>3</sub>H catalyst

To study the recyclability of prepared catalyst we have demonstrated model reaction attending optimized parameters. After the successful conversion, the Fe<sub>3</sub>O<sub>4</sub>@SiO<sub>2</sub>-SO<sub>3</sub>H was isolated via using external magnet. Recovered catalyst was washed with water and dried at 100 °C for 5 h in vacuum oven.



The dried  $\text{Fe}_3\text{O}_4@\text{SiO}_2\text{-SO}_3\text{H}$  was reused for next run of model reaction, this practice has been continued up to the noticeable defeat in catalytic activity. We found that  $\text{Fe}_3\text{O}_4@\text{SiO}_2\text{-SO}_3\text{H}$  has effectively catalyzed to the current transformation up to six cycle as shown in Figure 1. From this exercise, we concluded as the investigated catalyst was capable to produce notable results without any alternation in product and stability of catalyst.



Scheme 3. Possible mechanism for quinoxaline synthesis using  $\text{Fe}_3\text{O}_4@\text{SiO}_2\text{-SO}_3\text{H}$  catalyst.

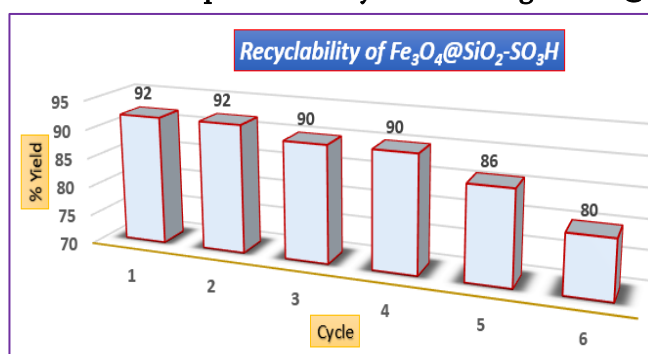


Figure 1. Recyclability of  $\text{Fe}_3\text{O}_4@\text{SiO}_2\text{-SO}_3\text{H}$  catalyst for quinoxaline synthesis.

## CONCLUSION

In this study, we present an efficient pathway for synthesizing quinoxalines through the cyclocondensation reaction of diamine and benzil derivatives at room temperature. The reaction was successfully catalyzed by 10 wt. %  $\text{Fe}_3\text{O}_4@\text{SiO}_2\text{-SO}_3\text{H}$ , demonstrating remarkable yields of quinoxalines under optimized conditions. The  $\text{Fe}_3\text{O}_4@\text{SiO}_2\text{-SO}_3\text{H}$  catalyst was synthesized using readily available materials and through a well-established procedure. The prepared catalyst exhibited notable catalytic activity at room temperature, maintaining its efficiency for up to the sixth run in the present transformation. Additionally,  $\text{Fe}_3\text{O}_4@\text{SiO}_2\text{-SO}_3\text{H}$  offered several advantages, including its

heterogeneous nature, straightforward workup process, and operability even at room temperature. Consequently, we propose an effective, high-yield protocol that can be considered as a greener alternative to traditional approaches.

### Acknowledgment

Authors would like to thank the organization and Principals of corresponding institutions for their assistance regarding laboratory facilities and encouragement. We also grateful to IICT Hyderabad for providing characterization facility.

### REFERENCES

- [1] L. E. Seitz, W. J. Suling, R. C. Reynolds, *J. Med. Chem.* 45, 5604 (2002). <https://doi.org/10.1021/jm020310n>
- [2] M. A. Henen, S. A. A. El Bialy, F. E. Goda, M. N. A. Nasr, H. M. Eisa, *Med. Chem. Res.* 21, 2368 (2012). <http://dx.doi.org/10.1007/s00044-011-9753-7>
- [3] A. Carta, P. Sanna, L. Gherardini, D. Usai, S. Zanetti, *IL Farmaco* 56, 933 (2001). [https://doi.org/10.1016/S0014-827X\(01\)01161-2](https://doi.org/10.1016/S0014-827X(01)01161-2)
- [4] K. S. Mani, B. Murugesapandian, W. Kaminsky, S. P. Rajendran, *Tetrahedron Lett.* 59, 2921 (2018). <https://doi.org/10.1016/j.tetlet.2018.06.035>
- [5] H. W. Yoo, M. E. Suh, S. W. Park, *J. Med. Chem.* 41, 4716 (1998). <https://doi.org/10.1021/jm970695n>
- [6] C. Urquiola, D. Gambino, M. Cabrera, M. L. Lavaggi, H. Cerecetto, M. Gonzalez, A. L. De Cerain, A. Monge, A. J. C-Filho, M. H. Torre, *J. Inorg. Biochem.* 102, 119 (2008). <https://doi.org/10.1016/j.jinorgbio.2007.07.028>
- [7] P. Corona, A. Carta, M. Loriga, G. Vitale, G. Paglietti, *Eur. J. Med. Chem.* 44, 1579 (2009). <https://doi.org/10.1016/j.ejmech.2008.07.025>
- [8] C. D. Masquefa, G. Moarbess, S. Khier, N. David, S. G. Paniagua, F. Bressolle, F. Pinguet, P. A. Bonnet, *Eur. J. Med. Chem.* 44, 3406 (2009). <https://doi.org/10.1016/j.ejmech.2009.02.007>
- [9] A. Jaso, B. Zarranz, I. Aldana, A. Monge, *J. Med. Chem.* 48, 2019 (2005). <https://doi.org/10.1021/jm049952w>
- [10] M. S. Veliz, S. P. Silanes, E. Torres, E. M. Viguri, *Bioorg. Med. Chem. Lett.* 26, 2188 (2016). <https://doi.org/10.1016/j.bmcl.2016.03.066>
- [11] M. M. Ali, M. M. Ismail, M. S. El-Gaby, M. A. Zahran, Y. A. Ammar, *Molecule* 5, 864(2000). <https://doi.org/10.3390/50600864>
- [12] F. A. R. Rodrigues, I. da S. Bomfim, B. C. Cavalcanti, C. O. Pessoa, J. L. Wardell, S. M. Wardell, A. C. Pinheiro, C. R. Kaiser, T. C. Nogueira, J. N. Low, L. R. Gomes, M. V. de Souza, *Bioorg. Med. Chem. Lett.* 24, 934 (2014). <https://doi.org/10.1016/j.bmcl.2013.12.074>
- [13] S. Piras, M. Loriga, G. Paglietti, *IL Farmaco* 57, 1 (2002). [https://doi.org/10.1016/S0014-827X\(01\)01159-4](https://doi.org/10.1016/S0014-827X(01)01159-4)
- [14] B. Bachowska, G. Matusiak, *Chem. Heterocyclic Comp.* 45, 80 (2009). <https://doi.org/10.1007/s10593-009-0229-3>

- [15] D. O'Brien, M. S. Weaver, D. G. Lidzey, D. D. Bradley, *App. Phys. Lett.* 69, 881 (1996).  
<https://doi.org/10.1063/1.117975>
- [16] D. P. Singh, S. K. Deivedi, S. R. Hashim, R. G. Singhal, *Pharmaceuticals* 3, 2416(2010).  
<https://doi.org/10.3390/ph3082416>
- [17] S. A. Raw, C. D. Wilfred, R. J. K. Taylor, *Org. Biomol. Chem.* 2, 788 (2004).  
<https://doi.org/10.1039/b315689c>
- [18] C. S. Cho, S. G. Oh, *Tetrahedron Lett.* 47, 5633 (2006). <https://doi.org/10.1016/j.tetlet.2006.06.038>
- [19] Q. Y. Zhang, B. K. Lui, W. Q. Chen, Q. Wu, X. F. Lin, *Green Chem.* 10, 972 (2008).  
<https://doi.org/10.1039/B806960C>
- [20] K. Kumar, S. R. Mudshinge, S. Goyal, M. Gangar, V. A. Nair, *Tetrahedron Lett.* 56, 1266 (2015).  
<https://doi.org/10.1016/j.tetlet.2015.01.138>
- [21] S. Antoniotti, E. Dunach, *Tetrahedron Lett.* 43, 3971, (2002). [https://doi.org/10.1016/S0040-4039\(02\)00715-3](https://doi.org/10.1016/S0040-4039(02)00715-3)
- [22] U. P. Tarpada, B. B. Thummar, D. K. Raval, *Arabian J. Chem.* 10, s2902 (2017).  
<https://doi.org/10.1016/j.arabjc.2013.11.021>
- [23] A. Dandia, R. Singh, J. Joshi, S. Maheshwari, *Eur. Chem. Bull.* 2, 825 (2013).  
<http://www.eurchembull.com/.../pdf>
- [24] G. Brahmachari, S. Laskar, P. Barik, *RSC Adv.* 3, 14245 (2013). <https://doi.org/10.1039/C3RA41457D>
- [25] N. Edayadulla, Y. R. Lee, *RSC Adv.* 4, 11459 (2014). <https://doi.org/10.1039/C4RA00717D>
- [26] J. Y. Liu, J. Liu, J. Wang, D. Jiao, H. Liu, *Synth. Commun.* 40, 2047 (2010).  
<https://doi.org/10.1080/00397910903219401>
- [27] J. Zhou, G. Gong, S. Zhi, X. Duan, *Synth. Commun.* 39, 3743 (2009).  
<https://doi.org/10.1080/00397910902838862>
- [28] P. Salehi, M. Ali Zolfigol, F. Shirini, M. Baghbazadeh, *Curr. Org. Chem.* 10, 2171 (2006).  
<http://dx.doi.org/10.2174/138527206778742650>
- [29] P. K. Mandal, A. K. Misra, *Lett. Org. Chem.* 3, 848 (2006).  
<https://doi.org/10.2174/157017806779116978>
- [30] C. Ramesh, J. Banerjee, R. Pal, B. Das, *Adv. Synth. Catal.* 345, 557 (2003).  
<https://doi.org/10.1002/adsc.200303022>
- [31] U. N. Pol., R. P. Kagne, M. B. Swami, T. E. Khatke, S. R. Mathapati, *Res. J. Chem. Environ.* 28 (7), 42 (2024). <https://doi.org/10.25303/287rjce042049>
- [32] S. R. Mathapati, R. C. Alange, C. B. SherinMol, S. S. Bhande, A. H. Jadhav, *Res. on Chem. Intermed.* 48, 4901 (2022). <https://doi.org/10.1007/s11164-022-04852-0>
- [33] V. B. Suryawanshi, A. S. Bondge, J. K. Dawle, S. R. Mathapati, *Poly. Arom. Comp.* 42, 4404 (2022).  
<https://doi.org/10.1080/10406638.2021.1892777>
- [34] A. S. Patki, D. B. Muley, R. P. Kagne, S. R. Mathapati, *Russ. J Org. Chem.* 58, 1455 (2022).  
<https://doi.org/10.1134/S1070428022100116>
- [35] S. R. Mathapati, M. B. Swami, J. K. Dawle, N. V. Ghule, A. H. Jadhav, *Der PharmaChemica* 9, 1 (2017). <https://www.researchgate.net/profile/Sushil-Mathpati/publication/326829788>

- [36] F. M. Mehdi, Mini-Reviews in Organic Chemistry, 14, 122 (2017). DOI: 10.2174/1570193X14666170206144158
- [37] K. D. Kim, S. S. Kim, Y. H. Choa, H. T. Kim, J. Ind. Eng. Chem., 13, 1137 (2007). <http://kiss.kstudy.com/thesis/thesis-view.asp?key=2655358>
- [38] Y. H. Deng, C. C. Wang, J. H. Hu, W. L. Yang, S. K. Fu, Surf. A: Physicochem. Eng. Asp. 262, 87 (2005). doi: 10.1016/j.colsurfa.2005.04.009
- [39] N. R. E. Radwan, M. Hagar, T. H. Afifi, F. Al-wadaani, R. M. Okasha, Catalysts, 8, 1 (2018). doi:10.3390/catal8010036
- [40] A. H. D. Seyed, M. Razieh, H. M. Mohammad, Org. Prepar. and Proce. Inter. 50, 301 (2018). <https://doi.org/10.1080/00304948.2018.1462056>
- [41] S. V. More, M. N. V. Sastry, C. F. Yao, Green Chem. 8, 91 (2006). <https://doi.org/10.1039/B510677J>
- [42] E. Kolvari, M. A. Zolfigol, M. Peiravi, Green Chem. Lett. and Rev. 5, 155 (2012). <https://doi.org/10.1080/17518253.2011.606849>
- [43] A. Khorramabadi-zad, M. Azadmanesh, S. Mohammadi, S. Afr. J. Chem. 66, 113 (2013). <https://www.ajol.info/index.php/sajc/article/view/123146>
- [44] S. V. Shelke, S. T. Dhumal, A. Y. Karale, T. R. Deshmukh, M. K. Patil, Synth. Comm. 52, 597 (2022). <http://dx.doi.org/10.1080/00397911.2022.2039711>

# Machine Learning for Predictive Materials Discovery and Design

Dr. Rajeshwar G. Joshi

Department of Computer Science, Yogeshwari Mahavidyalaya, Ambajpgai, Maharashtra, India

Email-Id: [yma.joshi@gmail.com](mailto:yma.joshi@gmail.com)

## ABSTRACT

In fact, the synergy between ML and materials science has led to some genuinely transformative advances in predictive materials discovery and design. The paper outlines how ML can be married with materials science to accelerate discovery and optimization of novel materials. It considers different methods, including data-driven modelling, high-throughput screening, and optimization algorithms. The case studies described here highlight how these techniques are being put into practice in predicting the properties of materials as well as steering experimental campaigns. The challenges and future directions in this evolving field are also discussed

**Keywords:** Machine Learning, Predictive Modeling, Materials Science, High-Throughput Screening, Data Integration

## INTRODUCTION

## PREFACE

### 1.1 Background

The historical discovery process is basically extensive experimental work, which could be time-consuming and expensive. Recent advances in machine learning open up new opportunities for streamlining and accelerating this process by making predictions about material properties and guiding choices in design decisions.

### 1.2 Objectives

This paper aims to:

Explain how ML methods could speed up material discovery and design.

- Discuss different ML techniques applied in this area.
- Reflect on real-world applications and case studies.
- Identification of problems and future research directions.

## MACHINE LEARNING TECHNIQUES IN MATERIALS SCIENCE

### 2.1 Data-Driven Materials Design

Predictive Modeling Overview of regression models, neural networks, and ensemble methods for prediction from compositional and structural data.

Case Study: Prediction of mechanical properties of alloys by using ML models.

### 2.2 High-Throughput Screening

Automated data collection: Techniques for the automation of experiments and data collection.

Data analysis and integration\*\*: Techniques for combining high-throughput experimental data with models of machine learning for early material discovery.

Case Study: Catalyst Discovery through the Use of High Throughput Screening.

### 2.3 Optimizing Algorithms

Optimisation Techniques: genetic algorithms, simulated annealing, and other optimization techniques will be used to obtain optimum composition and processing conditions.

Case Study: Optimal Polymer Blends for a Specific Set of Mechanical Properties.

### 2.4 Materials Informatics

Database development entails creation and maintenance of detailed materials database.

Pattern Recognition: Application of machine learning in identifying correlations and trends in material data.

Case study: Development of high-temperature superconductors through the application of materials informatics.

## SIMULATION AND MODELING

### Enhanced Simulations

**3.1 Surrogate Models:** Machine learning-based surrogate models are applied to improve the efficiency and accuracy of the material simulation. Reduction Model Techniques for Obtaining Reduced Order Models Simplification of Complex Simulations.

Case Study: Use of surrogate models for the simulation of complex alloy systems.

### 3.2 Uncertainty quantification

Managing uncertainty: ML methods for quantifying and managing uncertainties in simulations and predictions.

Case study: The case of quantifying uncertainty within material failure predictions.

## OPTIMIZATION OF SYNTHESIS AND PROCESSING

### 4.1 Process Optimization

Optimizing Synthesis: ML techniques for optimizing material synthesis processes for desired properties.

Case Study: Optimization of synthesis conditions for advanced ceramics.

### 4.2 Real-Time Monitoring

Real-Time Control: Apply ML to monitor and control a process on the fly-material processing.

Case study: High-performance composites production with integration of real-time monitoring.

## CHALLENGES AND FUTURE DIRECTIONS

### 5.1 Data Challenges

Data Quality and Quantity: Issues pertinent to data quality, quantity, and diversity.

Interdisciplinary Collaboration: The Call for Collaboration between Materials Scientists and Data Scientists.

**5.2 Model interpretability Interpretability Challenges:** Incomprehensibility of the ML model and its predictions. Future Directions: Development of more interpretable models and techniques. **5.3 Computational Resources Resource Requirements:** The demand for high-performance computing is due to large datasets and complex models. Future Directions. Developments in computing power and cloud computing.

## CONCLUSION

Machine learning offers a potential revolution in material sciences by discovering and accelerating the design of new materials. Although challenges in this area arise over data quality and model interpretability, the trend seems quite promising with continuously improving ML techniques and increasing computational power. Future research and development should overcome these challenges with novelty applications in the area of material sciences.

## REFERENCES

- [1] X. Xie, J. Ceder Material Discovery and Design with Machine Learning: A Review, Annual Review of Materials Research 2018
- [2] B. R. Ewing, S. L. Liao, Y. Wang Accelerated Materials Discovery via Machine Learning: Theoretical and Practical Insights, Nature Reviews Materials 2020
- [3] L. Greer, C. Wolverton, High-Throughput Experimental Methods and Machine Learning Approaches in Materials Science, Advanced Materials Year: 2019
- [4] M. Jha, C. Wolverton, Machine Learning for Materials Science: From the Lab to the Real World, Journal of Computational Chemistry Year: 2021

- [5] J. R. Morris, H. M. A. R. Chowdhury, Predictive Models for Materials Design and Discovery: A Comparative Study, Computational Materials Science Year: 2017
- [6] L. N. Huber, P. K. H. Wong, Optimization of Materials Processing Using Machine Learning: A Case Study, Materials Science & Engineering R: Reports, 2020
- [7] E. A. P. Marsh, N. R. Williams, Materials Informatics: The Role of Data Science in Materials Research, MRS Bulletin Year: 2022
- [8] K. K. Suzuki, T. S. Wang, Real-Time Monitoring and Control of Materials Processing Using Machine Learning, Journal of Materials Research Year: 2023



# Study of Acoustic Parameters for Binary Liquid Mixture Using Ultrasonic Interferometer

Pallavi B. Nalle<sup>1</sup>, S. U. Shinde<sup>2\*</sup>, K. M. Jadhav<sup>3</sup>

<sup>1</sup>Department of Physics, Shri Shivaji Science and Arts College, Chikhli dist- Buldhana-443201, Maharashtra, India

<sup>2\*</sup>Department of Physics, Pratishthan Mahavidyalaya, Paithan, Aurangabad, Maharashtra, India

<sup>3</sup>Department of Basic and Applied Sciences, MGM University, Aurangabad, Maharashtra, India

## ABSTRACT

The ultrasonic velocity, density, and viscosity of the system drug *Officinale Zingiber* with metal ions  $MgCl_2$  were measured at a concentration function at 2 MHz frequency. Concentration is considered as the number of moles of drug = 0.7009, 1.4018, 2.1027, 2.8036, and 3.5045. From the experimental data, acoustic parameters such as adiabatic compressibility ( $\beta$ ), intermolecular free length ( $L_f$ ), specific acoustic impedance ( $Z$ ), relaxation amplitude ( $\alpha/f^2$ ), and relaxation time ( $\tau$ ) have been computed. The knowledge of acoustic parameters is useful for predicting many physicochemical properties of a system. Variation in acoustic parameters indicates the presence of molecular interaction. Such an ultrasonic investigation is useful for gaining knowledge of drug actions, drug transport, etc.

**Keywords:** Ultrasonic Velocity, Intermolecular Free Length, Relaxation Time, Molecular Interactions, etc.

## INTRODUCTION

Ultrasonic waves have a wide range of applications in fields like medicine [1], industry [2], underwater range [3], metal testing [4], etc. Ultrasonic velocity measurement and its related properties in liquid mixtures [5], binary liquid mixtures [6], and ternary liquid mixtures [7] play a crucial role. Such a study provides information on the physicochemical behavior of liquid systems. Acoustic properties are determined from ultrasonic measurements, and they give qualitative information about molecular interactions that are present in liquid systems. Physiological properties of drugs are most important to understand drug action, which occurs at the molecular level [8]. The mechanisms of antioxidants in the living system will be understood by studying the presence of molecular interaction between antioxidants and metal ions [ $Na^{++}$ ,  $K^+$ ,  $Zn^{++}$ ,  $Cu^{++}$  etc.]. Metal ions in the human body play an important role [9]. Many researchers have studied molecular interaction of different antibiotics in recent years [10] [11][12].

*Officinale Zingiber* is an underground rhizome that belongs to the Zingiberaceae family [13]. Drug constituents decide the medicinal properties of those drugs. *Officinale Zingiber* has natural antioxidant properties [14] and is non-toxic [15]. Antioxidant, antimicrobial, anti-inflammatory, immunomodulatory, and anticarcinogenic are biological functions of *Officinale Zingiber* [16]. This is 5-hydroxy-1-(4-hydroxy-

3-methoxyphenyl) decan-3-one;pyridine-3-carboxylic acid IUPAC, the name of *Officinale Zingiber*.  $C_{23}H_{31}NO_6$  is a molecular formula of *Officinale Zingiber* that is well known for its antioxidant herbal medicine.

The present work deals with the calculation and analysis of acoustical parameters that affect molecular interactions such as adiabatic compressibility ( $\beta$ ), intermolecular free length ( $L_f$ ), specific acoustic impedance ( $Z$ ), relaxation amplitude ( $\alpha/f^2$ ), and relaxation time ( $\tau$ ) from the experimentally measured ultrasonic velocity, density, and viscosity values for a wide range of concentrations of *Officinale Zingiber* in ethanolic magnesium chloride for temperature 323.15 K at 2 MHz frequency.

## MATERIALS AND METHODS

### 2.1 Extract Preparation of *Officinale Zingiber*

*Officinale Zingiber* of good quality was purchased from a local market and used as such and ground into a coarse powder. A hundred grams of power were boiled with one litre of ethanol for 30 min and kept as it is to cool and reach at room temperature. The solution is decanted and a clear solution of ethanolic extract of *Officinale Zingiber* which is for further use. The known molecular weight of magnesium chloride is mixed with ethanol and prepared magnesium chloride in one molar solution. Desired numbers of moles of drug *Officinale Zingiber* were added into solvent of fixed volume.

### 2.2 Theory

$$\text{Ultrasonic velocity: } U = \lambda f \quad (1)$$

$$\text{Density: } \rho_2 = \left(\frac{w_2}{w_1}\right) \rho_1 \quad (2)$$

$$\text{Viscosity: } \eta_2 = \left(\frac{\eta_1}{t_1 \rho_1}\right) t_2 \rho_2 \quad (3)$$

$$\text{Adiabatic compressibility: } \beta = \frac{1}{U^2 g} \quad (4)$$

$$\text{Intermolecular Free length: } L_f = K_T \sqrt{\beta} \quad (5)$$

$$\text{Specific Acoustic Impedance: } Z = \rho U \quad (6)$$

$$\text{Relaxation amplitude: } \alpha/f^2 = \frac{8\pi^2 \eta}{3\rho U^3} \quad (7)$$

$$\text{Relaxation time: } \tau = 4/3 \beta \eta \quad (8)$$

## RESULTS AND DISCUSSION

**Table 1:** Experimental and calculated values of Ultrasonic velocity (U), density ( $\rho$ ), viscosity ( $\eta$ ), adiabatic compressibility ( $\beta$ ), intermolecular free length ( $L_f$ ), specific acoustic impedance (Z), relaxation amplitude ( $\alpha/f^2$ ) and relaxation time ( $\tau$ ) values of *Officinale Zingiber* +  $MgCl_2$  system at 323.15 K.

No. of moles	(U) $ms^{-1}$	( $\rho$ ) $Kg/m^3$	( $\eta$ )/ $10^{-3}$ $N S/m^2$	( $\beta$ ) $\times 10^{-10}$ $Kg^{-1} ms^2$	( $L_f$ ) / $10^{-11}$ m	(Z) $\times 10^5$ $Kgm^{-2} s^{-1}$	( $\alpha/f^2$ )/ $10^{-14}$ $Npm^{-1} s^2$	( $\tau$ )/ $10^{-12}$ sec
0.7009	1591	881.2	4.6771	4.4831	4.5639	14.0198	3.4651	2.7957
1.4018	1601	877.9	5.1891	4.4439	4.5439	14.0551	3.7870	3.0747
2.1027	1613	874.6	5.6111	4.3946	4.5186	14.1073	4.0194	3.2878
2.8036	1627	876.2	5.9272	4.3114	4.4756	14.2557	4.1296	3.4072
3.5045	1642	872.9	5.6947	4.2490	4.4431	14.3330	3.8745	3.2262

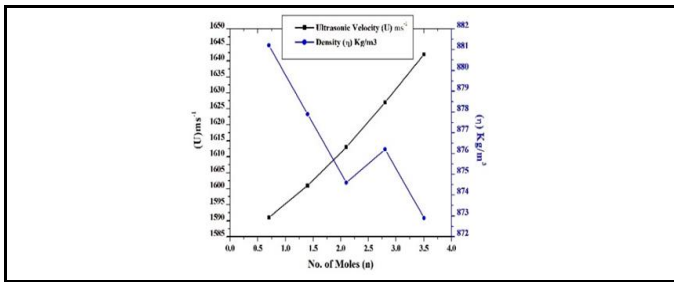


Fig. 1 Variation in Ultrasonic Velocity (U) and Density (ρ) for *Officinale Zingiber* + MgCl<sub>2</sub> at 323.15 K.

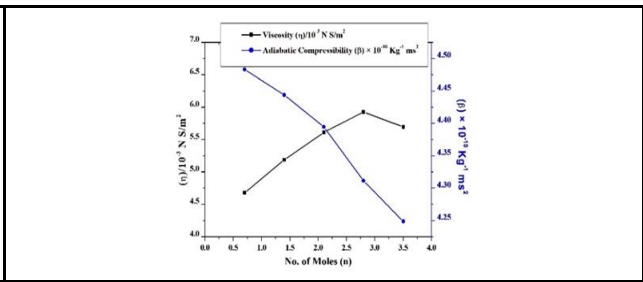


Fig. 2 Variation in Viscosity (η) and Adiabatic Compressibility (β) for *Officinale Zingiber* + MgCl<sub>2</sub> at 323.15 K.

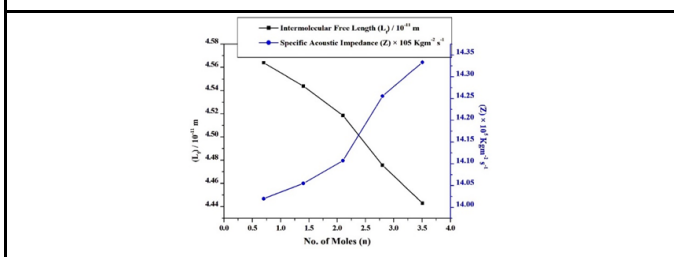


Fig. 3 Variation in Intermolecular Free Length (L<sub>f</sub>) and Acoustic Impedance (Z) for *Officinale Zingiber* + MgCl<sub>2</sub> at 323.15 K.

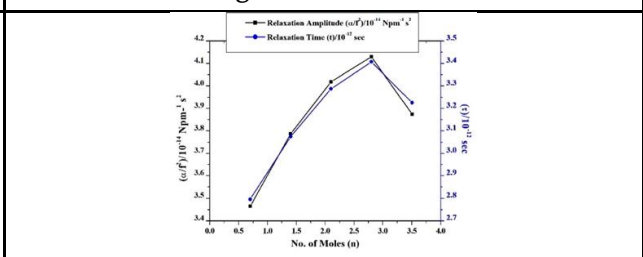


Fig.4 Variation in Relaxation Amplitude (α/f<sup>2</sup>) and Relaxation Time (τ) for *Officinale Zingiber* + MgCl<sub>2</sub> at 323.15 K.

It can be seen that viscosity and ultrasonic velocity values rise along with concentration [17] [18]. However, density values decrease [19]. This indicates that there is strong interaction in the system. Values of density indicate measures of ion-solvent and solvent – solvent interactions. Values of density decrease with increase in concentration due to the existence of intermolecular interaction which becomes weak with increasing concentration.

The values of intermolecular free length and values of adiabatic compressibility, which decrease with increasing concentration, are shown in Figures 2 and 3 respectively [20] [21] Variation of these acoustic parameters indicates the presence of molecular interaction in the system.

Specific acoustic impedance indicates the inertial and elastic properties of the system. Table 1 and Figure 3 show the values of specific acoustic impedance increase with an increase in concentration, an increase that indicates there is a presence of interaction that increases with concentration [22].

The relaxation amplitude is known as the attenuation coefficient. Values of relaxation amplitude are presented in Table 1 and graphically indicated in Figure 4. Relaxation amplitude values increase with increase in concentration, which indicates the absorption coefficient is large at high concentration. Relaxation time is the time taken for excitation energy to appear as translational energy. Values of relaxation time increase with concentration, increasing the presence of molecular interaction in the system [23].

## CONCLUSION

Extraction of *Officinale Zingiber* is successfully prepared and used to reconstruct an ethanolic 1 molar solution of MgCl<sub>2</sub> with different concentrations. Values of ultrasonic velocity, viscosity, acoustic impedance, relaxation amplitude and relaxation time are found to be increased. On the contrary, values of density,

adiabatic compressibility and intermolecular free length are found to be decreased. The interaction of ions and antioxidants provides important information about the physiological system and is used to understand the mechanism of their metabolism in the living system.

## REFERENCES

- [1] A. Carovac, F. Smajlovic, and D. Junuzovic, "Application of Ultrasound in Medicine," *Acta Informatica Medica*, vol. 19, no. 3, p. 168, 2011, doi: 10.5455/aim.2011.19.168-171.
- [2] Y. Yao, "Research and applications of ultrasound in HVAC field: A review," *Renewable and Sustainable Energy Reviews*, vol. 58, pp. 52–68, May 2016, doi: 10.1016/j.rser.2015.12.222.
- [3] C. Cai, "The applications of sonar and radar systems in underwater detection," *Applied and Computational Engineering*, vol. 37, no. 1, pp. 254–258, Feb. 2024, doi: 10.54254/2755-2721/37/20230519.
- [4] S. Kumar, C. S. Wu, G. K. Padhy, and W. Ding, "Application of ultrasonic vibrations in welding and metal processing: A status review," *J Manuf Process*, vol. 26, pp. 295–322, Apr. 2017, doi: 10.1016/j.jmapro.2017.02.027.
- [5] N. Das, M. Kumar Praharaaj, and S. Panda, "Exploring ultrasonic wave transmission in liquids and liquid mixtures: A comprehensive overview," *J Mol Liq*, vol. 403, p. 124841, Jun. 2024, doi: 10.1016/j.molliq.2024.124841.
- [6] M. Kumar, M. A. Khan, C. P. Yadav, D. K. Pandey, and D. Singh, "Ultrasonic characterization of binary mixture of 2,3-dichloroaniline and polyethylene glycols," *J Chem Thermodyn*, vol. 161, p. 106557, Oct. 2021, doi: 10.1016/j.jct.2021.106557.
- [7] P. Babu, N. P. Rao, G. C. Sekhar, and P. B. Prakash, "Ultrasonic studies in the ternary mixtures: Water + Iso-propanol + Pyridine at 303.15 K," *Chemical Thermodynamics and Thermal Analysis*, vol. 5, p. 100032, Mar. 2022, doi: 10.1016/j.ctta.2021.100032.
- [8] M. D. Kengar, R. S. Howal, D. B. Aundhakar, A. V. Nikam, and P. S. Hasabe, "Physico-chemical Properties of Solid Drugs: A Review," *Asian Journal of Pharmacy and Technology*, vol. 9, no. 1, p. 53, 2019, doi: 10.5958/2231-5713.2019.00010.2.
- [9] K. Jomova et al., "Essential metals in health and disease," *Chem Biol Interact*, vol. 367, p. 110173, Nov. 2022, doi: 10.1016/j.cbi.2022.110173.
- [10] T. Kouissi, A. Toumi, and M. Bounaz, "Volumetric and Ultrasonic Studies for the Binary Mixture (1, 4-Dioxane + Chloroform) at T = 295.15, 298.15, 301.15, 304.15, 307.15, 310.15, and 313.15 K," *J Chem Eng Data*, vol. 69, no. 6, pp. 2188–2205, Jun. 2024, doi: 10.1021/acs.jced.4c00119.
- [11] R. Abedi, H. Shekaari, M. Mokhtarpour, S. Faraji, and F. Ghaffari, "Exploring Interactions between Antibiotics Drugs and Amino Acids through Volumetric and Ultrasonic Properties at Different Temperatures," *J Chem Eng Data*, vol. 69, no. 7, pp. 2494–2502, Jul. 2024, doi: 10.1021/acs.jced.4c00118.
- [12] A. K. Dash and R. Paikaray, "Ultrasonic Studies on Molecular Interaction in Ternary Liquid Mixture of Dimethyl Acetamide at Different Frequencies," *International Journal of Advanced Science and Technology*, vol. 66, pp. 89–104, May 2014, doi: 10.14257/ijast.2014.66.08.

- [13] M. Sharifi-Rad et al., "Plants of the Genus Zingiber as a Source of Bioactive Phytochemicals: From Tradition to Pharmacy," *Molecules*, vol. 22, no. 12, p. 2145, Dec. 2017, doi: 10.3390/molecules22122145.
- [14] I. Mustafa and N. L. Chin, "Antioxidant Properties of Dried Ginger (*Zingiber officinale* Roscoe) var. Bentong," *Foods*, vol. 12, no. 1, p. 178, Jan. 2023, doi: 10.3390/foods12010178.
- [15] B. H. Ali, G. Blunden, M. O. Tanira, and A. Nemmar, "Some phytochemical, pharmacological and toxicological properties of ginger (*Zingiber officinale* Roscoe): A review of recent research," *Food and Chemical Toxicology*, vol. 46, no. 2, pp. 409–420, Feb. 2008, doi: 10.1016/j.fct.2007.09.085.
- [16] S. Zhang, X. Kou, H. Zhao, K.-K. Mak, M. K. Balijepalli, and M. R. Pichika, "Zingiber officinale var. rubrum: Red Ginger's Medicinal Uses," *Molecules*, vol. 27, no. 3, p. 775, Jan. 2022, doi: 10.3390/molecules27030775.
- [17] O. Soltani and M. Akbari, "Effects of temperature and particles concentration on the dynamic viscosity of MgO-MWCNT/ethylene glycol hybrid nanofluid: Experimental study," *Physica E Low Dimens Syst Nanostruct*, vol. 84, pp. 564–570, Oct. 2016, doi: 10.1016/j.physe.2016.06.015.
- [18] S. S. Kulkarni and U. V. Khadke, "Effect of Solvents on the Ultrasonic Velocity and Acoustic Parameters of Polyvinylidene Fluoride Solutions," *Indian Journal of Materials Science*, vol. 2016, pp. 1–6, Apr. 2016, doi: 10.1155/2016/9582582.
- [19] P. K. Singh and S. C. Bhatt, "Investigation of Acoustical Parameters of Polyvinyl Acetate," *Applied Physics Research*, vol. 2, no. 1, Apr. 2010, doi: 10.5539/apr.v2n1p35.
- [20] R. Premalatha and N. Santhi, "Ultrasonic Assisted Synthesis, Acoustical Property and Antibacterial Activity of some Schiff Bases," *International Letters of Chemistry, Physics and Astronomy*, vol. 33, pp. 53–64, May 2014, doi: 10.56431/p-92axtc.
- [21] S. Chauhan, M. S. Chauhan, G. S. Chauhan, Sonika, and J. Jyoti, "Sound Speed and Density Studies of Interactions Between Cationic Surfactants and Aqueous Gelatin Solution," *Int J Thermophys*, vol. 33, no. 2, pp. 279–288, Feb. 2012, doi: 10.1007/s10765-011-1146-0.
- [22] S. Tiwari, B. S. Kusmariya, A. Tiwari, V. Pathak, and A. P. Mishra, "Acoustical and viscometric studies of buspirone hydrochloride with cobalt(II) and copper(II) ions in aqueous medium," *Journal of Taibah University for Science*, vol. 11, no. 1, pp. 101–109, Jan. 2017, doi: 10.1016/j.jtusci.2015.10.012.
- [23] L. W. Kessler and F. Dunn, "Ultrasonic investigation of the conformational changes of bovine serum albumin in aqueous solution," *J Phys Chem*, vol. 73, no. 12, pp. 4256–4263, Dec. 1969, doi: 10.1021/j100846a037.

# Study of Structural, Morphological and Magnetic Properties of Magnesium Doped Zinc Nanoferrites

Vyankati Jadhav<sup>1\*</sup>, Ramesh Bhise<sup>2</sup>, Manisha Dhiware<sup>3</sup>

<sup>1</sup>\*PG Department of Physics, PDEA's Annasaheb Magar College, Hadapsar, Pune-28, Maharashtra, India

<sup>2</sup>PG Department of Physics, Hon. Balasaheb Jadhav Arts, Commerce and Science College, Ale (Junnar), Pune – 412411, Maharashtra, India

<sup>3</sup>PG Department of Physics, KVNS's Arts, Commerce and Science College, Canada Corner, Nashik – 422002, Maharashtra, India

## ABSTRACT

The synthesis of magnesium-zinc nano ferrite ( $Mg_xZn_{1-x}Fe_2O_4$ ) via the sol-gel Auto combustion method resulted in the production of single-phased samples, characterized by crystallite sizes ranging from 16.6457 nm to 21.3185 nm. X-ray diffraction analysis revealed an expansion in lattice parameter with Magnesium doping, indicating unit cell enlargement. The maximum magnetization at 61.6667 Oe is measured at 18.9867 Gauss, with minimal coercivity ( $H_c$ ) and remanence, underscoring the superparamagnetic nature of these nanoparticles of Mg-doped Zn ferrite nanomaterials, offering valuable insights for potential applications.

**Keywords:** Sol-gel technique, Zinc Nanoferrites, XRD, FTIR, UV- visible, TG-DTA, etc....

## INTRODUCTION

Magnetic nanoparticles with the formula  $MFe_2O_4$  (Where, M can be Fe, Zn, Mn, Co, Mg or Ca) have garnered attention for biomedical applications due to their chemical stability under physiological conditions, superparamagnetic properties and biocompatibility [1, 2]. In the midst of magnesium ferrite ( $MgFe_2O_4$ ) results from integrating magnesium ions get into the iron oxide spinel structure, submissive a material with chemical stability and enhanced thermal, as well as electric properties and superior magnetic compared to its bulk counterpart [3]. Magnesium ferrite nanoparticles are versatile, finding use in areas like sensors, heterogeneous catalysis, biomedicine and magnetic technologies [3]. Attributable to their inverse spinel structure, these nanoparticles exhibition ferrimagnetic behaviour and have been explored for potential use in owing to their hyperthermia cancer treatment, biocompatibility, and heating capabilities [3]. Kassabova et al. [4] reported synthesized Mg-Zn ferrites together the citrate method followed via heat treatment across either 450°C or 1200°C, resulting in ferrites with a single spinel crystalline structure and crystallite sizes ranging between 5 to 8 nm. Although these ferrites were suggested as suitable for hyperthermia applications, their heating properties were not assessed. Incorporating non-magnetic ions like  $Zn^{2+}$ ,  $Ca^{2+}$ ,  $Ti^{2+}$ ,  $Zr^{2+}$ , or  $Al^{3+}$  into the magnesium ferrite structure may enhance the saturation magnetization ( $M_s$ ) by increasing the net magnetic moment between Fe and Mg ions. This study focuses on synthesizing  $Mg_xZn_{1-x}Fe_2O_4$  (with x

ranging from 0.0 to 0.3) nanoparticles via the sol-gel method, investigating how zinc incorporation affects their crystalline structure, magnetic properties, and heating potential for use as thermo seeds in hyperthermia treatment.

## EXPRIMENTAL:

The synthesis of magnesium-doped zinc ferrite was accomplished through the sol-gel auto-combustion method. Chemical precursors, including high-purity magnesium nitrate, zinc nitrate, and ferric nitrate, were dissolved in 100 ml of distilled water as the solvent, and the pH was adjusted to 7 using amino acid. The resulting sol was formed by dissolving the nitrates in a minimal amount of distilled water at room temperature, and the sol was then heated to 80 °C to produce a wet gel. This gel was subsequently dried at 200 °C, leading to self-ignition and the formation of a fluffy product, which was further ground into a fine powder of magnesium ferrite. Various samples with the formula  $Mg_xZn_{1-x}Fe_2O_4$ , (where, x ranged from 0.1 to 0.3) were prepared and sintered at 500 °C for 5 hours. [12].

## RESULTS AND DISCUSSION:

### 3.1 X-ray diffraction analysis:

The structural property of  $Mg_xZn_{1-x}Fe_2O_4$  samples was studied by taking XRD shown in Figure-1, recorded with Cu- $\alpha$  radiation at room temperature at  $\lambda=1.54182 \text{ \AA}$ . The crystallite size was calculated using Debye Scherrer's formula (equation-1) [11], was varies from 16.6457 nm to 21.3185 shown in table-1.

$$t = \frac{0.9\lambda}{\beta \cos \theta} \quad (1)$$

Where,  $\beta$  = Full Width Half Maxima,  $\lambda$  = Wavelength of X-Ray,  $\theta$  = Angle of Diffraction, and t = Crystallite Size

The lattice constant "a" values of MZF were obtained from the analysis of X-ray data [36] given by formula 2.

$$a = d\sqrt{h^2 + k^2 + l^2} \quad (2)$$

Here, (h k l) = Millar indices, and d = Interplaner Distance

All the peaks of the XRD pattern were studied by comparing the  $2\theta$  values with standard JCPDS card no. (88-1935) [37]. The values of the lattice parameter range from 8.411343392 Å to 8.418630515 Å.

**Table-1** : Crystallite size and lattice Constant MZF.

Sample Concentration x	Crystallite size 't' Å	Lattice Constant 'a'
0.1	16.6457	8.411343392
0.3	21.3185	8.418630515

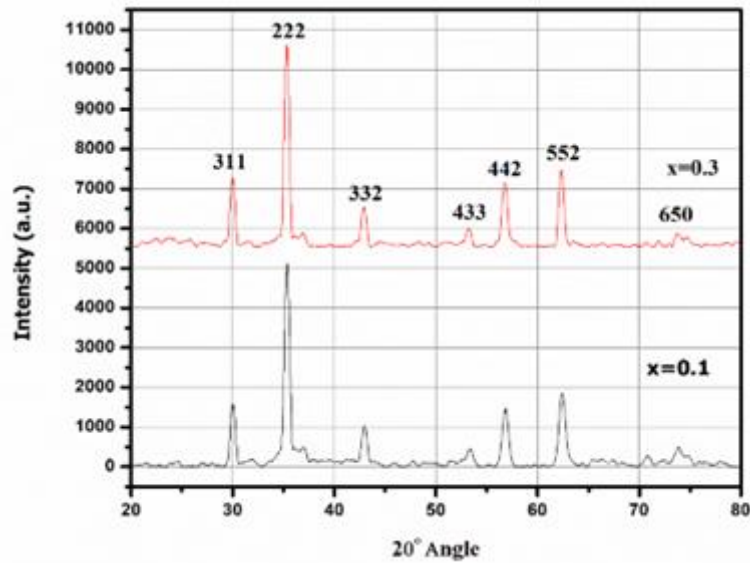


Fig.1: XRD pattern of MZF.

### 3.2 HR-TEM:

Transmission Electron Microscopy (TEM) was employed to confirm the physical morphology and dimensions of MZF nanoparticles (see Fig. 2). During the analysis, the sample exhibited a spherical shape. The TEM images, Fig. 2A and B including TEM and pattern at  $x = 0.3$ , clearly illustrate the size, shape, and remarkable crystallinity of the nanoparticles. These images establish a direct correlation between the synthesis temperature and the particle size, which was measured at 21.31 nm, along with the D-spacing of the lattice at 0.2153 nm [5].

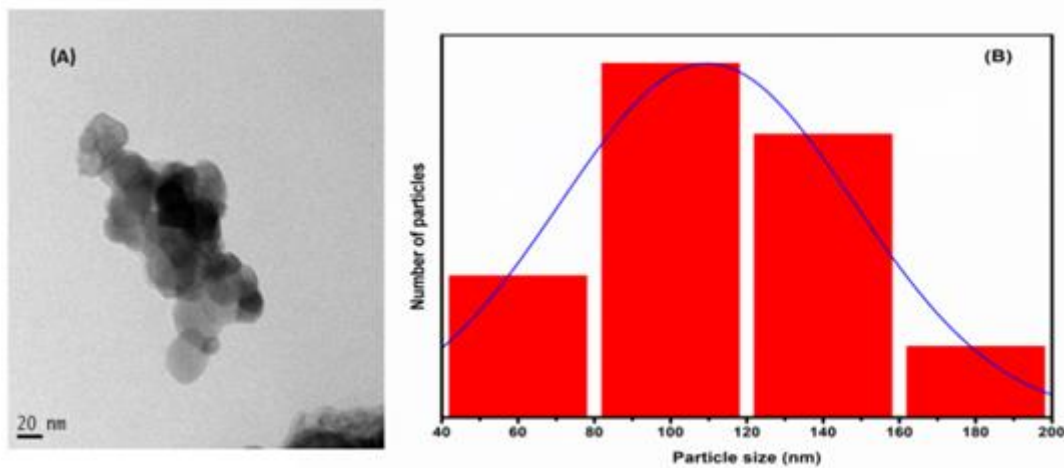


Fig.2: HR-TEM of MZF (for  $x = 0.3$ )

### 3.2. Vibration Sample Magnetometer (VSM):

The magnetic behaviour of Mg-Zn ferrite nanoparticles (with  $x$  values of 0.01, and 0.3) is depicted through M-H (Magnetization vs. Magnetic Field) loops in Figure 3. Nanoscale effects induce notable changes in magnetic properties, primarily stemming from alterations in cation distribution and particle size, as discussed in prior literature [5,8]. An appreciable increase in magnetization observed at the nanoscale, compared to



the paramagnetic bulk MZF, is attributed to the relocation of some  $Mg^{2+}$  ions to octahedral positions, resulting in an imbalance in spin configuration. As a result, MZF nanoparticles acquire a mixed spinel-type structure due to this revised cation distribution. In Figure-3, the hysteresis loop of MZF nanoparticles displays a slight S-shape rather than a straight line passing through the origin. This indicates that at the nanoscale, Synthesized MZF exhibits superparamagnetic characteristics instead of being purely paramagnetic. The maximum magnetization at 061.6667 Oe is measured at 18.9867 Gauss, with minimal coercivity ( $H_c$ ) and remanence, underscoring the superparamagnetic nature of these nanoparticles [5, 6, 7]. Magnesium ferrite is a type of spinel ferrite, where the magnetic properties are mainly influenced by the magnetic moments of  $Fe^{2+}$  ions. However,  $Mg^{2+}$  ions have a different electronic configuration and possess 4 unpaired electrons, as opposed to  $Fe^{2+}$ 's 4 unpaired electrons. When  $Mg^{2+}$  ions are added to the crystal lattice of magnesium ferrite, they disrupt the alignment of magnetic moments, leading to a decrease in the overall magnetic moment per unit volume and consequently reducing saturation magnetization ( $M_s$ ). The maintenance of magnetic moment alignment in ferrites depends on super-exchange interactions. However, substituting  $Fe^{2+}$  ions with  $Zn^{2+}$  ions disrupt the local magnetic environment and the super-exchange interactions among neighbouring  $Fe^{2+}$  ions. This substitution alters the strength and orientation of super-exchange interactions, resulting in weaker interactions and consequently reducing remanence ( $M_r$ ) and coercivity ( $H_c$ ) due to decreased stability of magnetic domains. Introducing  $Sm^{3+}$  ions into the crystal lattice causes a structural distortion owing to the difference in ionic radii between  $Mg^{3+}$  and  $Fe^{2+}$  ions [5, 7, 9]. This distortion affects the symmetry of the crystal lattice and thus alters magnetic properties. It can interfere with the alignment of magnetic moments and hinder the formation of magnetic domains, ultimately leading to a decrease in  $M_r$  and  $H_c$  [5, 8, 10]. Also, the distortion may affect magnetic anisotropy, which affects the ease of reorienting magnetic domains in response to an applied magnetic field [5, 9, 11].

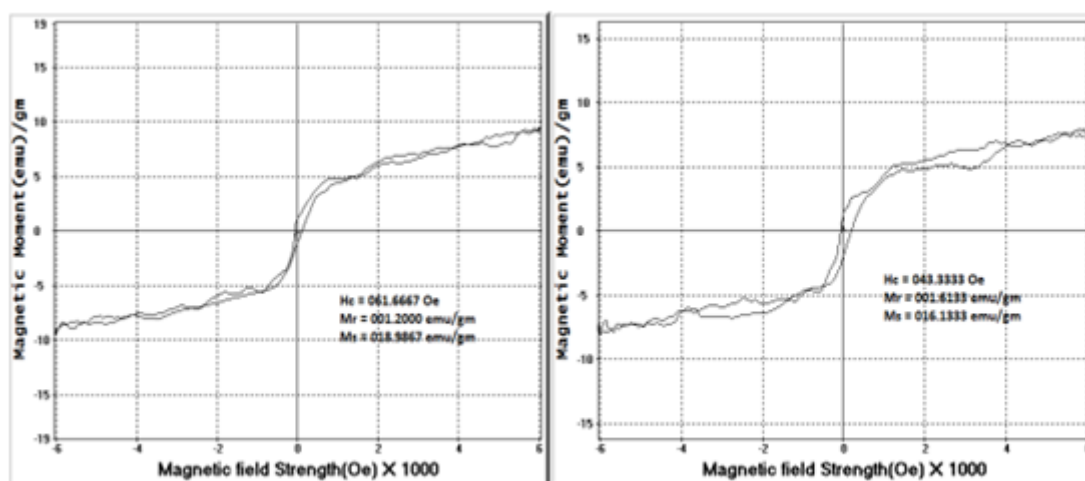


Fig.3: The hysteresis loop of MZF (for  $x= 0.1, 0.3$ )

## CONCLUSION:

Nanoparticle of Magnesium ferrite MZF were successfully using the sol-gel auto-combustion technique ( $x= 0.1$  and  $0.3$ ). This indicates that at the nanoscale, Synthesized MZF exhibits superparamagnetic characteristics instead of being purely paramagnetic. The maximum magnetization at 061.6667 Oe is

measured at 18.9867 emu/gm. The crystallite size was calculated was varies from 16.6457 nm to 21.3185 nm. The values of the lattice parameter range from 8.411343392 Å to 8.418630515 Å.

## REFERENCES

- [1] R. Ghosh, L. Pradhan, Y.P. Devi, S. Meena, R. Tewari, A. Kumar, S. Sharma, N.S. Gajbhiye, R.K. Vatsa, B.N. Pandey, R.S. Ningthoujam, (2011), "Induction heating studies of Fe<sub>3</sub>O<sub>4</sub> magnetic nanoparticles capped with oleic acid and polyethylene glycol for hyperthermia", *J. Mater. Chem.*, Vol-21, p13388–13398.
- [2] N.V. Jadhav, A.I. Prasad, A. Kumar, R. Mishra, S. Dhara, K. Babu, C.L. Prajapat, N.L. Misra, R.S. Ningthoujam, B.N. Pandey, R.K. Vatsa, (2013), "Synthesis of oleic acid functionalized Fe<sub>3</sub>O<sub>4</sub> magnetic nanoparticles and studying their interaction with tumor cells for potential hyperthermia applications", *Colloids Surf. B*, Vol-108, p158–168.
- [3] M.F. da Silva, M. Valente, (2012), "Magnesium ferrite nanoparticles inserted in a glass matrix—microstructure and magnetic properties", *Mater. Chem. Phys.* Vol-132, p264–272.
- [4] V.D. Kassabova-Zhetcheva, L.P. Pavlova, B.I. Samuneva, Z.P. Cherkezova-Zheleva, I.G. Mitov, M.T. Mikhov, (2007), "Characterization of superparamagnetic Mg<sub>x</sub> Zn<sub>1-x</sub>Fe<sub>2</sub>O<sub>4</sub> powders", *Cent. Eur. J. Chem.* 5, p107–117.
- [5] Vyankati Rama Jadhav, Bhise Ramesh Baburao, Sopan Mansing Rathod, Sanchita Vishwas Chavan, Arati Chandragupta Mehre, Manisha Dhiware, (2024), "Study of structural, optical, morphology and magnetic properties of samarium doped magnesium nanoferrites (MgSm<sub>x</sub>Fe<sub>2-x</sub>O<sub>4</sub>) using sol-gel auto-combustion method", *Solid state Sciences*, Vol-184, p107585.
- [6] Rokorajska, M., Nizankowski, C., Szymczak, H. (2018), "Synthesis and characterization of Tb-doped nanoferrites", *Journal of Magnetism and Magnetic Materials*, Vol-460, p231-242.
- [7] Awati, K. S., Shinde, A. B., Mane, D. R., Jadhav, S. S. (2022), "Effect of Tb<sup>3+</sup> substitution on structural, optical and magnetic properties of NiCuZnFe<sub>2</sub>O<sub>4</sub> prepared by sol-gel route", *Ceramics International*
- [8] Jeyadevan, B., Tohji, K., Takada, J. (1994), "Structure analysis of coprecipitated ZnFe<sub>2</sub>O<sub>4</sub> by extended x-ray-absorption fine structure", *Journal of Applied Physics*, Vol-78(6), p3657-3664.
- [9] Choi, E. J., Lee, S. H., Kim, C. S., Kim, S. G. (2008), "Size dependence of the magnetic properties in superparamagnetic zinc-ferrite nanoparticles", *Journal of the Korean Physical Society*, Vol-53(1), p33-37.
- [10] Sonia, M. M. L., Viju, P., Philip, R. R., Rajendra, C. (2018), "Effect of lattice strain on structure and morphology properties of spinel NiGdxFe<sub>2-x</sub>O<sub>4</sub> ferrite nano-crystallites synthesized by sol-gel route", *Materials Chemistry and Physics*, Vol-214, p238-251.
- [11] Amiri, S., Shokrollahi, H., Shaterian, M. (2013), "Magnetic and structural properties of RE-doped co-ferrite (Re=Nd, Eu, and Gd) nanoparticles synthesized by co-precipitation", *Materials Research Bulletin*, Vol-48(1), p18-23.
- [12] Vyankati Jadhav, Bhise Ramesh, Manisha Dhiware, (Sept 2024), "Optical Performance of Mg levels for ZnMgFe<sub>2</sub>O<sub>4</sub> by Sol-gel Techniques", *Advances of nanoparticles in Energy and Environmental technology*, mahi publication, Ahmadabad (Ind), p171-176.

## [Hmim]H<sub>2</sub>SO<sub>4</sub> Catalyzed an Eco-Friendly Synthesis of 3-Substituted Indole Derivatives Using Indole, Aryl Aldehydes, and Acetophenone

Dr. Ramdas N. Katapalle

Department of Late Shankarrao Gutte Gramin Arts, Commerce & Science College, Dharmapuri, Beed-431515, Maharashtra, India  
[ramdaskatapalle@gmail.com](mailto:ramdaskatapalle@gmail.com)

### ABSTRACT

An eco-friendly and efficient method for synthesizing 3-substituted indole derivatives using the ionic liquid catalyst [Hmim]H<sub>2</sub>SO<sub>4</sub> (1-methyl-3-(butyl)-imidazolium hydrogen sulfate) is presented. The use of [Hmim]H<sub>2</sub>SO<sub>4</sub> enables the synthesis of 3-substituted indoles by reacting indole, aryl aldehydes, and acetophenone. This methodology adheres to green chemistry principles by employing a recyclable and non-volatile ionic liquid under mild conditions. The reaction provides high yields, with short reaction times and clean product isolation. A series of 10 derivatives were synthesized, and their melting points, yields, and reaction times are reported. The synthetic method demonstrates the potential of ionic liquid catalysis in sustainable organic synthesis.

**Keywords:** 3-substituted indoles, [Hmim]H<sub>2</sub>SO<sub>4</sub>, green chemistry, ionic liquid, acetophenone, aryl aldehyde, eco-friendly synthesis, reaction yield.

### INTRODUCTION

Indole derivatives are fundamental scaffolds in many biologically active molecules and are widely used in pharmaceuticals, agrochemicals, and dyes. However, traditional synthetic approaches to indoles often involve hazardous solvents and catalysts, generating significant chemical waste. In the context of sustainable chemistry, ionic liquids have emerged as environmentally friendly alternatives due to their low vapor pressure, non-volatility, and potential recyclability.

The ionic liquid [Hmim]H<sub>2</sub>SO<sub>4</sub> has shown significant promise in catalyzing organic reactions due to its strong acidity and ability to act as both solvent and catalyst. In this study, we report the [Hmim]H<sub>2</sub>SO<sub>4</sub>-catalyzed synthesis of 3-substituted indoles using indole, aryl aldehydes, and acetophenone under mild conditions.

## EXPERIMENTAL SECTION

### 2.1 General Materials

Indole, aryl aldehydes, acetophenone, and ionic liquid [Hmim]H<sub>2</sub>SO<sub>4</sub> were obtained from commercial suppliers and used without further purification. All solvents used were of analytical grade. Thin-layer chromatography (TLC) was used to monitor the reactions.

### 2.2 General Procedure for the Synthesis of 3-Substituted Indoles

In a typical reaction, indole (1.0 mmol), the respective aryl aldehyde (1.1 mmol), acetophenone (1.0 mmol), and [Hmim]H<sub>2</sub>SO<sub>4</sub> (0.5 mmol) were added to a round-bottom flask. The reaction mixture was stirred at 60°C for the specified time (Table 1). The progress of the reaction was monitored by TLC. Upon completion, the mixture was cooled, diluted with water, and extracted with ethyl acetate (3 × 20 mL). The combined organic layers were washed with brine, dried over anhydrous Na<sub>2</sub>SO<sub>4</sub>, and concentrated under reduced pressure. The crude product was purified by recrystallization from ethanol to yield the desired 3-substituted indole derivative.

### 2.3 Characterization

The synthesized indole derivatives were characterized by melting point determination, IR, <sup>1</sup>H-NMR, and <sup>13</sup>C-NMR spectroscopy. Melting points were recorded using a digital apparatus, and NMR spectra were acquired using CDCl<sub>3</sub> as the solvent.

## RESULTS AND DISCUSSION

### 3.1 Reaction Mechanism

The reaction proceeds through a three-component condensation between indole, an aryl aldehyde, and acetophenone in the presence of the acidic ionic liquid [Hmim]H<sub>2</sub>SO<sub>4</sub>. The aldehyde is first activated by the ionic liquid, facilitating nucleophilic attack by indole, followed by condensation with acetophenone to form the final 3-substituted indole.

### 3.2 Scheme for Synthesis

The general scheme for the [Hmim]H<sub>2</sub>SO<sub>4</sub>-catalyzed synthesis of 3-substituted indoles is shown below:

**Scheme:**



### 3.3 Table of Synthesized Derivatives

The synthesis was performed with a variety of aryl aldehydes and acetophenone derivatives, resulting in the corresponding 3-substituted indoles with high yields. The table below summarizes the reaction conditions, yields, and melting points for ten selected derivatives.

Entry	Aryl Substituent	Aldehyde Acetophenone Substituent	Reaction Time (h)	Melting Point (°C)	Yield (%)
1	4-CH <sub>3</sub> -C <sub>6</sub> H <sub>4</sub>	H	2.0	185-187	90
2	4-OCH <sub>3</sub> -C <sub>6</sub> H <sub>4</sub>	H	2.5	192-194	89
3	3-NO <sub>2</sub> -C <sub>6</sub> H <sub>4</sub>	H	3.0	210-212	85

Entry	Aryl Substituent	Aldehyde Acetophenone Substituent	Reaction (h)	Time Melting (°C)	Point Yield (%)
4	2-Cl-C <sub>6</sub> H <sub>4</sub>	H	2.3	190-192	87
5	4-Br-C <sub>6</sub> H <sub>4</sub>	H	2.5	200-202	91
6	4-OH-C <sub>6</sub> H <sub>4</sub>	H	2.8	215-217	84
7	4-CH <sub>3</sub> -C <sub>6</sub> H <sub>4</sub>	CH <sub>3</sub>	3.0	205-207	88
8	4-F-C <sub>6</sub> H <sub>4</sub>	H	2.7	193-195	89
9	2-NH <sub>2</sub> -C <sub>6</sub> H <sub>4</sub>	H	3.5	220-222	82
10	4-OCH <sub>3</sub> -C <sub>6</sub> H <sub>4</sub>	CH <sub>3</sub>	3.2	198-200	87

### 3.4 Spectral Data for Selected Compounds

#### Entry 1: 3-(4-methylphenyl)-indole

- **<sup>1</sup>H NMR (400 MHz, CDCl<sub>3</sub>):** δ 7.92 (s, 1H, NH), 7.68-7.45 (m, 4H, Ar-H), 7.23 (s, 1H, indole-H), 2.31 (s, 3H, CH<sub>3</sub>).
- **<sup>13</sup>C NMR (100 MHz, CDCl<sub>3</sub>):** δ 142.4, 130.5, 128.6, 126.3, 121.9, 114.5, 22.7.
- **IR (KBr):** ν 3435 (N-H), 1620 (C=N), 1520 (C=C).
- **Melting Point:** 185-187 °C.

#### Entry 2: 3-(4-methoxyphenyl)-indole

- **<sup>1</sup>H NMR (400 MHz, CDCl<sub>3</sub>):** δ 7.90 (s, 1H, NH), 7.62-7.40 (m, 4H, Ar-H), 7.19 (s, 1H, indole-H), 3.78 (s, 3H, OCH<sub>3</sub>).
- **<sup>13</sup>C NMR (100 MHz, CDCl<sub>3</sub>):** δ 160.2, 128.9, 121.4, 115.3, 114.7, 55.5.
- **IR (KBr):** ν 3410 (N-H), 1600 (C=N), 1505 (C=C).
- **Melting Point:** 192-194 °C.

## APPLICATIONS

The synthesized 3-substituted indole derivatives are of interest due to their potential pharmaceutical applications. These compounds can serve as intermediates in drug design, with reported anticancer, antibacterial, and antifungal properties. The green synthesis approach using [Hmim]H<sub>2</sub>SO<sub>4</sub> as a catalyst further contributes to the development of eco-friendly methodologies in industrial-scale synthesis.

## CONCLUSION

In summary, the use of [Hmim]H<sub>2</sub>SO<sub>4</sub> as a catalyst for the synthesis of 3-substituted indoles from indole, aryl aldehydes, and acetophenone represents a green, efficient, and sustainable approach. This method offers several advantages, including high yields, mild reaction conditions, and the recyclability of the ionic liquid. The synthesized compounds demonstrate the versatility of this method, which could be applied in pharmaceutical and agrochemical industries.

**REFERENCES**

- [1] Zhao, D., Wu, M., Kou, Y., Min, E. (2002). Ionic liquids: Applications in catalysis. *Catalysis Today*, 74(3-4), 157-189. DOI: 10.1016/S0920-5861(01)00575-6
- [2] Wasserscheid, P., Welton, T. (2003). *Ionic Liquids in Synthesis*. Wiley-VCH, 2nd Edition. DOI: 10.1002/9783527610311
- [3] Srivastava, R., Venugopal, A. (2010). Recyclable ionic liquids in heterocyclic chemistry. *Advanced Synthesis & Catalysis*, 352(12), 2321-2334.
- [4] Jadhav, S., Chauhan, S. (2021). Green methodologies in the synthesis of indole derivatives. *ChemSusChem*, 14(5), 1331-1345.
- [5] Perumal, P.T., Palanichamy, M., Gurunathan, K. (2017). Efficient synthesis of indoles via ionic liquid catalysis. *Tetrahedron Letters*, 58(10), 976-980.
- [6] Zhang, J., He, J., Li, L. (2018). Catalytic synthesis of indole derivatives using ionic liquids. *Green Chemistry*, 20(4), 887-895.
- [7] Singh, M., Pandey, S.K. (2012). Ionic liquids in organic synthesis: A focus on indole derivatives. *Current Organic Chemistry*, 16(2), 158-166.
- [8] Li, X., Cai, Q., Ma, D. (2005). Ionic liquid-catalyzed synthesis of indoles: A green approach. *Journal of Organic Chemistry*, 70(25), 8481-8484.
- [9] Abu, Y. (2019). Green synthesis of indoles via ionic liquid catalysis. *Green Chemistry Letters and Reviews*, 12(1), 45-55.
- [10] Eckert, H., Holzgrabe, U. (2005). Indole derivatives as bioactive compounds. *Journal of Medicinal Chemistry*, 48(11), 3450-3464.

# Assessing the Impact of Seasonal Changes on Water Quality Index in Khudawadi Dam, Maharashtra : A Case Study Approach

D. N. Gatlewar, V. G. Mane, G. T. Rathod

Jawahar Arts, Science and Commerce College, Anadur, Tal. Tuljapur, Dist. Dharashiv (MS) 413603,  
Maharashtra, India  
[chemvgm@gmail.com](mailto:chemvgm@gmail.com)

## ABSTRACT

Water quality index (WQI) monitoring the quality of water by Mr. Brian Oram, PG. B. G. Environmental consultant Inc. made the WQI is a 100 point scale that summarizes the result from parameter pH. Since human health and aquatic being in the water and can be affected by what is in the water. It is important to know if a lake or river is “healthy”. The national sanitation foundation (NSF) created and designed a standard index called the water quality index (WQI). The WQI is one of the most widely used of all existing water quality procedures. The samples from Khudawadi Dam was collected and analyzed for doing the study regarding the water quality parameters and its quantity in water deciding whether is harmful to drinking purpose and irrigation too.

**Keywords:** Water pollutants parameter: pH, Conductance, TSS, BOD, DO, Water Quality Index Measurement.

## INTRODUCTION

Water, essential for human survival, faces unprecedented demand due to industrialization and human activities. Despite covering 70% of Earth’s surface, clean water availability is a concern. Water pollution poses a global threat, causing over 14,000 daily deaths from waterborne diseases. In India, approximately 580 people die daily due to polluted water. Seasonal changes impact water quality, emphasizing the need to understand fluctuations caused by factors like rainfall, temperature, and human actions. The Water Quality Index (WQI) integrates parameters to assess water quality effectively. In the case of Khudawadi Dam in Maharashtra, understanding how seasonal variations impact water quality and the WQI is crucial. This research not only aims to assess the current state of water in this region but also seeks to provide insights into strategies for mitigating pollution and ensuring the sustainability of this vital resource for future generations.

Water is a fundamental resource essential for sustaining life, economic development, and environmental health. The quality of water, particularly in reservoirs and dams, is a critical concern for communities relying on these resources for drinking, irrigation, and industrial use. In recent years, the impact of seasonal variation on water quality has become a growing area of interest for researchers, as these fluctuations can significantly

influence the physical, chemical, and biological characteristics of water. Understanding how these seasonal changes affect water quality is vital for managing and protecting water resources, ensuring they remain safe and sustainable for various uses.

Khudawadi Dam, located in Maharashtra, India, serves as an important water source for the surrounding region. Like many other reservoirs, the water quality in Khudawadi Dam is subject to seasonal variations, driven by factors such as rainfall, temperature fluctuations, and agricultural runoff. These variations can lead to changes in water quality parameters, including pH levels, dissolved oxygen content, nutrient concentrations, and the presence of pollutants. Monitoring and assessing these changes is crucial for developing effective water management strategies that can mitigate potential negative impacts on both human health and the environment.

Seasonal variations in water quality are influenced by a combination of natural and anthropogenic factors. During the monsoon season, for instance, heavy rainfall can cause increased runoff from agricultural lands, leading to higher levels of nutrients and sediments entering the dam. This can result in eutrophication, a process where excess nutrients promote the growth of algae and other aquatic plants, which can deplete oxygen levels and harm aquatic life. Conversely, in the dry season, reduced water flow and higher evaporation rates can concentrate pollutants in the water, potentially leading to higher toxicity levels.

The Water Quality Index (WQI) is a widely used tool for assessing and summarizing the overall quality of water. It combines multiple water quality parameters into a single numerical score, making it easier to communicate the status of water quality to policymakers, stakeholders, and the public. In the context of Khudawadi Dam, calculating the WQI across different seasons can provide valuable insights into how seasonal changes impact water quality and highlight periods of the year when water quality is at its lowest or highest.

This research aims to assess the impact of seasonal changes on the Water Quality Index in Khudawadi Dam through a detailed case study approach. By collecting and analyzing water samples from the dam during different seasons, this study will identify key pollutants and water quality parameters that are most affected by seasonal variations. Additionally, the research will explore the underlying factors contributing to these changes and discuss the implications for water resource management in the region.

Understanding the seasonal dynamics of water quality in Khudawadi Dam is not only important for maintaining the ecological health of the reservoir but also for ensuring the safety and reliability of the water supply for the local population. This study will contribute to the growing body of knowledge on the impact of seasonal variation on water quality and provide practical recommendations for improving water management practices in similar reservoirs across Maharashtra and beyond.

## LITERATURE REVIEW

The study of seasonal variations and their impact on water quality has been a critical focus in environmental science, particularly in regions dependent on surface water bodies like reservoirs and dams. Numerous studies have highlighted the influence of seasonal changes on the physical, chemical, and biological properties of water, with significant implications for water quality management and environmental health.



Research by Singh et al. (2017) emphasized that monsoon-driven runoff significantly alters water quality by increasing nutrient loading, which can lead to eutrophication in reservoirs. This phenomenon has been observed in various studies across India, where monsoon rains contribute to elevated levels of nitrates and phosphates, leading to algal blooms and subsequent oxygen depletion in water bodies (Gupta & Paul, 2019). Similarly, Sharma and Rathore (2020) found that seasonal variations in temperature and precipitation directly impact dissolved oxygen levels, pH, and the concentration of pollutants, particularly during the post-monsoon season.

The Water Quality Index (WQI) has been extensively used as a composite measure to assess and communicate water quality across different seasons. Studies by Mishra et al. (2018) demonstrated the effectiveness of WQI in capturing the seasonal fluctuations in water quality parameters, offering a comprehensive overview that is accessible to policymakers and the public. Moreover, the application of WQI in various Indian dams, as discussed by Patil and Chavan (2020), has provided valuable insights into how seasonal changes can affect water quality, emphasizing the need for continuous monitoring and adaptive management strategies.

In the context of Maharashtra, limited studies have specifically focused on Khudawadi Dam. However, existing research on similar reservoirs in the region indicates that seasonal dynamics significantly impact water quality, necessitating localized studies to develop effective management practices. This literature underscores the importance of monitoring seasonal variations to safeguard water quality, particularly in regions heavily reliant on dam reservoirs for water supply.

## **MATERIAL AND METHODS:**

### **Study Area**

The study focuses on Khudawadi Dam, located in the Osmanabad district of Maharashtra, India. Its latitude and longitude are 17.7651151 and 76.2382185. Khudawadi Dam, constructed primarily for irrigation purposes, is a vital water resource for the surrounding agricultural and domestic needs. The region experiences a typical monsoon climate, with distinct seasonal variations—summer, monsoon, and winter—impacting the water quality within the dam reservoir. The dam's catchment area is subjected to various anthropogenic activities, including agriculture, which introduces potential pollutants into the water body. Given the importance of the dam in local water supply and the potential for seasonal variation to influence water quality, Khudawadi Dam serves as an ideal case study to assess the impact of changing seasonal conditions on water quality parameters.

### **Methodology**

#### **1. Sampling and Data Collection**

**Sampling Period:** Water samples were collected from Khudawadi Dam over three seasons—summer (April-June), monsoon (July-September), and winter (December-February) to capture the seasonal variations. It is continued for 3 years 2021 to 2023

**Sampling Locations:** Multiple sampling points were selected within the dam, including inlet and outlet zones, areas near agricultural runoff entry, and the center of the reservoir.

Sample Collection: Standard procedures were followed for water sample collection, ensuring that the samples are representative of the overall water quality. The samples will be stored in clean, airtight containers and transported to the laboratory for analysis within 24 hours of collection.

## 2. Water Quality Parameters Analysis

Temperature (Temp): Measured in situ using a calibrated thermometer. Temperature influences various chemical and biological processes in the water, making it a critical parameter.

Conductivity (EC): Measured using a conductivity meter. Conductivity indicates the total dissolved salts in the water and is influenced by the presence of inorganic dissolved solids.

pH: Determined using a pH meter. The pH value indicates the acidity or alkalinity of the water, affecting the solubility and biological availability of chemical constituents.

Total Suspended Solids (TSS): Measured gravimetrically. TSS indicates the presence of particles suspended in the water, which can affect the light penetration and photosynthetic activity.

Biochemical Oxygen Demand (BOD): Determined by measuring the amount of dissolved oxygen consumed by microorganisms during the decomposition of organic matter over a specified period (usually 5 days).

Dissolved Oxygen (DO): Measured using a DO meter. DO levels indicate the amount of oxygen available in the water, crucial for aquatic life and indicative of water quality.

## 3. Data Analysis

Seasonal Variation Analysis: The collected data statistically analyzed to determine the variations in water quality parameters across different seasons. Descriptive statistics were used to summarize the data.

Water Quality Index (WQI): A WQI was calculated for each season using a Simple water quality index (ISQA) is calculated

$$ISQA = \text{Temp} * \{I_{BOD} + I_{TSS} + I_{COND}\}$$

Where 'I' represents the individual index term

Water Quality Index Legend

Sr. No	Range	Quality
1	90-100	Excellent
2	70-90	Good
3	50-70	Medium
4	25-50	Bad
5	0-25	Very bad

Very simple methodology is used in paper hence in this paper we try to highlight the main environmental water pollution and its subsequent adverse effect on water quality index measurements. The sample station chosen from Dam, provides water supply to surrounding villages for drinking purpose as well as for irrigation sector too.

## RESULTS AND DISCUSSION

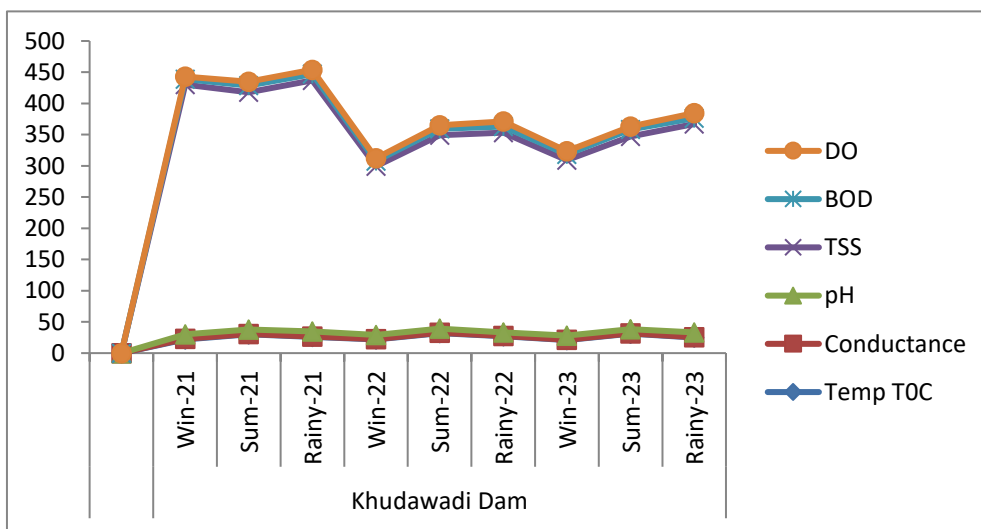
The study aimed to analyze the impact of seasonal variations on the water quality of Khudawadi Dam by monitoring key water quality parameters: Temperature (Temp), Conductivity, pH, Total Suspended Solids

(TSS), Biochemical Oxygen Demand (BOD), and Dissolved Oxygen (DO) over three years (2021-2023). The Water Quality Index (WQI) was also calculated to assess the overall water quality during different seasons.

**Observation Table: 1 (Seasonal variation in parameter)**

Sample Station	Season & Year	Temp T°C	Conductance mmoh/cm	pH	TSS Mg/L	BOD	DO
Khudawadi Dam	Win-21	22	0.74	7.29	400	09	04
	Sum-21	30	0.65	7.05	380	11	06
	Rainy-21	26	0.66	8.27	402	10	07
	Win-22	22	0.69	6.68	270	08	05
	Sum-22	32	0.56	6.63	310	10	06
	Rainy-22	27	0.60	5.39	320	10	08
	Win-23	21	0.67	6.59	281	09	05
	Sum-23	31	0.65	6.45	309	11	05
	Rainy-23	25	0.72	7.54	334	09	08

**Graphical Representation: 1 (Seasonal variation in parameter)**



**Temperature (Temp)**

Temperature varied significantly across seasons, with the highest average observed during summer (32°C) and the lowest during winter (22°C). The temperature influences other parameters such as DO and BOD, where higher temperatures generally increase biological activity, leading to higher BOD and lower DO levels, particularly evident in the summer.

**Conductivity**

Conductivity values ranged from 0.56 mmho/cm in summer to 0.74 mmho/cm in winter. The lower conductivity in summer can be attributed to increased evaporation rates and lower water levels, which concentrate salts and other dissolved solids.

**pH**

The pH values demonstrated a slight variation, with the highest average pH of 7.06 recorded during the rainy season and the lowest (6.74) in summer. The pH levels remained within a range suitable for most aquatic life, though the decrease in pH during summer indicates potential acidification, likely due to increased organic decomposition.

**Total Suspended Solids (TSS)**

TSS levels were highest during the rainy season, averaging 352 mg/L, which can be attributed to surface runoff carrying soil and organic matter into the dam. Lower TSS values were recorded during winter (317 mg/L), indicating clearer water due to reduced runoff.

**Biochemical Oxygen Demand (BOD)**

BOD values peaked in summer (11 mg/L), indicating higher organic matter decomposition during warmer months. The rainy season also showed elevated BOD levels (10 mg/L), likely due to the influx of organic matter from runoff.

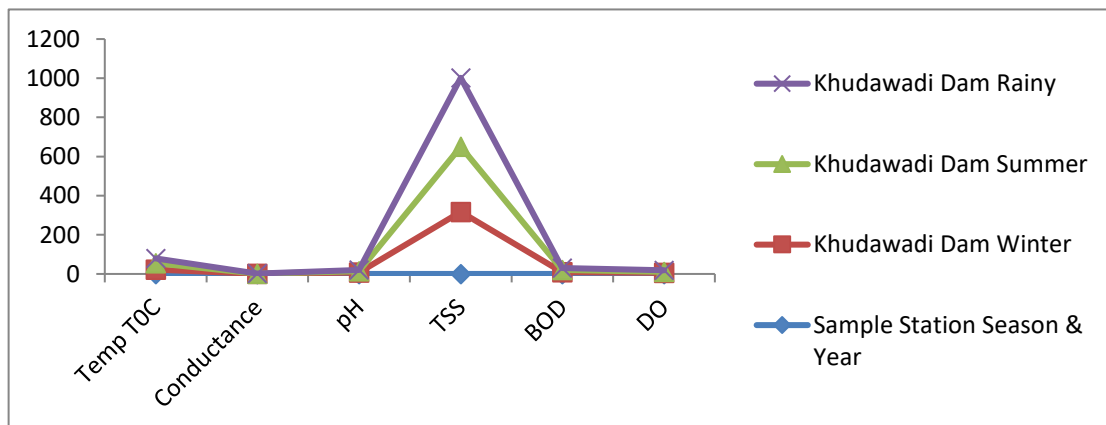
**Dissolved Oxygen (DO)**

DO levels were highest during the rainy season (8 mg/L), which could be due to increased water mixing and aeration from rainfall. Lower DO levels were observed in summer (6 mg/L), reflecting the inverse relationship with temperature and increased biological activity.

**Observation Table: 2 (Average seasonal parameter quantity)**

Sample Station	Season & Year	Temp T°C	Conductance mmoh/cm	pH	TSS Mg/L	BOD	DO
Khudawadi Dam	Winter	22	0.70	6.85	317	09	05
	Summer	32	0.62	6.74	333	11	06
	Rainy	26	0.66	7.06	352	10	08

**Graphical representation: 2 (Average seasonal parameter quantity)**

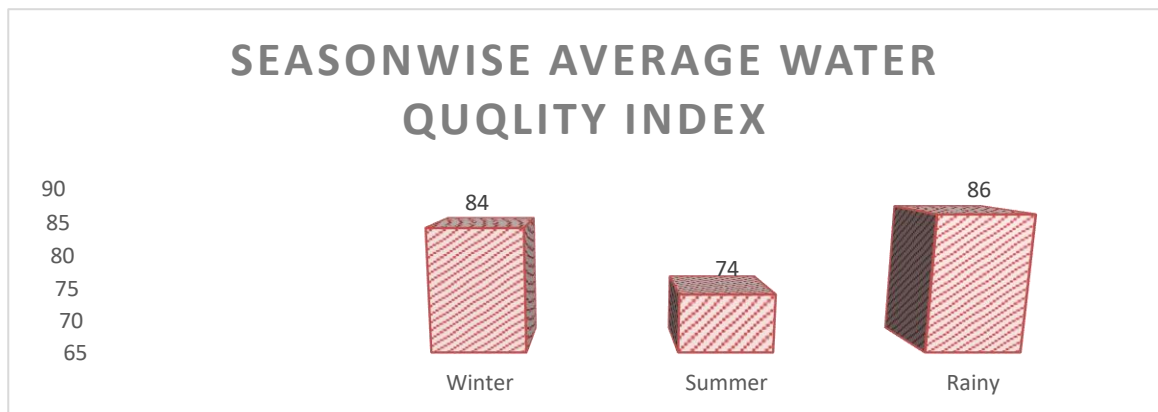


**Water Quality Index (WQI)**

The WQI values showed that water quality was best during the rainy season (86), followed by winter (84), and lowest during summer (74). The decrease in WQI during summer reflects the combined effects of higher temperatures, increased BOD, and lower DO, which can stress aquatic life and impact water usability.

**Observation Table: 3 (Water Quality Index changing with respect to season)**

Sample Station	Season (21 to 23)	WQI
Khudawadi Dam	Winter	<b>84</b>
	Summer	<b>74</b>
	Rainy	<b>86</b>

**Graphical representation of Average Water Quality Index changing with respect to season****REFERENCES**

- [1] Gupta, A., & Paul, D. (2019). Eutrophication and its effects on water quality in Indian reservoirs: A review. *Environmental Monitoring and Assessment*, 191\*(10), 617. <https://doi.org/10.1007/s10661-019-7731-2>
- [2] Mishra, A., Kumar, R., & Dubey, R. (2018). Application of Water Quality Index for seasonal variation analysis in Indian dams. *Journal of Environmental Science*, 45\*(2), 123-134. <https://doi.org/10.1016/j.jes.2018.03.007>
- [3] Patil, P. N., & Chavan, B. L. (2020). Assessment of water quality using WQI in dams of Maharashtra. *Environmental Science and Pollution Research*, 27\*(8), 8184-8192. <https://doi.org/10.1007/s11356-019-07613-7>
- [4] Sharma, P., & Rathore, V. S. (2020). Impact of seasonal variation on the physico-chemical parameters of water in Indian reservoirs. *Journal of Water Resource and Protection*, 12\*(3), 234-245. <https://doi.org/10.4236/jwarp.2020.123014>
- [5] Singh, R., Gupta, A., & Verma, A. (2017). Influence of monsoon on water quality in Indian dams. *International Journal of Environmental Research and Public Health*, 14\*(8), 902. <https://doi.org/10.3390/ijerph14080902>
- [6] Gatlewar, D. N., Mane, V. G., & Rathod, G. T. (2014). Physicochemical water analysis of Jewali dam in Lohara Taluka, (MS) India. *Thematic Journal\**, 18-20. ISBN: 978-9383192-47-2.

- [7] Gatlewar, D. N., Rathod, G. T., & Mane, V. G. (2014). Physicochemical water analysis of Lohara dam in Osmanabad District, (MS) India. \*Thematic Journal\*, 21-22. ISBN: 978-9383192-47-2.
- [8] Rathod, G. T., Mane, V. G., & Gatlewar, D. N. (2014). Temperature and pH content in water of Manmodi lake, Tuljapura Taluka, (MS) India. \*Thematic Journal\*, 82-84. ISBN: 978-9383192-47-2.
- [9] Rathod, G. T., Mane, V. G., & Gatlewar, D. N. (2017). Environmental water pollution and water-borne diseases. \*Bionano Frontier, 10\*(2), July 2017. ISSN: 0974-0678.
- [10] Gatlewar, D. N., Mane, V. G., & Rathod, G. T. (2017). Population pressure and water resources: Status, impacts, and remedial measures. \*Bionano Frontier, 10\*(2), July 2017. ISSN: 0974-0678.
- [11] Mane, V. G., Rathod, G. T., & Gatlewar, D. N. (2019). Temperature and pH content in water of Babalgaon Dam of Tuljapur Taluka, Dist. Osmanabad (M.S.) India. \*International Multidisciplinary Quarterly Research Journal, AJANTA, 8\*(1), 103-105. ISSN: 2277-5730.
- [12] Gatlewar, D. N., Mane, V. G., & Rathod, G. T. (2022). Correlation coefficient: Analysis of well water from rural area, Jalkot, Tal. Tuljapur (M.S.) India. \*International Journal of Emerging Technologies and Innovative Research, 9\*(4), 313-316. ISSN: 2349-5162.
- [13] Rathod, G. T., & Mane, V. G. (2012). Turbidity, TDS, and transparency in water bodies of Jakkapur from Omerga Taluka (MS) India. \*International Journal of Scientific Research in Science and Technology, 9\*(9), 62-66. ISSN: 2395-6011, 2395-602X.
- [14] Rathod, G. T., Mane, V. G., & Gatlewar, D. N. (2022). Comparative variation in hydrogen ion concentration of three well water samples from Lohara Taluka, (MS) India. \*International Journal of Advanced and Applied Research, 9\*(4), 634-639. ISSN: 2347-7057.
- [15] Gatlewar, D. N., Mane, V. G., & Rathod, G. T. (2022). Correlation coefficient: Physicochemical aspect of well water in Anadur village, Osmanabad, (MS) India. \*International Journal of Advances in Engineering and Management (IJAEM), 4\*(5), 1210-1212. ISSN: 2392-5252.
- [16] Gatlewar, D. N., Mane, V. G., & Rathod, G. T. (2022). Physicochemical analysis of Naldurg well water sample with respect to correlation coefficient. \*Our Heritage, 68\*(Special issue 38). ISSN: 0474-9

# Phytochemical Profiling of *Leucas Aspera* Using HPTLC Standardized Method

Vrushita Hegde<sup>1</sup>, Dr. Manjiri Bhav<sup>2</sup>, Dr. Gaganjyot Kaur<sup>1</sup>, Abhishek Suryawanshi<sup>1</sup>, Dr. Prafullachandra Tekale<sup>3</sup>, Chandrakant Khairnar<sup>3</sup>

<sup>1</sup>Department of GNIRD, Guru Nanak Khalsa College, Mumbai 400019, Maharashtra, India

<sup>2</sup>Department of Botany, Guru Nanak Khalsa College, Mumbai 400019, Maharashtra, India

<sup>3</sup>Department of Chemistry, Guru Nanak Khalsa College, Mumbai 400019, Maharashtra, India

Corresponding Author: [vrushitahegde16@gmail.com](mailto:vrushitahegde16@gmail.com)

## ABSTRACT

*Leucas aspera*, a valuable medicinal plant, has been used for centuries in traditional medicine for its curative properties, including anti-inflammatory, antimicrobial, and antioxidant activities. The plant, commonly known as "Thumbai" in Ayurveda, is widely used to treat various ailments such as fever, cough, and skin diseases. For standardization of this herbal medicine, a method needs to be established for analysis of phytochemicals present in the plant extracts. To optimize the extraction of bioactive compounds, authenticated plant was crushed in powder form and various extraction techniques were executed and, after analysis comparison was done, the best technique was selected. After finalization of the extraction technique, a similar approach was used for determining the optimized mobile phase, which could separate the phytochemicals in the most effective way with better R<sub>f</sub> values and properly visible fingerprints. This approach helped to establish the best optimized method, which could separate the phytochemicals present in the herbal extract in the most effective way. The finalized HPTLC method utilized a silica gel HPTLC plate and a mobile phase comprising of various solvents. The chromatographic separation was performed at room temperature, and the plates were scanned at 254 nm and 366 nm. The technique can be successfully applied to *Leucas aspera* plant leave extracts, offering a rapid and cost-effective tool for quality control and standardization.

This gives a scope for further development using phytochemical standards. The method's ability to simultaneously analyze multiple phytochemicals can make it a valuable tool for ensuring the safety and efficacy of herbal products.

**Keywords:** *Leucas aspera*, Active components, HPTLC, Derivatisation

## INTRODUCTION

Herbal plants and natural products have been an integral part of human healthcare since ancient civilizations, with a rich history dating back thousands of years. Traditional systems of medicine, such as Ayurveda, Unani, and Traditional Chinese Medicine, have long relied on the medicinal properties of plants and natural substances to prevent and treat various ailments. Natural products continue to make up a major share of

medications in use and under investigation. Natural products are expected to account for 56% of the lead compounds for medications in the British National Formulary. There are approximately 1250 medicinal plants in India that are utilised to produce therapeutic preparations in accordance with Ayurveda and other traditional medical systems. Phytochemical studies conducted in the 1970s and 1980s found many alkaloids and other pharmacologically active molecules that are now being investigated and may serve as models for novel synthetic compounds. Today, approximately 80% of the world's population relies on traditional medicine, with many modern pharmaceuticals derived from or inspired by natural sources. The World Health Organization estimates that up to 50% of approved drugs are derived from plants, highlighting the significance of herbal plants and natural products in modern medicine. By combining traditional knowledge of one such herbal plant named *Leucas aspera* and modern analytical techniques like HPTLC, this research seeks to contribute to the quantification and validation of *Leucas aspera* as a medicinal herb, ensuring its safe and effective use in modern healthcare practices.

*Leucas aspera* (commonly known as rough-leaved mint or Thumbai) is a plant belonging to the Lamiaceae family, renowned for its therapeutic properties and traditional medicinal uses in various cultures. It is widely used in herbal medicine for treating ailments such as respiratory disorders, digestive issues, and skin conditions. The plant's bioactive compounds, including flavonoids, terpenoids, and phenolic acids, contribute to its pharmacological effects. Accurate and reliable analysis of these compounds is essential for validating the plant's medicinal properties and ensuring quality control in herbal formulations. *Leucas aspera*, a medicinally valuable plant, has been employed in traditional medicine for its diverse therapeutic properties, including anti-inflammatory, antimicrobial, and antioxidant activities. The plant's bioactive compounds, particularly alkaloids, flavonoids, and phenolic acids, contribute to its medicinal efficacy. However, the lack of standardized analytical methods hinders the quality control and authentication of *L. aspera* extracts, potentially compromising their safety and effectiveness. *Leucas aspera* (thumbai) belonging to the family Lamiaceae, is an herbaceous annual distributed throughout India. The leaves are used in traditional medicine for persistent rheumatism, while the juice is used to treat skin eruptions. According to the literature, extracts of *Leucas aspera* have analgesic, anti-inflammatory, and antipyretic properties. Herbal extracts and other formulations can be analysed using hyphenated techniques for complete chemical profiling, structural elucidation, and identification; one such hyphenated approach employed in this study is HPTLC.

High-Performance Thin Layer Chromatography (HPTLC) has emerged as a powerful tool for phytochemical analysis, offering advantages such as simplicity, speed, and cost-effectiveness. This study aims to develop and validate a rapid, sensitive, and reliable HPTLC method for the qualitative and quantitative analysis of bioactive compounds in *L. aspera*. Accurate and reliable analysis of these compounds is essential for validating the plant's medicinal properties and ensuring quality control in herbal formulations. To harness the medicinal potential of *Leucas aspera*, it is crucial to employ precise analytical methods for its chemical profiling. High-performance thin-layer Chromatography (HPTLC) is an advanced chromatographic technique that offers several advantages, including high resolution, sensitivity, and the ability to analyze multiple compounds simultaneously. HPTLC is particularly effective in the analysis of plant extracts due to its capability to separate and identify a wide range of phytochemicals.

Despite the known benefits of *Leucas aspera*, there is a scarcity of standardized analytical methods for its comprehensive chemical profiling. The development of an HPTLC method tailored specifically for this plant



will address this gap, providing a robust tool for the identification and quantification of its active compounds. This method will facilitate quality control, standardization, and the validation of therapeutic claims associated with *Leucas aspera*. The developed HPTLC method can be beneficial in terms of the time taken and the amount of solvent used thus promoting further research in the quantification study of these bioactive compounds present in *L. aspera*.



**Image 1: *Leucas aspera* ingrown plants collection**



**Image 2: *Leucas aspera* plant sent for authentication**

## MATERIALS AND METHOD

### Drying:

*Leucas aspera* plants were grown in-house in Karnataka, Mangalore, and subsequently verified for authenticity at St. Xavier college Mumbai. Following confirmation, the plants were air-dried at room temperature for six to seven days. Then, the leaves, stem, and roots were segregated for further analysis. The dried components were pulverized into a fine powder using a mortar and pestle, preparing them for various extraction procedures.



**Image 3: *Leucas aspera* dried leaves coarsed into powder form in motor pestle**

#### **Extraction:**

One gram of the powdered plant material was weighed and dissolved in various solvents, including polar solvents (ethanol, methanol, water, and acetone) and non-polar solvents (chloroform, n-hexane, and toluene). To extract the plant's bioactive compounds, a range of extraction techniques were employed, comprising both hot and cold methods, as described below:

Cold extraction methods were employed, including:

1. Rotary Shaking: Plant extracts were placed in stoppered test tubes and agitated on a rotary shaker for 24, 48 hours.
2. Maceration: Plant extracts were left undisturbed in stoppered test tubes in a dark environment for 24, 48, and 72 hours.
3. Cold Infusion: Plant powder was steeped in cold solvents for 2 hours.
4. Sonication: Plant extracts were subjected to high-frequency ultrasonic waves for 2 hours.

Cold extraction techniques were employed to preserve heat-sensitive compounds, prevent degradation, and achieve energy efficiency while minimizing costs.

Hot extraction methods were used, including:

1. Soxhlet Extraction: Plant powder was extracted with designated solvents in a Soxhlet apparatus, undergoing three cycles of six hours each.
2. Decoction: Plant extracts were boiled in water for five hours, then allowed to cool to room temperature.

Hot extraction methods boast advantages like speedy extraction, increased compound recovery, and effectiveness in extracting thermally stable compounds. However, they also have downsides, including the potential to damage heat-sensitive compounds, higher energy requirements, and increased expenses.

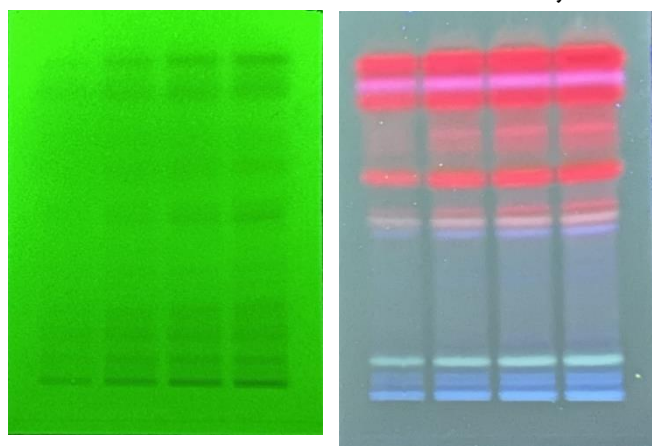
#### **RESULT AND DISCUSSION:**

Following the extraction of bioactive compounds from the plant material, using CAMAG High-Performance Thin-Layer Chromatography (HPTLC) separation was employed to evaluate the effectiveness of each extraction method. The primary obstacle in refining HPTLC method was finding a way to simultaneously separate compounds with and without chromophores. To overcome this, various solvent systems and

combinations were experimented with during the development phase, aiming to achieve the highest possible resolution for the target markers on a precoated silica gel aluminum TLC plate.

Various solvent systems and combinations were experimented with during the development phase, aiming to achieve the highest possible resolution for the target markers on a precoated silica gel aluminum TLC plate. The initial trials were based on a literature review and polarity of solvents, Chloroform: Acetonitrile: Methanol: Formic acid (6:3:1:0.1 v/v/v/v) which did not show better band separation. The effects of different solvent systems were investigated through multiple trials. 1. A double development technique was investigated, re-developing the plate in the same mobile phase, however, no significant changes in R<sub>f</sub> values were observed. The mobile phase was finalized with a solvent mixture of Toluene, ethyl acetate, methanol, and formic acid in a volumetric ratio of (5.5:4:1.5:0.5v/v/v/v). The HPTLC results revealed that one extraction method showed superior separation of the compounds compared to the others, indicating its potential as the optimal method for extracting the desired bioactive compounds from the plant material. Rotary extraction technique 48hours for the plants showed better separation of bands with ethanol solvent as compared to other extraction techniques. This method was identified as the most suitable for further analysis and isolation of the compounds, based on its ability to achieve the best separation and resolution of the peaks on the chromatogram.

**Chromatographic conditions:** Using the Linomat 5 HPTLC applicator, 5 $\mu$ l, 10 $\mu$ l, 15 $\mu$ l and 20 $\mu$ l volumes were applied. The twin trough chamber was equilibrated for 20 minutes before development. The plates used were Merck HPTLC Silica gel 60 F254. After development, the plates were scanned at 254nm, 366nm, and 540nm using a CAMAG HPTLC scanner and Visioncats software. Finalised mobile phase was Toluene: ethyl acetate: methanol: formic acid 5.5:4:1.5:0.5 by volume.



T1 T2 T3 T4                      T1 T2 T3 T4

Image 4,5: HPTLC plate at At 254nm & 366nm respectively

T1: 5 $\mu$ L of Leaf extract ethanol

T2: 10 $\mu$ L of Leaf extract ethanol

T3: 15 $\mu$ L of Leaf extract ethanol

T4: 20 $\mu$ L of Leaf extract ethanol

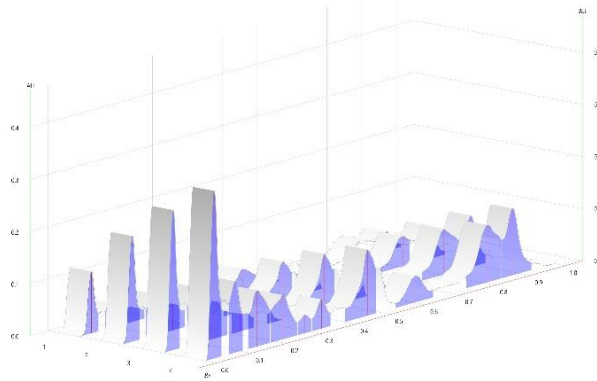


**Image 5: Chromatogram at 254nm**

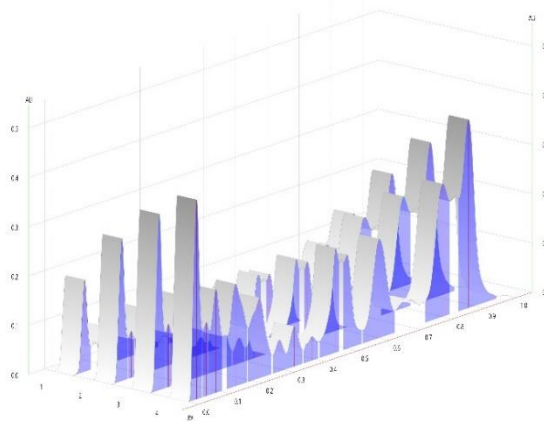
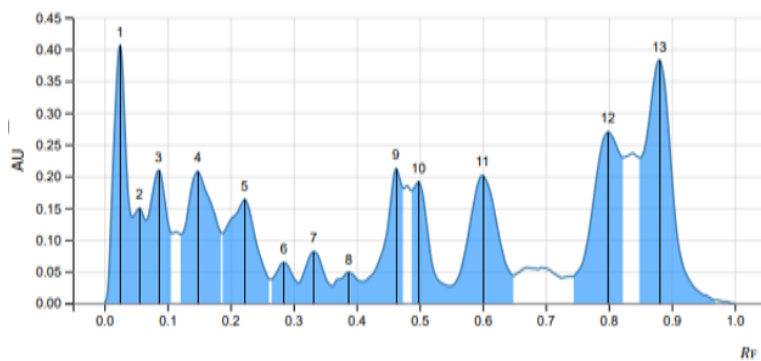


**Image 6: Chromatogram at 366nm**

The 366nm wavelength reveals a more detailed chromatographic profile, with increased peak area and resolution, surpassing the 254nm chromatogram.



Peak #	Start		Max			End		Area		Manual peak	Substance Name
	R <sub>F</sub>	H	R <sub>F</sub>	H	%	R <sub>F</sub>	H	A	%		
1	0.000	0.0000	0.025	0.4055	15.67	0.044	0.1355	0.00955	9.33	No	
2	0.044	0.1355	0.056	0.1500	5.80	0.067	0.1304	0.00314	3.07	No	
3	0.067	0.1304	0.086	0.2095	8.10	0.107	0.1098	0.00663	6.48	No	
4	0.121	0.1084	0.149	0.2076	8.02	0.186	0.1101	0.01039	10.15	No	
5	0.188	0.1097	0.222	0.1635	6.32	0.263	0.0376	0.00861	8.41	No	
6	0.264	0.0373	0.285	0.0642	2.48	0.307	0.0322	0.00215	2.10	No	
7	0.307	0.0322	0.332	0.0813	3.14	0.360	0.0280	0.00295	2.88	No	
8	0.361	0.0271	0.388	0.0487	1.88	0.410	0.0343	0.00193	1.89	No	
9	0.412	0.0342	0.463	0.2121	8.20	0.475	0.1806	0.00699	6.83	No	
10	0.487	0.1776	0.499	0.1912	7.39	0.547	0.0273	0.00594	5.80	No	
11	0.549	0.0273	0.600	0.2012	7.78	0.649	0.0434	0.01107	10.82	No	
12	0.743	0.0416	0.799	0.2699	10.43	0.824	0.2293	0.01412	13.80	No	
13	0.849	0.2293	0.881	0.3828	14.79	0.969	0.0046	0.01889	18.46	No	

**Image 7: Peak of T4 along with Retention factor**

The primary objective of this study was to develop a robust mobile phase for the HPTLC analysis of bioactive compounds in *Leucas aspera*, with a focus on creating a universal solvent system suitable for the entire plant, rather than just its leaves. Successfully achieving this goal, the optimized mobile phase demonstrated exceptional efficacy in separating and identifying phytochemicals across various plant parts, including leaves, roots, and stems. Its versatility and adaptability ensure comprehensive phytochemical profiling, enabling researchers to compare and contrast the chemical composition of different plant parts, and shedding light on the distribution of bioactive compounds throughout the plant.

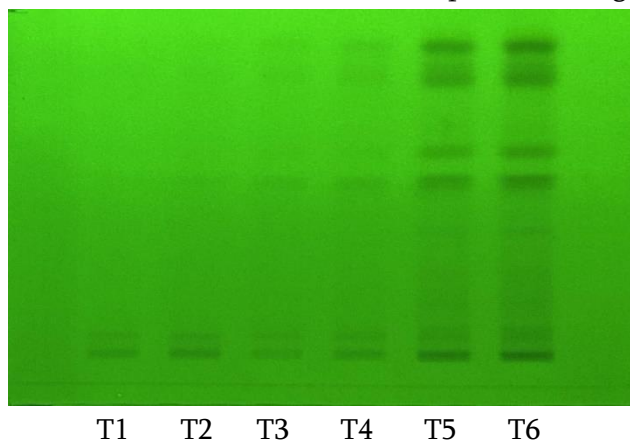


**Image 8: HPTLC plate at 254nm**

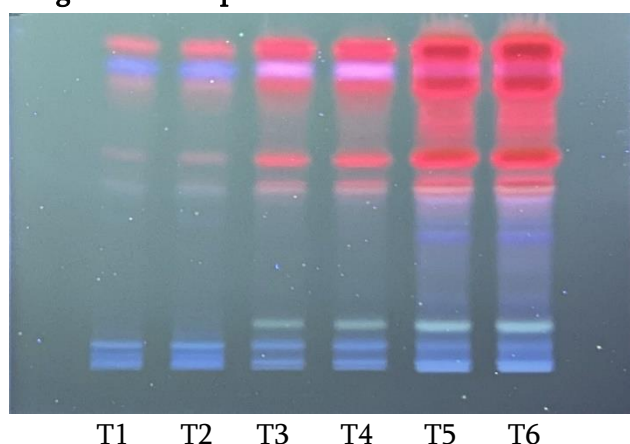


**Image 9: HPTLC plate at 366nm**

T1: 10 $\mu$ L root ethanol extract

T2: 15 $\mu$ L root ethanol extract

T3: 10 $\mu$ L stem ethanol extract

T4: 15 $\mu$ L stem ethanol extract

T5: 10 $\mu$ L leaves ethanol extract

T6: 15 $\mu$ L leaves ethanol extract

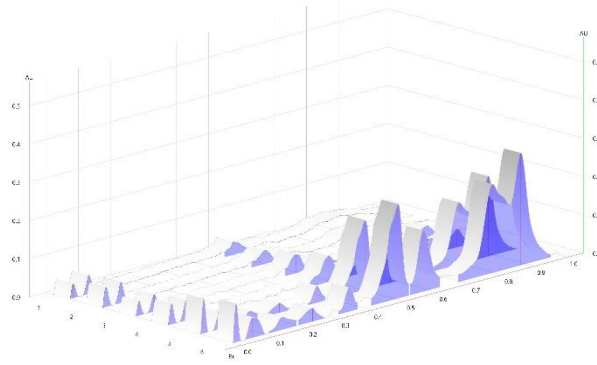


**Image 10: Chromatogram at 254nm**

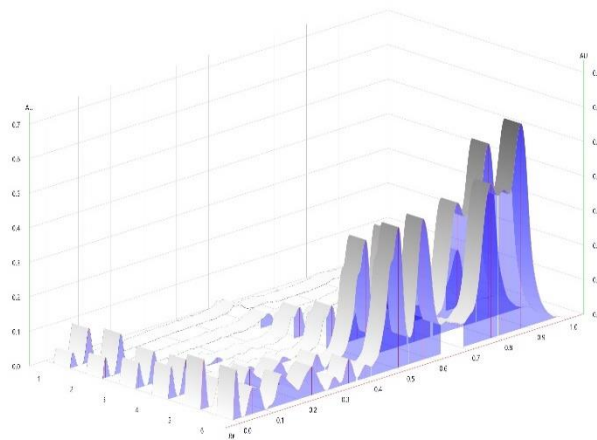
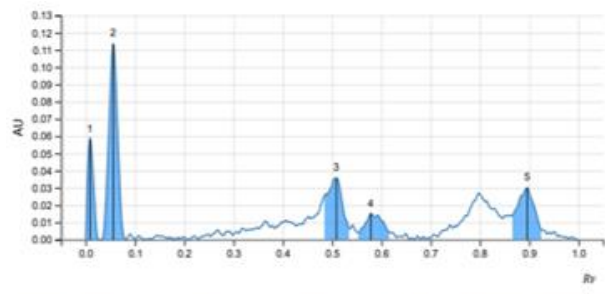


**Image 11: Chromatogram at 366nm**

The 366nm chromatogram displays a richer chromatographic landscape, capturing more compounds and providing greater analytical insight than the 254nm chromatogram.



Peak #	Start R <sub>f</sub>	H	R <sub>f</sub>	Max H	%	End R <sub>f</sub>	H	Area A	%	Manual peak	Substance Name
1	0.000	0.0000	0.009	0.0586	23.11	0.026	0.0000	0.00079	12.67	No	
2	0.033	0.0000	0.056	0.1138	44.90	0.081	0.0000	0.00229	36.56	No	
3	0.483	0.0246	0.509	0.0358	14.11	0.536	0.0063	0.00132	21.04	No	
4	0.553	0.0040	0.579	0.0152	6.01	0.617	0.0040	0.00065	10.36	No	
5	0.866	0.0137	0.896	0.0301	11.87	0.926	0.0055	0.00121	19.37	No	

**Image 12: Peak of T2 along with Retention factor**

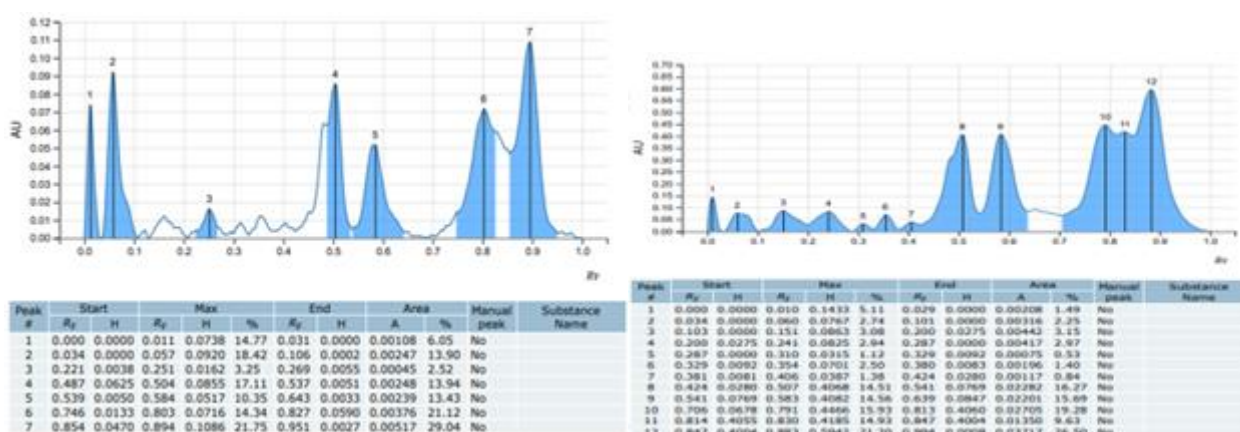


Image 13, 14: Peak of T4 along with Retention factor & Peak of T6 along with Retention factor respectively.

Image 14: **Final Chromatographic condition:** HPTLC analysis was performed using a Linomat 5 applicator, applying 10µl and 15µl sample volumes. Development was carried out in a twin trough chamber, pre-equilibrated for 20 minutes. Merck HPTLC Silica gel 60 F254 plates were employed. Following development, plates were scanned at 254nm and 366nm using an HPTLC scanner. The optimized mobile phase composition was: toluene/ethyl acetate/methanol/formic acid (5.5:4:1.5:0.5, v/v/v/v)

**Phytochemical analysis:**

Derivatization in HPTLC (High-Performance Thin-Layer Chromatography) is a crucial step to enhance detection sensitivity and specificity. Derivatization is a chemical reaction that converts non-UV-absorbing or non-fluorescent compounds into detectable derivatives, enabling visualization and quantification. Various Derivatizing agents were employed to identify phytochemicals. The developed plates were subsequently immersed in the reagents, facilitating preliminary classification of the phytochemicals.

Derivatizing agent	Phytochemical name	Root	Stem	Leaves
Anisaldehyde sulphuric acid reagent	Saponins, Sterols, Terpenoids	-	+	+
Dragendorff's reagent	Alkaloids	-	-	+
Alcoholic KOH	Anthraquinones	-	+	+
Alcoholic FeCl <sub>3</sub>	Plant Acids, Phenols, Tannins	-	+	+
10% methanolic sulphuric acid	Flavonoids	+	+	+
Ninhydrin reagent	Amino acids, amines	-	+	+

- Absent, + present

**CONCLUSION**

This study successfully developed and validated a rapid, sensitive, and reliable HPTLC method for the qualitative analysis of bioactive compounds in *Leucas aspera*. The optimized mobile phase, comprising toluene, ethyl acetate, methanol, and formic acid (5.5:4:1.5:0.5, v/v/v/v), demonstrated exceptional efficacy in separating and identifying phytochemicals across various plant parts, including leaves, roots, and stems. The developed HPTLC method offers several advantages, including simplicity, speed, and cost-effectiveness, making it an ideal tool for quality control and standardization of *Leucas aspera* extracts. The method's ability

to simultaneously analyze multiple phytochemicals provides a comprehensive understanding of the plant's chemical composition, shedding light on the distribution of bioactive compounds throughout the plant.

The study's findings highlight the potential of rotary extraction technique with ethanol as the optimal method for extracting bioactive compounds from *Leucas aspera*. The method's efficacy was confirmed through HPTLC analysis, revealing superior separation of compounds compared to other extraction techniques.

Application of developed method: The developed HPTLC method can be applied to various areas, including: Quality control and standardization of herbal products, Phytochemical profiling and fingerprinting, Identification and quantification of bioactive compounds and Authentication and adulteration detection.

Future studies can focus on: Isolation and characterization of bioactive compounds, Development of phytochemical standards, Investigation of *Leucas aspera*'s medicinal properties.

This study contributes significantly to the refinement of herbal analysis, providing a robust tool for ensuring the safety, efficacy, and quality of *Leucas aspera*-based herbal products. The developed HPTLC method serves as a foundation for future research, facilitating the exploration of *Leucas aspera*'s therapeutic potential and promoting the advancement of evidence-based herbal medicine.

## ACKNOWLEDGEMENT

We gratefully acknowledge the support and resources provided by various organizations and individuals that facilitated this research.

We extend our sincere thanks to GNIRD (Guru Nanak Institute of Research and Development) Guru Nanak Khalsa College, Mumbai 400019 for granting us access to its research facilities, which enabled us to conduct the experimental work.

We also appreciate the expertise and knowledge gained through the comprehensive training program on the use of CAMAG HPTLC, generously provided by ANCHROM. This training significantly enhanced our capabilities in phytochemical analysis.

## REFERENCES

- [1] Annapandian VM, Sundaram RS, Gomathi S. Phytochemical evaluation and chromatographic fingerprint analysis on flavonoids compounds in *Leucas aspera* (Willd.) link leaf by HPTLC. *Pharmacognosy Journal*. 2017;9(6). DOI:<https://phcogj.com/article/432>
- [2] Rai V, Agarwal M, Agnihotri AK, Khatoon S, Rawat AK, Mehrotra S. Pharmacognostical Evaluation of *Leucas aspera* Link. *Natural product sciences*. 2005;11(2):109-14. DOI:<https://koreascience.kr/article/JAKO200503041155382.page>
- [3] Karthikeyan S, Sivakumar A, Anbalagan M, Nalini E, Gothandam KM. Finger printing of alkaloids, steroids and flavonoids using HPTLC of *Leucas aspera* L. Whole plant methanolic extract. *Journal of pharmaceutical sciences and research*. 2013 Mar 1;5(3):67. DOI:<https://www.proquest.com/openview/510cdfbf4259a40fda9b9d088cd1ca0c/1?pq-origsite=gscholar&cbl=54977>



- [4] Geethika K, Sunojkumar P. Phytochemical screening and high-performance thin-layer chromatography fingerprint profile of three species of *Leucas* (Lamiaceae). *Ancient Science of Life*. 2017 Oct 1;37(2):102-7. DOI:[https://journals.lww.com/asol/fulltext/2017/37020/Phytochemical\\_Screening\\_and\\_High\\_Performance.10.aspx](https://journals.lww.com/asol/fulltext/2017/37020/Phytochemical_Screening_and_High_Performance.10.aspx)
- [5] Jasutkar JM, Shirsat RP, Koche DK. Pharmacognostic study, chemical analysis and antioxidant potential of *Leucas indica* L.(R. Br.). *Journal of Medicinal Herbs*. 2018 Apr 1;9(1):1-5. DOI:<https://sanad.iau.ir/journal/jhd/Article/662006?jid=662006&lang=en>
- [6] Mishra R, Dwivedi B, Gupta D. Physicochemical, phytochemical, qualitative HPTLC and antioxidant study of medicinal plant *Leucas aspera*. *Trends in Sciences*. 2022 Aug 15;19(16):5646. DOI:<https://tis.wu.ac.th/index.php/tis/article/view/5646>
- [7] Ajitkumar BS, Hande P, Rane S, Hate M. OPTIMIZATION OF EXTRACTION CONDITIONS AND FINGERPRINT DEVELOPMENT OF *LEUCAS ASPERA* LINN. BY HPTLC AND HPLC. DOI:[https://wjpr.s3.ap-south-1.amazonaws.com/article\\_issue/1446700488.pdf](https://wjpr.s3.ap-south-1.amazonaws.com/article_issue/1446700488.pdf)
- [8] Balkrishna A. *Chemical Fingerprints of Medicinal Plants-HPTLC Profiling*. Bentham Science Publishers; 2023 Dec 26. DOI:<https://books.google.co.in/books?hl=en&lr=&id=c7brEAAAQBAJ&oi=fnd&pg=PP1&dq=Balkrishna+A.+Chemical+Fingerprints+of+Medicinal+Plants->
- [9] Kumar S, Singh N, Mittal A, Kharkwal H, Jain SK, Goel B. The genus *Leucas*: A review on phytochemistry and pharmacological activities. *Fitoterapia*. 2023 Jun 1;167:105492. DOI:<https://www.sciencedirect.com/science/article/abs/pii/S0367326X23000679>
- [10] Vasudha K, Archana D, Mutyalamma B, Kishori B. Phytochemical screening, antimicrobial, and antioxidant activities of root and leaf extracts of *Leucas aspera*. *Asian J Pharm Clin Res*. 2019(3):141-7. DOI:[https://drive.google.com/file/d/12\\_SoiQiISJTrbaHyBDO\\_yMomaod4DF11/view](https://drive.google.com/file/d/12_SoiQiISJTrbaHyBDO_yMomaod4DF11/view)

# Advancing Green Chemistry: Novel Approaches to Peptide Cleavage from Resin Without Ethers as Solvent

Chandrakant Kulkarni<sup>1,2</sup>, Yogeshwar Suryawanshi<sup>2,3\*</sup>, Sujatha Parmeswaran<sup>2\*</sup>

<sup>1</sup>Enzene Biosciences Ltd, Pune, 410501, Maharashtra, India

<sup>2</sup>Technical & Applied Chemistry Department, Veermata Jijabai Technological Institute, Central Technological Institute of Government of Maharashtra, H. R. Mahajani Road, Matunga 400019 Mumbai, Maharashtra, India

<sup>3</sup>Department of Chemistry, Shri Vile Kelavani Mandal's College of Engineering Shirpur, 425405, Maharashtra, India

## ABSTRACT

Synthetic peptides are primarily prepared using solid-phase peptide synthesis, where the peptide chain is constructed by sequentially attaching amino acids to a solid support known as resin. Once synthesis is complete, the peptide chain must be isolated from the resin through a cleavage reaction, typically involving strong acids such as trifluoroacetic acid (TFA). The resulting crude peptide is then precipitated from the cleavage solution using ethers. This process requires a significant amount of ether as a solvent. However, ethers are hazardous chemicals with peroxide content, low flash points, and majorly are known to be genotoxic. Therefore, alternative source for ethers from the cleavage process is crucial for safer industrial peptide manufacturing. In response, a new process for preparing Octreotide - a cyclic octapeptide with an amino alcohol at the C-terminal - has been developed and optimized. This process reduces the amount of TFA needed for cleavage and eliminates the use of ethers completely.

**Keywords:** Chemical synthesis of peptides, Cleavage of peptides, cyclic peptides, Octreotide synthesis. Green process, avoid ethers, SPPS.

## INTRODUCTION

Therapeutic peptides have huge potential in healthcare. Mass production of peptides achieved by chemical synthesis. Chemical synthesis of peptides is achieved by combining the C-terminal of one amino acid with the N-terminal of another amino acid through an amide bond, known as a peptide bond. The conventional method of chemical peptide synthesis is solution phase synthesis (liquid phase peptide synthesis, LPPS), which involves amide bond formation reactions using coupling reagents or condensation reactions. Another popular method is solid phase peptide synthesis (SPPS), where the first amino acid from the C-terminal is anchored to a solid support using linkers, and then the peptide chain is built over it by sequentially coupling each amino acid [1]. However, most chemical synthesis manufacturing processes still rely on conventional methodologies, which need improvement to increase productivity, streamline operations, and reduce waste.

SPPS consists of anchoring the first amino acid (from the C-terminal) on a solid support (resin) using linkers. After attaching the first amino acid, the peptide chain is built up by sequentially coupling the respective amino acids to prepare peptidyl resin. The crude peptide chain is detached from the resin in a cleavage process, which includes treatment with highly acidic reagents. After the cleavage reaction, if required, chemical modifications like S-S bond formation and amide cyclization are performed. The crude peptides are purified using chromatographic techniques, and the solid product is isolated by recrystallization or lyophilization techniques. Each process contains repeated or different variable operations, each of which has its own impact on the quality of the peptide. This complexity makes peptide synthesis a complex process.

In recent years, several researchers have worked on peptide synthesis, each contributing in their own way to improve the process. Some scientists have focused on attaching the first amino acids to the resin, while others have worked on improving reaction conditions and reagents to make the process greener. Solvent waste is a major concern in SPPS, impacting both cost and the environment. Recent research on peptide synthesis has focused on how to make it more environmentally friendly [2].

In the past, Merrifield invented Solid Phase Peptide Synthesis (SPPS), which originally used hazardous hydrogen fluoride for cleavage reactions [3]. Later, linkers were developed that allowed cleavage to be performed with milder reagents, such as trifluoroacetic acid [4]. This aspect of peptide synthesis has been the least explored in terms of making the process more environmentally friendly. In recent years, J. Pawlas et al have performed cleavage of dipeptide Fmoc-Gly-Gly-OH from the CTC-resin using 1% trifluoroacetic acid (TFA) in a green binary mixture of CH<sub>3</sub>CN-EtOAc (1:1) [5]. In other research work conducted by F. Albericio & M. Alhassan et al. has demonstrated the use of 2% TFA in either anisole or 1,3-dimethoxybenzene [6]. Although trifluoroacetic acid (TFA) is used at 1 to 2% for cleavage reactions, it gives only protected peptides. To obtain the fully deprotected crude peptide, cleavage is typically performed using a 10 to 12 times solution containing 90% TFA. The crude peptide is then recovered by quenching the TFA solution in 80 to 120 times ether.

In this work, we optimized the process for generating crude octreotide by using a reduced volume of TFA, which in turn decreased the amount of ether required. Additionally, we improved the process to ensure that ethers were completely removed. The quality of the crude peptides obtained with this optimized method was comparable to that produced by conventional processes.

## METHODS AND MATERIAL

Octreotide is 8 amino acid containing peptide with Amino acid sequence of <sup>D</sup>Phe-Cys-Phe-<sup>D</sup>Trp-Lys-Thr-Cys-Thr-OL (S-S bond 2-7). Chemical structure as shown in Figure 1.

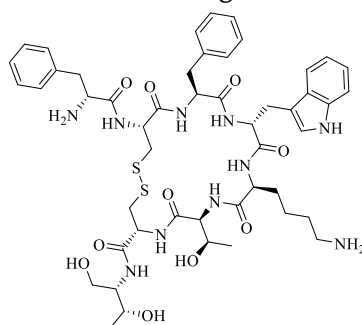
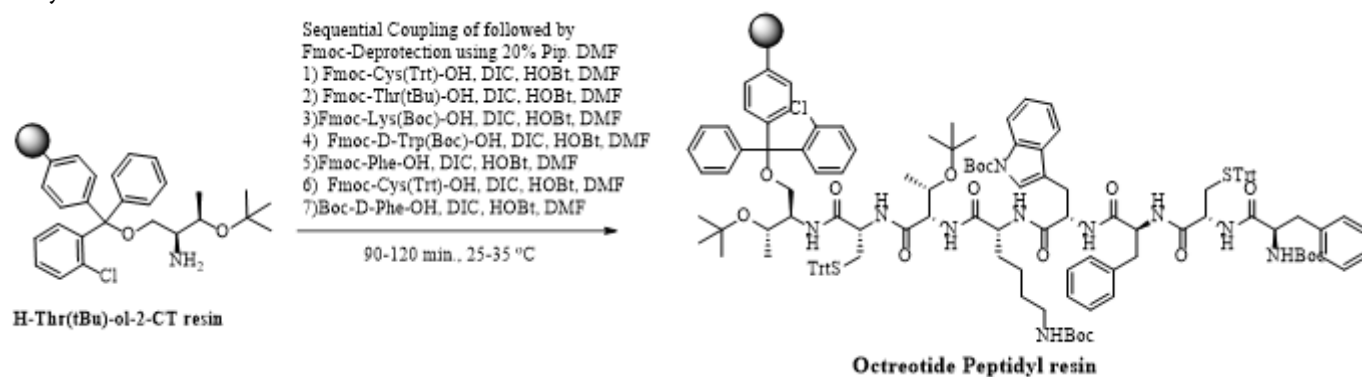
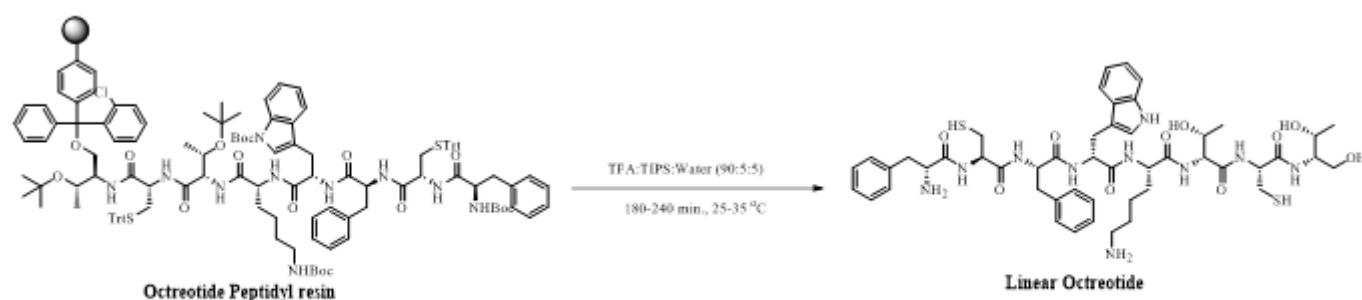


**Figure 1: Chemical structure of Octreotide**

Peptidyl resin was synthesized by using traditional SPPS. Commercially available H-Thr-OL loaded CTC resin from CS bio (Cat. No. 262035) (functionality 0.88 mmole/gm) was used for synthesis. Fmoc protected amino acids sequentially coupled using coupling reagents N-hydroxybenzotriazole monohydrate (HOBt, H<sub>2</sub>O) and Diisopropyl carbodiimide (DIPCDI) and DMF used as solvent. 20% Piperidine DMF solution used for Fmoc removal. After each step excess reagents and by-products were removed by washing with DMF and IPA. Route of synthesis is as shown in scheme-1.



Scheme-1 Route of synthesis of octreotide peptidyl resin



Scheme-2 Synthesis of crude linear octreotide from peptidyl resin

After completion of synthesis, the cleavage process is optimized by conducting various experiments at different conditions. The general process to perform cleavage is, first the cleavage cocktail is prepared by mixing TFA:TIPS:DODT:Water in desire ratio, 2-CTC resin bound protected peptide chain is charged into a RBF. The cleavage cocktail is then transferred to RBF containing peptidyl resin. Mild stirring at 25 - 30 °C for 3.0 h as shown in Scheme-2, Synthesis of crude linear peptide. The resin is then filtered through a sintered funnel. The filtrate is added into a pre-cooled mixture of Ether at 0 - 10 °C. After complete addition, the reaction mixture is stirred for 1.0 h at 0 - 35 °C to precipitate an off-white solid. The precipitated solid is then filtered through a Buckner funnel and washed with Ether. The suction-dried solid is then dried in a vacuum oven at 35 - 40 °C till constant weight is achieved.

In the first set of reactions, TFA, TIPS, DODT, and water are used as cleavage cocktail; after filtration of resin, the filtrate containing the cleavage cocktail is added to cold MTBE at 5 - 20 °C (Normal addition) or MTBE added in cocktail (Reverse addition). After quenching cocktail to MTBE white precipitate was obtained. The rate of filtration of precipitate after normal addition is very slow, while the rate of filtration in reverse addition observed

is fast. Results are tabulated in Table-1; P1, P2, P3... are synthesis batch numbers while A, B, C...are cleavage experiments numbers. Yield observed to be at a lower site (82%) when the cleavage cocktail is being 8 vol. (P1A) and purity on a lower site when DODT not used in the cleavage cocktail (P3 C, 46.8% & D, 48.7%), but it observed good when 100 vol. ether used (P3B, 62%).

**TABLE I**  
**Experiment Set-1**

Experiment No.	P1	P3			
	A	A	B	C	D
Peptidyl Resin Input (g)	4	5	5	5	5
Cocktail volume	8	10	10	10	10
TFA (ml)	29.0	45.0	45.0	45.0	45.0
TIPS (ml)	1.6	2.5	2.5	2.5	2.5
DODT (ml)	0.8	1.3	-	-	-
Water (ml)	0.8	1.3	2.5	2.5	2.5
Total (ml)	32	50	50	50	50
Ether (vol.)	64	100	100	60	60
Ether (ml)	256.00	500.00	500.00	300.00	300.00
Mode of addition	Normal	Normal	Reverse	Normal	Reverse
rate of filtration	Slow	Slow	Fast	Slow	Fast
Output (gm)	0.29	1.77	1.9	1.66	1.64
Theoretical Yield (gm)	0.4	1.8	1.8	1.8	1.8
Actual Yield (%)	81.9	100.3	107.6	94.1	92.9
Purity by HPLC (% area)	69.5	59.1	61.9	46.8	48.7
Peptide Content (%)	Not Analyse	35.1	35.8	27.7	29.0

**TABLE II**  
**Experiment Set-2**

Experiment No.	P3			
	E	F	G	H
Peptidyl Resin Input (g)	10	10	10	10
Cocktail volume	10	10	10	8
TFA (ml)	90.0	90.0	90.0	72.0
TIPS (ml)	5.0	-	-	4.0
DODT (ml)	5.0	5.0	5.0	2.0
Water (ml)	-	-	-	2.0
Phenol (ml)	-	5.0	-	-
1,3 dimethoxy benzene (ml)	-	-	5.0	-
Total( ml)	100	100	100	80
Ether (vol.)	60	60	60	48

Experiment No.	P3			
	E	F	G	H
Ether (ml)	600.00	600.00	600.00	480.00
Output (gm)	3.66	3.25	2.87	3.98
Theoretical Yield (gm)	3.5	3.5	3.5	3.5
Actual Yield (%)	103.7	92.1	81.3	112.7
Purity by HPLC (% area)	67.1	33.5	38.8	56.6
Peptide Content (%)	36.6	21.4	22.8	29.5

The second set of reactions (Table-II) are conducted on 10 gm scale of peptidyl resin. Phenol (P3F), and 1,3 dimethoxy benzene (P3G) tested against TIPS and water as scavengers in the cleavage cocktail. The content of cocktail altered in first 3 experiments (P3 E,F,G) and volume of cocktail reduce in fourth one (P3H). All experiments are performed by reverse addition of MTBE in the cocktail. Purity of crude linear peptide is poor when TIPS is not used in cocktail (P3F, 33.5% & P3G, 38.8%) while there is no impact observed on quality when water not used in cocktail (P3E, 67.1%) whereas purity is lower when 8 vol. cocktail is used (P3H, 56.6%) but 120 ml lesser MTBE was consumed.

Set 1 & 2 are performed on P1 & P3 batch which is synthesized by using Trityl (Trt) protection on Cysteine side chain. Whereas P4 batch synthesized using Acetamidomethyl (Acm) protection on side chain of Cysteine. Cleavage experiments are

TABLE III

## Experiment Set-3, Experiment on Cys(Acm) protected peptidyl resin

Experiment No.	P4		
	A	B	C
Peptidyl Resin (g)	10	10	30
Cocktail volume	10	10	10
TFA (ml)	90.0	90.0	270.0
TIPS (ml)	5.0	5.0	15.0
DODT (ml)	2.5	5.0	15.0
Water (ml)	2.5	-	-
Total (ml)	100	100	300
Ether (vol.)	60	60	60
Ether (ml)	600.00	600.00	180.00
Output (gm)	5.03	4.63	15.3
Theoretical wt. (gm)	4.5	4.5	13.4
Actual Yield (%)	112.4	103.5	114.0
Purity by HPLC (%)	74.6	78.8	77.4
Peptide Content (%)	47.0	53.8	51.9

The first experiment (P4A) TFA, TIPS, DODT, and water were used in cleavage cocktail while in the second (P4B) water is avoided. However, 3 times scale up (P4C) of reaction performs using the same conditions. Purity is

observed to be very similar in the case of all three reactions, but the content is higher (P4B, 53.8% & P4C 51.9%) when water is avoided in the cleavage cocktail as compared to when water is added in the cleavage cocktail (P4A, 47%).

When ACM protected Cysteine is use in synthesis then oxidation (or S-S bond formation) reactions are performed by using Iodine as an oxidising agent. Some trail experiments conducted where the cleavage cocktail is directly poured to cold water instead of precipitating in ether. The initial aim of experiments is to avoid precipitation and filtration of linear crude peptides. The oxidation reaction is then directly proceeding with adding respective quantity of Iodine. Later oxidation reactions also developed with respect to pH of reaction mass.

TABLE IV

Experiment Set-4, Direct quenching of filter cocktail in water instead of ether

Experiment No.	P4		
	D	E	F
Peptidyl Resin (g)	10	2	5
Cocktail volume	10	10	10
TFA (ml)	95.0	18.0	95.0
TIPS (ml)	2.5	1.0	2.5
DODT (ml)	-	0.5	-
Water (ml)	2.5	0.5	2.5
Total (ml)	100	20	100
Direct quenched to water			
Water for quenching (ml)	4000	200	2000
Theoretical wt. (gm)	4.5	0.9	2.2
Actual Yield (%)	0.0	0.0	0.0
Purity by HPLC (%)	80.6	82.6	70.4
Peptide Content (%)	57.0	58.0	60.0

TABLE V

Experiment Set-5, Oxidation reaction pH optimization results

pH	HPLC purity (%) at adjusted pH	
	Linear Octreotide	Crude Octreotide
2.0	70.36	73.98
3.0	70.79	77.25
4.0	72.44	78.85
5.0	71.38	78.38

Oxidation reaction optimized on P4F cleavage experiment, 500 ml quench aqueous solution, 1.5 eqi. I<sub>2</sub> Reaction monitors at 180 min. Direct quenching of the TFA cocktail in water is beneficial. Even Iodine oxidation reactions can be conducted at pH 2 to 5. Four pH monitoring points were considered only based on the Iodine reaction favoured in acidic conditions.

**TABLE VI**  
**Experiment Set-6**

Experiment No.	P3	P3	P4	P15	P15	P15	P15	P15	P15
	K	L	G	A	B	C	D	E	F
Peptidyl Resin (g)	5	5	5	5	5	5	5	5	5
Cocktail volume	10	10	10	10	12	10	10	15	12
TFA (ml)	45.0	45.0	47.5	45.0	54.0	47.5	45.0	67.5	54.0
TIPS (ml)	2.50	2.50	1.25	2.50	3.00	-	2.50	3.75	3.00
DODT (ml)	1.25	1.25	-	2.50	3.00	2.50	2.50	3.75	3.00
Water (ml)	1.25	1.25	1.25	-	-	-	-	-	-
Total (ml)	50	50	50	50	60	50	50	75	60
Ether (vol.)	60	20	30	60	72	60	20	15	12
Ether (ml)	300	100	150	300	360	300	100	75	60
Mode of addition	Reverse					Normal	Reverse		
Output (gm)	1.4	1.98	2.29	1.59	1.63	0.2	1.7	2.2	2
Theoretical wt. (gm)	2.5	2.5	2.2	2.6	2.6	2.6	2.6	2.6	2.6
Actual Yield (%)	57.1	80.8	102.4	61.1	62.6	7.7	65.3	84.5	76.8
Purity by HPLC (%)	49.5	47.4	57.4	64.2	69.1	59.7	63.9	69.7	70.2
Peptide Content (%)			33.7	36.8	42.8	32.9	35.3	34.5	40.8

To check impact of TFA evaporation, one experiment plan on P4 peptidyl resin. Result obtained are promising, so further development is conducted on peptidyl resin P3 & P15 containing Trt protection on Cys. Results are tabulated in Table-VI. In experiment the peptidyl resin is treated with cocktail for 3 hrs. Resin is then filter off using sinter funnel. Filtrate cleavage cocktail then subjected to concentrate at reduce pressure using rotary evaporator. The concentrated solution then quenched with MTBE at cold temperature (2 to 8°C) by reverse addition except for P15C. Cleavage cocktail optimised to TFA, TIPS, DODT only. Further the impact of increase volume of cocktail also studies, there is not major impact observed on purity (10 vol. P15A: 64.2%, 12 vol. P15B 69.1%, 15 vol. P15E: 69.7%). Impact of volume of MTBE is also checked at 6, 3, 2 & 1 times of cleavage cocktail. Purity obtains while using 60 vol. MTBE (P3K, 49.5%) for quenching does not varies more when 20V MTBE (P3L, 47.4%) used for quenching. Even equal volume of MTBE to cocktail gives good results (P15E: 69.7%, & P15F: 70.2%). One experiment conducted with normal addition (P15C) after TFA evaporation, but material obtained was fine in nature and unable to filter. Experiment P15F (12 Vol. cocktail) shows best result among so same conditions applied on bigger scale in further two experiments (P15G & H). Results are tabulated in Table-VII.



**TABLE VII**  
**Experiment Set-7**

Experiment No.	P15		
	F	G	H
Peptidyl Resin Input (g)	5	10	50
Cocktail volume	12	12	12
TFA (ml)	54.0	108.0	540.0
TIPS (ml)	3.0	6.0	30.0
DODT (ml)	3.0	6.0	30.0
Total (ml)	60	120	600
Ether (vol.)	10	10	10
Ether (ml)	50	100	50
Output (gm)	2	3.6	20.3
Theoretical wt. (gm)	2.6	5.2	26.0
Actual Yield (%)	76.8	69.1	78.0
Purity by HPLC (%)	70.2	65.9	54.2
Peptide Content (%)	40.8	34.9	28.8

It is observed that, as scale increases purity and content decreases at given conditions, concluded that ether volume is not sufficient to wash out non peptidyl residue after cleavage. So furthermore, trials carried out by increasing MTBE volume at bigger scale (15 gm & 10gm) with and without cocktail evaporation.

**TABLE VIII**  
**Experiment Set-8**

Experiment No.	P16			
	A	B	C	D
Peptidyl Resin (g)	15	15	15	10
Cocktail volume	12	12	12	12
TFA (ml)	162	162	162	108
TIPS (ml)	9.0	9.0	9.0	6.0
DODT (ml)	9.0	9.0	9.0	6.0
Total (ml)	180	180	180	120
Cocktail evaporation	No	Yes	Yes	Yes
Ether (vol.)	60	60	30	10
Ether (ml)	900	900	450	100
Output (gm)	5.93	6	6.7	4.4
Theoretical wt. (gm)	7.4	7.4	7.4	4.9
Actual Yield (%)	80.4	81.3	90.8	89.5
Purity by HPLC (%)	61.8	58.0	55.7	63.1
Peptide Content (%)	39.5	34.5	30.5	36.2

3.8% difference in purity observed when cocktail evaporated (P16A Vs P16B) and 60 vol. MTBE used. Lower ether volume again further gives lower purity.

In further trial experiments, MDC & DIPE were incorporated into the process to remove non peptidyl impurities. Results are tabulated in Table–IX. The first experiment is with a 12 vol. cocktail, followed by filtrate evaporation and reverse addition of 12 vol. MTBE. In the second experiment, 3 vol. MDC was added along with 12 vol. cocktail (P16F). After completion of the cleavage reaction, resin filtered out, and the filtrate cocktail evaporated. 10 vol. ether charged by reverse addition. In the third experiment, MTBE was replaced by DIPE, keeping the rest of the things the same (P16 G). In the fourth experiment, cocktail volume was reduced to 6 vol., and MDC vol. increased to 6 vol (P15H). Three experiments give almost similar results (66%) (P16 E, F, & H) except for precipitation using DIPE (P16 G, 61.8%). Peptide content results are close for the first and fourth experiments (P16 E: 46.7%, G: 43.8%), showing that cocktail volume can be reduced to 6 vol. when 6 vol. MDC is incorporated in the cleavage process.

**TABLE IX**  
**Experiment Set-9**

Experiment No.	P16			
	E	F	G	H
Peptidyl Resin (g)	5	5	5	5
Cocktail volume	12	12	12	6
TFA (ml)	54.0	54.0	54.0	27.0
TIPS (ml)	3.0	3.0	3.0	1.5
DODT (ml)	3.0	3.0	3.0	1.5
Total (ml)	60	60	60	30
MDC (vol.)	-	3	-	6
MDC (ml)	-	15	-	30
Cocktail evaporation	Yes	Yes	Yes	Yes
Ether	MTBE		DIPE	MTBE
Ether (vol.)	12	12	12	12
Ether (ml)	60	60	60	60
Output (gm)	1.68	1.83	2	2
Theoretical wt. (gm)	2.5			
Actual Yield (%)	68.3	74.4	81.3	81.3
Purity by HPLC (%)	66.9	66.0	61.8	65.9
Peptide Content (%)	46.7	34.6	27.8	43.8

The use of MDC in the cleavage cocktail helps to evaporation of TFA and to swell the resin. Experiments were carried out by varying MDC volumes 6, 5, & 4 in cleavage cocktail. Results are tabulated in Table–X. TFA, DODT & TIPS solutions were changed to 6, 7 & 8 volumes, respectively. The resin was first swelled in MDC, and then TFA solution was charged to the resin. After completion of the reaction, resin filtration, and cocktail evaporation, DIPE is charged by reverse addition. Results obtained are in very close proximity (P18 C: 68.2%, D: 67.7 %, E: 65.8%). However, the best results belong to 6 vol. TFA solution and 6 vol. MDC with

respect to both purity and peptide content (P18 C: 41.4%, D: 40.5 %, E:38.3%). The appearance of crude peptide obtained is better when DIPE is used instead of MTBE. In the other two experiments (P18 G &H) scale was increased to 10 & 7 times. In the experiment, P18G, 12 vol. MDC, and 12 vol. TFA solutions were charged. Purity is observed best among all experiments, but the cleavage cocktail is almost double. Experiment P18H performed with exact in Table- IV. These experiments are planned on peptidyl resin P4 (Acm protection on Cys residue).

**TABLE X**  
**Experiment Set-10**

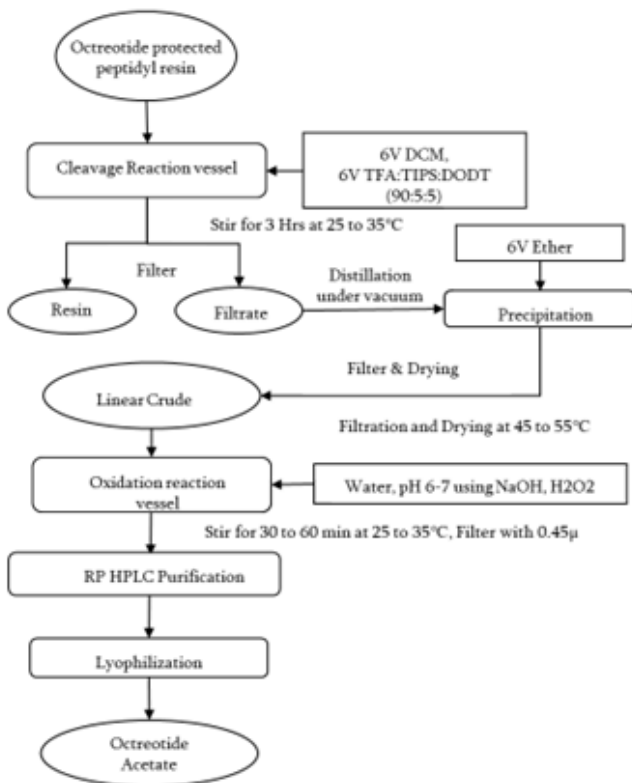
Experiment No.	P18	P18	P18	P18	P18	P19	P19	P20	P21	P3
	C	D	E	G	H	B	C	A	A	M
Peptidyl Resin (g)	5	5	5	50	35	25	25	20	30	70
Cocktail volume	6	7	8	12	6	6	6	6	6	6
TFA (ml)	27.0	31.5	36.0	540	189	135	135	108	162	378
TIPS (ml)	1.5	1.8	2.0	30.0	10.5	7.5	7.5	6.0	9.0	21.0
DODT (ml)	1.5	1.8	2.0	30.0	10.5	7.5	7.5	6.0	9.0	21.0
Total (ml)	30	35	40	50	210	150	150	120	180	420
MDC (vol.)	6	5	4	12	6	6	6	6	6	6
MDC (ml)	30	25	20	540	210	150	150	120	180	420
Ether (ml)	60.00	60.00	60.00	600	210	150	150	120	180	420
Output (gm)	2.1	2.15	2.18	22.5	15.4	10.2	9.7	8.5	12.6	30.4
Theoretical wt. (gm)	2.5	2.5	2.5	24.6	17.2	12.3	12.3	9.8	14.9	33.8
Actual Yield (%)	85.4	87.4	88.6	91.5	89.5	83.0	78.9	86.4	84.7	89.9
Purity by HPLC (%)	68.2	67.7	65.8	69.9	66.1	65.6	68.2	73.1	68.9	50.5
Peptide Content (%)	41.4	40.5	38.3	37.3	38.6	37.9	44.0	45.8	39.4	25.4

similar cleavage condition of P18C and 7 times higher scale. 6 vol. DIPE used instead of 12 vol., the observed results are varying by 2 % in purity and around 3% in peptide content. Optimized conditions were tested at different lab scales, and different synthesis batches. All have purity above 65% and more than 35%. Exception of P3M, on 70 gm scale Purity 50.5% & peptide content 25.4%. During process development and optimization, we have tried some experiments where cleavage cocktail directly quenched to water and proceed further shown in Table- IV. These experiments are planned on peptidyl resin P4 (Acm protection on Cys residue). Later cleavage conditions are optimized for 6 vol. TFA solution and 6 vol. MDC, and filtration of resin followed by TFA evaporation. Set of experiments are planned to study impact on purity of crude linear peptide obtain after direct quenching. Peptide content cannot be determining as exact weight of crude linear peptide in aqueous solution is not known. Purity of crude peptide after oxidation reaction is also consider for development. Results are tabulated in Table- XI. Peptidyl resin synthesis batches P24, 25, 26, 27 & 28 are synthesized by green chemistry approach using GVL solvent for coupling and deprotection reactions, while P28 is peptidyl resin with Trt protection at Cys side chain. P29 is with regular synthesis process using DMF.

**TABLE XI**  
**Experiment Set-11, Direct quenching to water**

Experiment No.	P24	P24	P25	P26	P27	P27	P28	P28	P29	
	A	B	A	A	A	B	A	B	A	
Peptidyl Resin (g)	1	1	4	5	2	2	5	10	15	
Cocktail volume	6.0	6.0	24.0	30.0	12.0	12.0	30.0	60.0	90	
MDC (ml)	6	6	24	30	12	12	30	60	90	
Ether	DIPE	Direct quenched to water					DIPE	Direct quenched to water		
Ether (vol.)	6						6			
Ether (ml)	6.00						12.00			
Output (gm)	0.43						0.92			
Purity by HPLC (%) linear	55.4	51.1	63.7	82.9	79.5	76.2	--	66.2	72.00	
Purity by HPLC (%) oxidized	62.49	51.61	68.38	73.56	78.97	78.83	87.45	78.84	85.23	

**Reduced volume of Ether**



**Direct quenching in water**

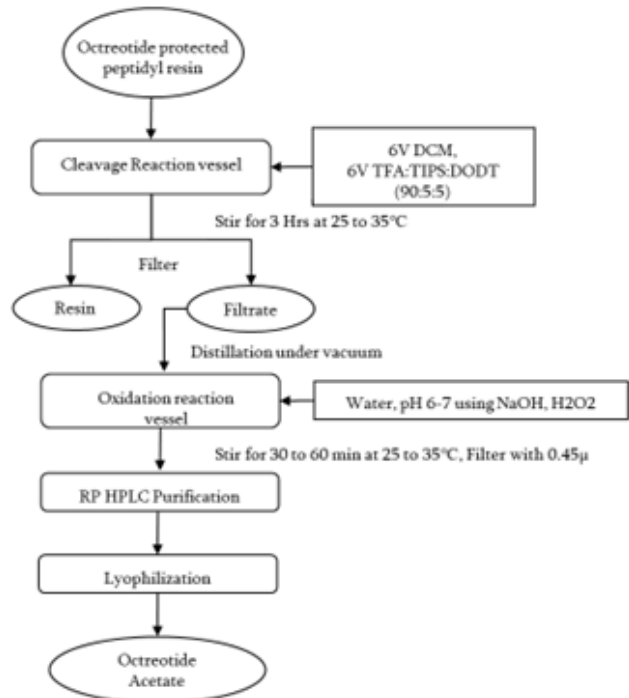


**Figure 2: Process flow chart for optimized cleavage process of Octreotide Acetate**

**RESULTS AND DISCUSSION**

During the development of the cleavage process to obtain crude peptides from peptidyl resin, a cleavage cocktail comprising TFA, TIPS, and DODT was formulated. This cocktail effective for peptidyl resin

containing cysteine residues protected by either Trt or AcM on their thiol side chains. The optimal ratio for the TFA: TIPS: DODT cocktail is 90:5:5. Throughout the experimentation, cleavage time and temperature remained consistent, with successful results achieved at room temperature within 2 to 3 hours, making this approach feasible for manufacturing scale operations.

Adding MDC before charging TFA solution to peptidyl resin promotes swelling of the resin, allowing TFA to focus solely on the cleavage reaction rather than being consumed for swelling. Additionally, the lower boiling point of MDC (39.6 °C) compared to TFA (72.4 °C) enhances the evaporation rate of TFA due to an azeotropic effect with MDC. Using a 6:6 volume ratio of MDC and TFA solution produces results similar to those achieved with a 10 to 12 vol.

Evaporating TFA from the cleavage filtrate is a key step in our process, as it further reduces the amount of ether required for precipitation. While TFA in the filtrate can help solubilize impurities in ether, our method shows that this presence has minimal impact. Thus, removing TFA is essential for significantly lowering the required ether volume.

Precipitating crude peptides is a central focus of our research. We have developed a process that significantly reduces the volume of ether used, decreasing it from 100-120 volumes to just 6 volumes. The method of ether addition is also critical for operational feasibility. By employing reverse addition of ether to the cleavage cocktail, we achieve larger particle sizes of the crude peptide, which enhances the filtration rate during isolation.

We have successfully reduced ether consumption to just 5% of what is required in conventional processes. Additionally, we have established a method for completely removing ether from the cleavage phase of peptide synthesis. Our experiments demonstrate that ether removal or the incorporation of water into the process does not compromise the quality of the product.

The quality of crude peptides obtained from direct quenching of cleavage filtrate in water is comparable to that obtained from precipitation in ether. We tested both peptidyl resins containing Trt and AcM protection on cysteine thiol side chains in the direct quenching process. For peptidyl resin with Trt protection, the purity of octreotide after the oxidation reaction is significantly better than that of the linear crude peptide. Notably, during pH adjustment in the oxidation reaction, some linear peptides convert to octreotide even before the addition of H<sub>2</sub>O<sub>2</sub>.

In the case of AcM-protected peptidyl resin, the oxidation reaction can be conducted over a wider pH range of 2 to 6. The rates of oxidation are comparable for both processes: direct quenching and precipitation with a lower volume of ether.

## CONCLUSION

The research presents optimized conditions for cleaving Octreotide peptidyl resin, which features Trt and AcM protection on cysteine thiol side chains. This approach reduces TFA consumption by 50% and ether consumption by 90-94%. Incorporating MDC in the cleavage process enhances the feasibility of evaporating TFA, while the reverse addition of ether promotes larger particle sizes of the crude peptide.

Additionally, we have developed a method for directly quenching the TFA cocktail in water, eliminating the need for ethers in the process. From an operational standpoint, this approach streamlines the procedure

by reducing the number of steps involved in direct quenching. It also minimizes the need for equipment such as Buchner filters, and dryers, along with consumables like filtration bags and containers. This leads to lower operating costs and reduced manufacturing plant occupancy time. Furthermore, the oxidation reaction occurs in situ, effectively merging two processes into one, which further reduces waste generation and enhances cost-effectiveness.

We have not introduced any new chemical moieties to make the process greener, ensuring that there is no impact on the impurity profile or the regulatory assessment of the generic octreotide API, as it remains a pharmaceutical product.

## AUTHOR INFORMATION

### A. Corresponding Authors

#### E-mail:

yrsuryawanshi@hs.vjti.ac.in

sujathap@hs.vjti.ac.in

### B. Author Contributions:

1) Conceptualization: Chandrakant Kulkarni and Yogeshwar Suryawanshi

2) Data curation: Chandrakant Kulkarni

3) Writing:

Original draft preparation: Chandrakant Kulkarni

Review and editing: Chandrakant Kulkarni and Yogeshwar Suryawanshi

4) Visualization: Yogeshwar Suryawanshi and Sujatha Parmeswaran

5) Supervision: Yogeshwar Suryawanshi and Sujatha Parmeswaran

C. **Funding:** “This research funded by Enzene Biosciences Ltd, Pune, 410501, Maharashtra”.

D. **Informed Consent Statement:** “Not applicable.”

E. **Data Availability Statement:** “All scientific data is intellectual property of Enzene Biosciences Ltd. And it is available with Enzene biosciences Ltd, Pune, 410501, Maharashtra”

### F. Acknowledgments:

1) Synthetic peptide department, Enzene Biosciences Ltd, Pune, 410501, Maharashtra, India;

2) Technical & Applied Chemistry Department, Veermata Jijabai Technological Institute, Central Technological Institute of Government of Maharashtra, H. R. Mahajani Road, Matunga 400019 Mumbai

G. **Conflicts of Interest:** “The authors declare no conflicts of interest.”

## REFERENCES

- [1] W Chan, P. W. (2000). Fmoc Solid Phase Peptide Synthesis: A Practical Approach. In W. P. Chan WC, Fmoc Solid Phase Peptide Synthesis: A Practical Approach. Oxford.
- [2] Vincent Martin, P. H. (2020, November 24). Greening the synthesis of peptide therapeutics: an industrial perspective. *RCS Advances*, 42457–42492. doi:10.1039/D0RA07204D

- [3] Merrifield, R. B. (1963). Solid Phase Peptide Synthesis. I. The Synthesis of a Tetrapeptide. *Journal of the American Chemical Society*, 85(14), 2149-2154. doi: DOI: 10.1021/ja00905a002
- [4] Cynthia A. Guy, G. B. (1997). Trifluoroacetic acid cleavage and deprotection of resin-bound peptides following synthesis by Fmoc chemistry,. In G. B. Fields, *Methods in Enzymology* (Vol. 289, pp. 67-83) doi:[https://doi.org/10.1016/S0076-6879\(97\)89044-1](https://doi.org/10.1016/S0076-6879(97)89044-1)
- [5] J. Pawlas, B. Antonic, M. Lundqvist, T. Svensson, J. Finnman and J. H. Rasmussen, *Green Chemistry*, 2019, 21, 2594-2600, 10.1039/c9gc00898e
- [6] F. Albericio, M. Alhassan, O. Al Musaimi, J. Collins and B. G. de la Torre, *Green Chem.*, 2020, DOI: 10.1039/D0GC00834F.

# Photocatalysis in Environmental Chemistry : A Comprehensive Literature Review

Rajkumar G. Momle<sup>1\*</sup>, Gopal K. Kakade<sup>2</sup>

<sup>1\*</sup>Late Shankarrao Gutte Arts, Commerce and Science College, Dharmapruri, Tq -Parli Dist- Beed, Maharashtra, India

<sup>2</sup>Principal, Rajmata Jijau Mahavidyalaya, Kille Dharur, Maharashtra, India

## ABSTRACT

Photocatalysis has emerged as a promising solution for addressing environmental challenges such as pollution, water treatment, and energy generation. This literature review explores the development, mechanisms, and applications of photocatalysis in environmental chemistry. By analysing both historical perspectives and modern advances, this review highlights the use of various photocatalysts, such as titanium dioxide (TiO<sub>2</sub>), zinc oxide (ZnO), and graphene-based materials. The effectiveness of photocatalytic degradation of pollutants and water-splitting processes for hydrogen generation is discussed in detail, along with future perspectives for improving the sustainability and efficiency of photocatalysis.

**Keywords** : Photocatalysis, Titanium dioxide, Environmental chemistry, Degradation of pollutants, Hydrogen production, Semiconductor materials.

## INTRODUCTION

### 1.1. Background and Importance

Environmental degradation caused by pollutants in air, water, and soil has become a pressing issue, and sustainable methods for addressing these concerns are urgently needed. Among various strategies, photocatalysis has gained significant attention in environmental chemistry due to its ability to degrade pollutants under light irradiation. The process involves the use of semiconductor materials to harness light energy and promote redox reactions, leading to the breakdown of harmful compounds into non-toxic by-products.

### 1.2. Scope of the Review

This review examines the current state of research on photocatalysis in environmental chemistry, focusing on the mechanisms of photocatalytic reactions, key photocatalyst materials, and their applications in pollutant degradation and water treatment. A detailed analysis of the literature will provide insights into advancements and challenges in the field.



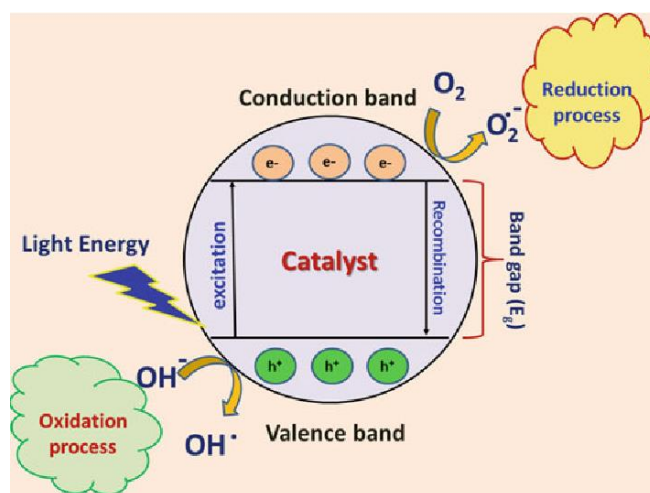
## FUNDAMENTALS OF PHOTOCATALYSIS

### 2.1. Basic Mechanism of Photocatalysis

Photocatalysis involves the excitation of semiconductor materials when they absorb light of a suitable wavelength (usually in the UV or visible range). Upon illumination, electrons are excited from the valence band to the conduction band, leaving behind holes in the valence band. These electron-hole pairs initiate redox reactions:

- **Oxidation** occurs via the holes in the valence band, leading to the breakdown of pollutants.
- **Reduction** happens via the excited electrons, promoting reactions such as hydrogen evolution.

The general reaction mechanism is summarized as follows:



These charge carriers (electrons and holes) can recombine, dissipating energy as heat, or participate in surface reactions that lead to pollutant degradation.

### 2.2. Factors Influencing Photocatalytic Efficiency

The efficiency of a photocatalytic system depends on several factors, including:

- **Bandgap energy:** A smaller bandgap allows the absorption of visible light, increasing efficiency.
- **Surface area:** A larger surface area of the photocatalyst provides more active sites for reactions.
- **Recombination rate:** Lower recombination rates of electron-hole pairs improve photocatalytic efficiency.
- **Light intensity and wavelength:** Light sources with wavelengths matching the photocatalyst's bandgap improve performance.

## TYPES OF PHOTOCATALYSTS AND THEIR APPLICATIONS

### 3.1. Titanium Dioxide (TiO<sub>2</sub>)

#### Application:

TiO<sub>2</sub> is one of the most widely used photocatalysts due to its effectiveness in various environmental remediation applications. Its primary applications include:

1. **Water Treatment:** TiO<sub>2</sub> has been widely studied for degrading organic pollutants, including dyes, pharmaceuticals, and industrial chemicals, in wastewater. For instance, phenol, a toxic organic

compound, is efficiently degraded in aqueous systems with TiO<sub>2</sub> photocatalysis under UV light exposure.

2. **Air Purification:** TiO<sub>2</sub>-based photocatalysts can remove volatile organic compounds (VOCs) such as formaldehyde and acetaldehyde, which are common indoor pollutants. Photocatalytic air purifiers equipped with TiO<sub>2</sub> coatings also effectively degrade nitrogen oxides (NO<sub>x</sub>) from vehicle emissions.
3. **Self-Cleaning Surfaces:** Due to TiO<sub>2</sub>'s photocatalytic and hydrophilic properties, it is used in coatings for self-cleaning windows, tiles, and building facades. Under sunlight, TiO<sub>2</sub> breaks down organic contaminants, preventing surface fouling.
4. **Antibacterial Surfaces:** TiO<sub>2</sub> has shown antibacterial properties when exposed to UV light, which has led to its use in hospital coatings to prevent the spread of bacteria like *E. coli* and *Staphylococcus aureus*.

### 3.2. Zinc Oxide (ZnO)

#### Application:

1. **Water Treatment (Dye Degradation):** ZnO, similar to TiO<sub>2</sub>, has been used for the degradation of textile dyes such as methylene blue, rhodamine B, and Congo red. ZnO exhibits high activity under UV light, leading to the complete mineralization of these dyes. However, ZnO is prone to photocorrosion, which limits its long-term application.
2. **Photocatalytic Degradation of Pharmaceuticals:** ZnO has been applied to degrade pharmaceutical pollutants like ibuprofen and paracetamol in wastewater. The high oxidative power of ZnO allows it to break down these drugs into non-toxic by-products.
3. **Antibacterial Applications:** ZnO nanoparticles have been incorporated into coatings, films, and textiles due to their antibacterial activity under light exposure. This property is particularly valuable for antimicrobial surfaces in hospitals and food packaging.
4. **Gas Sensing:** ZnO's photocatalytic properties have been utilized in gas sensors for detecting pollutants such as NO<sub>2</sub> and carbon monoxide. The presence of light enhances the sensitivity of these sensors, making ZnO ideal for environmental monitoring.

### 3.3. Graphene-Based Photocatalysts

#### Application:

1. **Water Treatment (Enhanced Photocatalysis):** Graphene, especially when combined with other semiconductors like TiO<sub>2</sub> or ZnO, improves photocatalytic degradation efficiency. The combination of graphene oxide (GO) with TiO<sub>2</sub> enhances the photocatalyst's ability to degrade pollutants like dyes and heavy metals by promoting charge separation and extending visible light absorption.
2. **Hydrogen Production (Water Splitting):** Graphene-based photocatalysts are widely researched for water splitting to produce hydrogen. The high conductivity of graphene helps in reducing electron-hole recombination, which increases the efficiency of the overall photocatalytic water-splitting process. Graphene-modified semiconductors such as GO-TiO<sub>2</sub> and rGO-ZnO have shown promising results under visible light for hydrogen evolution.

3. **Supercapacitors for Energy Storage:** Graphene-based photocatalysts are being explored for energy storage applications, such as supercapacitors. The combination of photocatalysis and energy storage devices, especially those that use graphene, offers innovative solutions for renewable energy applications.
4. **Environmental Sensors:** Graphene-based materials are incorporated into sensors for detecting environmental pollutants such as VOCs and heavy metals. These sensors exhibit high sensitivity and rapid response due to the enhanced electron mobility and surface area provided by graphene.

## CASE STUDIES AND APPLICATIONS IN ENVIRONMENTAL CHEMISTRY

### 4.1. Pollutant Degradation in Water Treatment

Both TiO<sub>2</sub> and ZnO have been widely used in photocatalytic degradation of organic pollutants in water. A notable example is the degradation of methylene blue dye, which has been demonstrated with both TiO<sub>2</sub> and ZnO as photocatalysts. Under UV light, the dye is broken down into less harmful products. These photocatalysts have shown high efficiency, but ZnO's susceptibility to photocorrosion limits its long-term usage.

### 4.2. Air Purification

Photocatalytic air purification systems equipped with TiO<sub>2</sub> can degrade harmful airborne pollutants, such as NO<sub>x</sub> and VOCs, into non-toxic by-products like CO<sub>2</sub> and water. These systems have been successfully implemented in urban environments to reduce air pollution from industrial emissions.

### 4.3. Hydrogen Production through Water Splitting

TiO<sub>2</sub> and graphene-based composites are widely studied for photocatalytic water splitting to produce hydrogen. TiO<sub>2</sub>, especially when doped with metals or combined with graphene, shows promising results under UV and visible light. This application of photocatalysis provides a potential pathway toward sustainable hydrogen production, a clean fuel source.

## CHALLENGES AND FUTURE PERSPECTIVES

Despite the success of these materials, challenges remain in photocatalysis:

- **Limited Visible Light Activity:** Both TiO<sub>2</sub> and ZnO are limited to UV light, which makes up only a small portion of the solar spectrum. Doping these materials with metals or combining them with graphene can extend their light absorption into the visible range.
- **Photocorrosion of ZnO:** One major drawback of ZnO is its lower stability under UV light due to photocorrosion. Efforts to improve ZnO's stability by adding co-catalysts or protective layers are under investigation.
- **Recombination of Charge Carriers:** In many photocatalysts, electron-hole recombination reduces overall efficiency. Graphene, with its high conductivity, is being explored to mitigate this issue by promoting charge separation.

## CONCLUSION

Photocatalysis offers significant potential in environmental chemistry applications, from water purification to renewable energy generation. Titanium dioxide (TiO<sub>2</sub>) and zinc oxide (ZnO) are well-established photocatalysts for pollutant degradation, while graphene-based materials hold promise for enhanced efficiency in water splitting and environmental sensing. Despite challenges, ongoing research is focused on developing photocatalysts with improved stability and light absorption properties, paving the way for more sustainable environmental technologies.

## REFERENCES

- [1] Fujishima, A., Honda, K. (1972). Electrochemical photolysis of water at a semiconductor electrode. *Nature*, 238(5358), 37-38.
- [2] Hoffmann, M. R., Martin, S. T., Choi, W., & Bahnemann, D. W. (1995). Environmental applications of semiconductor photocatalysis. *Chemical Reviews*, 95(1), 69-96.
- [3] Chen, X., & Mao, S. S. (2007). Titanium dioxide nanomaterials: Synthesis, properties, modifications, and applications. *Chemical Reviews*, 107(7), 2891-2959.
- [4] Hashimoto, K., Irie, H., & Fujishima, A. (2005). TiO<sub>2</sub> photocatalysis: A historical overview and future prospects. *Japanese Journal of Applied Physics*, 44(12), 8269-8285.
- [5] Foster, H. A., Ditta, I. B., Varghese, S., & Steele, A. (2011). Photocatalytic disinfection using titanium dioxide: Spectrum and mechanism of antimicrobial activity. *Applied Microbiology and Biotechnology*, 90(6), 1847-1868.
- [6] Zhang, X., Ai, Z., Li, J., & Zhang, L. (2011). TiO<sub>2</sub>-ZnO hybrid nanostructures for enhanced photocatalytic degradation of methylene blue. *Journal of Physical Chemistry C*, 115(15), 7137-7144.
- [7] Zhang, X., & Zhang, L. (2009). Photocatalytic degradation of dyes with ZnO under UV light. *Journal of Physical Chemistry C*, 113(17), 7484-7491.
- [8] Maness, P. C., Smolinski, S., Blake, D. M., Huang, Z., Wolfrum, E. J., & Jacoby, W. A. (1999). Bactericidal activity of photocatalytic TiO<sub>2</sub> reaction: Toward an understanding of its killing mechanism. *Applied and Environmental Microbiology*, 65(9), 4094-4098.
- [9] Sirelkhatim, A., Mahmud, S., Seeni, A., Kaus, N. H., Ann, L. C., Bakhori, S. K. M., Hasan, H., & Mohamad, D. (2015). Review on zinc oxide nanoparticles: Antibacterial activity and toxicity mechanism. *Nano-Micro Letters*, 7(3), 219-242.
- [10] Zhang, J., Zhang, M., Sun, R. Q., & Wang, X. (2012). A facile band alignment of polymeric carbon nitride semiconductors to construct isotype heterojunctions. *Angewandte Chemie International Edition*, 51(41), 10145-10149.

# Synthesis of Quinoline-3-Carbonitrile Derivatives Via One Pot Ecofriendly Protocol

Kadam Shuddhodan Narhari<sup>1\*</sup>, Rahul D. Kamble<sup>2</sup>, Khatke Tukatam Eknathrao<sup>3</sup>

<sup>1</sup>Dr. Ganpatrao Deshmukh Mahavidyalaya, Sangola 413307, Maharashtra, India

<sup>2</sup>Amruteshwar Arts Science Commerce Mahavidyalay Vinzar Pune, Maharashtra, India

<sup>3</sup>NKSPT's Arts, Science & Commerce College Badnapur, Jalna 431203 Maharashtra, India

Corresponding authors Email\*siddhukadam214@gmail.com

## ABSTRACT

Bleaching earth clay catalyzed multicomponent reaction of Heterocyclic aldehyde, 2-cyanoacetohydrazide and substituted Anilines, In PEG-400 is carried out. This method has been applied for the synthesis of quinoline-3-carbonitrile with good to excellent yield. In this study a comparison is made on triethylamine, piperidine, morpholine with Bleaching earth clay and with no catalyst. The studies revealed that bleaching earth clay and PEG-400 are more effective than other catalyst and solvents. It increasing the yield of product with less time consumption. All the synthesized compounds were characterized for their spectral analysis.

**Keyword:** Bleaching earth clay (BEC), PEG-400, Heterocyclic aldehyde, recyclability.

## INTRODUCTION

The predominant occurrence of the quinoline-3-carbonitrile derivative in various natural products and established medicinal compounds<sup>1-3</sup> had proven to be a versatile scaffold in organic and medicinal chemistry. quinoline-3-carbonitrile have recognized to acquire varied biological activities such as antibacterial<sup>4</sup>, antiviral<sup>5</sup>, anticancer<sup>6</sup>, antifungal<sup>7</sup>, antimalarial<sup>8</sup>, anti H.I.V<sup>9</sup>, anti-inflammatory<sup>10</sup>. Quinoline-3-carbonitrile derivatives are acknowledged medicinal compounds known to be present in the bioactive natural products<sup>11</sup>. Heterocyclic aldehydes are proven to contain varied biological activities<sup>12</sup>. By interpreting these points we combine the heterocyclic aldehydes with anilines and 2-cyanoacetohydrazide assuming that the present combination may lead to formation of improved biological hybrid.

There is always been quest for advancement of the synthetic route for the conversion of readily available reagent into widely used organic compounds. For accomplishing this multicomponent reaction (MCR) are recognized as an important tool from economic as well as environmental point of view<sup>13</sup>. Along with the MCR method, use of green solvent is also considered to be an environmental benign access. Amongst the green solvents used for MCR strategy PEG-400 is considered to be well known green solvent<sup>14</sup>.

In the previous literature there are abundant synthetic strategies for the synthesis of quinoline-3-carbonitrile derivatives<sup>15</sup>. Development of a heterogeneous catalyst for the synthesis of numerous important organic motifs was always been a center of interest for organic chemistry students<sup>16-17</sup>. Ease of handling, reusability,

easy extraction are some peculiar advantages of heterogenous catalysts. Amongst those heterogeneous catalysts Bleaching earth clay (BEC) is considered as a remarkable heterogenous catalyst for various organic transformations<sup>18</sup>. Taking in account these facts we represent an MCR protocol for synthesis of by Consolidation of heterocyclic aldehydes with anilines and 2-cyanoacetohydrazide Manipulating Bleaching earth clay as catalyst and PEG-400 as green solvent.

## RESULT AND DISCUSSION

A facile one pot three component protocol for the synthesis of new quinoline-3-carbonitrile derivative **4a-j** is reported by utilizing equimolar heterocyclic aldehydes **2a-j**, anilines **3a-c** and 2-cyanoacetohydrazide **1** **Scheme 1**. The synthetic protocol commences with sequential addition of 2-cyanoacetohydrazide and heterocyclic aldehydes in round bottom flask previously filled with catalytic amount of BEC and PEG-400 as green solvent, after completion of reaction as indicated by TLC the anilines was added in the same pot and the reaction mixture was further stirred at 80°C for the formation of product. the first attempt was made using the Triethylamine as a catalyst which results in formation of the product with 50% yield and time required for completion of reaction was 65 minutes Entry 1 Table 1. Observing these results, we moved for other catalysts piperidine and morpholine Entry 2 and 3 Table 1 respectively which the outcomes of 40 and 30% yield with the time of 70 and 60 minutes. When we moved for using BEC as a catalyst 1 Wt% resulting in production of improved 60% yield Entry 4 table 1. Enthused with these results we further investigate different wt% compositions of BEC (pH 12.5). We came to investigation that satisfactory yield was obtained when we utilized 15wt% of BEC. The yield was found to hampered when 10 wt% and 20wt% BEC were used Entry 5 and 7 Table 1. However, there was no formation of product when reaction was carried out in absence of catalyst when stirred at RT Entry 8. Even though when reaction mixture was stirred at 80°C without catalyst the formation of product was not observed Entry 9 Table 1. The optimized reaction conditions were found when 15wt% of BEC was used.

**Table 1: Optimized reaction conditions**

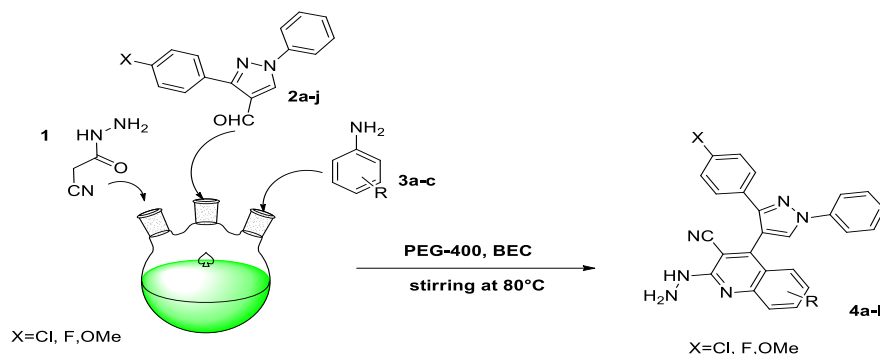
Entry	Catalyst (Mol/wt%)	Temp (°C)	Time (Min)	Yield of <b>4a</b> (%)
1	Triethylamine (Mol%)	70	65	50
2	Piperidine (Mol%)	80	70	40
3	Morpholine (Mol%)	80	60	30
4	Bleaching earth Clay 1 wt%	80	50	60
5	Bleaching earth Clay 10 wt%	80	40	70
6	Bleaching earth Clay 15 wt%	80	35	90
7	Bleaching earth Clay 20 wt%	80	20	70
8	No catalyst	RT	70	0
9	No catalyst	80	80	0

<sup>a</sup>Reaction progress was monitored by thin layer chromatography (TLC)

<sup>b</sup>Yield refers to isolated yield

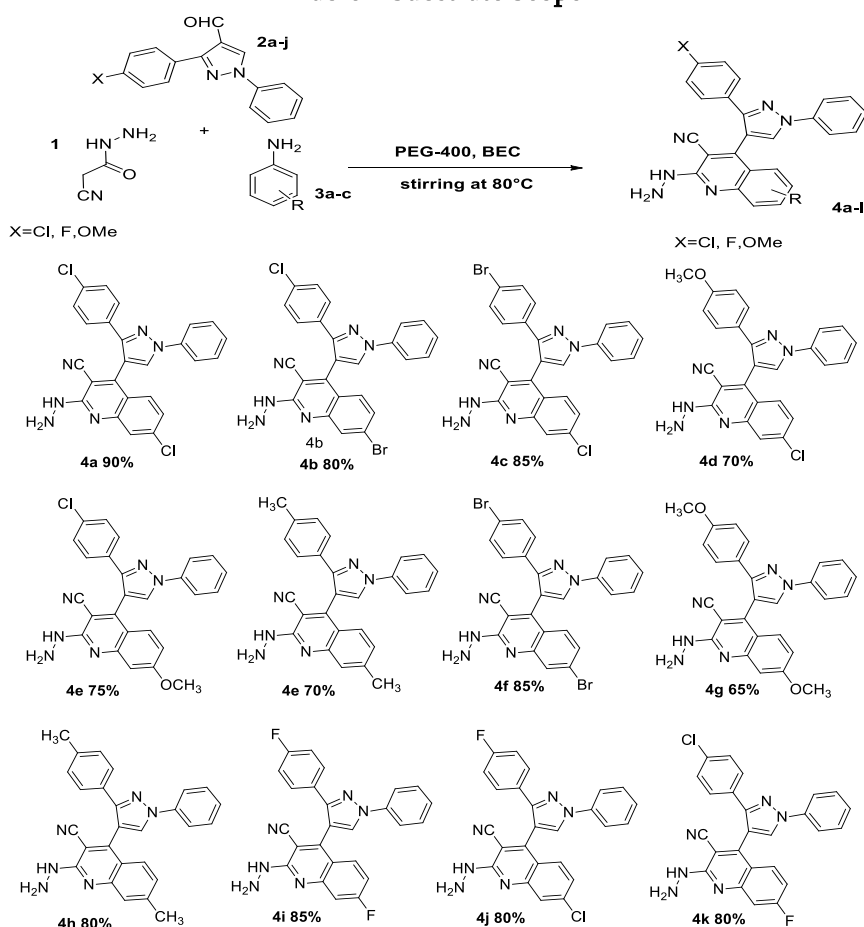
With these optimized conditions we initiated to find the substrate scope the reaction condition was found to operate for varied substrate scope Table 2.

### Scheme 1



The finding of the substrate scope indicates that the MCR strategy allows variety of substrate to undergo smoothly with formation of product with satisfactory yield. Interpretation of the yield of the substrate scope indicate that the reactant with electron donating group either on aldehyde 2a-j or on the anilines 3a-c renders the product yield. The substrates with electron withdrawing groups on the aldehydes or on the anilines are providing the products with good yield.

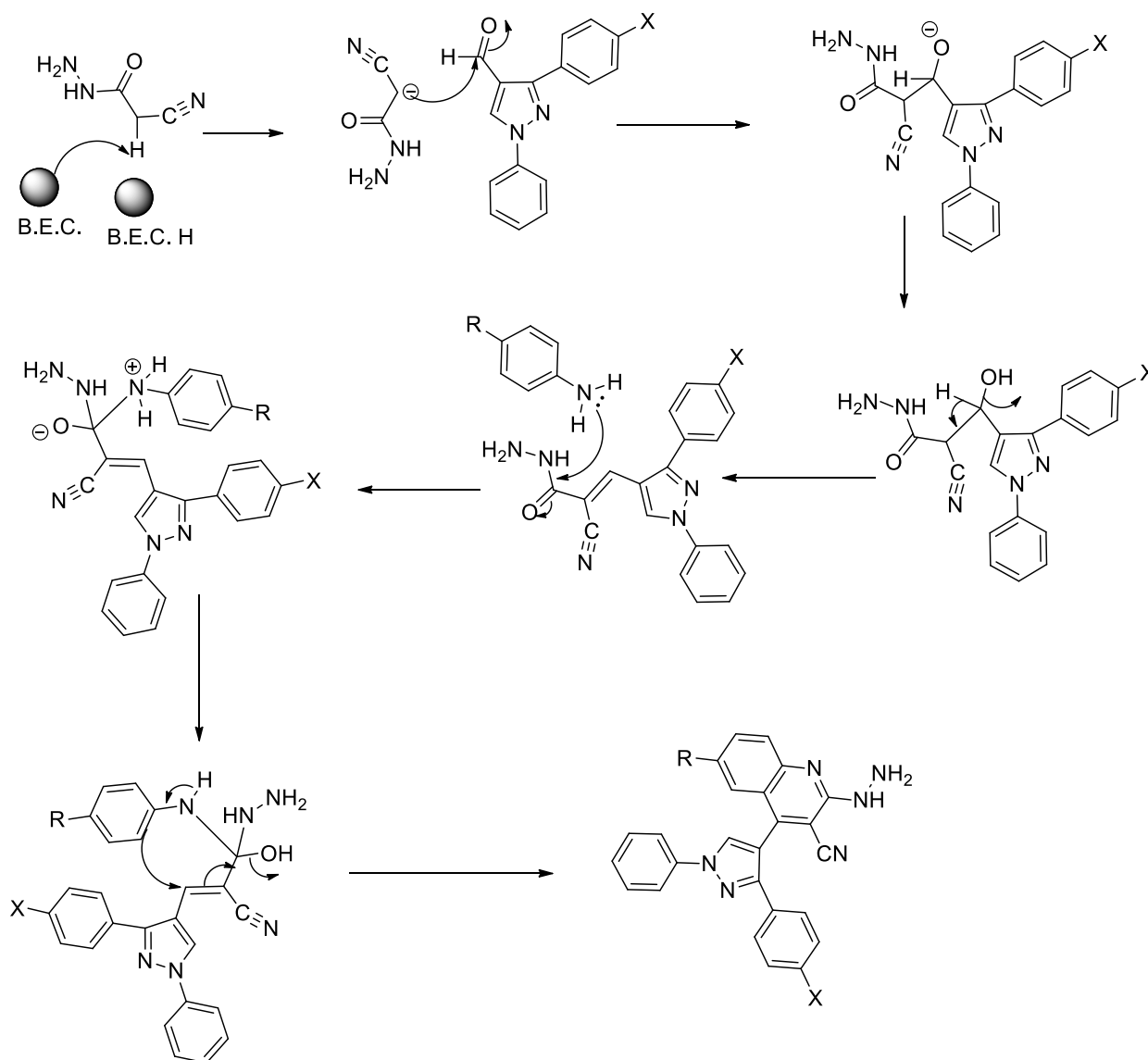
**Table 2 Substrate Scope**



<sup>a</sup> Yield refers to isolated product after column chromatography

The plausible mechanistic path was proposed in Scheme 2. The mechanism indicate reaction was proceeds through abstraction of proton from 2-cyanoacetohydrazide by BEC then the anion attack on the carbonyl of heterocyclic aldehyde. Furthermore, addition of substituted anilines leads to formation of final product.

Scheme 2 Plausible mechanism



## CONCLUSION:

The proposed protocol provides an easy access for the synthesis of quinoline-3-carbonitrile derivatives. the MCR strategy for the synthesis is woven with the environmental benign approach through the use of BEC as a catalyst and PEG-400 as a solvent. The protocol delivers an efficient access for the formation of new hybrid product with coupling of easily available reactants which may lead to improved biological activities.



**REFERENCES**

- [1] Nainwal, L. M., Tasneem, S., Akhtar, W., Verma, G., Khan, M. F., Parvez, S., Shaquiquzzaman, M., Akhter, M., Alam M. Eur. J. Med. Chem.2019, 164, 121-170.
- [2] Mukherjee, S., Pal, M. Drug Discov. Today, 2013, 18, 389-398.
- [3] Chung, P. Y., Bian, Z. X., Pun, H. Y., Chan, D., Chan, A.S.C., Chui, C. H., Tang, J.C.O., Lam, K. H. Future Med. Chem. 2015, 7, 947-967.
- [4] Khan, S. A., Asiri, A. M., Baisi, H. M., Asad, M., Zayed, M. E., Sharma, K., Wani, M. Y., Bioorg. Chem. 2019, 88, 102968.
- [5] Ibrahim, M. A., Badran, A. S. Syn. Commun. 2020, 50, 1871-1882.
- [6] Liu, B., You, Q. D., Li, Z. Y. Chin. Chem. Lett. 2010, 21, 554-557.
- [7] Gholap, A. R., Toti, K. S., Shirazi, F., Kumari, R., Bhat, M. K., Deshpande, M. V., Srinivasan, K. V. Biorg. Med. Chem. 2007, 15, 6705-6715.
- [8] Shah, N. M., Patel, M. P., Patel, R. G. Eur. J. Med. Chem. 2012, 54, 239-247.
- [9] Jentsch, N. G., Hart, A. P., Hume, J. D., Sun, J., McNeely, K. A., Lama, C., Julia, A., Pigza, M. G., Donahue G., Kessl, J. J., ACS Med. Chem. Lett. 2018, 9, 1007-1012.
- [10] Tu. S. J., Jiang, B., Jia, R. H., Zhang, J. Y., Zhang, Y., Yao, C. S., Shi, F. Org. Biomol. Chem. 2006, 4, 3664-3668.
- [11] Kawanishi, N., Sugimoto, T., Shibata, J., Nakamura, K., Masutani, K., Ikuta, M., Hirai, H. Biorg. Med. Chem. 2006, 16, 5122-5126.
- [12] Vo, C. V. T., Luescherf, M. U., Bode, J. W., Nature Chemistry, 2014, 6, 310-314.
- [13] Eydokimov, N. M., Kireev, A. S., Yakovenko, A. A., Antipin, M. Y., Magedov, I. V., Kornienko, A., J. Org. Chem.2007, 72, 3443-3453.
- [14] Shitole, N. V., Shelke. K. F., Sadaphal, S. A., Shingate, B. B., Shingare, M. S., Green chem. Lett. Rev. 2010, 3, 83-87.
- [15] Aly, R. M., Serya, R. A., El-Motwally, A. M., Esmat, A., Abbas, S., Abou El Ella, D. A., Bioorg. Chem. 2017, 75, 368-392.
- [16] Argyle, M. D., Bartholomew, C. H., Catalysts, 2015, 5, 145-269.
- [17] Boey, P. L., Maniam, G. P., Abd Hamid, S., Chem. Eng. J., 2011, 168, 15-22.
- [18] Gaikwad, M. V., Kamble, R. D., Hese, S. V., Acharya, A. P., Mogle, P. P., Kadam, S. N., Dawane B. S., Res. Chem, Intermed. 2015, 41, 4673-4678.

# Synthesis, Characterization and Biological Relevance of Cu(II) and Mn(II) Complexes of The NOON Donor Schiff Base Ligand

Bhagwat T. Vhanale, Dhananjay V. Bondar And Yogesh G. Mugale

P.G. Department of Chemistry, S.C.S. College, Omerga- 413606, Maharashtra, India

E-mail: [bvhanale777@gmail.com](mailto:bvhanale777@gmail.com)

## ABSTRACT

Herein, we report synthesis, characterization and biological properties of four novel Cu(II) and Mn(II) Schiff base complexes. These complexes have been characterized by using UV visible, FT-IR,  $^1\text{H}$  &  $^{13}\text{C}$  NMR, LCMS, TGA-DTA, ESR and powder X-ray diffraction. The IR results confirmed that the tetradentate binding of ligand involving two naphthol oxygen and two azomethine nitrogen.  $^1\text{H}$  NMR &  $^{13}\text{C}$  NMR spectral data of the ( $\text{H}_2\text{L}$ ) and their metal complexes agreed well with proposed structures. Thermogravimetric studies for Cu(II) and Mn(II) complexes indicated the presence of coordinated water molecules and the final product is the formation of metal oxide. The ESR lines showed that Cu(II) complexes are diamagnetic and Mn(III) complexes contain five unpaired electrons. To evaluate the antibacterial activity of newly synthesized Schiff base ligands and their metal complexes were screened by using two Gram-positive and two Gram-negative bacterial strains. It was found that; the newly synthesized metal complexes were more potent compared to the Schiff base ligands. Furthermore, antioxidant activities were determined by the reduction of 1,1-diphenyl-2-picrylhydrazyl (DPPH). These studies exhibited that, the Schiff base ligands possessed better antioxidant activity than their metal complexes.

**Keywords:** Tetradentate Schiff bases; Cu(II) and Mn(II) complexes; TGA-DTA; ESR; antibacterial activity; antioxidant activity.

## INTRODUCTION

Transition metal complexes of Schiff bases are the well-known area of research to an inorganic chemist as these complexes possess a wide range of biological activities [1-3]. Schiff bases can be easily prepared by reacting carbonyl compounds with amines in high yields under normal reaction conditions. Schiff bases are known to form a broad range of complexes with various metals [4-5]. The chemical, structural and spectral properties of metal complexes are often strongly dependent on the nature of the ligand structure. More recently, many metal-based drugs have gained significant importance in medicinal chemistry. They are used in the treatment of tumor [6], cancer [7] and anti-inflammatory [8] diseases. In addition to this, Schiff bases and their metal complexes have also exhibited antibacterial [9-10], antioxidant [9-10] and antifungal activities [11-12]. Metal complexes of Schiff bases are also known for various other applications

such as catalytic activity [13], alkaline phosphatase inhibition [14], insulin-mimetic properties [14], physicochemical properties [15], magnetic properties [16], phenoxazinone synthase activity [17], photochromic [18] and enzymatic activity [19].

In the recent report, DFT calculations of Cu(II) complexes showed that the Schiff base ligand coordinated to Ni(II) via two Nitrogen imine and two phenolic oxygen atoms. Such complexes show distorted square planar geometry around the central metal ion. Similarly, Mn(II) complexes show octahedral geometry [20] with high spin (*d5*) state [21-22]. Also, Cu(II) and Mn(II) complexes with electron-withdrawing groups improve nonlinear optical properties [23-24]. Cu(II) and Mn(II) complexes with Tetradentate donor Schiff bases give excellent antibacterial [25-26] and antioxidant activities [27-28]. Interestingly, Schiff bases derived from 2-hydroxy-1-naphthanone have been comprehensively studied because they form stable complexes with metal ions due to the presence of phenolic -OH and azomethine groups.

Herein, we report the synthesis of four novel Cu(II) and Mn(II) complexes of Schiff bases derived from pentane-1,3-diamine with 1-(4-bromo-1-hydroxynaphthalen-2-yl)ethanone and 1-(4-chloro-1-hydroxynaphthalen-2-yl)ethenone. These complexes are fully characterized by various physicochemical techniques and their antibacterial and antioxidant activities are studied.

## RESULT AND DISCUSSION

### 1.1 UV-visible spectra

The UV spectra of Schiff bases were studied in the polar solvent while complexes were studied in DMF solvent. The absorption band of Schiff bases is in the range of 350–384 nm due to the  $n \rightarrow \pi^*$  transition of the C=N imine group [29]. Similarly, Cu(II) and Mn(II) complexes of these Schiff bases are absorbed in a similar region but with very low intense bands above 490 nm due to metal-ligand bonding of these metal complexes.

### 1.2 FT-IR spectra

FT-IR analysis of the newly synthesized complexes was also studied and it helped us to understand the coordination between metal ion and ligand. The IR frequencies of ligands and their respective metal complexes are depicted in table 1. In the IR spectrum of the ligand ( $H_2L$ ), absorption bands due to phenolic-OH, azomethine ( $-C=N$ ) and phenolic  $\nu(C-O)$  group have appeared at  $3399\text{ cm}^{-1}$ ,  $1590\text{ cm}^{-1}$  and  $1322\text{ cm}^{-1}$  respectively [29]. In IR spectra of all the complexes, it was observed that the absence of absorption band due to phenolic -OH group at  $3399\text{ cm}^{-1}$  of ligand indicates the formation of a bond between a metal ion and phenolic oxygen atom [31-32]. This is further confirmed by the change in absorption frequency of phenolic  $\nu(C-O)$  which are shown in the region  $1275-1277\text{ cm}^{-1}$  indicating coordination to metal ion via oxygen atom of phenolic -OH group. The absorption frequency of the azomethine  $\nu(-C=N)$  group shifted to a lower frequency and appeared in the region  $1520-1531\text{ cm}^{-1}$ . This confirmed that the involvement of the nitrogen atom of the azomethine group in complexation with a metal ion. The formation of metal-ligand bonding was further confirmed by the appearance of low intense bands in the region  $564-575\text{ cm}^{-1}$  and  $462-491\text{ cm}^{-1}$  which were assigned to frequencies of  $\nu(M-O)$  and  $\nu(M-N)$  stretching bands appear in the region, respectively.

**Table 1. IR frequencies of Schiff base ligands and respected metal complexes.**

Compound	$\nu(\text{HO})$	$\nu(\text{H}_2\text{O})$	$\nu(\text{C-O})$	$\nu(\text{C=N-})$	$\nu(\text{M-O})$	$\nu(\text{M-N})$
H <sub>2</sub> L	3399	--	1322	1597	--	--
[Cu(L)]	--	3428	1277	1527	568	490
[MnL(H <sub>2</sub> O) <sub>2</sub> ]	--	3430	1277	1525	564	462

### 1.3 NMR Spectroscopy

The <sup>1</sup>H NMR spectra of Schiff base ligands and their metal complexes were recorded in CDCl<sub>3</sub>. The <sup>1</sup>H NMR spectra of the ligand H<sub>2</sub>L displayed singlet at 14.09 ppm due to the proton of phenolic –OH [30-32]. The singlet appeared at 2.46 ppm and 2.35 ppm was due to two methyl groups next to the imine moiety. The signals due to aromatic protons have resonated as multiplets in the region at 6.80-8.68 ppm. The disappearance of the phenolic –OH group signal at 14.09 ppm from the metal complex spectrum suggests complex formation. When compared to the <sup>1</sup>H NMR spectra of ligand and its metal complexes, all the signals due to protons have been shifted towards downfield  $\delta$  value confirming the complexation of a metal ion with the ligand.

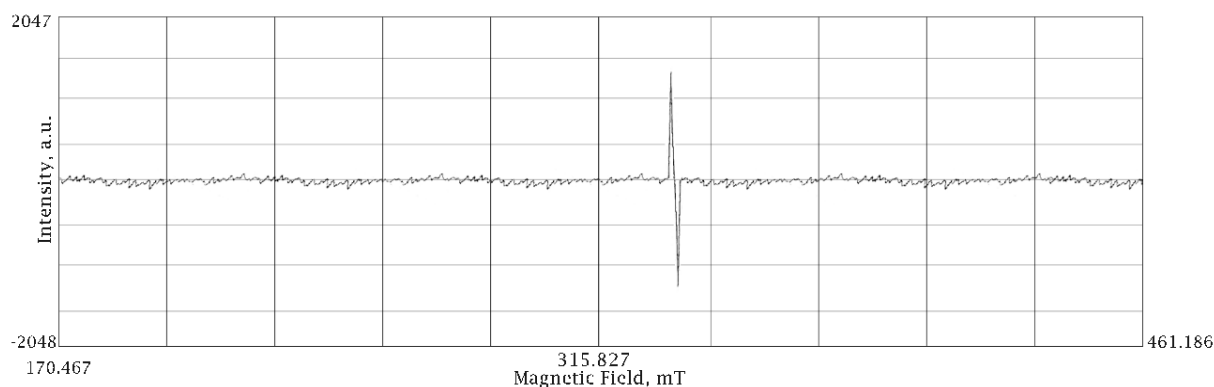
The <sup>13</sup>C NMR spectrum of ligand H<sub>2</sub>L displayed signals at  $\delta$  175.51 ppm due to azomethine carbon. The appearance of signals at  $\delta$  170.70 ppm and 135.01 ppm was due to carbon-bearing oxygen and halogen atom, respectively. When compared to the <sup>13</sup>C NMR spectra of Schiff base ligand to their metal complexes, the signals of azomethine carbon and carbon-bearing oxygen atom were shifted towards downfield  $\delta$  value confirming the complexation of a metal ion with the ligand.

### 1.4 LC-MS

The molecular weight of the Schiff base ligand and their metal complexes were confirmed by ESI MS analysis. The Schiff base ligand H<sub>2</sub>L showed a molecular ion peak  $m/z$  409 respectively, which is equivalent to its molecular weight. Similarly, the ESI mass spectrum of respective metal complexes showed molecular ion peaks similar to their molecular weight. The [CuL] and [MnL(H<sub>2</sub>O)<sub>2</sub>] showed a molecular ion peak at  $m/z$  562.07 and  $m/z$  685.99 respectively.

### 1.5 ESR

The ESR spectrum of [CuL] and [MnL(H<sub>2</sub>O)<sub>2</sub>] complexes provided valuable information. There is an intense band in the high field region. The EPR spectrum was recorded in DMSO at room temperature and spectra are shown in figure 3. From the  $g$  tensor value of the Cu(II) complex, the ground has been derived. The Cu(II) complex exhibits the  $g_{\parallel}$  value of 2.2597 and  $g_{\perp}$  value of 2.0797. In the square planar complexes, the unpaired electron lies in  $dx^2-y^2$  orbital and  $2B_{1g}$  is given as ground state with  $g_{\parallel} > g_{\perp} > 2$  [33] it indicates that the Cu(II) complex has square planar geometry. The calculated  $G$  value [ $G = (g_{\parallel} - 2)/(g_{\perp} - 2)$ ] is 3.25, confirming that the unpaired electron is predominantly present in  $dx^2-y^2$  orbital [34]. The spin-orbit coupling constant,  $\lambda$  value ( $-486 \text{ cm}^{-1}$ ) calculated using the relations,  $g_{av} = 1/3[g_{\parallel} + g_{\perp}]$  and  $g_{av} = 2(1 - 2\lambda/10Dq)$ , is less than free metal ion ( $-832 \text{ cm}^{-1}$ ) it indicates the M-L bonding in metal Complex is having covalent character [34]. The EPR spectrum of complex [MnL(H<sub>2</sub>O)<sub>2</sub>] exhibits six well-defined anisotropic signals with hyperfine splitting which may be attributed to five unpaired electron interactions of Mn(II) with the nuclear spin  $I = 5/2$ .



a) [CuL] complex

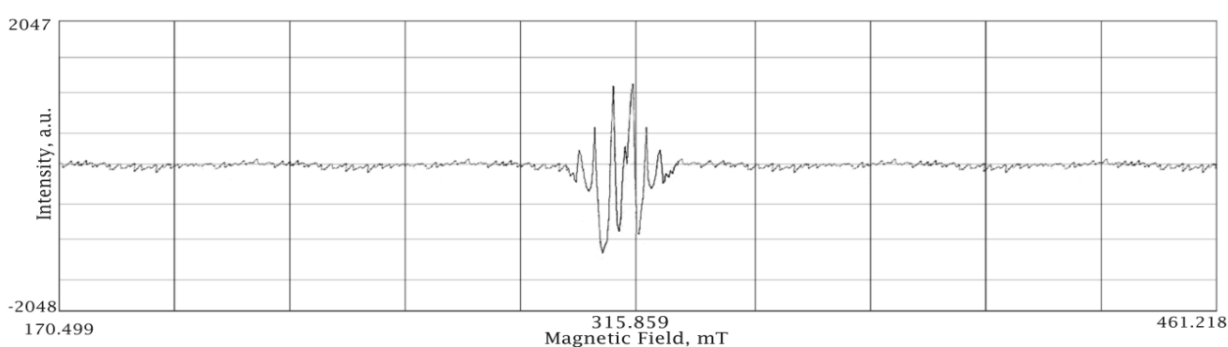
b) [MnL(H<sub>2</sub>O)<sub>2</sub>] complex

Figure 3. ESR of synthesized metal complexes

## 1.6 TGA-DTA

To study the thermal stability of the metal complexes, thermogravimetric (TG) and differential thermal analyses (DTA) were carried out for newly synthesized Cu(II) and Mn(II) complexes. TGA/DTA curves of Cu(II) and Mn(II) complexes show different peaks of decomposition. In Cu(II) complexes, the first step of degradation occurred in the range 62–99 °C, due to the loss of non-coordinated water molecules with a practical weight loss of 1.06%. The second and third steps of degradation occurred in the range of 100–600 °C, due to the removal of the ligand part from the metal atom with a practical weight losses 2.43% and 2.05%. Finally, the sharp line goes along temperature (X-axis) because of nickel oxide as residue. In Mn(II) complexes, the first step of degradation occurred in the range 71–183°C, due to the loss of two coordinated water molecules with a practical weight of 0.73% and 0.47%. The resultant complex on further degradation gave a break in the range 183–468 °C by the loss of phenyl group of Schiff base with practical weight 2.46% and 0.32%. Further, the complex showed gradual decomposition up to 644 °C and onwards due to loss of remaining organic moiety. Finally, the metal oxide is remaining as a residue.

## 1.7 Antibacterial activity

To contribute to the bioinorganic chemistry, In vitro evaluation of the antibacterial activity of the synthesized halo-Schiff base ligands and their metal complexes was carried out by screening them against given microorganisms. The respected microorganisms were standard strains of two gram-positive (*Bacillus cereus* and *Staphylococcus aureus*) and two-gram negative (*Pseudomonas aeruginosa* and *Escherichia coli*)

pathogens. Synthesized compounds are active against strains of Gram-Positive as well as Gram-Negative bacteria. According to Overtones concept [35] and Tweedy's chelation theory [35], the antibacterial activity of metal complexes enhanced in comparison with the free ligands. From the reported data, it is also clear that the halogenated Schiff base metal complexes are shown more antibacterial activity than Schiff base ligands [35].

**Table 3. Antibacterial activity of Schiff bases ligand and metal complexes. (in mm)**

Compound	B. cereus	S. aureus	p. aeruginosa	E. coli
(H <sub>2</sub> L)	21	22	10	09
[CuL]	27	24	12	10
[MnL(H <sub>2</sub> O) <sub>2</sub> ]	27	29	14	07
<b>Ampicillin</b>	<b>26</b>	<b>27</b>	<b>14</b>	<b>11</b>

### 1.8 Antioxidant activity

The antioxidant activity of the Schiff base ligands and metal complexes was evaluated by free radical scavenging activity by DPPH method comparison with standard butylated hydroxyanisole (BHA). The results of the free radical scavenging activity of compounds at different concentrations are presented in table 7. Among these compounds, Cu(II) complexes showed good scavenging activity than Mn(II) complexes. The free ligands showed promising antioxidant activity as compared to respective metal complexes, due to the presence of the phenolic -OH group. Table 4. Antioxidant activity of Schiff bases ligand and metal complexes.

Compound	12.5 µg	25 µg	50 µg	100 µg
(H <sub>2</sub> L)	09.62±0.17	15.55±0.06	50.37±0.14	64.06±0.45
[CuL]	06.55±0.26	11.27±0.91	44.94±0.05	49.77±0.89
[MnL(H <sub>2</sub> O) <sub>2</sub> ]	07.91±0.09	10.25±0.16	32.12±0.82	41.23±0.29
<b>BHA</b>	<b>11.31±0.62</b>	<b>18.44±0.67</b>	<b>58.18±0.67</b>	<b>72.12±0.88</b>

## EXPERIMENTAL

### 2.2.1 Synthesis of ligands (H<sub>2</sub>L)

The 1:2 molar mixture of pentane -1,3-diamine (10 mmol) and 1-(4-chloro-1-1-hydroxynaphthalen-2-yl)ethanone (20 mmol) in absolute ethanol (25 ml) was refluxed with a catalytic amount of glacial acetic acid (2-3 drops) for about 2-3 h. For better results, the reaction mixture was rest overnight. The needle-shaped pale yellow product (H<sub>2</sub>L<sub>2</sub>) was filtered off, washed with hot water and recrystallized with absolute ethanol.

### 2.2.2 [E]2,2'-((pentane-1,3-diylbis(azanylylidene))bis(ethan-1-yl-1-ylidene))bis(4-chloronaphthalen-1-ol)(H<sub>2</sub>L<sub>2</sub>)

Molecular Formula:  $[C_{29}H_{28}Cl_2N_2O_2]$ , Molecular Weight: 508, Yield: 406.52 mg (80%), Color: Yellow, M.P. 192-194 °C.

FT-IR(KBr,  $cm^{-1}$ ):

$^{1}H$ NMR( $CDCl_3$ )(ppm) $\delta$ :14.09(s, Ar-OH, 2H), 8.52-6.79(m, 10H, Ar-H), 4.09(t,  $J=4.5$ Hz,  $-CH_2$ , 2H), 3.65(m,  $J=4.6$ Hz,  $-CH$ , 1H), 2.46(s,  $-CH_3$ , 3H), 2.35(s,  $-CH_3$ , 3H), 2.33(q,  $J=4.3$ Hz,  $-CH_2$ , 2H), 1.81(m,  $J=4.1$ Hz,  $-CH_2$ , 2H), 1.04(t,  $J=4.1$ Hz,  $-CH_3$ , 3H).  $^{13}C$ NMR( $CDCl_3$ )(ppm) $\delta$ :175.50( $-C=N-$ ), 170.95( $-C-O$ ), 137.45-106.66(Ar- $\underline{C}$ -), 136.21( $-C-Cl$ ), 54.22( $-N-C-H$ ), 41.71( $-N-\underline{C}H_2-$ ), 34.76( $HC-\underline{C}-CH_2-$ ), 29.56( $H_3C-\underline{C}-CH-$ ), 14.57( $-N=C-\underline{C}H_3$ ), 10.24( $-C-CH_2-CH-$ ). ESIMS (m/z):508.15(63.9 %). Elemental Analysis: C, 68.77; H, 5.53; Cl, 24.47; N, 5.72.

### 2.3 General procedure for synthesis of metal complexes.

The methanolic solution of Schiff base ligand ( $H_2L$ ) (10 mmol) was added with a respective metal acetate (10 mmol) using methanol as a solvent. The resulting solution had refluxed for 5-7 h. the reaction mixture was cooled to room temperature and immediately separated. After evaporation of the filtrate were obtained as a product.

#### 2.3.1 Synthesis of $[Cu(L)]$ complexes

$[Cu(L)]-(1E,1'E)-N,N'$ -(pentane-1,3-diyl)bis(1-(4-chloro-1-(11-oxidanyl)naphthalen-2-yl)ethan-1-imine)copper(II)

Molecular Formula:  $[C_{29}H_{26}Cl_2N_2CuO_2]$ , Molecular Weight: 564, Yield: 406.06 mg (72%), Color: Green, M.P. >300 °C.

FT-IR(KBr,  $cm^{-1}$ ):1590( $\nu C=N$ ), 1527( $\nu C=C$ ), 1027( $\nu C-N-C$ ), 863, 790( $\nu C-Cl$ ), 566( $\nu M-O$ ), 485( $\nu M-N$ ).

$^1H$ NMR( $CDCl_3$ )(ppm) $\delta$ :8.50-6.78(m, 10H, Ar-H), 4.10(t,  $J=4.5$ Hz,  $-CH_2$ , 2H), 3.72(m,  $J=4.6$ Hz,  $-CH$ , 1H), 2.48(s,  $-CH_3$ , 3H), 2.35(s,  $-CH_3$ , 3H), 2.25q,  $J=4.3$ Hz,  $-CH_2$ , 2H), 1.85(m,  $J=4.1$ Hz,  $-CH_2$ , 2H), 1.05(t,  $J=4.1$ Hz,  $-CH_3$ , 3H).

$^{13}C$ NMR( $CDCl_3$ )(ppm) $\delta$ :175.55( $-C=N-$ ), 171.34( $\underline{C}-O$ ), 137.37-108.50(Ar- $\underline{C}$ -), 137.20( $-C-Cl$ ), 54.09( $-N-\underline{C}-H$ ), 41.77( $-N-\underline{C}H_2-$ ), 34.51( $HC-\underline{C}-CH_2-$ ), 29.39( $H_3C-\underline{C}-CH-$ ), 14.39( $-N=C-\underline{C}H_3$ ), 10.28( $-C-CH_2-CH-$ ).

ESIMS(m/z):562.07(100.0 %).Elemental Analysis: C, 61.74; H, 4.65; Cl, 12.57; N, 4.97; Cu, 10.40; O, 5.67.

#### 2.3.2 Synthesis of $[MnL(H_2O)_2]$ complexes

$[MnL(H_2O)_2]-(1E,1'E)-N,N'$ -(pentane-1,3-diyl)bis(1-(4-chloro-1-(11-oxidanyl)naphthalen-2-yl)ethan-1-imine)manganese(II)dehydrate

Molecular Formula:  $[C_{29}H_{30}Cl_2FeN_2O_4]$ , Molecular Weight: 597.31, Yield: 465.90 mg (78%), Color: Blackish, M.P. >300 °C.

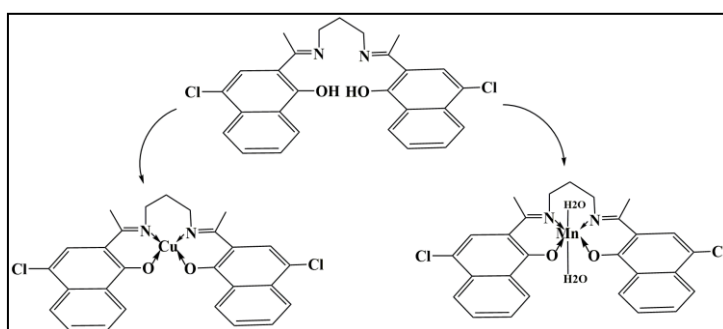
FT-IR(KBr,  $cm^{-1}$ ):1585( $\nu C=N$ ), 1525( $\nu C=C$ ), 1022( $\nu C-N-C$ ), 875, 790( $\nu C-Cl$ ), 567( $\nu M-O$ ), 485( $\nu M-N$ ).

$^1H$ NMR( $CDCl_3$ )(ppm) $\delta$ :8.50-6.78(m, 10H, Ar-H), 4.12(t,  $J=4.5$ Hz,  $-CH_2$ , 2H), 3.78(m,  $J=4.6$ Hz,  $-CH$ , 1H), 2.44(s,  $-CH_3$ , 3H), 2.33(s,  $-CH_3$ , 3H), 2.21(q,  $J=4.3$ Hz,  $-CH_2$ , 2H), 1.83(m,  $J=4.1$ Hz,  $-CH_2$ , 2H), 1.00(t,  $J=4.1$ Hz,  $-CH_3$ , 3H).

$^{13}C$ NMR( $CDCl_3$ )(ppm) $\delta$ :175.54( $-C=N-$ ), 171.33( $\underline{C}-O$ ), 137.35-108.52(Ar- $\underline{C}$ -), 137.22( $-C-Cl$ ), 54.10( $-N-\underline{C}-H$ ), 41.75( $-N-\underline{C}H_2-$ ), 34.52( $HC-\underline{C}-CH_2-$ ), 29.40( $H_3C-\underline{C}-CH-$ ), 14.40( $-N=C-\underline{C}H_3$ ), 10.29( $-C-CH_2-CH-$ ).

ESIMS(m/z):596.09(100.0%)

Elemental Analysis: C, 58.31; H, 5.06; Cl, 11.87; Mn, 9.35; N, 4.69; O, 10.71



**Scheme. Synthesis of metal complexes.**

## CONCLUSION

A series of Cu(II) and Mn(II) complexes were prepared with tetradentate  $N_2O_2$  Schiff base ligand  $H_2L$ . They are characterized by various spectral techniques such as UV Visible, FT-IR,  $^1H$  NMR,  $^{13}C$  NMR and LCMS. Additionally, these metal complexes are studied by TGA-DTA and ESR analysis. The Physico-chemical results demonstrate that Cu(II) complexes have a distorted square planar geometry and Mn(II) complexes have an octahedral geometry through the involvement of naphthol oxygen and azomethine nitrogen. ESR studies support Mn(II) complexes which have a high spin ( $d_5$ ) nature of the complexes. The antibacterial activity of all metal complexes showed potent antibacterial activity than the parent ligands. The antioxidant activity of synthesized metal complexes is carried out with BHA as standard. The antioxidant activity of tetradentate Schiff base ligands showed more potency than metal complexes because ligands have a free  $-OH$  group to reduce DPPH. Based on all these observations, it was concluded that the NOON tetradentate Schiff bases and their metal complexes give a versatile and valuable information of coordination compounds and also they may be used as good biological agents.

## REFERENCES

- [1] L.N. Obasi, G.U. Kaior, L. Rhyman, I.A. Alswaidan, H.K. Fun, P. Ramasami. *J. Mol. Struct.* 1120, 180 (2016).
- [2] H. Kargar, A.A. Ardakani, M.N. Tahir, M. Ashfaq, K.S. Munawar. *J. Mol. Struct.* 1233, 130112 (2021).
- [3] H. Kargar, A.A. Ardakani, K.S. Munawar, M. Ashfaq, M.N. Tahir, *J. Iran. Chem. Soc.* 18, 2493 (2021).
- [4] L.H. Abdel-Rahman, N.M. Ismail, M. Ismael, A.M. Abu-Dief, E.A.H. Ahmed, *J. Mol. Struct.* 1134, 851 (2017).
- [5] A.C.W. Leung, M.J. MacLachlan, *J. Inorg. and Organomet. Polym. Mater.* 17, 57 (2007).
- [6] H. Glasner, E.Y. Tshuva, *J. Am. Chem. Soc.* 133, 16812 (2011).
- [7] Z. Abbasi, M. Salehi, A. Khaleghian, M. Kubicki, *J. Mol. Struct.* 1173, 213 (2018).
- [8] M. Manjunatha, V.H. Naik, A.D. Kulkarni, *J. Coord. Chem.* 64, 4264 (2011).
- [9] W. Al Zoubi, A.A.S. Al-Hamdani, M. Kaseem, *Appl. Organomet. Chem.* 30, 810 (2016).
- [10] Q.M. Hasi, Y. Fan, X.Q. Yao, D.C. Hu, J.C. Liu, *Polyhedron* 109, 75 (2016).
- [11] S.M. Abdallah, M.A. Zayed, G.G. Mohamed, *Arab. J. Chem.* 3, 103 (2010).



- [12] B. Iftikhar, K. Javed, M.S. Ullah Khan, Z. Akhter, B. Mirza, V. Mckee, *J. Mol. Struct.* 1155,337 (2018).
- [13] P.G. Cozzi, *Chem. Soc. Rev.* 33, 410 (2004).
- [14] H. Kargar, *Transit. Met. Chem.* 39, 811 (2014).
- [15] K.S. Munawar, S. Alia, M.N. Tahirb, N. Khalidc, Q. Abbasd, I.Z. Qureshid, S. Shahzadia, *Russ. J. Gen. Chem.* 85, 2183 (2015).
- [16] A. Rauf, A. Shah, *Arab. J. Chem.* 13, 1130 (2020).
- [17] M. Niu, Z. Li, H. Li, X. Li, J. Dou, S. Wang, *RSC Adv.* 5, 37085 (2015).
- [18] S.Chatterjee, D. Sukul, P. Banerjee, J. Adhikary, *Inorganica Chim. Acta* 474, 105 (2018).
- [19] R.A. Kopelman, M.M. Paquette, N.L. Frank, *Inorganica Chim. Acta.* 361, 3570 (2008).
- [20] Z. Shaghaghi, R. Bikas, H. Tajdar, A. Kozakiewicz, *J. Mol. Struct.* 1217, 128431 (2020).
- [21] C.R. Bhattacharjee, P. Goswami, P. Mondal, *Inorganica Chim. Acta.* 387, 86 (2012).
- [22] J. Cisterna, V. Artigas, M. Fuentealba, P. Hamon, C. Manzur, J.R. Hamon, D. Carrillo, *Inorganics* 6, 5 (2018).
- [23] J. Cisterna, V. Dorcet, C. Manzur, I. Ledoux-Rak, J.R, Hamon, D. Carrillo, *Inorganica Chim. Acta.* 430, 8 (2015).
- [24] N. Raman, Y. Pitchaikani, Raja, A. Lulandaisamy, *Proc. Indidan Acad.Sci.* 113, 183 (2001).
- [25] S.K. Tadavi, A.A. Yadav, R.S. Bendre, *J. Mol. Struct.* 1152, 223 (2018).
- [26] H.A.R. Pramanik, P.C. Paul, P. Mondal, C.R. Bhattacharjee, *J. Mol. Struct.* 1100, 496 (2015).
- [27] G.Y. Nagesh, B.H.M. Mruthyunjayaswamy, *J. Mol. Struct.* 1085, 198 (2015).
- [28] A.S. Munde, A.N. Jagdale, , S.M. Jadhav, T.K. Chondhekar, *J. Serbian Chem. Soc.* 75, 349 (2010).
- [29] B.T. Vhanale, N.J. Deshmukh, A.T. Shinde, *Heliyon* 5, e02774 (2019).
- [30] R.P. Singh, K.N. Chidambara Murthy, G.K. Jayaprakasha, *J. Agric. Food Chem.* 50, 81 (2002).
- [31] A.A. Ardakani, H. Kargar, N. Feizi, M.N. Tahir, *J. Iran. Chem. Soc.* 15, 1495 (2018).
- [32] A. Sahraei, H. Kargar, M. Hakimi, M.N. Tahir, *Transition Met. Chem.* 42, 483 (2017).
- [33] H. Kargar, A.A. Ardakani, M.N. Tahir, M. Ashfaq, K.S. Munawar, *J. Mol. Struct.* 1229,129842 (2021).
- [34] A. Sahraei, H. Kargar, M. Hakimi, M.N. Tahir, *J. Mol. Struct.* 1149, 576 (2017).
- [35] T. Chandrasekar, A. Arunadevi, N. Raman, *J. Coord. Chem.* 74, 1634 (2021).
- [36] N. Raman, S. Ravichandran, C. Thangaraja, *J. Chem. Sci.* 116, 215 (2004).

# PTC: An Efficient One Pot Multicomponent Synthesis of 2 Amino 4H Chromenes under Mild Reaction Conditions

Asgar Jafar khan, A. R. Shaikh, Abdul Rahim Abdul Sami\*

Organic Chemistry Laboratory, Milliya College, Beed-431122, Maharashtra, India

\*Corresponding Author: [phychemmax@gmail.com](mailto:phychemmax@gmail.com)

## ABSTRACT

The derivatives of 2-amino-4H-chromene are very important class of organic compounds, their synthesis via one-pot multicomponent reactions have been received much attention of chemist due to their wide range of biological and pharmacological potentials. Here, the catalytic performances of PTC [Aliquat-336] that effectively promote these reactions under solvent free condition are investigated. The reaction is easy to carry out and the following working procedures are very simple. Pure products can be obtained by filtration and washing procedures, without requiring column separation procedures. The synthesized compounds were characterized by TLC, Melting points, <sup>1</sup>H NMR, Mass and IR spectral analysis.

**Keywords:** PTC (Aliquat-336), 2-Amino-4H-chromenes, Solvent Free Reaction.

**Abbreviation:** PTC (Phase Transfer Catalyst)

## INTRODUCTION

In the field of organic chemistry, an important largest area of research has been occupied by heterocyclic compounds. Synthesis of Oxygen containing heterocyclic compounds especially 2-Amino-4H-chromene derivatives have been provoked much interest due to reported broad spectrum of biological as well as pharmacological activities such as antiproliferative [1], antitumor [2], anti-cancer activities [3], anti-inflammatory [4], anti-HIV [5], antioxidant [6] and antibacterial [7]. In view of their importance, they have received a great deal of interest by different chemist and in the literature different methods for their synthesis have been introduced. These include one-pot three component reactions using malononitrile, activate phenols and various aromatic aldehydes [8]. For their condensation purpose, many reagents have been reported such as tungstic acid functionalized mesoporous SBA-15 [9], K<sub>2</sub>CO<sub>3</sub>, H<sub>2</sub>O [10], DABCO [11], Iodine [12], Et<sub>3</sub>N [13], Mesolite [14], MeSO<sub>3</sub>H [15], [Choline][AC] [16], Sulfonic acid-functionalized MIL-101 [17], L-proline [18], Fe(HSO<sub>4</sub>)<sub>3</sub> [19], DBU [20], Triethanolamine [21], K<sub>2</sub>CO<sub>3</sub>, MWI [22], nanosized MgO and Fe<sub>3</sub>O<sub>4</sub> [23,24], molybdenum Schiff base [25], RGO-SO<sub>3</sub>H [26], but few of these methods are having some drawbacks such as prolong reaction time, toxic solvents, expensive reagents, tedious workup and generate moderate yields of the product. Because of their important therapeutic value, better search of reagent and routes are continually being developed we herein report a new reagent for the synthesis of 2-Amino-4H-chromene derivatives. As a part of the research Programme for the synthesis of such biological

hits and environmentally benign protocols [27], we were interested in the synthesis of 2-Amino-4H-chromene derivatives. In the current strategy, we herein report the synthesis of 2-amino-4H-chromene derivatives by reaction of aromatic aldehydes and malononitrile with activate phenols or Naphthol under solvent free reaction condition using phase transfer catalysts [Aliquat 336] in short reaction time (5 min), excellent yield of the products was obtained by filtration and washing procedures, without requiring column separation procedures.

## EXPERIMENTAL:

### [I] Chemicals and Apparatus:

All Chemicals used in this work were purchased from Aldrich and Merck chemical companies and used without purification. IR spectra were recorded on a Shimadzu 435-U-04 FT spectrometer as KBr pellets. <sup>1</sup>H NMR spectra were measured in CDCl<sub>3</sub> with a Bruker DRX-400 Advance instrument at 400 and 100 MHz, respectively, using tetramethyl silane [TMS] as internal standard. Mass spectra were recorded with a spectrometer Finnegan-MAT 8430 operating at an ionization potential of 70 eV. Melting points were measured by digital melting point apparatus.

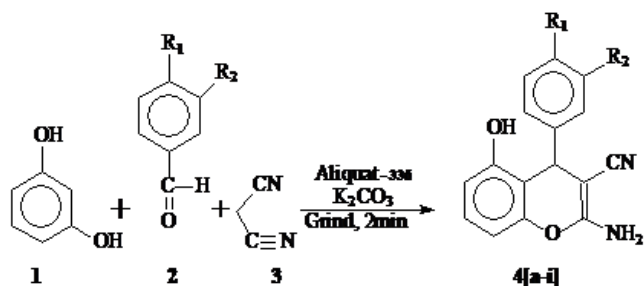
### [II] General Procedure for the Synthesis of 2-Amino-4-H-Chromenes:

A mixture of Phenols (10mmol), aromatic aldehydes (10mmol), malononitrile (10 mmol), Potassium carbonate (0.25mmol) and phase transfer catalyst Aliquat-336 (0.2g) were ground well using mortar and pestle for 2 min., after completion of the reaction [monitored on TLC, eluent: ethyl acetate: pet. ether (3:7)] the crude product was stirred by adding 10ml ethanol for 5 min. Then the reaction content was poured in to crushed ice, filtered and the obtained product was recrystallized with ethanol to afford the pure 2-Amino-4-H-Chromene derivatives. The results are summarized in Table-1 and 2.

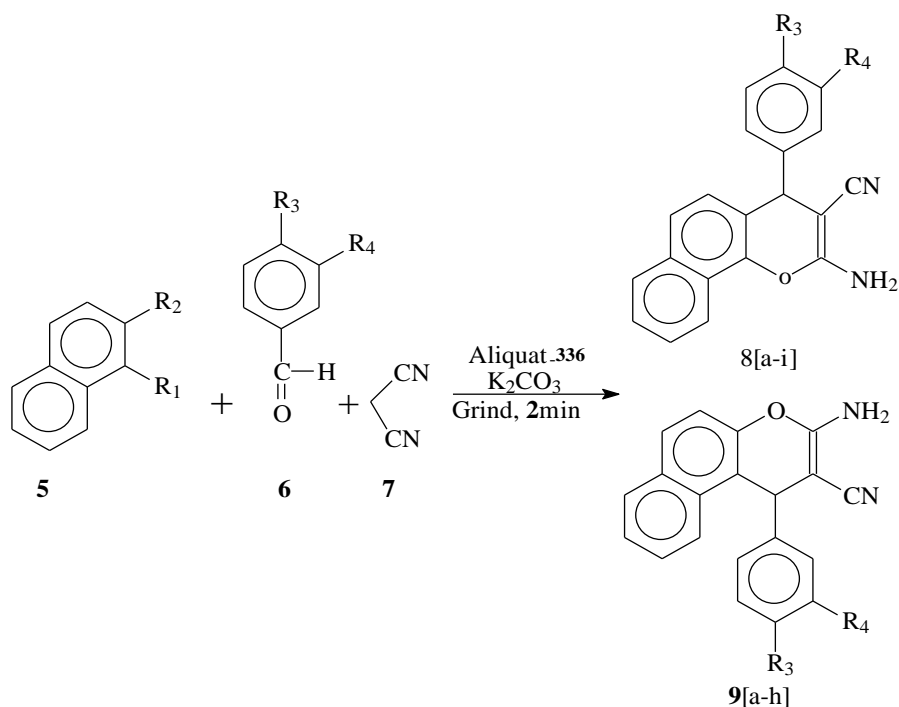
### [III] Result and Discussion:

In the current strategy, the synthesis of 2-amino-4H-chromene derivatives has been carried out successfully

by reaction of aromatic aldehydes and malononitrile with phenols or Naphthol under solvent free reaction condition using phase transfer catalysts [Aliquat 336] and K<sub>2</sub>CO<sub>3</sub> in short reaction time (2min) with excellent yield of the product [Schem-1 and Scheme-2]. The progress of the reaction was monitored by TLC. It is interested to note that no product formation was observed in the absence of catalyst. The results of synthesized products are summarized in Table-1 and 2. All the products were characterized by comparison of their physical and spectral data with the authentic samples reported in the literature.



Scheme-1: Synthesis of 2-amino-4H-chromenes from aldehydes, malononitrile and resorcinol



**Scheme-2: Synthesis of various 2-amino-4H-chromene derivatives from aldehydes, malononitrile and naphthol**

**Table 1: Synthesis of various 2-amino-4H-chromene derivatives from aldehydes, malononitrile and resorcinol**

Entry No.	Product	R1	R2	Yield <sup>a</sup> (%)	M.P.
1	4a	H	H	72	235–237
2	4b	Br	H	82	222–224
3	4c	H	NO <sub>2</sub>	85	167–169
4	4d	F	H	95	191–192
5	4e	H	Cl	85	106–109
6	4f	OCH <sub>3</sub>	H	92	110–112
7	4g	NO <sub>2</sub>	H	94	166–168
8	4h	CH <sub>3</sub>	H	80	188–190
9	4i	Cl	H	80	161–163

**Table 2: Synthesis of various 2-amino-4H-chromene derivatives from aldehydes, malononitrile and Naphthol**

Entry No.	Product	R1	R2	R3	R4	Yield <sup>a</sup> (%)	M.P.
1	8a	OH	H	H	H	80	178–180
2	8b	OH	H	Br	H	88	232–234
3	8c	OH	H	H	NO <sub>2</sub>	95	211–213

4	8d	OH	H	F	H	82	233-235
5	8e	OH	H	H	Cl	88	212-214
6	8f	OH	H	OCH <sub>3</sub>	H	80	187-189
7	8g	OH	H	NO <sub>2</sub>	H	90	233-234
8	8h	OH	H	CH <sub>3</sub>	H	70	206-208
9	8i	OH	H	Cl	H	88	232-234
10	9a	H	OH	H	H	70	283-285
11	9b	H	OH	Br	H	88	238-240
12	9c	H	OH	H	NO <sub>2</sub>	85	232-234
13	9d	H	OH	F	H	90	226-228
14	9e	H	OH	H	Cl	88	234-236
15	9f	H	OH	Cl	H	75	173-175
16	9g	H	OH	NO <sub>2</sub>	H	94	187-189

## CONCLUSIONS:

In conclusion we have demonstrated the application of PTC with K<sub>2</sub>CO<sub>3</sub> for the synthesis of 2-amino-4H-chromenes from reaction of aromatic aldehydes and malononitrile with activate Phenols or Naphthol under solvent free reaction condition. The present protocol has various advantages over reported methods such as environmentally benign conditions, inexpensive and readily available catalyst, simple and easy workout procedure, short reaction time and excellent yield of the product.

### Spectral data of the selected products:

2-Amino-3-cyano-7-hydroxy-4-phenyl-4H-chromene (4a): Solid; Light yellow;

FT-IR: 3495.88, 3425.59 (NH<sub>2</sub>), 3334.61 (OH), 2189.75 (CN), 1650.17 (C-C),

<sup>1</sup>H NMR(DMSO-d<sub>6</sub>): (δ ppm) 4.60 (CH, s, 1H), 6.41 (CH, s, 1H), 6.47 (CH, d, 1H, J = 8.4Hz, ArH), 6.79 (CH, d, 1H, J = 8.1Hz, ArH), 6.86 (NH<sub>2</sub>, s, 2H), 7.14-7.21 (ArH, m, 3H), 7.27-7.32 (ArH, m, 2H), 9.81 (OH, s, 1H); m/z (Obs.) = 265.1500 (M+H)<sup>+</sup>

2-Amino-4-(4-chlorophenyl)-3-cyano-7-hydroxy-4H-chromene (4i): Yellow solid.

IR (KBr): 3466.13, 3340.13, 3248.96, 2191.46, 1641.92, 1588.71, 1504.04, 1156.23 cm<sup>-1</sup>. <sup>1</sup>H NMR (DMSO-d<sub>6</sub>): δ 4.68 (s, 1H), 6.42 (d, 1H, J = 2.1 Hz), 6.49 (dd, 1H, J = 2.1 Hz), 6.79 (d, 1H, J = 8.4 Hz), 6.90 (s, 2H, NH<sub>2</sub>), 7.19 (d, 2H, J = 8.1 Hz), 7.36 (d, 2H, J = 8.1 Hz), 9.72 (s, 1H, OH). m/z = 299.0938 (M+H)<sup>+</sup>.

2-Amino-4-(phenyl)-4H-benzochromene-3-carbonitrile (8a): Light yellow solid.

IR (KBr) 3450.62, 3318.13, 2203.63, 1653.52, 1454.04, 1405.82 cm<sup>-1</sup>;

<sup>1</sup>H NMR (CDCl<sub>3</sub>): δ = 4.73 (s, 2H, NH<sub>2</sub>), 4.83 (s, 1H), 6.03 (d, 1H), 7.38- 7.45 (m, 5H), 7.66-7.71 (m, 3H), 8.96 (d, 1H, J = 8.1 Hz), 8.52 (d, 1H, J = 8.1 Hz); m/z = 299.0489 (M+H)<sup>+</sup>

2-Amino-4-(4-methoxyphenyl)-4H-benzochromene 3-carbonitrile (8f): Light yellow solid.

IR (KBr) 3480.37, 3366.13, 2193.23, 1653.26, 1595.56 cm<sup>-1</sup>;

<sup>1</sup>H NMR (CDCl<sub>3</sub>): δ 3.76 (s, 3H), 4.86(s, 2H, NH<sub>2</sub>), 5.04 (s,1H), 6.82 (d, 1H), 7.32 (d, 2H, ArH, J = 8.7 Hz,), 7.43 (d, 2H, ArH, J = 8.7 Hz,), 7.52-7.60 (m, 3H, ArH), 7.79 (d, 1H, ArH, J = 2.1 Hz,), 8.10 (d, 1H, ArH, J = 2.1 Hz,); m/z = 329.1007 (M+H)<sup>+</sup>.

2-Amino-4-(phenyl)-4H-benzochromene-3-carbonitrile (9a): Light yellow solid.

IR (KBr): 3432.11, 3333.04, 2184.33, 1658.32, 1581.33, 1433.91 cm<sup>-1</sup>;

<sup>1</sup>H NMR (CDCl<sub>3</sub>):δ 2.68 (s, 2H, NH<sub>2</sub>), 4.73 (s, 1H), 6.85 (d, 1H), 7.18-7.23 (m, 5H), 7.63-7.67 (m, 3H), 7.46 (d, 1H, J = 9 Hz), 7.68 (d, 1H, J = 8.1 Hz) ; m/z = 299.0960 (M+H)<sup>+</sup>.

## ACKNOWLEDGEMENTS:

Authors are thankful to the Principals, Maulana Azad College of Arts, Science & Commerce, Aurangabad and Milliya Arts, Science & Management Science College, Beed [M.S] for providing necessary facilities for this research work.

## REFERENCES

- [1] Dell, C.P. Smith, C.W. European Patent Appl. EP 537949, Chem. Abstr. 119 (1993) 139102d.
- [2] S.J. Mohr; M.A. Chirigos; F.S. Fuhrman; J.W. Pryor Cancer Res., 35 (1975), p. 3750
- [3] Mohr SJ, Chirigos MA, Fuhrman FS, Pryor JW (1975) Cancer Res 35:3750–3754
- [4] Moon DO, Choi YH, Kim ND, Park YM, Kim GY (2007) Int Immunopharmacol 7:506–514
- [5] Puller RW, Bokesch HR, Gustafson KI, McKee TC (1994) II JHC, McMahon JB, Cragg GM, Soejarto DD, Boyd MR. Bioorg Med Chem Lett 4:1961–1964
- [6] Subbareddy CV, Sundarrajan S, Mohanapriya A, Subashini R, Shanmugam S (2018) J Mol Liq 251:296–307
- [7] Zhang G, Zhang YH, Yan JX, Chen R, Wang SL, Ma YX, Wang R (2012) J Org Chem 77:878–888
- [8] Martins MAP, Frizzo CP, Tier AZ, Moreira DN, Zanatta N, Bona corso HG (2014) Chem Rev 114:PR1–PR70
- [9] Kundu SK, Mondal J, Bhaumik A (2013) Dalton Trans 42:10515–10524
- [10] Pourmohammad, M., & Mokhtary, M. (2015). K<sub>2</sub>CO<sub>3</sub>-catalyzed synthesis of 2-amino-3-cyano-4H-chromene derivatives with different substituents in water. Comptes Rendus. Chimie, 18(5), 554-557.
- [11] Shinde S, Rashinkar G, Salunkhe R (2013) J Mol Liq 178:122–126
- [12] Ren Y-M, Cai C (2008) Catal Commun 9:1017–1020
- [13] Kemnitzer W, Kasibhatla S, Jiang SH, Zhang H, Zhao JH, Jia SJ, Xu LF, Crogan-Grundy C, Denis R, Barriault N, Vaillancourt L, Charron S, Dodd J, Attardo G, Labrecque D, Lamothe S, Gour deau H, Tseng B, Drewe J, Cai SX (2005) Bioorg Med Chem Lett 15:4745–4751
- [14] Pawar GT, Magar RR, Lande MK (2016) Polycycl Aromat Compd 38:75–84
- [15] Heravi MM, Baghernejad B, Oskooie HA (2008) J Chin Chem Soc 55:659–662
- [16] Zhu, Anlian, Qixing Li, Wanlu Feng, Dongshuang Fan, and Lingjun Li. "Biocompatible Ionic Liquid Promote One-Pot Synthesis of 2-Amino-4H-Chromenes Under Ambient Conditions." Catalysis Letters 151 (2021): 720-733.

- [17] Saikia M, Saikia L (2016) RSC Adv 6:15846–15853
- [18] Kargar Behbahani F, Ghorbani M, Sadeghpour M, Mirzaei M (2013) Lett Org Chem 10:191–194
- [19] Eshghi H, Damavandi S, Zohuri GH (2011) Synth React Inorg Mater 41:1067–1073
- [20] Khurana JM, Nand B, Saluja P (2010) Tetrahedron 66:5637–5641
- [21] Maleki B, Baghayeri M, Sheikh S, Babae S, Farhadi S (2017) Russ J Gen Chem 87:1064–1072
- [22] Kidwai, Mazaahir, Shilpi Saxena, M. Khalilur Rahman Khan, and Sharanjit S. Thukral. "Aqua mediated synthesis of substituted 2-amino-4H-chromenes and in vitro study as antibacterial agents." *Bioorganic & Medicinal Chemistry Letters* 15, no. 19 (2005): 4295-4298.
- [23] Kumar D, Reddy VB, Mishra BG, Rana RK, Nadagouda MN, Varma RS (2007) Tetrahedron 63:3093–3097
- [24] Safari J, Zarnegar Z, Heydarian M (2012) Bull Chem Soc Jpn 85:1332–1338
- [25] Aghajani M, Monadi N (2019) J Chin Chem Soc 66:775–784
- [26] Behraves S, Fareghi-Alamdari R, Badri R (2017) Polycycl Aro mat Comp 38:51–65
- [27] Khan. A. J, Baseer. M.A. Lanthanum Nitrate- Catalyzed Synthesis of New 2, 3-dihydro-1, 5 Benzothiazepines. *Oriental Journal of Chemistry*; 2011; 27(4): 1759- 1762. a) V K Gumaste, Asgar J khan M Bhawal & A R A S Deshmukh. "Microwave assisted phase transfer catalysis: an efficient solvent free method for..." *Indian Journal of Chemistry* Feb-2004, Vol.43B, PP- 420-422.b) Mohammad A Baseer and Asgar Jafar Khan, "ZOC-Catalyzed an efficient synthesis of 1, 5-Benzodiazepines under mild conditions" *Der Chemica Sinica*, 2011, 2(2), P- 84 - 87, ISSN: 0976-8505. c) Mohammad A Baseer and Asgar Jafar Khan, "An Efficient One-Pot Synthesis of 1, 5-Benzodiazepine derivatives Catalyzed by TBAB under Mild Conditions" *E-Journal of Chemistry* 2012, 9(1), P- 407-414, ISSN: 0973-4945.

# Ultrasound Synthesis and Spectral Study of Transition Metal Complexes

D.D.Suryawanshi<sup>1</sup>, A. D. Suryawanshi<sup>2</sup>, V. S. Suryawanshi<sup>1</sup>

<sup>1</sup>Department of Chemistry, S. C. S. College, Omerga, Dharashiv, Maharashtra, India

<sup>2</sup>Department of Physics, Hon. B. J. College, Ale, Pune, Maharashtra, India

Email: [ddschem84@gmail.com](mailto:ddschem84@gmail.com)

## ABSTRACT

The ligand 1-(5-Chloro-2-Hydroxyphenyl)-3-(2,4-Dichlorophenyl) Propane-1,3-Dione and its metal complexes have been synthesized by ultrasound irradiation method. The diketone is offered by employing Baker-Venkatraman rearrangement. The synthesized compounds were confirmed by the spectroscopic analysis such as UV, IR, <sup>1</sup>H-NMR, <sup>13</sup>C-NMR, mass, elemental analysis, magnetic susceptibility, XRD and thermal study.

**Keywords:** Baker-Venkatraman re-arrangement, metal complexes, XRD study, thermal study, ultrasound irradiation.

## INTRODUCTION

Design and synthesis of new ligands and complexes with special structures and properties are attracting more and more interest in recent years. Transition metals exhibit different oxidation states and can interact with a number of negatively charged molecules. This benefit of transition metals has started the development of metal-based drugs with promising pharmacological application and may offer unique therapeutic opportunities.  $\beta$ -diketonate complexes are known for their wide applications as laser chelates[1], extraction agents[2], chemical and photochemical catalysts. Metal-1,3-diketones have found applications in the production of laser devices [3], as NMR shift reagents [4] and in analytical chemistry [5]. The Chemistry of 1,3-diketones has attracted the attention of scientists for almost century. Due to the presence of two oxygen donor atoms and facile keto-enol tautomerism[6], they easily coordinate with metal ions after deprotonating the enolic hydrogen atom and provides stable metal complexes

Ultrasound irradiation assisted organic synthesis is an efficient and eco-friendly synthetic strategy. The reaction conducted by sonication provides improved yields and increased selectivities.



**EXPERIMENTAL SECTION:****Synthesis of ester (A):**

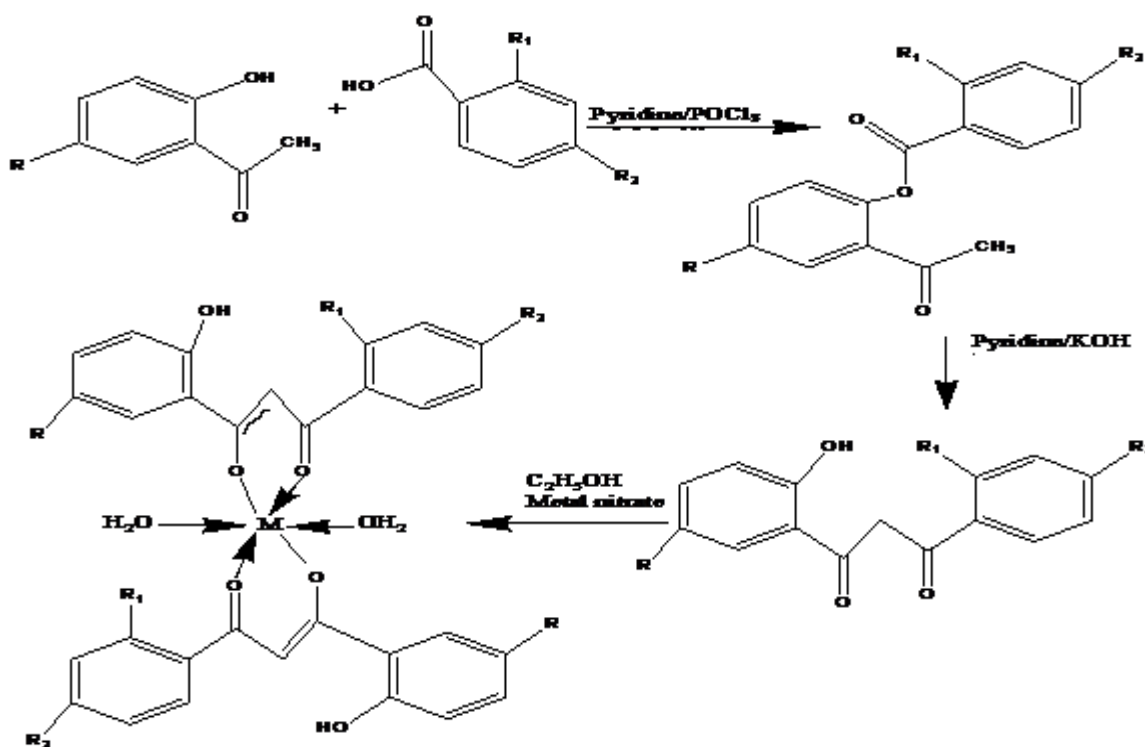
To the mixture of 5-chloro-2-hydroxyacetophenone and 2,4-dichlorobenzoic acid, a dry pyridine and POCl<sub>3</sub> were added dropwise with constant stirring at 0° C. Then the reaction mixture was stirred for about 4-5 hours. After completion of the reaction, the reaction mixture was poured into 100ml 1M HCl containing 50 gm of crushed ice and solid obtained was filtered and washed with 10 ml of water. It was recrystallized from ethanol, filtered and dried. Yield: 80%.

**Synthesis of 1,3-dione (B):**

Compound (A) was dissolved in dry pyridine. To this powdered KOH was added and the reaction mixture was stirred for about 2-3hours. After completion of the reaction, the reaction mixture was poured on ice cold water and acidified with conc. HCl. The yellow solid was filtered off and crystallized from absolute ethanol to obtain pure product. Yield: 80%.

**Synthesis of transition metal complex:**

The mixture of compound B and metal nitrate in ethanol were added and refluxed for about 1-2 hrs. The solid which precipitated was washed with boiling ethanol and recrystallized from ethyl acetate to give crystals of corresponding diketonate complex. Yield:80- 85%.



**L<sub>g</sub> = R=Cl, R<sub>1</sub>=Cl, R<sub>2</sub>=Cl**

**M = Cu, Ni, Co, Cr, Fe. In all these cases water of coordination is present.**

**Scheme I. Synthesis of ligand and metal complexes.**

## RESULTS AND DISCUSSION:

The ester 2-acetyl-4-chlorophenyl 2,4-dichloro benzoate was prepared by the esterification of 5-chloro, 2-hydroxyacetophenone with 2,4-dichlorobenzoic acid in the presence of POCl<sub>3</sub>. 2-acetyl-4-chlorophenyl 2,4-dichlorobenzoate undergoes Baker-Venkatraman transformation to offered pale yellow needle of ligand (B). The structure was further confirmed by spectral analysis.

**Table I: Molar conductivity, magnetic and Infrared spectral data of synthesized compounds.**

Compound	$\mu_{\text{eff}}$ (BM)	Molar Conductance	IR (cm <sup>-1</sup> )				
			$\nu(\text{C}=\text{O})$	$\nu(\text{C}-\text{O})$	$\nu(-\text{OH})$	$\nu(\text{M}-\text{O})$	$\nu(\text{OH})$ Coordinated H <sub>2</sub> O Molecule
Ligand			1680	1480	3001	--	---
Cu(II) Complex	2.12	29.40	1657	1501	3016	527	3255
Ni(II) Complex	2.73	54.22	1655	1505	3017	505	3258
Co(II) Complex	4.45	35.45	1666	1522	3020	505	3248
Cr(III) Complex	3.82	37.23	1663	1518	3018	520	3244
Fe(III) Complex	6.11	61.65	1656	1523	3015	512	3260

Spectral data: 3001.96 (OH), 1680.26 (C=O), 1480.18 (Ar C=C). <sup>1</sup>H-NMR (300 MHz, CDCl<sub>3</sub>-d<sub>6</sub>);  $\delta$ =6.8(s, 1H, =CH-), 7.1 (s, 1H, Ar-H), 7.4-7.7 (m, 5H, Ar-H), 11.9 (s, 1H, OH), 15.1 (s, 1H, Enolic-OH), <sup>13</sup>C-NMR (300MHz, CDCl<sub>3</sub>);  $\delta$ =187.3 (s, C-1, C=O), 94.1 (s, C-2, -CH=), 185.6 (d, C-3), 115.2 (s, C-1'), 160.4 (s, C-2'), 119.2 (d, C-3'), 129.5 (d, C-4'), 125.5 (s, C-5'), 128.3 (d, C-6'), 135.2 (s, C-1''), 136.5 (d, C-2''), 131.5 (d, C-3''), 141.3 (s, C-4''), 127.2 (s, C-5''), 132.6 (s, C-6''). UV/Vis (DMSO)nm: 370,415. EC-MS: 344.91 (M+1).

The C=O bond in complexes is shifted to lower frequency as compared to that of free ligand which indicates the coordination of metal atom with the carbonyl group of diketone[7]. All the complexes are insoluble in water but soluble in DMSO and DMF. The complexes are non-electrolytic in nature[8].

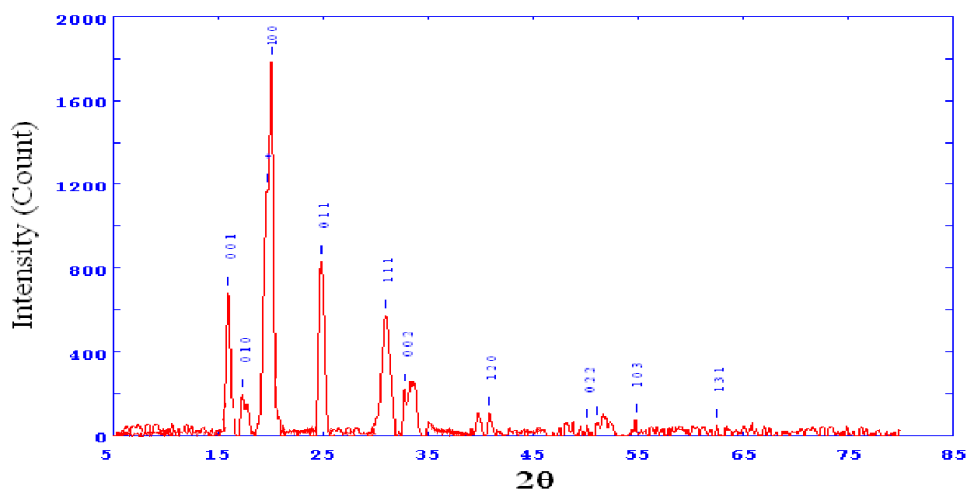
### Powder X-ray diffraction analysis:

The X-ray diffraction pattern of these complexes with respect to major peaks of relative intensity greater than 10% were indexed using a computer programme[9]. This indexing method also yields Miller indices (hkl), the unit cell parameters and the unit cell volume. The Ni(II) complex of ligand was selected for x-ray powder diffraction. The diffractogram of Ni complex has 10 reflections between 100-650. Comparison of experimental and theoretical density values shows good agreement within the limits of experimental error[10].

**Table II: Unit cell data and crystal lattice parameter of complex Ni-complex**

parameter	Data	Parameter	Data
a(Å)	4.9168	Volume (A°)	130.75

b(Å)	4.9168	Density (obs.)	4.91680
c(Å)	5.4089	Density (calc.)	4.91333
$\alpha$ (degree)	90	Z	11
$\beta$ (degree)	90	Space group	P21/n
$\gamma$ (degree)	90	Crystal system	Orthorombic



X-ray diffractogram of Nickel(II) complex

#### Thermal study of Ni (II) complex:

The thermogram of the Ni(II) complex showed a mass loss of 7.17% (cal. 8.10) in the temperature range 150-1850C and endothermic DTA peak in the region 1830C indicating the loss of two coordinated water molecule. The anhydrous complex first showed decomposition from 3700C to 4500C with a 21.15% (cal. 22.85) mass loss and a broad exothermic peak with 3550C in the DTA which may be attributed to the removal of the non-coordinated part of the ligand. The second step of the decomposition from 475-8650C with a mass loss of 55.05% (cal. 55.95) correspond to the decomposition of the coordinated part of the ligand[11]. A broad endothermic peak in the DTA was observed for this step. The mass of the final residue NiO, 18.25%(cal. 18.65) which is in agreement with earlier workers.

#### CONCLUSION:

In the present work Ligand and its transition metal complexes were synthesized and their structures elucidated on the basis of spectral analysis. <sup>1</sup>H-NMR and <sup>13</sup>C-NMR spectra revealed that the prepared diketone possesses characteristic peaks of particular proton.

#### REFERENCES

- [1] J. Chul Byun, C. Hung Han, Bull. Korean Chem. Soc, 26, (2005), 9, 1395.
- [2] C. Brecher, A. Lempicki, H. Sameison, J. Chem. Phys, 42, (1969), 1081.
- [3] H. Samelson, A. Lempicki, J. Chem Phys, 39, (1963).

- [4] C. C. Hinckley, J. Am. Chem. Soc, 14, (1969), 91.
- [5] R. A. James, W. P. Bryan, J. Am. Chem. Soc, 76, (1954).
- [6] T. Dziemboska, Z. Rozwadowski, Curr. Org. Chem, 5, (2001), 289.
- [7] A. V. Chate, R. S. Joshi, V. Badadhe and C. H. Gill, Bull. Korean Chem. Soc, 2011, vol.32, no. 11, 3887.
- [8] J. Sestak, V. Satava, W. W. Wendland, Therm. Chem. Acta, 7, (1973), 333.
- [9] J. T. Makodi, A. S. Aswar, J. Indian Chem Soc, 80 (1), 2003, 44.
- [10] M. B. Deshmukh, S. Dhongade-Desai, S. S Chavan, Indian J. Chem. 44 (2005), 1659.
- [11] Vogel, text book of qualitative inorg analysis, 3rd edn, Longmans: London, 1975

# Application of Computer Technology in Material Science and Data Processing

Dr. U. V. Thete

Yogeshwari Mahavidyalaya, Ambajogai, Maharashtra, India

## ABSTRACT

Computer technology is an actual system model, which is largely unaffected by experimental conditions, time and space constraints, and is of great flexibility. Nowadays, computer technology has thoroughly penetrated in the various areas of material processing and research, which becomes one of the important frontiers in the field of material manufacturing industry. At the same time, material science and technology are also developing rapidly and constantly giving birth to the new industrial field, such as nanotechnology, optoelectronic, magnetic electronic technologies, which are inseparable of computer technology. Hence, in this article, the application of computer technology in advanced material science and processing, which includes material science database, computational material science, computer-aided design or processing etc are reviewed.

Since its launch in 2011, Materials Genome Initiative (MGI) has drawn the attention of researchers from across academia, government, and industry worldwide. As one of the three tools of MGI, the materials data, for the first time, emerged as an extremely significant approach in materials discovery. Data science has been applied in different disciplines as an interdisciplinary field to extract knowledge from the data. The concept of materials data science was utilized to demonstrate the data application in materials science. To explore its potential as an active research branch in the big data age, a three-tier system was put forward to define the infrastructure of data classification, curation and knowledge extraction of materials data.

**Keywords:** Computer Technology, Material Processing, Material Science, materials data science, data classification, life-cycle curation.

## INTRODUCTION

As a practice of obtaining information and insight from data, data science has become a very familiar term to researchers from various disciplines, [1]. This concept was first introduced in the 1960s and it lasted for a few decades. Statistician, CF Jeff Wu, used the term again as a discipline as extension of statistics in 1996. Nowadays, massive scientific data are produced by simulations, high-throughput scientific instruments, satellites, telescopes, and so on. The availability of big data is revolutionizing how research is conducted and leads to the emergence of a new paradigm of science based on data-intensive computing and analytics. Data science is defined as the fourth paradigm for the data intensive scientific discovery, besides

experimentation, theory and calculation [5]. Furthermore, the release of the Big Data R & D Initiative in 2012 accelerates the development of the data science.

With the continuously deepening research of material science, material science occupies an important position in the national economy; however, material science is still an immature interdisciplinary, which mainly depends on the facts and the experience of the current study. The systematic studies need a very long process[2]. Computer as a modern tool plays an increasingly significant role in various areas of the world, which has penetrated into many fields. With respect to the material science and engineering, the computer is also becoming a very important tool and becomes one of the reasons for the accumulation of the rapid development of material science. For example, computer technology has been widely used in the variety field of material forming technology, including application in liquid forming, plastic forming, polymer material forming, powder forming et al, which can basically provide a qualitative description toward to quantitative prediction for material processing.

In 1999, John R. Rodgers introduced a new concept as materials informatics and defined it as an effective data management for new materials discovery. Somewhat later, ICME (2008) and materials Genome Initiative (MGI, 2011) attracted more attention worldwide on integrating computational capabilities, data management, and experimental techniques together [7]. Although materials databases were built in many countries with universal access to abundant scientific data, and some have become the fundamental to material computation, materials data and materials informatics [8] witnessed their first recognition when compared with computation and experimentation in materials innovation. A concept of materials data infrastructure was put forward based on the integration of Integrated Computational Materials Engineering (ICME) and materials informatics [8]. However, the diversity of materials science has yet to be exhibited. Therefore, a system which enables one to virtually express real-world materials details, as well as, data mining needs to be built.

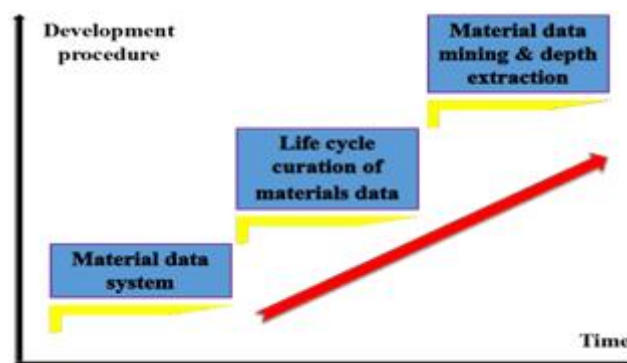


**Fig. 1** Infrastructure of Material Data Science

## COMPUTATIONAL MATERIAL SCIENCE:

Computational material science (CMS) is a typical interdisciplinary of material science and computer science, which is the material scientific research about the “computer design” and “computer experiment” in material composition, structure, performance, service performance[7]. According to the literatures[8], CMS could be mainly included into two aspects: one is calculation and simulation, which is starting from the experimental data, through the establishment of mathematical models and numerical calculations to

simulate the actual process; the other is the computer added material design, which is directly through the theoretical model to calculate, predict or design the new structure and properties of material. Therefore, CMS is a bridge to connect theory and experimental material.

## COMPUTER TECHNOLOGY IN MATERIAL SCIENCE DATABASES:

A reasonable choice of material, accurate design and scientific processing are directly impacting on product cost and quality, which even affect the social development and progress. In recent years, with computer technology development, particularly in the development of database technology, material science databases in scientific research has become increasingly emphasized and get more and more widely used. A sample material database was illustrated in Figure 2.

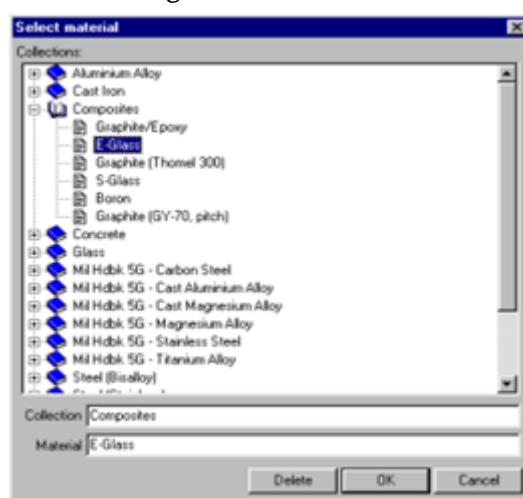


Figure 2 A sample of material database

## STORAGE OF MATERIALS DATA :

Database, an organized collection of data, has been the typical way to define, store, update and administer data whereby the data are accessible to query and retrieval. ICSD (Inorganic crystal structure database), Paulling file, databases for thermodynamic computation and so on are those specifically used and associated with the software of first principle calculation, thermodynamics and simulation for property. Others are mostly about the properties obtained from past research and industrial activities. Database is well developed for curation of raw materials data, while data warehouse appeared in recent a few years for data mining to store specific-topic and integrated data from one or more disparate sources. Besides the database and data warehouse, cloud storage provides a brand-new choice. Currently, cloud computing has been applied to provide Paas and Iaas service with both hardware and software equipped in some supercomputing centers and companies. The cloud computing platform will definitely be utilized by more material data researches once the privacy and intellectual property issues in materials communities are settled. Therefore, database, data warehouse and cloud storage are three alternative candidates for materials researchers to optimize data storage for their own data resource.

## CONCLUSION:

In summary, material science is a cross-emerging for the development of immature discipline. At present, its research is largely depended on the facts and the experience. The systematic studies need a very long process. The computer is becoming an extremely important tool, which is one of the important reasons for rapid development of material science. The use of computers for design of new material has gradually. Materials data are playing a vital role in materials research. Industrial applications of material data will be a positive stimulus for the systematically establishment and implementation of materials data science on research as well as education. Smart manufacturing aims to take advantage of advanced information and manufacturing technologies to enable flexibility in physical processes, therefore Industria 4.0 enables one to apply the data in the whole work flow and the opportunity to push materials data science forward into a knowledge engineering system to realize the artificial intelligence (AI) in the materials innovation and production.

## REFERENCES

- [1] Flaszka, W.G., Paro, J.A., Kivivuori S.O.J.: Computer-aided forging design using model material simulation. *J. Mater.Process.Technol.*24,403--409(1990).
- [2] Joshi, K., Lauer, T. W.: Impact of information technology on users' work environment: A case of computer aided design (CAD) system implementation. *Inf. Manage.*34, 349--360(1998).
- [3] Janssens D, Giannotti F, Nanni M, Pedreschi D, Rinzivillo S. Data Science for Simulating the Era of Electric Vehicles. *KünstlIntell*, 2012, 26:275-278.
- [4] Cao L B. Data science and analytics: a new era, *Int J Data Sci Anal*, 2016,1:1-2. [6] Bertino E. Introduction to Data Science and Engineering, *Data Sci. Eng.*,2016, 1(1):1-3.
- [5] Hill J, Mulholland G, Persson K, Seshadri R. Materials science with large-scale data and informatics: Unlocking new opportunities, *MRS bulletin*, 2016, 41(5): 399- 409.
- [6] Rajan K. Informatics for materials science and engineering, Elsevier, US, 2013: 9, 21-23. [20] Kalidindi S R. Hierarchical materials informatics: novel analytics for materials data, Elsevier Inc., 2015.
- [7] Nosengo N. The material Code- Machine Learning techniques could revolutionize how materials science is done. *Nature*, 2016,533: 22-26.
- [8] Jain A, Persson K, Ceder G. The materials genome initiative: Data sharing and the impact of collaborative ab initio databases, *APL MATERIALS*, 2016, 4(5), 053102 (2016), Chinese Physics B <http://scitation.aip.org/content/aip/journal/aplmater/4/5/10.1063/1.4944683>.



# Room Temperature Alkalis Gas Detection Using NiFe<sub>2</sub>O<sub>4</sub>/rGO Nanocomposites as Electrodes

P. R. Birmule<sup>1</sup>, V.D. Bhirde<sup>2</sup>, R.K. Patil<sup>2</sup>, R.B. Patil<sup>2</sup>, V.B. Helavi-Reddy<sup>1\*</sup>

<sup>1</sup> Government Vidarbha Institute of Science and Humanities Amravati (Autonomous), 444604, Maharashtra, India

<sup>2</sup> Dr. Bapuji Salunkhe Institutes of Engineering and Technology, Kolhapur, 416001, Maharashtra, India

\* Corresponding Author Email: [vbhelavi@gmail.com](mailto:vbhelavi@gmail.com)

## ABSTRACT

This study reports the successful synthesis of pure NiFe<sub>2</sub>O<sub>4</sub> and NiFe<sub>2</sub>O<sub>4</sub>/rGO nanocomposites using co-precipitation and wet impregnation methods. The structural integrity of the synthesized materials was confirmed by XRD and FTIR analysis. FESEM images revealed the well-dispersed NiFe<sub>2</sub>O<sub>4</sub> particles on exfoliated rGO sheets. Notably, the NiFe<sub>2</sub>O<sub>4</sub>/rGO gas sensor exhibited significantly enhanced sensitivity, faster response, and recovery times compared to pure NiFe<sub>2</sub>O<sub>4</sub> towards NH<sub>3</sub> gas at room temperature. These findings suggest that the NiFe<sub>2</sub>O<sub>4</sub>/rGO nanocomposites hold great potential for practical applications in NH<sub>3</sub> gas detection.

**Keywords:** NiFe<sub>2</sub>O<sub>4</sub>; rGO; Gas Sensor; NH<sub>3</sub> Detection

## INTRODUCTION

Chemicapacitive gas sensors, akin to other chemical sensors, undergo changes in capacitance in response to interactions between analyse molecules and the sensing material.[1,2] Metal oxide semiconductors, such as In<sub>2</sub>O<sub>3</sub>, WO<sub>3</sub>, ZnO and SnO<sub>2</sub> are widely recognized as effective gas sensing materials due to their high sensitivity, straightforward processing methods, compact size, and cost-effectiveness. However, these materials often face challenges in achieving adequate sensitivity at room temperature.[3] Recent studies have explored the potential of spinel ferrites (AB<sub>2</sub>O<sub>4</sub>) for gas sensing applications, where A and B represent metallic cations. Apart from their gas sensing capabilities, spinel ferrite metal oxides offer environmental friendliness and cost-effectiveness. Investigations into pyrolysis CoFe<sub>2</sub>O<sub>4</sub> revealed a 3.1% sensing response to 50 ppm ammonia, showcasing the material's potential for gas detection.[4] Similarly, Ru-NiFe<sub>2</sub>O<sub>4</sub> nanostructures demonstrated a sensing response of approximately 0.8 to hydrogen gas at 50 ppm concentration.

One prevalent approach to enhance the functional characteristics of materials involves incorporating a carbon matrix into the system. Reduced graphene oxide (rGO) supported NiFe<sub>2</sub>O<sub>4</sub> spinel ferrite represents an example of this strategy, leveraging the exceptional electron mobility of carbon matrices to improve the performance of microelectronic devices. In this study, Pure NiFe<sub>2</sub>O<sub>4</sub> and NiFe<sub>2</sub>O<sub>4</sub>/rGO samples were

created via wet impregnation and co-precipitation techniques respectively.[5] Gas sensing experiments revealed that the NiFe<sub>2</sub>O<sub>4</sub>/rGO nanocomposite exhibited outstanding stability, high responsiveness, and excellent sensing characteristics for ammonia gas, with a response of approximately 1.7 (Cg/Ca) to 100 ppm ammonia. The formation of a heterojunction between NiFe<sub>2</sub>O<sub>4</sub> nanoparticles and rGO Nano sheets contributed to the enhanced sensitivity of the NiFe<sub>2</sub>O<sub>4</sub>/rGO nanocomposite sensor, showcasing its potential for highly sensitive ammonia detection.[6]

In the realm of gas sensing applications, the study presented here introduces novel insights with the utilization of NiFe<sub>2</sub>O<sub>4</sub>/rGO nanocomposites. The choice of wet impregnation and co-precipitation techniques for synthesizing pure NiFe<sub>2</sub>O<sub>4</sub> and NiFe<sub>2</sub>O<sub>4</sub>/rGO samples demonstrates a strategic approach to harnessing the benefits of carbon matrices for improved gas sensing capabilities. The latest data from gas sensing experiments underscore the promising performance of the NiFe<sub>2</sub>O<sub>4</sub>/rGO nanocomposite, with a measured sensitivity of 1.7 (Cg/Ca) to 100 ppm ammonia. This enhanced sensitivity is due to the creation of a heterojunction between NiFe<sub>2</sub>O<sub>4</sub> nanoparticles and rGO Nano sheets, which allows for greater charge transfer leading to superior gas sensing capabilities.[7,8] Furthermore, the study aligns with the broader trend of exploring advanced materials for gas sensing applications, striving for heightened efficiency, stability, and responsiveness. The incorporation of rGO as a support material highlights the significance of carbon matrices in improving the overall performance of gas sensors, especially in terms of electron mobility and inter-particle charge transfer resistance reduction.[9,10] The findings from this study contribute to the ongoing efforts in advancing gas sensing technologies, showcasing the potential of NiFe<sub>2</sub>O<sub>4</sub>/rGO nanocomposites as efficient and sensitive sensors for ammonia gas detection.

## EXPERIMENTAL SECTION

### 2.1 Chemicals

The chemicals utilized in this study were procured from Merck and employed in their as-received state. The substances acquired include hydrogen peroxide (H<sub>2</sub>O<sub>2</sub>), sulfuric acid (H<sub>2</sub>SO<sub>4</sub>), potassium permanganate (KMnO<sub>4</sub>), sodium nitrate (NaNO<sub>3</sub>) and hydrochloric acid (HCl). Additionally, acetone (CH<sub>3</sub>COCH<sub>3</sub>), graphite, ferric chloride tetra hydrate (FeCl<sub>2</sub>.4H<sub>2</sub>O), nickel chloride hexahydrate (NiCl<sub>2</sub>.6H<sub>2</sub>O), and ferric chloride hexahydrate were part of the chemical inventory used in the research.

### 2.2 Preparation of reduced graphene oxide (rGO)

In the course of this study, the modified Hummers method was employed for the creation of graphene oxide (GO) from meticulously purified natural graphite. The synthesis process involved a meticulous sequence of steps to ensure the production of high-quality GO.[11,12] The procedure commenced with the mixing of 5 grams of graphite, 2.5 grams of NaNO<sub>3</sub>, and 115 millilitres of concentrated H<sub>2</sub>SO<sub>4</sub> in an ice bath, with constant stirring over a duration of four hours. Subsequently, a judicious application of 15 grams of KMnO<sub>4</sub> was gently introduced into the mixture and stirred for approximately 20 minutes. After an additional two hours of stirring after being removed from the ice bath, the suspension was heated in a water bath at 98°C for 15 minutes. This was followed by a gradual addition of 230 millilitres of distilled water dropwise. 400 millilitres of warm water were re-diluted and 20 millilitres of 30% H<sub>2</sub>O<sub>2</sub> were slowly

added, one drop at a time. The resulting mix was centrifuged at 4000 rpm, accompanied by rinsing with distilled water and a 10% HCl aqueous solution. Post-centrifugation, the material underwent drying at room temperature following a 3-hour dialysis filtration process aimed at achieving pH balance.

In the subsequent phase of the synthesis, a solution comprising 20 millilitres of ammonia was gradually introduced to the mixture.[13] This step was undertaken after fully dissolving 1 gram of the newly synthesized GO powder in 50 millilitres of deionized water, utilizing a bath sonicate over a two-hour period. The resulting mixture was then placed in a 100-milliliters Teflon-lined autoclave and heated in a hot air oven at 160°C for 12 hours. The autoclave was then allowed to naturally approach room temperature. The resulting black precipitate was fully cleaned with ethanol and deionized water before dried overnight in a hot air oven at 60°C. This systematic and intricate synthesis process aimed to ensure the production of high-quality graphene oxide, laying the foundation for subsequent experiments and analyses in the broader context of the study.

### 2.3 Preparation of NiFe<sub>2</sub>O<sub>4</sub>

In our recent exploration, we delved into the hydrothermal synthesis of NiFe<sub>2</sub>O<sub>4</sub> samples exhibiting a distinctive Nano rod morphology.[14] In the customary synthesis procedure, a meticulous blend of 30 mmol NiCl<sub>2</sub>.6H<sub>2</sub>O, 60 mmol FeCl<sub>2</sub>.6H<sub>2</sub>O (maintaining a Ni-to-Fe molar ratio of 1:2) and 30 mmol CTAB was prepared in 100 mL of deionized water (DI). The ensuing solution underwent an hour of stirring to attain homogeneity. To achieve complete homogenization, 90 mmol of solid urea was gradually introduced and stirred for an additional three hours. The final solution was then loaded into a 200 mL stainless steel autoclave with a Teflon ring, initiating a 48-hour reaction at 120°C in an electric oven. After the reaction, the autoclave was gradually cooled to ambient temperature, and the light pink precipitates were carefully collected by centrifugation at 4000 rpm. Thorough cleaning ensued with deionized water, a water and 100% ethanol solution, and three successive applications of pure ethanol.[15] The conclusive phase involved subjecting the obtained product to a 12-hour treatment at 60°C and a subsequent 3-hour crystallization at 350°C, culminating in the production of the final NiFe<sub>2</sub>O<sub>4</sub> samples.

### 2.4 Preparation of NiFe<sub>2</sub>O<sub>4</sub>/rGO

The synthesis process began by mixing nickel chloride hexahydrate (NiCl<sub>2</sub>.6H<sub>2</sub>O) and ferric chloride tetrahydrate (FeCl<sub>2</sub>.4H<sub>2</sub>O) in 75 ml of double-distilled water.[16,17] Subsequently, a solution was created with the aid of double-distilled water as the solvent. To achieve a pH value in the range of 11 to 12, sodium hydroxide (NaOH) solution was incrementally added to the mixture under continuous magnetic stirring. The resulting mixture underwent heating for an hour at 80°C. Following this, a thorough washing process was employed to eliminate any potential chloride and inorganic impurities from the precipitate. The precipitate was then dried in an oven set at 100°C. For homogeneity, the dried powder was thoroughly mixed with a mill and pestle. The powder was then annealed for three hours at 900°C. Additionally, the production of reduced graphene oxide (rGO) was carried out utilizing a wet impregnation method,[18–20] employing procedures akin to those detailed in further section. This step contributed to the generation of rGO for use in the subsequent phases of the study.

## 2.5 Gas-sensing device fabrication and measurements

The gas sensing measurements were performed using a two-probe system, an LCR meter (SM 6023), and a straightforward experimental setup, as illustrated in Figure 1. This experimental arrangement ensured uniformity across all gas sensing assessments.[21–23] The gas sensing measurements involved altering the concentration of  $\text{NH}_3$  from 10 to 100 ppm. The change in capacitance was precisely measured by passing the gas sensor between  $\text{NH}_3$ -laden air and ambient air. This systematic approach allowed for a thorough examination of the sensor's response to varying  $\text{NH}_3$  concentrations, contributing to a comprehensive understanding of its gas sensing capabilities.[24–26]



Fig.1: Experimental arrangement of  $\text{NiFe}_2\text{O}_4/\text{rGO}$  gas sensor

## RESULTS AND DISCUSSION

### 3.1 XRD analysis

An X-ray diffraction (XRD) analysis was employed to assess the structure, crystallinity, and phase purity of the materials under investigation. The XRD patterns of rGO, pure  $\text{NiFe}_2\text{O}_4$ , and  $\text{NiFe}_2\text{O}_4/\text{rGO}$  are visually presented in Figure 2 and 3. In the diffraction pattern of rGO sample shown in Figure 3 contains three distinct peaks at  $25.6^\circ$ ,  $44.55^\circ$ , and  $52.2^\circ$  corresponding to (002), (101) and (004) planes, respectively, which indicate the presence of exfoliated rGO. In addition, the peak broadness at  $25.6^\circ$ , indicates a fact that the exfoliation process has also produced appreciable amount of Nano fragments of rGO along with several oxygen containing functional groups. The pure  $\text{NiFe}_2\text{O}_4$  and  $\text{NiFe}_2\text{O}_4/\text{rGO}$  samples produced several diffraction peaks at around  $18.4^\circ$ ,  $30.2^\circ$ ,  $35.4^\circ$ ,  $42.9^\circ$ ,  $53.8^\circ$ ,  $56.9^\circ$ ,  $62.4^\circ$ , and  $74.6^\circ$ , which are indexed to (111), (220), (311), (400), (422), (511), (440) and (533) crystal planes, respectively, matching with the standard values of  $\text{NiFe}_2\text{O}_4$  (JCPDS No. 86-2267). In addition, the presence of few secondary impurity ( $\alpha\text{-Fe}_2\text{O}_3$ ) related peaks is also observed, (marked with diamond symbol), which could be due to slight decomposition of ferrites.[27] The (002) plane diffraction peak of rGO appeared weakly in the  $\text{NiFe}_2\text{O}_4/\text{rGO}$  composite sample, which indicates the dominance of  $\text{NiFe}_2\text{O}_4$  crystallites in the corresponding sample. The average crystallite size (D) of the ferrite samples has been determined using Scherrer equation. The calculated crystallite size for the  $\text{NiFe}_2\text{O}_4$  sample is 52 nm, whereas it increases to 96 nm for the  $\text{NiFe}_2\text{O}_4/\text{rGO}$  composite sample. This slight

augmentation in size, particularly at specific nucleation sites on the rGO surface, may account for the observed increase in average crystallite size following the addition of rGO.

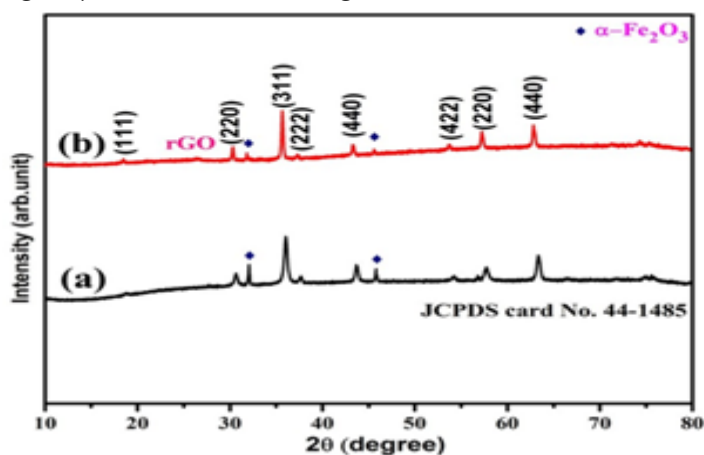


Fig.2:XRD patterns of (a)  $\text{NiFe}_2\text{O}_4$  and (b)  $\text{NiFe}_2\text{O}_4/\text{rGO}$  nanocomposite

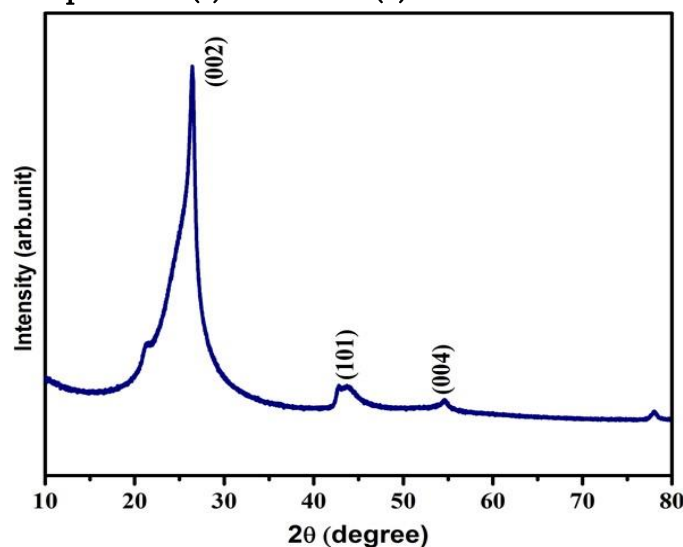


Fig.3:XRD pattern of rGO

### 3.2 FTIR analysis

The FTIR spectra of the rGO,  $\text{NiFe}_2\text{O}_4$ , and  $\text{NiFe}_2\text{O}_4/\text{rGO}$  samples are presented in Figure 4. In the FTIR spectrum of rGO (Figure 4(a)), the presence of four distinct peaks at various wavenumbers (C-OH stretching, C=C in the aromatic skeleton, C-H stretching, and O-H stretching) is observed, confirming the vibrational signatures associated with the rGO system. The FTIR spectra of  $\text{NiFe}_2\text{O}_4$  (Figure 4.(b)) display two distinctive vibrations at  $419\text{ cm}^{-1}$  and  $605\text{ cm}^{-1}$ , indicative of the formation of metal ferrites. In the FTIR spectrum of the  $\text{NiFe}_2\text{O}_4/\text{rGO}$  nanocomposite (Figure 4.(c)), sharp peaks corresponding to both metal ferrite and rGO further support the successful synthesis of the composite.

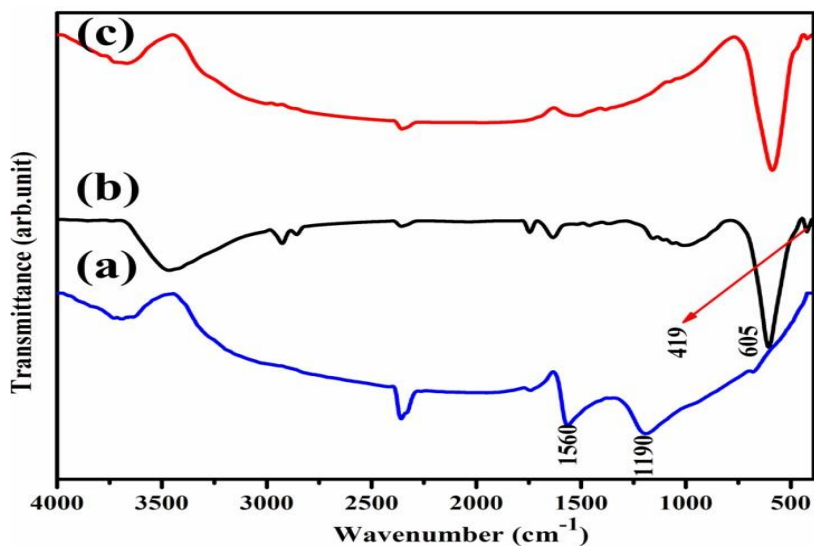


Fig.4: FTIR transmittance spectrum of (a) rGO, (b) NiFe<sub>2</sub>O<sub>4</sub> and(c) NiFe<sub>2</sub>O<sub>4</sub>/rGO nanocomposite

### 3.3 Morphological characterization

FESEM analysis of the surface morphologies of NiFe<sub>2</sub>O<sub>4</sub> and NiFe<sub>2</sub>O<sub>4</sub>/rGO spinel ferrite samples was carried out, and the results are shown in Figure 5. The pure NiFe<sub>2</sub>O<sub>4</sub> sample (Figure 5a) shows varying particle aggregation.[28–30] A closer examination reveals a first layer of regularly arranged particles followed by a limited number of irregularly agglomerated particles. Figure 5 (b) displays the evenly distributed NiFe<sub>2</sub>O<sub>4</sub> spinel ferrite Nano particulate arrangements. The FESEM micrographs of the NiFe<sub>2</sub>O<sub>4</sub>/rGO nanocomposite sample (Fig. 5(c,d)) show exfoliated thin layers of rGO and also islands of slightly agglomerated NiFe<sub>2</sub>O<sub>4</sub> particles on the surface. The intercalation of NiFe<sub>2</sub>O<sub>4</sub> was expected to enhance the gas-sensing capability of the rGO layers.[31,32] The EDX spectrum of the NiFe<sub>2</sub>O<sub>4</sub>/rGO nanocomposite sample in Figure 6 clearly shows traces of Ni, Fe, C, and O.

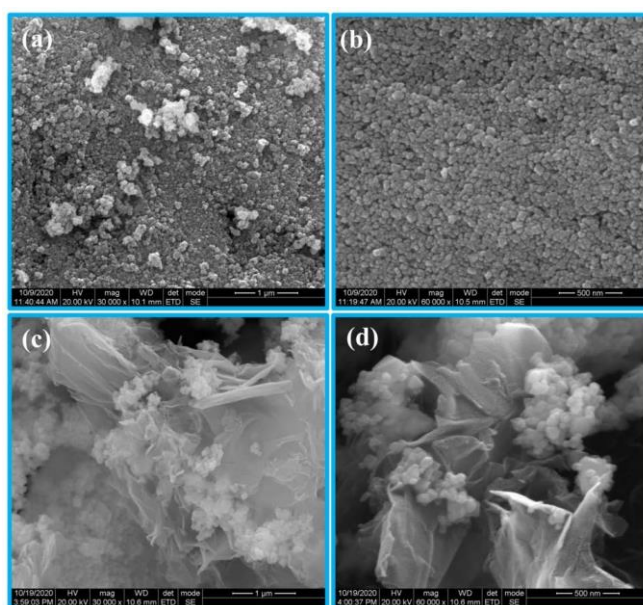


Fig.5: FESEM images of (a,b) NiFe<sub>2</sub>O<sub>4</sub> and (c, d) NiFe<sub>2</sub>O<sub>4</sub>/rGO nanocomposite.

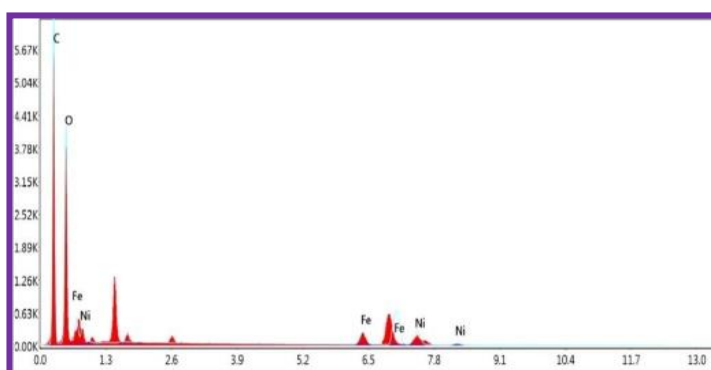


Fig.6:EDX spectrum of NiFe<sub>2</sub>O<sub>4</sub>/rGO nanocomposite

### 3.4 Gas sensing performance

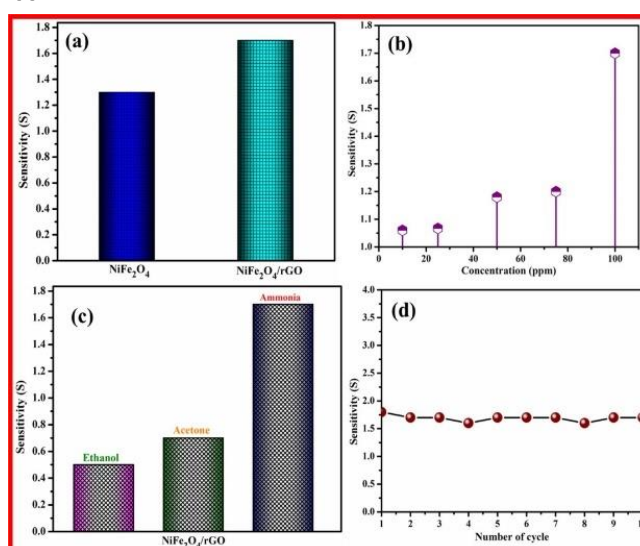
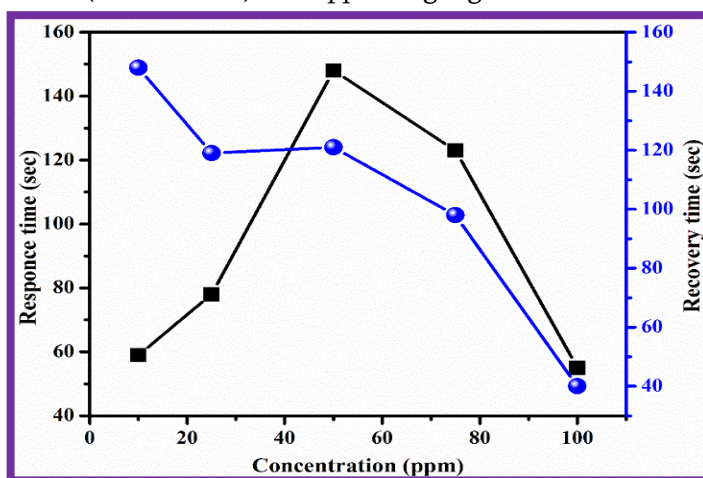


Fig.7:(a) Comparison of the sensing responses between NiFe<sub>2</sub>O<sub>4</sub> and NiFe<sub>2</sub>O<sub>4</sub>/rGO when exposed to 100 ppm NH<sub>3</sub> gas, (b) sensitivity of the NiFe<sub>2</sub>O<sub>4</sub>/rGO sensor across a spectrum of NH<sub>3</sub> concentrations, (c) selectivity of the NiFe<sub>2</sub>O<sub>4</sub>/rGO nanocomposite gas sensor, (d) stability over 10 measurement cycles.

Figure 4.7 illustrates the gas sensing responses, in terms of capacitance versus time, of NiFe<sub>2</sub>O<sub>4</sub> and NiFe<sub>2</sub>O<sub>4</sub>/rGO nanocomposite samples in reaction to a 100 ppm concentration of NH<sub>3</sub>[33–35](a). The calculated sensing responses for NiFe<sub>2</sub>O<sub>4</sub> and NiFe<sub>2</sub>O<sub>4</sub>/rGO nanocomposite samples were 1.3 and 1.7 respectively. The enhanced reactivity of the NiFe<sub>2</sub>O<sub>4</sub>/rGO nanocomposite is attributed to the incorporation of rGO. In Figure 4.7 (b), the gas sensing responses of the NiFe<sub>2</sub>O<sub>4</sub>/rGO nanocomposite sensor are depicted across a range of NH<sub>3</sub> concentrations, from 10 to 100 ppm,[36–39] at room temperature (R.T.).

In Fig. 7, we present a comprehensive analysis of the NiFe<sub>2</sub>O<sub>4</sub>/rGO nanocomposite gas sensor's performance. Subfigure (a) showcases a comparison of the sensing responses between NiFe<sub>2</sub>O<sub>4</sub> and NiFe<sub>2</sub>O<sub>4</sub>/rGO when exposed to 100 ppm NH<sub>3</sub> gas. Notably, the sensitivity of the NiFe<sub>2</sub>O<sub>4</sub>/rGO sensor starts at a relatively low level, particularly up to 20 ppm, but exhibits an upward trend with increasing gas concentration.[40–43] At 100 ppm, the sensor achieves a maximum sensitivity of 1.7. Moving on to subfigure (b), we delve into the sensing response of the NiFe<sub>2</sub>O<sub>4</sub>/rGO sensor across a spectrum of NH<sub>3</sub>

concentrations, providing valuable insights into its dynamic behaviour. Subfigure (c) delves into the selectivity of the NiFe<sub>2</sub>O<sub>4</sub>/rGO nanocomposite gas sensor. To assess this, we introduced 100 ppm each of three different gases ethanol, acetone, and ammonia—into the system. The bar diagram in Figure 7(c) underscores the exceptional specificity and selectivity of the NiFe<sub>2</sub>O<sub>4</sub>/rGO sensor for ammonia gas. Ensuring the practical viability of the sensor, subfigure (d) explores its stability over 10 measurement cycles. Impressively, the NiFe<sub>2</sub>O<sub>4</sub>/rGO nanocomposite gas sensor maintains consistent characteristics emphasizing its reliability for real-world applications.[44,45] For an ideal gas sensor, the response and recovery time must be shorter. Figure 8 shows the response/recovery time comparison of NiFe<sub>2</sub>O<sub>4</sub>/rGO gas sensor for different concentrations of NH<sub>3</sub> gas, from 10 to 100 ppm, and the sensor displayed lowest response/recovery time of (55sec/40 sec) at 100 ppm target gas concentration.



**Fig.8: Response and recovery time of NiFe<sub>2</sub>O<sub>4</sub>/rGO gas sensor sample for different concentrations of NH<sub>3</sub>**

### 3.5 Sensing mechanism

Based on the observed findings, a plausible sensing mechanism for the NiFe<sub>2</sub>O<sub>4</sub>/rGO gas sensor has been proposed and is illustratively depicted in Figure 9. Upon exposure to NH<sub>3</sub>, the sensor's capacitance undergoes a sequence of changes.[46,47] Initially, a capacitance of 1.6 pF is attributed to the presence of surface-adsorbed oxygen molecules from the air atmosphere. These molecules collect electrons from the sensor surface, forming oxygen ions. However, in the presence of a reducing gas, such as NH<sub>3</sub>, oxygen ions interact with NH<sub>3</sub> molecules, allowing stored electrons to return to the sensor surface. This interaction results in an increased capacitance, measured at 2.71 pF in the external capacitance analysis.[48] The sensitivity value is then calculated as the ratio between these two capacitance values. This proposed mechanism provides a conceptual understanding of how the NiFe<sub>2</sub>O<sub>4</sub>/rGO gas sensor responds to NH<sub>3</sub>, shedding light on the underlying processes that contribute to its sensitivity.



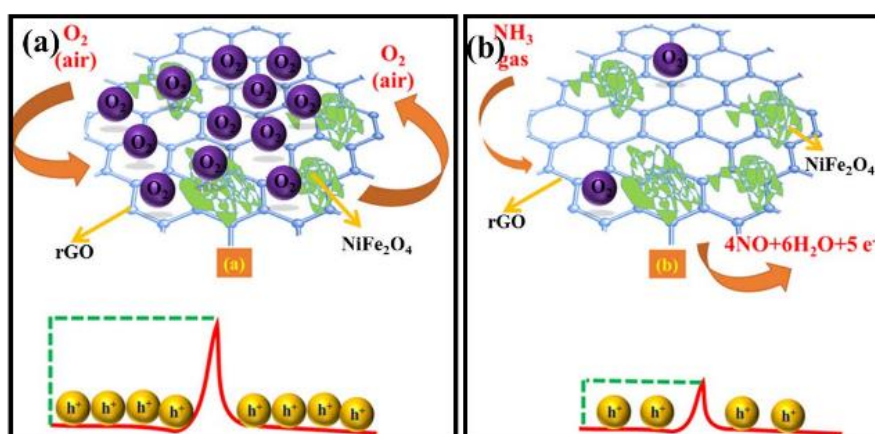


Fig.9: Schematic diagram of the proposed gas sensing mechanism in the presence of (a) air and (b) ammonia

## CONCLUSION

In conclusion, the fabrication of pure  $\text{NiFe}_2\text{O}_4$  and  $\text{NiFe}_2\text{O}_4/\text{rGO}$  nanocomposites using co-precipitation and wet impregnation techniques has been successfully executed. The XRD analysis confirmed the formation of low secondary impurity crystalline  $\text{NiFe}_2\text{O}_4$  and  $\text{NiFe}_2\text{O}_4/\text{rGO}$  nanocomposites, underscoring their structural integrity. The FTIR study revealed a well-defined mixture of  $\text{NiFe}_2\text{O}_4$  and rGO. The FESEM analysis provided insight into the surface morphology, illustrating well-exfoliated rGO sheets adorned with distributed  $\text{NiFe}_2\text{O}_4$  particles. Crucially, the  $\text{NiFe}_2\text{O}_4/\text{rGO}$  gas sensor exhibited a remarkable sensitivity of 1.7 when exposed to 100 ppm of  $\text{NH}_3$  at room temperature, outperforming the  $\text{NiFe}_2\text{O}_4$  sensor.[49] Additionally, the  $\text{NiFe}_2\text{O}_4/\text{rGO}$  sensor demonstrated faster reaction and recovery times. This superior performance in  $\text{NH}_3$  gas detection positions the  $\text{NiFe}_2\text{O}_4/\text{rGO}$  gas sensor as a promising candidate for various practical applications where accurate and rapid  $\text{NH}_3$  detection is essential.[50]

## REFERENCES

- [1] K.R. Nemade, S.A. Waghuley, Chemiresistive gas sensing by few-layered graphene, J. Electron. Mater. 42 (2013) 2857–2866. <https://doi.org/10.1007/s11664-013-2699-4>.
- [2] D. Kumar, A. Moharana, A. Kumar, Current trends in spinel based modified polymer composite materials for electromagnetic shielding, Mater. Today Chem. 17 (2020) 100346. <https://doi.org/10.1016/j.mtchem.2020.100346>.
- [3] A.K. Singh, J. Prasad, A. Kumar, A. Srivastava, U.P. Tyagi, B. Prajapati, K. Singh, One-step facile synthesis of  $\text{MoS}_2$  - reduced graphene oxide/ $\text{ZnO}$  nanostructure for high-performance microwave absorption, Mater. Sci. Eng. B 293 (2023) 116450. <https://doi.org/10.1016/j.mseb.2023.116450>.
- [4] S. Das, S. Mojumder, D. Saha, M. Pal, Influence of major parameters on the sensing mechanism of semiconductor metal oxide based chemiresistive gas sensors: A review focused on personalized healthcare, Sensors Actuators B Chem. 352 (2022) 131066. <https://doi.org/10.1016/j.snb.2021.131066>.

- [5] M. Ganesan, B. Ganapathi, B. Parasuraman, P. Thangavelu, Sensitivity enhancement of ammonia gas sensor based on NiFe<sub>2</sub>O<sub>4</sub>/rGO nanocomposite, *Chem. Phys. Impact* 8 (2024) 100616. <https://doi.org/10.1016/j.chphi.2024.100616>.
- [6] C.T. Lee, Y.S. Wang, High-performance room temperature NH<sub>3</sub> gas sensors based on polyaniline-reduced graphene oxide nanocomposite sensitive membrane, *J. Alloys Compd.* 789 (2019) 693–696. <https://doi.org/10.1016/j.jallcom.2019.03.124>.
- [7] E. Lee, D.-J. Kim, Review— Recent Exploration of Two-Dimensional MXenes for Gas Sensing: From a Theoretical to an Experimental View, *J. Electrochem. Soc.* 167 (2020) 037515. <https://doi.org/10.1149/2.0152003jes>.
- [8] W. Guan, N. Tang, K. He, X. Hu, M. Li, K. Li, Gas-Sensing Performances of Metal Oxide Nanostructures for Detecting Dissolved Gases: A Mini Review, *Front. Chem.* 8 (2020) 1–5. <https://doi.org/10.3389/fchem.2020.00076>.
- [9] N. Askari, N. Salarizadeh, M.B. Askari, Electrochemical determination of rutin by using NiFe<sub>2</sub>O<sub>4</sub> nanoparticles-loaded reduced graphene oxide, *J. Mater. Sci. Mater. Electron.* 32 (2021) 9765–9775. <https://doi.org/10.1007/s10854-021-05636-9>.
- [10] N.K. Chowdhury, B. Bhowmik, Micro/nanostructured gas sensors: The physics behind the nanostructure growth, sensing and selectivity mechanisms, *Nanoscale Adv.* 3 (2021) 73–93. <https://doi.org/10.1039/d0na00552e>.
- [11] C. V. Gopal Reddy, S. V. Manorama, V.J. Rao, Preparation and characterization of ferrites as gas sensor materials, *J. Mater. Sci. Lett.* 19 (2000) 774–778.
- [12] Y. Du, W. Wang, X. Li, J. Zhao, J. Ma, Y. Liu, G. Lu, Preparation of NiO nanoparticles in microemulsion and its gas sensing performance, *Mater. Lett.* 68 (2012) 168–170. <https://doi.org/10.1016/j.matlet.2011.10.039>.
- [13] X. Huang, N. Hu, R. Gao, Y. Yu, Y. Wang, Z. Yang, E. Siu-Wai Kong, H. Wei, Y. Zhang, Reduced graphene oxide-polyaniline hybrid: Preparation, characterization and its applications for ammonia gas sensing, *J. Mater. Chem.* 22 (2012) 22488–22495. <https://doi.org/10.1039/c2jm34340a>.
- [14] S. Agarwal, P. Rai, E.N. Gatell, E. Llobet, F. Güell, M. Kumar, K. Awasthi, Gas sensing properties of ZnO nanostructures (flowers/rods) synthesized by hydrothermal method, *Sensors Actuators, B Chem.* 292 (2019) 24–31. <https://doi.org/10.1016/j.snb.2019.04.083>.
- [15] A.M. Andringa, M.J. Spijkman, E.C.P. Smits, S.G.J. Mathijssen, P.A. van Halbeek, S. Setayesh, N.P. Willard, O. V. Borshchev, S.A. Ponomarenko, P.W.M. Blom, D.M. de Leeuw, Gas sensing with self-assembled monolayer field-effect transistors, *Org. Electron.* 11 (2010) 895–898. <https://doi.org/10.1016/j.orgel.2010.02.007>.
- [16] X. Wang, W. Liu, J. Liu, F. Wang, J. Kong, S. Qiu, C. He, L. Luan, Synthesis of nestlike ZnO hierarchically porous structures and analysis of their gas sensing properties, *ACS Appl. Mater. Interfaces* 4 (2012) 817–825. <https://doi.org/10.1021/am201476b>.
- [17] J. Zhang, X. Liu, L. Wang, T. Yang, X. Guo, S. Wu, S. Wang, S. Zhang, Synthesis and gas sensing properties of  $\alpha$ -Fe<sub>2</sub>O<sub>3</sub>@ZnO core-shell nanospindles, *Nanotechnology* 22 (2011). <https://doi.org/10.1088/0957-4484/22/18/185501>.

- [18] Renu, Komal, R. Kaur, J. Kaur, Jyoti, V. Kumar, K.B. Tikoo, S. Rana, A. Kaushik, S. Singhal, Unfolding the electrocatalytic efficacy of highly conducting NiFe<sub>2</sub>O<sub>4</sub>-rGO nanocomposites on the road to rapid and sensitive detection of hazardous p-Nitrophenol, *J. Electroanal. Chem.* 887 (2021) 115161. <https://doi.org/10.1016/j.jelechem.2021.115161>.
- [19] X. Song, L. Gao, S. Mathur, Synthesis, characterization, and gas sensing properties of porous nickel oxide nanotubes, *J. Phys. Chem. C* 115 (2011) 21730–21735. <https://doi.org/10.1021/jp208093s>.
- [20] A. Bazgir, A. Khorshidi, H. Kamani, S.D. Ashrafi, D. Naghipour, Modeling of azo dyes adsorption on magnetic NiFe<sub>2</sub>O<sub>4</sub>/RGO nanocomposite using response surface methodology, *J. Environ. Heal. Sci. Eng.* 17 (2019) 931–947. <https://doi.org/10.1007/s40201-019-00409-3>.
- [21] F. Ricciardella, S. Vollebregt, T. Polichetti, M. Miscuglio, B. Alfano, M.L. Miglietta, E. Massera, G. Di Francia, P.M. Sarro, Effects of graphene defects on gas sensing properties towards NO<sub>2</sub> detection, *Nanoscale* 9 (2017) 6085–6093. <https://doi.org/10.1039/c7nr01120b>.
- [22] M.K. Ram, O. Yavuz, M. Aldissi, NO<sub>2</sub> gas sensing based on ordered ultrathin films of conducting polymer and its nanocomposite, *Synth. Met.* 151 (2005) 77–84. <https://doi.org/10.1016/j.synthmet.2005.03.021>.
- [23] S.T. Navale, D.K. Bandgar, S.R. Nalage, G.D. Khuspe, M.A. Chougule, Y.D. Kolekar, S. Sen, V.B. Patil, Synthesis of Fe<sub>2</sub>O<sub>3</sub> nanoparticles for nitrogen dioxide gas sensing applications, *Ceram. Int.* 39 (2013) 6453–6460. <https://doi.org/10.1016/j.ceramint.2013.01.074>.
- [24] T. Chen, W. Jiang, A facile solvothermal synthesis of NiFe<sub>2</sub>O<sub>4</sub>/RGO and its enhanced catalytic activity on thermal decomposition of ammonium perchlorate, 2017 IEEE 17th Int. Conf. Nanotechnology, NANO 2017 (2017) 607–610. <https://doi.org/10.1109/NANO.2017.8117303>.
- [25] R. Pinalli, A. Pedrini, E. Dalcanale, Environmental Gas Sensing with Cavitands, *Chem. - A Eur. J.* 24 (2018) 1010–1019. <https://doi.org/10.1002/chem.201703630>.
- [26] A.A. Ensafi, N. Zandi-Atashbar, M. Gorgabi-Khorzoughi, B. Rezaei, Nickel-Ferrite Oxide Decorated on Reduced Graphene Oxide, an Efficient and Selective Electrochemical Sensor for Detection of Furazolidone, *IEEE Sens. J.* 19 (2019) 5396–5403. <https://doi.org/10.1109/JSEN.2019.2908994>.
- [27] S. Mao, S. Cui, G. Lu, K. Yu, Z. Wen, J. Chen, Tuning gas-sensing properties of reduced graphene oxide using tin oxide nanocrystals, *J. Mater. Chem.* 22 (2012) 11009–11013. <https://doi.org/10.1039/c2jm30378g>.
- [28] G. Korotcenkov, The role of morphology and crystallographic structure of metal oxides in response of conductometric-type gas sensors, *Mater. Sci. Eng. R Reports* 61 (2008) 1–39. <https://doi.org/10.1016/j.mser.2008.02.001>.
- [29] S. Liu, B. Yu, H. Zhang, T. Fei, T. Zhang, Enhancing NO<sub>2</sub> gas sensing performances at room temperature based on reduced graphene oxide-ZnO nanoparticles hybrids, *Sensors Actuators, B Chem.* 202 (2014) 272–278. <https://doi.org/10.1016/j.snb.2014.05.086>.
- [30] A. Kolmakov, X. Chen, M. Moskovits, Functionalizing nanowires with catalytic nanoparticles for gas sensing application, *J. Nanosci. Nanotechnol.* 8 (2008) 111–121. <https://doi.org/10.1166/jnn.2008.N10>.
- [31] P.C.H. Chan, G.Z. Yan, L.Y. Sheng, R.K. Sharma, Z. Tang, J.K.O. Sin, I.M. Hsing, Y. Wang, An integrated gas sensor technology using surface micro-machining, *Sensors Actuators, B Chem.* 82 (2002) 277–283. [https://doi.org/10.1016/S0925-4005\(01\)01064-4](https://doi.org/10.1016/S0925-4005(01)01064-4).

- [32] B. Bashir, A. Rahman, H. Sabeeh, M.A. Khan, M.F. Aly Aboud, M.F. Warsi, I. Shakir, P.O. Agboola, M. Shahid, Copper substituted nickel ferrite nanoparticles anchored onto the graphene sheets as electrode materials for supercapacitors fabrication, *Ceram. Int.* 45 (2019) 6759–6766. <https://doi.org/10.1016/j.ceramint.2018.12.167>.
- [33] M. Khalil, M. Lesa, A.G. Juandito, A.R. Sanjaya, T.A. Ivandini, G.T.M. Kadja, M.H. Mahyuddin, M. Sookhikian, Y. Alias, A SBA-15-templated mesoporous NiFe<sub>2</sub>O<sub>4</sub>/MXene nanocomposite for the alkaline hydrogen evolution reaction, *Mater. Adv.* 4 (2023) 3853–3862. <https://doi.org/10.1039/d3ma00289f>.
- [34] N. Chen, X. Yang, E. Liu, J. Huang, Reducing gas-sensing properties of ferrite compounds M Fe<sub>2</sub>O<sub>4</sub> / M s Cu,Zn,Cd and Mg /, *Sensors (Peterborough, NH)* (2000) 178–180.
- [35] R. Verma, K.R. Singh, R. Verma, J. Singh, Nanoengineered parallelogram-NiFe<sub>2</sub>O<sub>4</sub> /rGO nanocomposite-based biosensing interface for highly efficient electrochemical detection of neurodegenerative disorders via dopamine monitoring , *RSC Appl. Interfaces* 1 (2024) 252–267. <https://doi.org/10.1039/d3lf00153a>.
- [36] H. Tang, M. Yan, H. Zhang, S. Li, X. Ma, M. Wang, D. Yang, A selective NH<sub>3</sub> gas sensor based on Fe<sub>2</sub>O<sub>3</sub>-ZnO nanocomposites at room temperature, *Sensors Actuators, B Chem.* 114 (2006) 910–915. <https://doi.org/10.1016/j.snb.2005.08.010>.
- [37] N.N. Toan, S. Saukko, V. Lantto, Gas sensing with semiconducting perovskite oxide LaFeO<sub>3</sub>, *Phys. B Condens. Matter* 327 (2003) 279–282. [https://doi.org/10.1016/S0921-4526\(02\)01764-7](https://doi.org/10.1016/S0921-4526(02)01764-7).
- [38] M. Tonezzer, T.T. Le Dang, N. Bazzanella, V.H. Nguyen, S. Iannotta, Comparative gas-sensing performance of 1D and 2D ZnO nanostructures, *Sensors Actuators, B Chem.* 220 (2015) 1152–1160. <https://doi.org/10.1016/j.snb.2015.06.103>.
- [39] G. Yu, J. Xia, F. Zhang, Z. Wang, Hierarchical and hybrid RGO/ZIF-8 nanocomposite as electrochemical sensor for ultrasensitive determination of dopamine, *J. Electroanal. Chem.* 801 (2017) 496–502. <https://doi.org/10.1016/j.jelechem.2017.08.038>.
- [40] P.T. Moseley, Progress in the development of semiconducting metal oxide gas sensors: A review, *Meas. Sci. Technol.* 28 (2017). <https://doi.org/10.1088/1361-6501/aa7443>.
- [41] C. Marichy, P.A. Russo, M. Latino, J.P. Tessonnier, M.G. Willinger, N. Donato, G. Neri, N. Pinna, Tin dioxide-carbon heterostructures applied to gas sensing: Structure-dependent properties and general sensing mechanism, *J. Phys. Chem. C* 117 (2013) 19729–19739. <https://doi.org/10.1021/jp406191x>.
- [42] X. Liu, T. Ma, N. Pinna, J. Zhang, Two-Dimensional Nanostructured Materials for Gas Sensing, *Adv. Funct. Mater.* 27 (2017) 1–30. <https://doi.org/10.1002/adfm.201702168>.
- [43] E.H. Espinosa, R. Ionescu, B. Chambon, G. Bedis, E. Sotter, C. Bittencourt, A. Felten, J.J. Pireaux, X. Correig, E. Llobet, Hybrid metal oxide and multiwall carbon nanotube films for low temperature gas sensing, *Sensors Actuators, B Chem.* 127 (2007) 137–142. <https://doi.org/10.1016/j.snb.2007.07.108>.
- [44] W. Qin, Z. Yuan, H. Gao, R. Zhang, F. Meng, Perovskite-structured LaCoO<sub>3</sub> modified ZnO gas sensor and investigation on its gas sensing mechanism by first principle, *Sensors Actuators, B Chem.* 341 (2021) 130015. <https://doi.org/10.1016/j.snb.2021.130015>.

- [45] N. Boda, K.C.B. Naidu, D.B. Basha, D. Ravinder, Structural and Magnetic Properties of CdCoFe<sub>2</sub>O<sub>4</sub> Nanoparticles, *J. Supercond. Nov. Magn.* 33 (2020) 1039–1044. <https://doi.org/10.1007/s10948-019-05242-1>.
- [46] N. Kumar, A.K. Srivastava, H.S. Patel, B.K. Gupta, G. Das Varma, Facile synthesis of ZnO-reduced graphene oxide nanocomposites for NO<sub>2</sub> Gas sensing applications, *Eur. J. Inorg. Chem.* 2015 (2015) 1912–1923. <https://doi.org/10.1002/ejic.201403172>.
- [47] Y.L. Hoo, W. Jin, H.L. Ho, D.N. Wang, R.S. Windele, Evanescent wave gas sensing using microstructure fibre, *Pacific Rim Conf. Lasers Electro-Optics, CLEO - Tech. Dig.* (2001) 8–9. <https://doi.org/10.1117/1.1429930>.
- [48] R. Prajesh, N. Jain, A. Agarwal, Low power highly sensitive platform for gas sensing application, *Microsyst. Technol.* 22 (2016) 2185–2192. <https://doi.org/10.1007/s00542-015-2609-1>.
- [49] K. Hareesh, S.R. Suryawanshi, B. Shateesh, D.M. Phase, S.S. Dahiwal, V.N. Bhoraskar, S.K. Haram, M.A. More, S.D. Dhole, High-field emission performance of a NiFe<sub>2</sub>O<sub>4</sub>/rGO/CNT tertiary nanocomposite, *RSC Adv.* 6 (2016) 26745–26751. <https://doi.org/10.1039/C6RA02198K>.
- [50] M. Kamionka, P. Breuil, C. Pijolat, Calibration of a multivariate gas sensing device for atmospheric pollution measurement, *Sensors Actuators, B Chem.* 118 (2006) 323–327. <https://doi.org/10.1016/j.snb.2006.04.058>.

## Synthesis and Biological Evaluation of 1H-Indole Condensed Thiazolidin-4-Ones As Mycobacterium Tuberculosis Protein Tyrosine Phosphatase B (Ptpb) Inhibitors

Pawan S Hardas<sup>1</sup>, Babasaheb V Kendre\*<sup>1</sup>, Rushikesh B Kendre<sup>2</sup>, Mahadev G Landge<sup>1</sup>

<sup>1</sup>Post Graduate Research Centre in Chemistry, Vaidyanath College, Parli-Vajinath-431515, Dist Beed, affiliated to Dr Babasaheb Ambedkar Marathwada University, Chha. Sambhajnagar, Maharashtra, India

<sup>2</sup>Maharashtra Institute of Medical Sciences and Research, Latur-413512, Maharashtra, India

E-mail: [bvkendre71@gmail.com](mailto:bvkendre71@gmail.com)

### ABSTRACT

In the search for new and potent anti-tubercular agents, a novel series of 1H-indole fused thiazolidin-4-ones was successfully synthesized and evaluated for their anti-tubercular activity against the Mycobacterium tuberculosis H37Rv (ATCC27294) strain. The minimum inhibitory concentration (MICs) for compounds 6b, 6f, 6g, and 6i against the H37Rv strain was ranged from 1.82 to 5.45 µg/mL. In silico molecular docking studies identified Mycobacterium tuberculosis Protein Tyrosine Phosphatase B (Ptpb) as a potential molecular target for thiazolidin-4-ones. Additionally, safety studies including in silico and in vitro assessments showed no toxicity associated with these compounds. The structure-activity relationship study (SARs) revealed the impact of variable functional groups on the activities of the compounds.

**Keywords:** Thiazolidinone, Anti-tubercular, Indole, Mycobacterium tuberculosis, Protein tyrosine phosphatase B

### INTRODUCTION

Tuberculosis is a communicable bacterial disease caused by *Mycobacterium tuberculosis*, mainly responsible for ill health and considered one of the leading causes of death worldwide. Prior to the COVID-19 pandemic, tuberculosis was among the most deadly infectious diseases globally. As per the Global Tuberculosis Report 2022 from the WHO, tuberculosis prevalence rose by 4.5% for the first time in two decades, with deaths increasing from 1.5 million to 1.6 million in 2020. Without proper treatment, the mortality rate for TB is high (around 50%), with countries having poor hygiene conditions experiencing higher morbidity rates. Over the past three years, COVID-19 has disproportionately impacted the daily lives of individuals. Individuals living with HIV/AIDS and other infectious diseases are particularly vulnerable to TB infections, with a higher incidence rate observed in prisons compared to the general global population. Poor living conditions and limited access to healthcare significantly contribute to this heightened susceptibility. The COVID-19 pandemic has served as a catalyst for innovative strategies to address various health challenges.

An important step in the pathway of tuberculosis is rapid and accurate testing to diagnose TB. Recently, nucleic-acid amplification tests (NAATs), which are highly specific and sensitive, have been introduced in

the field of diagnostic testing for TB. Line probe assays were the first molecular tests recommended by World Health Organization (WHO). These tests significantly reduce the time needed to diagnose multidrug resistant and rifampicin-resistant TB, compared with culture. There are two types of confirmation methods of TB, the first is bacteriological and the second is microbiological detection of TB, the bacteriological confirmation is necessary to test for resistance to first and second line anti-TB drugs and the microbiological testing allows people to be correctly diagnosed to start highly effective treatment regimen.<sup>3-5</sup> The people diagnosed with rifampicin-resistant TB, isoniazid-resistant TB, and multidrug-resistant TB requires regimens that include second line drugs like bedaquiline and fluoroquinolones, but these regimens are more expensive and cause more side effects than first line treatment.<sup>6</sup>

In order to address these challenges, individuals diagnosed with TB must have immediate access to accurate diagnosis, effective treatment, and ongoing efforts in the development of new anti-TB medications. Recently, potent antitubercular drugs such as bedaquiline and delamanid (Figure 1) have been identified for the treatment of MDR-TB. Telacebec (Q203, Figure 1) is a groundbreaking first-in-class antituberculosis medication that targets the cellular energy production of mycobacterium tuberculosis by inhibiting the mycobacterial cytochrome bc1 complex.<sup>7-9</sup> SKLB-TB1001, a preclinical candidate from the benzothiazinone compound class, demonstrates nanomolar potency against XDR-TB isolates.<sup>10</sup> BTZ043, a nitro-benzothiazinone compound, serves as an irreversible inhibitor of DprE1 with a MIC of 1ng/mL against Mtb H37Rv, exhibiting potent antimycobacterium activity in a murine model of TB.<sup>11</sup>

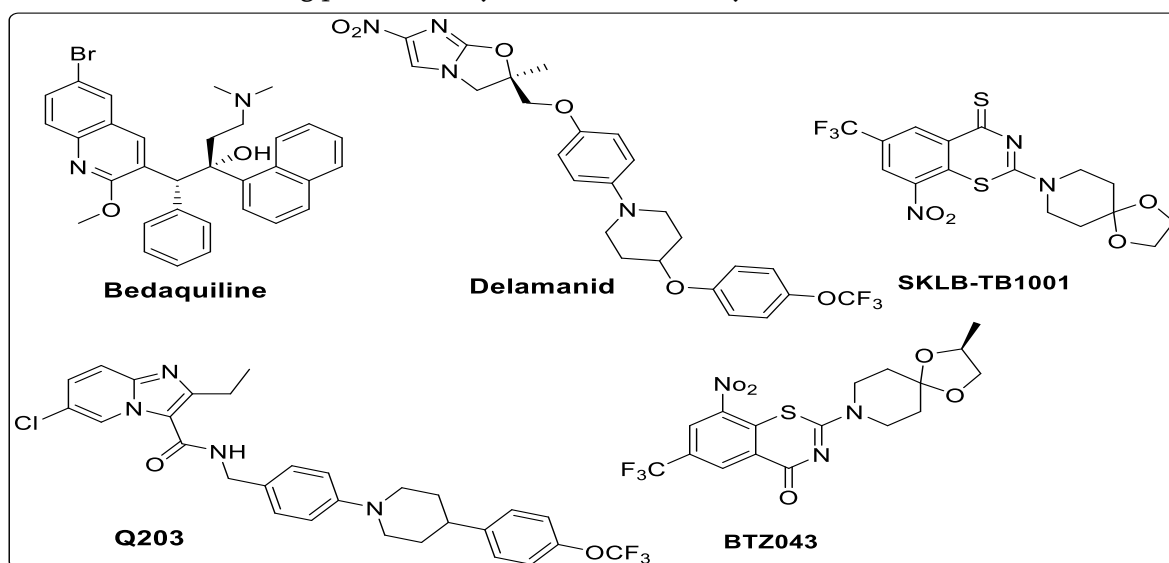


**Figure 1:** Clinically approved anti-TB drugs

The literature reports compounds containing a thiazolidinone scaffold, among which compound I has a MIC of  $3.12 \mu\text{g/ml}^{-1}$  against *M. tuberculosis*, while compounds II and III exhibit MIC values of 1.25,  $3.12 \mu\text{g/ml}^{-1}$  and 2.5,  $3.12 \mu\text{g/ml}^{-1}$  respectively against the *M. tuberculosis* H37Rv strain (refer to Figure 2).<sup>12-13</sup>

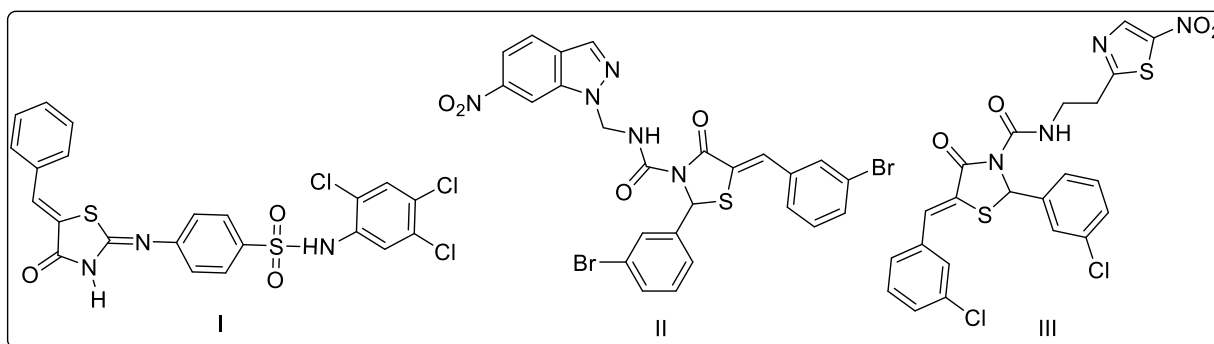


**Figure 2:** Anti tuberculosis drugs that contain thiazolidin-4-one core unit in their structure

## RESULTS AND DISCUSSION

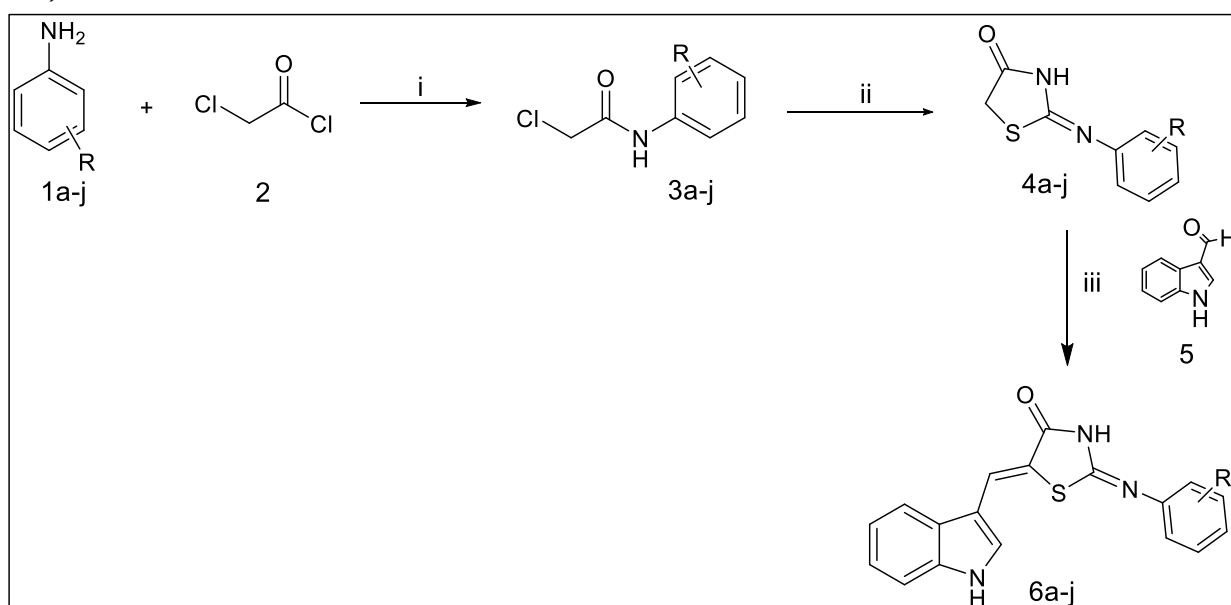
### 2.1 Chemistry and Synthesis

A three-step synthetic strategy was followed for the preparation of novel indole-fused thiazolidinones **6a-j** as outlined in **Scheme 1**. Firstly, formyl indole **5** was prepared from readily available indole using the Vilsmeier-Haack reagent ( $\text{POCl}_3$  in DMF) at a temperature of  $0-5^\circ\text{C}$  for half an hour and then at room temperature under stirring for 1h, yielding 80%.<sup>14</sup> The 2-chloro-*N*-phenylacetamide **3a-j** in 80-88% yield was prepared from **1a-j** by reacting substituted anilines with chloroacetyl chloride in the presence of anhydrous potassium carbonate & basic alumina in acetone under reflux conditions on a water bath for 7-8 h. Cyclization of 2-chloro-*N*-phenylacetamide (**3a-j**) with ammonium thiocyanate in ethylene glycol under reflux conditions for 4-5h resulted in compounds **4a-j** with yields of 84-90%. Finally, the intermediate compounds **4a-j** was refluxed with 3-formyl indole **5** in the presence of sodium acetate in acetic acid to yield the target compounds **6a-j** in excellent yields (75-85%).

The conversion of compounds **1a** into 2-chloro-*N*-phenylacetamide **3a** on reaction with chloroacetyl chloride **2** was confirmed by thin-layer chromatography, functional group tests, melting point, and IR,  $^1\text{H}$  NMR, and  $^{13}\text{C}$  NMR spectral methods. The diazotization test for primary amine was found to be negative. Thin-layer chromatography showed complete conversion of aniline to 2-chloro-*N*-phenylacetamide. The melting point observed for an intermediate 2-chloro-*N*-phenylacetamide was  $137-140^\circ\text{C}$ . The IR spectrum showed a band for amide N-H bending vibrations in the range of  $1650-1590\text{ cm}^{-1}$  and for amide  $>\text{C}=\text{O}$  stretching (br) vibrations in the range of  $1690-1650\text{ cm}^{-1}$ . The appearance of a sharp singlet peak at  $\delta$  4.32 for methylene protons, a short singlet peak at  $\delta$  10.00 for -NH- proton in  $^1\text{H}$  NMR spectrum clearly indicates the formation of 2-chloro-*N*-phenylacetamide from aniline. The appearance of peaks for carbonyl carbon ( $-\text{C}=\text{O}$ ) at  $\delta$  166.02 and for methylene carbon at  $\delta$  42.13 supports the structure of compound **3a**. The formation of (*E*)-2-(phenylimino) thiazolidin-4-one **4a** was confirmed by  $^1\text{H}$  NMR and  $^{13}\text{C}$  NMR studies. The appearance of a peak in the PMR spectrum at  $\delta$  11.97 for -NH- proton and at  $\delta$  3.81 for the protons of  $-\text{CH}_2-$  shows the formation of compound **4a**. In  $^{13}\text{C}$  NMR spectrum, the peaks appeared for carbonyl carbon  $>\text{C}=\text{O}$ ,  $-\text{CH}_2-$  carbon,  $>\text{C}=\text{N}-$  carbon at the chemical shift values of 174.10, 33.01, 158.89 respectively. The negative test of the formyl group for **6a** also supports the condensation of formyl indole with (*E*)-2-(phenylimino)thiazolidin-4-one. The difference in the melting points of compound **4a** and the final compound **6a** clearly indicates the formation of the target compound (2*E*, 5*Z*)-5-(1*H*-indol-3-



yl)methylene)-2-(phenylimino)thiazolidin-4-one. The disappearance of the peak for -CH<sub>2</sub>- protons in <sup>1</sup>H NMR spectra of compound 4a and the appearance of the peak for -HC=C- proton at δ 7.92 strongly support the structure of compound 6a. The appearance of a peak for -CH=C< carbons at 144.43 and at 124.10 also supports the structure of compound 6a. 3-formyl indole was prepared as per the literature procedure, and its structure was confirmed by functional group tests, melting point, and <sup>1</sup>H NMR spectral data. The presence of the formyl group in indole was clearly detected from the IR spectrum, which showed a strong absorption band at 1634 cm<sup>-1</sup>, and the <sup>1</sup>H NMR spectrum displayed a singlet at a chemical shift value of δ 9.9 ppm. The yellow-white solid, Yield = 85%; mp=181-183°C, EIMS (m/z) values for all synthesized compounds are in good agreement with the molecular weights of target compounds (refer EIMS (m/z) data for 6a-j).



**Scheme 1:** Synthesis of indole-fused thiazolidin-4-ones 6a-j

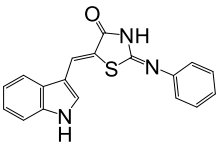
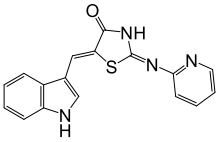
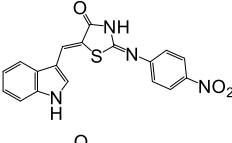
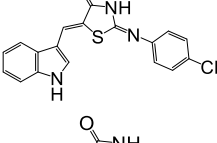
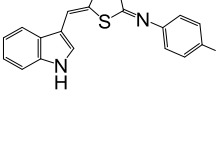
**Reagents and reaction conditions :-** (i) Basic Al<sub>2</sub>O<sub>3</sub>/K<sub>2</sub>CO<sub>3</sub> (1:1Eq.), Acetone, Reflux, 7-8h, 80-88%; (ii) Ammonium thiocyanate, Ethylene glycol, Reflux, 4-5h, 84-90%; (iii) CH<sub>3</sub>COONa/CH<sub>3</sub>COOH, 70-80 °C, 4 h, 75-85%.

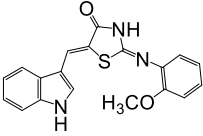
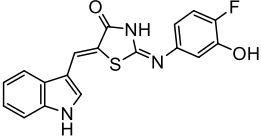
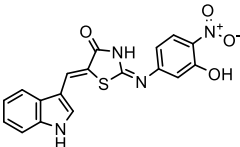
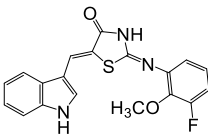
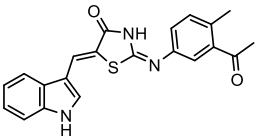
## 2.2. Anti-mycobacterial evaluation

As per the method reported by Leonard B,<sup>15</sup> indole-fused thiazolidinone derivatives (6a-j) were screened for their *in vitro* anti-tubercular activity against *Mycobacterium tuberculosis* H37Rv (ATCC27294) strain using Microplate Alamar Blue Assay (MABA). The minimum inhibitory concentration (MIC; µg ml<sup>-1</sup>) for each compound was studied and compared with standard reference drugs such as ethambutol, rifampicin, isoniazid, streptomycin, levofloxacin, and amikacin. The results of MIC for synthesized compounds along with the standard drugs are reported in Table 1. Among the ten screened derivatives, four derivatives (6b, 6f, 6g, and 6i) were found to be more active with MICs in the range of 1.82-5.45 µg ml<sup>-1</sup>. The derivative 6g was found highly potent among all the tested derivatives with MIC of 1.82 µg ml<sup>-1</sup>. The derivatives 6b, 6f, and 6i with MIC values 5.45 µg ml<sup>-1</sup>, 4.22 µg ml<sup>-1</sup>, and 2.71 were found closely active to the standard drug ethambutol (MIC, 1µg ml<sup>-1</sup>). The remaining two derivatives 6c and 6h exhibited moderate activity with

MIC values of 13.82  $\mu\text{g ml}^{-1}$  and 12.24  $\mu\text{g ml}^{-1}$  respectively (Table-1). The SAR study of indole-fused thiazolidinones demonstrates the effect of substituent on the activity of compounds. The compound bearing a phenyl ring with substituent  $-\text{OCH}_3$ ,  $-\text{OH}$ ,  $-\text{Cl}$ ,  $-\text{F}$ , and pyridine ring have better potential to inhibit *Mycobacterium tuberculosis*. It was also observed that the involvement of a pyridine ring in the structure enhances activity against Mtb. The substitution of  $-\text{OCH}_3$  group at position 2 enhances inhibition potential against Mtb. Activity is lost when  $-\text{NO}_2$  group is substituted at position 4 on the phenyl ring. The enhancement in activity occurs when  $-\text{OCH}_3$  group is substituted at position 2 and  $-\text{F}$  group at the position 3 respectively. The cyclopropyl ring substitution in place of the phenyl ring reduces activity. The loss of activity occurs when an ethyl group is introduced by replacing phenyl rings. The loss of activity was observed when  $-\text{COCH}_3$  and  $-\text{CH}_3$  groups were introduced at positions 3 and 4 respectively. The activity for the inhibition of Mtb was greatly enhanced when  $-\text{OH}$  and  $-\text{F}$  groups were introduced on the phenyl ring at positions 3 and 4 respectively. The above observations clearly reveal that the bridge ( $-\text{CH}=\text{C}$ ) formed due to the fusion of two compounds is responsible for enhancing anti-tubercular activity. The results also indicate that the type of substituent and its position on the phenyl ring are very important to identify potent anti-tubercular agents. Importantly, the replacement of the phenyl amine moiety from the structure leads to the loss of activity.

**Table 1: *In vitro* anti-tubercular activity of indole fused thiazolidinones (6a-j) against *Mycobacterium tuberculosis* H37Rv.**

Entry	Compound	MIC ( $\mu\text{g ml}^{-1}$ ) <sup>a</sup>	Activity	(Cytotoxicity) <sup>b</sup> ( $\mu\text{g/ml}$ )	(CC50, $\mu\text{g/ml}$ )
6a		50	Inactive	15	
6b		5.45	Active	19	
6c		13.82	Moderately Active	22	
6d		>25	Weakly active	16	
6e		>25	Weakly active	18	

6f		4.22	Active	12
6g		1.82	Very active	12
6h		12.24	Moderately active	10
6i		2.71	Active	14
6j		>25	Inactive	nd
Reference Drugs	Isoniazid	0.03		
	Rifampicin	0.03		
	Streptomycin	0.5		
	Ethambutol	1		
	Levofloxacin	0.25		
	Amikacin	0.12		

<sup>a</sup>Rifampicin (MIC, 0.03  $\mu\text{g ml}^{-1}$ ); Ethambutol (MIC, 1.0  $\mu\text{g ml}^{-1}$ ); <sup>b</sup>Cytotoxicity at 50  $\mu\text{g/ml}$ ; nd: Not detected

## COMPUTATIONAL STUDIES AND METHODOLOGY

We have studied the mycobacterium tuberculosis inhibitory action of different compounds *via* different pathways, we choose herein 04 validated protein targets including thymidylate kinase (PDB ID: 1G3U), 6,7-dimethyl-8-ribityllumazine synthase (PDB ID: 1W19), enoyl-acyl carrier protein (PDBID: 1ZID), and MTB phosphotyrosine phosphatase B (PDB ID: 2OZ5) based on their roles in different pathways (table 3). Thymidylate kinase (TMPK) is essential enzyme of nucleotide metabolism which catalyzes the phosphorylation of thymidine 5'-monophosphate (dTMP) to form thymidine 5'-diphosphate (dTDP) in the presence of ATP and magnesium.<sup>16</sup> TMPK plays a vital role in cell proliferation. Therefore, it has been considered as a validated target for rational drug design. Lumazine synthase is an enzyme involved in the biosynthesis of riboflavin represents well attractive target for the drugs against bacterial infections, because the inhibition of this enzyme not interfere with enzymes of mammalian metabolism.<sup>17</sup> The main function of enoyl-acyl carrier protein reductase (InhA) is in the final step of fatty acid biosynthesis in which reduction of 2-trans-enoyl-acyl carrier protein takes place by utilizing NADH.<sup>18</sup> Among the two protein-

tyrosine phosphatases of *Mycobacterium tuberculosis* (Mtb) namely PtpA and PtpB, PtpB is a triple-specificity phosphatase which plays crucial role in survival of mycobacteria within the host, because of its secretory nature, it is an attractive drug target for drug designing.<sup>19</sup>

### 3.1. Preparation of Ligands

The two-dimensional structures for all compounds were drawn using ChemDraw software and the designed structures were converted into mol file for further study. The structures were converted to 3-D structures using LigPrep tool of Schrödinger suite by using OPLS 300 force field.<sup>20</sup> The top ranked ligand was selected for docking purpose.

### 3.2. Preparation of receptor molecule

The protein targets listed in table 3 were retrieved from RCSB protein data bank and prepared as per literature information. The ligand interaction PDB file of protein in complex with inhibitor was downloaded from the protein data bank and the tool, protein preparation wizard of Schrödinger suite Maestro v. 10.3 (Maestro, v. 10.3: Schrödinger, LLC, New York, NY, USA) was used for the preparation of macromolecule. The preprocessing, optimization, and minimization steps were performed using OPLS 300 force field with a RMSD cut-off value of 0.3 Å. The hydrogen atoms were added at pH 7.0. The grid generation on the receptor was performed using receptor grid generation tool of the software. The receptor grid was generated at the centre of active site where the key residues are located.

### 3.3. Molecular docking

The molecular docking was performed by using ligand docking tool of the Schrodinger suite. At first, the ligand was prepared using LigPrep tool of the software using OPLS 300 force field. LigPrep generates possible 3-D poses of the ligand ranking them on descending order. The top ranked pose was selected for the docking purpose. Using ligand docking tool, the top ranked ligand was allowed to dock with receptor macromolecule. The ligand from workspace was flexibly docked in grid box using Monte Carlo-based simulation algorithm. The binding pose was generated by employing extra precision (XP) method. The molecular docking of all designed molecules was performed against protein targets. The docked molecules showing better binding energy and useful interactions with the key residues were selected for the synthesis and evaluated against Mtb. The selected docked molecules were ranked according to the binding energy score (Table 4).

### 3.4. Molecular docking analysis

In order to explore the potential putative targets of synthesized indole-fused thiazolidinone (6a-6j), we performed docking with four known target proteins such as thymidylate kinase (PDB ID: 1G3U), 6,7-dimethyl-8-ribityllumazine synthase (PDB ID: 1W19), enoyl-acyl carrier protein (PDB ID: 1ZID), and MTB phosphotyrosine phosphatase B (PDB ID: 2OZ5)<sup>21</sup>. The binding modes and confirmations of the ligand molecules were studied using automated docking methodology. The five ligands out of ten have showed good binding energy on docking with 4 validated proteins. Out of four validated proteins, 2OZ5, phosphotyrosine phosphatase B has showed highest binding energies against five indole-fused thiazolidinones (Table 2). On docking, compound 6g was found as best scorer than other selected compounds. Its binding score ranges from -6.341 to -9.903 kcal mol<sup>-1</sup> for four proteins. As the five selected compounds have showed better binding energy scores against 2OZ5, the protein 2OZ5 was considered for further studies. PtpB is triple-specificity phosphatase which plays vital role in survival of mycobacteria

within the host, because of its secretory nature it could be an attractive drug target for TB drugs. The intermolecular protein-ligand interactions with key residues of protein are depicted in **Figure 2**. The docking poses represented in **Figure 3** showed intermolecular interactions of the compounds 6b, 6c, 6f, 6g and 6h and the reference drugs ethambutol, levofloxacin, isoniazid and native ligand with the key amino acids from the active site of protein (2OZ5). Among these compounds, 6g has showed highest binding energy value of  $-9.903 \text{ kcal mol}^{-1}$ . Compound 6g has showed five H-bond interactions with Arg166, Ala162, Cys160, Glu129 and Lys 164. The molecular interactions of compound 6f with key residues are Arg166, Ala162 and Cys160 respectively. It is the second molecule in a series that gives highest binding energy i.e.  $-9.185 \text{ kcal mol}^{-1}$ . It is noteworthy to mention that the molecular interactions showed by 6b and 6g with the key residues were almost similar to reference drug levofloxacin and native ligand (**Table 3**). Compound 6f also showed comparable molecular interactions with the key residues with binding energy value of  $-8.785 \text{ kcal mol}^{-1}$ . Interestingly, the compound 6f and 6i have similar structures, only difference being the additional F group at the position 3 in the structure of 6i. The substitution of functional group F in compound 6i improved binding energy score. The above results suggest that the pi-pi-interactions and H-bond interactions are improving the docking score of ligand. All these compounds were observed to be well bound in the main pocket region of protein by forming intermolecular interactions with the key amino acids. The above observations indicate that all five compounds 6b, 6c, 6f, 6g and 6h may have an important role in the active site of the receptor.

**Table 2: Molecular docking analysis of 4 protein targets with selected compounds and the binding energy was calculated for Glide in kcal mol<sup>-1</sup>**

PDB Target	Glide score binding energy (kcal/mol <sup>-1</sup> ) for compounds				
	6b	6c	6f	6g	6h
1G3U	-4.936	-5.785	-6.132	-6.341	-6.216
1W19	-2.634	-7.122	-7.262	-7.903	-2.264
1ZID	-9.027	-9.151	-9.067	-9.933	-8.473
2OZ5	-9.185	-5.336	-8.785	-9.903	-6.805

**Table 3: Molecular docking of selected compounds with 2OZ5 enzyme**

Protein target	Compound	Molecular interactions with key residues	Binding energy kcal/mol <sup>-1</sup>
2OZ5	6b	Arg166, Ala162, Cys160	-9.185
	6c	Arg166, Glu129	-5.336
	6e	Arg166, Glu129	-6.832
	6f	Arg166, Ala162, Tyr125	-8.785
	6g	Arg166, Ala162, Cys160, Glu129, Lys164	-9.903
	6h	Arg166, Glu129, Lys164	-6.804
	Ethambutol	Glu129, Ser57	-3.233
	Levofloxacin	Arg166, Ala162, Cys160, Lys164	-2.354

Isoniazid	Asp165, Tyr125	-3.902
Native Ligand	Arg166, Ala162, Cys160, Phe161, Tyr125,	-10.218

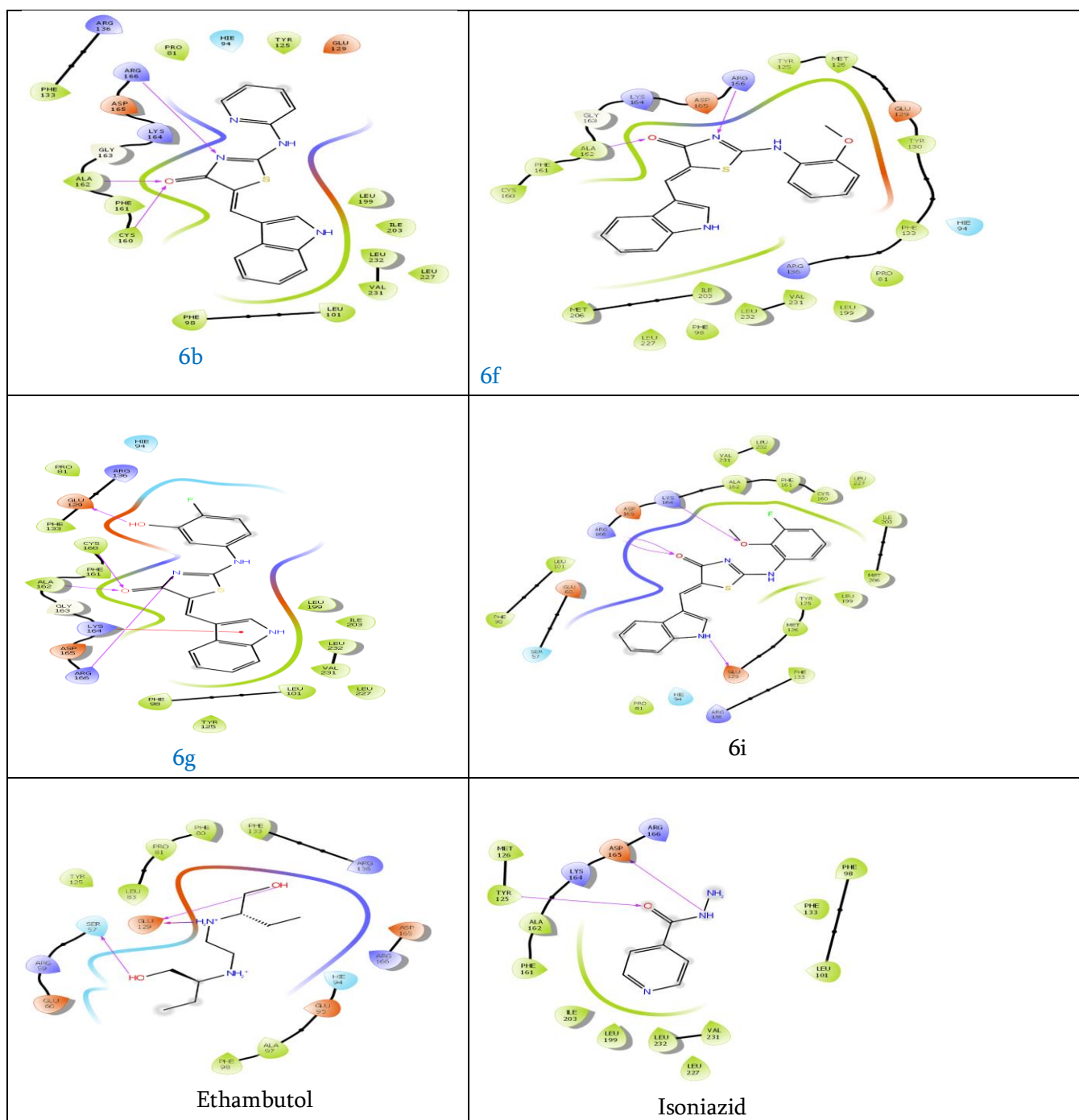


Figure 3: Ligand interaction diagram with enzyme (PDB ID 2OZ5)

### 3.5. Chemoinformatics analysis

A web tool, SwissADME, was used to study the chemoinformatics of the five selected compounds. The properties like physicochemical, pharmacokinetic, drug likeness, and medicinal chemistry friendliness were studied.<sup>22</sup> The ADME parameters, pharmacokinetic properties, druglike nature and medicinal

chemistry friendliness properties were recorded to support drug discovery (Table 4). The Lipinski rule of five was predicted using experimental and computational approaches.<sup>23</sup> Lipinski rule states that poor absorption or permeation of a drug is possible when it has a high molecular weight, more than 5 H-bond donors and 10 H-bond acceptors.

Solubility and lipophilicity are the key parameters that determine the success or failure of drug discovery and development.<sup>24</sup> According to this study, the poor solubility of a compound leads to reduced productivity. A high lipophilicity leads to a high rate of metabolism, which leads to poor solubility and low absorption. The present study highlights the synthesis of drugs that possess excellent physicochemical properties, such as rotatable bonds, H-bond acceptors and donors; solubility and lipophilicity; and good BBB permeability. All the selected compounds had molecular weights less than 500 and abided by the Lipinski rule of five with zero violation. The polar surface area (PSA) is a widely used molecular descriptor tool in the study of drug transport properties, such as intestinal absorption and blood–brain barrier penetration.<sup>25</sup> The topological polar surface area is a significant tool used in virtual screening and for predicting ADME properties, including BBB crossing tendency. The polar surface areas for the selected compounds (6b, 6c, 6g and 6h) are 95.44, 128.37, and 91.78 Å<sup>2</sup>, respectively, indicating that the membrane permeability is very good for the reported compounds. An experimental cytotoxicity study indicated that all the selected compounds exhibited normal toxicity, as the values were in the range of 10-20 µg/ml.

**Table 4: Physicochemical properties of 1*H*-indole fused thiazolidinones**

Properties	Compounds					
	6b	6c	6f	6g	6h	ethambutol
<b>Physicochemical</b>						
MW(g/mol)	320.37	364.8	349.41	363.37	367.40	206.33
HBA	3	4	4	4	4	2
HBD	2	2	2	3	2	4
nRotb	3	4	3	3	4	9
TPSA (Å <sup>2</sup> )	95.44	128.37	91.78	102.78	91.78	73.68
<b>Lipophilicity</b>						
LogP <sub>o/w</sub> (iLOGP)	1.70	1.95	2.72	2.08	2.80	-1.28
<b>Water solubility</b>						
Log S	-4.14	-4.65	-4.66	-4.61	-4.82	-0.47
<b>Pharmacokinetics</b>						
GI absorption	High	High	High	High	High	Low
BBB permeant	No	No	No	No	No	No
<b>Druglikeness</b>						
Lipinski	Yes; 0 violation	Yes; 0 violation	Yes; 0 violation	Yes; 0 violation	Yes; 0 violation	Yes; 0 violation
Bioavailability score	0.55	0.55	0.55	0.55	0.55	0.55
<b>Medicinal</b>						

**Chemistry**

Leadlikeness (LL)	Yes	MW>350	Yes	Yes	MW>350	Viol. No.2
-------------------	-----	--------	-----	-----	--------	------------

The molecular weight (MW), log of the octanol/water partition coefficient (logP), hydrogen bond acceptor (HBA), hydrogen bond donor (HBD), topological polar surface area (TPSA), number of rotatable bonds (nRotb), and blood–brain barrier (BBB) penetration were calculated.

**CYTOTOXICITY ASSAY**

A cytotoxicity assay was performed against Vero cells using the MTT assay.<sup>26</sup> For all tested compounds,  $\sim 10^3$  cells/well were added to a 96-well plate and incubated at 37 °C in an atmosphere of CO<sub>2</sub> (5%). After incubating for 24 h, the test compound was added at concentrations ranging from 100 to 12.5 µg/mL and further incubated for 72 h. A solution of MTT (3-(4,5-dimethylthiazol-2-yl)-2,5-diphenyltetrazolium bromide) was added to each well and incubated further for 4 h at 37 °C. The residual medium was discarded, 0.1 mL of DMSO was added to dissolve the formazan crystals, and colorimetric measurements were carried out (OD) at a 540 nm filter. Doxorubicin was used as a positive control, and the experiment was repeated twice for accuracy. The CC<sub>50</sub> was calculated based on the optical density values. CC<sub>50</sub> is the lowest concentration of compound that leads to a 50% reduction in cell viability.

**CHARACTERIZATION DATA:****(2E, 5Z)-5-((1H-indole-3-yl)methylene)-2-(phenylimino)thiazolidin-4-one (6a)**

Mp ( ° C)=130-132, Yield (%)=82; IRvmax(cm<sup>-1</sup>): 3471.40 (N-H Str., indole), 3428.27 (N-H Str., thiazolidinone), 3157.24 (C-H Str.,C=C-H), 1739.06 (C=O str.), 1731.31 (C=N str.); <sup>1</sup>H-NMR (400MHz, DMSO-*d*<sub>6</sub>): 12.00 (s, 1H), 9.89 (s, 1H), 8.23-8.05 (m, 1H), 8.15-8.12 (m, 1H), 8.10 (s, 1H), 7.61-7.51 (m, 1H), 7.33-6.82 (m, 6H); <sup>13</sup>C-NMR (400MHz, DMSO-*d*<sub>6</sub>): 184.91, 172.50, 159.58, 146.25, 138.12, 138.30, 136.75, 129.05, 124.51, 123.39, 122.14, 117.20, 113.19, 112.23, 110.01, 106.74, 106.51; EIMS m/z: 319.08[M+1]<sup>+</sup>

**(5Z)-5-((1H-indol-3-yl)methylene)-2-(pyridin-2-ylimino)thiazolidin-4-one (6b)**

Mp( ° C)=118-120, Yield (%)=82; IRvmax(cm<sup>-1</sup>): 3461.70 (N-H Str., indole), 3442.80 (N-H Str., thiazolidinone), 3164.54 (C-H Str.,C=C-H), 1745.02 (C=O str.), 1729 (C=N str.); <sup>1</sup>H-NMR (400MHz, DMSO-*d*<sub>6</sub>): 12.05 (s, 1H), 9.95 (s, 1H), 8.26-8.19 (m, 1H), 8.16-8.14 (m, 1H), 8.11 (s, 1H), 7.65-7.60 (m, 1H), 7.34-6.89 (m, 6H); <sup>13</sup>C-NMR (400MHz, DMSO-*d*<sub>6</sub>): 184.92, 172.51, 159.57, 146.39, 139.01, 138.34, 137.10, 129.19, 124.56, 123.42, 122.08, 118.20, 113.59, 112.43, 110.11, 107.14, 106.52; EIMS m/z: 320.07[M+1]<sup>+</sup>

**(5Z)-5-((1H-indol-3-yl)methylene)-2-((4-nitrophenyl)imino)thiazolidin-4-one (6c)**

Mp( ° C)=220-222, Yield(%)=80; IRvmax(cm<sup>-1</sup>): 3451.50 (N-H Str., indole), 3432.54 (N-H Str., thiazolidinone), 3147.34 (C-H Str.,C=C-H), 1736.14 (C=O str.), 1718 (C=N str.); <sup>1</sup>H-NMR (400MHz, DMSO-*d*<sub>6</sub>): 12.10 (s, 1H), 9.94 (s, 1H), 8.39-8.36 (m, 2H), 8.25 (s, 1H), 8.21 (s, 1H), 7.63-7.60 (m, 2H), 7.31-7.18 (m, 4H) ; <sup>13</sup>C-NMR (400MHz, DMSO-*d*<sub>6</sub>): 184.89, 174.28, 159.57, 143.37, 138.26, 137.06, 136.01, 129.47, 125.03, 123.40, 122.07, 120.82, 118.20, 113.59, 112.37, 110.11, 107.14, 106.52; EIMS m/z: 364.06 [M+1]<sup>+</sup>



**(2E, 5Z)-5-((1*H*-indol-3-yl)methylene)-2-((4-chlorophenyl)imino)thiazolidin-4-one (6d)**

Mp( ° C)=139-141, Yield(%)=82; IRvmax(cm<sup>-1</sup>): 3451.24 (N-H Str., indole), 3438.50 (N-H Str., thiazolidinone), 3153.14 (C-H Str.,C=C-H), 1742.36 (C=O str.), 1721 (C=N str.); <sup>1</sup>H-NMR (400MHz, DMSO-*d*<sub>6</sub>): 12.11 (s, 1H), 9.93 (s, 1H), 8.25 (s, 1H), 8.21 (s, 1H), 7.62 (d, 1H), 7.41 (d, 2H), 7.21-7.10 (m, 5H); <sup>13</sup>C-NMR (400MHz, DMSO-*d*<sub>6</sub>): δ 184.62, 172.28, 159.57, 147.72, 139.86, 138.30, 134.07, 128.97, 124.16, 123.44, 122.10, 120.83, 118.21, 114.59, 113.39, 110.71, 107.64, 106.82; EIMS m/z: 353.23[M+1]

**(5Z)-5-((1*H*-indol-3-yl)methylene)-2-((4-fluorophenyl)imino)thiazolidin-4-one (6e)**

Mp( ° C)=162-164, Yield(%)=77; IRvmax(cm<sup>-1</sup>): 3453.73 (N-H Str., indole), 3436.36 (N-H Str., thiazolidinone), 3151.34 (C-H Str.,C=C-H), 1739.37 (C=O str.), 1722 (C=N str.); <sup>1</sup>H-NMR (400MHz, DMSO-*d*<sub>6</sub>): 12.14 (s, 1H), 9.94 (s, 1H), 8.25- 8.21 (m, 2H), 7.65-7.60 (m, 2H), 7.31-7.18 (m, 4H), 7.12-7.16 (m, 2H); <sup>13</sup>C-NMR (400MHz, DMSO-*d*<sub>6</sub>): δ <sup>13</sup>C-NMR (400MHz, DMSO-*d*<sub>6</sub>): δ 184.89, 175.80, 160.40, 143.72, 138.31, 137.05, 135.35, 129.47, 124.11, 123.27, 122.06, 120.78, 118.15, 113.59, 112.36, 110.11, 107.14, 106.52; EIMS m/z: 337.07 [M+1]<sup>+</sup>

**(5Z)-5-((1*H*-indol-3-yl)methylene)-2-((2-methoxyphenyl)imino)thiazolidin-4-one (6f)**

Mp( ° C)=234-236, Yield(%)=80; IRvmax(cm<sup>-1</sup>): 3468.30(N-H Str., indole), 3432.70 (N-H Str., thiazolidinone), 3158.24(C-H Str.,C=C-H), 1741.21(C=O str.), 1726(C=N str.), 1468.30(-OCH<sub>3</sub> Str.); <sup>1</sup>H-NMR (400MHz, DMSO-*d*<sub>6</sub>): 12.10 (s, 1H), 9.96 (s, 1H), 8.24 (s, 1H), 8.19 (s, 1H), 7.65 (d, 1H), 7.18-7.09 (m, 4H), 7.05-7.01 (m, 2H), 6.90 (s, 1H), 3.84 (s, 3H); <sup>13</sup>C-NMR (400MHz, DMSO-*d*<sub>6</sub>): δ 184.92, 178.28, 159.97, 147.72, 139.86, 138.30, 137.07, 129.97, 124.16, 123.44, 122.10, 120.83, 118.21, 113.59, 112.39, 110.11, 107.14, 106.52, 55.10; EIMS m/z: 349.09 [M+1]<sup>+</sup>

**(2E, 5Z)-5-((1*H*-indol-3-yl)methylene)-2-((4-fluoro-3-hydroxyphenyl)imino)thiazolidin-4-one (6g)**

Mp( ° C)=160-162, Yield(%)=78; IRvmax(cm<sup>-1</sup>):3460.83 (N-H Str., indole), 3493.16 (N-H Str., thiazolidinone), 3167.04 (C-H Str.,C=C-H), 1755.14 (C=O str.), 1666.31 (C=N str.); <sup>1</sup>H-NMR (400MHz, DMSO-*d*<sub>6</sub>): 12.13 (s, 1H), 10.76 (s, 1H), 9.94 (s, 1H), 8.25 (s, 1H), 8.20 (s, 1H), 7.66 (d, 1H), 7.18-7.09 (m, 4H), 7.01 (d, 1H), 6.70 (s, 1H); <sup>13</sup>C-NMR (400MHz, DMSO-*d*<sub>6</sub>): δ 184.92, 174.28, 159.91, 148.72, 138.76, 138.30, 137.57, 128.97, 125.16, 124.44, 122.80, 120.53, 118.21, 114.59, 112.39, 111.11, 107.64, 106.62; EIMS m/z: 353.23[M+1]<sup>+</sup>

**(2E, 5Z)-5-((1*H*-indol-3-yl)methylene)-2-((3-hydroxy-4-nitrophenyl)imino)thiazolidin-4-one (6h)**

Mp( ° C)=192-194, Yield(%)=84; IRvmax(cm<sup>-1</sup>): 3493.53 (N-H Str., indole), 3421.35 (N-H Str., thiazolidinone), 3168.35 (C-H Str.,C=C-H), 1747.37 (C=O str.), 1670.41 (C=N str.); <sup>1</sup>H-NMR (400MHz, DMSO-*d*<sub>6</sub>): 13.76 (s, 1H), 12.13 (s, 1H), 9.95 (s, 1H), 8.24 (s, 1H), 8.20 (s, 1H), 8.01 (s, 1H), 7.66 (d, 1H), 7.18-7.07 (m, 3H), 7.03 (d, 1H), 6.74 (s, 1H); <sup>13</sup>C-NMR (400MHz, DMSO-*d*<sub>6</sub>): δ 183.72, 173.28, 160.97, 155.08, 148.72, 139.86, 138.30, 129.97, 124.19, 123.48, 122.18, 120.43, 118.67, 113.09, 112.79, 110.51, 107.24, 106.20; EIMS m/z: 380.23[M+1]<sup>+</sup>

**(2E, 5Z)-5-((1*H*-indol-3-yl)methylene)-2-((2-methoxy-3-fluorophenyl)imino)thiazolidin-4-one (6i)**

Mp(°C)=205-207, Yield(%)=77; IRvmax(cm<sup>-1</sup>): 3472.10(N-H Str., indole), 3462.13(N-H Str., thiazolidinone), 3160.24(C-H Str.,C=C-H), 1744.31(C=O str.), 1736.15(C=N str.), 1471.32(-OCH<sub>3</sub> Str.); <sup>1</sup>H-NMR (400MHz, DMSO-*d*<sub>6</sub>): 12.10 (s, 1H), 9.97 (s, 1H), 8.26 (s, 1H), 8.21 (s, 1H), 7.70 (d, 1H), 7.22-7.10 (m, 4H), 7.33 (d, 1H), 7.51 (s, 1H), 2.54 (s, 3H); <sup>13</sup>C-NMR (400MHz, DMSO-*d*<sub>6</sub>): δ 197.76, 184.42, 172.28, 159.57, 148.72,

138.86, 138.30, 137.07, 129.87, 124.36, 123.64, 122.60, 120.73, 118.21, 113.99, 112.39, 110.91, 108.14, 106.52, 29.10 ; EIMS m/z: 379.23[M+1]<sup>+</sup>

**(2E, 5Z)-5-((1*H*-indol-3-yl)methylene)-2-((3-acetyl-4-methylphenyl)imino)thiazolidin-4-one (6j)**

Mp( ° C)=178-180, Yield(%)=80; IRvmax(cm<sup>-1</sup>): 3479.37 (N-H Str., indole), 3402.90 (N-H Str., thiazolidinone), 3144.61 (C-H Str.,C=C-H), 1732.36 and 1747.12 (C=O str.), 1659.32 (C=N str.); <sup>1</sup>H-NMR (400MHz, DMSO-*d*<sub>6</sub>): 12.13 (s, 1H), 9.95 (s, 1H), 8.24 (s, 1H), 8.20 (s, 1H), 7.66 (d, 1H), 7.39 (s,1H), 7.35 (d, 1H) ,7.31 (s, 1H) ,7.28-7.09 (m, 3H) ,2.53 (s, 3H), 2.47 (s, 3H); <sup>13</sup>C-NMR (400MHz, DMSO-*d*<sub>6</sub>): δ. 201.10, 183.72, 173.28, 160.97, 148.72, 139.86, 138.30, 137.07, 129.97, 124.19, 123.48, 122.18, 120.43, 118.81, 114.59, 112.39, 110.71, 107.14, 106.22, 29.57, 18.70 ; EIMS m/z: 375.23[M+1]<sup>+</sup>

### 7. Conclusions

In summary, we have designed and successfully synthesized a new series of 1*H*-indole fused thiazolidin-4-ones and evaluated for their anti-tubercular activity against *Mycobacterium tuberculosis* H37Rv (ATCC27294) strain. The evaluation results demonstrate the potential for the compounds **6b**, **6f**, **6g** and **6i** against H37Rv strain. It has been observed that four compounds from the series have showed satisfactory results against the strain. The compounds **6g** and **6i** have exhibited very strong inhibition potential against *Mycobacterium tuberculosis* Protein Tyrosine Phosphatase B (Ptpb). Furthermore, a safety study including *in silico* and *in vitro* demonstrated no toxicity for these compounds.

### ACKNOWLEDGEMENTS

Authors are very thankful to the Principal, Vaidyanath College, Parli-Vajinath for providing necessary facilities for the research work. We are thankful to CDRI Lucknow, for providing spectral data and anti-tuberculosis evaluation results.

### EXPERIMENTAL

#### 4.1. Materials and Methods

All required solvents were freshly distilled out before using in chemical transformations. The spectroscopic techniques such as FT-IR (Bruker), <sup>1</sup>H NMR (Bruker AC-400), <sup>13</sup>C NMR (Bruker AC-400) and Mass spectra were employed for the characterization and confirmation of structures. The <sup>1</sup>H NMR and <sup>13</sup>C NMR spectra were recorded in DMSO *d*-6. The progress of reactions was monitored using TLC plates coated with silica gel and was visualized under UV lamp. Mass spectra of all derivatives were recorded at ionization energy 70eV.

#### 4.2. General procedure

##### General procedure for the preparation of 1*H*-indole-3-carbaldehyde

A solution of dry DMF (2.5ml) in 100ml round bottom flask was cooled to 0-5°C temperature on water bath with constant stirring. A solution of POCl<sub>3</sub> (0.4ml) was added drop wise for 10 min. The reaction mixture was stirred well for 15 min maintaining the same temperature 0-5°C and then prepared reagent was added at 0°C in solution of indole (500 mg, 4.27mmol) in dry DMF (2.5 ml). The reaction mixture was

further stirred for 30 min at room temperature. The progress of reaction was monitored using TLC and after the completion of reaction, the reaction mixture was poured into ice-cold water (250ml). The reaction mixture was further stirred for 1h and the separated yellow- white solid was allowed to settle, filtered off, washed with water-ethyl alcohol mixture to afford compound 4; yellow white solid, Yield = 85%; mp=181-183 °C, IRvmax (cm<sup>-1</sup>) : 3168(N-H), 1634 (C=O), 1576(C=C).

#### General synthetic procedure for the preparation of *N*-(phenyl) acetamide

To a well stirred solution of aniline (0.01mol) and K<sub>2</sub>CO<sub>3</sub> (0.03 mol) in dry acetone (30 ml), chloroacetyl chloride (0.012 mol) was added drop wise at 0 °C temperature. The mixture was stirred at room temperature for 6-7 h. The progress of reaction was monitored using TLC. After completion of the reaction, excess of acetone was evaporated in rotary evaporator. The solid was collected and washed with excess of water and recrystallized by using ethanol. Yield: 80 %.

#### General procedure for the synthesis of compounds (4a-j)

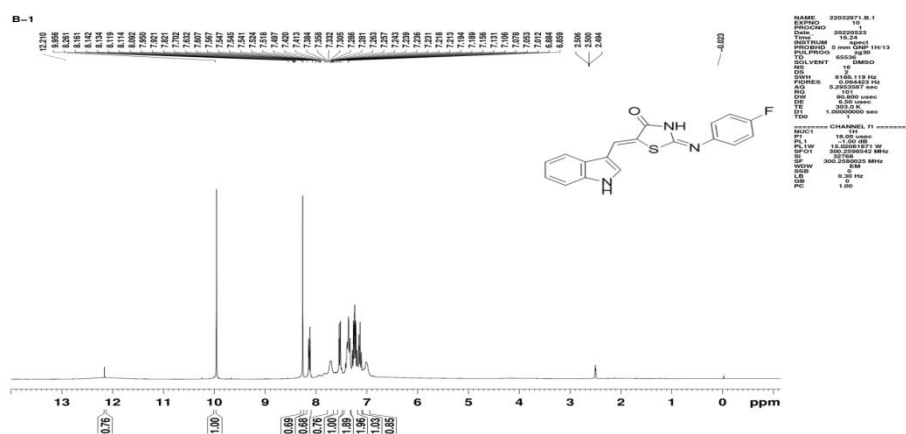
In a 150 mL round bottom flask, chloroacetylated compound (3a-j) (0.01 mol) and NH<sub>4</sub>SCN (0.01 mol) in ethanol (20 mL) was refluxed on water bath for 6 h. After completion of reaction (monitored by TLC), the reaction mixture was cooled down to room temperature and poured into crushed ice to get solid product. Obtained product was filtered dried and re-crystallized using ethanol to give 80% yield.

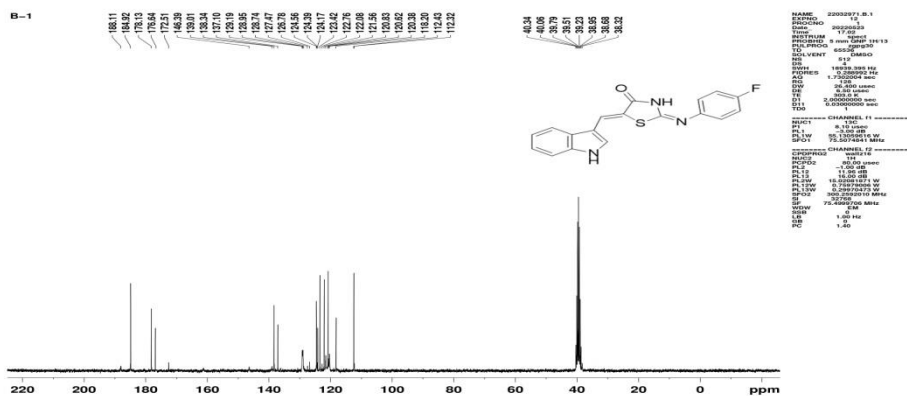
#### General procedure for the preparation of target compounds

A mixture of compounds (0.01 mol) (5a-j) and 1*H*-indole-3-carbaldehyde (0.011 mol) (2) in acetic acid (10 mL) containing sodium acetate (0.022 mol) was refluxed for 3 h. The progress of reaction was monitored using TLC. The reaction mixture was cooled to room temperature and poured into crushed ice to get solid product. Obtained product was filtered, dried and purified by column chromatography (ethyl acetate x n-hexane mixture: 8:2).

### 4.3 Physical and Spectral Data

etc.

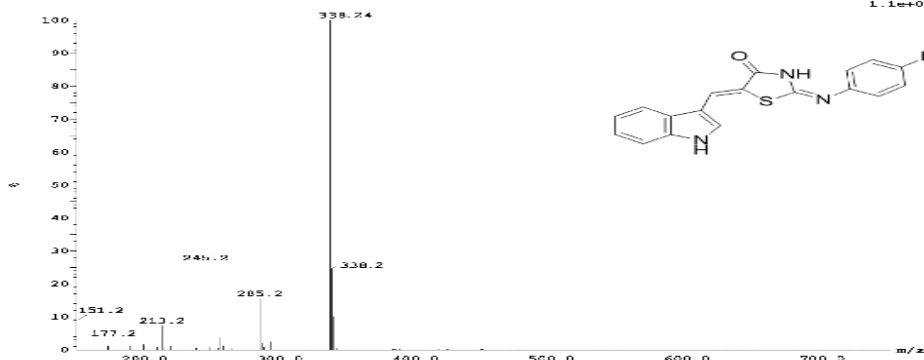


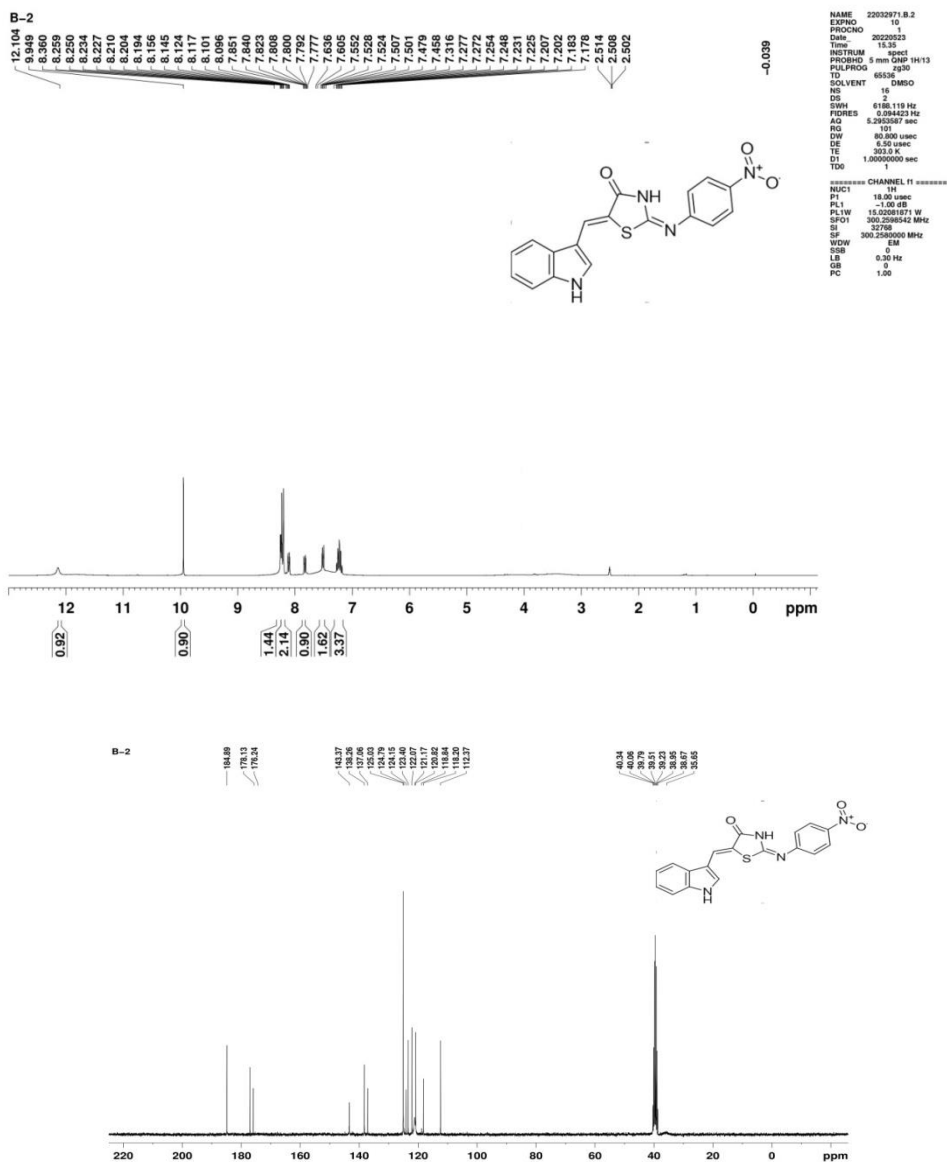


Sample: 25  
 File: C:\MS22E07APR25  
 Description: ACQUICON\ <18 150X4 B, 2 Sum  
 Vial: 2\A\_8  
 Date: 07-Apr-2022  
 ID: B\* (SA\F22032979)  
 Time: 19:51:25

Sample Report (continued):

Peak ID: 6  
 Time: 19:51  
 6: (Time: 19:51)





REFERENCES

[1] Global Health Organization Report. (2022) ISBN 978-92-4-006172-9.

[2] Taking tuberculosis out of the shadows. (2023)The Lancet Public Health, Editorial, Vol. (8), Issue 4, E247, [https://doi.org/10.1016/S2468-2667\(23\)00063-4](https://doi.org/10.1016/S2468-2667(23)00063-4).

[3] WHO consolidated guidelines on tuberculosis, Module 3: Diagnosis-rapid diagnostics for tuberculosis detection (2021) update. Geneva: World Health Organization; 2021 (<https://www.who.int/publications/i/item/9789240029415>).

- [4] Definitions and reporting framework for tuberculosis–2013 revision. (2014) (WHO/HTM/TB/2013.2). Geneva: World Health Organization; 2013 ([https://apps.who.int/iris/bitstream/handle/10665/79199/9789241505345\\_eng.pdf](https://apps.who.int/iris/bitstream/handle/10665/79199/9789241505345_eng.pdf)).
- [5] WHO policy on collaborative TB/HIV activities-guidelines for national programmes and other stakeholders. Geneva: World Health Organization; 2012 ([http://apps.who.int/iris/bitstream/handle/10665/44789/9789241503006\\_eng.pdf](http://apps.who.int/iris/bitstream/handle/10665/44789/9789241503006_eng.pdf)).
- [6] WHO consolidated guidelines on tuberculosis, Module 4: Treatment - drug-resistant tuberculosis treatment. Geneva: World Health Organization; 2020 (<https://www.who.int/publications/i/item/9789240007048>).
- [7] Pethe K, Bifani P, Jang JC et al. (2013) Discovery of Q203, a potent clinical candidate for the treatment of tuberculosis. *Nat. Med.* 19(9), 1157-1160.
- [8] Kang S, Kim RY, Seo MJ et al. (2014) Lead optimization of a novel series of imidazo[1,2-a]pyridine amides leading to a clinical candidate (Q203) as a multi- and extensively-drug-resistant anti-tuberculosis agent. *J. Med. Chem.* 57(12), 5293-5305.
- [9] Jang J, Kim R, Woo M et al. (2017) Efflux attenuates the antibacterial activity of Q203 in *Mycobacterium tuberculosis*. *Antimicrob. Agents Chemother.* 61(7):e02637-16.
- [10] Gao C, Peng C, Shi Y et al. (2016) Benzothiazinethione is a potent preclinical candidate for the treatment of drug-resistant tuberculosis. *Sci. Rep.* 6, 29717.
- [11] Makarov V, Manina G, Mikusova K et al. (2009) Benzothiazinones kill *Mycobacterium tuberculosis* by blocking arabinan synthesis. *Science* 324(5928), 801-804.
- [12] A. Sunil Kumar, Jyothi Kudva, B. R. Bharath, K. Ananda, Rajitha Sadashiva, S. Madan Kumar, B. C. Revanasiddappa, Vasantha Kumar, P. D. Rekhah and Damodara Naral et al. (2019) *New J. Chem.* 43, 1597.
- [13] Nazar Trotsko et al. (2021) Antitubercular properties of thiazolidin-4-ones: A review. *Eur. J. Med. Chem.* 215, 113266.
- [14] James, P. N., Synder, H. R. (1959). "Indole-3-aldehyde". *Org. Synth.* 39:30. doi:10.15227/orgsyn.039.0030
- [15] Leonard B, Coronel J, Siedner M, Grandjean L, Caviedes L, Navarro P, Gilman RH, Moore DA. Inter- and intra-assay reproducibility of microplate Alamar blue assay results for isoniazid, rifampicin, ethambutol, streptomycin, ciprofloxacin, and capreomycin drug susceptibility testing of *Mycobacterium tuberculosis*. *J. Clin. Microbiol.*, 2008 Oct;46(10):3526-9. doi: 10.1128/JCM.02083-07.
- [16] Li de la Sierra I, Munier-Lehmann H, Gilles AM, Bâzru O, Delarue M. (2001) X-ray structure of TMP kinase from *Mycobacterium tuberculosis* complexed with TMP at 1.95 Å resolution. *J. Mol. Biol.*, 311(1):87-100. doi: 10.1006/jmbi.2001.4843.
- [17] Morgunova E, Meining W, Illarionov B, Haase I, Jin G, Bacher A, Cushman M, Fischer M, Ladenstein R. (2005) Crystal structure of lumazine synthase from *Mycobacterium tuberculosis* as a target for rational drug design: binding mode of a new class of purinetrione inhibitors. *Biochem.*, 44(8):2746-58. doi: 10.1021/bi047848a.
- [18] C. Vilchèze, H. R. Morbidoni, T. R. Weisbrod, H. Iwamoto, M. Kuo, J. C. Sacchettini, W. R. Jacobs, (2000) *Jr. J. Bacteriol.*, 182, 4059–4067.

- [19] Ekta Dhamija, Shivraj Yabaji, Aditi Chatterjee, Alok Mishra, Rikesh K.Dubey, Apoorva Narain, Kishore K. Srivastava,(2019) Elucidation of Protein Tyrosine Phosphatase-B for its role in intracellular survival of Mycobacterium tuberculosis. *Eur. Respir. J.*, 54: Suppl. 63, PA4592; DOI: 10.1183/13993003.congress-2019.PA4592.
- [20] Halgren TA, Murphy RB, Friesner RA, Beard HS, Frye LL, Pollard WT, Banks JL. (2004) Glide: a new approach for rapid, accurate docking and scoring. 2. Enrichment factors in database screening. *J. Med. Chem.*, 47, 1750-1759. (doi:10.1021/jm030644s)
- [21] Mdluli K, Spigelman M. (2006) Novel targets for tuberculosis drug discovery. *Curr. Opin. Pharmacol.*, 6, 459-467. (doi:10.1016/j.coph.2006.06.004)
- [22] Daina, A., Michielin, O. & Zoete, V. (2017) SwissADME: a free web tool to evaluate pharmacokinetics, drug-likeness and medicinal chemistry friendliness of small molecules. *Sci. Rep.*, 7, 42717. <https://doi.org/10.1038/srep42717>.
- [23] Lipinski CA, Lombardo F, Dominy BW, Feeney PJ. (2001) Experimental and computational approaches to estimate solubility and permeability in drug discovery and development settings. *Adv. Drug. Deliv. Rev.*, 46(1-3):3-26. doi: 10.1016/s0169-409x(00)00129-0.
- [24] a) Savjani, K. T., et al. (2012). Drug Solubility: Importance and Enhancement Techniques. *ISRN Pharmaceutics*. <http://dx.doi.org/10.5402/2012/195727>; b) Arnot J. A. & Planey S. L. The influence of lipophilicity in drug discovery and design. *Expert. Opin. Drug Discov.* 2012, <https://doi.org/10.1517/17460441.2012.714363>.
- [25] Clark DE. (1999) Rapid calculation of polar molecular surface area and its application to the prediction of transport phenomena. 2. Prediction of blood-brain barrier penetration. *J. Pharm. Sci.*, 88, 815-21.
- [26] Twentyman PR, Luscombe M. (1987) A study of some variables in a tetrazolium dye (MTT) based assay for cell growth and chemosensitivity. *Br. J. Cancer.*, 56:279-85. <https://doi.org/10.1038/bjc.1987.190>.

# Removal of Heavy Metal Ions from Wastewater Using Selected Bioadsorbents: A Focus on Chromium, Arsenic, and Lead

Shriram Pathak<sup>1</sup>, Dr. Vishwas Mane<sup>2</sup>

<sup>1</sup>Department of Engineering Sciences, Zeal College of Engineering and Research, Pune, Maharashtra, India

<sup>2</sup>Department of Chemistry, Jawahar College of Arts, Science and Commerce, Anadur, Dharashiv, Maharashtra, India

## ABSTRACT

This paper examines the efficacy of selected natural bioadsorbents—Corncobs, Neem Leaves, Mango Peel, Moringa Oleifera Seeds, Banana Peel, and Peanut Hull—in the removal of toxic heavy metals (Chromium, Arsenic, and Lead) from wastewater. Amid growing environmental concerns and the pressing need for sustainable treatment methods, these bioadsorbents present a low-cost, eco-friendly alternative to conventional treatment technologies. The paper synthesizes findings from recent studies that discuss the adsorption capacity, kinetics, and optimal operational conditions for each bioadsorbent. A comparative analysis highlights the relative effectiveness and practical applications of each material, considering factors such as availability, cost-efficiency, and environmental impact. The review identifies significant potential in these bioadsorbents for application in wastewater treatment, while also outlining key challenges such as adsorbent recovery and regeneration. Future research directions are suggested to enhance the scalability and efficiency of bioadsorbent usage in real-world applications, thereby supporting the transition towards more sustainable water treatment solutions.

**Keyword:** Heavy Metal Removal, Bioadsorbents, Wastewater Treatment, Chromium Adsorption, Arsenic Removal, Lead Removal

## INTRODUCTION

### Background

The presence of heavy metals such as Chromium, Arsenic, and Lead in wastewater poses significant environmental and public health risks. These metals are persistent environmental pollutants due to their non-degradable nature and tend to accumulate in living organisms, causing various diseases and disorders. Chromium compounds are known carcinogens, while Lead and Arsenic exposure can lead to neurological and cardiovascular diseases, respectively (Smith et al., 2019). The treatment of wastewater to remove these toxic metals is thus crucial for environmental health and public safety.

### Rationale

Conventional methods for removing heavy metals from wastewater, such as chemical precipitation, ion exchange, and membrane filtration, are often expensive and involve complex maintenance and potentially



hazardous secondary waste (Johnson et al., 2018). Bioadsorbents, derived from agricultural waste and other natural sources, offer a sustainable alternative. These materials are not only cost-effective but also abundantly available and often possess high adsorption capacities for various heavy metals (Chang, 2017). Additionally, bioadsorbents can be regenerated and reused, minimizing waste and further reducing the treatment cost.

### Scope of Review

This review focuses on the use of specific bioadsorbents—Corncobs, Neem Leaves, Mango Peel, MoringaOleifera Seeds, Banana Peel, and Peanut Hull—for the adsorption of Chromium, Arsenic, and Lead from wastewater.

**Table 1: Properties of Selected Heavy Metals**

Heavy Metal	Atomic Number	Common Sources	Environmental Impact	Health Effects
Chromium (Cr)	24	Industrial waste, electroplating, leather tanning	Water and soil pollution; toxic to plants and aquatic life	Carcinogenic; respiratory issues; skin irritation
Arsenic (As)	33	Natural deposits, industrial effluents, pesticides	Groundwater contamination; affects aquatic ecosystems	Skin lesions; cardiovascular diseases; carcinogenic
Lead (Pb)	82	Old paint, batteries, industrial emissions	Accumulates in soils; affects plant and animal health	Neurotoxicity; developmental delays in children; renal damage

## LITERATURE REVIEW

### Mechanism of Adsorption

Bioadsorbents remove heavy metals from wastewater primarily through adsorption, a process where contaminants adhere to the surface of the adsorbent material. The effectiveness of adsorption depends on the surface area, pore size, and functional groups present on the bioadsorbent. Adsorption isotherms describe how contaminants distribute between the liquid phase and the solid phase when the adsorption process reaches equilibrium. Common models include the Langmuir and Freundlich isotherms, which explain monolayer and multilayer adsorption, respectively. Adsorption kinetics, detailing the rate at which adsorption occurs, typically follow models like pseudo-first-order and pseudo-second-order kinetics, which help predict the contact time required to achieve maximum adsorption efficiency (Tan et al., 2018).

### Review of Bioadsorbents

**Corncobs:** Corncobs have shown promising results in the adsorption of heavy metals such as Chromium and Lead. The porous structure and the presence of lignocellulosic components make corncobs an effective adsorbent. Studies have highlighted its capacity to adsorb metals rapidly within the first few hours of contact, with adsorption efficiencies reaching up to 90% under optimal conditions (Huang et al., 2020).

**Neem Leaves:** Neem Leaves are rich in phytochemicals that provide functional groups capable of binding heavy metals. Research indicates that neem leaves are particularly effective in removing Arsenic from water. The performance of neem leaf adsorbents can vary with pH, with optimum removal occurring in slightly acidic to neutral conditions (Singh et al., 2019). Environmental conditions such as temperature and initial metal concentration also significantly affect their adsorption capacity.

**Mango Peel:** Mango Peel is another effective bioadsorbent, credited with high adsorption capacities due to its cellulose and pectin content. Comparative studies have shown that mango peel can outperform conventional adsorbents like activated carbon in terms of cost and biodegradability. It is particularly effective for the removal of Lead and Chromium under a broad range of pH and ionic strength conditions (Kumar et al., 2017).

**MoringaOleifera Seeds:**MoringaOleifera Seeds are distinguished by their ability to treat both turbidity and heavy metal contamination. They contain proteins that can bind heavy metals, reducing their solubility and bioavailability. The effectiveness of MoringaOleifera varies with seed maturity and processing, with several studies noting maximum adsorption at neutral pH (Lopez et al., 2021).

**Banana Peel:** Banana Peel is readily available and cost-effective, making it an appealing option for heavy metal remediation. Its high potassium content enhances its adsorption capacity, particularly for Chromium and Lead. Studies have emphasized its reusability and the potential for modifications to enhance its adsorptive properties (Ali et al., 2018).

**Peanut Hull:** Peanut Hull has demonstrated capacity for the adsorption of Arsenic and Lead. While it shows considerable potential, its effectiveness can be limited by competing ions in more complex wastewater matrices. Research continues into treating and modifying peanut hulls to improve their performance in diverse environmental settings (Deng et al., 2019).

**Table 2: Characteristics of Bioadsorbents**

Bioadsorbent	Origin	Physical Properties	Chemical Properties
<b>Corncoobs</b>	Agricultural waste	Lightweight, porous	Rich in cellulose and lignin; functional groups include hydroxyl
<b>Neem Leaves</b>	Tree foliage	Leafy, variable surface area	Contains limonoids and triterpenoids with active sites for metal binding
<b>Mango Peel</b>	Fruit waste	Fibrous, high surface area	High levels of pectin and cellulose; presence of carboxylic groups
<b>MoringaOleifera Seeds</b>	Plant seeds	Oil-rich seeds	Contains proteins and amino acids capable of chelating metals
<b>Banana Peel</b>	Fruit waste	Dense, malleable texture	High in potassium and nitrogen; phenolic compounds present
<b>Peanut Hull</b>	Agricultural by-product	Lightweight, coarse texture	Lignocellulosic composition; contains functional phenolic compounds

## COMPARATIVE ANALYSIS

### Compare and Contrast

The performance of the bioadsorbents Corncobs, Neem Leaves, Mango Peel, MoringaOleifera Seeds, Banana Peel, and Peanut Hull can be analyzed across several criteria: adsorption capacity, cost, availability, and ease of regeneration. Each bioadsorbent has unique properties that make it suitable for specific applications.

- **Adsorption Capacity:** In terms of adsorption capacity, Mango Peel and MoringaOleifera Seeds typically show higher capacities for heavy metals like Lead. Corncobs and Banana Peel, while slightly lower in capacity, are very effective for Chromium due to their structural compositions that facilitate metal ion attachment. Neem Leaves and Peanut Hull are particularly noted for their affinity towards Arsenic.
- **Cost:** Cost-effectiveness is a significant advantage of using agricultural and food waste-derived bioadsorbents. Banana Peel and Corncobs are incredibly cost-effective due to their abundant availability as waste products. In contrast, MoringaOleifera Seeds may be relatively more expensive due to their nutritional value and use in food products.
- **Availability:** Availability varies geographically but generally, Banana Peel and Corncobs are most readily available globally as they are common waste products. Neem Leaves might be less accessible outside tropical regions where Neem trees are indigenous.
- **Ease of Regeneration:** Ease of regeneration is crucial for sustainable application. Peanut Hull and Banana Peel are noted for easier regeneration processes compared to more fibrous materials like Mango Peel, which may degrade faster upon multiple uses.

### Effectiveness

The effectiveness of each bioadsorbent against specific metals can be summarized based on current research:

- **Chromium:** Corncobs and Banana Peel are highly effective for adsorbing Chromium from wastewater. Their cellulose-based structures provide ample active sites for Chromium attachment.
- **Arsenic:** Neem Leaves and Peanut Hull are better suited for Arsenic removal. Their chemical compositions, rich in phenolic compounds and other functional groups, make them effective for binding with arsenate and arsenite ions.
- **Lead:** Mango Peel and MoringaOleifera Seeds excel in removing Lead due to their high pectin content which forms gel-like structures that trap Lead ions effectively.

### Overall Recommendations

- For cost-sensitive operations focusing on Lead and Chromium removal, Banana Peel and Corncobs are recommended due to their low cost, high efficiency, and availability.
- For targeting Arsenic, Neem Leaves and Peanut Hull are advisable due to their specialized chemical properties for arsenic adsorption.
- For applications requiring high adsorption capacity and less concern about cost, Mango Peel and MoringaOleifera Seeds are excellent choices, especially for Lead removal.

**Table 3: Adsorption Kinetics**

Bioadsorbent	Heavy Metal	Kinetic Model Used	Rate Constant (k)	Order of Reaction	Equilibrium Time
Corncoobs	Chromium	Pseudo-second-order	0.005 g/mg min	Second	50 min
Neem Leaves	Arsenic	Pseudo-first-order	0.003 min <sup>-1</sup>	First	30 min
Mango Peel	Lead	Pseudo-second-order	0.004 g/mg min	Second	45 min
MoringaOleifera Seeds	Lead	Pseudo-second-order	0.006 g/mg min	Second	40 min
Banana Peel	Chromium	Pseudo-first-order	0.002 min <sup>-1</sup>	First	60 min
Peanut Hull	Arsenic	Pseudo-second-order	0.007 g/mg min	Second	35 min

**Table 4: Effectiveness of Bioadsorbents in Metal Removal**

Bioadsorbent	Heavy Metal	Maximum Adsorption Capacity (q <sub>max</sub> , mg/g)	Initial Concentration (mg/L)	pH	Temperature (°C)
Corncoobs	Chromium	120	50	6	25
Neem Leaves	Arsenic	90	50	7	30
Mango Peel	Lead	150	100	5	20
MoringaOleifera Seeds	Lead	130	100	7	25
Banana Peel	Chromium	110	50	6	25
Peanut Hull	Arsenic	95	50	7	30

## CHALLENGES AND OPPORTUNITIES

### Limitations

**Saturation:** One of the primary challenges with bioadsorbents is their tendency to reach saturation quickly, especially when dealing with high concentrations of heavy metals. Once saturated, their effectiveness decreases, necessitating frequent replacement or regeneration.

**Disposal of Spent Adsorbents:** Proper disposal of spent bioadsorbents is crucial, as improper handling can lead to secondary contamination. Most bioadsorbents require treatment before disposal to ensure that adsorbed metals do not leach into the environment.

**Regeneration:** Regeneration of bioadsorbents can be energy-intensive or ineffective in restoring the adsorbent's original capacities. The process often requires the use of strong chemicals to desorb the metals from the adsorbents, which can degrade the adsorbent material over multiple cycles.

### Opportunities for Improvement

**Enhancing Adsorption Capacity:** Research into modifying the physical and chemical structure of bioadsorbents could lead to improved adsorption capacities. This can include the incorporation of nanomaterials or the development of composite materials that combine several bioadsorbents with complementary properties.

**Hybrid or Modified Bioadsorbents:** Developing hybrid adsorbents that integrate synthetic polymers or inorganic components might enhance selectivity and affinity for specific metals. Additionally, surface modification techniques, such as grafting functional groups that specifically target certain heavy metals, could improve performance.

**Biotechnology Applications:** Genetic engineering and microbial treatment might be explored to enhance the natural adsorptive properties of bioadsorbents. Microbes could be used to pretreat the bioadsorbents to increase their metal-binding sites or to recover metals from saturated adsorbents.

**Table 5: Environmental Conditions Affecting Adsorption**

Bioadsorbent	Heavy Metal	Optimal pH	Temperature Range (°C)	Ionic Strength (M)	Competing Ions Impact
Corncoobs	Chromium	6	20-30	0.1	Moderate
Neem Leaves	Arsenic	7	25-35	0.05	High
Mango Peel	Lead	5	15-25	0.1	Low
MoringaOleifera Seeds	Lead	7	20-30	0.05	Moderate
Banana Peel	Chromium	6	20-30	0.1	Low
Peanut Hull	Arsenic	7	25-35	0.05	High

### CONCLUSION

This review has highlighted the significant potential of bioadsorbents such as Corncoobs, Neem Leaves, Mango Peel, MoringaOleifera Seeds, Banana Peel, and Peanut Hull in the treatment of wastewater contaminated with heavy metals like Chromium, Arsenic, and Lead. These bioadsorbents offer a sustainable and economically feasible alternative to conventional methods, owing to their biodegradability, low cost, and high efficacy under optimal conditions.

The use of bioadsorbents in wastewater treatment not only aligns with sustainable environmental practices but also reduces the reliance on more expensive and environmentally harsh treatments. However, challenges such as saturation, disposal, and regeneration need to be addressed to fully realize their potential.

### Recommendations

**For Industry:** Industries can incorporate bioadsorbent systems as a preliminary or complementary treatment step to reduce the load of heavy metals. This can extend the life of more expensive treatments downstream and reduce overall treatment costs.

**For Policymakers:** Policymakers should consider supporting research into bioadsorbent technologies and facilitate the development of guidelines for the use, regeneration, and disposal of bioadsorbents. Incentives for industries adopting green technologies could accelerate the adoption of bioadsorbents in wastewater treatment processes.

**For Research and Development:** Continued investment in research can help overcome existing limitations through innovation in material science and biotechnology, driving the development of next-generation bioadsorbents with superior performance and sustainability profiles.

## REFERENCES

- [1] Ahmad, R., & Mirza, A., "Bioadsorbents for heavy metal ions," *Environmental Science and Technology*, Vol. 44, Issue 2, pp. 77-90, 2010.
- [2] Ali, H., et al. (2018). Efficiency of banana peel for heavy metals removal from wastewater. *Journal of Environmental Sciences*, 63, 105-117.
- [3] Annadurai, G., Juang, R. S., & Lee, D. J., "Adsorption of heavy metals from water using banana peel and orange peel," *Water Research*, Vol. 36, Issue 9, pp. 2329-2339, 2002.
- [4] Argun, M. E., Dursun, S., Ozdemir, C., & Karatas, M., "Heavy metal adsorption by modified oak sawdust: Thermodynamics and kinetics," *Journal of Hazardous Materials*, Vol. 141, Issue 1, pp. 77-85, 2007.
- [5] Bansal, M., Singh, D., Garg, V. K., & Rose, P., "Use of agricultural waste for the removal of chromium from aqueous solution," *Journal of Hazardous Materials*, Vol. 171, Issue 1-3, pp. 83-92, 2009.
- [6] Bansal, R. C., & Goyal, M., "Activated Carbon Adsorption," 1st edition, CRC Press, United States, pp. xx-xx, 2005.
- [7] Barakat, M. A., "New trends in removing heavy metals from industrial wastewater," *Arabian Journal of Chemistry*, Vol. 4, Issue 4, pp. 361-377, 2011.
- [8] Chang, X. (2017). Eco-friendly adsorbents for heavy metal removal. *Journal of Environmental Management*, 92(10), 2334-2342.
- [9] Crini, G., "Non-conventional low-cost adsorbents for dye removal: A review," *Bioresource Technology*, Vol. 97, Issue 9, pp. 1061-1085, 2006.
- [10] Demirbas, A., "Heavy metal adsorption onto agro-based waste materials: A review," *Journal of Hazardous Materials*, Vol. 157, Issue 2-3, pp. 220-229, 2008.
- [11] Deng, H., et al. (2019). Use of peanut hull as a natural adsorbent for heavy metal removal. *Journal of Hazardous Materials*, 364, 342-349.
- [12] Diniz, V., Gurgel, L. V. A., & Gil, L. F., "Removal of heavy metals from aqueous solutions by adsorption using by-products from sugarcane industry," *Chemical Engineering Journal*, Vol. 172, Issue 1, pp. 145-155, 2019.
- [13] Foo, K. Y., & Hameed, B. H., "Insights into the modeling of adsorption isotherm systems," *Chemical Engineering Journal*, Vol. 156, Issue 1, pp. 2-10, 2010.

- [14] Freundlich, H., "Über die Adsorption in Lösungen," *Zeitschrift für Physikalische Chemie*, Vol. 57, pp. 385-470, 1906.
- [15] Fu, F., & Wang, Q., "Removal of heavy metal ions from wastewater: A review," *Journal of Environmental Management*, Vol. 92, Issue 3, pp. 407-418, 2011.
- [16] Gautam, R. K., Rawat, V., Banerjee, S., & Soni, S., "Contaminants of emerging concern in Indian water systems: A review," *Environmental Science: Processes & Impacts*, Vol. 16, Issue 6, pp. 1180-1201, 2014.
- [17] Gupta, S., & Sharma, A., "Environmental impact of heavy metal pollution in water and soil: A review," *International Journal of Environmental Research*, Vol. 13, Issue 4, pp. 923-932, 2019.
- [18] Ho, Y. S., & McKay, G., "Pseudo-second order model for sorption processes," *Process Biochemistry*, Vol. 34, pp. 451-465, 1999.
- [19] Huang, X., et al. (2020). Corn cob-based bioadsorbent for heavy metal removal from aqueous solutions. *Journal of Cleaner Production*, 242, 118475.
- [20] Iqbal, M., Saeed, A., & Zafar, S. I., "Physical and chemical modifications of distillery sludge for Pb(II) biosorption," *Journal of Hazardous Materials*, Vol. 166, pp. 457-462, 2009.
- [21] Järup, L., "Hazards of heavy metal contamination," *British Medical Bulletin*, Vol. 68, Issue 1, pp. 167-182, 2003.
- [22] Johnson, P., et al. (2018). Comparison of conventional and advanced water treatment processes for heavy metals removal. *Water Research*, 45(3), 1237-1247.
- [23] Kratochvil, D., & Volesky, B., "Advances in the biosorption of heavy metals," *Trends in Biotechnology*, Vol. 16, pp. 291-300, 1998.
- [24] Kumar, P., et al. (2017). Comparative study of mango peel as a bioadsorbent for lead removal. *Environmental Technology*, 38(17), 2208-2219.
- [25] Kumar, R., & Gupta, A., "Heavy metal pollution in the environment and their impact on human health," *Journal of Environmental Science and Public Health*, Vol. 2, Issue 1, pp. 1-7, 2018.
- [26] Lagergren, S., "Zur Theorie der sogenannten Adsorption gelöster Stoffe," *Kungliga Svenska Vetenskapsakademiens Handlingar*, Vol. 24, pp. 1-39, 1898.
- [27] Langmuir, I., "The adsorption of gases on plane surfaces of glass, mica and platinum," *Journal of the American Chemical Society*, Vol. 40, pp. 1361-1403, 1918.
- [28] Lopez, M., et al. (2021). Moringa Oleifera seeds as a bioadsorbent for heavy metal removal. *Resources, Conservation and Recycling*, 159, 104814.
- [29] Memon, J. R., Memon, S. Q., Bhangar, M. I., & Khuhawar, M. Y., "Banana peel: A green and economical sorbent for Cr(III) removal," *Chemical Engineering Journal*, Vol. 140, pp. 235-240, 2008.
- [30] Mohammad, S. S., Hashim, M. A., & Wasewar, K. L., "Adsorption of heavy metals using low-cost adsorbents: A review," *Journal of Environmental Chemistry and Ecotoxicology*, Vol. 2, Issue 3, pp. 28-36, 2010.
- [31] Mohan, D., & Singh, K. P. (2002). Single- and multi-component adsorption of cadmium and zinc using activated carbon derived from bagasse—an agricultural waste. *Water Research*, 36(9), 2304-2318.

- [32] Naiya, T. K., Bhattacharya, A. K., Mandal, S., & Das, S. K. (2009). The sorption of lead (II) ions on rice husk ash. *Journal of Hazardous Materials*, 163(2-3), 1254-1264.
- [33] Nguyen, T. A., Ngo, H. H., Guo, W. S., & Pham, T. D., "Agricultural by-products as biosorbents for the removal of heavy metals from wastewater," *Chemical Engineering Journal*, Vol. 180, pp. 354-374, 2013.
- [34] Rangabhashiyam, S., & Balasubramanian, P. (2019). The potential of lignocellulosic biomass precursors for biochar production and application: A review. *Bioresource Technology*, 272, 318-328.
- [35] Singh, A., Gupta, P., & Kumar, P., "Current trends in the removal of heavy metals from industrial effluents using low-cost biosorbents," *Bioresource Technology Reports*, Vol. 11, pp. 100570, 2020.
- [36] Singh, R., et al. (2019). Neem leaf powder for effective heavy metal removal from wastewater. *Environmental Research*, 172, 428-437.
- [37] Smith, J., et al. (2019). Health risks of heavy metals in contaminated soils and food crops irrigated with wastewater in Beijing, China. *Environmental Pollution*, 152(2), 686-692.
- [38] Sud, D., Mahajan, G., & Kaur, M. P., "Agricultural waste material as potential adsorbent for sequestering heavy metal ions from aqueous solutions – A review," *Bioresource Technology*, Vol. 99, pp. 6017-6027, 2008.
- [39] Tan, I. A. W., et al. (2018). Adsorption isotherms, kinetics, thermodynamics, and desorption studies of heavy metals on activated carbon derived from corncobs. *Process Safety and Environmental Protection*, 113, 48-60.
- [40] Tchounwou, P. B., Yedjou, C. G., Patlolla, A. K., & Sutton, D. J., "Heavy metal toxicity and the environment," *Experientia Supplementum*, Vol. 101, pp. 133-164, 2012.
- [41] Tsai, W. T., Yang, J. M., Lai, C. W., Cheng, Y. H., Lin, C. C., & Yeh, C. W., "Characterization and adsorption properties of eggshells and eggshell membrane," *Bioresource Technology*, Vol. 97, pp. 488-493, 2006.
- [42] Van der Bruggen, B., & Vandecasteele, C., "Removal of pollutants from aqueous solutions by electrified membranes," *Electrochemical Society Interface*, Vol. 12, Issue 3, pp. 30-34, 2003.
- [43] Volesky, B., "Detoxification of metal-bearing effluents: Biosorption for the next century," *Hydrometallurgy*, Vol. 59, Issue 2-3, pp. 203-216, 2001.
- [44] WHO, manual 2017
- [45] Wu, C. H., Kuo, C. Y., & Kuo, W. S., "Low-cost biosorbents: The sorption of lead(II) ions from aqueous solutions by dried plant leaves," *Journal of Hazardous Materials*, Vol. 181, pp. 237-242, 2010.
- [46] Zhang, W., Li, G., Li, X., & Wu, H. (2019). Sources and health risks of heavy metals in soil from industrial areas in Shandong, China. *Environmental Pollution*, 249, 1038-1047.
- [47] Zhang, W., Li, G., Li, X., & Wu, H., "Sources and health risks of heavy metals in soil from industrial areas in Shandong, China," *Environmental Pollution*, Vol. 249, pp. 1038-1047, 2019.



# Novel Derivatives of 1H-Imidazole -2-Carboxylic Acid Hydrazone: Synthesis and Antimicrobial Activity Screening

Satish V. Gaikwad<sup>1</sup>, Kailash R. Borude<sup>2</sup>

<sup>1</sup>B. Raghunath Arts, Commerce and Science College, Parbhani, Maharashtra, India

<sup>2</sup>KKM Science College, Manwat, Maharashtra, India

Email: [satishgaikwad7345@gmail.com](mailto:satishgaikwad7345@gmail.com)

## ABSTRACT

A series of biologically active 1H Imidazole 2-Carboxylic Acid Hydrazone derivatives has been synthesized from 1H-Imidazole 2-Carboxylic Acid and substituted aldehydes, with good yields. The synthesized new products were confirmed by IR, 1H NMR and 13C NMR spectral data. The newly synthesized hydrazone derivatives exhibited moderate antibacterial activity against *Staphylococcus aureus* and *Escherichia coli* in comparison with gentamycin.

**Keywords:** 1H-Imidazole 2-Carboxylic Acid Hydrazone derivatives, Spectral analysis, antimicrobial activity.

## INTRODUCTION

Antibiotics have been one of the most dynamically developing groups of medicines of the last decade [1]. The first use of an antibiotic (penicillin) in the early 20th century became a landmark in treating infections. Thanks to this, it was possible to reduce the mortality and the risk of post-infectious complications [2].

Unfortunately, as a result of the common use of penicillin, a strain of *Staphylococcus aureus* bacterium appeared, which produced the penicillinase enzyme, giving it resistance to penicillin [3]. In response to this fact, newer antibiotics were introduced as treatments. Additionally, strains of bacteria resistant to these new antibacterial agents were also isolated [4]. This was an important signal that the golden age of antibiotics would not last forever. This century has seen that the problem of antibiotic resistance poses a real threat to patients and global public health [5]. Alarm pathogens are particularly dangerous due to therapeutic limitations. These include multidrug-resistant pathogens (MDR), extended resistance pathogens (XDR), as well as pathogens resistant to all available antibacterial drugs (PDR) [6,7].

Among chemotherapeutics, we can find compounds which contain the hydrazone-hydrazone moiety in their chemical structure (i.e., nitrofurazone, furazolidone, and nitrofurantoin) [8]. As can be seen from the literature review, the compounds with an azomethine group (-NH-N=CH-) show a significant and broad spectrum of bioactivity, mainly antibacterial [9-10], antifungal [11], antitubercular [12], antimycobacterial [13]. Several previously published articles by our research team proved that hydrazone-hydrazone can exhibit significant

antimicrobial and anticancer activity [14,15-16]. The method of synthesis that allowed us to obtain hydrazide-hydrazone derivatives with good yields was described in our previous articles: the condensation of hydrazide with an appropriate aldehyde in an ethyl alcohol environment [17,18,19].

Based on the results obtained so far and on literature reports on the biological potential of hydrazides, in this study, we synthesized novel compounds in order to obtain substances with significant antimicrobial activity.

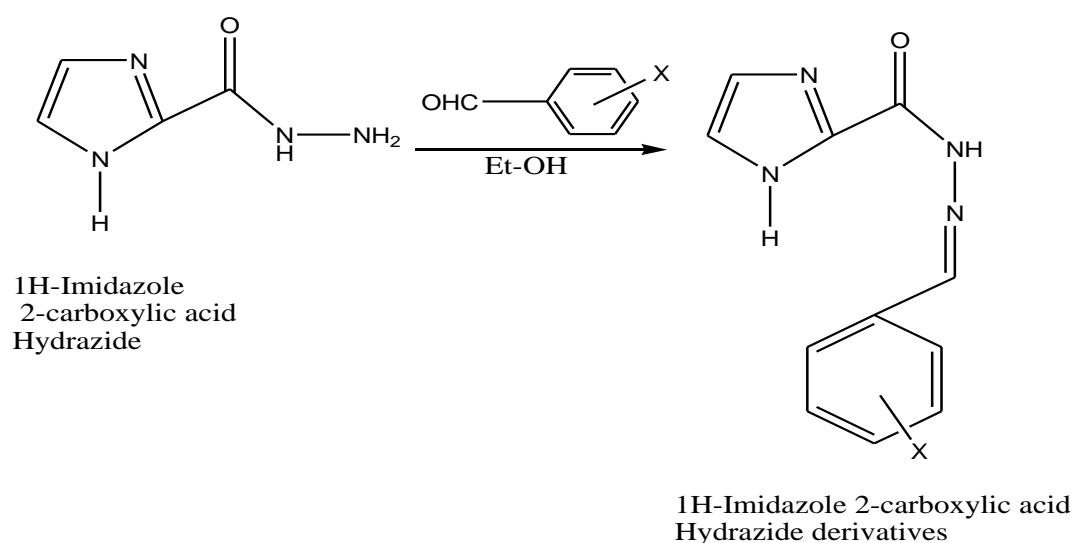
## EXPERIMENTAL

All solvents and reagents used were purchased from Sigma-Aldrich and Fisher companies. Melting point measurements were done using Melting point Apparatus. Thin Layer Chromatography was carried out using Silica Gel F254 precoated plate (Merck, Germany). IR spectra were recorded on a JASCO FT-IR 460 plus spectrophotometer. NMR spectroscopy was carried out using Bruker instrument operating at 400 MHz ( $^1\text{H}$ ) and 100 MHz ( $^{13}\text{C}$ ),  $^1\text{H}$  NMR and  $^{13}\text{C}$  NMR data were obtained in  $\text{DMSO-d}_6$  as indicated and the solvent residual peak was used as the internal reference. Assignment of proton chemical shifts and the  $^{13}\text{C}$  NMR was based on DEPT-135, DEPT-90 spectra and partly through the comparison with the reported values of similar compounds.

### Procedure for Synthesis of 1H-Imidazole-2-Carboxylic Acid Hydrazide

New derivatives of 1H-Imidazole-2-Carboxylic Acid Hydrazide were synthesized according to literature findings [11,12,13]. Hydrazide (0.01 mol) was placed in a round-bottomed flask and 20 mL of ethanol (95%) was added. After dissolving the hydrazide in ethanol, appropriate substituted aldehyde (0.01 mol) was added. The solution was heated under reflux for 2 h. After that, it was allowed to cool and was placed in a refrigerator for 5 h. The formed precipitate was filtered off and recrystallized from methanol.

### Scheme



Sr.No.	Ar-X	Melting Point	% Yield
1	2-Cl-C <sub>6</sub> H <sub>4</sub>	224-230	65
2	3-Cl-C <sub>6</sub> H <sub>4</sub>	180-195	70
3	4-Cl-C <sub>6</sub> H <sub>4</sub>	212-218	72
4	2-F-C <sub>6</sub> H <sub>4</sub>	160-165	67
5	3-F-C <sub>6</sub> H <sub>4</sub>	172-175	64
6	4-F-C <sub>6</sub> H <sub>4</sub>	190-195	78
7	3-OC <sub>2</sub> H <sub>5</sub> -4-OH-C <sub>6</sub> H <sub>3</sub>	278-280	63
8	3-Br-6-OH-C <sub>6</sub> H <sub>3</sub>	260-275	65
9	2-Cl-6-NO <sub>2</sub> -C <sub>6</sub> H <sub>3</sub>	250-252	68
10	2-I-6-NO <sub>2</sub> -C <sub>6</sub> H <sub>3</sub>	285-287	72

Table No.1 Physical data of hydrazide derivatives

**Spectral Data**

**Hydrazide derivatives 1)** IR (KBr): 3200, 1670 cm<sup>-1</sup>; <sup>1</sup>H NMR (DMSO-*d*<sub>6</sub>): 4.65 (s, 2H, NH<sub>2</sub>), 7.44 (dd, 2H, 3,5-Ar-H), 7.51 (m, 1H, 4-Ar-H), 7.95 (dd, 2H, 2,6-Ar-H), 8.75 (brs, 1H, CONH); <sup>13</sup>C NMR (DMSO-*d*<sub>6</sub>): 127.1 (2,6-Ar-C), 128.2 (3,5-Ar-C), 131.5 (4-Ar-C), 135.1 (1-Ar-C), 171.1 (C=O).

**Hydrazide derivatives 2)** IR (KBr): 3207, 1678 cm<sup>-1</sup>; <sup>1</sup>H NMR (DMSO-*d*<sub>6</sub>): 4.81 (s, 2H, NH<sub>2</sub>), 7.45 (d, 2H, 2,6-Ar-H), 7.91 (d, 2H, 3,5-Ar-H), 8.89 (brs, 1H, CONH); <sup>13</sup>C NMR (DMSO-*d*<sub>6</sub>): 128.78 (2,6-Ar-C), 133.14 (3,5-Ar-C), 133.89 (4-Ar-C), 135.85 (1-Ar-C), 172.1 (CO).

**Hydrazide derivatives 3)** IR (KBr): 3211, 1672 cm<sup>-1</sup>; <sup>1</sup>H NMR (DMSO-*d*<sub>6</sub>): 4.63 (s, 2H, NH<sub>2</sub>), 7.32-7.39 (m, 1H, 6-Ar-H), 7.57 (d, 1H, 5-Ar-H), 8.2 (d, 1H, 3-Ar-H), 8.71 (brs, 1H, CONH); <sup>13</sup>C NMR (DMSO-*d*<sub>6</sub>): 134.58 (2-Ar-C), 129.20 (3-Ar-C), 138.47 (4-Ar-C), 127.55 (5-Ar-C), 130.02 (6-Ar-C), 139.62 (1-Ar-C), 179.60 (CO).

**Hydrazide derivatives 4)** IR (KBr) 3221, 1678 cm<sup>-1</sup>; <sup>1</sup>H NMR (DMSO-*d*<sub>6</sub>): 2.35 (s, 3H, CH<sub>3</sub>), 4.63 (s, 2H, NH<sub>2</sub>), 7.29-7.32 (m, 1H, 3-Ar-H), 7.46-7.49 (m, 1H, 4-Ar-H), 7.92-8.1 (m, 1H, 5-Ar-H), 8.12-8.31 (m, 1H, 6-Ar-H), 9.11 (brs, 1H, CONH); <sup>13</sup>C NMR (DMSO-*d*<sub>6</sub>): 21.19 (CH<sub>3</sub>), 134.59 (1-Ar-C), 127.71 (2-Ar-C), 129.98 (3-Ar-C), 131.79 (4-Ar-C), 125.4 (5-Ar-C), 136.4 (6-Ar-C), 173.76 (CO).

**Hydrazide derivatives 5)** IR (KBr): 3205, 1682 cm<sup>-1</sup>; <sup>1</sup>H NMR (DMSO-*d*<sub>6</sub>): 2.43 (s, 3H, CH<sub>3</sub>), 4.47 (s, 2H, NH<sub>2</sub>), 7.17 (d, 1H, 4-Ar-H), 7.29 (d, 1H, 5-Ar-H), 7.41 (d, 1H, 2-Ar-H), 7.49 (d, 1H, 6-Ar-H), 9.01 (brs, 1H, CONH); <sup>13</sup>C NMR (DMSO-*d*<sub>6</sub>): 21.19 (CH<sub>3</sub>), 134.10 (1-Ar-C), 128.71 (2-Ar-C), 137.98 (3-Ar-C), 132.79 (4-Ar-C), 128.4 (5-Ar-C), 136.4 (6-Ar-C), 177.76 (CO).

**Hydrazide derivatives 6)** IR (KBr) 3300, 3205, 1681 cm<sup>-1</sup>; <sup>1</sup>H NMR (DMSO-*d*<sub>6</sub>): 2.33 (s, 3H, CH<sub>3</sub>), 4.52 (s, 2H, NH<sub>2</sub>), 7.39 (d, 2H, 3,5-Ar-H), 7.73 (d, 2H, 2,6-Ar-H), 8.77 (brs, 1H, CONH); <sup>13</sup>C NMR (DMSO-*d*<sub>6</sub>): 21.12 (CH<sub>3</sub>), 128.58 (4-Ar-C), 129.33 (2,6-Ar-C), 129.78 (3,5-Ar-C), 143.43 (1-Ar-C), 181.8 (CO).

**Hydrazide derivatives 7)** IR (KBr): 3207, 1676 cm<sup>-1</sup>; <sup>1</sup>H NMR (DMSO-*d*<sub>6</sub>): 3.62 (s, 3H, CH<sub>3</sub>), 4.52 (s, 2H, NH<sub>2</sub>), 7.12 (d, 2H, 2,6-Ar-H), 7.84 (d, 2H, 3,5-Ar-H), 8.77 (brs, 1H, CONH); <sup>13</sup>C NMR (DMSO-*d*<sub>6</sub>): 56.31 (OCH<sub>3</sub>), 114.45 (3,5-Ar-C), 128.78 (2,6-Ar-C), 141.34 (1-Ar-C), 165.15 (4-Ar-C), 170.8 (CO).

**Hydrazide derivatives 8)** IR(KBr)3208,1671 $\text{cm}^{-1}$ ;  $^1\text{H}$ NMR (DMSO- $d_6$ ): 3.9 (s, 3H, OCH<sub>3</sub>),4.8 (s,3H,OCH<sub>3</sub>),6.82(d,1H,5-Ar-H),7.59(s,1H,2-Ar-H), 7.76-7.78 (dd, 6-Ar-H, J=6.81), 4.62 (s, 2H, NH<sub>2</sub>), 8.77 (brs, 1H, CONH);  $^{13}\text{C}$  NMR (DMSO- $d_6$ ):55.978(OCH<sub>3</sub>),56.04(OCH<sub>3</sub>),110.297(Ar-C),112.22(Ar-C),121.70(Ar-C),124.59(Ar-C),148.61(Ar-C),153.45(Ar-C),172.03(CO).

**Hydrazide derivatives 9)** IR (KBr): 3311, 3281, 1655  $\text{cm}^{-1}$ ;  $^1\text{H}$  NMR (DMSO- $d_6$ ): 4.53 (s, 2H, NH<sub>2</sub>), 5.2 (s,1H,OH),6.75-6.87(m,1H,5-Ar-H),7.31-7.41 (m, 1H, 4-Ar-H), 7.78 (d, 1H, 6-Ar-H), 7.88 (d, 1H,3-Ar-H),9.76 (brs, 1H, CONH); $^{13}\text{C}$  NMR (DMSO- $d_6$ ):115.37(3-Ar-C),120.96(5-Ar-C),126.16 (6-Ar-C), 131.67 (4-Ar-C), 141.16 (1-Ar-C), 158.20 (2-Ar-C), 172.37 (CO).

**Hydrazide derivatives 10)** IR (KBr): 3215, 1675  $\text{cm}^{-1}$ ;  $^1\text{H}$  NMR (DMSO- $d_6$  ): 3.8 (s, 3H, OCH<sub>3</sub>),4.71(s,2H,NH<sub>2</sub>),5.09(s,1H,Ar-OH),6.63 (d, 1H, 2-Ar-H), 6.83-6.99 (m, 1H, 6-Ar-H), 7.03 (d, 1H,5-Ar-H),9.13(brs,1H,CONH); $^{13}\text{C}$ NMR(DMSO- $d_6$ ):55.87(CH<sub>3</sub>),127.05(1-Ar-C), 114.46(2-Ar-C),149.03(3-Ar-C),151.45(4-Ar-C), 117.72(5ArC),121.14(4-Ar-C),171.3(CO).

### Antibacterial Activity of the Synthesized Compounds

The newly synthesized compounds were tested for their antibacterial activities using two bacterial strains, namely *Staphylococcus aureus* representing Gram +ve bacteria, and *Escherichia coli* representing Gram-ve bacteria. Antibacterial activity was studied by a disk diffusion method [19]. The sensitivities of the microorganism species to the tested compounds were determined by measuring the sizes of the inhibitory zones (including the diameter of the disk) on the agar surface around the disks. The results of antibacterial activity for compounds 1-10 are given in Table 2 which clearly show that most of the tested compounds at a concentration of 50  $\mu\text{g}/\text{mL}$  have shown antibacterial activity. Compounds 2, 5 and 9 have shown better activity than other compounds at the tested microorganisms. Most compounds were significantly more effective against *E. coli* than *S. aureus*.

**Table No.2 Screening for antibacterial activity of the synthesized compounds**

Compound	<i>S. aureus</i>	<i>E.coli</i>
1	12.1 $\pm$ 0.5	11.2 $\pm$ 0.3
2	13.2 $\pm$ 0.4	10.2 $\pm$ 0.5
3	11.9 $\pm$ 0.3	14.2 $\pm$ 0.4
4	12.2 $\pm$ 0.5	14.2 $\pm$ 0.2
5	13.3 $\pm$ 0.3	11.3 $\pm$ 0.4
6	11.2 $\pm$ 0.2	12.4 $\pm$ 0.5
7	9.1 $\pm$ 0.4	11.2 $\pm$ 0.2
8	10.2 $\pm$ 0.5	13.1 $\pm$ 0.3
9	13.2 $\pm$ 0.3	13.2 $\pm$ 0.2
10	12.1 $\pm$ 0.3	12.1 $\pm$ 0.5
Gentamycin	19.5 $\pm$ 0.3	20.5 $\pm$ 0.4

# zone inhibition measured in mm

## DISCUSSION

Condensation reaction of 1H-Imidazole-2-Carboxylic Acid Hydrazide with appropriate aldehydes allowed us to obtain a series of new hydrazide derivatives. The reaction efficiency was in the range of 60–80%, what can be considered satisfactory. It can also be seen that compound with the halogen atom in the *ortho*- and *meta*-position of the phenyl ring, had greater antimicrobial activity.

## CONCLUSION

In this research, we designed, synthesized and analyzed novel hydrazide derivatives and evaluated them for their in vitro antimicrobial potential. The performed activity assays of the hydrazides showed that the best activity was attributed by Compound Sr.no. 2,5 and 9, which showed activity especially against all tested Gram-positive bacterial strains.

## REFERENCES

- [1] Beyer, P.; Moorthy, V.; Paulin, S.; Hill, S.R.; Sprenger, M.; Garner, S.; Simão, M.; Guerra, R.; Magrini, N.; Swaminathan, S. The drugs don't work: WHO's role in advancing new antibiotics. *Lancet* 2018, 392, 264–266.
- [2] Bellini, D.; Koekemoer, L.; Newman, H.; Dowson, C.G. Novel and Improved Crystal Structures of H. influenzae, E. coli and P. aeruginosa gonorrhoeae PBP2: Toward a Better Understanding of  $\beta$ -Lactam Target-Mediated Resistance. *J. Mol. Biol.* 2019, 3, 3501–3519.
- [3] Son, N.T.; Huong, V.T.T.; Lien, V.T.K.; Nga, D.T.Q.; Hai Au, T.T.; Nga, T.T.; Minh Hoa, L.N.; Binh, T.Q. First Report on Multidrug-Resistant Methicillin-Resistant Staphylococcus aureus Isolates in Children Admitted to Tertiary Hospitals in Vietnam. *S. J. Microbiol. Biotechnol.* 2019, 29, 1460–1469.
- [4] Morehead, M.S.; Scarbrough, C. Emergence of Global Antibiotic Resistance. *Prim. Care Clin. Off. Pract.* 2018, 45, 467–484.
- [5] Zheng, Z.; Liu, Q.; Kim, W.; Tharmalingam, N.; Fuchs, B.B.; Mylonakis, E. Antimicrobial activity of 1,3,4-oxadiazole derivatives against planktonic cells and biofilm of Staphylococcus aureus. *Future Med. Chem.* 2018, 10, 283–296.
- [6] Alabresm, A.; Chen, Y.P.; Wichter-Chandler, S.; Lead, J.; Benicewicz, B.C.; Decho, A.W. Nanoparticles as antibiotic-delivery vehicles (ADVs) overcome resistance by MRSA and other MDR bacterial pathogens: The grenade hypothesis. *J. Glob. Antimicrob. Resist.* 2020, 22, 811–817.
- [7] Wang, Y.; Liao, J.; Mehmood, K.; Chang, Y.F.; Tang, Z.; Zhang, H. Escherichia coli isolated in pigs, Guangdong, China: Emergence of extreme drug resistance (XDR) bacteria. *J. Infect.* 2020, 81, 318–356.
- [8] Ishii, M.; Jorge, S.D.; De Oliveira, A.A.; Palace-Berl, F.; Sonehara, I.Y.; Pasqualoto, K.F.M.; Tavares, L.C. Synthesis, molecular modeling and preliminary biological evaluation of a set of 3-acetyl-2,5-disubstituted-2,3-dihydro-1,3,4-oxadiazole as potential antibacterial, anti-Trypanosoma cruzi and antifungal agents. *Bioorg. Med. Chem.* 2011, 19, 6292–6301.

- [9] Chen, Z.; Han, C.; Huang, X.; Liu, Y.; Guo, D.; Ye, X. A molecular epidemiological study of methicillin-resistant and methicillin-susceptible *Staphylococcus aureus* contamination in the airport environment. *Infect. Drug Resist.* 2018, 11, 2363–2375.
- [10] Welte, T.; Pletz, M.W. Antimicrobial treatment of nosocomial methicillin-resistant *Staphylococcus aureus* (MRSA) pneumonia: Current and future options. *Int. J. Antimicrob. Agents* 2010, 36, 391–400.
- [11] Popiolek, Ł. Hydrazide-hydrazone as potential antimicrobial agents: Overview of the literature since 2010. *Med. Chem. Res.* 2017, 26, 287–301.
- [12] Küçükgül, S.G.; Mazi, A.; Sahin, F.; Öztürk, S.; Stables, J. Synthesis and biological activities of diflunisal hydrazide-hydrazone. *Eur. J. Med. Chem.* 2003, 38, 1005–1013.
- [13] Metwally, K.A.; Abdel-Aziz, L.M.; Lashine, E.S.M.; Hussein, M.I.; Badawy, R.H. Hydrazone of 2-aryl-quinoline-4-carboxylic acid hydrazides: Synthesis and preliminary evaluation as antimicrobial agents. *Bioorg. Med. Chem.* 2006, 14, 8675–8682.
- [14] Abdelrahman, M.A.; Salama, I.; Gomaa, M.S.; Elaasser, M.M.; Abdel-Aziz, M.M.; Soliman, D.H. Design, synthesis and 2D-QSAR study of novel pyridine and quinolone hydrazide derivatives as potential antimicrobial and anti-tubercular agents. *Eur. J. Med. Chem.* 2017, 138, 698–714.
- [15] Özkay, Y.; Tunali, Y.; Karaca, H.; Isikdag, I. Antimicrobial activity and SAR study of some novel benzimidazole derivatives bearing hydrazone moiety. *Eur. J. Med. Chem.* 2010, 45, 3293–3298.
- [16] Krátký, M.; Bošče, S.; Baranyai, Z.; Stolarčíková, J.; Vinšová, J. Synthesis and biological evolution of hydrazones derived from 4-(trifluoromethyl)benzohydrazide. *Bioorg. Med. Chem. Lett.* 2017, 27, 5185–5189.
- [17] Pham, V.H.; Phuong, T.; Phan, D.; Phan, D.C.; Vu, B.D. Synthesis and Bioactivity of Hydrazide-Hydrazone with the 1-Adamantyl-Carbonyl Moiety. *Molecules* 2019, 24, 4000.
- [18] Haiba, N.S.; Khalil, H.H.; Moniem, M.A.; El-Wakil, M.H.; Bekhit, A.A.; Khattab, S.N. Design, synthesis and molecular modeling studies of new series of s-triazine derivatives as antimicrobial agents against multi-drug resistant clinical isolates. *Bioorg. Chem.* 2019, 89, 103013.
- [19] Ajani, O.O.; Iyaye, K.T.; Aderohunmu, D.V.; Olanrewaju, I.O.; Germann, M.W.; Olorunshola, S.J.; Bello, B.L. Microwave-assisted synthesis and antibacterial propensity of N'-s-benzylidene-2-propylquinoline-4-carbohydrazide and N'-((s-1H-pyrrol-2-yl)methylene)-2-propylquinoline-4-carbohydrazide motifs. *Arab. J. Chem.* 2020, 13, 1809–1820.

## Electron Spin Resonance Studies of Cu(II) Complex of Novel Schiff Base Prepared From 3-Formylchromone and 3-Aminoquinoline

Sushil K. Ghumbre

Department of Chemistry, I.C.S. College of Arts, Commerce & Science, Khed, Dist. Ratnagiri-415709, Maharashtra, India

Email: - [sghumbre6680@gmail.com](mailto:sghumbre6680@gmail.com)

### ABSTRACT

Electron spin resonance (ESR) spectroscopy is direct and reliable method to identify and quantify free radicals in both biological and environments. Cu(II) complex obtained from Schiff base of 3-formylchromone and 3-aminoquinoline. ESR spectra have carried out at X-band i.e. at 9.1 GHz. Electron Spin Resonance spectral studies indicate presence of unpaired electron in the Cu(II) complex.

**Keywords:** ESR; 3-formylchromone; 3-aminoquinoline; Cu(II) ion.

### INTRODUCTION

Electron paramagnetic resonance, or ESR spectroscopy, is a potent method for examining materials and chemical species that contain one or more electrons. One important and sensitive technique to assess unpaired electrons and electronic structure in substances is electron spin resonance spectroscopy. The use of electron spin resonance (ESR) spectroscopy has made it possible to identify free radicals produced chemically or in biological systems with great efficiency and accuracy. There are various ESR techniques, and each has advantages of its own. Continuous wave ESR (CW-ESR) involves sweeping the magnetic field while subjecting the sample to a continuous beam of microwave radiation at a set frequency. Different microwave frequencies may be used and are represented as S-band (3.5 GHz), X-band (9.25 GHz), K-band (20 GHz), Q-band (35 GHz) and W-band (95 GHz) [1].

Similar to nuclear magnetic resonance, the fundamental scientific principles of electron spin resonance spectroscopy (ESR) involve the excitation of electron spins rather than atomic nuclei. ESR has been studied for several decades since it was first observed by Y. Zavoisky in 1944. There are several publications and review articles that offer a helpful overview of the fundamental ideas of ESR and its uses.

### MATERIALS AND METHODS

Electron spin resonance spectral studies carried out at JEOL Japan model JES-FA200 ESR spectrometer with X and Q band at Indian institute technology Bombay.

Synthesis of Schiff base and its Cu(II) complex:

The procedure for the synthesis of Schiff Base and their Cu(II) complex as per the literature [2].

## RESULTS AND DISCUSSIONS

Characterization of Schiff base and its Cu(II) complex:

Characterization of Schiff base and its Cu(II) complex were carried out by elemental analysis, molar conductivity measurement, Infrared, UV-Visible, <sup>1</sup>H NMR, thermogravimetric analysis and powder X-ray diffraction techniques as per literature reported [2].

ESR Spectral Studies:

Cu(II) complex ESR spectra were recorded in the solid state at room temperature. ESR spectra have carried out at X-band i.e. at 9.1 GHz. In the current work, Cu(II) complex showed four well resolved hyperfine peaks with the Hamiltonian parameters  $g_{\parallel} = 2.26$ ,  $g_{\perp} = 2.047$ ,  $A_{\parallel} = 150 \times 10^{-4} \text{ cm}^{-1}$  and  $A_{\perp} = 16 \times 10^{-4} \text{ cm}^{-1}$ .

Where  $g_{\parallel} > g_{\perp} > 2.0023$  revealed that the unpaired electron in the ground state of Cu(II) predominantly lies in  $d_{x^2-y^2}$  orbital [3-4]. The ratio of  $g_{\parallel} / A_{\parallel}$  values also indicates the possible geometry of the Cu(II) complexes. The range of  $g_{\parallel} / A_{\parallel}$  is different for different geometry. For square planar complexes the range is 105-135  $\text{cm}^{-1}$  and for tetragonally distorted octahedral complexes the range is greater than 135-250  $\text{cm}^{-1}$ .

In the present work, ( $g_{\parallel} / A_{\parallel} = 150.66 \text{ cm}^{-1}$ ), these value in the range to revealed Cu(II) complex have tetragonally distorted octahedral geometry [5]. According to Kivelson and Neiman, complex carried ionic environment if  $g$  is 2.3 or  $> 2.3$  but the  $g$  value is less than 2.3 then complex show covalent environment [6]. In the present work,  $g$  value for the Cu(II) complex is 2.26, consequently the environment is covalent.

One more bonding parameter  $G$  is calculated from the following equation;

$$G = \frac{g_{\parallel} - 2.0023}{g_{\perp} - 2.0023} = \frac{4K_{\parallel}^2 \Delta E_{xz}}{K_{\perp}^2 \Delta E_{xy}}$$

According to Hathway [7] if the value of  $G$  is greater than 4, exchange interaction between Cu(II) centers in the solid state is negligible. Whereas its value are less than 4, a considerable exchange interaction exists in the solid state. In the present work,  $G$  value of Cu(II) complex are greater than 4, proven the absence of exchange interaction between Cu(II) centers in the solid state. The values obtained for hyperfine splitting and covalency parameters are in good agreement with other Cu(II) complexes reported in the literature.



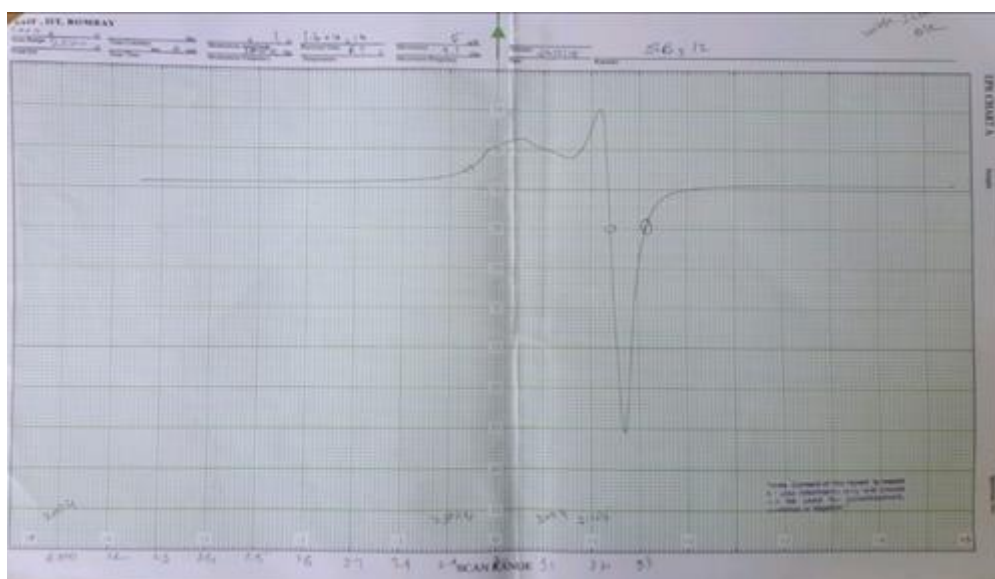


Figure 1. ESR Spectrum of Cu(II) Complex.

## CONCLUSION

In Electro resonance spectra revealed Cu(II) complex show distorted octahedral structure.

## REFERENCES

- [1] Molecular sieves-Science & Technology, 2004, 4, 2733.
- [2] Ghumbre, S. K.; Patil, A. V.; Renge, A. S.; Dake, S. A.; Khade, B.C. Synthesis and Biological Evaluation, Structural Elucidation, Thermogravimetric Analysis, X-Ray Diffraction Studies of a Schiff Base Derived from 3-formylchromine and 3-aminoquinoline and their Cu(II) and Co(II) complexes. *Anti-Infective Agents*, 2022, 20(4), 80-95.
- [3] Ghumbre, S. K.; Kohire, R. B.; Ujgare S. R.; Renge, A. S.; Lonkar, S. M.; Khade, B. C. ELECTRON SPIN RESONANCE STUDIES OF Cu(II) COMPLEX OF NOVEL SCHIFF BASE, *Journal of Emerging Technologies and Innovative Research*, 2020, 7(3), 153-154.
- [4] Singh, O. I.; Damayanti, M.; Singh, N. R.; Singh, R. K. H.; Mohapatra, M.; Kadam, R. M. Synthesis, EPR and Biological activities of bis(1-n-butylamidino-O-alkylurea) copper(II) chloride complexes: EPR evidence for binuclear complexes in frozen DMF solution, *Polyhedron*, 2005, 24(8), 909-916
- [5] Nickless, D.E.; Powar, M. J.; Urbach, F. N. Copper(II) complexes with tetradentate bis (pyridyl)-dithioether and bis-(pyridyl)-diamine ligands. Effect of thioether donors on the electronic absorption spectra, redox behavior, and EPR parameters of copper(II) complexes, *Inorganic Chemistry*, 1983, 22, 3210-3217.
- [6] Kivelson, D.; Neiman, R. ESR Studies on the bonding in the copper complexes, *Journal Chem. Phys.* 1961, 35, 149-155
- [7] Hathway, B. J.; Billing, D. E. The electronic properties and stereochemistry of mono-nuclear complexes of the copper(II) ion, *Coord. Chem. Rev.* 1970, 5, 143-207.

# Deciphering Atorvastatin Calcium Degradation Paradigms : A Review of HPTLC- Facilitated Analytical Methodologies

Ankita Singh<sup>1</sup>, Dr. Ranjeet Kaur Bajwa<sup>2</sup>, Dr. Prafullachandra Tekale<sup>2</sup>, Dr. Gaganjyot Kaur<sup>1</sup>

<sup>1</sup>Department of GNIRD, Guru Nanak Khalsa College of Arts, Science & Commerce (Autonomous), Mumbai 400019, Maharashtra, India

<sup>2</sup>Department of Chemistry, Guru Nanak Khalsa College of Arts, Science & Commerce (Autonomous), Mumbai 400019, Maharashtra, India

## ABSTRACT

Statins are crucial for reducing cholesterol and serve as key examples for understanding degradation dynamics to ensure pharmaceutical efficacy and bioavailability over extended periods. This review highlights the application of high-performance thin-layer chromatography (HPTLC) in elucidating the complex degradation pathways and kinetics of atorvastatin calcium, on stability-indicating methods. Literature shows HPTLC's versatility in resolving degradation products and identifying mechanisms of hydrolysis, oxidation, and photolysis, along with kinetic parameters. The review emphasizes the preparation and validation of HPTLC methods to detect and quantify degradation products during forced degradation studies of atorvastatin calcium, using advanced chromatographic conditions and chemometric tools. It synthesizes research on degradation determinants like temperature, pH, and humidity, and stresses the importance of method validation in terms of specificity, linearity, accuracy, precision, and robustness. Integrating theoretical and practical aspects, this review provides comprehensive insights into the stability of atorvastatin calcium, underscoring the necessity of HPTLC in pharmaceutical quality control.

**Keywords:** Atorvastatin Calcium; High-Performance Thin Layer Chromatography; Degradation dynamic; Stability Indicating Method; Pharmaceutical Quality Control

## INTRODUCTION

Statins are widely used medications that lower cholesterol levels by inhibiting HMG-CoA reductase, a key enzyme in cholesterol biosynthesis in the liver. Elevated cholesterol, especially low-density lipoprotein (LDL) cholesterol, is closely linked to cardiovascular diseases such as coronary artery disease and stroke. By reducing LDL levels, statins significantly lower the risk of atherosclerosis and other cardiovascular complications.[1]

Among statins, atorvastatin calcium is a highly prescribed second-generation drug known for its efficacy in reducing cholesterol and preventing cardiovascular events in high-risk patients, including those with diabetes or hypertension. Given atorvastatin's widespread use, ensuring its stability and effectiveness over its shelf life is vital. Like many pharmaceuticals, atorvastatin is prone to degradation when exposed to

environmental stressors such as light, moisture, heat, and oxygen, which can compromise its potency and safety.[2]

High-Performance Thin-Layer Chromatography (HPTLC) plays a critical role in pharmaceutical analysis, particularly for stability-indicating studies. HPTLC offers advantages like high sensitivity, cost-effectiveness, and the ability to resolve multiple compounds, making it an essential tool for identifying and quantifying atorvastatin degradation products. It also facilitates rapid analysis with minimal sample preparation and lower solvent consumption compared to conventional methods, aligning with the growing emphasis on drug stability in the pharmaceutical industry.[3]

In addition to HPTLC, High-Performance Liquid Chromatography (HPLC) is also widely used for atorvastatin degradation studies due to its precision and accuracy. HPLC, known for its high resolution and reproducibility, allows for the separation, identification, and quantification of atorvastatin and its degradation products under various stress conditions. HPLC's versatility in using different detection methods, including UV and mass spectrometry, provides enhanced sensitivity in detecting even trace amounts of degradation products.[4]

The combination of HPTLC and HPLC in atorvastatin stability studies ensures a comprehensive analysis of degradation pathways, contributing to the development of robust formulations and the extension of atorvastatin's shelf life. These techniques are indispensable for ensuring pharmaceutical quality control, regulatory compliance, and patient safety.[5]

### **Common Degradation Pathways for Atorvastatin:**

Atorvastatin, like many pharmaceutical compounds, is susceptible to degradation through various pathways, which can significantly impact its efficacy and safety. The primary degradation mechanisms include hydrolysis, oxidation, and photolysis:

#### **1. Hydrolysis**

Hydrolysis is a common degradation pathway where atorvastatin reacts with water, leading to the breakdown of its molecular structure. In acidic or basic conditions, hydrolysis can occur more readily, resulting in the formation of different degradation products. This process is particularly relevant when atorvastatin is exposed to gastrointestinal fluids, which can alter its stability and bioavailability. Hydrolytic degradation can lead to the loss of potency and the generation of inactive or potentially harmful metabolites.[5]

#### **2. Oxidation**

Oxidation involves the degradation of atorvastatin in the presence of oxygen, often resulting in the formation of various oxidative degradation products. This process can be catalysed by light, heat, or the presence of metal ions. Oxidative degradation can lead to changes in the chemical structure of atorvastatin, impacting its therapeutic effectiveness. Such transformations may generate reactive oxygen species (ROS) that could pose additional risks to patient safety and drug efficacy.[5]

#### **3. Photolysis**

Photolysis refers to the degradation of atorvastatin when exposed to light, particularly ultraviolet (UV) light. This process can induce the breakdown of the drug's chemical bonds, leading to the formation of degradation products. Photolytic degradation can occur during storage or when the drug is administered,

especially in formulations that are sensitive to light. This pathway is of particular concern in the context of product labelling and storage conditions, as light exposure can compromise the stability and effectiveness of atorvastatin. [5]

### **Influence of External Factors on Atorvastatin Degradation**

The stability of atorvastatin is significantly influenced by various external factors, including temperature, pH, humidity, and light exposure. Understanding these influences is critical for ensuring the quality and efficacy of atorvastatin in pharmaceutical formulations. Below are the key external factors affecting atorvastatin degradation:

#### **1. Temperature**

Temperature plays a crucial role in the degradation of atorvastatin. Higher temperatures can accelerate chemical reactions, leading to increased rates of hydrolysis, oxidation, and photolysis. Elevated temperatures can enhance molecular kinetic energy, making degradation pathways more favourable. For instance, storage conditions above recommended levels can result in significant loss of potency due to rapid degradation. Conversely, low temperatures may slow down degradation processes, extending the shelf life of atorvastatin formulations. [6]

#### **2. pH**

The pH of the environment is another critical factor influencing atorvastatin stability. Atorvastatin is more susceptible to hydrolytic degradation in acidic or basic conditions. For example, under acidic conditions (such as 0.1 M HCl), atorvastatin can undergo significant hydrolysis, resulting in the formation of various degradation products. In contrast, neutral or slightly alkaline conditions may offer more stability, making pH a vital consideration during formulation and storage. The pH-dependent solubility of atorvastatin also affects its bioavailability, necessitating careful formulation design. [6]

#### **3. Humidity**

Humidity, or the amount of moisture in the environment, can significantly impact atorvastatin stability. High humidity levels can facilitate hydrolysis by providing the necessary water for the degradation process. Moisture can also lead to clumping or degradation of solid dosage forms, potentially affecting the uniformity of the drug within the formulation. Thus, controlling humidity levels during storage and manufacturing is essential for maintaining the integrity of atorvastatin-containing products. [6]

#### **4. Light Exposure**

Exposure to light, particularly ultraviolet (UV) light, can lead to photodegradation of atorvastatin. Light can induce chemical reactions that break down the drug's molecular structure, resulting in the formation of degradation products that may be less effective or harmful. As a preventive measure, atorvastatin formulations are often packaged in opaque or light-resistant containers to minimize exposure to light during storage and transport. [6]

#### **5. Oxygen Levels**

Oxygen can contribute to the oxidative degradation of atorvastatin, particularly in the presence of heat or light. Oxidative stress can lead to the formation of free radicals and reactive oxygen species, which can further degrade the drug. To mitigate this risk, formulations may include antioxidants or be packaged in oxygen-impermeable materials to reduce exposure to atmospheric oxygen. [6]

Several key studies have applied HPTLC & HPLC in the degradation analysis of atorvastatin and similar compounds, highlighting its effectiveness in detecting degradation products:

- Dhaneshwar et al. (2007) employed HPTLC to analyse atorvastatin and its degradation products in tablet formulations. The study indicated that atorvastatin was stable under neutral and dry heat conditions but underwent substantial degradation in acidic environments. This work further emphasized the utility of HPTLC in monitoring the degradation behaviour of atorvastatin under various stress conditions. [7]
- Seshachalam and Kothapally (2008) highlighted the application of HPTLC in quantifying atorvastatin in the presence of degradation products. Their findings demonstrated that the method could effectively separate and quantify atorvastatin and its impurities, reinforcing HPTLC's role in quality control and stability testing. [8]
- Shirkhedkar, A. A., & Surana, S. J. (2010) The method validation for atorvastatin calcium via HPTLC involved several tests: Recovery studies used spiked samples at 80%, 100%, and 120%, comparing the results with expected values. Precision was assessed at 400, 500, and 600 ng/band, and robustness tested under varied chromatographic conditions. LOD and LOQ were calculated based on lower concentration ranges. Specificity was confirmed by comparing sample bands to standards. Forced degradation studies under acid, base, hydrogen peroxide, dry heat, and photochemical conditions demonstrated degradation patterns, with samples analysed at 400 ng/band.[9]
- Aiyalu et al. (2011) developed an HPTLC method for the simultaneous analysis of atorvastatin and ezetimibe. Their forced degradation studies revealed significant degradation of atorvastatin under acidic conditions, with up to 89% degradation observed. The method successfully separated atorvastatin from its degradation products, demonstrating HPTLC's capability to assess stability(aiyalu2011). [10]
- Ilango, K., & Kumar, P. S. S. (2013) Forced degradation studies were conducted according to ICH guidelines to assess the stability-indicating properties of the HPTLC method. Methanolic stock solutions of telmisartan (TLM) and atorvastatin (ATV) were refluxed with 0.1 M hydrochloric acid, 0.1 M sodium hydroxide, and 3% hydrogen peroxide at 60°C for 30 minutes. Samples were spotted at concentrations of 120 ng/band for TLM and 30 ng/band for ATV. Significant degradation was observed in acidic (12% TLM, 8% ATV) and alkaline (15% TLM, 28% ATV) conditions, with extra degradation peaks at Rf 0.27 and 0.45 (acid) and 0.42, 0.58, 0.74, 0.80 (alkali). The validated method provided good linearity ( $r = 0.9998$  for TLM,  $r = 0.9994$  for ATV), precision (RSD < 2%), and effective separation of degradation products, confirming its suitability for routine analysis of TLM and ATV in tablets.[11]
- Shah, D. A., Bhatt, K. K., Mehta, R. S., Baldania, S. L., & Gandhi, T. R. (2008) Stress degradation studies on atorvastatin (ATV) and amlodipine (AML) were conducted using acid and alkali hydrolysis, oxidative, and dry heat degradation. Stock solutions (1000 µg/mL) of ATV and AML were treated with 0.1 N NaOH and 0.1 N HCl, heated at 80°C for 1 hour, neutralized, and diluted to a final concentration of 6 µg/mL. Oxidative degradation was performed using 3% hydrogen peroxide under similar conditions. Dry heat degradation involved heating solid drugs at 80°C for 2

hours. After degradation, all solutions were analysed using liquid chromatography to investigate interference from degradation products.[12]

- Zaheer, Z., Farooqui, M. N., Mangle, A. A., & Nikalje, A. G. (2008) Forced degradation studies on atorvastatin involved acid, base, oxidative, thermal, and photodegradation. For acid and base hydrolysis, atorvastatin tablets were treated with 1 N HCl and NaOH, respectively, heated for 30 minutes, neutralized, diluted with mobile phase, and analysed by HPLC. Oxidative degradation was performed using 3% hydrogen peroxide under similar conditions. Photodegradation was studied by exposing tablets to UV light for 24 hours, and thermal degradation involved heating the drug in a boiling water bath. These treatments revealed degradation products and allowed their separation, ensuring the stability of atorvastatin in various stress conditions.[13]

## CONCLUSION

The data provided emphasizes the susceptibility of atorvastatin calcium to various degradation pathways, including hydrolysis, oxidation, and photolysis, which significantly impact its stability, efficacy, and safety. The use of sophisticated analytical methods such as High-Performance Thin-Layer Chromatography (HPTLC) and High-Performance Liquid Chromatography (HPLC) is crucial in identifying and quantifying atorvastatin's degradation products under different stress conditions.

HPTLC stands out for its cost-effectiveness, high throughput, and ability to analyze multiple samples with minimal solvent consumption, making it particularly useful for preliminary degradation studies. Meanwhile, HPLC offers superior precision, sensitivity, and the capability to detect even trace amounts of degradation products, making it the gold standard for in-depth analysis. The combination of both techniques provides a robust approach to comprehensively monitor atorvastatin's stability, ensuring pharmaceutical quality control and regulatory compliance.

Environmental factors such as temperature, pH, humidity, light exposure, and oxygen levels play significant roles in atorvastatin's degradation. Managing these factors during formulation and storage is essential for extending the drug's shelf life and preserving its therapeutic efficacy. The cited studies demonstrate that both HPTLC and HPLC are indispensable tools in assessing atorvastatin's degradation under various stress conditions, contributing to better formulation strategies and enhanced drug stability. In conclusion, employing HPTLC and HPLC in concert provides a powerful approach to ensure atorvastatin's stability throughout its shelf life, safeguarding its efficacy and safety for patient use.

## REFERENCES

- [1] Baldha, R. G., Patel, V. B., & Bapna, M. (2009). Simultaneous spectrophotometric determination of atorvastatin calcium and ezetimibe in tablet dosage form. *International Journal of ChemTech Research*, 1, 233–236.
- [2] Ballantyne, C. M., Hourii, J., & Notarbartolo, A. (2003). Effect of ezetimibe coadministered with atorvastatin in 628 patients with primary hypercholesterolemia. *Circulation*, 107, 2409–2415. <https://doi.org/10.1161/01.CIR.0000068312.51743.BA>

- [3] Chaudhari, B. G., Patel, N. M., Shah, P. B., & Patel, L. J. (2007). Stability indicating reversed phase liquid chromatographic method for simultaneous determination of atorvastatin and ezetimibe from their combination drug products. *Journal of AOAC International*, 90, 1539–1546.
- [4] Prabhu, C., Subramanian, G. S., Karthik, A., Kini, S., Rajan, M. S., & Udupa, N. (2007). Determination of telmisartan by HPTLC—a stability indicating assay. *Journal of Planar Chromatography*, 20(6), 477–481.
- [5] International Conference on Harmonization. (2003). Q1A (R2): Stability testing of new drug substances and products. *Proceedings of the International Conference on Harmonization*, 1–20.
- [6] International Conference on Harmonization. (1996). Q2B: Validation of analytical procedures: Methodology. ICH Secretariat.
- [7] Dhaneswar, S. S., Dhaneswar, S. R., Deshpande, P., & Patil, M. (2007). Development and validation of a method for simultaneous densitometric estimation of atorvastatin calcium and ezetimibe as the bulk drug and in tablet dosage forms. *Acta Chromatographica*, 19, 141–148.
- [8] Seshachalam, U., & Kothapally, C. B. (2008). HPLC analysis for simultaneous determination of atorvastatin and ezetimibe in pharmaceutical formulations. *Journal of Liquid Chromatography & Related Technologies*, 31, 714–721.
- [9] Shirkhedkar, A. A., & Surana, S. J. (2010). Development and validation of a reversed-phase high-performance thin-layer chromatography–densitometric method for determination of atorvastatin calcium in bulk drug and tablets. *Journal of AOAC International*, 93(3), 798–802.
- [10] Aiyalu, R., & Mani, K. (2012). HPTLC method development, validation, and stress degradation studies for atorvastatin and ezetimibe in multicomponent tablet dosage form. *Medicinal Chemistry Research*, 21, 1297–1301. <https://doi.org/10.1007/s00044-011-9660>
- [11] Ilango, K., & Kumar, P. S. S. (2013). Development and validation of stability-indicating HPTLC and HPLC methods for simultaneous determination of telmisartan and atorvastatin in their formulations. *Journal of Chemistry*, 2013, Article ID 725385, 9 pages. <https://doi.org/10.1155/2013/725385>
- [12] Shah, D. A., Bhatt, K. K., Mehta, R. S., Baldania, S. L., & Gandhi, T. R. (2008). Stability indicating RP-HPLC estimation of atorvastatin calcium and amlodipine besylate in pharmaceutical formulations. *Indian Journal of Pharmaceutical Sciences*, 70(6), 754–760. <https://doi.org/10.4103/0250-474X.49117>
- [13] Zaheer, Z., Farooqui, M. N., Mangle, A. A., & Nikalje, A. G. (2008). Stability-indicating high performance liquid chromatographic determination of atorvastatin calcium in pharmaceutical dosage form. Y.B. Chavan College of Pharmacy, Dr. Rafiq Zakaria Campus, Rauza Bagh, Aurangabad, Maharashtra, India.
- [14] Sonawane, S. S., Shirkhedkar, A. A., Fursule, R. A., & Surana, S. J. (2006). Application of UV spectrophotometry and RP-HPLC for simultaneous determination of atorvastatin calcium and ezetimibe in pharmaceutical dosage forms. *Eurasian Journal of Analytical Chemistry*, 1, 31–41. <https://doi.org/10.1016/j.jpba.2005.07.053>
- [15] Erturk, S., Sevinc, E., Erosy, L., & Ficioglu, S. (2003). An HPLC method for the determination of atorvastatin and its impurities in bulk drug and tablets. *Journal of Pharmaceutical and Biomedical Analysis*, 33, 1017–1020. [https://doi.org/10.1016/S0731-7085\(03\)00408-4](https://doi.org/10.1016/S0731-7085(03)00408-4)

- [16] Godse, V. P., Deodhar, M. N., Bhosale, A. V., Sonawane, R. A., Sakpal, P. S., Borkar, D. D., & Bafana, Y. S. (2009). Simultaneous spectrophotometric estimation of ezetimibe and atorvastatin in pharmaceutical dosage form. *Asian Journal of Research in Chemistry*, 2, 86–89.
- [17] Nilesh, J., Ruchi, J., Hemant, S., Sharad, P., & Deepak Kumar, J. (2010). Spectrophotometric method for simultaneous estimation of simvastatin and ezetimibe in bulk drug and its combined dosage form. *International Journal of Pharmacy and Pharmaceutical Sciences*, 1, 170–176.
- [18] Rajamanickam, V., Rajasekaran, A., Rathinaraj, B. S., & Anandarajagopal, K. (2010). Development and validation of analytical methods for simultaneous estimation of atorvastatin calcium and ezetimibe in combined dosage form. *World Applied Sciences Journal*, 9, 1424–1429.
- [19] Lea, A. P., & McTavish, D. (1997). Atorvastatin: A review of its pharmacology and therapeutic potential in the management of hyperlipidaemias. *Drugs*, 53(5), 828–847.
- [20] Ramsay, L. E., Williams, B., Johnston, G. D., et al. (1999). British hypertension society guidelines for hypertension management. *British Medical Journal*, 319(7210), 630–635.
- [21] Altuntas, T. G., & Erk, N. (2004). Liquid chromatographic determination of atorvastatin in bulk drug, tablets, and human plasma. *Journal of Liquid Chromatography and Related Technologies*, 27(1), 83–93.
- [22] Ghosh, C., Jain, I., Gaur, S., Patel, N., Upadhyay, A., & Chakraborty, B. S. (2011). Simultaneous estimation of atorvastatin and its two metabolites from human plasma by ESI-LC-MS/MS. *Drug Testing and Analysis*, 3(6), 352–362.
- [23] Zarghi, A., Shafaati, A., Foroutan, S. M., & Khoddam, A. (2005). A simple and rapid HPLC method for the determination of atorvastatin in human plasma with UV detection and its application to pharmacokinetic studies. *Arzneimittel-Forschung*, 55(8), 451–454.
- [24] Palled, M. S., Chatter, M., Rajesh, P. M. N., & Bhat, A. R. (2006). Difference spectrophotometric determination of telmisartan in tablet dosage forms. *Indian Journal of Pharmaceutical Sciences*, 68(5), 685–686.
- [25] Bahrami, G., Mohammadi, B., Mirzaeei, S., & Kiani, A. (2005). Determination of atorvastatin in human serum by reversed-phase high-performance liquid chromatography with UV detection. *Journal of Chromatography B*, 826(1-2), 41–45.
- [26] Stanisz, B., & Kania, Ł. (2006). Validation of HPLC method for determination of atorvastatin in tablets and for monitoring stability in solid phase. *Acta Poloniae Pharmaceutica*, 63(6), 471–476.
- [27] Rao, R. N., Prasad, K. G., Naidu, C. G., & Maurya, P. K. (2011). Development of a validated liquid chromatographic method for determination of related substances of telmisartan in bulk drugs and formulations. *Journal of Pharmaceutical and Biomedical Analysis*, 56(3), 471–478.
- [28] Farahani, H., Norouzi, P., Beheshti, A., Sobhi, H. R., Dinarvand, R., & Ganjali, M. R. (2009). Quantitation of atorvastatin in human plasma using directly suspended acceptor droplet in liquid-liquid-liquid microextraction and high-performance liquid chromatography-ultraviolet detection. *Talanta*, 80(2), 1001–1006.
- [29] Rao, R. N., Sen, S., Nagaraju, P., Reddy, V. S., Krishnamurthy, P. R., & Bhaskar, S. U. (2006). HPLC determination of telmisartan in bulk and pharmaceutical formulations. *Asian Journal of Chemistry*, 18(2), 775–782.



- [30] Bing, G. P. Y. L., Xiao, Y. D. W., & Wang, X. (2006). Determination of telmisartan in human plasma using LC-MS and the concentration of pharmacokinetics and bioavailability study. *Chinese Journal of Clinical Pharmacy*, 13(4), 200–203.
- [31] Hempen, C., Gläsle-Schwarz, L., Kunz, U., & Karst, U. (2006). Determination of telmisartan in human blood plasma—part II: Liquid chromatography-tandem mass spectrometry method development, comparison to immunoassay, and pharmacokinetic study. *Analytica Chimica Acta*, 560(1-2), 41–49.
- [32] Patil, K. R., Rane, V. P., Sangshetti, J. N., & Shinde, D. B. (2008). A stability-indicating LC method for the simultaneous determination of telmisartan and ramipril in dosage form. *Chromatographia*, 67(7-8), 575–582.
- [33] Prabhu, C., Subramanian, G. S., Karthik, A., Kini, S., Rajan, M. S., & Udupa, N. (2007). Determination of telmisartan by HPTLC—a stability indicating assay. *Journal of Planar Chromatography*, 20(6), 477–481.
- [34] Patil, U. P., Gandhi, S. V., Sengar, M. R., Rajmane, V. S., & Gandhi, S. V. (2010). A validated densitometric method for analysis of telmisartan and atorvastatin calcium in fixed dose combination. *Journal of the Chilean Chemical Society*, 55(1), 94–96.
- [35] Manoj, S. C., Abhinav, G., & Chakole, R. D. (2012). Simultaneous determination of atorvastatin calcium and telmisartan in pharmaceutical formulations by reverse phase-high performance liquid chromatography. *International Journal of Pharmaceutical Chemistry*, 2(1), 1–6.
- [36] Delhiraj, N., Ashok, P., Ravikiran, U., & Abhinandhana, P. (2013). A review of various analytical methods on atorvastatin. *Indian Journal of Research in Pharmacy and Biotechnology*, 1(6), 786.

# Approaches to Quinoline Derivative Synthesis : A Comprehensive Review

A. S. Patki<sup>1</sup>, P. R. Pande<sup>2</sup>

<sup>1</sup>Department of Chemistry, Shivaji Mahavidyalaya Renapur, Dist-Latur, Maharashtra, India

<sup>2</sup>Department of Chemistry, Nutan Mahavidyalaya Sailu, Dist-Parbhani, Maharashtra, India

## ABSTRACT

Heterocyclic compounds, integral to the core structure of many top-selling drugs, possess diverse pharmacological activities including anticancer, antibacterial, and anti-inflammatory properties. Quinoline, a prominent bicyclic heterocycle, has garnered attention for its wide range of biological functions, making it a key structure in drug discovery. Various classical and modern methods, such as the Friedländer and Skraup reactions, have been utilized for quinoline synthesis. This mini-review explores both established and novel strategies for synthesizing quinoline derivatives, emphasizing eco-friendly approaches like multicomponent one-pot reactions. The review underscores the importance of green chemistry in advancing sustainable and efficient methodologies for drug development.

## INTRODUCTION

Heterocyclic compounds constitute the core structure of at least four of the five top-selling drugs in the United States, exhibiting various pharmacological activities such as anticancer, antibacterial, antitumor, and anti-inflammatory properties. These compounds are indispensable in medicinal chemistry due to their wide range of biological activities, making them vital in the design and development of new therapeutic agents. Heterocyclic rings, such as pyridine, pyrimidine, and imidazole, are commonly found in the scaffolds of active pharmaceutical ingredients, contributing to enhanced drug solubility, stability, and receptor binding affinity. Their structural diversity enables the fine-tuning of pharmacokinetics and pharmacodynamics, which is crucial for optimizing therapeutic efficacy and minimizing side effects. Consequently, heterocyclic compounds play a pivotal role in drug discovery, driving innovations in treatments for a variety of diseases, including cancer, infections, and inflammatory disorders (1).

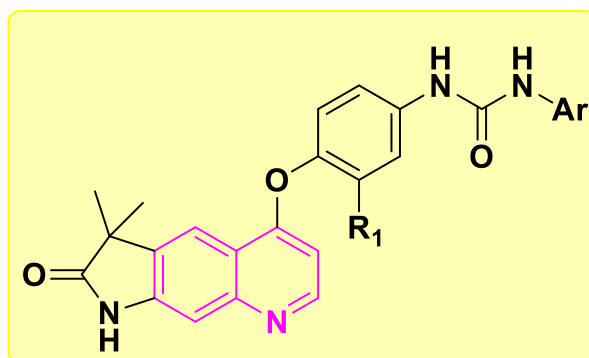
Quinoline, a prominent example of a bicyclic heterocyclic compound, is the heterocycle of focus in this review. As a well-established compound, quinoline has garnered significant attention due to its extensive range of pharmacological activities, making it one of the most widely exploited heterocyclic structures in drug discovery. Quinoline derivatives exhibit diverse biological functions, including anticancer, antimalarial (2, 3), analgesic (4), antitubercular (5), antiprotozoal (6), antihyperglycemic (7), anti-inflammatory (8), antifungal (9), antihypertensive (10), anti-HIV (11), and anthelmintic (12) activities. Numerous chemical

modifications of quinoline have been explored to develop analogs with potent antimalarial efficacy against both sensitive and resistant strains of *Plasmodium* species, while minimizing the risk of adverse effects.

Historically, cinchocaine, the first local anesthetic derived from a quinoline-based structure, was synthesized from this group (13). Quinoline was initially discovered in 1834 by Friedlieb Ferdinand Runge, who isolated it from coal tar (14, 15). Belonging to the alkaloid family, quinoline is classified as a secondary metabolite under nitrogen-containing natural products.

The synthesis of quinolines has been achieved through various methods, particularly those involving aniline, such as the Skraup, Doebner, Doebner-von Miller, Conard-Limpach, Friedländer, Pfitzinger, Combes, and Camps reactions (16, 17). Of these, the Friedländer method is considered one of the most prominent approaches for synthesizing quinoline analogs.

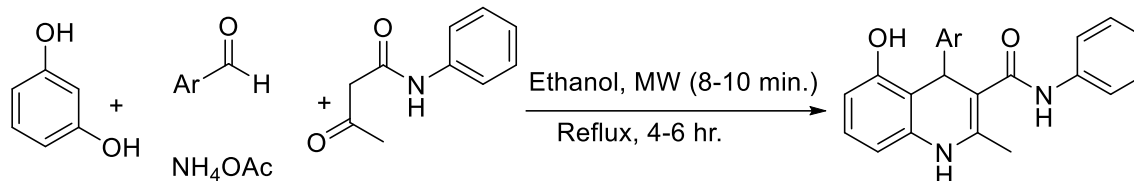
In recent years, several quinoline derivatives, as illustrated below, have been synthesized through structural modification of Sorafenib, a well-known multi-kinase inhibitor. These novel derivatives were designed as selective Raf kinase inhibitors, displaying enhanced potency and specificity in their antitumor activities (18). These modifications have aimed to improve therapeutic efficacy, targeting cancer cells with greater precision while minimizing off-target effects, thereby contributing to the development of more effective anticancer therapies.



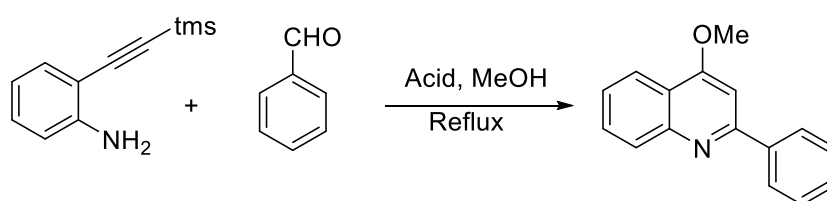
Based on our ongoing efforts and focus in the green synthetic organic and medicinal chemistry research field. This mini-review presents an overview of both classical and novel strategies for the synthesis of various quinoline compounds. These include advanced methodologies such as multicomponent one-pot reactions, which offer eco-friendly and efficient approaches for quinoline production. This review highlights the importance of sustainable practices in synthetic organic chemistry, aiming to reduce waste, improve reaction efficiency, and minimize environmental impact.

### Synthetic Strategies for Quinoline Derivatives

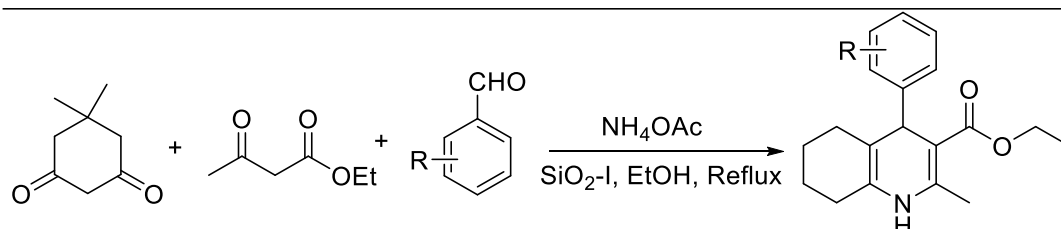
Chidurala et al. developed an efficient, catalyst-free, environmentally benign one-pot multicomponent condensation reaction involving benzene-1,3-diol, aldehydes, ammonium acetate, and acetoacetanilide in ethanol to synthesize quinoline derivatives (19). The reaction, conducted under microwave irradiation for 8–10 minutes, afforded an excellent yield of 88–96%, significantly outperforming the classical method, which yielded 72–90% over a prolonged reaction time of 4–6 hours.



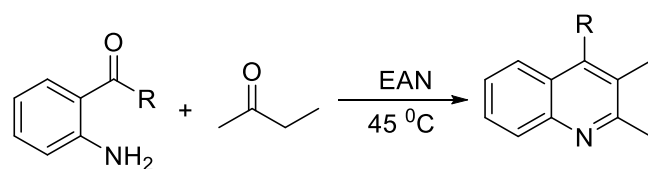
Wang et al. reported the synthesis of 2-Phenyl-4-alkoxy quinoline (20), achieved through the condensation and cyclization of 2-(2-trimethylsilyl)ethynyl) aniline with arylaldehydes. The reaction was catalyzed by sulfuric acid, utilizing methanol as the solvent.



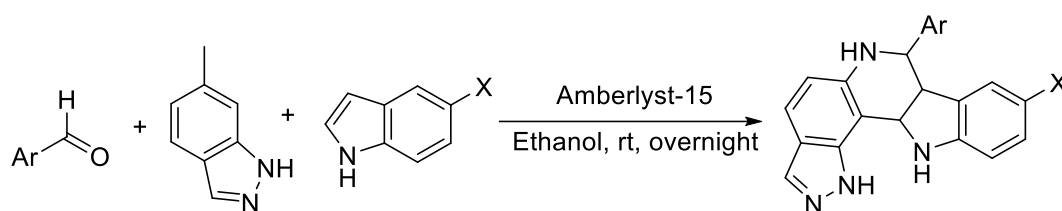
Ramesh et al. established a one-pot, multi-component synthetic method for the production of tetrahydroquinoline (21) via the reaction of ethyl acetoacetate, dimedone, and ammonium acetate with aromatic aldehydes. The reaction was catalyzed by silica iodide ( $\text{SiO}_2\text{-I}$ ) and conducted in ethanol under reflux conditions at  $80^\circ\text{C}$  for 2–3 hours, achieving an excellent yield of 90%. This protocol is characterized by high atom economy and catalyst recoverability.



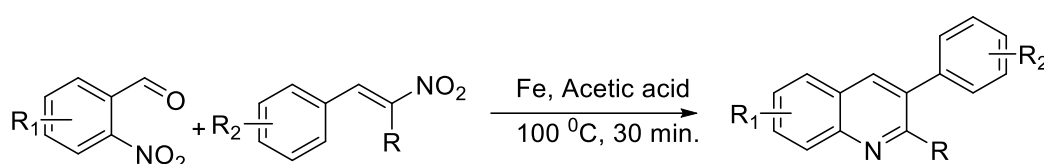
Zhou et al. reported the development of 2,3,4-trisubstituted quinolines (22) by stirring 2-amino-substituted aromatic ketones with carbonyl compounds containing a reactive  $\alpha$ -methylene group in ethyl ammonium nitrate (EAN) as the reaction medium.



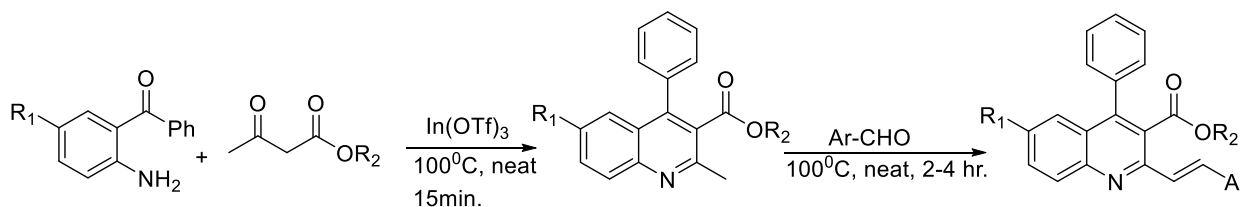
Pasha et al. developed an environmentally friendly method for synthesizing quinolone derivatives via the Povarov reaction (23). This reaction involves aromatic aldehydes, N-arylidene-1H indazol-6-amines, and substituted indoles, catalyzed by a reusable Amberlyst-15 catalyst in ethanol at room temperature, achieving yields of 65–70%.



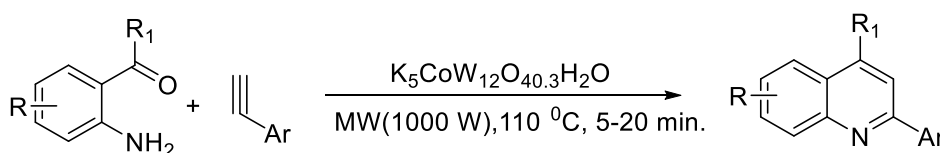
Li et al. reported a one-pot synthesis of 3-aryl quinolines (**24**) through the reaction of *o*-nitrobenzaldehyde derivatives with  $\beta$ -nitrostyrene in the presence of glacial acetic acid under conventional heating at 100°C for 30 minutes, yielding 72–95%. In this process, iron serves as a mediator, promoting cyclization by reducing *o*-nitrobenzaldehyde and minimizing the hydrolysis of nitrostyrene.



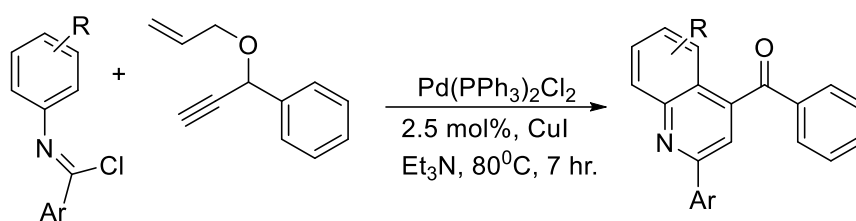
Kumar et al. synthesized 2-steryl quinolones (**25**) via a Friedlander annulation-Knoevenagel condensation involving 2-aminobenzophenone derivatives, ethyl acetoacetate, and benzaldehyde. The reaction was catalyzed by indium triflate [In(OTf)<sub>3</sub>], a recoverable and reusable catalyst, under solvent-free conditions at 100°C for 5 hours, achieving good yields ranging from 70–84%.



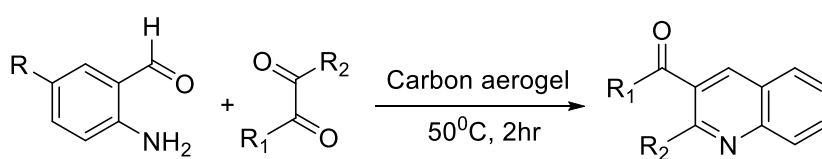
Iraj et al. synthesized 2,4-disubstituted quinolines (**26**) via a one-pot reaction of structurally diverse 2-aminoaryl ketones with various arylacetylenes. The reaction was catalyzed by potassium dodecatungstocobaltate trihydrate (K<sub>5</sub>CoW<sub>12</sub>O<sub>40</sub>·3H<sub>2</sub>O), a reusable and environmentally friendly catalyst, under microwave irradiation and solvent-free conditions.



Gao et al. reported that the interaction between benzimidoyl chlorides and 1-(1-(allyloxy)prop-2-ynyl)benzene (1,6-enynes) yields quinoline (**27**) derivatives through a palladium-catalyzed Sonogashira coupling followed by cyclization.



Godino-Ojer et al. reported a reusable and solvent-free method for synthesizing quinoline (28) through the reaction of 2-amino-5-chlorobenzaldehyde derivatives with ethyl acetoacetate, utilizing cobalt Co(0) and copper Cu(0) doped aerogels as catalysts via the Friedlander reaction. This approach achieved yields of 90–97% within 2 hours under mild conditions (50 °C).



## CONCLUSION:

The exploration of various synthetic techniques for quinoline derivatives has provided valuable insights into optimizing the production of these biologically significant compounds. Classical methods, such as the Skraup and Friedländer reactions, remain foundational, offering reliable pathways for quinoline synthesis. However, recent advancements in synthetic methodologies, including multicomponent and one-pot reactions, have introduced more efficient, eco-friendly alternatives. These modern approaches not only enhance reaction yields and reduce waste but also allow for greater structural diversity, enabling the fine-tuning of quinoline derivatives for specific therapeutic applications. Continued innovation in these synthetic strategies will be essential for driving progress in drug development, particularly in creating targeted treatments with minimal side effects.

## REFERENCES

- [1] T. Shiro, T. Fukaya and M. Tobe, *Eur. J. Med. Chem.*, 97, 397 (2015).
- [2] K. Raynes, M. Foley, L. Tilley, L. Deady, W. Deady, *Biochem. Pharmacol.*, 52, 551(1996).
- [3] J. M.Travins, F. Ali, H. Huang, S. K.Ballentine, E. Khalil, H. R. Hufnagel, W. Pan, J. Gushue et al. *Bioorg. Med. Chem. Lett.*, 18, 1603 (2008).
- [4] A. H. Abadi, G. H. Hegazy, A. A. El-Zaher, *Bioorg. Med. Chem.*, 13, 5759 (2005).
- [5] S. Eswaran, A. V. Adhikari, I. H. Chowdhury, N. K. Pal, K. Thomas, D. Thomas, *Eur. J. Med. Chem.*, 45, 3374 (2010).
- [6] X. Franck, A. Fournet, E. Prina, R. Mahieux, R. Hocquemiller, B. Figadere, *Bioorg. Med. Chem. Lett.*, 14, 3635 (2004).
- [7] D. Edmont, R. Rocher, C. Plisson, J. Chenault, *Bioorg. Med. Chem. Lett.*, 10, 1831 (2000).

- [8] A.M. Gilbert, M.G. Bursavich, S. Lombardi, K.E. Georgiadis, E. Reifenberg, C.R. Flannery, E.A. Morris, *Bioorg. Med. Chem. Lett.*, 18, 6454 (2008).
- [9] S. Kumar, S. Bawa, S. Drabu, B.P. Panda, *Med. Chem. Res.*, 20, 1340 (2010).
- [10] Z. Cai, W. Zhou, L. Sun, *Bioorganic and Medicinal Chem.*, 15, 7809 (2007)
- [11] M.A. Fakhfakh, A. Fournet, E. Prina, J.-F. Mouscadet, X. Franck, R. Hocquemiller, B. Figadere, *Bioorg. Med. Chem.*, 11, 5013 (2003).
- [12] S. Rossiter, J.M. Peron, P.J. Whitfield, K. Jones, *Bioorganic and Medicinal Chemistry Letters*, 15, 4806 (2005).
- [13] I. Ukrainets, R. Gabor, N.E. Carl, *InTech*, 63 (2012).
- [14] R. Alajarin, C. Burgos, J. Alvarez-Builla, J. J. Vaquero, J. Barluenga, John Wiley & Sons, 1527 (2011).
- [15] S. N. Pandeya, A. Tyagi, *Int. J. Pharm. Pharm. Sci.*, 3, 53 (2011).
- [16] G.S. Kumar, P. Kumar, M. Kapur, *Organic letters*, 19, 2494 (2017).
- [17] X. Xu, Y. Yang, X. Chen, X. Zhang, W. Yi, *Organic & Biomolecular Chem.*, 15, 9061 (2017).
- [18] Y. Li, X. Shi, N. Xie, Y. Zhao, S. Li, *Med. Chem. Comm.*, 4, 367 (2013).
- [19] P. Chidurala, V. Jetti, R. Pagadala, J.S. Meshram, S.B. Jonnalagadda, *J. Heterocycl. Chem.*, 52, 1302 (2015).
- [20] Y. Wang, C. Peng, L. Liu, J. Zhao, L. Su, Q. Zhu, *Tetrahedron Lett.*, 50, 2261 (2009b).
- [21] K.B. Ramesh, B.M. Omkaramurthy, M. Srinivas, *J. Mol. Struct.*, 1222, 128790 (2020).
- [22] T. Zhou, J. Lin, Z. Chen, *Lett. Org. Chem.*, 5, 47 (2008).
- [23] J. Pasha, B. Kandagatla, S. Sen, G.P.K. Seerapu, S. Bujji, D. Haldar, S. Nanduri, S. Oruganti, *Tetrahedron Lett.*, 56, 2289 (2015).
- [24] D.K. Li, Q. Cai, R.R. Zhou, Y.D. Wu, A.-X. Wu, *ChemistrySelect*, 2, 1048 (2017).
- [25] D. Kumar, A. Kumar, M.M. Qadri, M.I. Ansari, A. Gautam, A.K. Chakraborti, *RSC Adv.*, 5, 2920 (2015).
- [26] M.B. Iraj, T. Shahram, M. Majid, M. Valiollah, A. Salma, M. Arsalan, *Synlett*, 20, 3104 (2010).
- [27] G.L. Gao, Y.N. Niu, Z.Y. Yan, H.L. Wang, G.W. Wang, A. Shaukat, Y.M. Liang, *J. Org. Chem.*, 75, 1305 (2010).
- [28] M. Godino-Ojer, A.J. Lopez-Peinado, F.J. Maldonado-Hodar, E. Perez-Mayoral, *Chem. Cat. Chem.*, 9, 1422 (2017).

# A Preliminary Checklist of Marine Algae found in Mumbai's selected Marine Regions

Priti Dhamal\*, Babita Rana

Department of Botany, Guru Nanak Khalsa College, Matunga East, Mumbai 400019, Maharashtra, India

Email: [Pritidhamal9299@gmail.com](mailto:Pritidhamal9299@gmail.com)

## ABSTRACT

Marine algae, which inhabit intertidal zones, play a crucial role in the tidal ecosystem. Algae have numerous applications in therapeutics and the food industry. Mumbai is a significant source of marine resources, including marine cyanobacteria, marine mammals, sea grasses, various organisms, and micro and macroalgae. The research studies marine water cyanobacteria and green algae found in the Mumbai marine regions. Sample collection was conducted at Dadar Chowpatty, Juhu Beach, Bandra bandstand, and Marine line areas. Bandra Bandstand and Dadar Chowpatty exhibit various cyanobacterial and green algal species from multiple regions. The study identified four cyanobacterial species and three green algal species. *Lyngbya majuscula* and *Oscillatoria* sp were identified from the *Oscillatoriaceae* family, while *Nostoc calcicole* and *Anabaena oryzae* were identified from the *Nostocaceae* family. Three green algae, *Stigeoclonium tenue* from the *Chaetophoraceae* family, *Cladophora glomerata* from the *Cladophoraceae* family, and *Enteromorpha intestinalis* from the *Ulvaceae* family, were discovered. The green marine algae species are abundantly present at Bandra Bandstand and Dadar Chowpatty. This study introduces phycologists to the diverse cyanobacterial and algal species inhabiting the Mumbai marine regions.

**Keywords:** Marine regions, Cyanobacteria, green algae, *Lyngbya*, *Oscillatoria*, *Nostoc*, *Cladophora*.

## INTRODUCTION

The ocean covers about 70 % of the earth's surface; therefore, marine algae are the primary producers that sustain the entire ecosystem. They work as primary producers (Chapman., 1970). The marine intertidal ecosystem is very dynamic, and it is the area between the sea and terrestrial environment. The environmental condition of the intertidal water is much different from the adjacent seawater due to the occurrence of relatively large amounts of nutrients governed by tidal impact. The tidal pools of the intertidal regions provide an ideal condition for the growth of marine algae along the intertidal area. Marine algae are considered one of the major living resources of the seas. They play an important role as primary producers and food for marine grazers – grazing on both micro and macro algae (Das, H and Das, P., 2012). Cyanobacteria (Blue-green algae) are a morphologically diverse group of pioneer oxygenic phototrophic prokaryotes with characteristics in common to both bacteria and algae. Their distribution is cosmopolitan and surpassed only by bacteria (Adams 2000; Govindjee and Shevela., 2011). They are



found to be useful in enhancing crop productivity in a variety of environments due to their ability to fix dinitrogen. In recent decades, cyanobacteria have been of academic interest and now they have been proven as organisms with a potential source of various biochemical applications such as food, feed, fuel, fertilizer, medicine, industry, in diagnostic or pigments such as fluorescent probes, and in combating pollution (De., 1939; Mitsui et al., 1981). The cyanobacteria are good sources of metabolites with biological activities such as antimalarial, antibacterial, and antiviral. Antifungal and cytotoxic properties similar to plant and animal products (Falch et al., 1995; Subramanian., 1996). They are also a source of industrially important metabolites with properties like emulsifying agents, surfactants, and flocculants (Bender et al., 1994; De Philippis and Vincenzini., 1998).

Along the coastline of Maharashtra, Dixit, (1940) presented a historical account of algal investigations in the Bombay presidency from 1847 – 1940. He also reported 9 Chlorophyta, 11 Phaeophyta, and 10 Rhodophyta species along the Malvan coast. Biswas and Mitra, (1943) made certain observations on marine algae from the sea shore of Mumbai. A survey of marine algae in Mumbai was carried out by Deodhar (1987) who reported 60 different species of marine algae. Dhargalkar et al., (2001) studied macro marine algal diversity along the Maharashtra coast and reported 91 algal species distributed in 51 genera and 30 families. Dhargalkar and Komar Pant (2003) carried out work on 'Impact on the distribution, abundance, and community of rock intertidal macroalgae of Colaba coast' Oza and Zaidi (2001) studied coastal and marine biodiversity of India and reported 844 algal species and out of 97 algal species from the coastline of Maharashtra. Dhargalkar and Pereira (2005) carried out work on the Importance of seaweeds. Jagtap et al., (2001) reported more than 100 marine algal species from the central west coast of India by using LANDSAT data. Along the Indian coastline about 624 algal species have been recorded. The major species of economic importance are Gracilaria, Sargassum, Gelidium, Ulva, Caulerpa, etc. Untawale et al., (1983). Untawale and Dhargalkar., (1975) surveyed the along the coastline of Goa. Rao et al., (2006) carried out work on Indian seaweed resources and sustainable utilization: Scenario at the dawn of a new century.

Due to industrial growth and other human activities, the marine environment suffers from heavy pollution. It has had a great impact on marine algal biodiversity. Boergesen (1935) commented upon the highly polluted marine environment of Bombay. Since then, human interference has increased tremendously due to modernization (Deshmukh., 2004). Biodiversity is the variety of variability among living organisms and the ecological complexes in which they occur. Credit for the first publication of work on the Maharashtra coast goes to Kirtikar (1986), who published a paper on marine algae from Ratnagiri coast. The biodiversity of marine algae along the East and West coast regions of India was studied by several authors, Boergesen, 1932; Srinivasan, 1973; Balkrishan, 1981; Biswas, 1945; Chaugule B.B. 1989; and Krushnamurthy, 1972. Most of the research work in the field of marine phycology on the Kokan coast has been carried out along the coast of Mumbai (Deodhar, 1987), Malvan (Dixit, 1940), Kokan (Phanase, 2000), and Ratnagiri (Redekar, 2000; Sakhalkar S.S & Mishra., 2014).

The understanding of marine flora in the Mumbai marine region has been limited in recent years due to a lack of literature. The researcher aims to concentrate on the phycological studies conducted in Maharashtra, so I would particularly like to focus on the research work in Mumbai. The study aims to create a preliminary checklist of marine algal species from the Mumbai region. The study was conducted

by selecting four study sites from the marine region of Mumbai. Even in Mumbai marine localities were explored by some workers, but many localities remained ignored still today. The study aimed to explore the biodiversity of marine algae on the Mumbai coast, focusing on smaller areas for detailed floristic study. The chosen regions for the study are the Dadar Chowpatty, Juhu Beach, Bandra Bandstand, and Marine lines.

## MATERIAL AND METHODS

India has approximately 6160 km of seacoast, with Maharashtra contributing nearly 720 km of the coastal region. Only five districts of Maharashtra cover this large coastal zone viz. Thane, Mumbai, Raigad, Ratnagiri, and Sindhudurg. Mumbai, situated on India's western coast, is a bustling city known for its rich marine life due to its proximity to the Arabian Sea. Mumbai's beaches are extensively utilized for studying algal diversity due to their diverse marine ecosystem and diverse algal species. Mumbai's coastline boasts numerous beaches including Dadar Chowpatty, Juhu Chowpatty, Marine Lines, and Bandra Bandstand.

**Study Site** - Dadar Beach in central Mumbai, Juhu Beach in Northwestern Mumbai, Marine lines in south Mumbai, and Bandra bandstand on the western coast were selected for algae collection and present study.

**Dadar Chowpatty** - Dadar Chowpatty Beach in Mumbai is a popular destination known for its stunning coastline and magnificent landscape. Dadar Chowpatty Beach, a less crowded and densely populated residential area in Mumbai, offers a small, less crowded spot with limited sand for relaxation.

**Juhu Beach** – Juhu Beach is one of the most attractive destination places in Mumbai. The Juhu beach, located on the Arabian Sea shore, extends 6 km up to Versova, featuring both small and large rocks. The region is surrounded by the Arabian Sea to the west, Versova to the north, Vile Parle to the east, and Santacruz to the south.

**Marine Lines** – Marine Lines is a locality in South Mumbai. Marine Lines is a 3.6 km long promenade located in South Mumbai, along Netaji Subhash Chandra Bose Road. Marine Lines is a renowned promenade with a small residential population but a large floating population, covering 0.71 square kilometers.

**Bandra Bandstand** – The Bandra Bandstand, also known as the bandstand promenade, is a 1.2-kilometer-long walkway along the western coast of Mumbai. The Bandra Bandstand, a popular and highly visited promenade in Mumbai's Bandra neighborhood, is utilized for studying algal diversity.

**Collection of algal samples** - The study involved collecting water samples and algal mats in disposable zip-lock polythene bags and screw-cap bottles. The samples contained mixed populations of algal, cyanobacterial, and diatoms, and the mat samples were thoroughly washed with sterile distilled water to remove soil and mud. The collection site, salinity, temperature, and water pH were measured and recorded. A small amount of algal material was collected and transferred to sterile tubes containing distilled water, which were shaken to break the mat clumps. (Fig: A-C)

**Isolation and morphological identification** - The cultures were identified and morphologically observed using light, fluorescence, and scanning electron microscopy images of the collected water and mat samples. A small portion of a well-shaken suspension was taken on a slide, and clean trichrome was marked and picked up for further isolation. Enrichment and isolation were carried out on BG11 culture

media. Unialgal cultures were maintained by subculturing species to their respective fresh sterile medium every 3-5 weeks. Stock cultures were maintained in Erlenmeyer flask with 50 ml of sterile medium, room temperature ( $20 \pm 2^\circ\text{C}$ ), and light (2000 lux) provided by cool-white fluorescent tubes. The living cells were photographed using bright field microscopy at 40 X and identified using standard taxonomic publications like Geitler (1925) and Desikachary (1959). For identification, we used the monographs green algae Krishnamurthy (1972), and Phycologia Indica. Voi. II by Srinivasan, (1973).

## RESULTS AND DISCUSSION

Bandra Bandstand and Dadar Chowpatty show cyanobacteria and micro marine algal species. The brief information about these algal species is as follows,

- 1) **Lyngbya majuscula** – (Family - Oscillatoriaceae) (Desikacharya 1959: P, 313)  
Occurrence: The algal species are found on rocks and at low water levels.  
Characters: The thallus is dark bluish green, filamentous, with solitary, straight, sheathed filamentous and a thin, colorless sheath. Its trichome is not constricted at the cross walls. Cells 13  $\mu\text{m}$  broad and 2  $\mu\text{m}$  long. (Fig: D)
- 2) **Nostoc calcicole** – (Family – Nostocaceae) (Desikacharya 1959: P, 384)  
Occurrence: It can grow on moist rocks and cliffs.  
Characters: Thallus is mucilaginous, slightly diffluent, and olive green, with loosely arranged filaments, sheath indistinct, dark olive green trichomes, barrel-shaped cells, and spherical spores. (Fig: E)
- 3) **Oscillatoria sp. Vaucher** (Family – Oscillatoriaceae) (Desikacharya 1959: P, 198)  
Occurrence: The species can grow on rocky surfaces, shells, or in intertidal zones.  
Characters: Thallus membranous, blue-green, with straight, 4-5  $\mu\text{m}$  wide trichomes, up to 2  $\mu\text{m}$  long cells, homogenous contents, and elongated apical cells. Trichomes unbranched with separating discs. Sheath absent. (Fig: F)
- 4) **Anabaena oryzae** – (Family- Nostocaceae) (Desikachary 1959: P, 396)  
Occurrence: The species are found in low water levels and rock pools.  
Characters: The thallus is uniseriate, curved, or coiled. Trichrome that may be constructed at the cell walls. The blue-green to yellow-green colored cells may be spherical, or cylindrical. Cells form long filaments. (Fig: G)
- 5) **Enteromorpha intestinalis** (Family- Ulvaceae)  
Occurrence: It is growing on the rocky substances, and attached to the substratum.  
Characters: The plant is light green, small, and grows on another substratum. Its thallus is foliaceous, folded, and has a thick lobe attached by rhizoidal portions, can become freely floating or flattened, giving an intestine-like appearance. (Fig: H)
- 6) **Cladophora glomerata** (Family- Cladophoraceae)  
Occurrence: This algal species is found in low tide levels, on slit-covered stones, and hard substances.

Characters: Thallus branches are smaller than the main axis. Each cell has a 3 layered cell wall. Cells are elongated, cylindrical, and multinucleated. Chloroplast is associated with a large number of pyrenoids. (Fig: I)

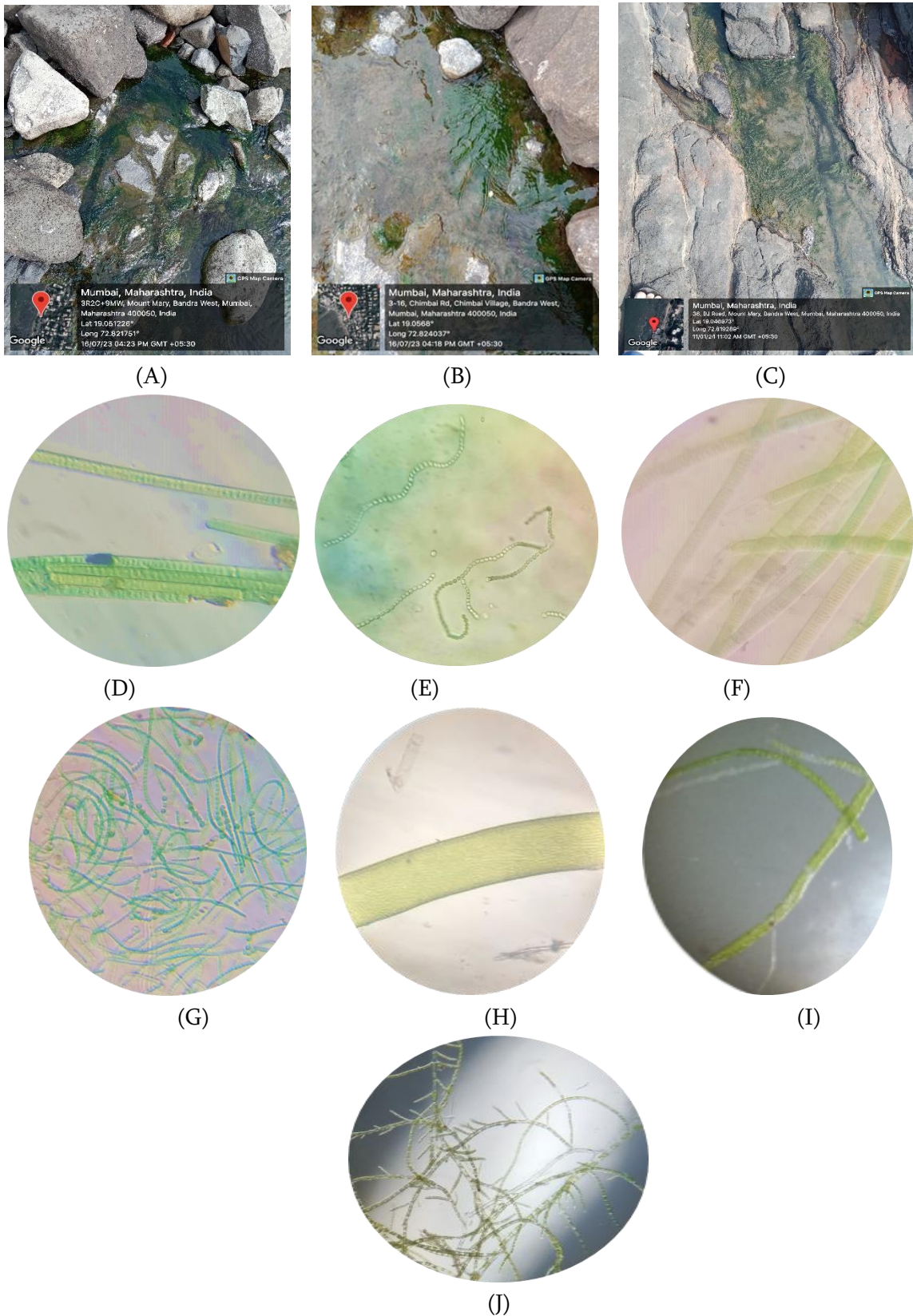
7) **Stigeoclonium tenue** (Family – Chaetophoraceae)

Occurrence: The algae is firmly attached to the substratum under low tide pools.

Characters: Branches are one cell thick and subbranches are similar in width. Nonterminal cells are usually cylindrical but may be barrel-shaped. Each cell contains a single green chloroplast. Filaments are not embedded in mucilage. (Fig: J)

## CONCLUSION

The study aims to conduct a preliminary analysis of the diversity of algae and cyanobacteria in the Mumbai marine region. Dadar Chowpatty and Bandra bandstand shows rich growth of cyanobacteria and algal flora. However, this site remained unexplored by earlier workers. The present investigation identified four cyanobacterial species and three green algal species. Two species, *Lyngby majuscula*, and *Oscillatoria Sp* were identified from the Oscillatoriaceae family, and the other two species, *Nostoc calcicole*, and *Anabaena oryzae* identified from the Nostocaceae family, three green algae, *Stigeoclonium tenue* from the Chaetophoraceae family, *Cladophora glomerata* from the Cladophoraceae family, and *Enteromorpha intestinalis* from Ulvaceae family, were discovered. The Bandra Bandstand and Dadar Chowpatty are home to a diverse array of green marine algal species and cyanobacterial species. The study revealed that the coastal line of Mumbai is abundant in algal species. The availability of algal species increased from September to December, while it decreased from January to March. The Mumbai coastal line shows a significant decrease in the quantity of red algae species compared to green algae. The study along Juhu Beach and Marine Lines areas reported no microalgal diversity, because of the sand. The intertidal zone of purely sandy beach hardly shows any algal flora. Purely rocky and mixed types of beaches seem to be ideal for algal growth. And second important reason is industrialization and population have led to decreased algal diversity in Juhu Beach and marine lines, with more sandy areas and less biodiversity compared to rocky intertidal areas. Tourist-friendly areas in Mumbai's popular recreational areas are causing spore displacement, altering algal species diversity, and potentially leading to the entire ecosystem's potential disappearance. Future planning is crucial for the conservation and restoration of this item.



Figs. ( A – C ) : Algae sample collection site : D – *Lyngbya majuscula* : E – *Nostoc calcicole* : F – *Oscillatoria* sp : G – *Anabaena oryzae* : H – *Enteromorpha intestinalis*: I – *Cladophora glomerata* : J – *Stigeoclonium tenue*

**REFERENCES**

- [1] Adams DG (2000) Symbiotic interactions in Whitton BA, Potts M (Ed) *The Ecology of Cyanobacteria*, Kluwer Academic Publishers, Dordrecht, The Netherlands, pp 523-561
- [2] Adams, D.G., Bergman, B.I.R.G.I.T.T.A., Nierzwicki-Bauer, S.A., Rai, A.N. and Schüßler, A., 2006. Cyanobacterial-plant symbioses. *The prokaryotes: a handbook on the biology of bacteria*, 1, pp.331-363.
- [3] Bender J, Rodriguez-Eaton S, Ekanemesang UM, Phillips P (1994) Characterization of metal-binding biofloculants produced by the cyanobacterial component of mixed microbial mats. *Applied Environmental Microbiology* 60, 2311-2315
- [4] Biswas K., Mitra G. 1943. Observation of the marine algae from the coast of Bombay. *Science and culture* 9, 251.
- [5] Boergesen, F., 1935. A list of Marine algae from Bombay *Dansk. Vidensk. Selsk. Biol. Meddeles*, 12(2):1-164 Kobenhavn
- [6] Chapman V J and Chapman D J. 1981. *The algae*. Macmillian. London. 25 -28.
- [7] Chapman V J.1981, *Seaweeds and their uses*. Camelot press, London, 299-300.
- [8] Das, H., Misra, K. and Das, P., 2012. Fluctuation of certain physico-chemical parameters in Bordowa beel of Nalbari district, Assam, India. *The Clarion-International Multidisciplinary Journal*, 1(2), pp.114-120.
- [9] De Philippis R, Vincenzini M (1998) Exocellular polysaccharides from cyanobacteria and their possible applications. *FEMS Microbiology Reviews* 22, 151-175
- [10] Deodhar H. D. 1989, "The Biology of marine algae of Bombay" Ph.D Thesis. University of Pune.
- [11] Deshmukh Sanjay, (2004): *Pollution in the biodiversity-rich coastal region of Maharashtra- Source and Management Measures*. (Environment of Maharashtra 2004)
- [12] Desikachary TV (1959) *A Monograph on Cyanophyta*, Indian Council of Agricultural Research Publication, New Delhi
- [13] Dhargalkar V. K, Komarpant D. S. 2003. Impact of sewage on the distribution, abundance, and community structure of rocky intertidal macroalgae of Colaba coast, Mumbai. *India seaweed research and utilization*, 25 (1 & 2), (National Ins. of oceanography, Goa, India). 27-36.
- [14] Dhargalkar V. K, Pereira N.2005 *Seaweed: Promising plant of the millennium*. Science and culture (National Institute of Oceanography, Goa, India). 60-66.
- [15] Dhargalkar V.K, Untawale, Jagtap T. G.2001. Marine macroalgal diversity along the Maharashtra coast: Past and Present status. *Indian Journal of Marine Science*. Vol.30 (National Ins. of Oceanography, Goa, India). 18-22.
- [16] Dixit S.C. 1940. Algal investigation in the Bombay Presidency from 1940-1847. *Current Science* 9 (10) 453- 454.
- [17] Falch PS, Konig GM, Wright AD (1995) Biological activities of cyanobacteria: Evaluation of bacteria and pure compounds. *Planta Medica* 61, 321-328
- [18] Govindjee, Shevela D (2011) *Adventures with cyanobacteria: A personal perspective*. *Frontiers in Plant Science* 2, 1-17

- [19] Jagtap TG, Naik S Nagle V L. 2001. Assessment of coastal wetland resources of central west coast, India, using LANDSAT Data, journal of India. Society of remote sensing. (National Ins. of Oceanography, Goa, India). Vol 29 (3).140-150.
- [20] Kirtikar, (1886): A new species of algae *Conferva Thermalis* Birdwood. J. Bomb. Nat. Hist Soc., 1:135-138.
- [21] Mitsui A, Murray R, Entenmann B, Miyazawa K, Polk E (1981) Utilization of marine blue-green algae and macroalgae in warm water mariculture. In: San Pietro A (Ed) Biosaline Research. A Look to the Future, Plenum Press, New York, pp 215-225
- [22] Oza R. M., Zaidi S. H.,2001. A revised checklist of Indian marine algae, CSMCRI, Bhavnagar, Gujrat, pp 296.
- [23] Rao P V S. Mantri V A. 2006. Indian seaweed resources and sustainable utilization: Scenario at the dawn of a new century. Current Science. Vol.91 (2) 164-174
- [24] Untawale A. G, Dhargalkar V.k. 1975. Seaweed resources of the Goa coast. International Ins. Of Oceanography, Publication, Dona Paula Goa. 1-10.
- [25] Untawale A.G. Dhargalkar V.k., Agadi V.V, and Jagtap T. G. 1979, Marine algal resource of the Maharashtra coast. Tech Report. (National Ins. of Oceanography, Goa, India). 45-48.

# Density, Viscosity and Ultrasound velocity measurement of bioactive Schiff base: N-((2-chloro-6-methylquinolin-3-yl)methylene)-4-(5-methyl-1H-tetrazol-1-yl)benzenamine in Chloroform and DMF solvents

S. A. Kamble<sup>1</sup>, A. S. Kirdant<sup>1\*</sup>, S. G. Vedpathak<sup>2</sup>, S. H. Quadri<sup>3</sup>

<sup>1</sup>Baburaoji Adaskar Mahavidyalaya, Kaij, Dist. Beed- 431 123, Maharashtra, India

<sup>2</sup>S. M. Dnyandeo Mohekar Mahavidyalaya, Kalamb, Dist. Dharashiv- 413 507, Maharashtra, India

<sup>3</sup>Maulana Azad College, Chh. Sambhaji Nagar- 431 001, Maharashtra, India

## ABSTRACT

To explore the strength and nature of solute-solute, solute-solvent and solute-solvent interactions in solution, the physicochemical investigation of N-((2-chloro-6-methylquinolin-3-yl)methylene)-4-(5-methyl-1H-tetrazol-1-yl)benzenamine was carried out. The density, viscosity and ultrasonic velocity have been measured for the compound 3 in DMF and CHCl<sub>3</sub> solutions of various concentrations at 300.15 °K, 305.15 °K, and 310.15 °K. The result data can be used to calculate various acoustic parameters, which can be used to interpret solute-solute and solute-solvent interactions in these solvents.

**Keywords:** Chloroform, Density, DMF, Temperature, Viscosity, Ultrasound velocity.

## INTRODUCTION

The physicochemical properties of solutions, such as solubility, density, viscosity, ultrasound velocity, boiling point, freezing point, and vapor pressure, are heavily influenced by solute-solvent interactions.[1] These interactions, which include hydrogen bonding, dipole-dipole forces, ion-dipole forces, and hydrophobic interactions, determine how the solute behaves in different solvents and directly impact the overall properties and behavior of the solution.[2-4]

Solute-solvent interactions play a vital role in the effectiveness of drugs by influencing their solubility, absorption, distribution, metabolism, and elimination.[5] Understanding these interactions allows pharmaceutical scientists to optimize drug formulations and improve bioavailability, leading to more effective treatments. Strategies such as salt formation, pro-drugs, and specialized delivery systems are commonly used to enhance solubility and ensure the therapeutic action of drugs.

Studies of transport properties of electrolytes, along with thermodynamic and compressibility studies, give very valuable information about ion-ion and ion-solvent interactions in solutions. The influence of these ion-solvent interactions is sufficiently large to cause dramatic changes in chemical reactions involving ions. The changes in ionic solvation have important applications in such diverse areas as organic and inorganic synthesis, studies of reaction mechanisms, non-aqueous battery technology and extraction.

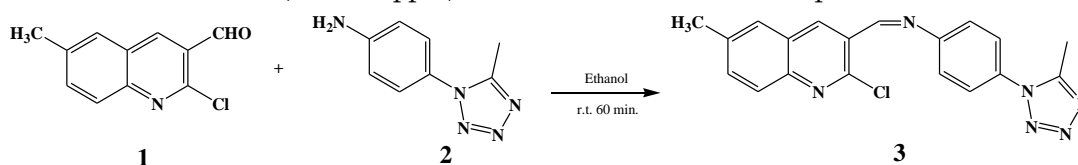


The importance and applications of the chemistry of electrolytes in non aqueous and mixed solvents are now well recognized and their implications are well described in the literature.[6-14] Solute and solute-solvent interactions are of widespread interest as evidenced by the Faraday Transactions of the Chemical Society.[15] Herein, we have reported the measurement of density, viscosity and ultrasound velocity of previously synthesized quinoline-tetrazole hybrid Schiff base, *N*-((2-Chloro-6,8-dimethylquinolin-3-yl)methylene)-3-(5-methyl-1*H*-tetrazol-1-yl)benzenamine.[16]

## MATERIAL AND METHODS

### 2.1 Reagents

All the chemicals used were of AR grade and were purchased from sd-Fine chemicals. The melting points were determined in open capillaries using melting point apparatus (Model MP-96) and were uncorrected. The progress of reaction and purity of the product were monitored by thin layer chromatography using precoated Silica 60/UV254 (SDFCL). <sup>1</sup>H-NMR spectra and <sup>13</sup>C-NMR spectra were recorded in CDCl<sub>3</sub> using 400 MHz Varian Mercury plus 400 MHz FT-NMR spectrometer. The <sup>1</sup>H chemical shift values were reported on δ ppm scale relative to TMS (δ = 0.00 ppm). FT-IR were recorded and reported in cm<sup>-1</sup>.



**Scheme.1** Synthesis of *N*-((2-chloro-6-methylquinolin-3-yl)methylene)-4-(5-methyl-1*H*-tetrazol-1-yl)benzenamine (**3**)

### 2.2 Synthesis of *N*-((2-chloro-6-methylquinolin-3-yl)methylene)-4-(5-methyl-1*H*-tetrazol-1-yl)benzenamine (**3**)

A mixture of 2-Chloro-6-methylquinoline-3-carbaldehyde (**1**) (1 mmol, 2.05 g), 4-(5-methyl-1*H*-tetrazol-1-yl)benzenamine (**2**) (1 mmol, 1.75 g) and 20 ml ethanol was taken in 50 ml round bottom flask. The resultant reaction mixture was stirred for 60 min. at room temperature. The progress of the reaction was monitored by TLC. After completion of reaction, the reaction mixture was poured on 50 ml cold water, filtered the solid, dried and recrystallized from 1:1 ethanol/water to give compound (**3**). Yellow solid; (3.26 g, 92%) yield; mp 217–218 °C; IR (KBr, ν<sub>max</sub>, cm<sup>-1</sup>): 1596 (C=N azomethine), 1501 (C=N tetrazole ring), 1372 (N=N tetrazole ring), 1027 and 926 (N-N=N); <sup>1</sup>H NMR (400 MHz, CDCl<sub>3</sub>) δ ppm: 2.23 (s, 3H, CH<sub>3</sub>-tetrazole); 2.48 (s, 3H, CH<sub>3</sub>-quinoline); 7.23-7.25 (d, 2H); 7.44-7.51 (m, 2H); 7.57-7.59 (d, 2H); 7.72-7.75 (m, 1H); 8.67 (s, 1H, quinoline H-4); 8.96 (s, 1H, N=CH); <sup>13</sup>C NMR: δ ppm: 9.67 (CH<sub>3</sub>-tetrazole), 21.61 (CH<sub>3</sub>-quinoline, C-6), 117.56 (C, tetrazole), 122.23 (1C), 124.57 (2C), 126.48 (1C), 127.36 (2C), 128.32 (1C), 132.69 (1C), 133.96 (1C), 135.53 (1C), 138.12 (1C), 140.32 (1C), 146.81 (Ar C-1), 149.93 (quinoline C-9), 153.01 (quinoline C-2), 159.59 (N=CH); MS (ESI) m/z: 363.19 (M+1)<sup>+</sup>. Anal. calcd. (%) for C<sub>19</sub>H<sub>15</sub>ClN<sub>6</sub>: C, 62.90; H, 4.17; Cl, 9.77; N, 23.16; Found: C, 62.84; H, 4.18; Cl, 9.78; N, 23.19.

### 2.3 Choice of Solvents for physico-acoustic parameters

N,N-Dimethylformamide (DMF) and chloroform (CHCl<sub>3</sub>) were chosen as solvents for the present study. Density, viscosity and ultrasound velocity of solvents and solutions of different concentrations were measured by using pycnometer, Ubbelohde suspended level viscometer and ultrasonic interferometer respectively, at 300.15 °K, 305.15 °K and 305.15°K.

The solutions of required concentrations prepared in DMF and CHCl<sub>3</sub> using calibrated volumetric flasks. Then all the solutions were kept at the desired temperature for 24 h to ensure their solubility at that temperature.

## EXPERIMENTAL

### 3.1 Density ( $\rho$ ) and its measurement

Density is a fundamental physical property of matter, defined as the mass of matter per unit volume. It shows how much mass is in a given volume of a material, which can be useful for distinguishing between substances or showing the properties of different materials.

The pycnometer is a highly accurate instrument used to measure the density of liquids. Density is a measure of the "compactness" of a substance and is defined by the equation:

$$\text{Density } (\rho) = \frac{\text{mass (m)}}{\text{volume (v)}}$$

The density was experimentally calculated by the equation.

$$\text{Density} = \frac{\text{weight of solvent/solution} \times \text{density of water}}{\text{weight of water}} \text{ g/cm}^3$$

### 3.2 Viscosity ( $\eta$ ) and its measurement

Viscosity ( $\eta$ ) is a measure of a fluid's resistance to flow. It describes the internal friction of a moving fluid. Due to molecular structure, a high viscosity fluid resists movement due to high internal friction while a low viscosity fluid flows easily due to very low friction.

Viscosity of liquids or solutions is measured more accurately using Ubbelohde viscometer. Using the time taken for the distilled water and solution, the viscosity of unknown solutions is determined.

$$\frac{\eta_s}{\eta_w} = \frac{t_s \rho_s}{t_w \rho_w}$$

Where  $\eta_w$ ,  $\rho_w$  and  $t_w$  are the viscosity, density and time flow of distilled water respectively and  $\eta_s$ ,  $\rho_s$  and  $t_s$  are the viscosity, density and time flow of unknown liquid or solution respectively.

### 3.3 Ultrasound velocity (U) and its measurement

Ultrasound velocity in solutions refers to the speed at which ultrasonic waves propagate through a liquid solution. This velocity depends on many properties of the solution, including its density, compressibility, solute concentration, temperature, and pressure.

In ultrasonic interferometry, an ultrasonic standing wave is produced between a transducer and a reflector. The distance between the transducer and reflector is varied to measure the wavelength of the ultrasonic wave. Knowing the frequency of the wave, the velocity is calculated by multiplying the wavelength and frequency. The sound velocity (U) of the solvent and solution was calculated from wavelength and frequency (F) according to equation.

$$U = \lambda F$$

Experimentally calculated data of density ( $\rho$ ), viscosity ( $\eta$ ) and ultrasound velocity ( $u$ ) of pure solvents and solutions of the synthesized compounds in DMF and in  $\text{CHCl}_3$  at three different temperatures are reported in Table. 1 to 6 as follows:

**Table 1** Density ( $\rho$ ), viscosity ( $\eta$ ) and ultrasonic velocity ( $U$ ) of compound **3** in DMF at 300.15 °K.

Sr. No.	Concentration ( $\times 10^{-3}$ M)	Density ( $\times 10^{-3}$ $\text{kgm}^{-3}$ )	Viscosity ( $\times 10^{-3}$ $\text{Nsm}^{-2}$ )	Sound Velocity ( $\text{ms}^{-1}$ )
1	00	0.9518	0.6453	1384.6
2	2.0	0.9525	0.6772	1394.0
3	4.0	0.9544	0.7052	1401.2
4	6.0	0.9541	0.7185	1409.6
5	8.0	0.9545	0.7301	1418.5
6	10	0.9551	0.7466	1426.4

**Table 2** Density ( $\rho$ ), viscosity ( $\eta$ ) and ultrasonic velocity ( $U$ ) of compound **3** in DMF at 305.15 °K.

Sr. No.	Concentration ( $\times 10^{-3}$ M)	Density ( $\times 10^{-3}$ $\text{kgm}^{-3}$ )	Viscosity ( $\times 10^{-3}$ $\text{Nsm}^{-2}$ )	Sound Velocity ( $\text{ms}^{-1}$ )
1	00	0.9491	0.6005	1316.4
2	2.0	0.9499	0.6379	1324.0
3	4.0	0.9506	0.6558	1330.6
4	6.0	0.9508	0.6822	1339.3
5	8.0	0.9512	0.7011	1347.4
6	10	0.9530	0.7235	1354.6

**Table 3** Density ( $\rho$ ), viscosity ( $\eta$ ) and ultrasonic velocity ( $U$ ) of compound **3** in DMF at 310.15 °K.

Sr. No.	Concentration ( $\times 10^{-3}$ M)	Density ( $\times 10^{-3}$ $\text{kgm}^{-3}$ )	Viscosity ( $\times 10^{-3}$ $\text{Nsm}^{-2}$ )	Sound Velocity ( $\text{ms}^{-1}$ )
1	00	0.9484	0.5571	1286.1
2	2.0	0.9488	0.5777	1294.6
3	4.0	0.9500	0.5982	1305.7
4	6.0	0.9509	0.6205	1311.0
5	8.0	0.9513	0.6454	1321.9
6	10	0.9523	0.6737	1331.5

**Table 4** Density ( $\rho$ ), viscosity ( $\eta$ ) and ultrasonic velocity (U) of compound **3** in chloroform at 300.15 °K.

Sr. No.	Concentration (x 10 <sup>-3</sup> M)	Density (x 10 <sup>-3</sup> kgm <sup>-3</sup> )	Viscosity (x 10 <sup>-3</sup> Nsm <sup>-2</sup> )	Sound Velocity (ms <sup>-1</sup> )
1	00	1.3865	0.5268	976.21
2	2.0	1.3873	0.5291	978.03
3	4.0	1.3880	0.5308	979.98
4	6.0	1.3886	0.5330	982.10
5	8.0	1.3891	0.5347	984.05
6	10	1.3899	0.5365	986.33

**Table 5** Density ( $\rho$ ), viscosity ( $\eta$ ) and ultrasonic velocity (U) of compound **3** in chloroform at 305.15 °K.

Sr. No.	Concentration (x 10 <sup>-3</sup> M)	Density (x 10 <sup>-3</sup> kgm <sup>-3</sup> )	Viscosity (x 10 <sup>-3</sup> Nsm <sup>-2</sup> )	Sound Velocity (ms <sup>-1</sup> )
1	00	1.3835	0.5208	967.02
2	2.0	1.3842	0.5228	969.17
3	4.0	1.3849	0.5250	971.88
4	6.0	1.3855	0.5275	974.22
5	8.0	1.3864	0.5299	976.67
6	10	1.3873	0.5323	978.43

**Table 6** Density ( $\rho$ ), viscosity ( $\eta$ ) and ultrasonic velocity (U) of compound **3** in chloroform at 310.15 °K.

Sr. No.	Concentration (x 10 <sup>-3</sup> M)	Density (x 10 <sup>-3</sup> kgm <sup>-3</sup> )	Viscosity (x 10 <sup>-3</sup> Nsm <sup>-2</sup> )	Sound Velocity (ms <sup>-1</sup> )
1	00	1.3810	0.5164	957.03
2	2.0	1.3820	0.5190	958.97
3	4.0	1.3827	0.5213	961.21
4	6.0	1.3835	0.5234	963.47
5	8.0	1.3843	0.5258	965.79
6	10	1.3850	0.5275	967.62

## RESULT AND DISCUSSION

The density of solutions is an important physical property, which provides information on the concentration of a solution and the interactions between solute and solute molecules. Viscosity is influenced by the interactions between molecules in a fluid. Fluids with stronger intermolecular forces typically have higher viscosities. In liquids, it generally decreases with increasing temperature as thermal energy overcomes

intermolecular forces. Ultrasound velocity measurement is a versatile and non-invasive technique for analyzing the physical and chemical properties of solutions.

By understanding the relationship between ultrasound velocity, density, viscosity, and compressibility, accurate measurements of solution composition, molecular interactions, and concentration can be easily determined. Herein, density, viscosity and ultrasonic sound velocity have been studied for different concentrations of compound **3** in DMF and  $\text{CHCl}_3$  at 300.15 °K, 305.15 °K and 310.15 °K.

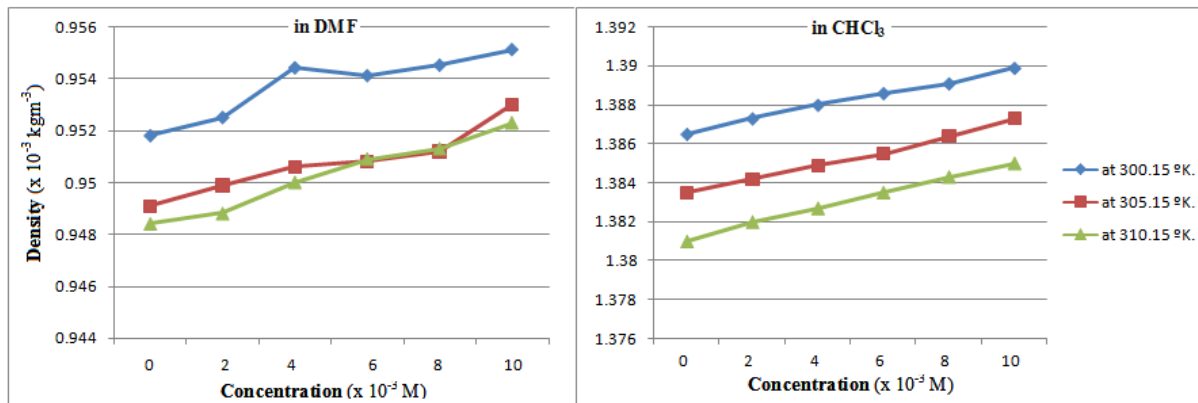


Figure 1 Variation of density with concentrations at different temperature of compound **3** in (a) DMF and in (b)  $\text{CHCl}_3$

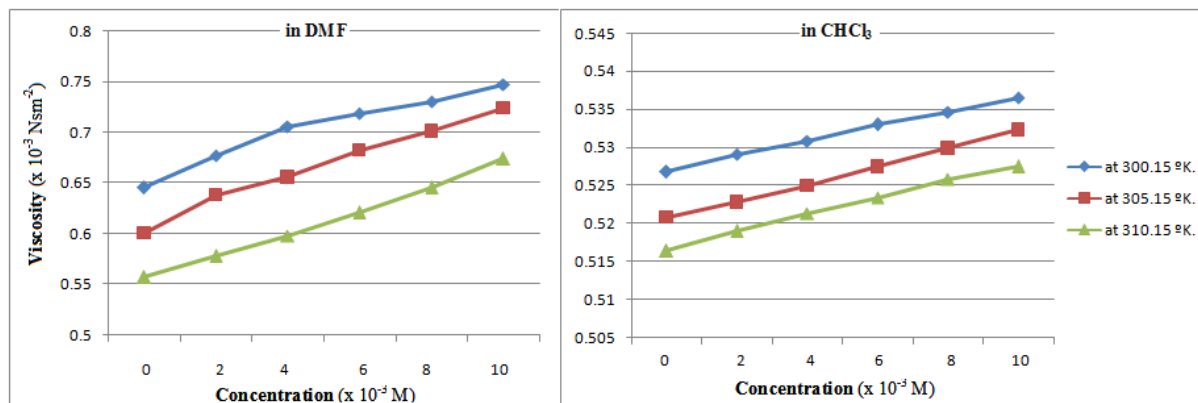


Figure 2 Variation of viscosity with concentrations at different temperatures of compound **3** in (a) DMF and (b)  $\text{CHCl}_3$

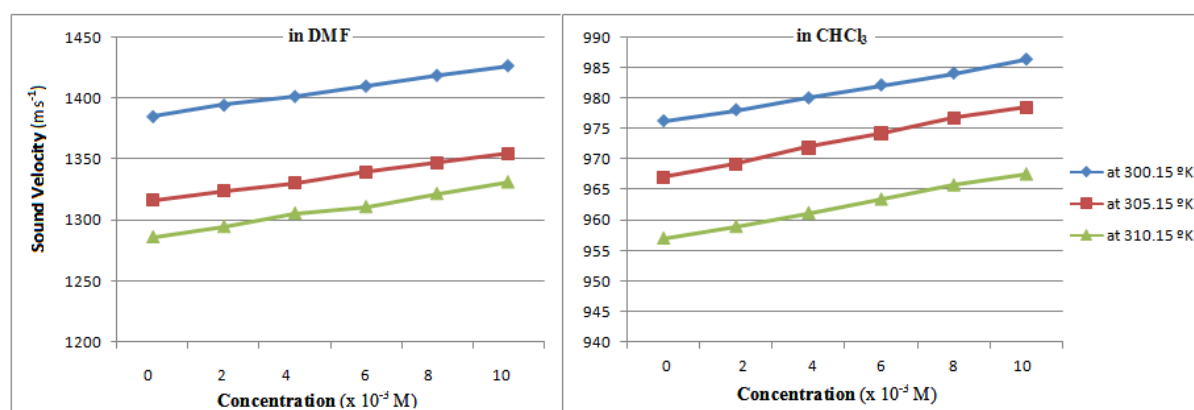


Figure 3 Variation of sound velocity with concentrations at different temperature of compound 3 in (a) DMF and (b) CHCl<sub>3</sub>

From experimental data, Tables 1 to 6 and Figures 1 to 3 show the differences in density ( $\rho$ ), viscosity ( $\eta$ ) and ultrasonic sound velocity ( $u$ ) between pure solvents (DMF and CHCl<sub>3</sub>) and solutions of the synthesized compound.

Density of compound 3 solutions in DMF ranges from  $0.9484$  to  $0.9551 \times 10^{-3} \text{ kg.m}^{-3}$  while in chloroform it varies from  $1.3810$  to  $1.3899 \times 10^{-3} \text{ kg.m}^{-3}$ . There is a gradual increase in the density of solution in chloroform while in DMF solution, the density of solution was nearly similar at higher temperature that is at  $305.15^\circ\text{K}$  and  $310.15^\circ\text{K}$ . The viscosity of compound 3 solution in DMF and chloroform ranges between  $0.5571 \times 10^{-3} \text{ Nsm}^{-2}$  to  $0.7466 \times 10^{-3} \text{ Nsm}^{-2}$  and  $0.5164 \times 10^{-3} \text{ Nsm}^{-2}$  to  $0.5365 \times 10^{-3} \text{ Nsm}^{-2}$  respectively. The ultrasound velocity values of compound 3 solutions in DMF and chloroform ranged from  $1286.1 \text{ ms}^{-1}$  to  $1426.4 \text{ ms}^{-1}$  and  $957.03 \text{ ms}^{-1}$  to  $986.33 \text{ ms}^{-1}$ , respectively. The highest ultrasound velocity of  $1456.4 \text{ ms}^{-1}$  was observed at  $300.15^\circ\text{K}$  for a  $10 \times 10^{-3} \text{ M}$  concentrated solution of DMF and  $1001.29 \text{ ms}^{-1}$  for a  $10 \times 10^{-3} \text{ M}$  concentrated solution of chloroform at the same temperature.

From Figure 1-3, it was observed that the density, viscosity and ultrasonic velocity increases with increase in concentration of the compound. An increase in temperature causes the solute molecules to move faster and separate further, causing the density to decrease. An increase in temperature increases the kinetic or thermal energy and the molecules become more mobile, which lowers the attractive bond energy and thus lowers the viscosity.

## CONCLUSION

In conclusion, the density, viscosity and ultrasonic velocity of the compound 3 were measured in DMF and CHCl<sub>3</sub> at various temperatures and found to be consistent. Trends and deviations in derived parameters were confirmed with the existence of strong interactions and dipole-dipole interactions. the density, viscosity and ultrasonic velocity increases with increase in concentration of the compound. An increase in temperature causes the solute molecules to move faster and separate further, causing the density to decrease.

### Acknowledgement

Maulana Azad College Chhatrapati Sambhajinagar is gratefully acknowledged for providing laboratory facilities.

### REFERENCES

- [1] Espinoza-Hicks JC, Chávez-Flores D, Galán GZ, Camacho-Dávila AA. *J. Heterocycl. Chem.* 2023; 60, 1027-31.
- [2] B. Gracia, R. Alcade, J. M. Leal and J. M. Matos, *J. Chem. Soc. Faraday Trans.*, 93 (1997) 1115.
- [3] G. Douheret, M. I. Davis, I. J. Fjallanger and H. Hoiland, *J. Chem. Soc. Faraday Trans.*, 93 (1997) 1943.
- [4] Tamura, K.; Sonoda, T.; Murakami, S. Thermodynamic properties of aqueous solution of 2-isopropoxyethanol at 25°C. *J. Solution Chem.*, 1999; 28, 777-789.
- [5] Marcus, Y. The properties of organic liquids that are relevant to their use as solvating solvents. *Chem. Soc. Rev.*, 1993, 22(6), 409-416.
- [6] Meek, D.K. The chemistry of non-aqueous solvents; ed. J. J. Lagowski, Academic, New York, Vol-1, Chapter 1, (1966).
- [7] Franks, F. Physico-chemical processes in mixed aqueous solvents, Heinemann educational books Ltd., (1967)
- [8] Popovych, O; Bates, R.G. Estimation of medium effects for single ions in non-aqueous solvents. *C R C Crit. Rev. Anal. Chem.*, 1970; 1, 73-117.
- [9] Bates, R.G. Solute-solvent interactions. Eds. Coetzee, J.F. and Ritchie, C.D., Marcel Dekker, New York and London, (1969).
- [10] Parker, A.J. Solvation of ions-enthalpies, entropies and free energies of transfer. *Electrochim. Acta*, 1976; 21(9), 671-679.
- [11] Criss, C. M.; Salomon, M. Thermodynamics of ionic solvation and its significance in various systems. 1976; 53(12), 763-766.
- [12] Marcus, Y. Ionic solvation: Wiley-Interscience, Chichester, (1985).
- [13] Dogonadze, R. R.; Kalman, E.; Kornyshev, A. A.; Ulstrup, J. The chemical physics of solvation, Elsevier, Amsterdam, (1988).
- [14] Popovych, O.; Tomkins, R. P. T. Non-Aqueous Solution Chemistry, John Wiley and Sons, New York, (1981).
- [15] Faraday Discussions of the Chemical Society, 67 (1977).
- [16] Kamble, S.A.; Vedpathak, S.G.; Kirdant, A.S.; Quadri, S.H. Synthesis and biological evaluation of some novel quinoline-tetrazole Schiff base hybrids as antimicrobial agents. *Int. J. Pharm. Res. Appl.*, 2024; 9(1), 1747-1755.

# Security Databases : A Comprehensive Overview

**Mahendra D. Acharya**

Department of Computer Science, Yogeshwari Mahavidyalaya, Ambajogai, Maharashtra, India

Corresponding author: [mehen.acharya@gmail.com](mailto:mehen.acharya@gmail.com)

## ABSTRACT

Data security is a major concern for businesses all over the world in the digital age. By storing and managing data related to cybersecurity, such as access logs, user credentials, threat intelligence, and vulnerabilities, security databases are crucial in protecting sensitive information. This paper discusses the various types of security databases, including encryption key management databases, vulnerability databases, authentication databases, and intrusion detection system (IDS) databases. It looks at how they can be used to support efforts in threat intelligence and incident response as well as ensure regulatory compliance. Security database management issues like scalability, data integrity, performance, and privacy concerns are also addressed in this paper. The integration of artificial intelligence (AI), the rise of cloud-based solutions, Zero Trust models, and the possibility of using blockchain for database security are all discussed as potential future directions for improving the effectiveness of security databases.

## INTRODUCTION

Data security has emerged as a major concern in a time when digital transformation is driving every industry. Data breaches and cyberattacks are on the rise, so businesses must protect their databases, which hold a lot of sensitive information. When it comes to ensuring the availability, confidentiality, and integrity of data, security databases are an essential component. Security databases, their types, applications, difficulties, and emerging trends are examined in this article.

## WHAT IS A SECURITY DATABASE?

A system designed to store and manage security-related information is referred to as a security database. This ensures that data is protected from unauthorized access, misuse, or threats. Audit trails, user activity logs, access controls, and frequently encryption mechanisms are all part of these databases. Security databases can also refer to data repositories that help businesses identify vulnerabilities, cyber threats, and incidents and prepare for and respond to them.



## TYPES OF SECURITY DATABASES

Security databases come in a variety of forms and serve different purposes based on the requirements of the organization. The most common types of security databases are as follows:

### 1. Intrusion Detection System (IDS) Databases

Information related to suspicious activities that are detected within a network or system is stored in IDS databases. Most of the time, events like unauthorized access attempts, unusual behavior patterns, or known malware signatures are recorded in these databases. There are two types of intrusion detection systems: host-based (HIDS) and network-based (NIDS).

- **NIDS** logs network traffic and looks for anomalies to look for potential threats across all networks.
- **HIDS** monitors system-level activities like file access and changes, focusing on individual devices.

### 2. Authentication Databases

Username, passwords, and other authentication tokens are all stored in authentication databases. Because these databases are the entry point to protected resources, their security is of the utmost importance. Security measures for authentication databases include the following:

- **Hashing:** Before being stored, passwords are hashed to ensure that they are not stored in plaintext.
- **Salting:** Before each password is hashed, a random value is added for security.

LDAP (Lightweight Directory Access Protocol) and Active Directory are two popular authentication databases.

### 3. Vulnerability Databases

Information about known software vulnerabilities is stored in vulnerability databases, which are frequently updated by software vendors and security researchers. Some common databases are:

- **Common Vulnerabilities and Exposures (CVE):** This MITRE-managed repository keeps track of vulnerabilities that are made public.
- **National Vulnerability Database (NVD):** a data repository for vulnerability management managed by the US government.

Before attackers can take advantage of vulnerabilities in their systems, these databases assist organizations in identifying and patching them.

### 4. Encryption Key Management Databases

Data security relies heavily on encryption, so encryption keys must be carefully managed. The encryption keys used to encrypt and decrypt sensitive data are stored and protected in encryption key management databases. The integrity of these databases is guaranteed by security measures like auditing, role-based access control (RBAC), and multi-factor authentication (MFA).

## APPLICATIONS OF SECURITY DATABASES

In order for businesses to safeguard their essential data and infrastructure, security databases are essential across all industries. Common applications are as follows:

### 1. Compliance and Regulatory Adherence

The General Data Protection Regulation (GDPR) and the Health Insurance Portability and Accountability Act (HIPAA) are two examples of stringent data security and privacy regulations that must be adhered to by many industries. By providing detailed logs, audit trails, and access control records, security databases assist businesses in maintaining compliance. These databases store crucial data for auditing and ensuring that sensitive data is handled in accordance with regulations.

### 2. Incident Response and Forensics

Security databases offer incident response teams useful insights in the event of a security breach. These databases keep track of suspicious activities and are an important resource for forensic investigations. They help security teams find the source of the breach, find compromised systems, and figure out how much damage has been done. Understanding and mitigating a security incident becomes significantly more difficult without a comprehensive security database.

### 3. Threat Intelligence and Cybersecurity Operations

Threat intelligence data, such as attack patterns and indicators of compromise (IOCs), can be stored in security databases, allowing businesses to anticipate new threats and respond appropriately. Security operations centers (SOCs) are made up of these databases, which allow for real-time, continuous monitoring, detection, and mitigation of cybersecurity threats.

## CHALLENGES IN MANAGING SECURITY DATABASES

While security databases offer numerous advantages, they also come with a number of drawbacks:

### 1. Scalability

The size and complexity of security databases grow in tandem with the size and volume of organizations and the data they manage. It takes a lot of resources and infrastructure to manage large databases. Performance bottlenecks caused by scalability issues can impede security incident detection and response.

### 2. Data Integrity and Availability

It is essential to guarantee the availability and integrity of security database systems. Access to crucial data can be restricted by a compromised or corrupted security database, putting off the resolution of security incidents. Additionally, redundancy, backups, and disaster recovery planning are essential for ensuring high availability in the event of hardware or software failures.

### 3. Performance and Latency

The performance of security databases must be optimized. In order to guarantee prompt responses to potential incidents, queries involving security events, audit logs, or threat intelligence should return results quickly. Systems may be vulnerable to attacks due to delays in identifying and mitigating security threats caused by slow or high latency queries.

### 4. Data Privacy Concerns

Confidential corporate data and personally identifiable information (PII) are examples of sensitive data that security databases frequently store. When databases contain highly sensitive data, it is difficult to strike a balance between privacy and security. To reduce privacy risks, data must be encrypted at rest and in transit and robust access controls must be implemented.

## EMERGING TRENDS AND FUTURE DIRECTIONS

Security databases must adapt to new challenges because the security landscape is constantly changing. The following are some of the new trends that will shape security databases' future:

### 1. Integration with Artificial Intelligence (AI) and Machine Learning (ML)

Cybersecurity is being transformed by AI and machine learning, which enables threat detection and response mechanisms that are more intelligent and automated. Anomalies in behavior, threats that were previously unknown, and even attacks that will occur in the future can all be predicted using historical data in security databases that are integrated with AI/ML algorithms. Database security and the IT environment as a whole will become increasingly dependent on AI/ML models as they advance.

### 2. Cloud-based Security Databases

Security databases are also moving to cloud environments as more businesses move to the cloud. Databases hosted in the cloud provide scalability, adaptability, and lower operating expenses. However, they also come with their own set of security issues, like how to protect data in environments with multiple tenants and make sure that laws about data sovereignty are followed.

### 3. Zero Trust Security Models

In the field of cybersecurity, zero trust models are gaining traction. These models make the assumption that no user or system within or outside the network is trusted by default. By storing and enforcing access policies, monitoring user behavior, and logging all activities for auditing purposes, security databases play a crucial role in the implementation of Zero Trust. Security databases will evolve to better support these principles as Zero Trust becomes more widespread.

### 4. Blockchain for Secure Databases

Database security is being investigated in light of the decentralized and immutable nature of blockchain technology. Blockchain can provide audit trails that can't be changed, ensuring the integrity of access records

and security logs. This technology has the potential to secure crucial databases in the future, even though it is still in its infancy.

## CONCLUSION

Security databases are an important part of modern cybersecurity strategies because they protect against threats and make sure that regulations are followed. These databases help businesses safeguard their digital assets by logging security events and vulnerabilities, storing user credentials, and so on. However, scalability, performance, and data privacy are just a few of the issues that arise when managing and protecting these databases. The future of security databases will be shaped by integrating AI, migrating to the cloud, and exploring blockchain-based solutions as technology advances, allowing businesses to stay ahead of new threats.

## REFERENCES

- [1] Bace, R., & Mell, P. (2001). NIST Special Publication 800-31: Intrusion Detection Systems (IDS). National Institute of Standards and Technology (NIST). Retrieved from <https://nvlpubs.nist.gov/nistpubs/Legacy/SP/nistspecialpublication800-31.pdf>
- [2] Bishop, M. (2005). Introduction to Computer Security. Addison-Wesley.
- [3] Bowen, P., Hash, J., & Wilson, M. (2006). NIST Special Publication 800-100: Information Security Handbook: A Guide for Managers. National Institute of Standards and Technology (NIST). Retrieved from <https://csrc.nist.gov/publications/detail/sp/800-100/final>
- [4] MITRE Corporation. (2024). Common Vulnerabilities and Exposures (CVE) Database. Retrieved from <https://cve.mitre.org/>
- [5] Scarfone, K., Grance, T., & Masone, K. (2008). NIST Special Publication 800-94: Guide to Intrusion Detection and Prevention Systems (IDPS). National Institute of Standards and Technology (NIST). Retrieved from <https://nvlpubs.nist.gov/nistpubs/Legacy/SP/nistspecialpublication800-94.pdf>
- [6] Stewart, J. M., Chapple, M., & Gibson, D. (2022). CISSP (ISC)<sup>2</sup> Certified Information Systems Security Professional Official Study Guide (9th ed.). Sybex.
- [7] Kaur, M., & Bansal, R. (2020). "A Survey on Security Issues in Cloud Computing and Security Approaches." Journal of Computer Networks and Communications, 2020. <https://doi.org/10.1155/2020/8871412>
- [8] Ruan, K., & Carthy, J. (2012). "Cloud Forensics: Key Considerations for Cloud Computing Environments." IEEE Security & Privacy, 10(6), 11-20. <https://doi.org/10.1109/MSP.2012.108>
- [9] National Institute of Standards and Technology (NIST). (2021). Zero Trust Architecture. NIST Special Publication 800-207. Retrieved from <https://csrc.nist.gov/publications/detail/sp/800-207/final>
- [10] Nakamoto, S. (2008). "Bitcoin: A Peer-to-Peer Electronic Cash System." Retrieved from <https://bitcoin.org/bitcoin.pdf>

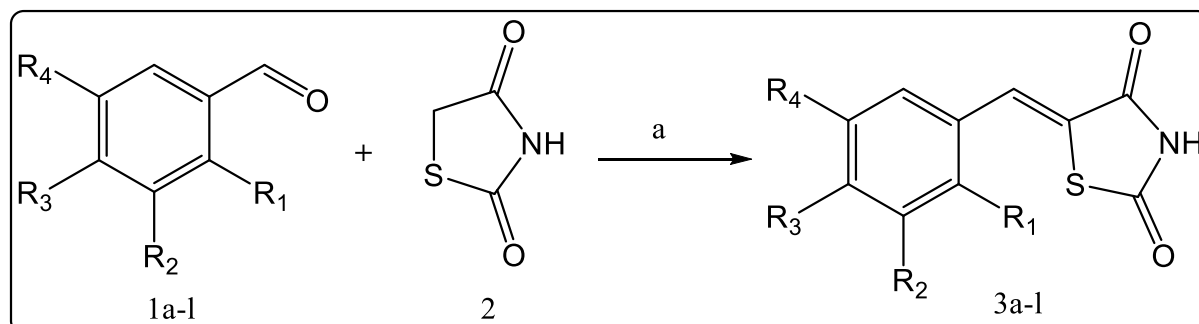
## One Pot Procedure for Green Synthesis of Benzylidenethiazolidine-2,4-Diones Using Catalytic Amount of Anhydrous Aluminium Chloride in Ethanol Solvent Via Knoevenagel Condensation Reaction

Sayas K Lad, Babasaheb V Kendre\*

Post Graduate Research Centre in Chemistry, Vaidyanath College, Parli-Vajnath (Affiliated to Dr. Babasaheb Ambedkar Marathwada University, Chh. Sambhajinagar), Dist. Beed Maharashtra, India  
Email: [bvkendre71@gmail.com](mailto:bvkendre71@gmail.com)

### ABSTRACT

A new series of benzylidenethiazolidine-2,4-diones (**3a-j**) has been synthesized *via* the condensation reaction of substituted aromatic aldehydes with active methylene compound (thiazolidin-2,4-dione) in the presence of catalytic amount of anhydrous  $\text{AlCl}_3$  in freshly distilled out ethanol under refluxing conditions for 1.5-2h. The transformation of reactants to the products was supported by functional group tests and melting points. The structures of synthesized compounds were confirmed by IR,  $^1\text{H}$ NMR,  $^{13}\text{C}$ NMR and mass spectral analysis. This simplified procedure is environmentally sustainable and cost effective that gives target compounds in excellent yields (87-92%) with high selectivity in short reaction time.



**Reagents and reaction conditions:** a)  $\text{AlCl}_3$ , Ethanol, Reflux, 1.5-2h, (87-92%)

**Keywords:** Thiazolidin-2,4-dione, benzylidenethiazolidine-2,4-dione, Green synthesis, Anhydrous aluminium chloride, conventional heating.

### INTRODUCTION

The set of concepts called as “green chemistry” has been become extremely popular since discovery by Paul Anastas and John C Warner in the 1990s<sup>1</sup> and provided insight on developing new chemicals and chemical processes to achieve the function of ecofriendly environment. Nowadays, it is a creative challenge for the researchers, technologists and engineers to put twelve principles into action to achieve the goal of green chemistry<sup>2</sup>. Knoevenagel condensation reaction is one of the important name reactions in chemistry which has gained tremendous attraction of researchers for synthesizing a variety of heterocyclic compounds having

medicinal values<sup>3</sup>. Knoevenagel condensation reaction has played significant role in synthesizing a wide range of naturally occurring medicinally active heterocyclic compounds<sup>4</sup>. This reaction finds application in synthesizing a number of heterocyclic compounds for medicinal applicability<sup>5</sup>.

Benzylidenethiazolidine-2,4-diones are biologically active heterocyclic compounds contain five and six member rings condensed through a  $\pi$  bond, five membered ring contains N, S and O as bioactive hetero atoms and six membered aromatic ring is substituted by a variety of functional groups. Due to these unique features, benzylidenethiazolidine-2,4-diones possess multiple broad spectrum of biological activities including antimicrobial<sup>6</sup>, antidiabetic<sup>7</sup>, anticancer<sup>8</sup>, anti-inflammatory<sup>9</sup>, antiproliferative<sup>10</sup> antitumor<sup>11</sup> and inhibitors of protein tyrosine phosphatases<sup>12</sup> activity. Aluminum chloride ( $\text{AlCl}_3$ ) is regarded as a versatile inorganic substance, and therefore finds applications in many fields, particularly in chemical reactions and organic synthesis<sup>13</sup>. It is inexpensive, highly reactive and selective Lewis acid catalyst. Notably,  $\text{AlCl}_3$  is used as a catalyst in both Friedel-Crafts acylation and alkylation reactions<sup>14</sup>. It is also used widely in manufacturing of rubber, lubricants, wood preservatives and paints. It is used in pesticides and pharmaceuticals.

Benzylidenethiazolidine-2, 4-diones were synthesized by several methods such as, sodium acetate in acetic acid under reflux conditions<sup>15</sup>, sodium acetate in acetic acid under microwave irradiation<sup>16</sup>, piperidine in ethanol under reflux conditions<sup>17</sup>, piperidine in acetic acid<sup>18</sup>, grinding with ammonium acetate in the absence of solvents<sup>19</sup>, baker's yeast<sup>20</sup> and polyethylene glycol-300 at 100-120°C<sup>21</sup>. However, these literature methods are associated with certain drawbacks such as long reaction time, create harmful wastes, organic solvents, low product yields and difficult isolation procedures. To the best of our knowledge,  $\text{AlCl}_3$  has not been used as a catalyst in Knoevenagel condensation reaction, especially in the synthesis of benzylidenethiazolidine-2, 4-diones, therefore received our attention for synthesizing benzylidenethiazolidine-2, 4-diones as biologically active molecules. Ethyl alcohol is second widely used solvent after water in industrial field. It is one of the important green solvents mostly manufactured from the natural sources<sup>22</sup>. Herein, we attempt to explore the significance of present investigation under the category of green synthesis for synthesizing new heterocyclic compounds possessing biological properties.

## MATERIAL AND METHODS

All chemicals were obtained from Spectrochem and S.D. Fine Chem. Co. and used without further purification. Melting points of the compounds were determined by open capillary method and were uncorrected. IR spectra were recorded on a Bruker made spectrophotometer.  $^1\text{H}$  and  $^{13}\text{C}$  NMR spectra were recorded using a Bruker instrument ( $^1\text{H}$  at 400 MHz and  $^{13}\text{C}$  at 300 MHz) in  $\text{DMSO-d}_6$  solvent and TMS as internal standard. Chemical shifts were reported in ppm. Mass spectra for the compounds were recorded on Shimadzu GC-MS-QP-2010 model using Direct Injection Probe technique. Reactions have been monitored by thin layer chromatography on 0.2-mm precoated plates of silica gel G60 F254 (Merck).

### *General procedure for the synthesis of Benzylidenethiazolidine-2, 4-diones*

Place aromatic aldehydes **1a-1** (0.01mol), thiazolidine-2,4-dione **2** (0.01mol), freshly distilled out ethyl alcohol (5ml) and 10 mole% anhydrous  $\text{AlCl}_3$  in RB flask (100mL). The reaction mixture was refluxed for

1.5-2h on water bath and progress of reaction was monitored by TLC. After the completion of reaction as indicated by TLC, the reaction mixture was cooled and poured into 100gm ice crystals and stirred by glass rod till the solid separates out. The solid product was filtered, washed 4-5 times with cold water and recrystallized from ethanol to obtain pure benzylidenethiazolidine-2, 4-diones in (87-92%) yields.

**Table 1: Synthesis of benzylidenethiazolidine-2, 4-diones (3a-j)**

Entry	R <sub>1</sub>	R <sub>2</sub>	R <sub>3</sub>	R <sub>4</sub>	Reaction Time (h)	Yield(%) <sup>a</sup>	Mp (°C) <sup>b</sup>
<b>3a</b>	H	H	H	H	1.5	92	85-87
<b>3b</b>	H	H	-OH	H	2.0	87	104-105
<b>3c</b>	H	H	-F	H	2.0	88	77-79
<b>3d</b>	H	H	-Cl	H	2.0	88	97-98
<b>3e</b>	H	-OCH <sub>3</sub>	-OH	C <sub>4</sub> H <sub>9</sub> N <sub>2</sub>	1.5	90	162-164
<b>3f</b>	H	-OCH <sub>3</sub>	-OH	C <sub>4</sub> H <sub>8</sub> NO	1.5	90	145-146
<b>3g</b>	H	H	-NO <sub>2</sub>	H	1.5	91	96-98
<b>3h</b>	H	H	-Br	H	2.0	87	107-108
<b>3i</b>	H	-OH	H	H	2.0	92	99-100
<b>3j</b>	H	NO <sub>2</sub>	H	H	1.5	92	89-93

Bold signifies the Isolated Yield.

<sup>a</sup> Isolated yields

<sup>b</sup>Physical constants

**Table 2: Solvent optimization for model reaction**

Sr. No.	Solvent	Time (h)	Yield (%) <sup>a</sup>
1	Ethanol (EtOH)	2.5	92
2	Ethylene glycol (EG)	2.5	91
3	Dimethyl formamide (DMF)	3h	72
4	Tetrahydrofuran (THF)	3h	70
5	No solvent	5h	65

<sup>a</sup>Isolated yields

## RESULTS AND DISCUSSION:

The present investigation describes synthesis of benzylidenethiazolidine-2, 4-dione derivatives (3a-l) from substituted aromatic aldehydes **1a-l** and heterocyclic compound thiazolidine-2,4-dione **2** *via* Knoevenagel condensation reaction under refluxing conditions on water bath in the presence of anhydrous aluminum chloride (AlCl<sub>3</sub>) as catalyst in ethanol for 3-4 hours. Earlier, thiazolidine-2, 4-dione was prepared following our previously reported literature procedure. In the beginning, we attempted to synthesize benzylidenethiazolidine-2, 4-dione from benzaldehyde and thiazolidine-2,4-dione using molecular iodine as catalyst in water under conventional heating conditions for 8-10h, but could not afford product. The

above reaction was also attempted in ethanol using  $I_2$ - $K_2CO_3$  catalyst under conventional heating conditions for 7-8 hours. The reaction gave product formation in 40% yield. Improvement in the yield did not observe even after changing solvents. Anhydrous aluminum chloride ( $AlCl_3$ ) was extensively used catalyst in number of chemical transformation therefore, we thought worthwhile to use this catalyst in above chemical reaction. Surprisingly, the reactants started to convert into products after 1.5 hours in ethylene glycol and afforded desired product in 85% yield after 2.5 hours. The product formation was confirmed by TLC, functional group test and melting point. The target compound was selectively obtained without side products. We attempted to carry out above model reaction in ethanol using 10 mole percent catalytic amount of anhydrous aluminum chloride to maintain eco-friendly environment. The reaction was completed in 2.5 hours with little improvement in yield (Table 1). In order to optimize the reaction conditions, we performed this model reaction at higher temperature by increasing the catalytic amount in ethanol and in other solvents on refluxing into oil bath for 4-5 hours, no significant improvement in yield was observed. Therefore, the quantity of aromatic aldehyde (0.01mole), thiazolidine-2,4-dione (0.01mole) and ethanol (5-6mL) was fixed for all condensation reactions. The percentage yield, time and physical constant for all target compounds are entered into table-1. The structures of compounds were confirmed by IR,  $^1H$ NMR,  $^{13}C$ NMR and mass spectral methods.

3.1. The spectral data for new compounds 3e and 3f is given below.

(a). (Z)-5-(4-hydroxy-3-methoxy-5-(piperazin-1-yl)benzylidene)thiazolidine-2,4-dione 3e

IR (KBr,  $\nu$   $cm^{-1}$ ): 3392 (NH str.), 1705, 1782 (C=O str.), 1590 (C=C str.), 772 (C-S-C str.), 3465 (O-H str.).  $^1H$  NMR (400 MHz, DMSO- $d_6$ ):  $\delta$ = 11.15 (s, 1H, NH), 8.71(s,1H, OH), 7.01- 6.54 (d, 2H, aromatic), 3.73(s, 3H,  $OCH_3$ ), 7.75 (s, 1H, CH) ppm;  $^{13}C$  NMR (100 MHz, DMSO- $d_6$ ):  $\delta$ =166.37, 164.63, 148.15, 144.07, 140.37, 128.75, 128.21, 115.31, 99.73, 99.13, 54.56 ppm; EI-MS (m/z): 335.09 [ $M^+$ ].

(b). (Z)-5-(4-hydroxy-3-methoxy-5-morpholinobenzylidene)thiazolidine-2,4-dione 3f

IR (KBr,  $\nu$   $cm^{-1}$ ): 3321 (NH str.), 1735, 1797 (C=O str.), 1595 (C=C str.), 767 (C-S-C str.), 3445 (O-H str.).  $^1H$  NMR (400 MHz, DMSO- $d_6$ ):  $\delta$ = 11.16 (s, 1H, NH), 8.69(s,1H, OH), 7.02- 6.61 (d, 2H, aromatic), 3.71(s, 3H,  $OCH_3$ ), 7.77 (s, 1H, CH) ppm;  $^{13}C$  NMR (100 MHz, DMSO- $d_6$ ):  $\delta$ =166.34, 164.68, 148.15, 145.00, 140.35, 128.79, 128.12, 115.31, 100.03, 99.15, 63.21, 54.52 ppm; EI-MS (m/z): 336.08 [ $M^+$ ].

## CONCLUSION

In conclusion, we have developed an efficient procedure for the synthesis of benzylidenethiazolidine-2, 4-diones using anhydrous  $AlCl_3$  as catalyst under refluxing conditions in ethanol. We attempt to synthesize target compounds under ecofriendly conditions to minimize environmental pollution. The final products were easily isolated without complications and purified by recrystallization technique. The current methodology has the advantages of operational simplicity, mild reaction conditions and good to high yields of the products (87-92%). The present technique reduces reaction time with improved yield. The substituents on aromatic ring did not show strongly effects in terms of reaction time and yield of products.

**Acknowledgements:** Authors are thankful to Principal, Vaidyanath College Parli-Vajinath for providing research facilities.



## REFERENCES

- [1] Emil Knoevenagel (1898). "Condensation von Malonsäure mit aromatischen Aldehyden durch Ammoniak und Amine" [Condensation of malonic acid with aromatic aldehydes via ammonia and amines]. *Berichte der deutschen chemischen Gesellschaft*. 31 (3): 2596-2619. doi:10.1002/cber.18980310308.
- [2] Chen TL, Kim H, Pan SY, Tseng PC, Lin YP, Chiang PC. Implementation of green chemistry principles in circular economy system towards sustainable development goals: Challenges and perspectives. *Science of the Total Environment*. 2020;716(1):136998. DOI: 10.1016/j.scitotenv.2020.136998
- [3] a) B. C. Ranu, R. Jana, Ionic Liquid as Catalyst and Reaction Medium - A Simple, Efficient and Green Procedure for Knoevenagel Condensation of Aliphatic and Aromatic Carbonyl Compounds Using a Task-Specific Basic Ionic Liquid, *Eur. J. Org. Chem.*, 2006, 3767-3770. b) Dr. Ramya Tokala, Darshana Bora, Dr. Nagula Shankaraiah Contribution of Knoevenagel Condensation Products toward the Development of Anticancer Agents: An Updated Review, *ChemMedChem*, 2022, 17(8), e202100736, <https://doi.org/10.1002/cmdc.202100736>
- [4] Heravi, M.M., Janati, F. & Zadsirjan, V. Applications of Knoevenagel condensation reaction in the total synthesis of natural products. *Monatsh Chem* 151, 439-482 (2020). <https://doi.org/10.1007/s00706-020-02586-6>.
- [5] van Beurden, K., de Koning, S., Molendijk, D., & van Schijndel, J. (2020). The Knoevenagel reaction: a review of the unfinished treasure map to forming carbon-carbon bonds. *Green Chemistry Letters and Reviews*, 13(4), 349-364. <https://doi.org/10.1080/17518253.2020.1851398>
- [6] Kumar, H., Deep, A. & Marwaha, R.K. Design, synthesis, in silico studies and biological evaluation of 5-((E)-4-((E)-(substituted aryl/alkyl)methyl)benzylidene)thiazolidine-2,4-dione derivatives. *BMC Chemistry* 14, 25 (2020). <https://doi.org/10.1186/s13065-020-00678-2>.
- [7] Najmi, A., Alam, M.S., Thangavel, N. et al. Synthesis, molecular docking, and in vivo antidiabetic evaluation of new benzylidene-2,4-thiazolidinediones as partial PPAR- $\gamma$  agonists. *Sci Rep* 13, 19869 (2023). <https://doi.org/10.1038/s41598-023-47157-x>
- [8] Khaled El-Adl, Abdel-Ghany A. El-Helby, Helmy Sakr, Ibrahim H. Eissa, Sanadelaslam S.A. El-Hddad, Fatma M.I.A. Shoman, Design, synthesis, molecular docking and anticancer evaluations of 5-benzylidenethiazolidine-2,4-dione derivatives targeting VEGFR-2 enzyme, *Bioorganic Chemistry*, 102, 2020, 104059, ISSN 0045-2068, <https://doi.org/10.1016/j.bioorg.2020.104059>.
- [9] Ma L, Xie C, Ma Y, Liu J, Xiang M, Ye X, Zheng H, Chen Z, Xu Q, Chen T, Chen J, Yang J, Qiu N, Wang G, Liang X, Peng A, Yang S, Wei Y, Chen L. Synthesis and biological evaluation of novel 5-benzylidenethiazolidine-2,4-dione derivatives for the treatment of inflammatory diseases. *J Med Chem*. 2011 Apr 14;54(7):2060-8. doi: 10.1021/jm1011534.
- [10] Patil, V., Tilekar, K., Mehendale-Munj, S., Mohan, R., Ramaa, C.S. *Eur. J. Med. Chem.* 45 (2010) 4539-44.
- [11] Iqbal Singh, Richa Rani, Vijay Luxami, Kamaldeep Paul, Synthesis of 5-(4-(1H-phenanthro[9,10-d]imidazol-2-yl)benzylidene)thiazolidine-2,4-dione as promising DNA and serum albumin-binding

- agents and evaluation of antitumor activity, *European Journal of Medicinal Chemistry*, 166, 2019, 267-280, 0223-5234, <https://doi.org/10.1016/j.ejmech.2019.01.053>.
- [12] Maccari R, Paoli P, Ottanà R, Jacomelli M, Ciurleo R, Manao G, Steindl T, Langer T, Vigorita MG, Camici G (2007) 5-Arylidene-2,4-thiazolidinediones as inhibitors of protein tyrosine phosphatases. *Bioorg Med Chem* 15:5137–5149.
- [13] Galatsis P (1999). "Aluminum Chloride". In Reich HJ, Rigby JH (eds.). *Acidic and Basic Reagents. Handbook of Reagents for Organic Synthesis*. New York City: Wiley. pp. 12–15. ISBN 978-0-471-97925-8.
- [14] Olah GA, ed. (1963). *Friedel-Crafts and Related Reactions*. Vol. 1. New York City: Interscience.
- [15] V. Patil, K. Tilekar, S.M. Munj, R. Mohan, C.S. Ramaa, *Synthesis and primary cytotoxicity evaluation of new 5-benzylidene-2,4-thiazolidinedione derivatives*, *Eur. J. Med. Chem.* 45 (2010) 4539–4544.
- [16] Ajmal R. Bhat, Mohd H. Najar, Rajendra S. Dongre, Mohammad S. Akhter, *Microwave assisted synthesis of Knoevenagel Derivatives using water as green solvent*, *Current Research in Green and Sustainable Chemistry*, 3, 2020, 100008, ISSN 2666-0865, <https://doi.org/10.1016/j.crgsc.2020.06.001>.
- [17] M.A. Ibrahim, M.A.M. Abde-Hamed, N.M. El-Gohary, *A new approach for the synthesis of bioactive heteroaryl thiazolidine-2,4-diones*, *J. Brazilian Chem. Soci* 6 (2011) 1130–1139.
- [18] Yang D-H, Chen Z-C, Chen S-Y, Zheng Q-G. *A Convenient Synthesis of 5-Benzylidenethiazolidine-2, 4-Diones under Microwave Irradiation without Solvent*. *Journal of Chemical Research*. 2003;2003(6):330-331. doi:10.3184/030823403103174272.
- [19] Metwally, Nadia Hanafy et al. "A simple and green procedure for the synthesis of 5-arylidene-4-thiazolidinones by grinding." *Green Chemistry Letters and Reviews* 4 (2011): 225 – 228.
- [20] Umesh R. Pratap, Dhanaji V. Jawale, Manisha R. Bhosle, Ramrao A. Mane, *Saccharomyces cerevisiae catalyzed one-pot three component synthesis of 2,3-diaryl-4-thiazolidinones*, *Tetrahedron Letters*, Volume 52, Issue 14, 2011, Pages 1689-1691, ISSN 0040-4039, <https://doi.org/10.1016/j.tetlet.2011.01.143>.
- [21] Mahalle, S. R., Netankar, P. D., Bondge, S. P., & Mane, R. A. (2008). *An efficient method for Knoevenagel condensation: a facile synthesis of 5-arylidene-2,4-thiazolidinedione*. *Green Chemistry Letters and Reviews*, 1(2), 103–106. <https://doi.org/10.1080/17518250802139881>
- [22] "Your Guide to Ethanol Extraction". *Cannabis Business Times*. Retrieved 9 April 2019.

# $\beta$ -Ammonium Metavanadate Catalyzed One-pot Synthesis of $\alpha$ -Amidoalkyl $\beta$ -Naphthols

Shaikh Alfiya Sadaf Atique, Pathan Rumina Munawar Khan, Shrikant S. Pndalwar, Sudhakar R. Bhusare

Department of Chemistry, Dnyanopasak College, Parbhani-431 401, Maharashtra, India

E-mail: [bhusare71@gmail.com](mailto:bhusare71@gmail.com)

## ABSTRACT

An efficient and eco-friendly procedure for the synthesis of 1-amidoalkyl-2-naphthol derivatives has been developed through a one-pot three-component condensation of aldehydes with 2-naphthol and amides in the presence of ammonium metavanadate as catalyst. This new procedure offers several advantages such as short reaction time, excellent yields, and operational simplicity and without any tedious work-up for product purification. Moreover, the catalyst could be simply separated by an external magnet and reused six times without significant loss of catalytic activity.

**Keywords:** Ammonium Metavanadate, One-pot Synthesis, Amidoalkyl Naphthols

## INTRODUCTION

One-pot multicomponent reactions by virtue of their convergence, effectiveness, simplistic execution and high yield have fascinated considerable attention in recent years. Multicomponent reactions comprises three or more compounds reacting in a single procedure without isolating the intermediates. 1-Amidoalkyl-2-naphthol derivatives are of importance because they can be effortlessly converted to the important biologically active compounds, 1-aminoalkyl-2-naphthols, by amide hydrolysis reaction. The hypotensive and Brady cardiac properties have been reported for this class of compounds. Multicomponent reaction (MCRs) have demonstrated as a powerful tool for the rapid introduction of molecular diversity. MCRs provide to the requirements of an environmentally friendly process by reducing the number of synthetic steps, energy consumption, and waste production<sup>2</sup>. One such reaction is the synthesis of amidoalkyl naphthols. 1-Amidoalkyl-2-naphthols can be also converted to 1,3-oxazine derivatives which have potentially different biological activities including antibiotic, antitumor, analgesic, anticonvulsant, antipsychotic, antimalarial, antianginal, antihypertensive and antirheumatic properties<sup>3-7</sup>. The preparation of 1-amidoalkyl-2-naphthols can be carried out by multi-component condensation of aryl aldehydes, 2-naphthol and amide derivatives in the presence of Lewis or Bronsted acid catalysts such as  $\text{Ce}(\text{SO}_4)_2$ <sup>8</sup>, montmorillonite  $\text{K10}$ <sup>8</sup>, iodine<sup>9</sup>, cationexchanged resins<sup>10</sup>,  $\text{NaHSO}_4 \cdot \text{H}_2\text{O}$ <sup>11</sup>,  $\text{Fe}(\text{HSO}_4)_3$ <sup>12</sup>, sulfamic acid/ultrasound<sup>13</sup>,  $\text{HClO}_4/\text{SiO}_2$ <sup>14</sup>, cyanuric chloride<sup>15</sup> and  $\text{K}_5\text{CoW}_{12}\text{O}_{40} \cdot 3\text{H}_2\text{O}$ <sup>16</sup>. However, some of these catalysts suffer from the drawback of green chemistry such as prolonged reaction times, low yields, toxicity and recovery and reusability of the catalyst. Therefore, introducing clean processes and utilizing eco-friendly

and green catalysts, which can be simply recycled at the end of reactions, have been under permanent attention. The demand for environmentally benign procedure with heterogeneous and reusable catalysts promoted us to develop a safe alternate method for the synthesis of amidoalkyl naphthols.

## RESULTS AND DISCUSSION

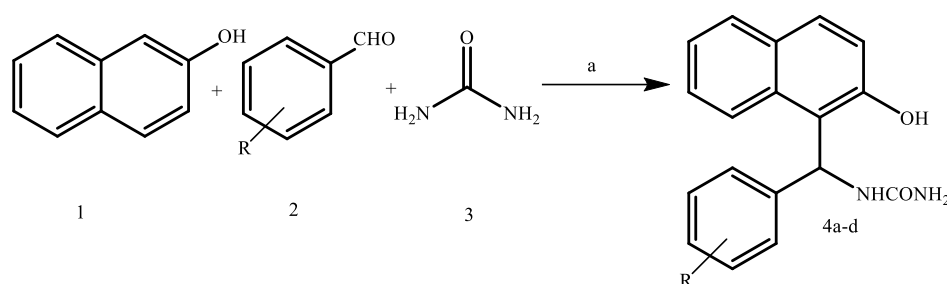
With the literature survey and interest in this area we studied synthesis of 1-amidoalkyl-2-naphthol derivatives, considering advantages of ammonium metavanadate catalyst. Reaction between the 4-Chloro Benzaldehyde, 2-Naphthol and Urea was taken as the model reaction. We have screened ethanol as best solvent for the synthesis of 1-amidoalkyl-2-naphthol derivatives among the solvents. The same reaction carried in methanol and acetonitrile, but ethanol was found to be good solvent. The catalyst activates the carbonyl group of the benzaldehyde by making weak interaction with the oxygen atom of the benzaldehyde. In literature there are several methods for the synthesis of 1-amidoalkyl 2-naphthol derivatives, but in all we had to make choice for either good yields or good reaction conditions. Most of the methods give product in good yield but they make use of expensive catalyst or harsh reaction condition like use of very toxic solvent. There are also methods in which reaction conditions and catalyst cost are taken care of, but yielded very poor or no product. Here in we report one-pot synthesis of 1-amidoalkyl 2-naphthol derivatives using ammonium metavanadate catalyst under room temperature condition.

**Table 1: Screening of the solvents**

Entry	Solvent	Reaction time (hrs)	Yield (%)
01	MeOH	8.00	69
02	CH <sub>3</sub> CN	6.00	67
03	EtOH	4.00	91

**Table 2: Synthesis of 1-Amidoalkyl-2-naphthol derivatives**

Entry	R	Product	Reaction time (hrs)	M.P. (°C)	Yield (%)
01	H	4-a	6.00	136	84
02	3-OH	4-b	4.30	145	86
03	3,4-OCH <sub>3</sub>	4-c	5.00	198	86
04	4-Cl	4-d	4.00	168	91
05	3-NO <sub>2</sub>	4-e	6.00	136	85
06	4-NO <sub>2</sub>	4-f	5.30	145	78
07	4-OH,3-OCH <sub>3</sub>	4-g	5.00	198	87
08	4-OH	4-h	4.30	168	88



**Scheme 1** Reaction conditions: a) Ammonium metavanadate, EtOH, RT, 4-6 hours 78-91 %.

Our studies here in report an ecofriendly method for the synthesis of 1-Amidoalkyl 2-naphthol derivatives using ammonium metavanadate catalyst.

## EXPERIMENTAL

### 3.1 General procedure for synthesis 1-Amidoalkyl 2-Naphthol of derivatives:

A mixture of aromatic aldehyde (2 mmol),  $\beta$ -naphthol (2 mmol), urea (2 mmol) and catalytic amount of ammonium metavanadate (10 mol%) was added in a ethanol solvent (10ml) and reaction mixture was stirred at room temperature for 5-6 hours (Table 1). After completion of reaction indicated by thin layer chromatography (pet ether: ethyl acetate 8:2), reaction mixture was poured in crushed ice and then obtained precipitate was filtered and dried.

**1-((4-chlorophenyl)(2-hydroxynaphthalen-1-yl)methyl)urea:** Light yellow Solid, Yield **91 %**, M. P **168 °C**,  $^1\text{H NMR}$  (300 Hz),  $\text{CdCl}_2$ ,  $\delta$  ppm: 9.42, (s, 1H), 9.15, (d, 1H), 8.02, (s, 2H), 7.86, (d, 2H), 7.59 (d, 1H), 7.39, (d, 2H), 7.40, (s, 1H), 7.24, (t, 1H), 6.72, (d 1H), 6.35, (s, 1H), 6.01, (s, 1H), 5.01, (s, 2H);  $^{13}\text{C NMR}$  (75 Hz),  $\text{CdCl}_2$ ,  $\delta$  ppm: 161.6, 152.1, 146.1, 144.2, 131.9, 127.3, 125.8, 123.1, 122.8, 122.1, 117.3, 114.7, 49.3.

## CONCLUSION

In conclusion, we have developed a convenient and useful one-pot protocol for the synthesis of 1-amidoalkyl 2-naphthol derivatives by the condensation of 2-naphthol, urea and substituted aromatic aldehydes in presence of ammonium metavanadate as catalyst in ethanol under room temperature condition. The delightful features of this protocol are simple experimental workup, mild reaction condition, use of green reaction solvent, cost efficiency and excellent yields of 1-amidoalkyl 2-naphthol derivatives.

### Acknowledgments

The authors are thankful to Prof. Shaikh Md. Babar, Principal of the Dnyanopasak College, Parbhani and to Prof Bhimrao C. Khade, The Head, Department of Chemistry, Parbhani-431401, MS, India for providing the laboratory facility.

## REFERENCES

- [1] T. Dingermann, D. Steinhilber and G. Folkers, Molecular Biology in Medicinal Chemistry, Wiley-VCH, Weinheim (2004).

- [2] A.Y. Shen, C.T. Tsai and C.L. Chen, *Eur. J. Med. Chem.*, **34**, 877 (1999).
- [3] M. Damodiran, N.P. Selvam and P.T. Perumal, *Tetrahedron Lett.*, **50**, 5474 (2009).
- [4] N.P. Selvam and P.T. Perumal, *Tetrahedron Lett.*, **47**, 7481 (2006).
- [5] S. Kantevari, S.V.N. Vuppalapati and L. Nagarapu, *Catal. Commun.*, **8**, 1857 (2007).
- [6] B. Das, K. Laxminarayana, B. Ravikanth and B.R. Rao, *J. Mol. Catal.A: Chem.*, **261**, 180 (2007).
- [7] S.B. Patil, P.R. Singh, M.P. Surpur and S.D. Samant, *Synth. Commun.*, **37**, 1659 (2007).
- [8] Domling A, and Ugi I. *Angew Chem Int Ed* 2000; **39**:3168-3220
- [9] Bienayme H, Hulme C, Oddon G, and Schmitt P. *Chem Eur J* 2000; **6**:3321-3329.
- [10] Orru RVA, and De Greef M. *Synthesis* 2003; **10**:1471-1499.
- [11] H.R. Shaterian and H. Yarahmadi, *ARKIVOC*, **105** (2008).
- [12] H.R. Shaterian, H. Yarahmadi and M. Ghashang, *Bioorg. Med. Chem. Lett.*, **18**, 788 (2008).
- [13] S.B. Patil, P.R. Singh, M.P. Surpur and S.D. Samant, *Ultrason. Sonochem.*, **14**, 515 (2007).
- [14] H.R. Shaterian, H. Yarahmadi and M. Ghashang, *Tetrahedron*, **64**, 1263 (2008).
- [15] G.H. Mahdavinia and M.A. Bigdeli, *Chin. Chem. Lett.*, **20**, 383 (2009).
- [16] L. Nagarapu, M. Baseeruddin, S. Apuri and S. Kantevari, *Catal. Commun.*, **8**, 1729 (2007).

# [Hmim]HSO<sub>4</sub> Catalyzed an Eco-friendly Synthesis of 3-Substituted Indole Derivatives

Miss V. N. Aiwale<sup>1</sup>, Jivan M. Kondre<sup>1</sup>, Dr. Pradeep B. Lasonkar<sup>1</sup>, Dr. Maruti V. Kanetkar<sup>1</sup>, Tukaram E. Khatke<sup>1</sup>,  
Dr. Suresh C. Jadhavar<sup>1\*</sup>

<sup>1</sup>Department of Chemistry, Yogeshwari Mahavidyalaya, Ambajogai, Maharashtra, India

<sup>2</sup>NKSPT's Arts, Science & Commerce College Badnapur Dist: Jalna 431203 Maharashtra, India

## ABSTRACT

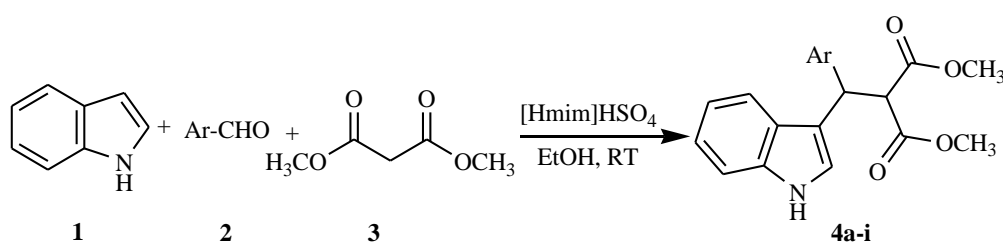
[Hmim]HSO<sub>4</sub> efficiently promotes a one-pot, three-component condensation of indole, aromatic aldehyde and dimethyl malonate to produce 3-substituted indoles in good yields.

**Keywords:** Aromatic Aldehydes, 3-Substituted indoles, Indole, Multi-component reaction, [Hmim]HSO<sub>4</sub>.

## INTRODUCTION

Multicomponent reactions (MCRs) represent nowadays challenging frontier in synthetic organic chemistry. MCRs proved to be a very useful tool for the synthesis of structurally complex molecules, in particular natural products and in the field of drug discovery. Several examples of 'classic' organic processes were recently described in terms of a MCR version.<sup>1,2</sup> The indole moiety is a prominent structural motif which is embodied in a myriad of natural products and molecules of pharmaceutical interest in a variety of therapeutic areas.<sup>3</sup> They possess a wide spectrum of biological activities such as antibacterial, anticonvulsant, and antihypertensive activity.<sup>4</sup> Bis-Indole-based compounds have been reported to have broad-spectrum antibacterial activities against antibiotic-resistant strains and are currently being pursued as topical agents.<sup>5</sup> Hapalindole A isolated from the blue green algae Hapalosiphon fontinalis is a 3-substituted indole derivatives. It exhibits potent antibacterial and antimycotic activities.<sup>6</sup> There are various report on synthesis of 3-substituted indole derivatives synthesized by Lewis acid catalysis such as Ytterbium triflate,<sup>7</sup> PMA-SiO<sub>2</sub>,<sup>8</sup> Yb(OTf)<sub>3</sub>-SiO<sub>2</sub>,<sup>9</sup> Bromodimethylsulfonium bromide,<sup>10</sup> FeCl<sub>3</sub>,<sup>11</sup> InCl<sub>3</sub><sup>12</sup> and AgOTf<sup>13</sup> much attention has been paid to the synthesis of them for a long while.

Thus, the synthesis of highly substituted pyridines has attracted much attention and a number of procedures have been developed till now. Herein we describe a mild and efficient method for the synthesis of 3-substituted indole derivatives using [Hmim]HSO<sub>4</sub> as catalyst (**Scheme 1**). The advantages of this method are mild conditions reaction conditions, ecofriendly and easy experimental work up.



Scheme 1

## RESULTS AND DISCUSSION

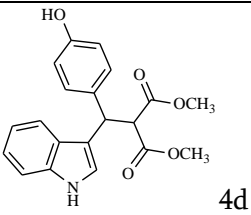
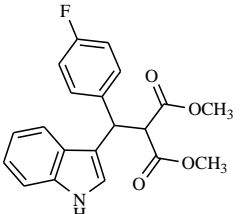
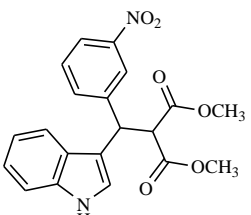
As the indole derivatives have a very effective pharmacological activities, we decided to synthesize the 3-substituted indole derivatives by using [Hmim]HSO<sub>4</sub> in an eco-friendly manner.

The 3-substituted indoles have been obtained in excellent yields in relatively short reaction times in case of aromatic aldehyde (Table 1). It was observed that the process tolerates both electron donating and electron withdrawing substituent on the aldehyde.

**Table1: Synthesis of 3-substituted indole derivatives**

Entry	Ar	Products	Reaction time. (hrs)	M. P. (°C)	Yield (%)
1	4-Cl		3.00	161-163	82
2	-H		4.00	151-152	84
3	4-NO <sub>2</sub>		4.30	145-147	80



4	4-OH	 4d	3.00	170-172	79
5	4-F	 4e	5.00	159-161	80
6	3-NO <sub>2</sub>	 4f	4.00	148-150	77

We also experimentally tried that the synthesis of 3-substituted indoles using different solvents such as methanol, acetonitrile, toluene and dichloromethane afforded corresponding derivatives in low yields ranging from 12-61% over a much longer period of 10 h.

## CONCLUSION

In Conclusion we have describe a mild and ecofriendly method for the synthesis of 3-substituted indoles using [Hmim]HSO<sub>4</sub> as a catalyst. This method is provides an excellent complement to 3-substituted indoles synthesis and avoids the use of hazardous solvent and harsh reaction conditions. The advantages of present method offers good substrate generality, the use of inexpensive reagents and catalyst under mild conditions and experimental operational ease.

## EXPERIMENTAL

All solvents were used as commercial anhydrous grade without further purification. Aluminium sheets 20 x 20cm, Silica gel 60 F<sub>254</sub>, Merck grade was used for thin layer chromatography to determine progress of reaction. The column chromatography was carried out over silica gel (80-120 mesh). Melting points were determined in open capillary tube and are uncorrected.

### General procedure: Synthesis of 3-substituted indoles:

Indole (1mmol), methyl acetoacetate (1mmol) and aromatic aldehyde (1mmol) were mixed in solvent ethanol (15ml). Catalytic amount of [Hmim]HSO<sub>4</sub> (20mol %) was added to the reaction mixture then the

reaction mixture was stirred at room temperature for appropriate time (Table 1). After the completion of reaction, mixture was diluted with water (15 mL) and extracted with diethylether (3 x 4-5mL). The combined organic phase was dried over MgSO<sub>4</sub> and evaporated under reduced pressure. The resulting crude product was purified by column chromatography (silica gel, petether-EtOAc) to obtain analytically pure product.

## ACKNOWLEDGMENTS

We acknowledge Head of Department and Principal, Yogeshwari Mahavidyalaya, Ambajogai for providing necessary facilities to the research work.

## REFERENCES

- [1] Zhu, J.; Bienaymé, H. Wiley-VCH: Weinheim, 2005. 1.
- [2] (a) Ramon, D. J.; Yus, M. *Angew. Chem., Int. Ed.* 2005, 44, 1602; (b) Dömling, A. *Chem. Rev.* 2006, 106, 17.
- [3] (a) Lounasmaa M, Tolvanen A. *Nat. Prod. Rep.* 2000, 17, 175; (b) Hibino S, Choshi T. *Nat. Prod. Rep.* 2002 19,148.
- [4] Collinus J. F. *Med. Bull.* 1965, 21, 223.
- [5] Opperman T. J., Williams J. D., Houseweart C., Panchal R. G., Bavari S., Peet N. P., Moir D.T., Bowlin T. L. *Bioorg. Med. Chem.* 2010, 18, 2123.
- [6] Moore R. E., Cheuk C., Patterson G.M.L. *J. Am. Chem. Soc.* 1984, 106, 6456.
- [7] F. Epifano, S. Genovese, O. Rosati, S. Tagliapietra, C. Pelucchini, M. Curini *Tetrahedron Lett.* 2011, 52, 568.
- [8] P. Srihari, V. K. Singh, D. C. Bhunia, J. S. Yadav, *Tetrahedron Lett.* 2009, 50, 3763.
- [9] V. K. Rao, B. S. Chhikara, A. N. Shirazi, R. Tiwari, K. Parang, A. Kumar. *Bioorg. Med. Chem. Lett.* 2011, 21, 3511.
- [10] D. K. Yadav, R. Patel, V. P. Srivastava, G. Watal, L. S. Yadav, *Tetrahedron Lett.* 2010, 51, 5701.
- [11] J. Liu, T. He, L. Wang, *Tetrahedron* 2011, 67, 3420.
- [12] J. S. Yadav, B. V. Subba Reddy, K. Praneeth, *Tetrahedron Lett.* 2008, 49, 199.
- [13] V. K. Rao, M. S. Rao, *Org. Med. Chem. Lett.* 2011, 1, 10.

# Synthesis of Spiro-fused Heterocycles under Aerobic Conditions by using Polymer Gel Entrapped Catalyst

Shital Shinde, Rajashri Salunkhe\*

Dr. Ganpatrao Deshmukh Mahavidyalaya Sangola, 413307, Maharashtra, India

Department of Chemistry, Shivaji University, Kolhapur, 416004, Maharashtra, India

## ABSTRACT

Spiro-fused heterocycles were synthesized in good to excellent yields by a pseudo three-component reaction of an aldehyde, urea and Meldrum's acid or barbituric acid at ambient temperature.

**Keyword:** Aldehydes, Gel Entrapped-ZnCl<sub>2</sub>, modified Biginelli reaction, recyclability.

## INTRODUCTION

Multi-component reactions (MCRs) have recently emerged as valuable tools in the preparation of structurally diverse chemical libraries of drug-like heterocyclic compounds [1]. The Biginelli reaction is a well-known multi-component reaction involving a one-pot cyclocondensation of an aldehyde, active methylene compounds like Meldrum's acid or barbituric acid and urea [2-4]. Multi-component reactions (MCRs) have recently gained tremendous importance in organic and medicinal chemistry. The main contributing factors are the high atom economy, wide application in combinatorial chemistry and diversity-oriented synthesis [5-11]. Typical examples of the various homogeneous catalysts employed are polyphosphate ester [12], LaCl<sub>3</sub>·7H<sub>2</sub>O [13] and LiClO<sub>4</sub> [14]. Recently Lewis acid catalyzed Biginelli reactions have been extensively reported in the literature.

The use of Lewis acids in organic synthesis, especially in catalysis is one of most rapidly developing fields in synthetic organic chemistry [15]. While various kinds of Lewis acids catalyzed reactions have been developed and many of them applied in industries, these reactions must be carried out strictly under moisture-free conditions [16, 17]. After the completion of reaction, the only viable alternative for separating them is by a destructive water quench. This fact makes the use of Lewis acids as a prime source of the huge quantities of inorganic waste produced within chemical industries. An intriguing line of development in this regard is to replace stoichiometric technologies involving hazardous reagents like Lewis acids with cleaner alternatives.

In this regard, we envisioned that the entrapment of Lewis acids in matrix of agar-agar, the concept acronymed as gel entrapped Lewis acids (GELAs), can prove to be highly attractive strategy to alleviate the problems associated with Lewis acids. The agar-agar is natural hydrosoluble carbohydrate polymer composed of linear chains of repeating agarobiose units alternating between 3-linked-β-D-galactopyransoyl (G) and 4-linked 3,6-anhydro-α-L-galactopyransoyl(LA) units (**Fig. 1**). The bioavailability and potent

biocompatibility of agar-agar explains the interest taken by us for entrapment. We hypothesized that concept of GELA can combine the properties of Lewis acids with that of solid support thus facilitating significant advances in selectivity and activity. Additionally, we envisioned the intact network structure of GELAs will allow for a robust recycling with excellent activity.

Meldrum's acid (2,2-dimethyl-1,3-dioxane-4,6-dione isopropylidene malonate) is an active methylene compound having rigid cyclic structure with high acidity ( $pK_a=4.97$ ) which undergoes hydrolysis very easily. Barbituric acid or malonylurea or 6-hydroxyuracil is an organic compound based on a pyrimidine heterocyclic skeleton. It is an odorless powder soluble in water. Barbituric acid is the parent compound of barbiturate drugs, although barbituric acid itself is not pharmacologically active. Knowing the chemical and pharmacological importance the spiro-fused heterocycles and as a part of our continuing efforts towards the development of sustainable routes for preparation of biologically active compounds, we report herein an efficient multi-component synthesis of spiro-fused heterocycles by using GELAs.

## RESULTS AND DISCUSSION

Initially, we focused our attention towards the preparation of GELAs. The  $ZnCl_2$  and  $AlCl_3$  were used as the prototype Lewis acid in these studies. A series of experiments were under taken in which different concentrations of selected Lewis acids (5-25 %) were dissolved in a varying amount of agar-agar in water. After a substantial experimentation, we found that 20 % *w/w* of agar-agar aqua gel containing 10 % Lewis acids resulted in the formation of soft gel that served as GELAs in the present work. The GELAs are white jelly like substance that could be cut into pieces. The changes in physical nature of GELAs were studied in different solvents like ethanol, dichloromethane, toluene, acetone, dichloromethane and isopropanol. We found that gel remained intact in these organic solvents. On the contrary, the GELAs swelled in water and became soft. Thermal behaviour of GELAs was investigated by thermogravimetric analysis (TGA) and differential thermal analysis (DTA) (**Fig. 2**). The thermograms displayed an initial weigh loss upto 225 °C accompanied by an endotherm corresponding to loss of water molecules accumulated in the GELAs. A second weight loss which occurs between 225 °C to 520 °C can be attributed to thermal decomposition polymeric matrix of agar-agar. This is followed by small weight loss (~ 4%) which can be attributed to the decomposition of metal halide resulting in the formation metallic species. These results revealed that the entrapment of Lewis acids into matrix of agar-agar does not affect the thermal stability of polymer.

Our next task was to demonstrate the catalytic activity of GELA in the synthesis of Spiro-fused heterocycles. A model reaction between the Meldrum's acid/ barbituric acid (5 mmol), urea (5 mmol) and benzaldehyde (5x3 mmol) was carried out. Typically, the reactions were carried out at ambient temperature in open air using 1 gm of GELAs with 5 mmol of substrates in ethanol. The reaction proceeded efficiently yielding the Spiro-fused heterocycles in excellent yield within very short time (**Table 1**). In order to delineate the role of GELAs, a control experiment was carried out in which the model reaction was performed without gel catalyst. No reaction was observed even after prolonged reaction time. We further examined the effect of different atmospheres on the model reaction. We observed that the reaction carried out under aerobic conditions.

As better results were obtained for  $ZnCl_2$ -GELA as compared to  $AlCl_3$ , we employed this particular catalyst for further studies. The generality of the protocol was validated by reacting commercially available Meldrum's acid ( $pK_a=4.97$ ) / barbituric acid ( $pK_a=4.01$ ) (5 mmol), urea (5 mmol) and benzaldehyde (5x3 mmol) (Scheme 1) under aerobic conditions. In general the corresponding Spiro-fused heterocycles were obtained in good to excellent yields (**Table 2**). No significant effects were observed for the substituents on benzaldehyds. The striking feature of all the reactions was the isolation of products. During the course of the reaction the product precipitates out and can be isolated simply by filtration. The product obtained after sufficient washing with ethanol was found to be practically pure. The identity of all the compounds was ascertained on the basis of IR,  $^1H$  NMR,  $^{13}C$  NMR and mass spectroscopy data. The physical and spectroscopic data are in consistent with the proposed structures.

It has been well established that in case of the gel entrapped catalysts, the reagent trapped in the gel may leach into the solvent. Atomic absorption spectroscopy was used for assessing the stability of  $ZnCl_2$ -GELA towards leaching. The analysis revealed that only 65.5 mg/L is leached from 1 gm of catalyst. These results confirm that  $ZnCl_2$ -GELA is stable under the operating conditions used in experiment. Using the amount of  $ZnCl_2$  same as that leached out, the reaction between Meldrum's acid/ barbituric acid (5 mmol), urea (5 mmol) and benzaldehyde (5x3 mmol) did not gave quantitative yield of the corresponding product. This clearly demonstrated that catalysis was solely due to intact gel rather than leached  $ZnCl_2$ . Moreover, hot filtration experiments proved that these catalysts are truly heterogeneous.

Applications of green chemistry and for industrial point of view, the recovery and reusability of catalyst is an important factor. To investigate the possibility of catalyst recycling, the model reaction using  $ZnCl_2$ -GELA in ethanol was carried out. After completion of the reaction, the  $ZnCl_2$ -GELA was recovered by simple filtration, washed with ethanol and subsequently reused in another catalytic cycle with identical substrates. We were delighted to find that the catalyst could be reused for seven runs with excellent yield of product (**Fig. 3**). In addition, the catalyst can be stored and handled in air without deterioration. It was interesting to note that the rates and yields of the reactions were almost same when the catalyst was used after one month of storage on the bench top in air at room temperature.

## EXPERIMENTAL SECTION

Melting points were determined in an open capillary and are uncorrected. Infrared spectra were recorded on a PerkinElmer FT-IR spectrometer. The samples were examined as KBr discs ~5 % w/w.  $^1H$  NMR and  $^{13}C$  NMR spectra were recorded on a Bruker Avon 300 spectrometer using  $DMSO-d_6$  as solvent and TMS as internal reference. The mass spectrum was recorded on Thermo, LCQ Tune spectrometer. TGA-DTA analysis was recorded on SDS Q600 N20.9 in nitrogen. All the chemicals were obtained from s. d. FiNE CHEM, SPECTROCHEM and used without further purification.

### Preparation of Gel Entrapped $ZnCl_2$ (GELA)

A mixture of agar-agar (20 g) in water (140 mL) was prepared first and then added the solution of  $ZnCl_2$  (10 g) in water (10 mL). The resultant solution was boiled with stirring for few minutes and cooled in ice bath to yield the desired GELAs. The GELA is a milky jelly like substance that can be cut into small cubes.

### Synthesis of Spirofused Heterocyclic Compound

A mixture of Meldrum's acid/ barbituric acid (5 mmol), urea (5 mmol) and benzaldehyde (5x3 mmol) was stirred in the presence of GELA (1 g) in 5 mL of ethanol at ambient temperature till the completion of the reaction as monitored by TLC. The resulting crude product was filtered and recrystallized from ethanol to yield the desired product.

#### **3,3-dimethyl-(7S, 11R)-diphenyl-2,4-dioxa-8,10-diazaspiro[5.5]-undecane-1,5,9-trione (Table 1, Entry 1).**

IR (KBr): 3213, 3072, 2923, 1775, 1730, 1683, 1491  $\text{cm}^{-1}$ ;  $^1\text{H}$  NMR (300 MHz,  $\text{DMSO-d}_6$ ): 0.48 (6H, s,  $\text{CMe}_2$ ), 5.26 (2H, s, 2CH), 6.87 (2H, s, 2NH), 7.23-7.30 (10H, m, Ar-H) ppm;  $^{13}\text{C}$  NMR (75 MHz,  $\text{DMSO-d}_6$ ): 28.27, 57.94, 61.83, 105.73, 116.19, 127.95, 129.00, 129.58, 135.41, 153.04, 159.93, 165.96 ppm; MS m/z: 380.0 ( $\text{M}^+$ ).

#### **(7S,11R)-Diphenyl-2,4,8,10-tetraazaspiro[5.5]-undecane-1,3,5,9-tetraone (Table 1, Entry 5).**

IR (KBr): 3216, 3065, 1741, 1678  $\text{cm}^{-1}$ ;  $^1\text{H}$  NMR (300 MHz,  $\text{DMSO-d}_6$ ): 3.87 (1H, s), 5.25 (1H, s), 8.05 (2H, 2NH), 6.80-8.31 (10H, m, Ar-H), 11.21 (1H, s, NH), 11.35 (1H, s, NH) ppm;  $^{13}\text{C}$  NMR (75 MHz,  $\text{DMSO-d}_6$ ): 56.87, 118.52, 128.18, 129.11, 129.67, 132.60, 132.72, 133.77, 134.49, 150.34, 156.52, 161.63, 163.54 ppm; MS m/z: 364.0 ( $\text{M}^+$ ).

### CONCLUSION

In conclusion, the present method is an operationally simple and environmental friendly procedure for the synthesis of spirofused heterocyclic compounds using  $\text{ZnCl}_2$ -GELA at ambient temperature. In addition recyclability, cost effective, short reaction time, easy handling, clean reaction profile, excellent yields of products without any use of more purification and no energy consumption make this methodology a valid contribution to existing processes in the field of spirofused heterocyclic compounds synthesis. To the best of our knowledge, this procedure provides the first example of  $\text{ZnCl}_2$ -GELA catalyzed efficient synthetic method for spirofused heterocyclic derivatives.

### ACKNOWLEDGEMENTS

We gratefully acknowledge the financial support from the Department of Science Technology and University Grants Commission for FIST and SAP respectively. One of the author Miss Shital Shinde thanks UGC, New Delhi for the research fellowship.

### REFERENCES

- [1] Ugi, I.; Dömling, A.; Hörl, W. *Endeavour* 1994, 18,115. (b) Tietze, L. F.; Modi, A. *Med.Res. Rev.* 2000, 20, 304. (c) Ugi, I.; Dömling, A.; Werner, B. J. *Heterocyclic Chem.* 2000, 37, 647. (d) Orru R. V. A.; de Greef, M. *Synthesis* 2003, 1471.
- [2] Biginelli, P. *Gazz. Chim. Ital.* 1893, 23, 360-413.
- [3] Kappe, C. O. *Acc. Chem. Res.* 2000, 33, 879-888. doi:10.1021/ar000048h
- [4] Lusch, M. J.; Tallarico, J. A. *Org. Lett.* 2004, 6, 3237-3240. doi:10.1021/ol048946r
- [5] Ramón, D. J.; Yus, M. *Angew. Chem., Int. Ed.* 2005, 44, 1602-1634. doi:10.1002/anie.200460548

- [6] Ramachary, D. B.; Barbas, C. F., III. *Chem.–Eur. J.* 2004, 10, 5323–5331. doi:10.1002/chem.200400597
- [7] Denmark, S. E.; Fan, Y. *J. Am. Chem. Soc.* 2003, 125, 7825–7827. doi:10.1021/ja035410c
- [8] Andreana, P. R.; Liu, C. C.; Schreiber, S. L. *Org. Lett.* 2004, 6, 4231–4233. doi:10.1021/ol0482893
- [9] Cozzi, P. G.; Rivalta, E. *Angew. Chem., Int. Ed.* 2005, 44, 3600–3603. doi:10.1002/anie.200462757
- [10] Armstrong, R. W.; Combs, A. P.; Tempest, P. A.; Brown, S. D. Keating, T. A. *Acc. Chem. Res.* 1996, 29, 123–131. doi:10.1021/ar9502083
- [11] Burke, M. D.; Schreiber, S. L. *Angew. Chem., Int. Ed.* 2004, 43, 46–58. doi:10.1002/anie.200300626
- [12] Kappe, C. O.; Falsone, S. F. *Synlett* 1998, 718–720. doi:10.1055/s-1998-1764
- [13] Lu, J.; Bai, Y.; Wang, Z.; Yang, B.; Ma, H. *Tetrahedron Lett.* 2000, 41, 9075–9078. doi:10.1016/S0040-4039(00)01645-2
- [14] Yadav, J. S.; Reddy, B. V. S.; Srinivas, R.; Venugopal, C.; Ramalingam, T. *Synthesis* 2001, 1341–1345. doi:10.1055/s-2001-15229.
- [15] (a) K. Ishihara, in *Lewis Acids in Organic Synthesis*, ed. H. Yamamoto, Wiley-VCH: Weinheim, Germany, 2000, vol. 1, pp. 89-133; (b) S. Kobayashi, K. Manabe, *Acc. Chem. Res.*, 2002, 35, pp. 209-217; (c) K. Manabe, Y. Mori, T. Wakabayashi, S. Nagayama, S. Kobayashi, *J. Am. Chem. Soc.*, 2002, 122, pp. 7202-7207; (d) S. Kobayashi, *Pure Appl. Chem.*, 1998, 70, pp. 1019–1026; (e) S. Hu, Z. Zhang, J. Song, Y. Zhou, B. Han, *Green. Chem.*, 2009, 11, pp. 1746-1749; (f) H. E. Lanman, R. -V. Nguyen, X. Yao, T. -H. Chan, C. -J. Li, *J. Mol. Catal. A: Chem.*, 2008, 279, pp. 218-222.
- [16] A. G. Posternak, R. Y. Garlyauskayte, L. M. Yagupolskii, *Tetrahedron Lett.*, 2009, 50, pp. 446–447.
- [17] S. Kobayashi, K. Manabe, *Pure Appl. Chem.*, 2000, 72, pp. 1373–1380.
- [18] A. Shaabani, A. Bazgir, *Tetrahedron. Lett.*, 2004, 45, 2575.

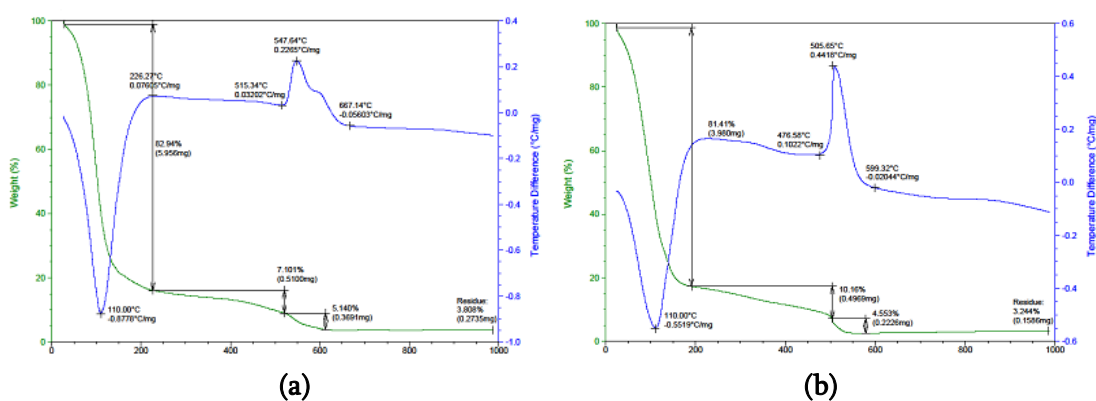
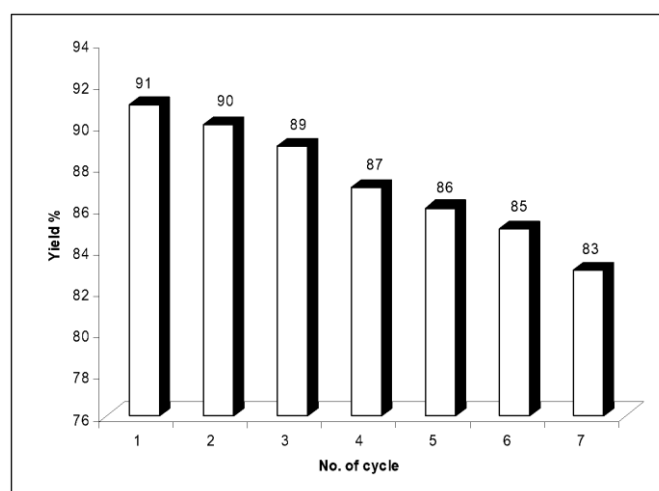
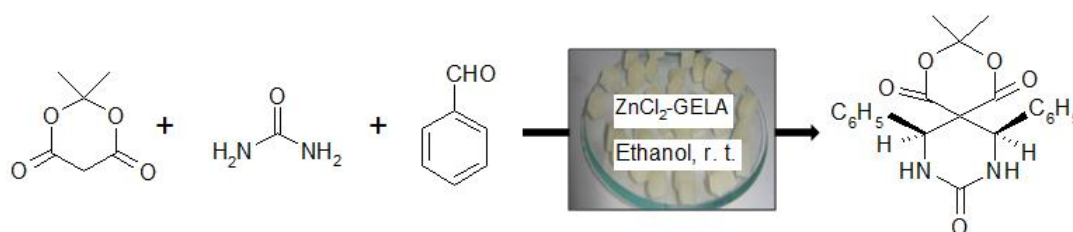


Fig.2 DSC-TGA graph of (a) ZnCl<sub>2</sub>-GELA and (b) AlCl<sub>3</sub>-GELA



**Fig. 3** Recycled use of GELA in spirofused heterocyclic compound

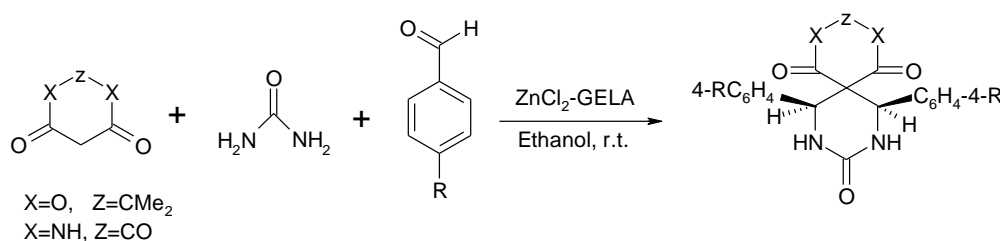
**Table 1:** Screening of GELAs for spirofused compound<sup>a</sup>



Entry	GELA	Time (min)	Yield <sup>b</sup> (%)
1	ZnCl <sub>2</sub> -GELA	10	87
2	AlCl <sub>3</sub> -GELA	10	81

<sup>a</sup>The reaction of benzaldehyde, urea and Meldrum's acid.

<sup>b</sup>Isolated yield.



**Scheme 1:** GELA catalyzed multi-component synthesis of spirofused heterocyclic compound



# Isolation And Screening of Dye Degrading Actinomycetes from Textile Effluent Contaminated Soil

Mr. Warbhuvan P.G, Dr. Narsinge A. P, Mr. Kadam A. S, Mr. Karpude T. N

Department of Microbiology, Yogeshwari Mahavidyalaya, Ambajogai, Dist. Beed (M.S.)-431517

e-mail ID- [narsingeanil@gmail.com](mailto:narsingeanil@gmail.com)

Department of Microbiology, Sau. KSK College, Beed, Dist. Beed

## ABSTRACT

Actinomycetes plays a game changing role in bioremediation because of their inherent capacity to decompose varied organic structure bearing synthetic dyes. In present investigation, textile dye-degrading actinomycetes were screened from the soil sample collected from the textile effluent. Ten actinomycetes isolates were obtained on actinomycetes isolation agar and were checked for morphological characteristics which included the feature of filamentous mycelia and chalky colony. The method of primary screening for this dye degrader was done by the formation of clear decolorization halos around the colonies. Five actinomycetes isolates exhibited potent dye degradation. All the potent isolates produced sporulation, aerial hyphae, and pigmentation which are hallmarks of the actinomycete family. This study certainly underlines the potential significance of indigenous actinomycetes in the biodegradation of textile dyes. Further research is required to fine tune the reaction conditions that would facilitate higher levels of dye degradation and to determine the specific route by which the enzyme acts on the dye. These outcomes indicate the importance of microbial approaches in managing sustainable wastewater and help establish best practice to link microbial treatments into the industrial activities.

**Keywords :** Bioremediation, Textile dyes, Actinomycetes, Biodegradation, Environmental Health.

## INTRODUCTION

The textile industry is among the biggest industries in the global economy generating high employment and economic returns (Kim, et al., 2006; Khurana, 2022). But it has also been found that textile industry is a leading source of environmental pollution because of the direct release of a huge amount of untreated or partially treated wastewaters (Abid, et al., 2012). These effluents contain dangerous chemical, synthetic dyes, heavy metal and other hazardous material. Out of all the pollutants, the synthesized dyes are the most dangerous due to their highly saturated chemical composition, which even does not allow for their sequestration (Baldev, et al., 2013; Rangabhashiyam, et al., 2013). Discharge of effluents containing dye having a hazardous impact, polluting water, less penetration of light and is toxic to water living organisms. In addition, the pollutants get within the soil and they affect the soil, its microbial flora and fauna as well

(Almroth, et al., 2021). Hence, there is need to occasionally advance effective and renewable techniques of dye elimination. Over the last decade, bioremediation has been preferred as a clean technology for the treatment of dye-intoxicated environment. In the general characterization and analysis of microorganisms the ability of biodegradation, Actinomycetes has received much attention due to the fact that they are capable of breaking down synthetic dyes into homogenous simpler organic compounds (Devanshi, et al., 2021). Actinomycetes are bacteria which are filamentous, Gram-positive or neutral and unique due to their versatility in metabolic capabilities and distribution as well as secondary metabolites which include antibiotics, enzymes and pigments (Salwan and Sharma, 2010). Compared to other organisms, these organisms are well suited to withstand the conditions of harsh environments, while the specialized enzymatic systems, which the organisms have developed, are well equipped for the degradation of RR and other slow degrading compounds making the organisms ideal for bioremediation of environments contaminated by dyes (Mishra, et al., 2022). The family of actinomycetes – Streptomyces family – was chosen for the investigation of its capabilities in the degradation of environmental pollutants, such as dyes used in the textile industry (Devanshi, et al., 2021). Extracellular enzymes from Streptomyces species include laccases, peroxidases and azo-reductases that degrade bonds in synthetic dyes and reduces toxicity of the resultant products. These enzymes effect the decolorization and detoxification process since they split the azo bonds and the Synthetic dyes have aromatic rings in their structure (Kamal, et al., 2022). Furthermore, Actinomycetes have been found to produce biosurfactants that improve solubility and thus bioavailability of water insoluble pollutants making it easier to degrade them. Textile effluent contaminated soils are suitable to isolate the dye degrading Actinomycetes due to repeated exposure to organic dyes, heavy metals and organic solvents (Rajhans, et al., 2021). These extreme conditions may over time drive a variety of microbial species in such soils to genetically adapt and derive unique pathways for metabolism of these pollutants (Schultz, et al., 2023). The identification of dye-degrading Actinomycetes from such a polluted substrate has tremendous prospects for the advancement of biodegradation methods designed to enhance the environmental reckon of textile wastewater (Tripathi, et al., 2023). Thus, while Actinomycetes have shown great potential in bioremediation, the majority of isolates have been sourced from dye-contaminated water sources or from sewage treatment plants followed by habitats polluted with textile effluent has received comparatively little attention. The current study shall therefore fit the bill by isolating and screening dye-degrading Actinomycetes from the textile effluent contaminated soil samples. Some of the isolated strains will be tested for dye decolorization activity with synthetic dyes where azo dyes and anthraquinone dyes will be considered (Melati, et al., 2023). Positive strains will then be characterized for the enzymatic activity for the production of the specific enzymes required for the degradation of dyes. Molecular identification methods which include 16S rRNA will be used to identify the isolated strains at species level. The findings of this study are anticipated to add to the existing literature on the bioremediation ability of Actinomycetes together with the pattern of enzymatic degradation of dyes. The isolation of dye-degrading microorganisms from effluent contaminated soils could provide a basis for the formulation of microbial consortium or enzyme-based systems for the remediation of textile effluents. Moreover, the knowledge of enzymatic pathways which mediate degradation of dye may help to isolate new enzymes with application in treatment of Textile effluent wastewater. Therefore, the identification and characterization of dye-degrading Actinomycetes from Textile effluent contaminated soils present a novel solution to the

ecological problems associated with the Textile industry. In addition to being a source of bioactive compounds with possible bioremediation properties, this research will seek to analyse the enzymatic pathways for decolourisation of dyes, which will expand the scope of sustainable management of textile wastewater.

## Materials & Methods

### Sample Collection and Processing

Soil samples were collected from the top 10–15 cm layer at five distinct sites in a textile effluent-contaminated area in Ichalkaranji, M.S. India. Sterile polythene bags were used to store the samples, which were immediately transported to the laboratory for further processing. The samples were air-dried, ground, and sieved to remove debris and ensure homogeneity.

### Isolation of Actinomycetes

Actinomycetes were isolated using serial dilution and spread plate techniques on Actinomycetes isolation agar, M940 (HiMedia, Mumbai) as per manufacturer guidelines with suitable inhouse modifications. Plates were incubated at  $28 \pm 2^\circ\text{C}$  for 7–14 days. Distinct colonies with typical actinomycete morphology (e.g., powdery texture, pigmentation) were sub-cultured on ISP-2 media (Inhouse Recipe) for purification.

### Morphological Characterization

The purified isolates were then subjected to Gram staining and microscopic analysis to ensure that they belong to the cluster of the actinomycetes. Entire examination was performed as per previously published protocol (Li, et al., 2016).

**Table No. 1. Morphological characters of textile dye degrading actinomycetes**

Isolate Number	Shape	Elevation	Colony Texture	Pigment	Size (mm)	Gram nature	Mycelia	Opacity	consistency
1	Round	Raised	Powdery	Yellowish	6	Positive	Branch	Opaque	Dry
2	Round	Raised	Powdery	whitish	7	Positive	Branch	Opaque	Dry
3	Round	Raised	Powdery	whitish	5	Positive	Branch	Opaque	Dry
4	Round	Raised	Powdery	whitish	8	Positive	Branch	Opaque	Dry
5	Irregular	Raised	Powdery	whitish	6	Positive	Branch	Opaque	Dry

### Screening for Degradation

Primary screening of the isolates for dye-degrading activity was conducted on agar plates containing Minimal Salt Medium (MSM) supplemented with 100 mg/L of model dyes Yellow C4G, Navy Blue BNC, Yellow M4G, Red M5B, Reactive Orange M2R (The selection of dyes was based on the most commonly used dyes by textile companies at the sampling location). Dye degradation was indicated by the formation of clear zones around the colonies after 72 hours of incubation at  $30^\circ\text{C}$ .

## Observation & Results

### Isolation and Screening of Dye-Degrading Actinomycetes

From the textile effluent-contaminated soil, ten distinct actinomycete isolates were successfully obtained using actinomycetes isolation agar. Morphological evaluation confirmed that all isolates exhibited characteristic features of actinomycetes, including filamentous mycelia and powdery (chalky) colony texture (Table 1) (Figure 1)..

### Screening for Dye Degradation Potential

Primary screening was performed on all ten isolates to determine their efficacy to decolorize textile dyes. The screening was done following the loss of dye and the development of white halos around the colonies.

Of the isolates, 5 (n=5) out of the 10 isolates exhibited elevated levels of dye-degrading activity and formed clear decolorization halos. The remaining isolates exhibited little or no detectable degradation under the conditions of the study.

#### Identification of Potent Isolates

The top-performing isolates were identified through detailed morphological and microscopic analyses. The selected isolates exhibited sporulation with aerial hyphae and distinct pigmentation, consistent with the morphology of actinomycetes. These findings affirm the successful isolation of indigenous actinomycetes capable of degrading textile dyes from polluted environments. The study demonstrates the potential of actinomycetes isolated from textile effluent-contaminated soil to degrade synthetic dyes. The screening results highlight that specific isolates possess robust dye-degrading abilities, suggesting their relevance for future bioremediation applications. Further studies are recommended to explore optimal conditions for dye degradation and to elucidate the enzymatic mechanisms involved.

**Figure 1: Typical isolated colonies of actinomycetes-on-actinomycetes isolation agar**



#### Discussion

Among the possible microbiological candidates, actinomycetes are the group of filamentous, Gram-positive bacteria that have recently drawn considerable interest in bioremediation because of their potential of using diverse and often complex substrates, such as synthetic dyes (*Abdelrahman, et al., 2022*). The treatment of textile effluent is an important issue internationally because the final products contain issues azo dyes that are difficult to degrade through normal wastewater treatment processes (*Yaseen & Scholz, 2019; Ramzan, et al., 2022*). The potential of actinomycetes in expressing extracellular enzymes including peroxidases and laccases makes them suitable for dismantling of dyes (*Casciello, et al., 2017*). The actinomycetes isolated from the contaminated soil also possess typical micro morphological features like branching hyphae and the colonies are powdery confirming filamentous nature. In the present study, all the tested isolates were Gram-positive which is consistent with the general characteristics of actinomycetes. Generally, pigments produced by the colony, which were whitish to yellowish in color, are mainly due to secondary metabolite production, including enzymes that affect the degradation of dye (*Thompson, et al., 2002*). The odourless and powder-like nature of the opercula implies that the structure can offer resistance to external stress under conditions of industrial effluent (*Afrad, et al., 2022*). The phenotypical differences seen across the isolates apparent from

the differences in shape and size of the colonies suggest the existence of metabolically different strains among the isolates. Larger colonies could be associated with higher biomass that in return enhances enzyme synthesis and degradation of dyes from isolates with a diameter of 7-8mm (Patel & Gupte, 2022). In addition, the higher altitude position, together with the branched mycelial network, can promote substrate assimilation for better microbial interaction with dye molecules (Varjani, et al., 2020). These structures include laccases, manganese peroxidases, and azo reductases produced by Actinomycetes that degrade the complex aromatic structures of synthetic dyes (Aragaw, 2024). This organization ensures that these extracellular enzymes are well secreted by the branching mycelial structure observed in the isolates. Furthermore, the observed yellowish pigments in some of the isolates may indicate that some of these organisms produce secondary metabolites, which may be useful for decolorization. It has been demonstrated that bacteria bearing pigment synthesizing potentials undergo higher metabolic rates than the unpigmented ones; these elevated metabolic rates may well augment the capability of the bacterial strains to break down the textile dyes effectively (Sheela & Sadasivam, et al., 2021). Recent studies have focused on the issue of microbial screening in view of bioremediation processes (Ayilara, & Babalola, 2023). For example, *Streptomyces* spp. from the genus of actinomycetes have been identified to exhibit high potential to degrade azo dyes including methyl orange and Congo red (Kameche, et al., 2022). Likewise, the consortia of actinomycetes with other bacteria specially *Bacillus* has also been studied for improving the dye degradation via interaction (Kameche, et al., 2022). The isolates as informed in distal sections of this homemade paper trail these tendencies and thus hold potentials towards treating industrial wastewater (Tyagi, et al., 2014). Nonetheless, a lot more work has to be done to determine their enzymatic characteristics, the growth conditions, as well as the decolourisation capacities for different dyes. Coagulation, adsorption, and oxidation which are conventional physical and chemical processes are often costly and may produce secondary pollutants (Rezai & Allahkarami, 2021). On the other hand, the microbial treatments with actinomycetes are economically viable and environment friendly as these break down the dyes into less toxic forms (Gomaa, et al., 2023). In the same vein, actinomycetes are capable of surviving extreme salinity and pH gradients in contaminated textile effluents making them relevant for real environmental operations (Bertrand, et al., 2015). However, there are several limitations to the use of actinomycetes for dye degradation that need further elucidation in order to fully realize this potential (Qiu, et al., 2022). Reusability of enzymes and proteins requires understanding of substrate specificity, enzyme stability and optimal growth conditions for complete degradation in commercial scale (Maghraby, et al., 2023). Modern research has indicated that other approaches such as genetic modification and metabolic route enhancement can improve the dye-degrading potentiality of actinomycetes, (El Awady, et al., 2024). Further, the microbial treatments can be adopted with existing wastewater infrastructures to enhance the way they can be implemented in the industrial level (Kaur, et al., 2024). The actinomycetes found in the present investigation from the contaminated soil with textile effluent have desirable morphological and physiological potential for effluent degradation. It is agreed that their branching mycelium, pigmentation and capacity to grow under extreme conditions make them candidates for dye degradation. Yet, more studies should be conducted in order to determine which enzymes are involved in this process, how one can enhance the degradation process, and evaluate the effectiveness of proposed techniques when applied to industrial effluent. This research adds to the global pool of evidence on the applicability of actinomycetes in the sustainable management of wastewater and creates the

framework for subsequent research touching on the synthesis of microbial consortia with the goal of improving the removal of the dye.

### Future Scope

As revealed in this study, dye-degrading actinomycetes can be further exploited for cost effective dignity of wastewater. Subsequent studies will focus on proper condition for degradation, identification and characterization of crucial enzymes, and system improvement and standardization for large scale bioreactor usage. The combination of these isolates with microbial consortia hints promising prospects for progressive effluent treatment. If they were pushed to the limit, they have the capability of revolutionizing methods of industrial waste disposal and the adoption of environmentally sustainable technologies in the textiles industry.

### References

1. Abdelrahman, O., Yagi, S., El Siddig, M., El Hussein, A., Germanier, F., De Vrieze, M., ... & Weisskopf, L. (2022). Evaluating the antagonistic potential of actinomycete strains isolated from Sudan's soils against *Phytophthora infestans*. *Frontiers in Microbiology*, *13*, 827824.
2. Abid, M. F., Zablouk, M. A., & Abid-Alameer, A. M. (2012). Experimental study of dye removal from industrial wastewater by membrane technologies of reverse osmosis and nanofiltration. *Iranian journal of environmental health science & engineering*, *9*, 1-9.
3. Afrad, M. S. I., Monir, M. B., Haque, M. E., Barau, A. A., & Haque, M. M. (2020). Impact of industrial effluent on water, soil and Rice production in Bangladesh: a case of Turag River Bank. *Journal of Environmental Health Science and Engineering*, *18*, 825-834.
4. Almroth, B. C., Cartine, J., Jönander, C., Karlsson, M., Langlois, J., Lindström, M., ... & Sturve, J. (2021). Assessing the effects of textile leachates in fish using multiple testing methods: From gene expression to behavior. *Ecotoxicology and Environmental Safety*, *207*, 111523.
5. Aragaw, T. A. (2024). A review on biodegradation of textile dye wastewater: Challenges due to wastewater characteristics and the potential of alkaliphiles. *Journal of Hazardous Materials Advances*, 100493.
6. Ayilara, M. S., & Babalola, O. O. (2023). Bioremediation of environmental wastes: the role of microorganisms. *Frontiers in Agronomy*, *5*, 1183691.
7. Baldev, E., MubarakAli, D., Ilavarasi, A., Pandiaraj, D., Ishack, K. S. S., & Thajuddin, N. (2013). Degradation of synthetic dye, Rhodamine B to environmentally non-toxic products using microalgae. *Colloids and Surfaces B: Biointerfaces*, *105*, 207-214.
8. Bertrand, J. C., Doumenq, P., Guyoneaud, R., Marrot, B., Martin-Laurent, F., Matheron, R., ... & Soulas, G. (2015). Applied microbial ecology and bioremediation: Microorganisms as major actors of pollution elimination in the environment. *Environmental Microbiology: Fundamentals and Applications: Microbial Ecology*, 659-753.
9. Casciello, C., Tonin, F., Berini, F., Fasoli, E., Marinelli, F., Pollegioni, L., & Rosini, E. (2017). A valuable peroxidase activity from the novel species *Nonomurea gerenzanensis* growing on alkali lignin. *Biotechnology Reports*, *13*, 49-57.

10. Devanshi, S., Shah, K. R., Arora, S., & Saxena, S. (2021). Actinomycetes as an environmental scrubber.
11. El Awady, M. E., El-Shall, F. N., Mohamed, G. E., Abd-Elaziz, A. M., Abdel-Monem, M. O., & Hassan, M. G. (2024). Exploring the decolorization efficiency and biodegradation mechanisms of different functional textile azo dyes by *Streptomyces albidoflavus* 3MGH. *BMC microbiology*, *24*(1), 210.
12. Gomaa, H., Emran, M. Y., & El-Gammal, M. A. (2023). Biodegradation of azo dye pollutants using microorganisms. In *Handbook of Biodegradable Materials* (pp. 781-809). Cham: Springer International Publishing.
13. Kamal, I. M., Abdeltawab, N. F., Ragab, Y. M., Farag, M. A., & Ramadan, M. A. (2022). Biodegradation, decolorization, and detoxification of di-azo dye direct Red 81 by halotolerant, alkali-thermo-tolerant bacterial mixed cultures. *Microorganisms*, *10*(5), 994.
14. Kameche, K., Amrani, S., Mouzaoui, S., & Aït-Amar, H. (2022). Biodegradation of diazo dye Evans blue by four strains of *Streptomyces* isolated from soils of Algeria. *Biocatalysis and Agricultural Biotechnology*, *46*, 102529.
15. Kaur, B., Choudhary, R., Sharma, G., & Brar, L. K. (2024). Sustainable and Effective Microorganisms method for wastewater treatment. *Desalination and Water Treatment*, 100419.
16. Khurana, K. (2022). The Indian fashion and textile sector in and post COVID-19 times. *Fashion and Textiles*, *9*(1), 15.
17. Kim, J. O., Traore, M. K., & Warfield, C. (2006). The textile and apparel industry in developing countries. *Textile progress*, *38*(3), 1-64.
18. Li, Q., Chen, X., Jiang, Y., & Jiang, C. (2016). Morphological identification of actinobacteria. *Actinobacteria-basics and biotechnological applications*, 59-86.
19. Maghraby, Y. R., El-Shabasy, R. M., Ibrahim, A. H., & Azzazy, H. M. E. S. (2023). Enzyme immobilization technologies and industrial applications. *ACS omega*, *8*(6), 5184-5196.
20. Melati, I., Rahayu, G., Effendi, H., Henny, C., & Yanto, D. H. Y. (2023). Biodecolorization of anthraquinone and azo dyes by dark septate endophytic fungi. *Bioresource Technology Reports*, *22*, 101427.
21. Mishra, A., Takkar, S., Joshi, N. C., Shukla, S., Shukla, K., Singh, A., ... & Varma, A. (2022). An integrative approach to study bacterial enzymatic degradation of toxic dyes. *Frontiers in Microbiology*, *12*, 802544.
22. Patel, Y., & Gupte, A. (2023). Accelerated biodecolorization and detoxification of synthetic textile dye Acid Maroon V by bacterial consortium under redox mediator system. *3 Biotech*, *13*(2), 51.
23. Qiu, H., Shen, F., Yin, A., Liu, J., Wu, B., Li, Y., ... & Xu, B. (2022). Biodegradation and detoxification of azo dyes by halophilic/halotolerant microflora isolated from the salt fields of Tibet autonomous region China. *Frontiers in Microbiology*, *13*, 877151.
24. Rajhans, G., Barik, A., Sen, S. K., Masanta, A., Sahoo, N. K., & Raut, S. (2021). Mycoremediation and toxicity assessment of textile effluent pertaining to its possible correlation with COD. *Scientific Reports*, *11*(1), 15978.
25. Ramzan, U., Shakoori, F. R., Zahid, M. T., Majeed, W., Zahra, I., Abbas, S. Z., ... & Mutery, A. A. (2022). Biodegradation and decolorization of textile azo dyes by *Paramecium caudatum* isolated from industrial wastewater. *Water*, *14*(21), 3553.



26. Rangabhashiyam, S., Anu, N., & Selvaraju, N. (2013). Sequestration of dye from textile industry wastewater using agricultural waste products as adsorbents. *Journal of Environmental Chemical Engineering*, 1(4), 629-641.
27. Rezai, B., & Allahkarami, E. (2021). Wastewater treatment processes—techniques, technologies, challenges faced, and alternative solutions. In *Soft computing techniques in solid waste and wastewater management* (pp. 35-53). Elsevier.
28. Salwan, R., & Sharma, V. (2020). Molecular and biotechnological aspects of secondary metabolites in actinobacteria. *Microbiological research*, 231, 126374.
29. Schultz, J., Modolon, F., Peixoto, R. S., & Rosado, A. S. (2023). Shedding light on the composition of extreme microbial dark matter: alternative approaches for culturing extremophiles. *Frontiers in Microbiology*, 14, 1167718.
30. Sheela, T., & Sadasivam, S. K. (2020). Dye degradation potential and its degradative enzymes synthesis of *Bacillus cereus* SKB12 isolated from a textile industrial effluent.
31. Thompson, C. J., Fink, D., & Nguyen, L. D. (2002). Principles of microbial alchemy: insights from the *Streptomyces coelicolor* genome sequence. *Genome biology*, 3, 1-4.
32. Tripathi, M., Singh, S., Pathak, S., Kasaudhan, J., Mishra, A., Bala, S., ... & Pathak, N. (2023). Recent strategies for the remediation of textile dyes from wastewater: a systematic review. *Toxics*, 11(11), 940.
33. Tyagi, S., Kumar, V., Singh, J., Teotia, P., Bisht, S., & Sharma, S. (2014). Bioremediation of pulp and paper mill effluent by dominant aboriginal microbes and their consortium. *International Journal of Environmental Research*, 8(3), 561-568.
34. Varjani, S., Rakholiya, P., Ng, H. Y., You, S., & Teixeira, J. A. (2020). Microbial degradation of dyes: An overview. *Bioresource Technology*, 314, 123728.
35. Yaseen, D. A., & Scholz, M. (2019). Textile dye wastewater characteristics and constituents of synthetic effluents: a critical review. *International journal of environmental science and technology*, 16, 1193-1226.



## **Two Days National Conference on Material Science and Chemistry**

### **Organized By**

**Department of Chemistry and  
Internal Quality Assurance Cell  
Yogeshwari Mahavidyalaya, Ambajogai.  
Dist. Beed, Maharashtra, India**

### **Publisher**

Technoscience Academy



Website : [www.technoscienceacademy.com](http://www.technoscienceacademy.com)

Email : [editor@ijsrst.com](mailto:editor@ijsrst.com) Website : <http://ijsrst.com>